Molecular and physiological responses to elevated temperatures in *Arabidopsis thaliana* and barley

Dissertation zur Erlangung des Doktorgrades der Naturwissenschaften (Dr. rer. nat.)

der

Naturwissenschaftlichen Fakultät III
Agrar- und Ernährungswissenschaften,
Geowissenschaften und Informatik

der Martin-Luther-Universität Halle-Wittenberg

vorgelegt von

Frau Bellstädt, Julia
Geb. am 23.03.1989 in Dessau-Roßlau

Verteidigungsdatum: 21.11.2022
Gutachter: Prof. Dr. Marcel Quint, Prof. Dr. Jutta Ludwig-Müller

Für meinen Freund Dirk und meine Eltern

Abstract

Temperature is a major factor governing the distribution and seasonal behavior of plants. Being sessile, plants are highly responsive to small differences in temperature. Plant growth and development are adjusted accordingly, collectively referred to as thermomorphogesis. In the light of climate change, especially plant behavior in response to elevated ambient temperatures is of increasing interest not only for fundamental science but also for plant breeding. Our understanding of temperature signaling has recently been progressing, mainly by exploiting temperature-sensitive hypocotyl elongation in the model plant *Arabidopsis thaliana*. However it remained unknown, how different shoot organs elevated temperature perceive. Furthermore, temperature signaling in roots are not understood at all.

My thesis aimed to dissect temperature signaling on an organ level. Specifically, I investigated whether cotyledons, hypocotyls, and roots sense changes in temperature autonomously as sensing, signal transduction, and growth responses might be spatially separated between organs. While focusing on *A. thaliana*, studied similar responses in the major crop *Hordeum vulgare* (barley). By assessing warmth-induced growth in barley, I analyzed whether the responses identified in *A. thaliana* can be transferred to distantly related crops.

In Arabidopsis, I found that hypocotyl elongation in response to elevated temperatures depends on temperature sensing in the cotyledons. In the regulation of this process phytohormones such as auxin and brassinosteroids play a key role. Thus an increase in temperature triggers a cotyledon-derived mobile auxin signal, which is transmitted via the petioles to the hypocotyls where it induces the biosynthesis of brassinosteroids to elicit cell elongation.

In contrast, the temperature-induced root elongation seems to be partially independent of the shoot. However, the absence of defective root elongation responses in shoot thermomorphogenesis mutants suggests a mode of action that differs between the two organs. While cell elongation is the dominating factor of warmth-induced growth in the shoot, root thermomorphogenesis is primarily caused by cell divisions. Thus, shoots and roots are probably utilizing different distinct temperature signaling pathways. Furthermore, genetic and pharmacological analyses suggest that the stimulation in cell division rate at elevated temperature may be largely due to an increase in intracellular auxin levels, possibly by up-regulating auxin biosynthesis. Moreover, my experiments revealed that elevated temperatures in the root may altering the activity of the auxin efflux carrier PIN-FORMED 2 (PIN2), and promoting the degradation of the AUXIN/INDOLE-3-ACETIC ACID (AUX/IAA) family of transcriptional repressors.

The third part of my work attempts to improve our understanding of thermomorphogenesis in barley. Therefore, a non-invasive, medium-throughput phenotyping system was used to screen a set of 48 juvenile wild barley introgression lines (S42ILs) for the temperature-sensitive shoot and root growth. Generally, among the 25 measured phenotypic traits, the majority seem to be positively affected by elevated temperatures. Through a quantitative trait loci (QTL) analysis, a total of 122 QTLs associated with 16 phenotypic traits were detected. Among them, several genomic "hotspots" were identified which may control correlated root and shoot traits, indicating certain genetic coordination between these plant tissues. Overall, results represent the first step towards a comparative understanding of thermomorphogenesis in plants.

Keywords: Arabidopsis, barley, hypocotyl, cotyledons, roots, thermomorphogenesis, brassinosteroids, auxin, temperature, sensing, signaling, response

Abstract – Deutsche Version

Für die jahreszeitliche Entwicklung und Verbreitung von Pflanzen spielt der Faktor Temperatur eine wesentliche Rolle. Als festsitzende (sessile) Lebewesen sind Pflanzen gezwungen auf widrige Umweltbedingungen wie Temperaturerhöhungen mit veränderten Wachstum zu reagieren. Diese Prozesse werden unter dem Begriff ,,Thermo-morphogenese" zusammengefasst. Vor allem im Rahmen des Klimawandels ist das Verstehen dieser Anpasssungsmechanismen nicht nur für die Grundlagenforschung, sondern auch für die Pflanzenzüchtung relevant. Durch intensive Forschung an der Modellpflanze *Arabidopsis thaliana* konnte in den letzten Jahren ein breites Wissen über die grundlegenden molekularen Signalwege generiert werden. Grundlage für diese Erkenntnisse waren übeUS stainingrwiegend Beobachtungen am Modellphänotyp der temperaturinduziereten Hypokotylverlängerung. Wie die anderen Pflanzenorgane, neben dem Hypokotyl, erhöhte Temperaturen wahrnehmen, ist hingegen kaum untersucht. Insbesondere über die Temperaturreaktionen in der Wurzel ist nur wenig bekannt.

In meiner Dissertation habe ich daher versucht, mich bei der Betrachtung der entsprechenden Prozesse nicht nur auf den Spross zu beschränken, sondern auch weitere Pflanzenorgane, wie die Wurzel und die Keimblätter (Kotyledonen) mit einzubeziehen. Konkret bin ich der Frage nachgegangen, ob Kotyledonen, Hypokotyl und Wurzel in der Lage sind, erhöhte Temperaturreize autonom wahrzunehmen und darauf zu reagieren oder ob diese Prozesse räumlich voeinander getrennt erfolgen. Dabei habe ich neben den Untersuchungen an der Modellpflaze *A. thaliana,* Temperaturphänotypen der Nutzpflanze *Hordeum vulgare* (Gerste) analysiert. Die Experimente an Arabidopsis

ergaben, dass die Hypokotylverlängerung unter erhöhten Temperaturen von der Temperaturwahrnehmung in den Kotyledonen abhängt. In der Regulation dieser Prozesse spielen Phytohormone wie Auxin und Brassinosteroide eine wesentliche Rolle.So löst die Temperaturwahrnehmung ein mobiles Auxin-Signal aus, das über die Petiolen zum Hypokotyl weitergeliet wird, wo es die Biosynthese von Brassinosteroidenen induziert, um Zellstreckungsprozesse auszulösen.

Im Gegensatz dazu scheint die Wurzel in der Lage, Temperaturreize teilweise autonom wahrzunehmen zu können und darauf zu reagieren.. Da Mutationen von bekannten, am Temperatursignalweg im Spross, beteiligten Genen nur geringfügige Auswirkungen auf das Längenwachstum in der Primärwurzel hatten, wird vermutet, dass die Wurzel auf andere, vom Spross verschiedene Signalwege zurückgreift. Ebenfalls dafür spricht die Beobachtung, das für das temperaturinduzierten Längenwachstum im Hypokotyl vorwiegend die Zellstreckung verantwortlich gemacht werden kann, während die Verlängerung der Wurzel unter erhöhten Temperaturen eher durch gesteigerte Zellteilungsprozesse hervorgerufen wird. Die Ergebnisse aus meinen genetischen und pharmakologischen Analysen lassen auch vermuten, dass der Anstieg in der Zellteilungsrate unter erhöhten Temperaturen weitgehend auf einen Zunahme in der intrazellulären Auxinkonzentration zurückzuführen ist, möglicherweise durch eine Hochregulierung Auxin-Biosynthese. ErhöhteTemperaturen scheinen zudem die Ativität des Auxin-Efflux-Carriers PIN-FORMED2 (PIN2) zu verändern und den Abbau der AUXIN/INDOLE-3-ACETIC ACID (AUX/IAA)-Familie von Transkriptionsrepressoren zu fördern.

Schließlich sollte der dritte Teil meiner Arbeit dazu beitragen, unser Verständnis der Thermomorphogenese in Gerste zu verbessern. Dazu wurde ein nicht-invasives Hochdurchsatz-Phänotypisierungssystem verwendet, um ein Set aus 48 Introgressionslinien (S42ILs) auf temperatursensitive Spross- und Wurzelphänotypen zu screenen. Generell scheint die Mehrheit der 25 untersuchten phänotypischen Merkmale positiv von erhöhten Temperaturen beeinflusst zu werden. Durch eine quantitative Trait-Loci (QTL)-Analyse wurden insgesamt 122 QTLs entdeckt, die mit 16 phänotypischen „Traits" assoziiert werden können. Darunter wurden mehrere genomische "Hotspots" identifiziert, die möglicherweise korrelierte Wurzel- und Sprossmerkmale kontrollieren. Das deutet auf eine gewisse genetische Abhängigkeit zwischen diesen beiden Pflanzenorganen hin. Insgesamt tragen die Ergebnisse der Dissertation zu einem besseren Verständnis über die Grundlagen der Thermomorphogenese bei Pflanzen bei.

Schlüsselwörter: Arabidopsis, Gerste, Hypocotyl, Kotyledonen, Wurzel, Thermomorphogenese, Brassinosteroid, Auxin, Temperatur, Signalwahrnehmung, -transduktion und Reakation

Index

V

1. Introduction

1.1 Building a bridge from basic plant research to applied agriculture to cope with "global warming"

The climate on earth is changing rapidly, mainly due to increased atmospheric concentrations of greenhouse gases, such as carbon dioxide. One central symptom of climate change are rising temperature levels on Earth. The average temperature of the last five years was 1.1°C higher than the pre-industrial average (as defined by the Intergovernmental Panel on Climate Change (IPCC)). The impacts of climate change can be observed in extreme habitats on earth, such as arctic ice caps melting. However, climate change is also visible in our immediate environments around us, such as Halle (Saale) and Leipzig. Data collected from three different meteorological stations in Halle/Saale (Saxony-Anhalt) and Leipzig (Saxony) (University campus Heide-Süd geological garden, Leipzig/Schkeuditz, Leipzig-Holzhausen) in the period from 2010 to 2019 showed that the annual average daytime temperatures (AVDT) rose by 0.16°C per year on average and which led to a total increase of 1.27°C within this period (Figure 1A). These findings are in line with the data of Deutscher Wetterdienst (DWD). Furthermore, AVDT did not fall below 10°C since the two warmest years on record, 2014 and 2015 (Copernicus Climate Change Service, ECMWF, 2019)(See Figure 1B).
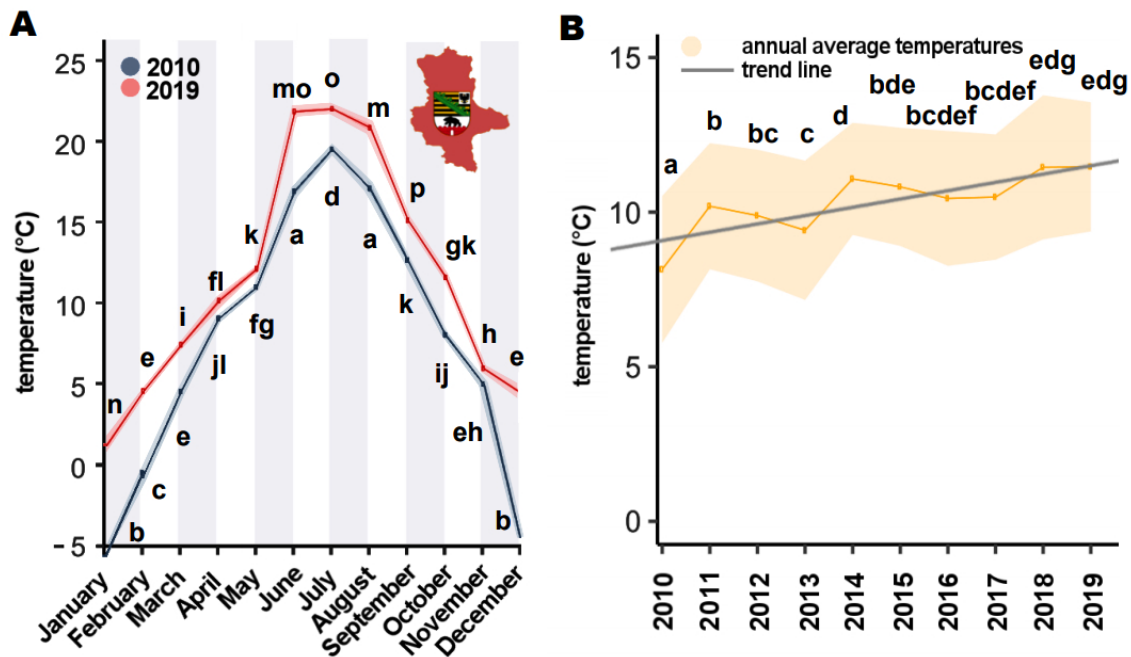
Figure 1. Global warming effects in Halle/ Leibzig (Saxonia Anhalt). **A** Average monthly air temperature in 2010 and 2020. **B** Annual average air temperature from 2010 to 2019 with trend line for plotted data. **A-B** The shadowed ribbon denotes the SE. Different letters denote statistical differences with $p < 0.05$ as assessed by one-way ANOVA and Tukey's honestly significant difference (HSD) posthoc test.

Based on these data climate change might raise the AVDTs (See trend line Figure 1B). Furtjhermore, the rise in temperature might be particularly evident in the winter months (Figure 1A). The average temperatures between 2010 and 2019 in the three locations were higher in winter seasons than in summer seasons. These effects are seen worldwide (NOAA climate.gov). However, the December/January warming trend in Halle (Saale) and Leipzig since 2010 has been nearly 0.26°C per year. This could mean that we will have fewer below-freezing days in winter. This increase in temperature influences the development of both our native flora and the cultivated crops. For instance, temperature changes may affect the timing and production of flowering, as well as the plant reproductive output and quality (Thuzar et al., 2010 Nicole et al., 2011, Gillman et al., 2019, Lippmann et al., 2019). From this point of view, global warming will have far-reaching impacts on food security in many parts of the world.

To tackle global warming, plant researchers have focused on the identification of solutions that minimize the negative impacts of climate change on food crops. Plant breeding is an essential tool in promoting global food security. Moreover, fundamental plant science is increasingly gaining interest from plant breeding research since multiple insights from the model plant *A. thaliana* can be transferred to crop plants. The more we know about how plants work, how they evolve, the genes underlying adaptive variation, and other topics, the better is their capacity to develop sustainable agriculture and to understand the impacts of agriculture on natural plant diversity. In this context, this thesis aimed to contribute to analyzing temperature response mechanisms in the root and shoot in the dicot model plants *A. thaliana* and barley.

1.2. Thermomorpgogenesis

1. 2.1 Definition

Together with light, temperature is one of the most critical environmental factors that impact plant development and physiological processes. Just a slight increase in temperature of two degrees considerably affects the growth and productivity of many plant species, including crops. However, *p*lants can adapt their growth and development to temperature changes. In *A. thaliana*, high temperature induces elongation growth of hypocotyls and petioles, upward leaf movement (thermonastic movement), biomass allocation, and thinned leaves (Gray et al., 1998, Quint et al., 2016) (Figure 2).
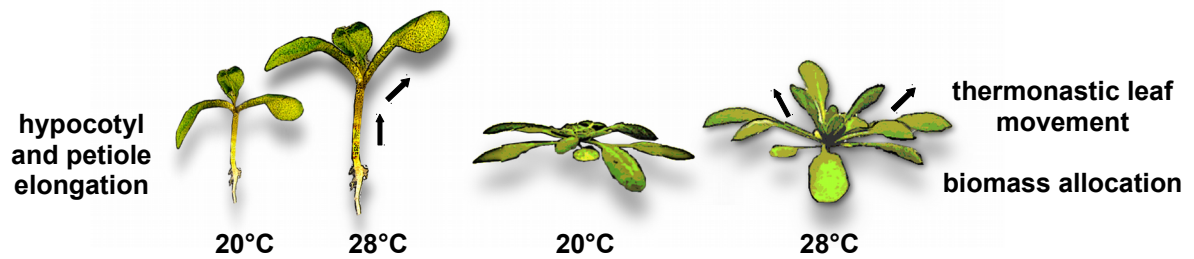
Figure 2. Temperature-induced shoot growth in *Arabidopsis thaliana*. Hypocotyl elongation, petiole elongation (left) and rosette opening, thermonastic leaf movement (right) in response to elevated ambient temperature.

These temperature-induced morphological changes are collectively termed thermomorphogenesis (Erwin et al., 1989). Adaptations to temperature are effective survival strategies exhibited by diverse plant species to dissipate body heat under suboptimal temperature conditions. (Crawford et al., 2012). These thermal responses of plants might be observable in almost all developmental stages, including Seed germination, vegetative growth, floral transition, and fruit dehiscence and the underlying molecular mechanisms (e.g., transcriptional, posttranscriptional, and protein levels) (Quint et al., 2016, Ibañez et al., 2017, Casal and Balasubramanian, 2019). Most of the current knowledge about hermomorphogenesis signaling pathways based on the temperature-induced hypocotyl elongation of the model plant *A. thaliana*.

However, the above-ground parts are not exclusively affected by increased ambient temperatures. As the soil absorbs up to 51% of light radiation (Zhao et al. 2017, Rickels et al. 2011), soil temperatures possibly have a similar effect on root growth (root thermomorphogenesis) as air temperatures have on shoot growth. In this context, root growth might be affected by warm temperatures, either directly or indirectly, via temperature-induced shoot growth (i.e. sink-source relations like root-to-shoot water and nutrient supply and shoot-to-root carbon supply) and the distribution of assimilates in the root (Heckathorn et al., 2013). In general, roots play critical roles in plant survival in environments with high soil temperatures due to their lower optimum temperature range for growth or lower acclimation potential to extreme conditions (Nielsen, 1974).

Moreover, the numerous functions of roots, which are essential for shoot growth (uptake of water and nutrients and synthesis and translocation of hormones such as cytokinin and Abscisic acid (ABA)), are susceptible to heat stress (McMichael and Burke, 1999). Temperature-induced root growth has been investigated much less than above-ground parts of plants, mainly due to experimental challenges (McMichael and Taylor, 1987). Consequently, very little is known about the mechanisms controlling root development at higher soil temperatures.

1.3 Temperature perception

Until recently, the molecular mechanisms of temperature perception and signaling remained unknown. However, our understanding of temperature sensing and signaling is progressing mainly by investigating the model plant *A. thaliana* at this moment. Accordingly, several putative candidates for thermosensors and sensing mechanisms are currently discussed. Thus, it is highly likely that multiple sensors, rather than a single sensor, are responsible for the perception of temperature changes in Arabidopsis plants. Furthermore, it is unknown whether all thermoresponsive tissues can sense ambient temperature changes. Alternatively, sensing, signaling, and growth responses might be distinct from the responding tissues and organs. Such spatiotemporal specificities have been demonstrated previously for other regulatory contexts, including light responses mediated by phytochromes (for review, See Montgomery, 2016). Thus further studies are necessary to identify and elucidate such spatial-specific sensing and signaling mechanisms.

1.3.1 In the hypocotyls

Several studies on the model plant *A. thaliana* provided insights in the molecular signaling pathways causing temperature-induced hypocotyl elongation. Key components of the thermomorphogenesis perception signaling pathway are described in more detail in the next two chapters and are summarized in Figure 3. The first step in thermal response is sensing or perception of temperature signals by plants. To sense a wide spectrum of light irradiation spanning from ultraviolet B (UV-B) to far-red wavelengths, plants are equipped with different highly specialized photoreceptors. The photoreceptor phytochrome B (phyB) has been currently proposed as the major integrators of temperature signals, which simultaneously function as primary red-light photoreceptors in plants. During the night, increases in temperatures revert the light-activated far-red absorbing form (Pfr) of phyB to the inactive red light absorbing form (Pr) in a light-independent process called thermal reversion or dark reversion (Figure 3, Sweere, 2001, Klose et al., 2015, Legris et al., 2016). Thus, more rapid reversion of the active form of phyB to the inactive form may promote the derepression of the repressive action of the PHYTOCHROME INTERACTING FACTORs (PIFs), central players in phytochrome-mediated light and temperature signaling networks (Castillon et al., 2007). Besides, blue light represses thermomorphogenesis via its receptor CRYPTOCHROME1 (CRY1, Ma et al., 2016) and UVB-RESISTANCE8 (UVR8) under UV light (Hayes et al., 2017). Another group of

temperature-sensitive blue light receptors are phototropins and the F-box protein ZEITLUPE (ZTL), which will not be discussed in this chapter (For more detailed information, See references Fujii et al., 2017, Somers et al., 2004). The involvement of several other putative temperature sensors has been discussed in the literature, such as the thermodynamic change of plasma membrane fluidity, calcium ion channels or histone-DNA interactions. An alteration of temperature directly causes structural changes in general membrane lipid conformation, which coincided with changes in the activity of the plasma membrane-bound proteins and membrane fluidity. This in turn can have an impact on the signal transduction process. (Plieth, 1999, DA Los et al., 2004, Vigh et al., 2007, Ruelland and Zachowski, 2010, Schroda et al., 2015).

In contrast, it has been speculated that specific calcium ion channels function as fundamental second messengers (Steinhorst and Kudla, 2014) and could connect temperature stimuli with inner cellular mechanisms. However, another strong candidate for a potential thermosensor seems to be the histone variant H2A.Z (H2A histone family member Z) that mediates genome-wide transcriptional changes to ambient temperature by chromatin remodeling. Elevated temperatures decrease the H2A.Z concentration at the nucleosomes associated with the auxin biosynthesis genes such as *YUCCA8 (YUC8)*. (Boden et al., 2013, Proveniers and Van Zanten, 2013) This allows chromatin accessibility for the central temperature-signaling component PHYTOCHROME INTERACTING FACTOR 4 (PIF4), promoting gene expression followed by auxin accumulation and shoot thermomorphogenesis (Koini et al., 2009, Franklin et al., 2011, Sun et al., 2012). Thus, H2AZ seems to act as a thermostat for correct temperature perception by modulating gene expression via chromatin remodeling (Cortijo et al., 2017, Kumar et al., 2010, van der Woude et al., 2019). Furthermore, epigenetic changes such as histone de-acetylation mediated by HISTONE DEACETYLASE 9 (HDA9) can facilitate the H2A.Z eviction (Lee et al., 2014, van der Woude et al., 2019).

Finally, I will address the role of the clock in the temperature-induced regulation of hypocotyl growth. Some essential clock compounds, including CIRCADIAN CLOCK-ASSOCIATED1 (CCA1), LATE ELONGATED HYPOCOTYL (LHY), and TIMING OF CAB EXPRESSION1/PSEUDO-RESPONSE REGULATOR1 (TOC1/PRR1) participate in temperature sensing and interact with PIF4 (Edwards et al., 2005, Gould et al., 2006). As temperature increases, LHY protein levels increase and this in turn slows the clock to compensates the temperature-induced acceleration of other reactions in the organism. Thus, plants are able to maintain a robust rhythms with a period close to a 24h- cycle (Balasubramanian and Weigel, 2006, Lutz et al., 2015, Sureshkumar et al., 2016). Since the molecular and supramolecular mechanisms are masked by thermodynamic effects (enzyme activity increase by 3.5-fold

for a 10°C temperature rise (Q10, Franklin and Wigge, 2014), it is challenging to identify the initial receptor or source of the thermomorphogenesis perception signaling network, Possibly a combination of different factors could initiate downstream responses.
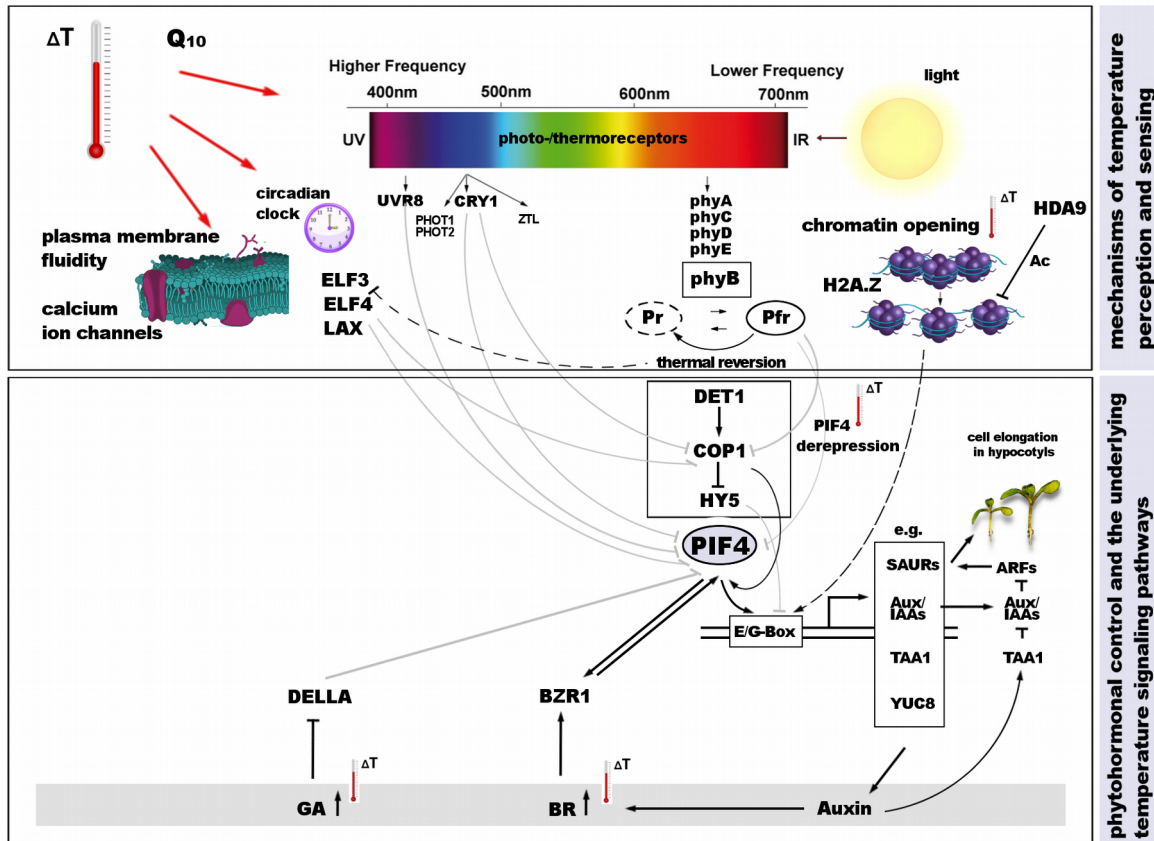
Figure 3. Integration of hormone signaling, light signaling, circadian clock and high ambient temperature in regulating plant thermoresponsive and periodic growth. Arrows indicate positive regulation, bars indicate negative regulation, solid lines indicate direct regulation, dashed lines indicate indirect regulation, light gray lines indicate reduced impact on temperature response (Model with reference to the review of Dai Vu et al. 2019).

1.3.2 In the root

Currently, it is unknown whether shoots and roots share common components in thermomorphogenesis. In general, *PHYTOCHROME A, B, D* and *E* (*phyA*, *phyB*, *phyD*, *phyE*) are expressed in the *A. thaliana* root. *phyB* mutants produced fewer lateral roots (Salisbury et al., 2007). Moreover, *phyB* and *phyA* single and double mutants exhibit shortened primary roots under normal conditions compared with wild-type plants (Correll and Kiss, 2005, Silva-Navas et al., 2015). Besides, *CRYPTOCHROME1* and *2* (*CRY1, CRY2)* are also expressed in *A. thaliana* roots and act as regulators in primary root elongation under blue light. CRY2 has inhibitory effects on primary root growth by modulation of free auxin levels and auxin distribution (Canamero et al., 2006, Mo et al., 2015). In contrast, the ultraviolet-B receptor UVR8 has been discovered to

inhibit lateral root development via the regulation of (MYB DOMAIN PROTEIN 73/77) (MYB73/ MYB77) (Yang et al., 2019). Several shoot-active light receptors are also expressed in the root which suggests their potential role in root temperature perception/ signaling. Additionally, it was recently shown that the temperature-sensitive clock component EARLY FLOWERING 4 (ELF4) moves from shoot to root to regulate the period of the root clock in a temperature-dependent manner (Chen et al., 2019). Furthermore, the fact that 2d-old seedlings of the *pHDA9::GUS* line (H2A histone family member Z (H2A.Z)) regulator) exposed to elevated temperatures revealed a strong *HISTONE DEACETYLASE 9 (HDA9)* promoter activity in the root (van der Woude et al., 2019), indicates a relevant function of this gene similar to the shoot in the process of root thermomorphogenesis. Overall, these findings reinforce the assumption that some regulatory components involved in temperature responses in hypocotyls might be shared with the root.

1.4 Temperature signaling

1.4.1 In the hypocotyls

While phyB and other phys is seen as the key receptor for high-temperature perception at the moment, the temperature-regulated basic HELIX-LOOP-HELIX (bHLH) transcription factor PHYTOCHROME-INTERACTING FACTOR 4 (PIF4) (See lower part Figure 3) might act as a core component of downstream temperature signaling. PIF4 regulates levels of auxin by controlling THE expression of key auxin biosynthesis genes (*YUCCA8 (YUC8)*, *TRYPTOPHAN AMINOTRANSFERASE OF ARABIDOPSIS 1* (*TAA1*), and *CYTOCHROME P450 FAMILY 79B (CYP79B2))* and thus auxin-induced hypocotyl elongation at elevated temperatures (Koini et al., 2009, Stavang et al., 2009).

This change in auxin concentrations results in increased expression of auxin responsive genes such as *AUXIN/ INDOLE-3-ACETIC ACID (Aux/IAA)* genes and *SMALL AUXIN UPREGULATED RNAs (SAURs)* (Gray et al., 1998, Franklin et al., 2011, Sun et al., 2012). Hence, Aux/IAA repressors are recruited to auxin receptors and then degraded via the ubiquitin- proteasome pathway (Benfey, 2002, Hellmann et al., 2002). This degradation allows AUXIN RESPONSE FACTORs (ARFs) to repress the expression of auxin-responsive genes (Benfey, 2002).

Auxin could theoretically induce elongation growth without additional players. Based on genetic, biochemical, and pharmacological experiments, it was recently reported that auxin action in thermomorphogenesis depends on the brassinosteroid (BR)-activated transcription factor *BRASSINAZOLE-RESISTANT1* (BZR1) and its homolog

BRI1-EMS-SUPPRESSOR1, which activate elongation growth downstream of auxin (Ibañez et al., 2018, Martínez et al., 2018). BZR1 function may involve heteromerization with other transcription factors such as ARFs and PIF4 (Oh et al., 2012, 2014), affecting preferences for specific cis-element-binding sites (Martínez et al., 2018).

Besides auxin and BR, the growth-promoting hormone gibberelic acid (GA) is also involved in hypocotyl growth under warm conditions. Temperature promotes GA increase which leads to degradation of growth-repressive DELLA proteins (Feng et al., 2008, de Lucas et al., 2008, Gallego-Bartolome et al., 2012, Oh et al., 2012, Wang et al., 2012, Bai et al., 2012, Li et al., 2012). The current models suggest that this process can be carried out largely independently of auxin and BR signaling (Stavang et al., 2009).

However, the temperature-induced inactivation of phyB results in a derepression of PIF4, which initiates temperature responses (Franklin et al., 2011). The thermal reversion or dark reversion might happen primarily in the dark or under low fluence rates. It was observed at higher fluence rates if the temperature is strong enough (Legris et al., 2016). In addition to photoreceptors in temperature sensing, multiple components of the photomorphogenesis and circadian clock pathways were also found to regulate theactivity of PIF4 in thermomorphogenesis. This includes DE-ETIOLATED1 (DET1), E3 ubiquitin ligase CONSTITUTIVE PHOTOMORPHOGENESIS1 (COP1), ELONGATED HYPOCOTYL5 (HY5) (Oyama et al., 1997, Ang et al., 1998, Holm et al., 2002, Andronis et al., 2008, Delker et al., 2014, Nozue et al., 2015, Gangappa and Botto, 2016, Park et al., 2017, Gangappa et al., 2017) or EARLY FLOWERING3 (ELF3) (Thines, 2010, Mizuno, 2014, Nieto, 2014). While the DET1/COP1 complex may promoting *PIF4* expression and stabilizing the PIF4 protein via yet unknown mechanisms (Delker et al., 2014, Gangappa and Kumar, 2017). HY5, which is also a downstream target of DET1 and COP1, acts as a negative regulator of thermoresponses by competing with PIF4 for binding to the promoters of growth genes and thereby suppressing their expression (Gangappa et al., 2017). Elevated temperature leads to a decrease in HY5 activity result-ing in reduced HY5 binding. Thus, the activity of PIF4 target genes is increased (Delker et al., 2014, Gangappa and Kumar, 2017, Zhou et al., 2019). In addition, PIF4 protein interacts with circadian clock components, such as ELF3, but in an Evening Complex (EC) -independent manner. This interaction prevent PIF4 from activating its transcriptional targets (Nieto et al., 2015). PIF4, in turn, leads to the degradation of ELF3 protein. This event is mediated indirectly by the rapid thermal reversion of phyB at warm temperatures.

1.4.2 In the root

Similar to temperature perception, the mechanisms underlying temperature-induced signaling in the roots are still barely understood. The fact that the *PHYTOCHROME INTERACTING FACTOR4/5) pif4/pif5* double mutant did not show any difference in temperature-induced root elongation compared to wild-type plants (Yang et al. 2016, Martins et al., 2017), indicates that PIF4/PIF5 do not link temperature sensing with growth responses in roots. Since *PIF4/5* are members of multigene families, it is still possible that other family members are involved in temperature-mediated root elongation. Thus, the involvement of other PIF family cannot be excluded at this moment.

Furthermore, direct light exposure was found to enhance *ELONGATED HYPOCOTYL5 (HY5)* transcript level in the roots and inhibit root growth. The amount of the *HY5* gene product, in turn, might be modulated by DET1 and COP1 in the root (Zhang et al., 2019). In addition, Sassi et al. (2012) supposed that in the ROOT APICAL MERISTEM (RAM), COP1 might directly target PIN-FORMED 2 (PIN2) for degradation through ubiquitination (e.g., during root gravitropism). Furthermore, Iqbal et al. (2017) demonstrated that CONSTITUTIVE PHOTOMORPHOGENESIS1 (COP1) affects the PIN1 and PIN2 intracellular localization by modulating the activity of the actin cytoskeleton in the root under light conditions. PIN2 in the root were also regulated by blue light receptor PHOTOTROPIN1 (PHOT1) via the NON-PHOTOTROPIC HYPOCOTYL3 (NPH3)-based signal transduction process in response to blue light. Thus, PHOT1 in root tissues acts to adjust the polar auxin transport in cortical cells of the root apex transition zone (Wan et al., 2012)*.*

However, whether these light signaling cues also play a role in the temperature signaling machinery, similar to the hypocotyls, remains to be investigated.

Apart from the question about the roles and functions of the main actors of the light signaling in temperature-induced root response, there are some issues still need to be clarified, such as the hormonal regulation of root growth at elevated temperatures.

Generally, the roots are known to be regulated by various phytohormones to cope with different environmental stresses such as drought or high salinity (Grieneisen et al., 2007, Petrasek et al., 2006, Sassi et al., 2012). Nevertheless, the role of phytohormones in the regulation of root growth under warmth is poorly understood, with differing and sometimes controversial results (Lewis et al., 2011, Li et al., 2015, Mao et al., 2016, Sun et al., 2014, Xu et al., 2013, Zheng et al., 2011). Especially the involvement of auxin in temperature response in primary root elongation is a controversial topic. Temperature shift experiments (e.g., shift plant growing at 20°C to 28°C for additional days) highlighted the adaptive relevance of auxin for temperature-induced primary root growth (Hanzawa et al., 2007,

Zhu et al., 2018). In that case, it was suggested that altered auxin levels enhance root growth by increasing meristem size and cell number caused by faster rate of cell division (Hanzawa et al., 2007, Zhu et al., 2018).

This is in line with the general knowledge about the biological function of auxin in the root. High levels of auxin maintain stem cell activities in the quiescent center (QC) (Grieneisen et al., 2007), to regulate the size of the meristematic zone where active cell division occurs. In contrast, auxin minimum at the last meristematic cell functioned as a signal that positions the TRANSITION ZONE (TZ) and pushes meristematic cells to differentiation (Kong et al., 2018). The phytohormone, cytokinin, in turn acts as a counterpart of auxin to diminish auxin concentration by positive regulation of auxin catabolism and polar auxin transport toward the root-shoot junction to maintain the balance between auxin-promoted cell division (Blilou et al., 2005), and cytokinin-promoted cell differentiation (Loio et al., 2008). Furthermore, Auxin minima in TZ cells initiate cell elongation in the following elongation zone, which merges without sharp boundaries with the maturation zone (Nultsch, 2001) (Figure 4).
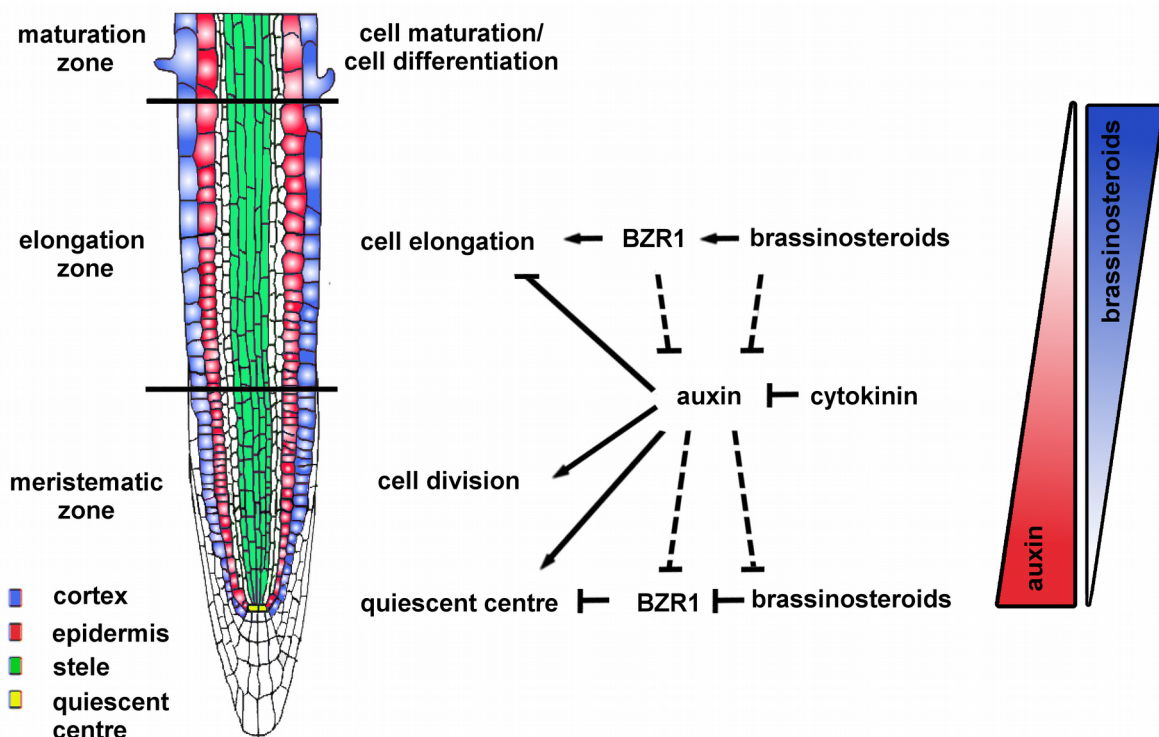
Figure 4. Schematic representation of the cell types in longitudinal and radial cross-sections and spatiotemporal action of BR and auxin in the root-regulating. While longitudinal axis of the root apex (RAM) is organized into the meristematic zone, elongation zone and maturation zone, the epidermis, cortex and stele exhibit radial symmetry. Antagonistic actions of BR and auxin maintains the spatiotemporal balance between cell division and cell elongation (modified from Chaiwanon et al., 2015).

In contrast to the studies that performed temperature-shift experiments for their analysis, Martins et al. (2017) have proposed that root growth under constant temperature conditions is regulated independently of auxin and PIN2. Accordingly, the length of MERISTEMATIC ZONE (MZ) was decreased at elevated temperatures compared to the wild-type. Thus, there is some indication that different physiological and probably also molecular mechanisms occur in primary roots of plants shifting to elevated temperatures or staying at a constant temperature. In contrast, Feraru et al. (2019) monitored temperature-induced root growth under constant temperatures and supported the findings based on shift experiments. Moreover, they revealed that elevated temperatures regulate PIN-LIKES 6 (PILS6) abundance, modulating nuclear auxin signaling rates in roots and subsequently root growth. Thus, to better understand the substantial discrepancy between the data, further independent investigations are required. Here, it must be especially clarified whether temperature-shift and constant temperature treatments could have different impacts on root growth.

Besides auxin, brassinosteroids (BR) and gibberellic acids (GA) play crucial roles in high temperature-induced hypocotyl elongation. However, Chaiwanon and Wang's (2015) results showed that BR and auxin work, in contrast to the synergistic effects in the shoot, antagonistically in Arabidopsis roots (Chaiwanon and Wang, 2015). Figure 4 visualizes the spatiotemporal distribution of auxin and BR. While cell division is maintained in the proximal meristem by the presence of high auxin concentrations and subsequently enhanced auxin signaling, a high level of BR and enhanced BR signaling in the transition-elongation zones is necessary to promote root cell elongation (Oh et al., 2014, Chaiwanon and Wang, 2015). Nevertheless, a minimum of BR in the QC and MZ must maintain stem cell and meristem size (Chaiwanon and Wang, 2015). Moreover, Chaiwanon and Wang (2015) showed that genes in the root regulated by BR and auxin are mostly direct target genes of BZR1. This indicates that shoots and roots share partially similar BR signaling pathways (e.g. BRASSINAZOLE-RESISTANT1 *(*BZR1)-mediated signaling pathway).

However, little is known about the influence of BR signaling on controlling root growth under warm temperature conditions. Martins et al. (2017) examined this issue for the first time. Their results demonstrated that the stability and the abundance of the BR receptor BRASSINOSTEROID INSENSITIVE 1 (BRI1) in the primary root might be reduced likely by regulating BRI1 ubiquitination. In contrast to the hypocotyls, this might negatively affect the regulation of BR signaling and root growth. Furthermore, Martins et al. (2017) observed no significant changes in mRNA accumulation of *BRI1*, *BRASSINOSTEROID INSENSITIVE 1-associated receptor kinase1 (BAK1), BRI1-EMS-SUPPRESSOR1 (BES1), BZR1*, which are the key factors in BR signaling in

their whole-genome RNA-seq experiment. Fei et al. (2019) monitored a downregulation of the *BRI1* transcript level at elevated temperatures. A downregulation were also observed in the levels of *ARABIDOPSIS RESPONSE REGULATORS1 and 12* (*ARR1* and *ARR12)*, affecting cytokinin signaling. An opposite effect was detected for the level of the repressors of GA signaling *DELLA* genes and GA biosynthesis genes (*GIBBERELLIN 3-OXIDASE 2* (*GA3OX2)*, *GIBBERELLIN 2-OXIDASE1* and *4 (GA2OX1*, *GA2OX4)*), which were upregulated. Based on these result gibberellins seem to positively regulate root growth at elevated temperatures (Fei et al., 2019). On the other hand, experiments of Camut et al. (2019) suggested that temperature-induced increase of GA_{12}, a precursor of the bioactive gibberellins, in the root will be used as a suitable source for the shoot to maintain temperature-induced hypocotyl elongation. In contrast, the potential role of gibberellin in temperature-induced root growth is not yet fully understood.

Although it cannot be ruled out that thermomorphogenesis sensing and signaling partially differs between roots and shoots, a common set of mechanisms and potential candidates for temperature sensing and signaling known from the shoot might also be involved in the root growth. Nevertheless, the molecular mechanisms governing root responses to elevated temperatures are largely unknown and require further studies.

1.5 Transfer genetic approaches in Arabidopsis thermomorphogenesis research to monocot crops

Recent studies mainly discussed the molecular regulation of plant development and growth at elevated temperatures in the dicot model plant *A. thaliana*. Thus, an important question is whether the identified mechanisms are relevant in other species, including monocot crops? The availability of genome assemblies with high-confidence sequences for rice, maize, wheat, and barley, allow the identification of phenotype-associated gene orthologs in monocots.

Thus, some temperature effects in monocot crops were already investigated, such as the effect of high temperature on yield and the role of H2A histone family member Z (H2A.Z) in *Brachypodium distachyon* (Boden et al., 2013), the role of phyB in rice anther development and pollen viability (Sun et al., 2017), or the role of auxin in male sterility caused by high temperature in wheat (Sakata et al., 2010).

Nevertheless, further studies are needed to determine whether the mechanism in temperature sensing and signaling identified in *A. thaliana* are also functionally conserved in other plant species like crops.

Having a completely sequenced and well-annotated genome and well-developed transformation methods, barley seemed to be a logical choice for a model system to study temperature responses in root and shoot. In this context, mapping quantitative trait loci (QTL) is a promising approach to detect marker-trait associations in the model system. QTL mapping study investigates a phenotype against genotypic variations to find the genetic variant (QTL) that contributes to the variation in the phenotype (Kim et al., 2009). This is achieved by a statistical correlation between the genotypic data (usually molecular markers) and the phenotypic data (trait measurements) for a quantitative trait of a population of individuals. Although QTL analysis gives low resolution, it gives high statistical power for detecting a QTL. One benefit of QTL mapping is to detect loci with large effects on phenotypic variation in a trait of interest and loci with small effects. Thus, if the trait of interest is governed by rare alleles, QTL mapping would be the method of choice. Using this approach, I can identify genes that affect the relevant traits but will not point to specific genomic loci (i.e. Single Nucleotide Polymorphisms (SNPs)). Using Introgression Line (IL) populations is an ideal approach for increasing the resolution and speed up mapping and target gene discovery. Thus QTL identification and fine mapping are more efficient. In a set of ILs (IL library), each of these ILs carried a single marker-defined segment that originates from a donor plant (DP) in a homogeneous elite genetic background. ILs can be generated by repeated backcrossing and marker-assisted selection covered by the contigs of ntrogressed segments from the DP (Yunbi Xu, 2010). The advantage of ILs compared to other mapping approaches are that they consist of homozygous lines. Thus, IL libraries can be phenotyped repeatedly and used for the simultaneous mapping of many traits. Another advantage of using ILs compared to the conventional population is that they have a high percentage of the genome of the homozygous recipient plant (RP) and a low percentage of the introgressed DP genome. Herein, epistatic effects from the donor parent are eliminated. To resolve the complexity of quantitative traits, ILs have another key advantage in reducing polygenic traits by dissecting them into a set of monogenic loci Peleman and Van-der-Voort, 2003). This increases the reliability of measuring phenotypic traits. Furthermore, in most cases with ILs, QTLs are typically mapped in smaller intervals than by classical QTL mapping, which simplified large-scale gene identification, fine-mapping, cloning, and molecular characterization of QTLs (Li et al., 2005, Tian et al., 2006). ILs with a QTL of interest can be easily backcrossed to various lines to investigate interactive effects. Several IL libraries are now available in barley, maize, rice, soybean, and wheat. Von Korff et al. (2004) developed an advanced backcross doubled haploid population (301 BC_2DH lines) from a cross between the German spring barley cultivar 'Scarlett' (*Hordeum vulgare* (*Hv*)) and the Israeli wild-barley accession *Hordeum vulgare ssp. Spontaneum* (hereafter abbreviated

with *Hsp*) 'ISR42-8' (See Figure 5). As von Korff et al. (2004) described, a pre-selection step, based on genotype data of 98 Simple sequence repeats (SSR) markers, was carried out in the BC_2DH generation. A set of 40 candidate introgression lines were selected from a population consisting of 301 lines and backcrossed once again with 'Scarlett' (BC_3) to further reduce the portion of the *Hsp* genome and minimize the target introgression. The $BC_3S_{4,6}$ originated from BC_3 plants by further rounds of subsequent selfing, genotype verification, and marker-assisted selection (Schmalenbach et al., 2008, Schmalenbach et al., 2009, Schmalenbach and Pillen, 2009). In order to increase the recombination events within the target QTL interval, Schmalenbach et al. (2011) developed for most introgression lines a high-resolution mapping population (S42IL-HR) segregating within the introgressed region. 73 S42ILs-HR were developed by backcrossing the S42ILs with the recurrent parent followed by two selfings (BC_4S_2). The S42IL set represents 87.3% of the wild barley genome, where each line contains, on average, 3.3% of the donor genome. Based on redundancies in the introgressed segments, a total set of 47 ILs for phenotyping experiments is sufficient to cover 87.3% of the donor genome. The power of the S42IL library to detect QTL was demonstrated in several studies where *Hordeum vulgare ssp spontaneum (Hsp)* alleles were associated with a broad spectrum of traits like testability (Schmalenbach et al., 2011), root and shoot related parameters (Hoffmann et al., 2012, Naz et al., 2012), grain parameters and yield-related traits (Schnaithmann and Pillen, 2013, Honsdorf et al., 2017, Arifuzzaman et al., 2014), nutrient accumulation (Reuscher et al., 2016, Soleimani et al., 2017) as well as drought stress tolerance traits (Honsdorf et al., 2014) in greenhouse trials. So far, little is known about the influence of exotic barley alleles on root and shoot response under elevated temperatures. In this work, I examined the effect on 43 ILs of the S42IL library grown in different ambient temperatures.

Altogether, the results of QTL analysis for temperature responses in the root and shoot in the S42IL population could complement our current knowledge of thermomorphogenesis perception-signaling network gained predominantly in *A. thaliana*. Furthermore, the analysis helps identify orthologues and paralogues of Arabidopsis genes associated with temperature responses, which are conserved in both species, monocot/dicot differences, and barley-specific differences in temperature responses. In any case, the findings could provide an important basis for further investigation of the function of genes probably involved in plant thermomorphogenesis, including crops.
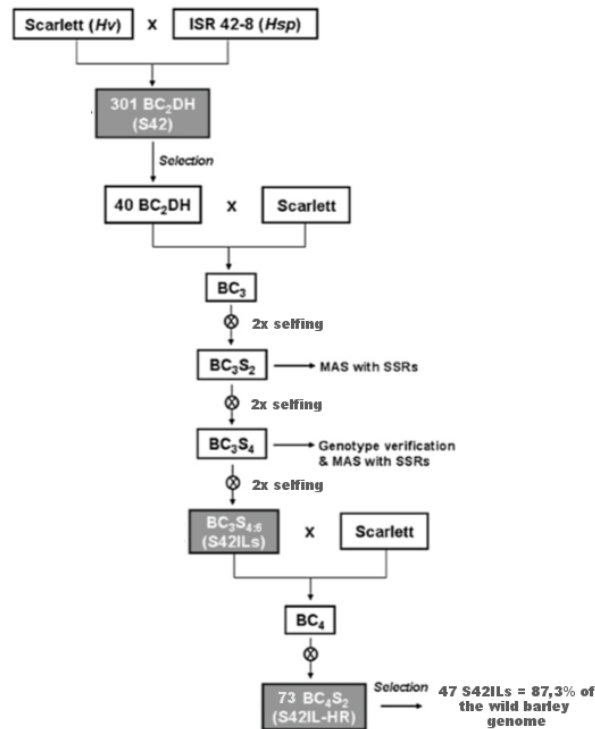
Figure 5. Strategy for developing introgressions lines and high-resolution mapping populations from the wild barley cross 'Scarlett' × 'ISR42-8'. In order to select a set of introgression lines (BC$_3$S$_{4,6}$), different techniques combining backcrossing, repeated selfing, and marker-assisted selection was used. High-resolution mapping populations (S42IL-HR) were finally developed by backcrossing the BC$_3$S$_{4,6}$ with the recurrent parent followed by two selfings. For future QTL analysis,fine-mapping and cloning of interesting genes a set of 47 S42Ils were selcted which cover 87.3%, of the donor genome (modified from Schmalenbach et al. 2008, Schmalenbach et al. 2009, Schmalenbach et al. 2011).

2. Objectives

This study aimed to investigate plant thermomorphogenis in roots and shoots. In recent years, scientists have uncovered a series of genes and biological pathways at the interface between temperature-induced growth responses and temperature perception/ signaling (See Figure 3). However, it remained unclear whether the known temperature signaling pathways, operate during temperature-induced hypocotyl elongation growth, are transferable to the other plant organs (the cotyledons/petioles and the roots). Alternatively, sensing, signaling, and/or responses could be spatially separated and tissue- or organ-specific. The argument for such spatial separations in temperature perception/ signaling is supported by the observation of previous studies related to organ-specific sha- de avoidance, which showed local spatial separation of shade perception within cotyledon and shade signaling within the hypocotyls (Michaud et al., 2017, Pantazopoulou et al., 2017).

The first chapter of this thesis aims at answering these questions. Furthermore, understanding the temperature-induced physio-morphological and molecular changes in

the root is still elusive. Thus, investigating these complex processes in roots, and the root zones, was the goal of the second chapter.

Although studies in the dicotyledonous model plant *A. thaliana* build the basis of the current understanding of plant thermomorphogenesis, the availability of a high-quality reference genome assembly for barley is now also present. It allows establishing similar approaches for monocots (Chapter III).

Thus, the objectives of my work were:

1. To explore the spatial relationships in sensing, signaling, and growth responses to elevated temperatures, especially in the aerial part of plants (hypocotyls and cotyledons), using a combination of genetic, physiological, and pharmacological approaches.

2. To identify the molecular mechanisms involved in the regulation of root temperature responses, using cell biology, physiological, and quantitative genetic approaches.

3. To systematically profile root architecture traits in a broad set of barley introgression lines of the S42IIs population in response to elevated temperatures using a non-invasive, medium-throughput imaging system (GrowScreen-PaGe).

4. To detect genomic regions associated with phenotypic data from temperature-induced root growth assays with the introgression line collection S42ILs by following a quantitative trait locus (QTL) analysis approach.

3. Materials and Methods

3.1 Materials

3.1.1 Chemicals

Modified Hoagland solution for *Hordeum vulgare* experiment

Reagent	MW	Concentration (mM)	V 1M stock/liter	V 0.5 M stock/liter	g/liter	1000x stock	per 12l box ml	per 12l box
$Ca(NO_2)_2$ $4H_2O$	236.15	2	2				24	
MES 1-hydrat	213.25	2.4			0.5118			6.142
K_2SO_4	174.26	0.7		1.4			16.8	
$MgSO_4$ 7 H_2O	246.47	0.5	0.5				6.0	
KCL	74.55	0.1			0.00746			0.089
KH_2PO_4	136.09	0.1	0.1				1.2	
NaEDTA $C_{10}H_{14}N_2$-Na_2O_8 $2H_2O$	372.24	0.05			0.018612			0.223
$FeSO_4$ $7H_2O$	278.02	0.05			0.013901			0.167
H_3BO_3	61.83	0.01			0.000618	0.618		
$MnSO_4$ H_2O	169.02	0.0005			0.000085	0.085		
$CuSO_4$ $5H_2O$	249.69	0.0002			0.00005	0.050	12	
$ZnSO_4$ 7 H_2O	287.55	0.0001			0.000029	0.029		
$(NH_4)_6Mo_7O_{24}$ $4H_2O$	1235,86	0.00001			0.000012	0.012		

Adjust to pH 5.8 with 1M KOH(~8ml)

Make up nutrient solution in 12l deionized water (instructions from Nagel et al. 2009)
Note: For the repetition in Halle, 48l nutrient solution per box were used and prepared. In both experiments the solution were replaced every week.

1x PBS

Dissolve the following in 800ml distilled H_2O.

8g NaCl (137mM)

0.2g KCL (2.7mM)

1.44g Na_2HPO_4 (10mM)

0.24g KH_2PO_4 (1.8mM)

Adjust to pH 7.4 with NaOH

Sterilise by autoclaving.

(Sambrook et al., 2001)

3.2 Growth Conditions

Chapter I and II

Arabidopsis thaliana Seeds were surface sterilized with 70% ethanol solution and shaken overhead for 5 min, followed by a second sterilization step with 34%-NaClO-Triton-X-100 for 8 min. Thereafter Seeds were washed four times with sterile Milli-Q water. Sterilized Seeds were stratified in Eppendorf tubes (2.0 ml) filled with Milli-Q water for 3d at 4°C before sowing in all experiments. seedlings were grown on solid Arabidopsis solution (ATS) nutrient medium including 1.5% (w/v) Suc (Lincoln et al., 1990) on vertically oriented plates under long-day (LD) conditions (16h of light/8h of dark) with 90 µmol m^{-2} s^{-1} photosynthetically active radiation (PAR) from white fluorescent lamps (T5 4000K). The Petri dishes were sealed with Parafilm to ensure sufficient moisture during germination.

Chapter III

Barley Seeds were surface sterilised in 1% NaClO (w/v) for 15 min and rinsed 10 times with deionised water. In all experiments, Seeds were pre-germinated between two wetted filter paper sheets (MN713, Macherey-Nagel GmbH & Co KG) within Petri dishes. The Petri dishes were sealed with Parafilm M and placed at 16°C for 4d in darkness to promote and synchronise germination. Pregerminated Seeds of each genotype were randomly chosen and transfered to vertically oriented plates with germination papers. Plates were placed into the container filled withnutrient solution. The first 4d containers were completely covered with aluminum foil (for more details See 3.3.2) In the experiments plants were grown in a controlled Walk-In Chamber at 16°C or 24°C (day/night) air temperature, 70% relative air humidity and 16 h/8h light/dark cycles and a light intensity of ~200 mmol m^{-2} s^{-1} (PAR) at plant level. The light panels in the growth

cabinet (Conviron Adaptis A1000) for the repetition experiment could only adjusted to 120 µmol m^{-2} s^{-1} photosynthetically active radiation (PAR).

3.3 Plant Material

Chapter I and II

If not differently describe, Genotypes used in this chapters were obtained from the Nottingham Arabidopsis Stock Centre (NASC, http://arabidopsis.info): *yuc1-D* (Zhao et al., 2001), *wei8-1 tar1-1* (N16412, Stepanova et al., 2008), *tir1-1 afb2-3* (N69691, Parry et al., 2009), *35S:PIF4-HA* (Nozue et al., 2007), *pifQ* (N66049, Leivar et al., 2008), *bzr1-1D-OX* (Oh et al., 2014), *bri1-4* (N3953, Noguchi et al., 1999), *phyABCDE* (Hu et al., 2013), *YHB* (p35S:AtphyBY276H in *phyA-201 phyB-5*, Su and Lagarias, 2007)*, yucQ (*Chen et al. 2014*), cpd (*N301993*, Rosso et al. 2003)*, *dwf4-102* (N520761, Nakamoto et al, 2006), *bes1-1* (SALK_098634*,* He et al. 2005)*, *bsk3-1* (N65990, Tang et al. 2008), *bsl1-1* (N684838, Alonso et al. 2003), *pgp4-1* (N16269, Terasaka et al., 2005), *pin2-1* (SALK_091142, Abas et al. 2006), *axr5-1/iaa11* (Yang et al. 2004), *msg2-1/iaa19* (Tatematsu et al., 2004, Overvoorde et al., 2005), *slr1-1/iaa14* (Fukaki, et al., 2002), *pin3-4* (Friml et al. 2003), *pin4-2* (Friml et al., 2002), *cry2-1* (NASC N3732, Lin et al. 1998), *cry1 (hy4)* (NASC N6955).The *pin3 pin4 pin7* m,utant was generated by successive crosses of *pin3-5* (Friml et al., 2003), *pin4-3* (Friml et al., 2002), and *pin7-1* (Friml et al., 2003). The *bsu1 bsl1* mutant line was generated by crossing two SALK T-DNA insertion lines [single lines ordered from NASC: T-1983(NASC N682181 SALK_030721C) and T-1984 (NASC N684838 SALK_051383C) (Kim et al. 2009). To generate the quadruple loss-of-function mutant of *bsu1, bsl1/BSL2, 3-amiRNA,* the double mutant of *bsu1-1* (SALK_030721) and *bsl1-1* (SALK_051383) was transformed with an artificial microRNA construct targeting both BSL2 and BSL3 genes *(BSL2,3-amiRNA)* (Kim et al. 2009). wild-type strains were Col-0 (N1092), Ws-2 (N28827), Rrs-7 (N22688), and Ler-0 (NW20). Tomato (*Solanum lycopersicum var. cerasiforme 'WV 106'*) was kindly provided by Stefan Bennewitz (IPB), and cabbage (*Brassica oleracea*, N29002) was obtained from NASC., Triple mutant *tir1-1 afb2-3 afb3-4* (N69653) was generated by crossing *afb2-3* (CS69651) and *afb3-4* (CS69652) into *tir1-1* (CS3798) and was obtained by NASC. The Cytrap marker lines were kindly given to me by Dr. Masaaki Umeda and are described in (Yin et al., 2014). The Seeds carried the *CYCB1:GUS* reporter gene construct (Ferreira et al. 1994) were kindly supplied by Dr. Carolin Delker. The *R2D2* (Liao et al. 2015) reporter line was obtained from Dr. Luz

Irina Calderón Villalobos. This reporter combines *RPS5A*-driven DII fused to n3×Venus and *RPS5A*-driven mDII fused to ntdTomato on a single transgene (See Liao et al. 2015).

Chapter III

Accordingly to Honsdorf et al. (2014), for the medium-throughput non-invasive phenotyping of plant architecture traits using the experimental set-up, GrowScreen-PaGe (Paper Germination) in chapter III, 74 wild barley ILs of the S42ILs library and the recipient parent 'Scarlett' were used (See Supplemental data Table S11). In addition, I chose the line S42IL-176 from the original set of 73 introgression lines (S42ILs) developed by Schmalenbach et al. (2011), since this line already revealed intersting root phenotypes (Naz et al., 2014). The S42ILs were derived from a cross between the German spring barley cultivar 'Scarlett' and the Israeli wild barley accession 'ISR42-8'. The 48 ILs possess few *Hsp* (*Hordeum vulgare ssp. spontaneum*) chromosome segments and were selected based on simple sequence Repeats (SSR) and single-nucleotide polymorphisms (SNP) genotyping to represent a large portion, 87.3%, of the 'ISR42-8' genome (Schmalenbach et al. 2011). Repeated backcrossing and MAS procedure are explained in Schmalenbach et al. (2008).

3.3 Plants biology techniques

3.3.1 Temperature Response of hypocotyls, petioles or roots in Arabidopsis

Chapter I

Organ-specific temperature responses were determined in 8d-old seedlings grown at 20°C or 28°C. For detached organ growth, 4d-old seedlings grown at 20°C were dissected to obtain roots or hypocotyls. Isolated organs were placed on ATS medium including 1.5% (w/v) Suc and cultivated at 20°C or 28°C for additional 3 or 4d. All measurements were made from digital photographs of plates using RootDetection (www.labutils.de) and depict the total length of the analyzed organ. Hypocotyl elongation in tomato and cabbage was assessed in 11d-old plants. seedlings were cultivated for 8d at 20°C prior to a shift at 28°C for additional 3d. Cotyledons were either detached or seedlings were left intact at the time of the shift. Control plants remained at 20°C. Because of high variability in the germination and growth of tomato and cabbage individuals in the first 8d, hypocotyl length for each seedling was calculated as the increase in length after transfer to higher temperature

(Δlength = length at 11d – length at 8d). All experiments were repeated at least 2 times, data of one representative experiment is shown.

Chapter II

For quantification of temperature-induced primary root length, lateral root and root hair growth, 7d-old seedlings were used which had been grown on sterile ATS medium including 1.5% (w/v) Suc. The plates were placed in a vertical position to allow downward root growth. Primary root length were photographed and measured similar to the hypocotyl length measurments using Root Detection software. Based on the same pictures lateral root number were countered for the entire root below the shoot-root junction. For root hair density measurments (i.e. the number of root hairs per unit root length), root hairs in a 1 mm root segment at the beginning of the maturation zone were countered. Plant materials were cleared in chloral hydrate, and roots were imaged with a Zeiss axioplan 2 stereomicroscope fitted with a AxioCam HRc using a differential interference contrast (DIC) objective. For the time scale experiments plant had been grown for 12d on sterile ATS medium including 1.5% (w/v) Suc and were photographed on a fixed camera station every day until day ten. The first image was taken at day two after germination, because at this time point, roots at both temperatures reached a certain length which allowed accurate quantification. With the aim to See the overall trend in primary root growth at different temperatures more clearly, the primary root length at day 12 was additionally quantified. All experiments were repeated at least 2 times, data of one representative experiment is shown.

3.3.2 Phenotyping of barley root and shoot growth of S42ILs with GrowScreen-PaGe

Before starting the experiment the containers, rigid plates and frames were cleaned and desinfected using 1% (V/V) Menno-Florades for 48h to prevent fungal growth. After washing with tap water, the containers with the frames for the rigid plates were filled with 12L of one-third strength modified Hoagland solution (stock solution, 5 mM KNO3, 5 mM Ca(NO3)2, 2 mM MgSO4, 1 mM KH2PO4, plus FeHEDTA and trace elements, Hoagland and Arnon 1950) and the nutrient solution was replaced weekly. Pregerminated barley seedlings with a radicle of 0.2-0.3 mm in length were transfered to germination paper and fixed to the rigid plate. The seedlings were placed more or less in the centre of the germination paper. For the fixation of the seedling, it was covered with a stripe of filter paper with two fold-back butterfly clips. Due to the high tension of the filter paper,

seedlings were pressed on the germination paper and could not fall down. Another seedling was attached the same way on the other side of the rigide plate. Then the plates were placed into the container and fitted into the frame assembly with 25 (Jülich) or 50 (Halle) slots. After all 25 or 50 plates were placed into the containers, which was filled with 12l nutrient solution (Jülich) or 48l (Halle) in such a way that approximately 5cm of the bottom of the germination paper was constanly submerged in the nutrient solution. The containers were completely covered with aluminum foil and placed inside the Walk-In Chamber experiment1) or growth cabinet (Conviron Adaptis A1000). After two days, at the level of the fixed seedlings, a gap was left in the cover, so that the shoot could established. With a portable imaging station with fixed positions of two cameras and illumination and a frame to load the plates with the plants, high-resolution image (based on RGB imaging) of the plants were taken every second day for 6 time point after fixation. The image processing and analysis were automated. A barcode label positioned on each side of the plate allows the automatic identification of each plant and to sort and store the images automatically. seedling root system analysis was conducted using the image based software, GROWSCREEN-Root, which is described in more detail by Nagel et al. (2009). With the software, data of parameters of root systems already described was collected (e.g. length of main root). The software used RGB image analysis procedures and measure root system traits via colour contrasts between roots and the artificial background. Due to the fact that often parts of individual roots are closely spaced or overlap, quantification of the number of main, lateral roots is challenging for the software. In such cases, the RGB images were post-processed by hand. For the second experiment measurements were performed using Image J software (NIH, USA, https://imagej.nih.gov/ij and root detection software).

3.3.4 Cell measurements

Hypocotyl cell lengths were determined by staining seedlings with 10 µg mL^{-1} propidium iodide (Sigma-Aldrich) for 5 min, while data of root cell length were collected by staining seedlings with 10 µg ml^{-1} propidium iodide (Sigma-Aldrich) for 30 sec. Subsequent microscopic analyses were performed using a Zeiss LSM 700 AxioObserver (Laser 555 nm, Plan-Neofluar 20x/0.50 Ph2). Measurements on the hypocotyl were performed on all individual cells of a consecutive cortex cell file from the first cell after the root-shoot junction upward to the shoot apical meristem (SAM). In contrast, cell measurements on the roots were carried out separately for each root zone or for an entire root. In this

regard, for the meristematic zone the length of all cells of a consecutive cortex cell file from the quiescent center (QC) upward to the first noticeably elongated cell which were larger than broad (accordingly to the definition used in Dello Ioio et al. (2007)) were measured. For the analysis of cell length of the elenogation zone, only the cells of a consecutive cortex cell file from the first cell which is larger than broad to the last cell which is in the neighborhood of the first epidermal cell with visible root hair bulge (García-González et al. 2021), were measured. Corresponding to the definition of the maturation zone, the length of all cells of a consecutive cortex cell file in the region from the first visible root hair bulge to the root-shoot junction were considered. For the determination of the cell number and cell length of hypocotyls and the root zones, propidium iodide stained hypocotyls and roots were placed on a glass cover slip for imaging using the LSM 700 ZEN software. For the entire root scans three independent seedlings were analyzed. For the analyses of cell morphology changes in the hypocotyls at 20°C and 28°C, as well as for the separately analyses of the root zones 7 to 10 independent seedlings per experiment were used. In general, experiments were carried out two to three times with similar results, of which one representative experiment is shown.

3.3.5 EdU-based proliferation assay

For root tip labeling, Arabidopsis seedlings which had been grown for 2d, 5d or 7d on sterile ATS agar plates with 1.5% (w/v) Suc at 20°C or 28°C were transferred to 24-well plates filled with ATS liquid media including 1.5% (w/v) Suc and 10 µM EdU (5-Ethynyl-2′-deoxyuridine) (Invitrogen *cat no: C10637*). In this solution mixture seedlings were incubated for further 30min at 20°C or 28°C. For a negative control of cell division, some of the 7d-old seedlings were additionally treated with Aphidicolin (12 µg/mol) together with EdU (final volume of 3ml solution). Aphidicolin is a DNA polymerase inhibitor and blocks cell cycle progression of the majority of cells at the $G1/S$-phase. To minimize temperature changes, transferation of root to the 24-well plates occurred insight the same growth cabinets. The light, humidity and day length condition in the growth cabinets were similar to the other experiments (See above). seedlings were then fixed for 30 min at room temperatures. Fixation solution consists of 4% (w/v) formaldehyde solution in phosphate buffered saline (PBS) with 0.1% Triton X-100. Thereafter, fixer was washed with PBS (3 × 10 min) and seedlings were incubated in EdU detection cocktail according to the Life Technologies™ Supported Protocol for the Click-iT® Plus EdU Imaging Assay (Invitrogen *cat no: C10637)* for 30 min followed by PBS washes. The root tips were cut and placed on to a glass slide and covered with cover slip. Then, fluorescent confocal

imaging was performed using a Zeiss LSM 700 confocal microscope (Zeiss, Gottingen, Germany) using 40x water / NA1.2 objective. Counterstaining of cell walls was used during image acquisition by staining roots in 10 µM propidium iodide for 30 s. For Hoechst labeled cells, the excitation was at the combined 351 and 364 nm lines of a Spectra-Physics 164-05 argon ion laser (Spectra-Physics, Inc., Mountain View, Calif.). Images were anonymously analyzed. HOECHTS positive cells (Green) were countered. For the analyses seven to 10 independent seedlings per experiment were used. In general, experiments were carried out two times with similar results, of which one representative experiment is shown.

3.3.6 Cell proliferation assays with *Cytrap* line

Seeds of the DUAL CORE MARKER SYSTEM (Cytrap) expressing pHTR2::CDT1a(C3)-RFP and pCYCB1::CYCB1-GFP was provided by Dr Masaaki Umeda (Nara Institute of Science and Technology, Japan). pHTR2::CDT1a (C3)-RFP and pCYCB1::CYCB1-GFP fluorescence was visualised by a Zeiss LSM 700 confocal microscope (Zeiss, Gottingen, Germany) using 40x water / NA1.2 objective, exciting at 488 nm and at 559 nm, respectively. Cells expressing pHTR2::CDT1a (C3)-RFP (Red), which monitors the cell cycle phases from S-phase to late G2-phase and cells expressing pCYCB1::CYCB1-GFP (Green) which track cells in the G2-phase to M-cell cycle phase were separately countered. For time-lapse imaging experiment cell of the meristematic zone of 7d-old roots were investigated for GFP and RFP-positive cells 30 min, 1, 3 and 6 hour after the light went on. For the IAA treatment assays using *Cytrap* line, seedlings were germinated and grown on ATS medium containing 1.5% suc with or without 0.01nM IAA for 7d and investigated for RFP-positive cells 1 hour after the light went on. seedlings were fixed at the selected time points for 20 min in 4% (w/v) paraformaldehyde in PBS (pH 7.4), washed twice with PBS and placed in 0.5% (v/v) TritonX-100 in PBS. For the negative control some seedlings were treated with 1 µM Aphidicolin (H_2O) at 1 hour before harvesting. For these analyses seven independent seedlings per experiment were used. In general, experiments were carried out two times with similar results, of which one representative experiment is shown.

3.3.7 Cell proliferation assays with *R2D2* line and analysis

Seedlings of the *R2D2* (Ratiometric version of 2 D2's) fluorescent reporter line (Liao et al. 2015) which express a Venus-tagged auxin degradable reporter protein

(DII:n3xVenus) under control of an RPS5A promoter along with an RFP-tagged undegradable protein (mDII:ntdTomato) grown for 7d on ATS medium containing 1.5% suc. Images were taken (1h after dawn) from up to 10 individual roots for each analysis in Image J using a LSM700 inverted confocal microscope with a 40× water objective lens. GFP (green fluorescent protein) and VENUS were excited using an argon-ion laser, whereas tdTomato (tandem dimer Tomato), RFP (red fluorescent protein). Emissions were detected sequentially with ZEN to prevent crosstalk between fluorophores. Excitation and detection of fluorophores were configured in two separate channels. GFP was excited at 488 nm and detected at 498–530 nm. DII-VENUS was excited at 508–543 nm and tdTomato was excited at 561 nm and detected at 597–696 nm. For Quantification DII signal was normalized against mDII. Therefore, ImageJ polygon tool was used to delineate regions of interest (ROI) in the root tip. Fluorescence was measured as mean grey value. All channels were exported as separate TIFFS and converted to 32-bit images and mean grey value measured using the 'set measurement' function in ImageJ. The resultant DII channel was divided by the resultant mDII channel. 7 independent seedlings per experiment were used for this assay and two times repeated.

3.3.8 Hormone/Inhibitor treatments

Except for the indole-3-acetic acid (IAA) and N-1-naphthylphthalamic acid (NPA) treatment assays on the shoot (Chapter I), seedlings were germinated and grown on ATS medium containing 1.5% suc with different concentrations of Hormones/Inhibitors specified for each assay. Hormones or inhibitors were added to the ATS liquid medium after autoclaving and cooling in the following concentrations:

Compound	Supplier-Cat.no	Solvent	Working concentration
Propiconazole	Sigma-45899	Methanol	0.5, 1, 3 µM
Paclobutrazol	Sigma-46046	Ethanol 70%	0.25, 0.5, 1, 5 µM
Yucasin	sc-233161	DMSO	1, 5, 10, 50, 70, 100 µM
L-kynurenin	Sigma-K8625	DMSO	1, 5, 10, 50, 70, 100 µM
Fluridone	Sigma-45511	Ethanol 70%	0.5, 1, 5,10, 20, 30, 50 µM
Lovastatin	Sigma-438185	DMSO	10, 50, 100, 500, 10000 nM
Silver nitrate	Roth-7908.1	H_2O	3, 5, 7.5, 10 µM
1-N-Naphthylph-thalamic (NPA)	Duchefa-N0926.0250	DMSO	100 µM
Aphidicolin	Sigma-178273	H_2O	1µM
Epibrassinolide	Sigma-E1641	Ethanol 70%	0.05nM, 5nM, 100nM
Indole-3-Acetic-Acid	Duchefa-I0901.0025	DMSO	1mM, 1nM, 0.01nM
Picloram	Sigma-5575	DMSO	1µM

*For all root growth assays with IAA treatments, agar plates were additionally covered with yellow plastic plates to prevent IAA degradation from light.

3.3.8.1 IAA and NPA Treatment Assays with lanolin and tissue stripes

Seedlings were grown in LD conditions at 90 µmol m^{-2} s^{-1} for IAA application and at 30 µmol m^{-2} s^{-1} for N-1-naphthylphthalamic acid (NPA) treatments to allow for longer petiole growth for application of NPA plasters. In both experiments, seedlings were initially grown at 20°C for 7d prior to the pharmacological treatment. For IAA application, 1 mM IAA in lanolin paste (Sigma-Aldrich) was applied to cotyledons. For NPA treatments, thin strips of tissue were soaked in lukewarm ATS medium with or without the addition of 100 µm NPA and carefully placed across petioles. For both experiments, seedlings were subsequently cultivated for an additional 3d at 20°C or 28°C in the respective light conditions.

3.3.9 GUS staining

For β-glucuronidase (GUS) staining and sectioning of the primary root, I followed the procedure described by Gsperini et al. 2015), vertically grown 7d-old seedlings (1h after dawn) were carefully transferred to GUS staining solution (50 mM sodium phosphate buffer pH 7.0, 0.1% Triton X-100, 3 mM $K4Fe(CN)_6$, 3 mM $K_3Fe(CN)_6$, 0.5 mg/ml X-Gluc) and incubated at 37°C in the dark for 2–4 h. For imaging the primary root tip, the reaction was stopped by replacing the staining solution with 50 mM sodium phosphate buffer pH 7.0. Roots were then immediately mounted in freshly prepared chloral hydrate: glycerol: water solution (8:2:1). roots were imaged with a Zeiss axioplan 2 stereomicroscope fitted with a AxioCam HRc using a differential interference contrast (DIC) objective.

3.4 Molecular biology methods

3.4.1 RNA Extraction, cDNA Synthesis, and qRT- PCR

Chapter I

Col-0 seedlings were cultivated at 20°C for 7d in LD photoperiods (16/8 h) in 30 µmol m^{-2} s^{-1} (PAR). seedlings were shifted to 28°C at Zeitgeber time (ZT) 16 and harvested after 8 h at ZT24. seedlings were dissected by cutting off cotyledons (with petioles) and roots to allow organ-specific expression analysis. Dissection was performed either before or after the temperature shift at ZT16 or ZT24, respectively. Control seedlings remained at 20°C and were harvested and dissected at the same time points.

Chapter II

After surface-sterilization and stratifiecation, Seeds were placed on ATS medium and grown for 5d under long day photoperiods (16h light/ 8 dark) and 95 μmol m^{-2}s^{-1} white light at 20°C or 28°C. At ZT1 (1h after dawn) plant material of the meristematic zone and elongation zone were harvested with an ordinary scalpel in a time frame of 1h (N=100). The regions were defined as already described. To provide higher accuracy in harvesting of the special tissues a standard binocular microscope were used.

In all cases total RNA was extracted from three biological replicates using the NucleoSpin RNA Plant Kit (Macherey-Nagel). First-strand cDNA was synthesized using the PrimeScript RT Reagent Kit (Perfect Real Time) from Takara Bio. qPCR analyses were performed on an AriaMx Real-Time PCR System (Agilent) using Absolute Blue Low Rox Mix (Thermo Fisher Scientific). *At1g13320* was used as a reference gene (Czechowski et al., 2005) for the shoot tissues and AT4G05320 for the root tissues (Hu et al., 2020). Relative expression levels for each analyzed gene were calculated as 2(Ct reference gene-Ct gene of interest). Oligonucleotide primers used in the analysis are listed in Supplemental data Table S1.

3.4.2 Transcriptome Profiling

Arabidopsis seedlings (Rrs-7, N22688) were cultivated for 5 d at 20°C in LD conditions with 120 μmol m−2 s−1 PAR. seedlings were either kept at 20°C or shifted to 28°C for 24 h prior to dissection of the plant material into cotyledons, hypocotyls, and roots. For each seedling organ sample, material for three biological replicates was harvested. RNA was extracted using the RNeasy Plant Mini Kit (Qiagen). RNA samples were further processed and hybridized to the ATH1-121501 microarray by the NASC microarray hybridization service. Raw data were processed with the simpleaffy R package to obtain robust multichip average-normalized log2 expression levels using default settings (See Bellstaedt et al., 2019, Supplemental Data Set S3). The eBayes function of the limma R package (See Bellstaedt et al., 2019, Supplemental Data Set S4) was used to compute log2 FCs, *t* values, and *P* values and to correct *P* values for multiple testing. Genes were considered to be differentially regulated if the 28°C expression values showed a |log2 FC| > 1 and an fdr < 0.01 compared with expression levels at 20°C (See Bellstaedt et al., 2019, Supplemental Data Set S1).

3.5 Statistical Analyses

3.5.1 In Arabidopsis

Chapter I and II

Statistical differences were assessed by one-way ANOVA and Tukey's HSD posthoc test, using built-in functions of the statistical environment R (R Development Core Team, 2018). Different letters in graphs denote statistical differences at $p<$ 0.05. Graphs were generated using the ggplot2 R package.

3.5.1.1 Hierarchical Clustering and MDS

The log2 FC data of differentially expressed genes (DEGs) with significant expression responses in at least one organ were subjected to hierarchical clustering in R using the hclust function of the gplots package with Euclidean distances and complete linkage. The heat map was generated using the heatmap.2 function of the gplots package.
Multidimensional scaling (MDS) was performed in R using the build-in cmd scale function with $k=$ 2 dimensions. Pairwise Pearson correlations (cor) among all individual array samples were computed using the normalized log2 expression levels of DEGs, and $1 - cor$ served as a distance measure in the MDS.

3.5.1.2 GO Term Analysis

GO enrichment of DEGs was assessed using PANTHER version 14.0 (Mi et al., 2017). Arabidopsis Genome Initiative (AGI) codes of genes with |log2 FC| > 1 and fdr < 0.01 were analyzed for different gene sets (See Bellstaedt et al., 2019, Supplemental Data Set S2). Enrichment of GO terms was tested using default test settings (Fisher's exact test and false discovery rate correction) for the PANTHER Biological Process Data Set.

3.5.2 In barley

3.5.2.1 Descriptive Statistic

Chapter III

Descriptive statistical parameters were calculated with R Studio (Version 0.99.903) and Microsoft Excel (version 2015) and SAS Enterprise Guide 4.2 (SAS Institute (2008). Boxplots were generated using the ggplot2 R package. Different letters in graphs denote statistical differences in all phenotypic traits at $p < 0.05$, based on the analysis of variance (one-way ANOVA) and Tukey's HSD posthoc test.

Analysis were carried out in the statistical environment R (R Development Core Team, 2018), as well as the generation of the histograms using the hist() function. Normal distribution of each phenotypic trait was assessed using a Kolmogorow-Smirnow test, a Shapiro–Wilk test and Anderson-Darling test (*https://statistikguru.de/rechner/normalvertei-lung-rechner.html*). The coefficient of variation (CV) in percentage was calculated as: CV = (SD/m) × 100, in which "SD" is the standard deviation, and "m" is the mean for a trait. Therfore I used Microsoft Excel functions (version 2015). Heritabilities across treatments were calculated as

$$h^2 = V_G/[\ V_G + V_{GT}/t + V_{GE}/e + V_{GET}/et + V_R/etr].$$

The terms V_G, V_{GT}, V_{GE}, V_{GET} and V_R represent the genotypic, genotype x treatment, genotype x environment, genotype x environment x treatment, and error variance components, respectively, calculated with procedure VARCOMP (SAS Institute, 2008). The terms t, e, and r indicate the number of treatments, experiments and replicates, respectively.

3.5.2.2 Correlation analysis

Pearson correlation coefficients were calculated using Hmisc and cor R packages (Harrell, 2016, R Core Team, 2015). The correlogram was plotted with the corrplot R package (Wei and Simko, 2016). "rcorr()" function from "Hmisc" package give out outputs of r values, n number of observations analysed in the data matrix and *p*-values of all pair-wise correlations. r values with $0.2 \leq |\ r\ | \leq 0.5$, $0.5 < |\ r\ | < 0.8$ and $|\ r\ | \geq 0.8$ were defined as weak, moderate and strong, respectively. A correlogram combined with its respective r-values was produced by using "corrplot ()" function of "corrplot" package. Correlation network of traits was calculated using R (R Core Team, 2018).

3.5.2.3 Hierarchical Clustering and PCA

In addition, trait responses (means) of the S42ILs across treatments in root or shoot were subjected to hierarchical clustering in R using the hclust function of the gplots package with Pearson distances and complete linkage. The heat map was generated using the heatmap.2 function of the gplots package.

PCA was performed to determine the overall traits distinctiveness, and to investigate the relationships between the traits. PCA was performed using the software SigmaPlot ver. 13 (Systat Software Inc.). Venn diagrams were generated by the web-tool Draw Venn Diagram. Available online: *http://bioinformatics.psb.ugent.be/webtools/Venn/*.

3.5.2.3 Statistical methods for QTL detection

Subsequently, a post-hoc Dunnett test was carried out to compare LSmeans between the introgression lines and the control genotype 'Scarlett'. Next, the obtained raw P values of the Dunnett test were adjusted for multiple testing by FDR implemented in procedure MULTTEST. In case the LSmeans of an introgression line was significantly different from 'Scarlett' across treatments or within a single treatment with *P(FDR)*< 0.05, a line-by-trait association was accepted. The relative performance (RP) of each introgression line compared to 'Scarlett' was calculated as follows:

$$RP(IL)=100\times\frac{[LSMeans(S42IL)-LSMeans('Scarlett')]}{LSMeans('Scarlett')}$$

For each trait the LSMeans were calculated separately for 16°C or 24°C, respectively. All lines were of interest which were insignificant at 16°C and significant at 24°C for the investigated trait. Finally, a significant line-by-trait association effect is assumed to be caused by a QTL, located within the introgressed chromosomal segment of the IL. If two overlapping ILs show a similar line-by-trait association effect (same sign of effect), the causative QTL is assumed to be located within the overlapping segment of the two S42ILs.

4. Results

4.1 Chapter I: Spatial relationships in sensing, signaling, and growth responses to elevated temperature in the aerial part of plants

4.1.1 Organ-specific transcriptome analysis in responses to elevated temperatures

Increases in ambient temperature affect numerous growth and developmental traits in flowering plants (Quint et al., 2016). Among these changes, temperature-induced elongation of hypocotyls, petioles, and roots are hallmark responses (Figure 6A-D). The hypocotyl phenotype has been used to unravel the underlaying molecular principles already described. However, it is unclear whether all elongating organs are regulated similarly or have the capacity to sense and responde to ambient temperature changes autonomously. Alternatively, sensing, signaling, and growth responses may be distinct processes that are spatially separated and tissue- or organ-specific. Such spatiotemporal specificities have been demonstrated previously for other regulatory contexts, including light responses mediated by phytochromes (See Montgomery, 2016).
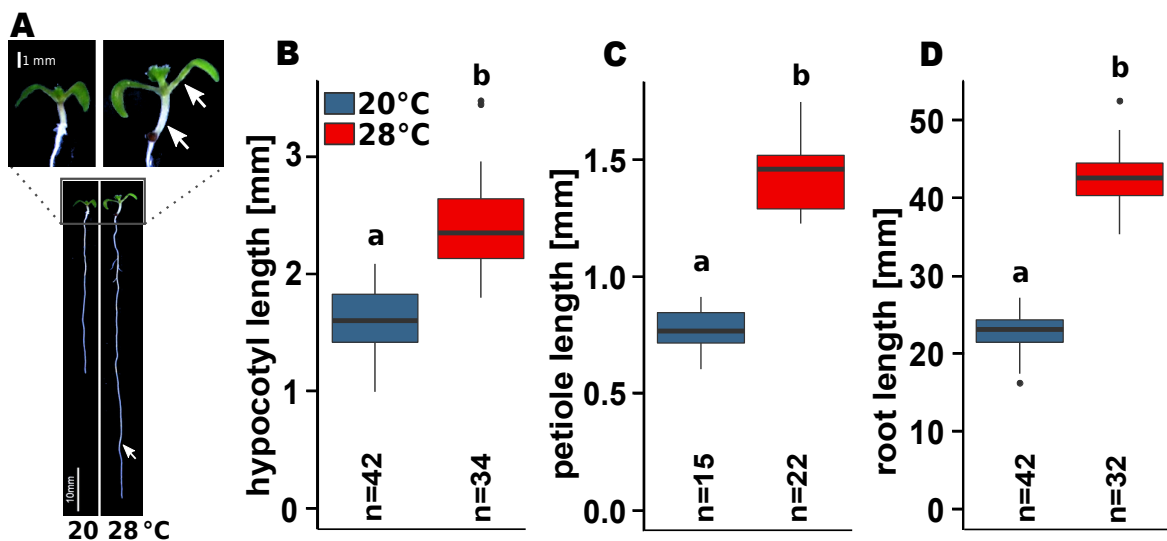
Figure 6. Thermomorphogenesis in seedling organs. A Representative pictures from the corresponding temperature assay. White arrows show the relavant plant organs. Temperature-induced elongation of (**B**) hypocotyls, (**C**) petioles and (**D**) roots in 8d-old Col-0 seedlings grown at 20°C or 28°C. Experiments were performed in LD (16/8h) conditions under 90 µmol m^{-2} s^{-1} white fluorescent light. Box plots show medians and interquartile ranges of total organ lengths, outliers (greater than 1.5× interquartile range) are shown as black dots. Different letters denote statistical differences at $p< 0.05$ as assessed by one-way ANOVA and Tukey's honestly significant difference (HSD) posthoc test. Experiments were repeated once with similar results (adapted from Bellstaedt et al. 2019).

However, to get the first idea about any tissue or organ specificities and interactions in signaling among organs, I reanalyzed an existing microarray data set, generated in the Quint Lab in 2014, in which gene expression of cotyledons, hypocotyls and roots of 5d-old temperature-treated or untreated Rrs-7 seedlings (24h 20°C vs. 28°C) were measured. The Venn diagram (Figure 7A) depicts the numbers of genes differentially expressed in all three tissues after 28°C temperature treatment for 24 h compared with the 20°C control. Of all 944 differentially expressed genes (DEGs), the majority are specific for cotyledons

(633) and roots (349), while only 77 DEGs belongs to the hypocotyl group. Even more, for unknown reasons, the number of overlapping DEGs between roots and cotyledons were, considerably higher (64) compared to the number of overlapping genes between the aerial tissue parts of the plants (40). However, there were very few DEGs (24) shared between all three organs, indicating a structural heterogeneity in gene expression between the different organs in response to elevated temperatures.
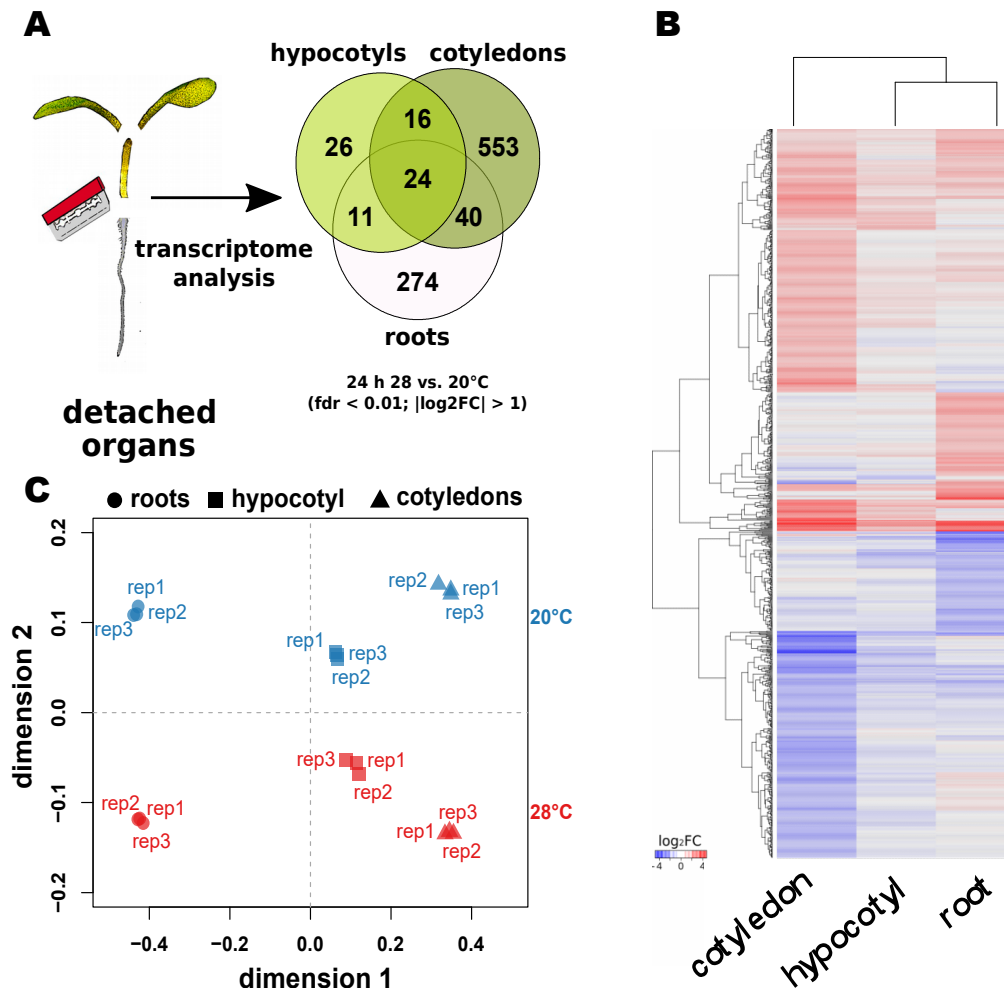
Figure 7. Temperature-induced transcriptome responses in 6d-old seedlings. A Venn diagrams show overlap in differential gene expression after 24 h at 28°C versus control seedlings at 20°C (|log2 fold change [FC]||>1, false discovery rate [fdr]<0.01). **B** Hierarchical clustering of DEGs using Euclidian distances of log2 fold change data. multidimensional scaling of DEGs (shown in **C**) based on the pairwise Pearson correlation (1- *cor*) among all individual biological replicates. (adapted from Bellstaedt et al. 2019)

To identify functional relationships between the DEGs of the three tissue samples, I performed a gene ontology (GO) enrichment analysis. Annotation of DEGs showed that GO terms overrepresented in genes with differential temperature responses in all three tissues primarily comprised stress-relevant categories (e.g., reactive oxygen species and response to heat or temperature stimulus, see Bellstaedt et al., 2019, Supplemental data

set Table S1, S2, S3, S4) and included gene encoding heat shock proteins (e.g., *AT3G12580*, *AT5G52640*, and *AT5G12020*). While the organ-specific gene sets were partially enriched in similar GO terms, each organ also contained a variety of specifically enriched GO terms (See Bellstaedt et al., 2019, Supplemental data set Table S1, S2, S3, S4). Interestingly, the "response to hormone" category was significantly enriched in cotyledons but not in hypocotyls or roots (See Bellstaedt et al., 2019, Supplemental data set Table S1, S2, S3, S4). In contrast, the GO term "response to ethylene" was only enriched in DEGs specific for roots. These results provide evidence for differences at the signaling level between organs. Overall, the GO term analysis revealed possible organ specificity in transcriptional responses to elevated temperatures. However, the classification of genes was made using strict cut-off values ($|log2 fold| < 1$ and $fdr > 0.01$) and may thus exclude genes that only marginally fail to meet these criteria. Therefore, we performed a hierarchical cluster analysis of all genes that showed differential expression in at least one tissue (n = 946, See Bellstaedt et al., 2019, Supplemental data set Table S1) . Most genes clustered because of their distinct expression response in either roots or cotyledons, whereas the hypocotyl expression response seemed generally less pronounced (Figure 7B), which is in line with the generally low number of DEGs in this organ (Figure 7A). I further assessed the pattern of the organ-specific expression using a multidimensional scaling (MDS) approach on the DEG set (n=946). I found that two dimensions were sufficient to separate the individual biological replicates into distinct groups (Figure 7C). Dimensions 1 and 2 separated the samples according to tissue type and temperature, respectively. Furthermore, dimension 1 separated the root samples from the two shoot organs (Figure 7C). While these results indicated a high degree of organ specificity in the temperature response of root and shoot tissues, analysis of the response 24h after the stimulus (at midday) is likely too late to assess the overlap among initial signaling events. In accordance with currently reported expression patterns of central regulators of plant growth, such as PIF4 (Nozue et al., 2007, Nomoto et al., 2012), which displayed a narrow peak at dawn in long-day (LD), I chose for all further experiments a sampling time point immediately before dawn. Nevertheless, based on this finding, it is difficult to make more specific conclusions regarding the microarray dataset, which I used. For the same reason (different harvesting time point), the comparability to other available datasets is limited. Taken together, microarray data provide extensive evidence for different organ specificities in response to elevated temperatures, including local differences in temperature signaling mechanisms and regulation of organ development.
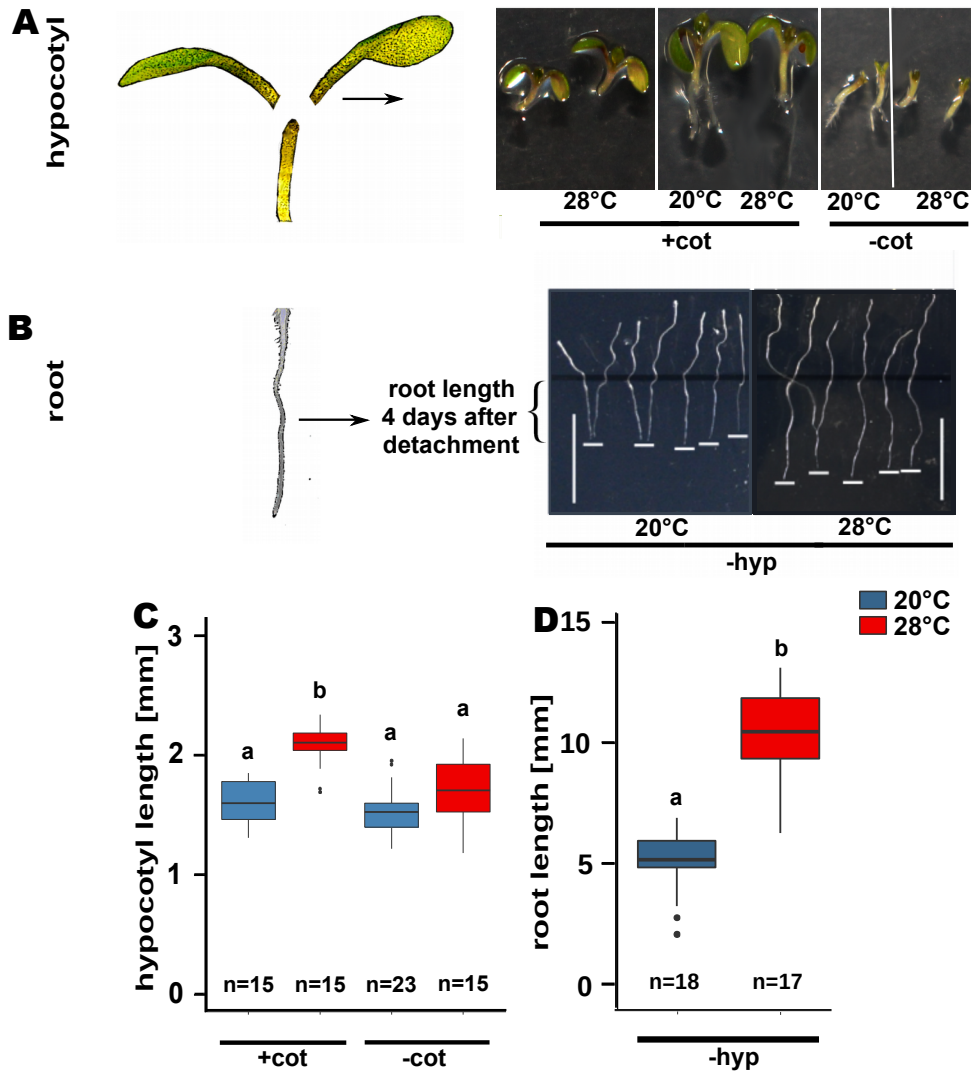
Figure 8. Elongation responses of detached seedling organs. A-D Petioles and cotyledons or whole shoots were removed from 4d-old Col-0 seedlings grown at 20°C. Subsequently, detached organs were placed on growth medium and cultivated for an additional 4d at 20°C or 28°C. Representative pictures of **(A)** hypocotyls with or without cotyledons (cot) and **(B)** roots without hyocotyls (hyp) from the corresponding temperature assay. Black line marks the starting point for measuring. Scale bar = 10 mm. **C** TIHE of hypocotyls without root and with or without cotyledons. **D** TIRE of roots without hypocotyls. Experiments were performed in LD (16/8 h) conditions under 90 µmol m^{-2} s^{-1} white fluorescent light. Box plots show medians and interquartile ranges of total organ lengths, outliers (greater than 1.5× interquartile range) are shown as black dots. Different letters denote statistical differences at $p < 0.05$ as assessed by one-way ANOVA and Tukey's honestly significant difference (HSD) posthoc test (adapted from Bellstaedt et al., 2019).

4.1.2 The ability for temperature-induced elongation growth in detached organ seedling

Based on these global observations, I next tested dissected plant organs for temperature-induced elongation growth. Therefore, roots and hypocotyls (with or without cotyledons and roots) were removed from 4d-old single wild-type (WT) seedlings and cultivated for additional 4d on ATS with sugar at 20°C or 28°C (Figure 8A,B). Generally,

detached organs grew well if provided with sucrose as an external energy source. In the absence of any shoot tissue, detached roots were still able to elongate at 28°C proportionally more than at 20°C (Figure 8A,C). In contrast, albeit hypocotyls continued to elongate, they did not show a thermomorphogenic response when cotyledons and petioles were removed from the seedling regardless of the presence or absence of the root (Figure 8A,B). However, I observed that the deviations in hypocotyl length between detached and undetached organ seedlings will become more pronounced when the root remains intact (Supplementary Figure S1). These observations indicated two things. First, it seems that roots can autonomously sense and respond to temperature (Figure 8B,D). Whether similar sensing and signaling mechanisms regulate temperature-induced growth responses in root and shoots is unknown and will be further discussed in Chapter II. Secondly, data suggest that temperature-induced hypocotyl growth probably depends on the presence of cotyledons. This reinforced the idea of spatial regulation of temperature sensing and signal transduction pathways in aerial parts of plants. Since much more is known about the molecular mechanisms underlying the regulation of temperature-induced hypocotyl growth, I first focused my analysis on this plant organ.

4.1.3 Separation of temperature perception and growth response in hypocotyls

A possible explanation for the dependency of the hypocotyl response on the presence of cotyledons could be the separation of temperature sensing and possibly also signaling from the actual growth response. Hypocotyls may be unable to sense differences in temperature themselves. Instead, they may rely on long-distance signaling triggered by thermosensing events taking place in the cotyledons. To test this hypothesis, I analyzed the temperature-mediated hypocotyl elongation of intact seedlings and seedlings with detached cotyledons on the cellular level. Hypocotyl growth during normal Arabidopsis development occurs via cell elongation and cell division. I therefore measured cell length and counted the cell number of individual cells of one cortical cell layer from the first cell after the root-shoot junction upward to the shoot apical meristem (SAM) by using laser scanning microscopy (LSM). Confocal imaging of hypocotyl cells (Figure 9A) showed that temperature-induced cell elongation in wild-type plants occurred when seedlings were intact. However, this reaction was considerably reduced in seedlings with detached cotyledons, confirming the necessity of a cotyledon-derived signal to induce cell elongation (Figure 9B) that ultimately results in longer hypocotyls (Figure 9C). Hypocotyls also showed an increase in cell number, indicating that warm ambient temperature stimulates a moderate increase also in cell division (Figure 9D). As this response was not

affected by the removal of cotyledons, temperature-induced cell division in hypocotyls seems to occur independently of a cotyledon-derived signal. Comparing the cell number and length of Arabidopsis seedlings at the embryo maturation stage (4d after vernalization, day0) and a vegetative stage (7d after sowing) (See Supplementary Figure S2), demonstrates that cell division processes in hypocotyls are almost completed by then. Therefore post-embryonic hypocotyls have a comparably higher capacity for cell expansion to promote elongation growth at warmth. Thus, cell elongation seems to be the primary determinant of hypocotyl thermomorphogenesis, while cell division plays a rather minor role. Taken together, apparently in Arabidopsis cotyledons (and/or upper petioles) are not only the primary sites for thermosensing (Kostaki et al., 2010) but also the source of a signal that drives temperature-induced hypocotyl elongation.

4.1.4 Auxin connects temperature sensing in cotyledons with hypocotyl growth

It was unclear which signal molecule moves from temperature-induced cotyledons via the petioles to the hypocotyls to promote cell elongation. One obvious candidate messenger to fulfill such a function is auxin. As illustrated in Figure 3, PHYTOCHROME INTERACTING FACTOR 4 (PIF4), which is the key transcription factor in hypocotyl themomorphogenesis, is able to induce auxin biosynthesis genes in response to elevated temperature (Franklin et al., 2011). Moreover, at the cellular level, auxin is an essential regulator of temperature-induced cell division as well as for elongation (Gray et al., 1998). As such, auxin seems to be an excellent candidate for a mobile signal that regulates temperature-induced elongation of hypocotyl cells. To address this issue, I used both pharmacological and genetic approaches, as the next section will show.

4.1.5 Auxin mediated efflux from induced cotyledons to the hypocotyl: a pharmacological analysis

To interrupt cotyledon-derived auxin transport to the hypocotyls, 1-N-naphthylphtalamic acid (NPA), a polar auxin transport inhibitor, was locally applied to petioles of 7d-old intact seedlings (Figure 10A), which were subsequently shifted to elevated temperatures or stayed at control temperatures. After two days hypocotyl length, cell length, and cell number were quantified using confocal microscopy. As expected, NPA application
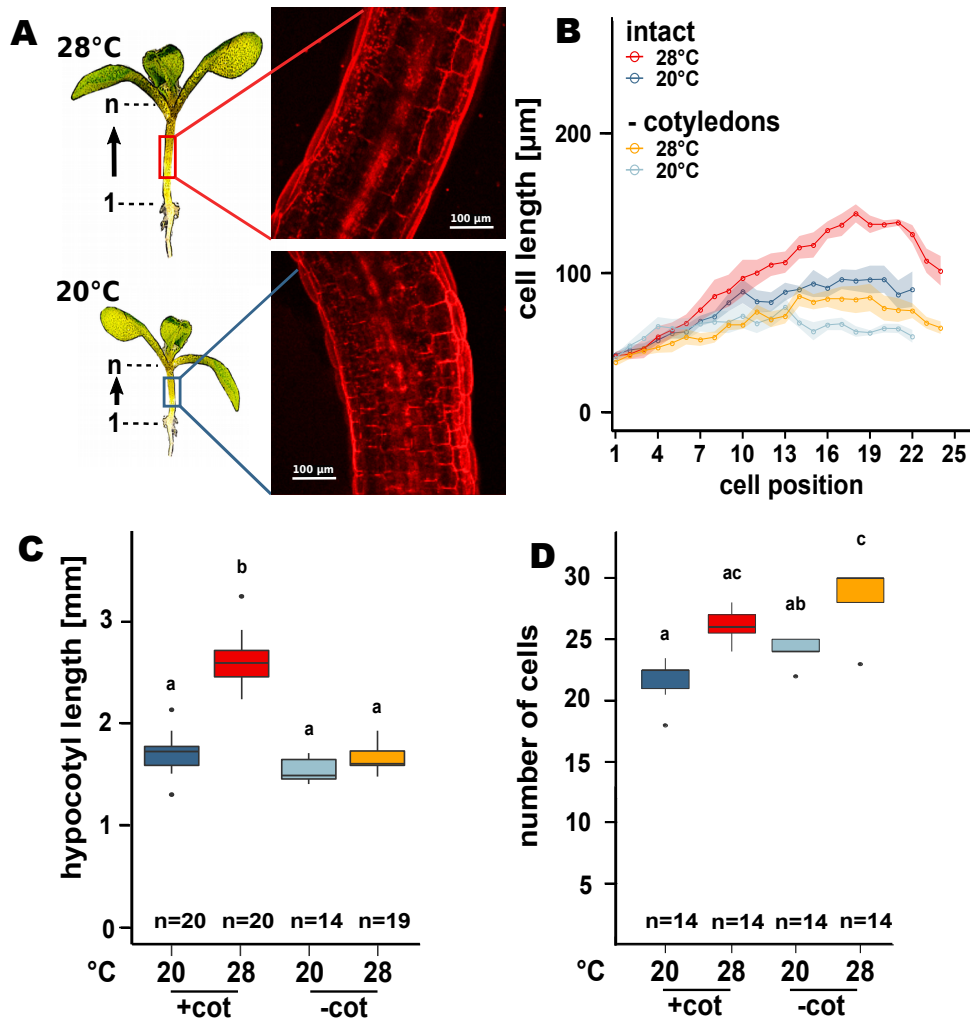
Figure 9. Cell anylsis of detached seedling organs. A Lengths of individual cells in a consecutive hypocotyl cortex cell file were determined via confocal microscopy of propidium iodide-stained seedlings. **B** Effects of cotyledon detachment on hypocotyl cell length, **(C)** hypocotyl length and **(D)** hypocotyl cell number in one consecutive cortex cell file. **A-D** Col-0 seedlings were grown at 20°C for 4d. Petioles and cotyledons were removed or seedlings were left intact prior to a shift to 28°C for an additional 3d. Experiments were performed in LD conditions (16/8 h) under 90 μmol m^{-2} s^{-1} white fluorescent light. Control plants in experiments were treated similarly but were grown at 20°C for the whole time instead of shifting to 28°C. Bold lines in ribbon plots **(B)** show mean lengths of individual cells in a consecutive cortex cell file from the first cell after the root-shoot junction (1) upward to the shoot apex (20+). The shadowed ribbon denotes the SE. Box plots show medians and interquartile ranges; outliers (greater than 1.5× interquartile range) are shown as black dots. Different letters denote statistical differences at $p < 0.05$ as assessed by one-way ANOVA and Tukey's HSD posthoc test (modified from Bellstaedt et al., 2019).

essentially phenocopied the physical detachment of cotyledons and inhibited temperature-induced cell elongation (Figure 10B) as well as total hypocotyl elongation (Figure 10C), while cell division was not affected (Figure 10D). Collectively, these data indicate that auxin is the sought-for mobile signal that links temperature sensing in cotyledons with elongation responses in the hypocotyls. In any case, auxin or auxin transport from the cotyledons seems to be needed. To test whether auxin movement is also sufficient to induce temperature mediated cell elongation in hypocotyls, I transferred 4d-old plants grown at 20°C on unsupplemented medium either as intact wild-type seedlings or as seedlings with detached cotyledons to medium containing the synthetic

auxin picloram. It was expected that auxin could restore temperature responsiveness in hypocotyls even in the absence of cotyledons (Figure 10E). On the other hand, it was recently proposed (Ibañez et al., 2018, Martínez et al., 2018*) that increased auxin level in thermomorphogenesis induces BR biosynthesis and signaling, which in turn activates elongation growth in the hypocotyls downstream of auxin. Thus, I assumed that in similar detached organ experiments, the exogenous addition of epi-brassinolide, a biologically active BR, should also partially compensate for the lack of cotyledon-derived auxin in the hypocotyl. Indeed, either hormone phenocopied temperature-induced hypocotyl elongation in seedlings with detached cotyledons.

Together, these experiments might suggest that auxin is the mobile signal that connects thermosensing in the cotyledons with growth responses in the hypocotyl in a BR dependent manner. This mechanism seems to be of general biological relevance, as the effect of cotyledon removal observed in Arabidopsis was also detected in other flowering plant species. Both tomato (*Solanum lycopersicum*, see Supplementary Figure S3A) and cabbage (*Brassica oleracea*, Supplementary Figure S3B) seedlings failed to show hypocotyl thermomorphogenesis when cotyledons were removed before the exposure to elevated temperatures.

4.1.6 Auxin mediated efflux from temperature-induced cotyledons to the hypocotyl: mutant-based analysis

Pharmacological experiments have been complemented by genetic approaches (knock-out, rescue, gain of function experiments). First, I explored the TIHE of different mutants, defective in auxin biosynthesis or signaling. The loss of function auxin biosynthesis mutant *wei8-1 tar1-1,* which displays strong defects in *TRYPTOPHAN AMINOTRANSFERASE OF ARABIDOPSIS1 (TAA1)* and its close homolog *TRYTOPHAN AMINOTRANSFERASE RELATED 1 (TAR1)*, indeed failed to elongate hypocotyl cells, as well as the auxin receptor mutant *tir1-1 afb2-3*, which lacks two of the six auxin co-receptor (F-box proteins) (Figure 11). Further substantiating these observations, local application of Indole-3-Acetic Acid (IAA) (dissolved in lanolin paste) to cotyledons of the *wei8-1 tar1-1* auxin biosynthesis mutant was sufficient to partially restore the elongation response to elevated temperature (Figure 12). Accordingly, the dominant gain-of-function, auxin overproducing *YUCCA1* mutant (*yuc1-D*), which produces an excess of auxin, also showed a hyperelongation of hypocotyl cells. Furthermore, *yuc1-D* seedlings retain temperature responsiveness to a certain extent also in the absence of cotyledons

(Figure 12), indicating that an ectopic generation of auxin can overcome the lack of the cotyledon-derived signal. A similar trend was observed for all auxin mutants tested when cellular proliferation was examined (See Supplementary Figure S4). Taken together, both *TAA1*-regulated auxin biosynthesis and *TIR1/AFB*-Mediated auxin signaling are both required to promote temperature-induced hypocotyl cell elongation and cell division as described in previous studies. Moreover, I demonstrated that a temperature-dependent cotyledon-derived mobile auxin signal seems to be necessary to promote cell elongation in hypocotyls.
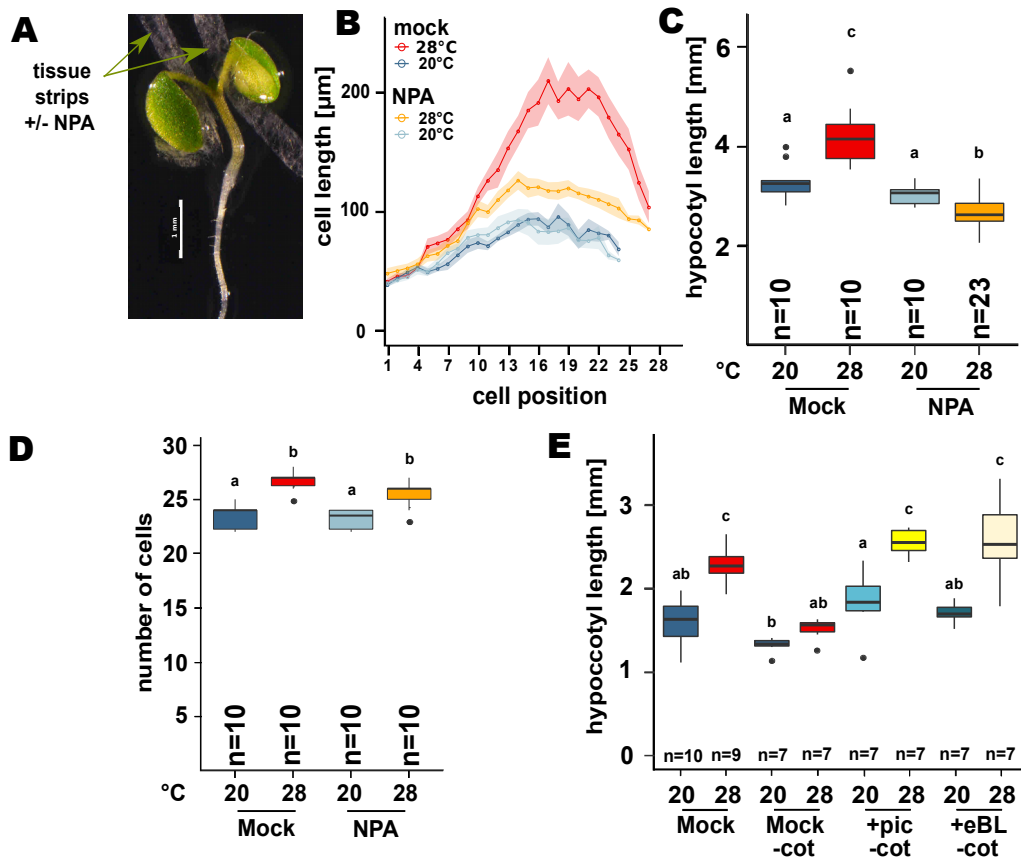
Figure 10. Rescue and inhibition of TIHE effects in seedlings with detached or intact cotyledons with addition of synthetic auxin picloram, epi-brassinolide and NPA. A Localized block of auxin transport by application of thin tissue strips soaked in medium with or without 100 µm NPA. **B - D** Cell length **(B)**, total hypocotyl length **(C)**, and cell number **(D)**. Lengths of individual cells and number in a consecutive hypocotyl cortex cell file were determined via confocal microscopyof propidium iodide-stained Col-0 seedlings. **E** Total hypocotyl length of intact seedlings (+cot) or with detached cotyledons (−cot) in the presence or absence of 1 µm picloram (pic) or 100 nm epi-brassinolide (eBL). 4d-old seedlings grown at 20°C were transferred to medium containing the respective hormones and cultivated at 20°C or 28°C for an additional 3d. Experiments were performed in LD conditions (16/8 h) under 90 µmol m^{-2}s^{-1} white fluorescent light. Control plants in experiments were treated similarly but were grown at 20°C for the whole time instead of shifting to 28°C. Bold lines in ribbon plots **(B)** show mean lengths of individual cells in a consecutive cortex cell file from the first cell after the root-shoot junction (1) upward to the shoot apex. The shadowed ribbon denotes the SE. Box plots show medians and interquartile ranges; outliers (greater than 1.5× interquartile range) are shown as black dots. Different letters denote statistical differences at *p*< 0.05 as assessed by one-way ANOVA and Tukey's HSD posthoc test (modified from Bellstaedt et al., 2019).

Figure 11. Temperature-induced cell and hypocotyl elongation in selected auxin mutants. Effects of cotyledon detachment on hypocotyl cell length in one consecutive cortex cell file and hypocotyl length in Col-0 (**A,C,E,G**), *wei8-1 tar1-1* (**B,C**), *tir1-1 afb2-3* (**D,E**) and *yuc1-D* (**F,G**).seedlings were initially grown in LD (16/8 h) under 90 µmol m^{-2} sec^{-1} white fluorescent light at 20°C for 4d. **A-G** Petioles and cotyledons were removed or seedlings were left intact prior to a shift to 28°C for additional 3d. Control plants were treated similarly but grown at

40

Figure 12. Exogenous auxin on cotyledons restore auxin-deficient response in hypocotyls at elevated temperatures. A Representative pictures of lanolin-treated wild-type and mutant seedlings. **B** Total hypocotyl lengths of 10d-old seedlings with or without localized application of 1 mM IAA in lanolin paste to cotyledons. 7d-old seedlings grown at 20°C were treated with lanolin paste and transferred to 28°C for an additional 3d. Experiments were performed in LD conditions (16/8 h) under 90 μmol m^{-2}s^{-1} white fluorescent light. Control plants in experiments were treated similarly but were grown at 20°C for the whole time instead of shifting to 28°C. Scale bar = 100 μm. Box plots show medians and interquartile ranges, outliers (greater than 1.5× interquartile range) are shown as black dots. Different letters denote statistical differences at $p < 0.05$ as assessed by one-way ANOVA and Tukey's HSD posthoc test (modified from Bellstaedt et al. 2019)

4.1.7 Cell elongation and division are regulated by the same signaling pathway

To further examine the functional linkage between auxin signaling and temperature sensing in cotyledons on the one hand and auxin signaling and temperature signaling in the hypocotyl, on the other hand (Figure 13B), I analyzed the effects of warm temperatures on cell division and cell elongation in detached and undetached mutant plants, defective in central players which regulate the shoot thermomorphogenesis response. PHYTOCHROME INTERACTING FACTORs (PIFs) are basic HELIX-LOOP-HELIX (bHLH) transcription factors previously shown to regulate plant growth in response to changes in temperature. A quadruple *pif* mutant (*pifq*), lacks *PHYTOCHROME INTERACTING FACTOR 1, 3, 4, 5* (*PIF1,3,4,5)* activity displayed cell and hypocotyl elongation patterns, and a cell division behavior at 28°C that strongly phenocopied that of *wei8-1 tar1-1* seedlings indepedent of detached or undetached cotyledons (Figure 13C,D). Thus, as previously suggested PIFs, especially PHYTOCHROME INTERACTING FACTOR4 (PIF4), are important in temperature-induced hypocotyl elongation (TIHE). Among other things, PIF4 directly stimulates IAA biosynthesis by binding to the promoters of genes involved in the indole-3-acetaldoxime (IAOx) and indole-3-pyruvic acid (IPA) pathways, including *TRYPTOPHAN AMINOTRANSFERASE OF ARABIDOPSIS 1* (*TAA1*) (Franklin et al. 2011, Sun et al. 2012). To further assess the potential spatial specificities of PIF4, I also inspected the effect of cotyledon detachment on the temperature response in *PIF4* gain-of-function mutants. *35S:PIF4* hypocotyls hyperelongated in seedlings with intact cotyledons (Figure 13E) at both temperatures. If cotyledons were removed before the temperature shift, hypocotyls of seedlings grown at 20°C were still longer than in the wild-type. The TIHE effect at 28°C was abolished (Figure 13E), indicating that at 20°C PIF4 can serve as a general regulator of elongation growth if ectopically expressed in relevant tissues. Interestingly, the TIHE response at 28°C is lost in the absence of cotyledons. Hence, the primary role of PIF4 in elevated temperatures seems to indeed reside in the cotyledons, where its activity is derepressed by the inactivation of photoreceptors (e.g., phyB) (Figure 14B).

Similarly to the *pifq* phenotype, seedlings that express a constitutively active light and temperature receptor phytochrome B (phyB) variant (*YHB*) have less (Figure S6B) and shorter hypocotyl cells (Figure 14C) than the corresponding wild-type. Furthermore, hypocotyl cells fail to elongate and divide in response to temperature, confirming that the derepression of PIF4 via inactivation of *phyB* is a prerequisite for hypocotyl

thermomorphogenesis. Accordingly, the *phytochrome A,B,C,D* (*phyABCDE)* mutant shows hyperelongated hypocotyl cells regardless of the cultivation temperature (Figure 14E). In conclusion, based on the phenotype of mutants tested, especially the phenotypes of *wei8-1 tar1-1* and detached *yucca1 dominant* (*yuc1-D*) mutant seedlings, it is most likely that cotyledon-derived auxin triggers temperature-induced cell enlargement in hypocotyls. In contrast, cell division appears to be primarily activated by auxin, which is produced by the shoot apical meristem but seems to be regulated by the same signaling pathway.
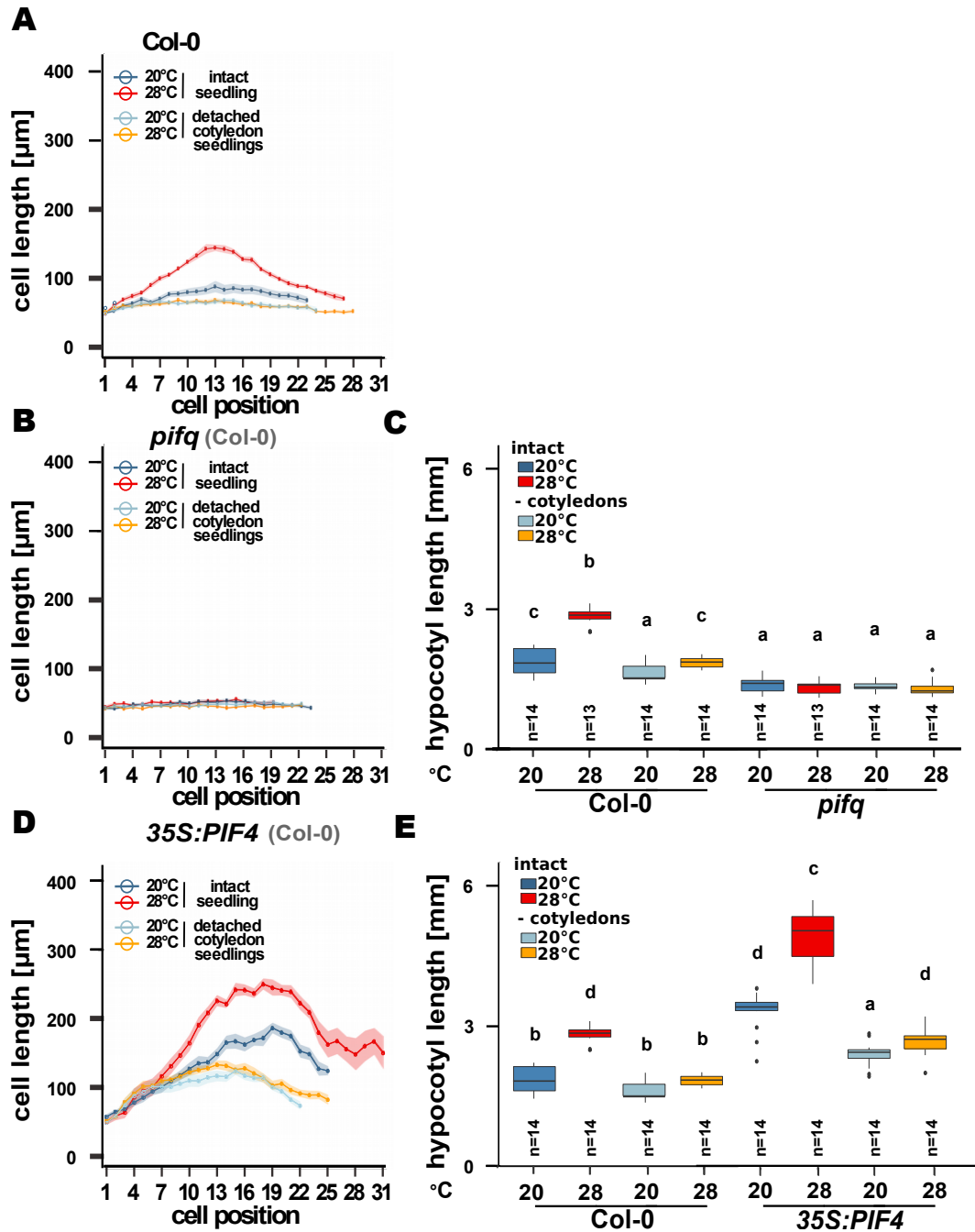
Figure 13. Temperature-induced cell and hypocotyl elongation in mutants of thermomorphogenesis regulators. A-E Effects of cotyledon detachment on hypocotyl cell length in one consecutive cortex cell file and hypocotyl length in Col-0 **(A, C, E**), *pifq* (**B, C**) *and 35S:PIF4* (**D,E**). Seedlings were grown at 20°C for 4d. Petioles and cotyledons were removed or seedlings were left intact prior to a shift to 28°C for an additional 3d. Experiments were performed in LD conditions (16/8 h)

Figure 14. Temperature-induced cell and hypocotyl elongation in mutants of photomorphogenesis regulators. A-E
Effects of cotyledon detachment on cell length in one consecutive cortex cell file and hypocotyl length in Ler-0 (**A,C,E**), *YHB* (**B,C**) and *phyABCDE* (**D,E**), seedlings were grown at 20°C for 4d. Petioles and cotyledons were removed or seedlings were left intact prior to a shift to 28°C for an additional 3d. Experiments were performed in LD conditions (16/8 h) under 90 µmol m^{-2} s^{-1} white fluorescent light. Control plants in all experiments were treated similarly but were grown at 20°C

44

or the whole time instead of shifting to 28°C. Bold lines in ribbon plots (**C,E**) show mean lengths of individual cells in a consecutive cortex cell file from the first cell after the root-shoot junction (1) upward to the shoot apex. The shadowed ribbon denotes the SE. Box plots show medians and interquartile ranges, outliers (greater than 1.5× interquartile range) are shown as black dots. Different letters denote statistical differences at $P < 0.05$ as assessed by one-way ANOVA and Tukey's HSD posthoc test (modified from Bellstaedt et al. 2019).

4.1.8 BZR1-mediated hypocotyl thermomorphogenesis requires local permissive temperature sensing

It was recently reported that auxin action in thermomorphogenesis depends on the brassinosteroid (BR)-activated transcription factor BRASSINAZOLE-RESISTANT1 (BZR1) and its homolog BRI1-EMS-SUPPRESSOR 1 (BUS1), which activate elongation growth downstream of auxin (Ibañez et al., 2018, Martínez et al., 2018). BZR1 function may involve heteromerization with other transcription factors such as AUXIN RESPONSE FACTORs (ARFs) and PHYTOCHROME NTERACTING FACTOR4 (PIF4)(Oh et al., 2012, 2014), which can affect preferences forspecific *cis*-element binding sites (Martínez et al., 2018). To determine potential spatial specificities in BZR1 action, I also performened cotyledon detachment experiments for *bzr1-1D-OX* gain of function lines in response to elevated temperatures. Hypersensitivity of *bzr1-1D-OX* can be largely attributed to hyperelongated hypocotyls at 28°C (Figure 15D). In dissected seedlings, *bzr1-1D-OX* still displayed temperature-induced hypocotyl elongation comparable to the wild-type. Since detached *bzr1-1D-OX* hypocotyls are deprived of cotyledon-derived thermosensing via phytochromes and PIF4, this suggests the presence of asecond independent thermosensor. This unknown sensor possibly provides a permissive signal that gates cotyledon-derived signaling in the hypocotyls. Numerous molecular mechanisms have the capacity to serve as thermosensors (for review, See Vu et al., 2019). One possible candidate for a permissive temperature sensor gating BZR1 function in the hypocotyl could be constituted by changes in the chromatin structure (Figure 15B). Thermomorphogenesis has been shown to require chromatin remodeling that involves histone deacetylation (Tasset et al., 2018) and the eviction of the H2A.Z histone variants (H2A histone family member Z) (Kumar and Wigge, 2010). To study potential fortissue sepcific role of H2A.Z in plant, the tissue specific themomorphogenesis, I analyzed temperature induced hypocotyl elongation of mutant plants defective in SWR1 chromatin remodeling complex (CRC) component ACTIN-RELATED PROTEIN6 (ARP6) (Deal et al., 2007) with or without cotyledons (Knock-out (KO)). In Arabidopsis, three genes encode the pool of H2A.Z proteins and there are no completely null triple *H2A.Z* mutants available, which complicates genetic work (Coleman-Derr and Zilberman, 2012). Other studies have

verified that ARP6 is required for proper H2A.Z incorporation into nucleosomes and *arp6* mutants phenocopy *H2A.Z* mutants, making *arp6* mutants a logical proxy for H2A.Z mutants in my genetic study (Sura et al., 2017, March-Diaz et al., 2008, Berriri et al., 2016). The *arp6-1* mutants which is unable to form H2A.Z histone variants is hypersensitive to temperature which results in an exaggerated elongation of hypocotyls (Figure 15D). While *arp6-1* mutant retain the ability for temperature responses in the hypocotyl, the hyperelongation at 28°C is abolished when cotyledons are detached prior to the temperature shift. Although this needs to be substantiated with complementary experimental approaches, the results illustrate that cotyledon-derived signaling converges with chromatin-mediated processes in the regulation of hypocotyl thermomorphogenesis. It remains to be clarified whether other components of chromatin remodeling or entirely different signaling processes may be involved in the permissive autonomous sensing of elevated temperatures in thehypocotyl. In this context the role of HISTONE DEACETYLASE 9 (HDA9) should be clarified. Van der Woude et al. (2019) showed that HDA9 stimulates auxin-dependent thermomorphogenesis in *A. thaliana* by mediating H2A.Z depletion (See Introduction). HDA9 protein levels are increased in young seedlings in warmth and mediate histone deacetylation at nucleosomes of *YUCCA8* (*YUC8*) gene. This deacetylation event proposedly reduced H2A.Z levels, which allows for PIF4 binding to the *YUC8* promoter and transcriptional activation. However, it seems that HDA9 acts independent of the plant thermosensor phytochrome B (phyB). Thus, it is likely that HDA9 is part of a novel thermosensing pathway (Van der Woude et al., 2019). Detached organ experiments with an *HDA9* overexpression line imply a certain dependency of a cotyledon-derived signal similar to ARP6. While the *hda9-1* mutant retained the ability to respond to elevated temperature in the hypocotyl (that is what we See also in the literature, See Van der Woude et al. 2019), hypocotyl elongation of *HDA9-OX* is increased compared to the wild-type at 28°C (Figure 15E). In contrast, the hyperelongation at 28°C is reduced without cotyledons. These observations highlighted the link between HDA9 and chromatin remodeling on the one hand, but also indicate a certain dependence on a signal coming from the cotyledons.
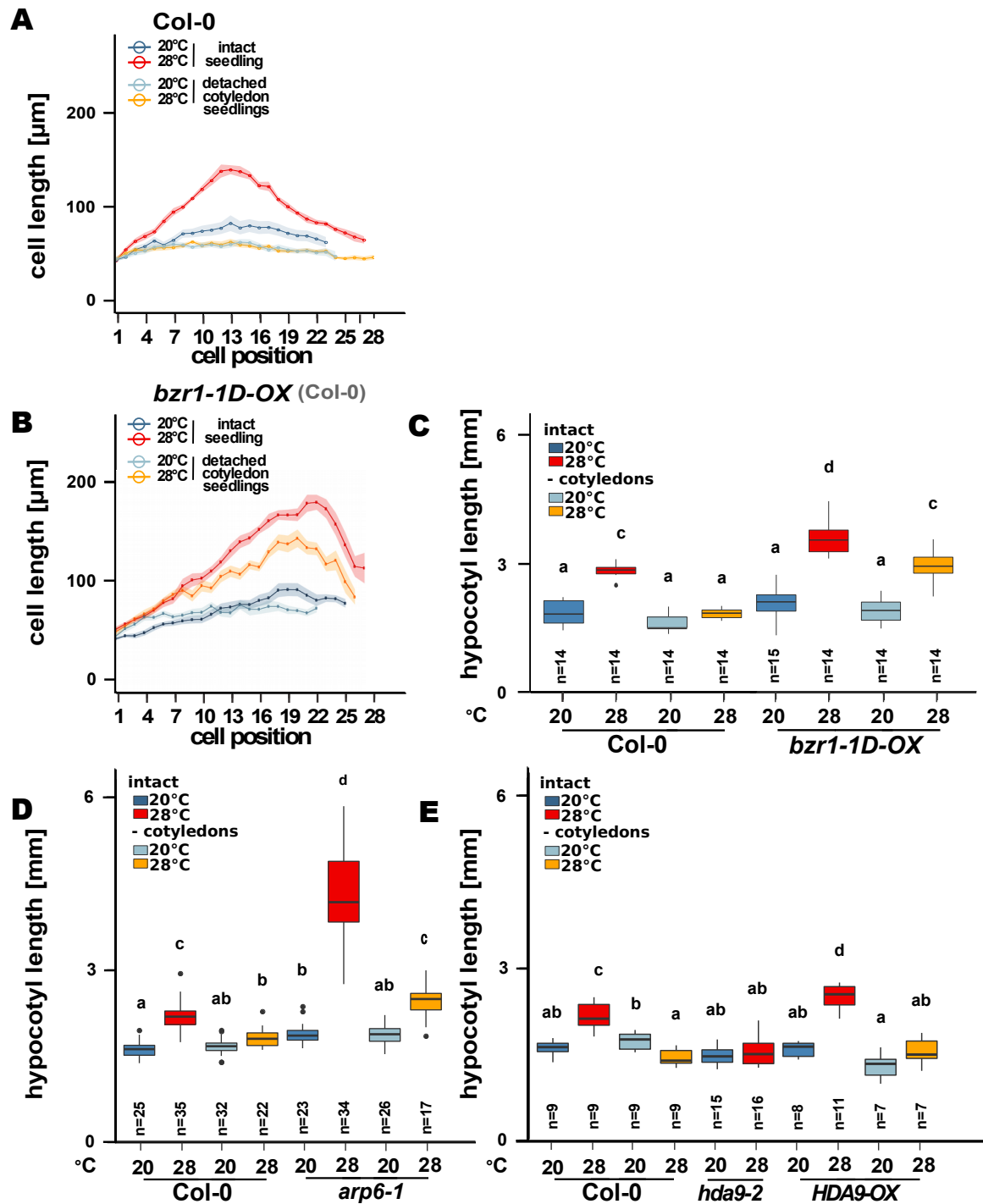
Figure 15. Temporal temperature-induced changes in chromatin structure might enable gating of BZR1 function in the hypocotyl. A-E Effects of cotyledon detachment on hypocotyl cell length in one consecutive cortex cell file and total hypocotyl length in *Col-0* (**A,C,D,E**), *bzr1-1D-OX* (**B,C**) *arp6-1* (**D**), *arp6-1* and *HDA9-OX* (**E**). seedlings were grown at 20°C for 4d. Petioles and cotyledons were removed or seedlings were left intact prior to a shift to 28°C for an additional 3d. Experiments were performed in LD conditions (16/8 h) under 90 μmol m^{-2} s^{-1} white fluorescent light. Control plants in all experiments were treated similarly but were grown at 20°C for the whole time instead of shifting to 28°C. Bold lines in ribbon plots (**B**) show mean lengths of individual cells in a consecutive cortex cell file from the first cell after the root-shoot junction (1) upward to the shoot apex. The shadowed ribbon denotes the SE. Box plots show medians and interquartile ranges, outliers (greater than 1.5× interquartile range) are shown as black dots. Different letters denote statistical differences at *p*< 0.05 as assessed by one-way ANOVA and Tukey's HSD posthoc test (modified from Bellstaedt et al. 2019).

4.1.9 Organ-specific expression analysis in response to elevated temperatures by qPCR

Based on the physiological observations, I next investigated the potential effects of a mobile auxin signal on the transcriptional activation of thermoresponsive genes. seedlings were dissected in cotyledons and hypocotyls either before or after an 8h temperature stimulus of 28°C to seedlings previously grown at 20°C (Figure 16A). In this experimental setup, seedlings dissected after the temperature shift were able to send a mobile auxin signal from the cotyledons to the hypocotyl. Obviously, this was not possible in seedlings that were dissected before temperature treatment. To first test the relevance of temperature-induced auxin biosynthesis in cotyledons versus hypocotyls, we quantified transcript levels of the thermoresponsive auxin biosynthesis gene *YUCCA8* (*YUC8*). As shown in Figure 16B, *YUC8* was thermoresponsive in cotyledons but not in hypocotyls. Furthermore, expression levels of *YUC8* at elevated temperature were several fold higher in cotyledons in comparison with hypocotyls (Figure 16B), suggesting that thermoresponsive induction of auxin biosynthesis is most relevant in cotyledons rather than in hypocotyls. We then inspected the need for a mobile auxin signal in the induction of thermoresponsive auxin *INDOLE-3-ACETIC ACID INDUCIBLE 19* (*IAA19*) and auxin/BR response genes that are relevant for cell elongation (*SAUR19* and *SAUR20*, Spartz et al., 2012). Hypocotyls that were excised from seedlings after a temperature stimulus showed a strong temperature response in *Small auxin-up RNA 19, 20* (*SAUR19*, *SAUR20)*, and *IAA19* (Figure 16B), indicative of a successfully transmitted auxin signal from the cotyledons to the hypocotyl. In contrast, the induction was absent if cotyledons were detached prior to the shift to higher temperatures, confirming that auxin has to be translocated to the hypocotyl to induce growth-relevant genes in elevated temperatures. This mode of regulation strongly resembles processes involved in the regulation of hypocotyl elongation in response to shade (i.e. reduced blue light) or vegetative shade (Keuskamp et al., 2011, Procko et al., 201, Procko et al., 2016, Nito et al., 2015). Whether temperature perception also shows local spatial preferences within cotyledon and leaf areas similar to the sensing of vegetative shade (Michaud et al., 2017, Pantazopoulou et al., 2017) remains to be clarified. Collectively, these results imply that the predominant function of PHYTOCHROME INTERACTING FACTOR4 (PIF4) in thermomorphogenesis may be the induction of auxin biosynthesis genes in the cotyledons. Auxin synthesized in the cotyledons then travels to the hypocotyl, where it triggers BR-dependent cell elongation. If it were that simple, there would be no

need for thermoresponsive induction of *PIF4* transcription in hypocotyls. We observed that in response to temperature, *PIF4* was significantly induced in both cotyledons and hypocotyls (Figure 16C). While the absolute expression level was higher in cotyledons, the induction of expression in hypocotyls may be a consequence of the proposed BRASSINAZOLE-RESISTANT1 (BZR1)-mediated feed-forward regulation (Ibañez et al., 2018) to enable a cooperative interaction of BZR1 and PIF4 in the transcriptional regulation of growth-promoting genes in hypocotyls. The presence of PIF4 may be relevant to fully express *BZR1* function, as the interaction with PIF4 seems to affect the specificity for different target *cis*-elements (Martínez et al., 2018).
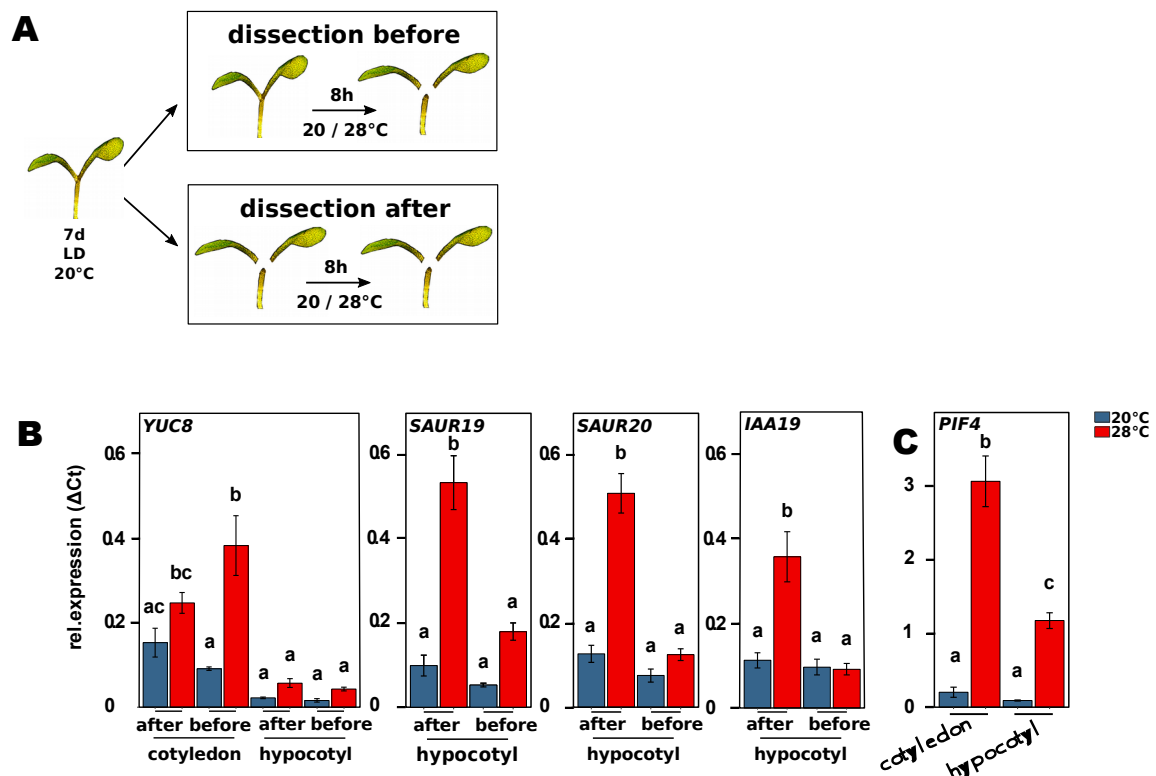
Figure 16. Organ-specific expression analysis of auxin- and growth-related genes. A-C Col-0 seedlings cultivated for 7d at 20°C were transferred to 20 or 28°C at ZT 16 for 8 h prior to harvesting of cotyledons and hypocotyls for expression analysis. seedlings were either dissected after or before the temperature shift including the removal of the root. **B** Genes relevant for auxin biosynthesis *YUC8*, hypocotyl elongation (*SAUR19* and *SAUR20*) and an auxin response gene (*IAA19*) were assessed in hypocotyl samples. **C** RT-qPCR expression analysis of the gene *PIF4* was assessed for cotyledons and hypocotyls. seedlings were grown in LD (16/8h) conditions under 30 µmol m-^{2} sec-^{1} white fluorescent light. RT-qPCR analyses were performed on 3 independent biological samples. Bar plots show mean values, error bars denote SE. Different letters denote statistical differences at $p < 0.05$ as assessed by one-way ANOVA and Tukey HSD post hoc test (modified from Bellstaedt et al. 2019).

In conclusion, there are two most important findings of this chapter. The first concerns the question whether spatiotemporal separation in sensing and/or signaling governs temperature-induced cell elongation in the hypocotyls, while the second relates to the processes in roots at elevated temperatures. Based on a combination of genetic, transcriptomic, physiological and pharmacological experiments, I could demonstrate that

temperature-induced cell elongation requires temperature sensing in the cotyledons, where a mobile signal, which might be auxin, is generated that delivers the growth stimulus to the hypocotyl. All the data discussed in this session are summarized in a model (See Figure 51A). Hence, shoot temperature responses require both local and systemic processes. In contrast, a distinct elevated temperature signaling mechanisms must exist in roots. Roots might be able to sense and respond to temperature independently of other organs.

4.2 Chapter II: Influence of elevated temperature on root growth

Following a similar approach to the investigations of the aerial parts of plants, I explored the impact of elevated ambient temperatures on root growth parameters. Beside quantifying variations in primary root length at elevated temperatures, experiments to study temperature-induced changes in lateral root number and root hair density (defined by the number of root hairs per 5 mm root length) were carried out. At 28°C, all three quantified root growth traits were significantly increased compared lower temperatures (Figure 17A-D). Lateral root elongation on plants exposed to elevated temperatures was already observed by Quint et al. (2009). Although root hair density was most affected by an increase in ambient temperature (~70% increase at 28°C), my research focussed on studying temperature-induced root elongation (TIRE) which is a more easily and robust measurable phenotype.

To study root growth dynamics in primary root elongation to warmth, time scale experiments were performend (from 2d to 12d after sawing).Time-course analysis revealed a significant increase in primary root length at 28°C from day 4 to day 5 (Figure 18A). Correlation between primary root elongation and temperature might indicate a direct influence of temperature on root growth processes such as cell proliferation or cell expansion. The values of the relative root growth calculated for each time point, showing an increase from day 2 to day 5 of up to ~120%, while from day 6 to day 12 the values increased up to ~200% (Figure 18B). Contrasting the acceleration of primary root growth after 6d at 28°C, the growth rates between 2d to 4d and 8d to 10d were quite similar. The observation that the root lengths did not differ significantly between 20 and 28°C during the first three days after sawing, indicates that either the root requires a certain amount of time to react to temperature differences or that the plants must have reached a certain development stage to perceive temperature differences.

However, only in the period between 5 and 7d, the growth rates were significantly different. Likely, growth processes have been adapted to elevated temperatures during the last time interval. Based on this data, I chose day 7, for my further analysis of cellular characteristics, unless otherwise described, as the maximal growth rate at each temperature was reached. As such, roots are already in or near a steady growth state and therefore easier to compare and analyze. Furthermore, it will reduce the potential for complications resulting from differing levels of root development.

Figure 17. Temperature-induced root responses at elevated temperatures. A-B Representative picture from the corresponding temperature-induced root elongation assay and light-microscopy images from root hair measurements at 20°C or 28°C. Temperature-induced (**C**) elongation in primary roots, (**D**) emergence of lateral roots and (**E**) formation of root hairs of 7d-old seedlings, grown at constant temperatures of 20°C or 28°C. Scale bar: 10mm. Experiments were performed in LD (16/8h) conditions under 90 µmol m^{-2} s^{-1} white fluorescent light. Box plots show medians and interquartile ranges of total organ lengths; outliers (greater than 1.52 interquartile range) are shown as black dots. Different letters denote statistical differences at $p<0.05$ as assessed by one-way ANOVA and Tukey's honestly significant difference (HSD) posthoc test.

4.2.1 The effect of elevated temperature on cell division and cell elongation in developing roots under constant temperatures

Warmth-induced promotion of primary root growth must result from increased cell division and/or cell elongation. To investigate how these processes are affected by elevated temperature, I explored the of temperature-induced root elongation for each day of plant

growth until day 7 on cellular level. I measured the root zone length, cell number, and cell length of the meristematic zone (MZ), elongation zone (EZ) and maturation zone (MaZ) of a consecutive cell file (See Figure 4).
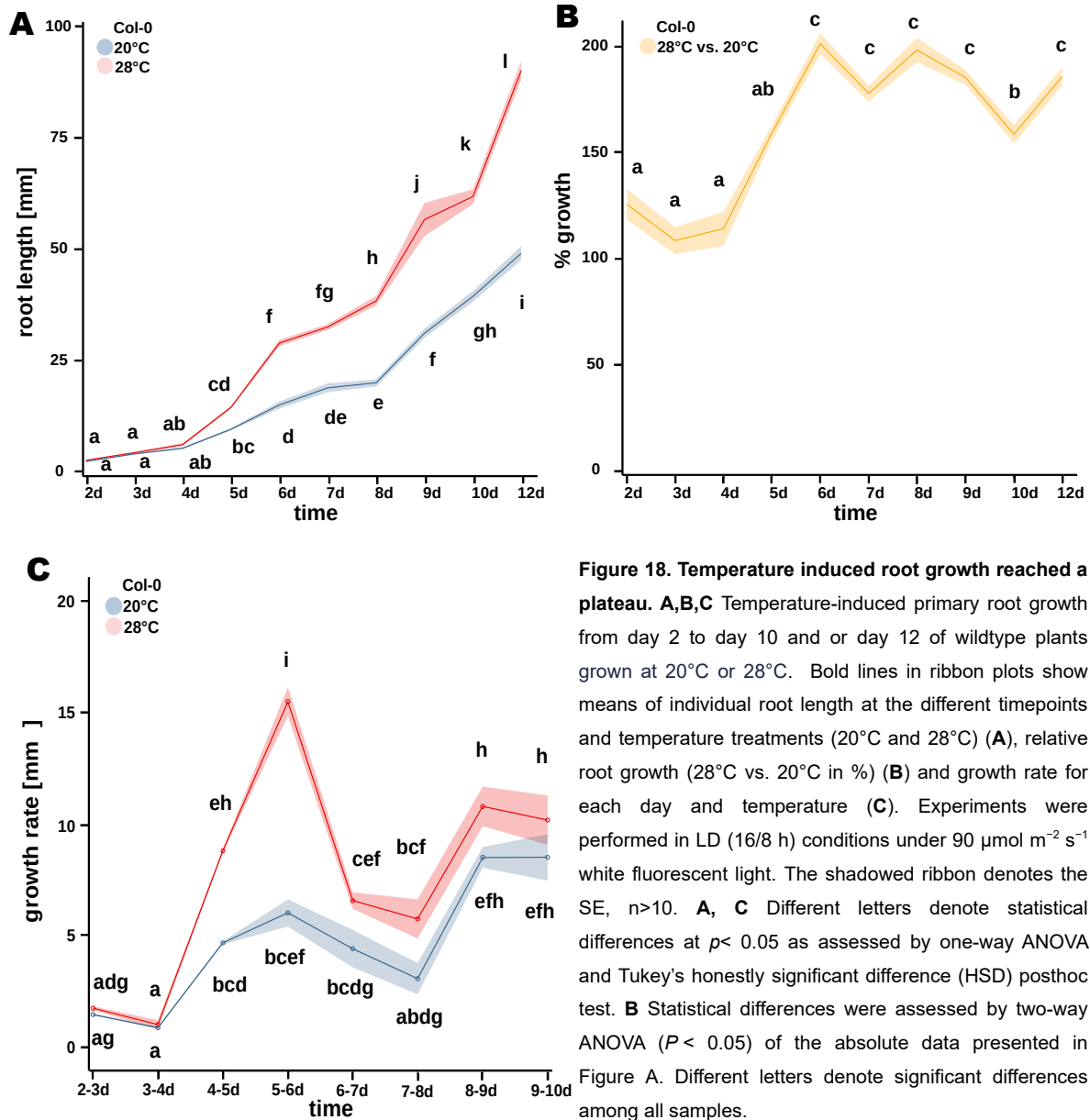
Figure 18. Temperature induced root growth reached a plateau. A,B,C Temperature-induced primary root growth from day 2 to day 10 and or day 12 of wildtype plants grown at 20°C or 28°C. Bold lines in ribbon plots show means of individual root length at the different timepoints and temperature treatments (20°C and 28°C) (A), relative root growth (28°C vs. 20°C in %) (B) and growth rate for each day and temperature (C). Experiments were performed in LD (16/8 h) conditions under 90 µmol m^{-2} s^{-1} white fluorescent light. The shadowed ribbon denotes the SE, n>10. A, C Different letters denote statistical differences at $p < 0.05$ as assessed by one-way ANOVA and Tukey's honestly significant difference (HSD) posthoc test. B Statistical differences were assessed by two-way ANOVA ($P < 0.05$) of the absolute data presented in Figure A. Different letters denote significant differences among all samples.

The results showed that the total length and the cell number of the MZ of plants subjected to elevated temperature slightly increased until day 6, but then stagnated at day 7 and lagged behind the level of plants cultivated at 20°C (Figure 19A-C). Although some significant differences in meristem size and the cell number were found between 20°C and 28°C, they were not substantial to explain the large existing variation in primary root length. Thus, the TIRE-effect of 28°C-grown plants seems unlikely to result from an increase in cell division. Therefore, it is assumed that the TIRE-phenotype must cause

temperature-induced changes in cell elongation in the EZ at 28°C. Interestingly, cell elongation in the EZ was also not fundamentally affected by elevated temperatures. While the total zone length of the EZ was slightly increased at 28°C until day 6, the total zone length and cell number at the time points after that were similar at both temperatures (Figure 19D-F). Furthermore, although the last two cells of the EZ of roots grown at 28°C, were always significantly longer than those at 20°C (Figure 19G), the average length of the cells across the complete EZ was nearly the same. TIRE assays revealed tremendous differences in primary root length between 20°C and 28°C (Figure 17C), which could not be explained from these findings.

However, the rate of cell production by a meristem has two distinct components: the number of dividing cells and the time in which a meristematic cell may take to complete the cell cycle and devide (Beemster et al., 1998). If the cell doubling time (cell division rate) in root meristematic zone is reduced at elevated temperatures, the total amount of cells in the MaZ, which is directly affected by the changes in the distal root zones, should be increased. Indeed, the number of cells in the MaZ were significantly increased at 28°C (Figure 20). Although the cells in the MaZ were also slightly longer at elevated temperatures, the differences in cell numbers between 20°C and 28°C were even more pronounced. Under elevated temperatures, the MaZ consists of twice as many cells compared to plants grown at 20°C (Figure 20C). These observations implicate that cell division in the MZ, nonetheless, must play a role in temperature-induced root elongation. Since the total length and cell number of the MZ revealed non-essential effects in cell growth, and only reasonable explanation left is an increase of the cell division rate in the MZ. This, for example, was shown by the results of some kinematic measurements at elevated temperatures of Yang et al. (2016) in *A. thaliana* and Alarcón et al. (2017) in maize. Hence, the root seems to respond to warmth differently from the shoot, mainly increasing cell expansion. The finding that the MZ shortens at elevated temperatures while the final cell number increased could be interpreted as an effect of temperature adaptation. Reduction in meristem size at elevated temperature might be a useful mechanism for plants to handle extra cells, save energy and operate more efficiently (Yang et al., 2016). The observation that the increase in cell number in the MaZ decreases after day 4, which is the time point when the MZ was starting to reduce, will support this hypothesis (See Figure 20, Figure S7). At 20°C, the number of cells increases evenly and stays roughly constant. However, overall cell division processes appear to be going faster at elevated temperatures.
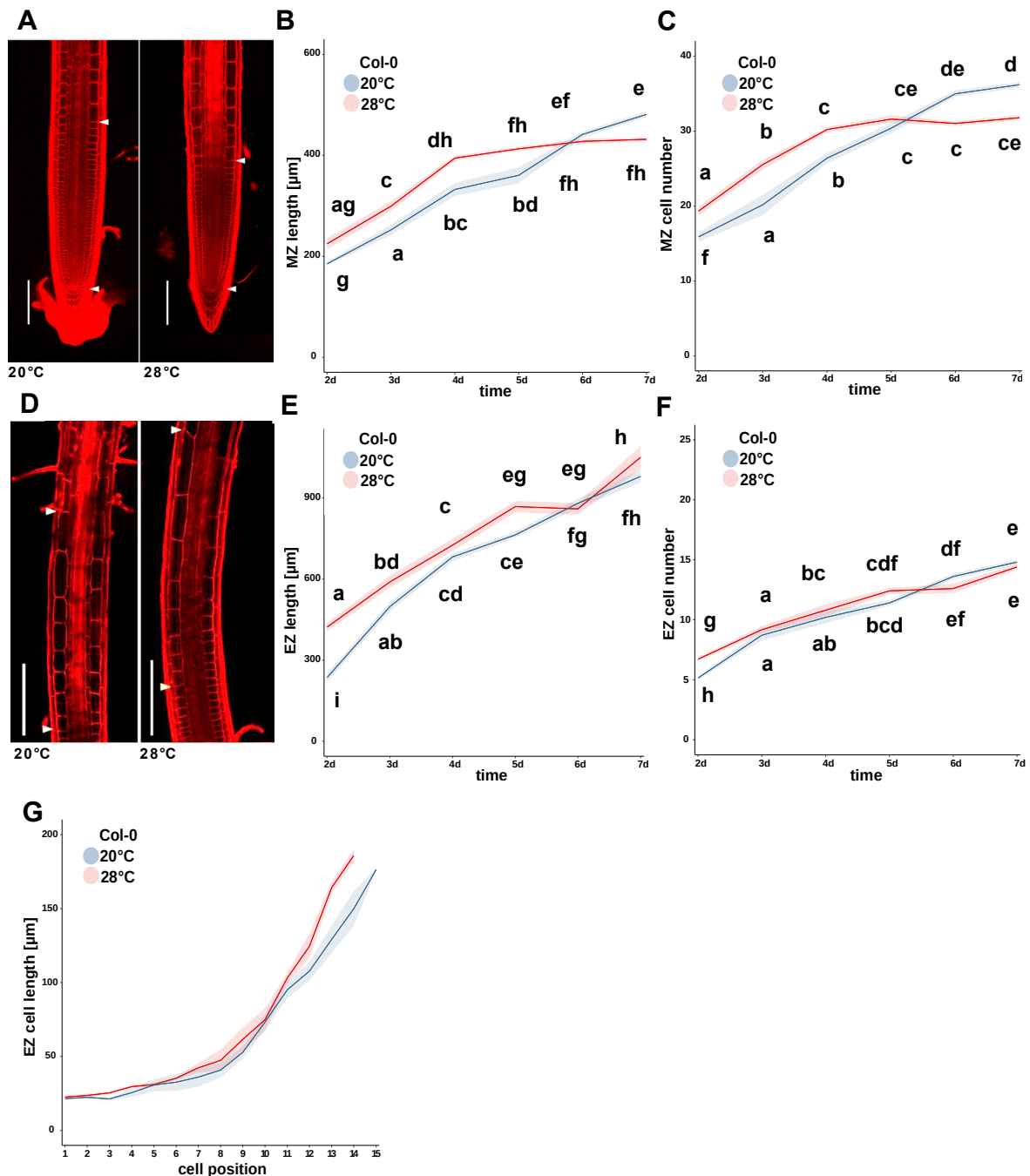
Figure 19. Temperature-induced cellular changes in the meristematic zone and elongation zone. Representative pictures of **A** meristematic zone, **D** elongation zone of 7d-old wild-type plants grown at 20°C and 28°C. Scale bars: 100µm. Cell files were determined via confocal microscopy of propidium iodide-stained seedlings. Temperature- induced elongation (**B**) and cell production (**C**) of the meristematic zone. Temperature- induced elongation (**E**), cell production (**F**) and cell elongation (**G**) of the elongation zone. Roots of wild-type seedling grown at 20°C or 28°C were determined over a time course of 7 days, starting with 2 days after germination. All Experiments were performed in LD (16/8 h) conditions under 90 µmol m^{-2} s^{-1} white fluorescent light. Bold lines in ribbon plots show means of length, number, cell length of the two different zones on 5 different time points (**B,C,E,F**) or the individual cell length in a consecutive cortex cell file from the first cell which is longer than broad to the region of the first visible root hair bulge (**G**). The shadowed ribbon denotes the SE. Different letters denote statistical differences at *p*< 0.05 as assessed by one-way ANOVA and Tukey's honestly significant difference (HSD) posthoc test.
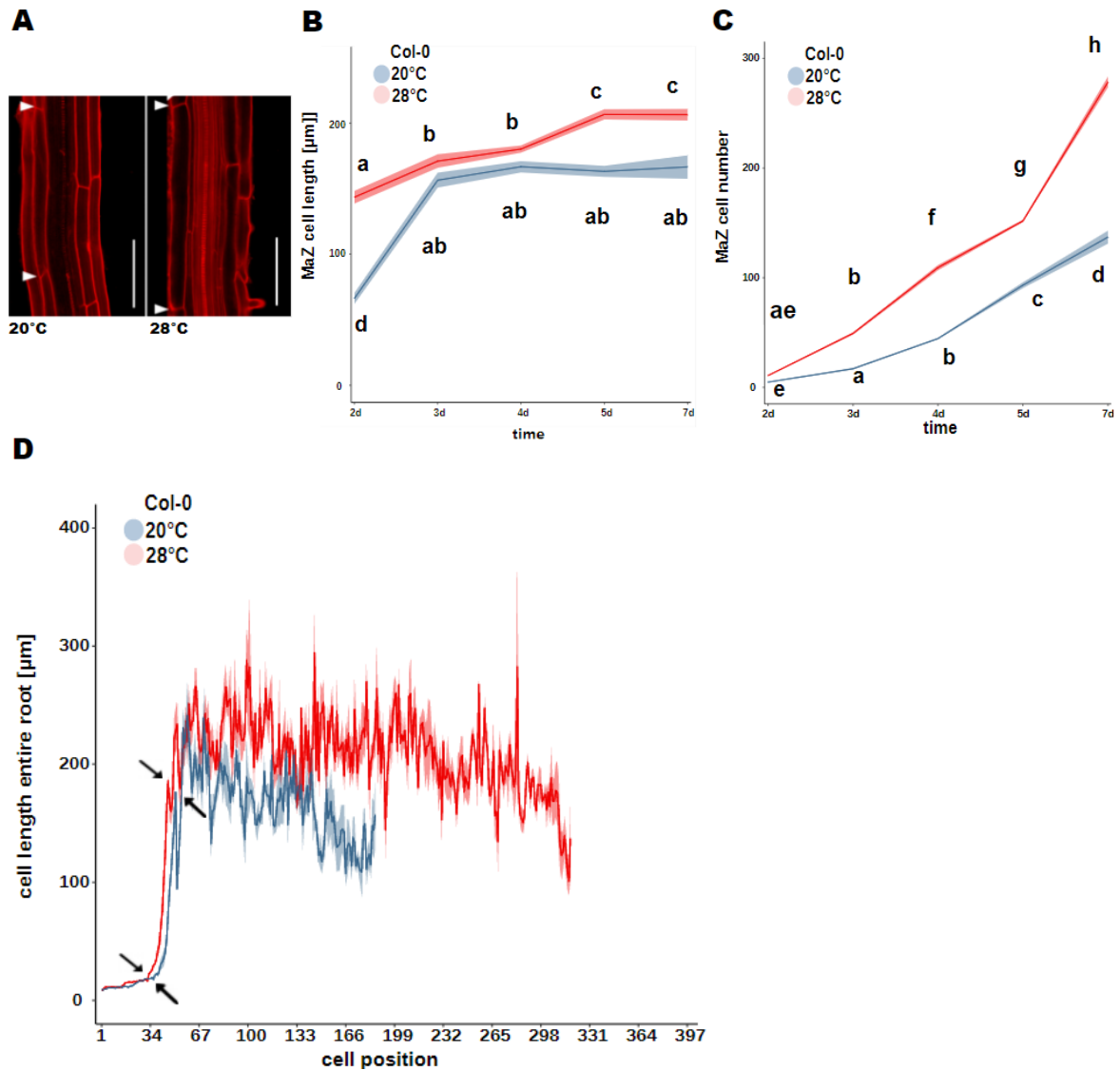
Figure 20. Cellular pattern in the maturation zone. Representative pictures of **A** maturation zone of 7d-old wild-type plants grown at 20°C and 28°C. Scale bars: 100μm. Cell files were determined via confocal microscopy of propidium iodide-stained seedlings. **B** Cell length and **(C)** cell number of the maturation zone. **D** cell length of all cells in the root from QC upward to the root-shoot junction (n<5). Roots of wild-type seedling grown at 20°C or 28°C were determined over a time course of 7 days, starting with 2 days after germination. All Experiments were performed in LD (16/8 h) conditions under 90 μmol m⁻²s⁻¹ white fluorescent light. Bold lines in ribbon plots show means of cell number and length of the maturation zones on 5 different time points (**B,C**) or the cell length in a consecutive cortex cell file from the first cell after the QC upward to the root-shoot junction (**D**) The shadowed ribbon denotes the SE. Different letters denote statistical differences at $p < 0.05$ as assessed by one-way ANOVA and Tukey's honestly significant difference (HSD) posthoc test.

4.2.2 Temperature-induced root growth can be largely explained by temperature-sensitive cell division

As cell division in the MZ is strongly affected by elevated ambient temperatures, I next examined the mitotic activity in the root apical meristem. Although the MZ was not affected by temperature concerning length and number of cells therein, increased cell division rate at high temperature would generate more cells in a given time. Ultimately, this would

result in a higher number of cells in the MaZ and thus, a longer primary root. To monitor cell division rates at different temperatures, I stained 2, 5, and 7d-old seedlings grown at 20°C and 28°C with a thymidine analogue, 5-ethynyl-2′-deoxyuridine (EdU). Edu is a popular nonradioactive marker for identifying *de* novo DNA synthesis in proliferating cells during the S-phase of the cell cycle (Kotogány et al., 2010). It can, therefore, be used as a marker for cell proliferation. When EdU-labeled cells divide, each progeny cell also contains EdU-labeled nuclei (green). Consequently, the more often cells divide, the higher the number of cells with green fluorescence protein (GFP) signal, indicating a higher cell division rate. According to the growth curve data in Figure 18A and B, there was no statistical difference between the number of positively stained cells at 20°C and 28°C on the second day. In contrast, the Edu staining revealed a significant increase of dividing cells at 28°C compared to 20°C at day 5 and 7. These results indicate that elevated temperatures can increase cell division events in *A. thaliana* after the second day of germination (Figure 21A-C). As a negative control, I treated roots with the DNA polymerase inhibitor aphidicolin, which has been shown to induce cell cycle arrests. As expected, fluorescence signals indicating positive EdU incorporation could not be detected (Figure 21B).

4.2.3 Temperature effect on cell cycle stages

Increasing cell number in roots grown at 28°C compared to 20°C without time shifts can only be explained by decreased cell cycle duration. That cell cycle duration shortens with increasing temperatures could be observed in several species, such as maize (Francis and Barlow, 1998) or onion roots (Lopez-Saez et al., 1966, Cuadrado et al., 1989). To determine whether elevated temperatures affecting specific cell cycle phase transitions, the relative abundance of cells in the different phases of the cell cycle should be measured. Therefore, I used the dual-colour marker system "*Cytrap*" (Yin et al., 2014). The *Cytrap* line carries a part of Arabidopsis Chromatin Licensing And DNA Replication Factor 1a (*CDT1a*) to the Red Fluorescent Protein (RFP) gene. Another part of the *Cytrap* line is the G2/M- specific cyclin B1 marker, which is fused to the Green Fluorescent Protein (GFP,) gene. (Aki et al., 2016). Both part allows visualization of the S-phase and G2 to M cell cycle stages (See Figure 22).

Cytrap seedlings were cultivated for seven days at 20°C or 28°C and harvested (n=9) at ZT0 (Zeitgeber Time,1 hour (h) after lights on), ZT1 (1.30h after dawn) , ZT2 (2h after dawn), ZT3 (3h after dawn), and ZT6 (6h after dawn). Fluorescent images were taken, and red and green fluorescent cells were counted. My preliminary work has mostly

focussed on cell detection in the S-phase and G2/M-phase since both fluorescence signals were clearly quantifiable.

A
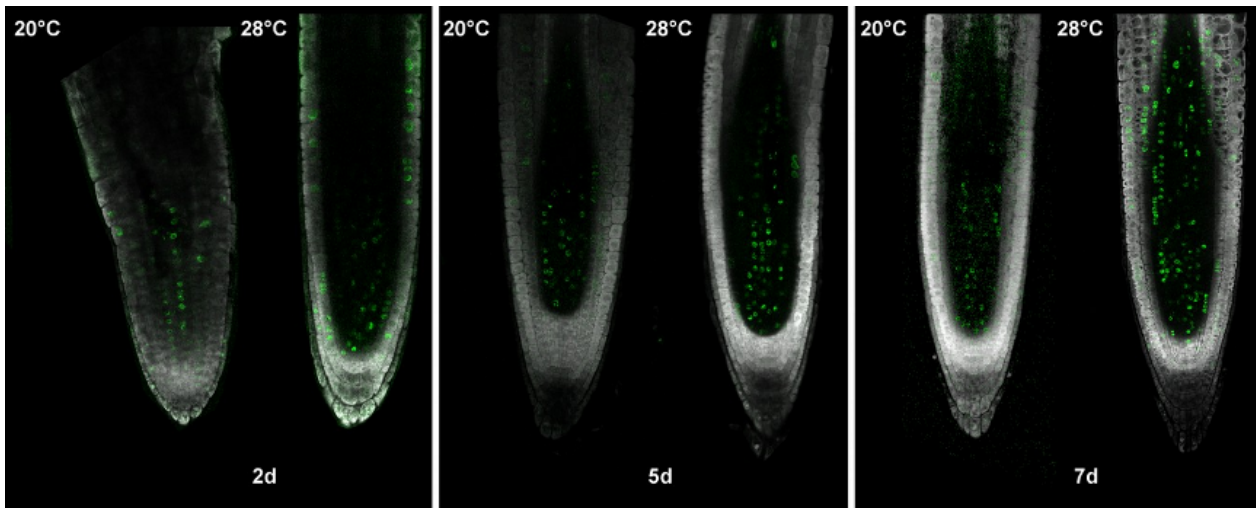
B
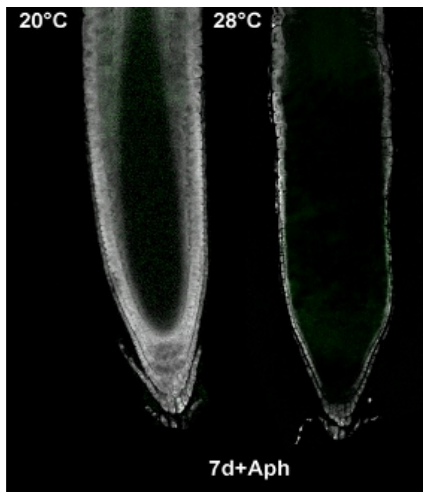
C
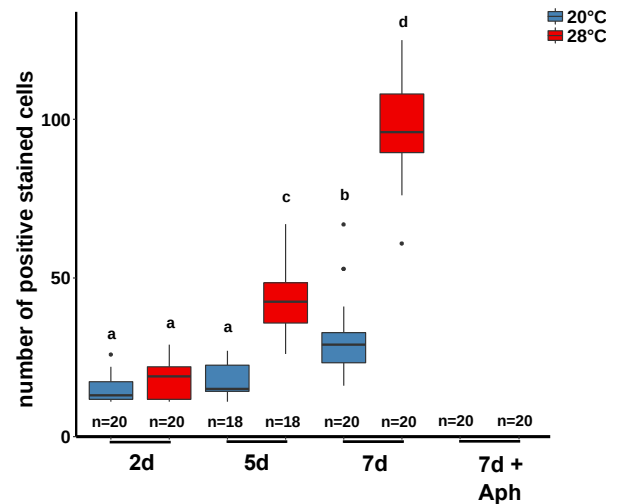
Figure 21. Elevated temperature stimulates cell divison events. A, B, C temperature-induced cell division activity after 2, 5, 7d in roots of wild-type seedlings at 20°C or 28°C, stained with 5-ethynyl-2′-deoxyuridine (EdU) and with propidium iodide (PI) after fixation. Negative control of cell division by additionally adding aphidicolin (Aph). Root apical meristems (RAM) were determined via Laser scanning microscopy and ImageJ. **A** Representative pictures of the EdU-stained RAMs at three time points at 20°c and 28°C and **(B)** after adding Aphidicolin. All experiments were performed in LD (16/8 h) conditions under 90 µmol m^{-2}s^{-1} white fluorescent light. **C** Box plots show medians and interquartile ranges of total organ lengths; outliers (greater than 1.52 interquartile range) are shown as black dots. Different letters denote statistical differences at $p < 0.05$ as assessed by one-way ANOVA and Tukey's honestly significant difference (HSD) posthoc test.

~3h

~1h

M-phase
(Cell division)

G₁-phase
(Growth)

G₂-phase
(Growth and preparation for mitosis)

~6h

S-phase
(DNA synthesis)

~8h

Figure 22. Schematic representation of the stages in the cell cycle in the Arabidopsis root cell with the corresponding biological functions. Time-lapse imaging of epidermal cells under standard conditions in the root meristem of Arabidopsis plants revealed that a typical rapidly proliferating plant cell with a total cycle time, the G1 phase might last about 6 h, S-phase to late G2-phase or early M-phase about 8 h, and M about 3 h (modified from Aki et al., 2016).

I observed that the number of RFP-positive cells in root apical meristems (RAMs) of roots cultivated at 28°C was significantly increased already 30 min after ZT0 compared to the cells in RAMs of roots grown at 20°C. This observation might indicate that elevated temperature affect the timing of entry into the S-phase. (See Figure 23A,C). However, after 3 h, the red fluorescent signal in the cells of RAMs of 28°C plants gradually disappeared, while the signal in RAMs can be measured significantly longer in 20°C plants. These data suggest that elevated temperature stimulates an earlier entry of RAM cells in the S-phase cell cycle and an earlier exit from this cell cycle stage.

However, consistent with the earlier exit of S-phase cells at 28°C, the number of cells with green G2/M fluorescent expression was significantly increased after 1h compared to the RAMs of roots grown at 20°C, suggesting an earlier entry into the G2/M-phase (See Figure 23B,D). Approximately up to 7 cells more were in the G2/M-phase at 28°C compared to 20°C at ZT0 (Zeitgeber Time,1 hour after lights on). At ZT2 (1.30h after dawn) and ZT3 (3h after dawn) at 28°C, the average number of cells with green fluorescence signal remained at the same level as ZT0 at 28°C.

In contrast, the number of green cells in the RAM of plants cultivated at 20°C increased strongly from ZT1 to ZT3 and then remained roughly the same at ZT6 (6h after dawn) as ZT3. This observation contradicts a bit with the results from cell analysis (Figure 21), which indicates a higher cell division rate at elevated temperatures. One explanation for these results could be that the cells in the MZ of plants grown at 28°C might finish mitosis earlier than cells at 20°C and push the cells into the next root zone. Alternatively, it is also

possible that the time point where the number of cells in the G2/M-phase at 28°C reached the maximum was located between ZT1 and ZT2.

Taken together, temperature-induced root elongation might likely be due to earlier entry into and faster exit from both the S-phase of the cell cycle ,as well as the cell division phase (M-phase). Based on these results, it is most likely that temperature-induced root elongation is caused by a shortening of the cell cycle, which is possibly due to temperature-induced increase of the enzymatic activity (Draeger et al., 2017) However, data also indicated that the S-phase duration shortens and possibly also the length of the G2/M-phase in *A. thaliana* as observed in different species (Tardieu and Granier, 2000). It can be assumed that the acceleration in the S- and G2/M-phase duration can also be seen for the other cell phases, although that has to be shown. In addition to the length of the cell cycle, the initiation time point of the cell cycle during the day seems to also play a role. Based on the results of long-term growth rate experiments and the findings of the cell cycle experiments (especially for the S-phase), it is most likely that elevated temperatures might also affect the clock regulation of the cell cycle during the day. Thus, it can be assumed that the clock-regulated cell cycle will be synchronized with the environmental conditions to preserve its timing function over a range of temperatures, as shown for zebrafish cells (Lahiri et al., 2005). Accordingly, Chen et al. (2019) showed that high temperatures decrease the movement of ELF4 from shoot to root, leading to a faster root clock and potentially a faster cellcycle in meristematic cells.

4.2.4. Regulation of temperature-mediated growth promotion

4.2.4.1 Role of known thermo-sensitive regulators during temperature responses in the root

As described in Figure 3, the warm-temperature response is regulated in a phyB-dependent manner in hypocotyls. Increases in ambient temperature promote phyB's Pfr to Pr dark/thermal reversion that releases the inhibitory function of phyB in hypocotyl elongation. phyB, in turn, operates via the key transcriptional regulator PIF4. Temperature-induced inactivation of phyB allows PIF4 accumulation (Koini et al., 2009, Stavang et al., 2009). The COP1-SPA complex regulates PIF4 activity via its negative regulators HY5 and ELF3 (Park et al., 2017, Delker et al., 2014, (Koini et al., 2009, Kumar et al., 2012, Franklin et al., 2014). To determine whether root responses to elevated temperature involve the same machinery as in the hypocotyls, I next investigated

the primary root length of mutants, which have defects in genes involved in shoot temperature responses.

elf3 and *hy5* mutants*,* as well as *35:PIF4* overexpression lines, for example, exhibit enhanced shoot growth at elevated temperatures. However, these mutants showed only weak alterations in root responses to elevated temperatures (Figure 24A,B).
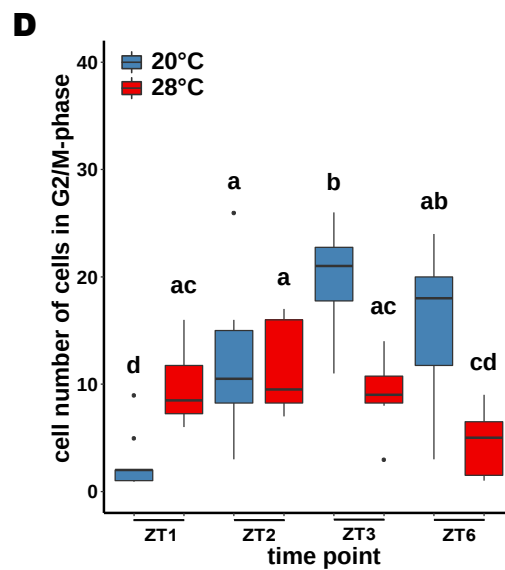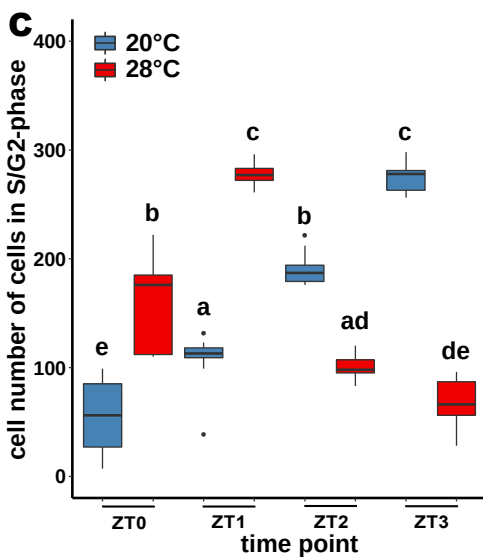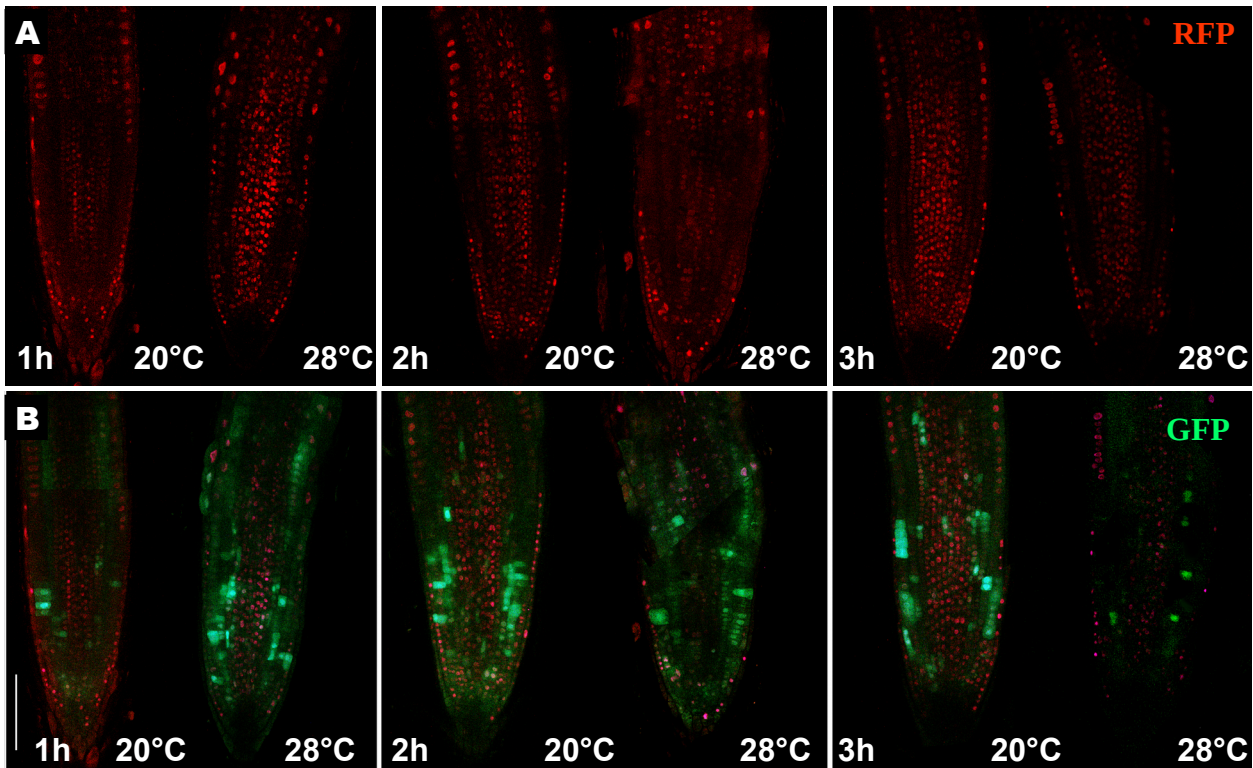
Figure 23. Temperature effects on the cell cycle phases in the meristematic zone. A-C Time series analyses of cell cycle progression in the MZ of *Arabidopsis thaliana* roots using the dual-color marker system "Cytrap." Cells in the RAM of 7d-old seedlings cultivated at constant temperatures (20°C/28°C) were observed at ZT0 (1h after dawn), ZT1 (1.30h)

Figure 23 (Continued). after lights on), ZT2 (2h after dawn), ZT3 (3h after dawn) and ZT6. Representative pictures are shown in **(A-B)**. *pHTR2:CDT1a (C3)–RFP* (RFP) and *pCYCB1:CYCB1-GFP* (GFP) that label *cells* in S/G2- **(C)** and G2/M- **(D)** phase were identified and seperately countred. All Experiments were performed in LD (16/8h) conditions under 90 µmol m^{-2} s^{-1} white fluorescent light. Box plots show medians and interquartile ranges, outliers (greater than 1.52 interquartile range) are shown as black dots. Different letters denote statistical differences at $p < 0.05$ as assessed by one-way ANOVA and Tukey's honestly significant difference (HSD) posthoc test.

Even *pifQ* roots respond similarly to the wild-type to warmth (Figure 24A,B). Likewise, *phyABCDE* thermosensory mutants, which display a constitutive warm temperature response in the hypocotyls (Legris et al., 2016), showed no apparent defects in temperature response in the root (Figure 24C,D). Vice versa, the a constitutively active *phyB* mutant (*YHB*) (Legris et al., 2016) had no impact on the temperature-induced root elongation (Figure 24C,D). Altogether, these data suggest that TIRE is regulated by signaling mechanisms different from what has been described for hypocotyls.

4.2.4.2 Pharmacological inhibition of JA, ET, Auxin and BR action can reduce temperature-induced root growth

Phytohormones are important regulators of root growth and development in general. Previous studies of *A. thaliana* roots have shown that different hormones, such as auxin, cytokinin (CK), abscisic acid (ABA), brassinosteroids (BR), ethylene (ET), gibberellic acid (GA), and jasmonates (JA) control organ growth by regulating specific growth processes such as cell proliferation, differentiation, or expansion in different tissues (Ubeda-Tomás et al. 2012). In order to understand which of these main hormones regulate root growth at elevated temperatures, a pharmacological approach was chosen by either adding exogenous biosynthesis inhibitors (if available) to growth media or adding hormones of different concentrations to growth media in TIRE assays. In the context of this work, pharmacological inhibition of JA biosynthesis during temperature-induced root growth could not be investigated at this point. To determine any involvement of JA in temperature-induced root elongation, further research is needed. However, ABA and GA biosynthesis inhibitors (paclobutrazol and fluridone, respectively) showed only mild effects, lovostatin (CK inhibitor), silvernitrate (ET inhibitor), propiconazole (BR inhibitor) and a combination of L-kynurenin and yuccasin (auxin inhibitor) had severe effects on root growth, especially at 28°C (Figure 25A-B). This probably suggests that the de novo synthesis of GA and ABA under my conditions play a minor role in root responses to elevated temperatures. In contrast,

Prerostova et al. (2020) showed that in *A. thaliana* roots, the ABA content decreased in the case of heat stress.

Transcriptome analysis of Fei et al. (2019) revealed an upregulation of gibberellin biosynthesis genes (GA3OX2, GA2OX1, and GA2OX4) and a downregulation of genes encoding DELLA proteins (RGL3 and RGA) in roots of plants grown at elevated temperature. In this regard, the results of Camut et al. (2019) implicate that root- synthesised GAs could be used as an available source for shoot thermomorphogenesis response. However, whether and what role these hormones might play in root temperature responses have to be seen. Nevertheless, based on my results, I focused on investigating of auxin, ET, BR, CK.

In contrast to he GA and ABA inhibitors tested, a rapid decrease in root elongation of wild-type seedlings at 28°C was observed after the application of the selected auxin, ET, BR, CK biosynthesis inhibitors (Figure 25C-F), especially at low concentrations. Thus, there might be a connection between auxin, ET, BR, Ck and root development at elevated temperatures. However, the auxin, ET, BR, CK inhibitors do also drastically affect root growth at 20°C. Therefore, It is difficult to distinguish between pleiotropic effects of the inhibition and changes caused by temperature increases. In this regard, my data must viewed with caution and thus will be further examined using a complementary mutant-based reverse genetics approach.

4.2.4.3 Low concentration of auxin and BR promote temperature induced root growth

Davies et al. (2007) have shown that auxin and BR positively affect *A. thaliana* root growth under optimum temperature conditions (20°C+/-2). In contrast, both low and high concentrations of ethylene (ET) (Qin et al., 2019, Abts et al., 2017), cytokinin (CK) (Laplaze et al., 2007), and jasmonate (JA) (Kamińska et al., 2018) treatments inhibit primary root growth (Müssig et al., 2003). Hence, I next investigated whether TIRE can be increased by adding low doses of biologically active indole-3-acetic acid (IAA) and/or a synthetic BR epi-brassinolide (epi-BL). While Belkhadir et al. (2010) and Sun et al. (2010) showed that root growth of wild-type plants increased in response to treatments with low concentrations of epi-BL (0.05nM) or IAA (0.01nM) at standard conditions (16 hr of light and 8 hr 22°C/ 20°–24°C continuous light), no considerable changes in root elongation were observed under our conditions at 20°C combined with or without pharmacological treatments. However, the root lengths increased significantly at 28°C when 0.01nM IAA

(Figure 26A-C) or 0.05nM epi-BL (Figure 26D-F) was included in the growth medium, whereby the effect of the hormones on root growth was considerably weaker when compared to the hypocotyl (Ibañez et al. 2018). In contrast, concentrations above 0.01nM IAA or 0.05nM epi-BL had a root growth inhibitory effectin *A. thaliana* independent of temperature treatments. These observations suggest that temperature mediated increase in root elongation can be further boosted by adding of exogenous BR and/or auxin. Nevertheless, it must be noted that a promoting effect was observed only for low (physiological) levels of exogenously added hormones (Figure 26A-F). Overall, it seems that auxin and BR might be involved in the temperature responses in the root.
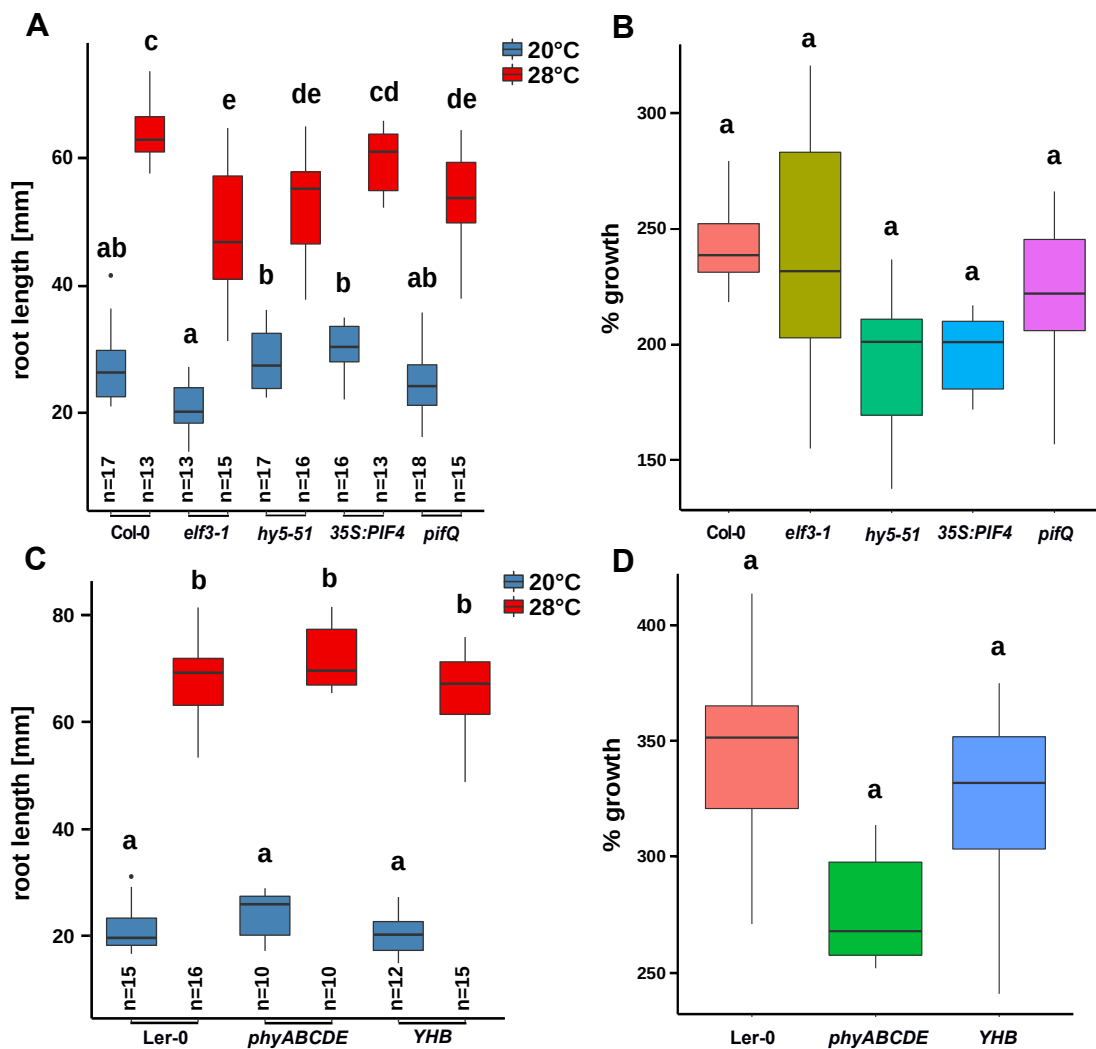
Figure 24. Temperature induced root response of different thermomorphogenesis and photomorphogenesis mutants. A Box plots show relative (28°C/20°C in %, **B,D**) or absolute (**A,C**) root length of thermomorphogenesis mutants *elf3-1, hy5-51, 35S:PIF4, pifQ* (**A,B**) and photomorphogenesis mutants *phyABCDE, YHB* (**C,D**). All seedlings were grown for 7d. in LD (16/8 h) conditions under 90 µmol m^{-2} s^{-1} white fluorescent light. **A,B** Box plots show medians and interquartile ranges, outliers (greater than 1.52 interquartile range) are shown as black dots. Different letters denote statistical differences at *p*< 0.05 as assessed by one-way ANOVA and Tukey's honestly significant difference (HSD) posthoc test. **B,D**

63
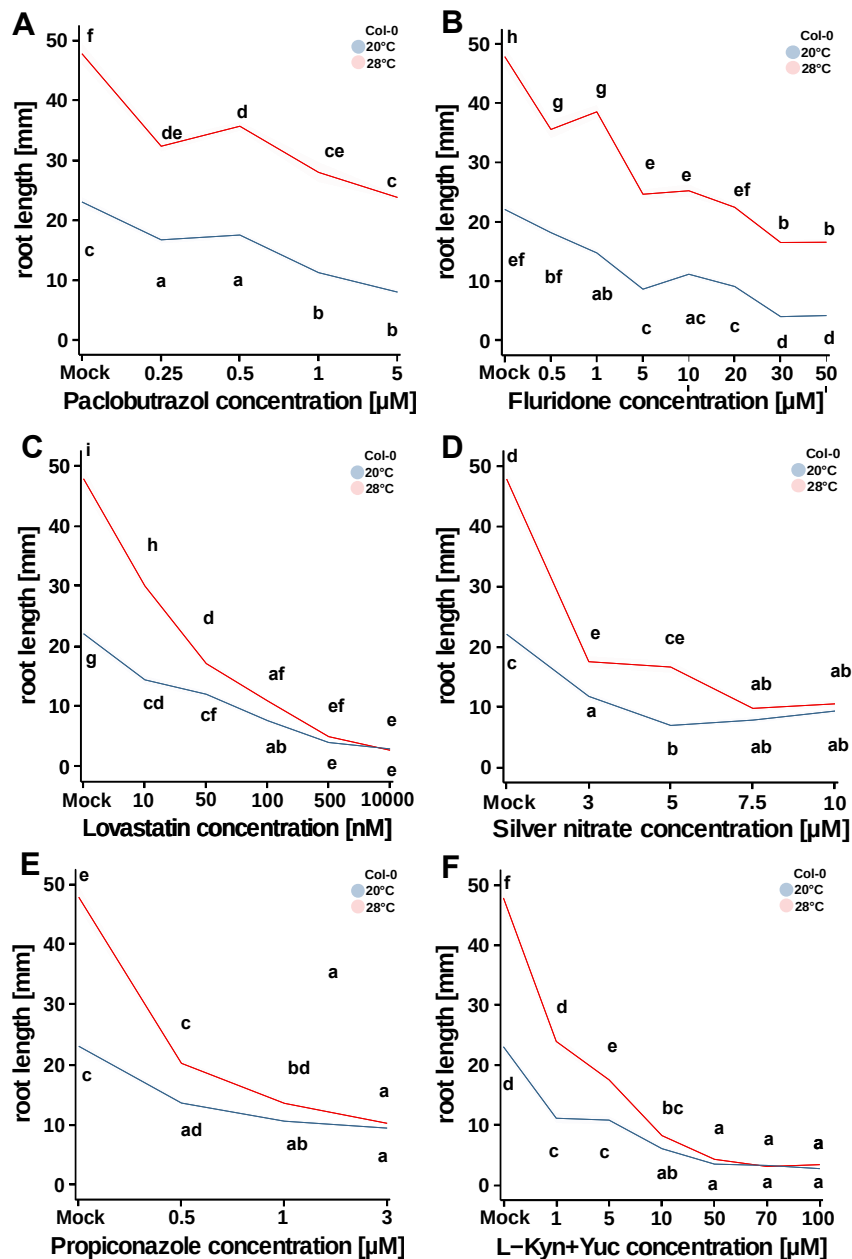
Figure 25. Effects of specific hormone inhibitors on temperature induced root growth. **A-F** root length of 7d-old Col-0 plants grown at 20 or 28 °C treated with different concentrations of (**A**) Gibberellin (GA) biosynthesis inhibitors Paclobutrazol, (**B**) Abscisic acid biosynthesis inhibitor Fluridone, **(C)** Cytokinin biosynthesis inhibitor Lovastatin, **(D)** Ethylene biosynthesis inhibitor Silver nitrate, (E) Brassinosteroid biosynthesis inhibitor Propiconazole, **(F)** Auxin biosynthesis inhibitor L-kynurenine combined with Yucasin. All Experiments were performed in LD (16/8 h) conditions under 90 µmol m^{-2}s^{-1} white fluorescent light. Bold lines in ribbon plots show means of root length under different hormone inhibitor concentrations. The shadowed ribbon denotes the SE. Different letters denote statistical differences at $p < 0.05$ as assessed by one-way ANOVA and Tukey's honestly significant difference (HSD) posthoc test. n> 20.
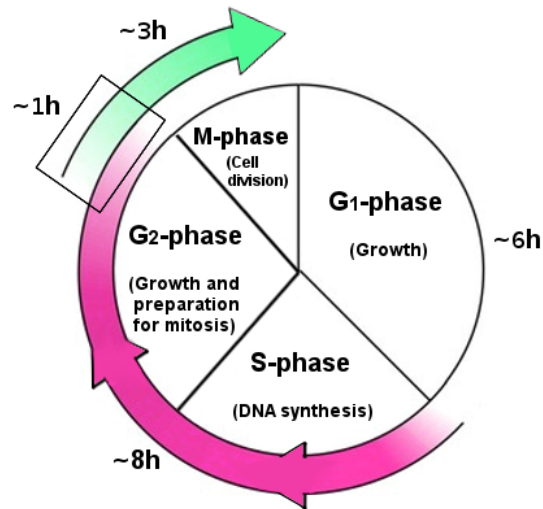
4.2.5 Impact of auxin and BR-related mutations on temperature induced root growth

In addition to verifying the results of the pharmacological experiments presented so far, implying that auxin, cytokinin (CK), brassinosteroids (BR), ethylene (ET) have a certain impact on root growth at elevated temperatures, I used a mutant-based reverse genetic approach. I screened different hormone mutants defective in biosynthesis and/or signaling for abnormal temperature responses in root elongation. For most of these chosen BR (Figure S9C,D) and auxin mutants (Figure S9A,B) a temperature-responsive hypocotyl phenotype had previously been described (Ibanez et al., 2017). This leads to the question of whether similar genes could regulate temperature-induced root responses. The following assays were performed under the same conditions as in the other TIRE assays. Although some ET- and JA-deficient mutants were also significantly reduced at elevated temperatures compared to the wild-type (Data for other hormone mutants are appended in Figure S9), I focused on investigating the role of auxin and BR in root thermomorphogenesis. The results will be presented and discussed in the following. However, It cannot be excluded that JA and ET might also be involved in parts of root thermomorphogenesis signaling pathways.

4.2.6 BR seems to play a minor role in root thermomorphogenesis

Investigating the impact of BR on root growth in *A. thaliana* seedlings under elevated temperatures, the root elongation of different BR biosynthesis, and BR signaling mutants were analysed in further temperature assays (Figure 27). If temperature-induced root elongation is affected by BR, root length of *bri1 (BRASSINOSTEROID INSENSITIVE1)* BR receptor mutant should be significantly different from wild-type at warmth. However, this could not be observed (Figure 28A-C). Although the roots of *bri1*-mutant were significantly reduced at 20°C, as previously reported (Noguchi et al., 1999, Gou et al., 2012, Sun et al., 2017), the relative temperature response behaved similarly to that of wild-type roots. This observation rather indicates that warmth interferes with primary root growth independent of BRI1-dependant signaling, which contradicted the assumptions of Martins et al. (2017). Since the two BRI1 homologs, BRI1-like 1 and 3, play partially redundant roles with BRI1 (Cano-Delgado et al. 2004, Wei et al. 2008), BR-dependent regulation in the root may be activated by other BR receptors such as BRL1 and BRL3 at elevated temperature . If temperature-induced root elongation is modulated by functional BR signaling, downstream BR signaling mutants should show defective temperature-induced root elongation. Therefore, I tested other BR-signaling mutants,

including mutants of BR signaling kinases and phosphatases (See Figure 27) and transgenic lines, in which one of the key transcription factors of the BR signaling pathway, BZR1 or BES1, was constitutively active.
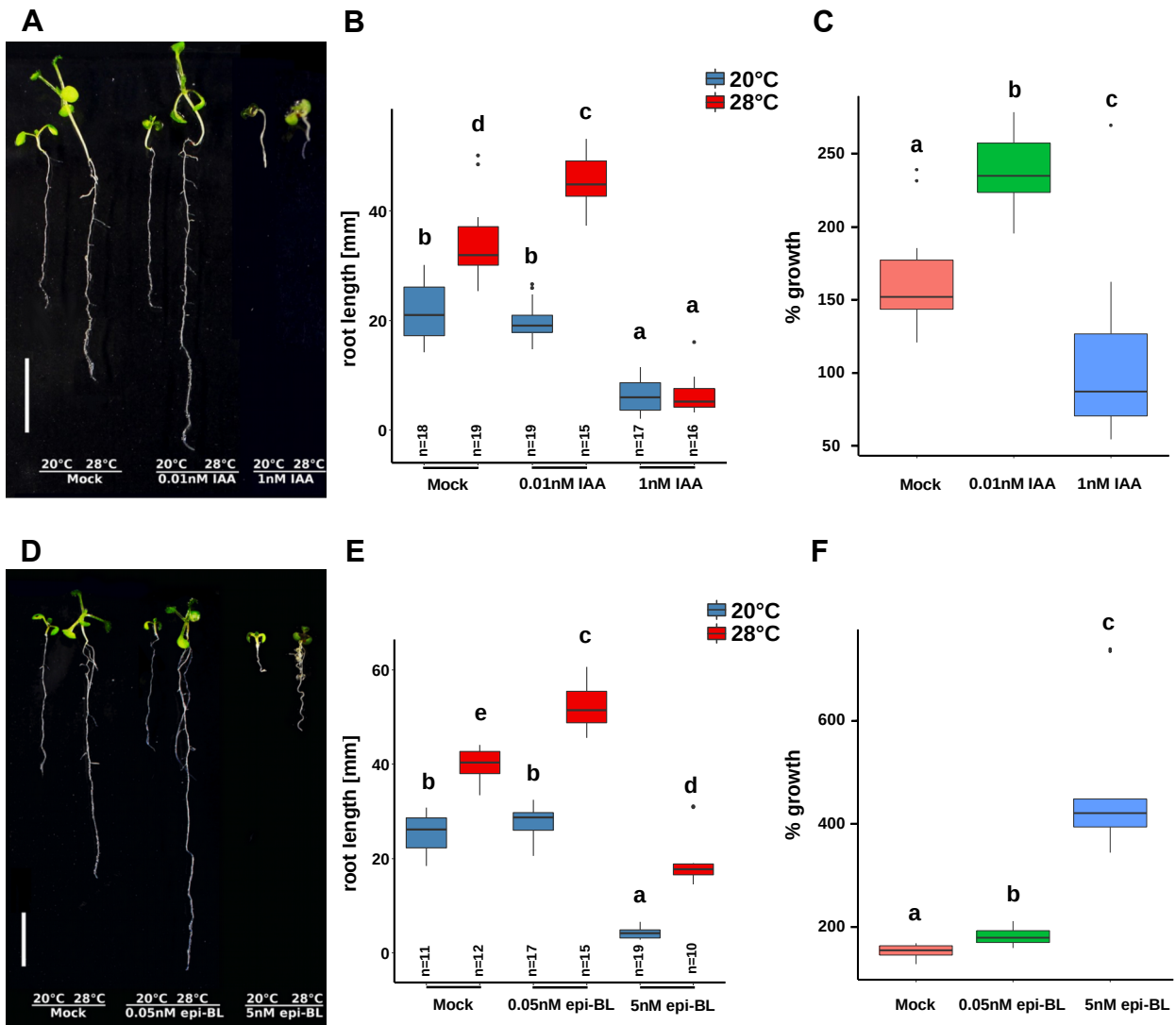
Figure 26. Effects of specific hormones on temperature induced root growth. **A,D** Representative pictures of plants from corresponding TIRE-assays. Scale bars: 10mm. (Figure **B, E**) Box plots show relative (28°C/20°C in %; **C,F**) or absolute (**B,E**) root length o 7d-old Col-0 seedlings grown at 20°C or 28 °C treated with low or high concentrations of IAA (**A-C**) or epi-BL (**D-F**) or without treatment (Mock). All Experiments were performed in LD (16/8 h) conditions under 90 µmol m^{-2} s^{-1} white fluorescent light. **A-C** Agar plates were additionally covered with yellow plastic plates. Box plots show medians and interquartile ranges; outliers (greater than 1.53 interquartile range) are shown as black dots. B,E Different letters denote statistical differences at $p < 0.05$ as assessed by one-way ANOVA and Tukey's honestly significant difference (HSD) posthoc test. **C,F** Statistical differences were assessed by two-way ANOVA ($p < 0.05$) of the absolute data presented in Figure **B,E**. Different letters denote significant differences among all samples.

Although some of these signaling mutants tested (*bsu1-1*, *bsu1 bsl1*, *bsuq*) displayed reduced root growth in the presence of elevated temperatures, the defects were less severe than in hypocotyls (See Figure 28, Figure S9). All mutants affected in BR signaling still were able to respond to temperature stimulus. Equally, the constitutive activation of BR responses in *bes1-D* and *bzr1-1D-Ox* does not show substantial effects on TIRE response compared to the wild-type (Figure 28D-F, S10), as well as the *bes1-1* knockout mutant (Figure S10). These data indicate that the BR signaling pathway where BZR1 acts downstream of BRI1 might be not sufficient for temperature mediated root responses. Nevertheless, the significant decrease in absolute root length at 20°C and 28°C of *bes1-D*, clearly shows that a fully functional BR signaling is necessary for general root growth, as described in the literature (Chaiwanon and Wang, 2015, González-García et al., 2011, Hacham et al., 2011, Mussig et al., 2003). Additional components might be required to enhance root growth responses to temperature. Recent work claimed that BR signaling negatively regulates root responses to temperature elevation (Martins et al., 2017). This suggestion was not confirmed by my results. On the contrary, BR positively regulated TIRE (Figure 28E-F).
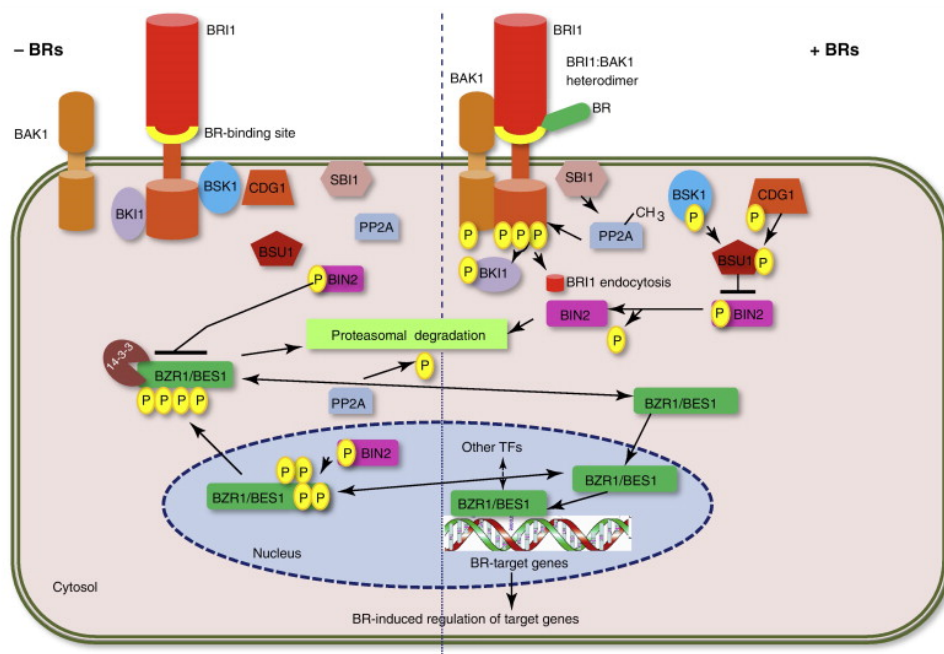
Figure 27. Model of brassinosteroid signaling pathway. In the absence of BR, BRI1 KINASE INHIBITOR 1 (BKI1) suppresses the receptor kinase BRI1, and the BRASSINOSTEROID INSENSITIVE 2 (BIN2), which is a GSK3-like kinase, phosphorylates BZR1/BES1 proteins and inactivates them (left side). Upon brassinosteroid (BR) binding, BKI is dissociated from the intracellular kinase domain of BRI1 (Wang and Chory 2006), and BRI1 forms a heterodimeric complex with BRASSINOSTEROID INSENSITIVE 1-ASSOCIATED RECEPTOR KINASE 1 (BAK1) to autophosphorylate and sequentially trans-phosphorylate each other, leading to full activation of the receptor complex (Wang et al., 2008, Bojar et al., 2014, Oh et al., 2009). To transduce the extracellular signal to the downstream components, the activated BRI1 receptor complex phosphorylates several receptor-like cytoplasmic kinases, including the BRI1 SUBSTRATE KINASEs (BSKs), BSKs then activate the nucleocytoplasmic phosphatase called BRI1 SUPPRESSOR 1/BSU1-LIKE (BSU1/BSL) by phosphorylating the

Figure 27 (Contined). latter (Tang et al., 2008, Kim et al., 2009, 2011) Phosphorylated BSU1/BSL, in turn, dephosphorylates the negative regulator BRASSINOSTEROID-INSENSITIVE 2 (BIN2), a cytoplasmic glycogen synthase kinase-3 (GSK3)-like kinase, inactivates its kinase activity and directs the BIN2 protein to the subsequent degradation in a proteasome-dependent manner (Li et al., 2001, 2002, Kim et al., 2009, Tang et al., 2011). Inactivation of BIN2,allows the dephosphorylation of the downstream plant-specific transcription factors BRASSINAZOLERESISTANT 1 (BZR1) and BRI1-EMS-SUPPRESSOR 1 (BES1), which are released from cytosolicretention by 14-3-3 phosphopeptide-binding proteins and can therefore translocate to the nucleus to regulate BR-responsive transcriptional program (Wang et al., 2002, Yin et al., 2002, 2005, He et al., 2005, Gampala et al., 2007, Tang et al., 2011). (Sikander Pal Choudhary et al., 2012).

Since the results of the pharmacological experiments showed that a low concentration of epi-BL has a stimulating effect on TIRE response, I also investigated root elongation of different biosynthesis mutants at warm conditions. The BR-deficient *cpd* and *dwf4-102* mutants (Figure 29), carrying loss-of-function mutations in the *CONSTITUTIVE PHOTOMORPHOGENESIS AND DWARFISM (CPD)* and *DWARF4 (DWF4)* genes, respectively. Both mutant lines displayed wild-type temperature-mediated root elongation (Figure 29A-C), similar to the observations of Martins et al. (2018). These findings indicate that warm conditions interfere with root growth independently of BR biosynthesis, which would contradict the root measurements of the pharmacological experiments. One explanation for this discrepancy in data may be due to the non-physiological distribution of exogenously applied hormone epi-BL. Under the given experimental setup, plants were grown on the surface of ATS agar plates containing different concentrations of hormones or inhibitors. Thus, each part of the root was equally affected by the synthetic stimulator epi-BL and elicitation of an "artificial" response, which does even less reflect the natural (in vivo) mechanism of action. Alternatively, other possible as yet unknown components of BR biosynthesis may be more prominently involved. Especially in this regard, further analysis will be necessary.

In general, gene-based approaches are more precise (Guan, 2012) than pharmacological approaches. Thus, my conclusion relies in particular on the results of the TIRE assays with BR biosynthesis and signaling mutants. Hormonal pathways are interconnected by a complex network of interactions and feedback circuits that determines the outcome of the individual hormone and cannot be considered separately via single gene mutation. Nevertheless, the results of these experiments could be important indicators for future research.
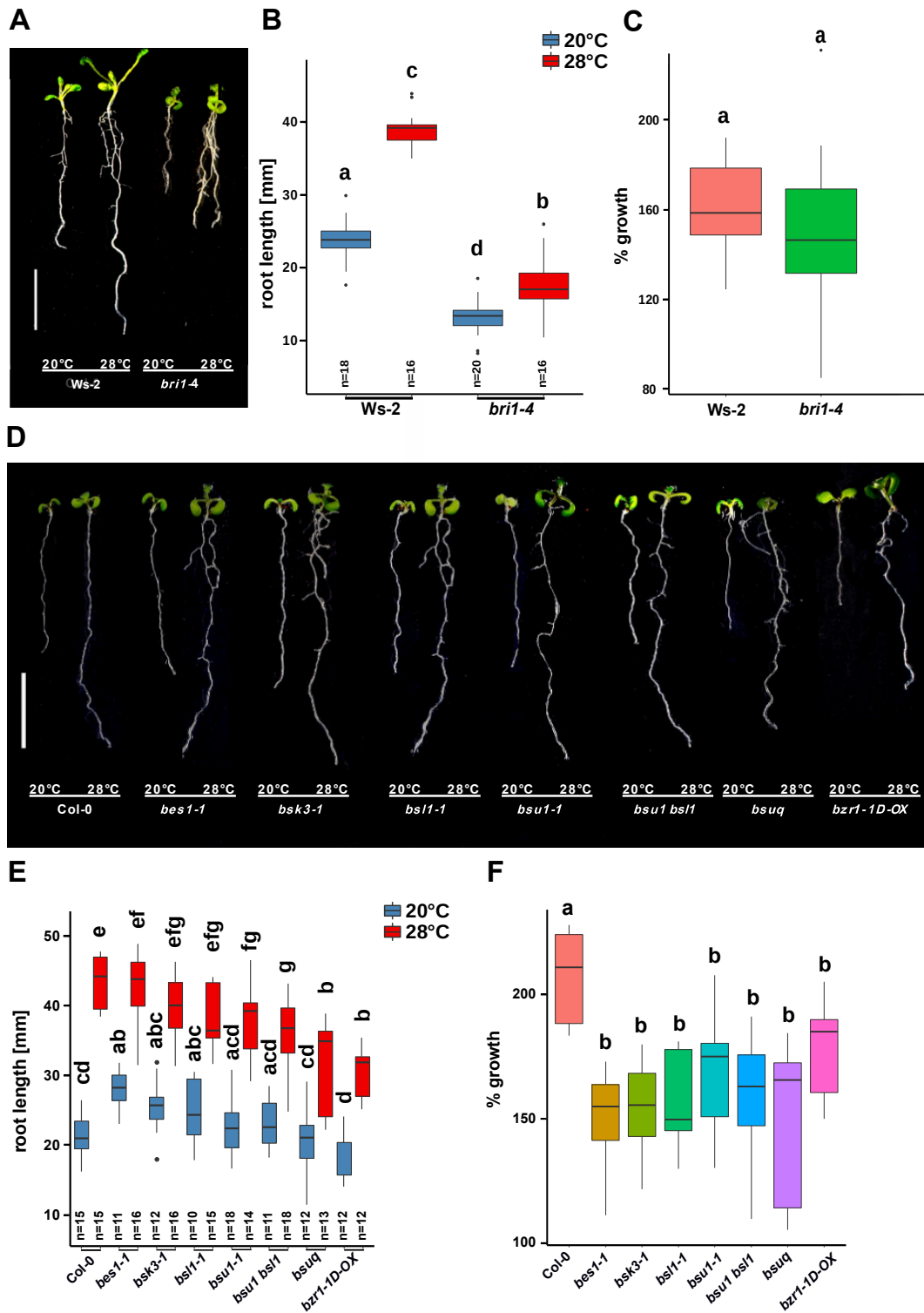
Figure 28. Impact of BR signaling genes on the temperature induced root growth. **A,D** Representative pictures of plants from corresponding TIRE assays (**B,E**). Scale bars: 10mm. **A-F** Box plots show relative (28°C/20°C in %, C,**F**) or absolute (**B,E**) root length of 7d-old wild-type plants (Col-0, Ws-2) and BR mutants (*bri1-4, bes1-1, bsk3-1, bsl1-1, bsu1-1, bsu1,bsl1, bsuq, bzr1-1D-OX)* grown at 20°C or 28 °C under LD (16/8 h) and 90 μmol m^{-2} s^{-1} white fluorescent light. **B,C,E,F** Box plots show medians and interquartile ranges, outliers (greater than 1.52 interquartile range) are shown as black dots. **B,E** Different letters denote statistical differences at *p*< 0.05 as assessed by one-way ANOVA and Tukey's honestly significant difference (HSD) posthoc test. **C,F** Statistical differences were assessed by two-way ANOVA (*p*< 0.05) of the absolute data presented in Figure B,E. Different letters denote significant differences among all samples.

In summary, data revealed a general involvement of BR signaling in regulating primary root elongation independent of temperatures, as described previously (Müssig et al., 2003, Wei et al., 2016, Vukasinovic et al., 2020). But specifically for genetic analysis of BR mutants, it can be supposed that BR signaling and biosynthesis are of minor importance for regulating temperature-induced root elongation.
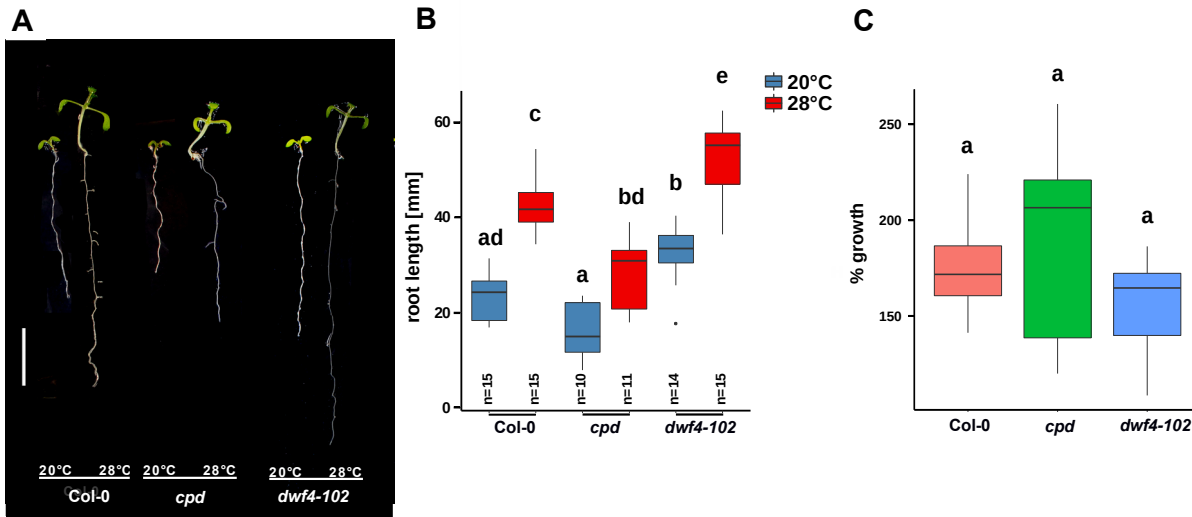
Figure 29. Impact of BR biosynthesis genes on the temperature induced root growth. **A** Representative picture of plants from corresponding TIRE assay (**B**) Scale bars: 10mm.. Box plots show relative (28°C/20°C in %) (**C**) or absolute (**B**) root length of 7d-old wild-type plants and BR biosynthesis mutants *cpd, dwf4-102* grown at 20°C or 28 °C under LD (16/8 h)and 90 μmol m^{-2} s^{-1} white fluorescent light. Agar plates were additionally covered with yellow plastic plates. **B,C** Box plots show medians and interquartile ranges; outliers (greater than 1.52 interquartile range) are shown as black dots. **B** Different letters denote statistical differences at *p*< 0.05 as assessed by one-way ANOVA and Tukey's honestly significant difference (HSD) posthoc test. **C** Statistical differences were assessed by two-way ANOVA (*p*< 0.05) of the absolute data presented in Figure **B** (left) Different letters denote significant differences among all samples.

4.2.7 Auxin biosynthesis, signaling and transport are required for the temperature-induced root growth

The endogenous auxin indole-3-acetic acid (IAA) is another major plant growth regulator (Davies et al., 2010), which is important for response to elevated temperatures in the aerial parts of the plant (Gray et al., 1998, Franklin et al., 2011, Sun et al., 2012). However, the underlying hormone-based mechanisms in the root are controversially discussed. While several studies suggest that elevated temperatures also affect root growth in an auxin-dependent manner (Hanzawa et al., 2013, Wang et al., 2016, Fei et al., 2017), the experiments of Martins et al. (2018) showed the opposite. For that reason and the results of my pharmacological experiments, indicating that low concentrations of IAA can stimulate temperature responses in the root (Figure 26), I

investigated TIRE effects of different auxin biosynthesis and signaling mutants at elevated temperatures under the conditions described above. However, the selected auxin mutants (Figure 31) responded under our conditions quite different to temperature stimuli. Although the absolute root length of the auxin signaling mutant tir1-1 afb2-3, which lacks two of the six auxin co-receptor F-box proteins, is generally highly reduced at 20°C as well as 28°C, the relative temperature response was similar to wild-type plants (Figure 31A). Based on this observation, I can conclude that auxin perception through the TIR1/AFBs pathway might play a minor role in root thermomorphogenesis, reinforcing the idea of a TIR1/AFB-independent auxin signaling pathway.
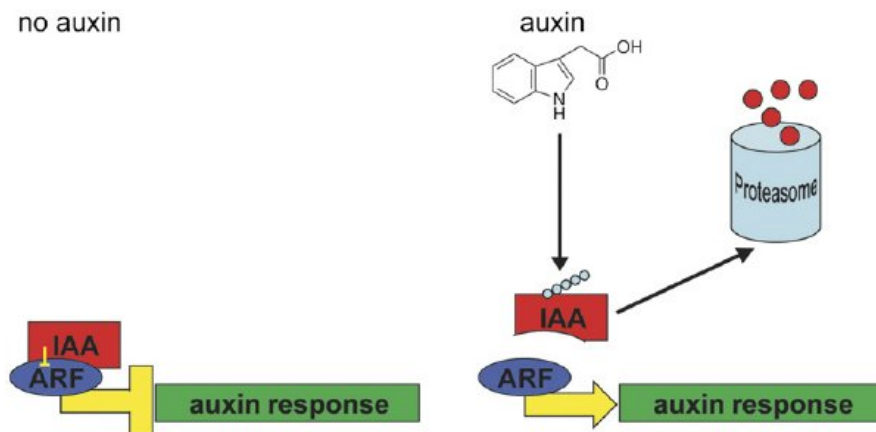
Figure 30. The ARF-Aux/IAA auxin response pathway. In the absence of auxin (left side), Aux/IAAs repress the activity of ARF transcription factors which activating the auxin-responsive genes.In the presence of auxin, the Aux/IAA repressors are targeted for ubiquitin-dependent proteasomal degradation by the SCF (Skp1-Cul1-Rbx1-Fbox protein) E3 ubiquitin ligase. The auxin-dependent degradation of the Aux/IAAs relieves inhibition of ARF activity and results in expression of auxin-responsive genes. As these genes also include the Aux/IAA-encoding genes, this mechanism provides a negative feedback loop for control of auxin signaling (Mockaitis,2008, Hayashi,2012). (Bargmann et al. 2009)

On the other hand, it is possible that other AFBs, besides TIR1 and AFB2, influence temperature promoted auxin-mediated root elongation. But since mutants that are entirely incapable of perceiving auxin are lethal, it is challenging toevaluate the role of challenging to evaluate the role of auxin in root responses to warmth. Moreover, higher-order auxin receptor mutants, such as *tir1-1 afb2-3 afb3-4* (Figure S11) displayed pleiotropic defects, which lead to inconclusive results In general, the *AUX/IAAs* are transcriptional repressors that, in the absence of auxin, bind and repress *AUXIN RESPONSE FACTORs (ARFs)*, transcription factors located on the promotors of auxin response genes (See Figure 30). In this context, investigation of *aux/iaa* mutants is a reasonable choice because the degron motif in these mutants is mutated, which affects the interaction between TIR1/AFBs and AUX/IAAs and prevents AUX/IAAs from degradation, resulting in a quasi-constitutive inhibition of auxin response. If auxin signaling is important in temperature response in the root, at least some of these *AUX/IAA (AUXIN/INDOLE-3-ACETIC ACID)* mutants should

display root growth defects at elevated temperatures in TIRE assays. Indeed, in contrast to *tir1-1 afb2-3, t*emperature-induced root response was decreased in the gain-of-function *AUX/IAA* mutants axr5-1/iaa1, *msg2-1/iaa19* and *slr1-1/iaa14.* These genes are involved in lateral root formation (Muto et al., 2007). However, primary root elongation seems to be also affected at elevated temperatures. The root length of all mutants was significantly reduced at 28°C compared to the wild-type (Figure 31D-F). This, in turn, suggests that temperature-induced root elongation might depend on a normally functioning auxin signaling pathway and is therefore consistent with the pharmacological data (Figure 25). Why loss-of-function mutations and gain-of-function mutation did not respond oppositely could not be conclusively clarified. Since the pharmacological results described above indicate activation of auxin biosynthesis in the root during temperature treatments, I additionally investigated the primary root growth of different auxin biosynthesis mutants such as the loss-of-function mutants *wei8-1 tar1-1/wei8-4*, which display defects in the *TRYPTOPHAN AMINOTRANSFERASE OF ARABIDOPSIS1 (TAA1)* and its close homolog *TRYPTOPHAN AMINOTRANSFERASE RELATED 1 (TAR1)* at 20°C and 28°C. Similarly, I analysed the TIRE of *yucQ* (*YUCCA Quatruple*), in which all five YUCCAs *(YUC3, YUC5, YUC7, YUC8* and *YUC9)* genes have been silenced. These five YUC genes showed distinct expression patterns during root development (Chen et al. 2014). Indeed, Figure 31A-C shows that the *wei8-1 tar1-1* and *yucQ* mutations resulted in a slight decrease in temperature response. But like most other auxin mutant lines described so far, primary root growth was not only affected at high temperature but also at 20°C control conditions. To confirm my observation that high levels of IAA have inhibiting effects on primary root growth at elevated temperatures, I tested also the YUCCA-overexpressing mutant line (*yuc1-D*). This line is distinguished by a high level of free endogenous IAA. Although the root length of the mutant line is reduced at both temperatures related to the wild-type, the relative temperature response of the roots is in deed also decreased (Figure 31A-C)*.*
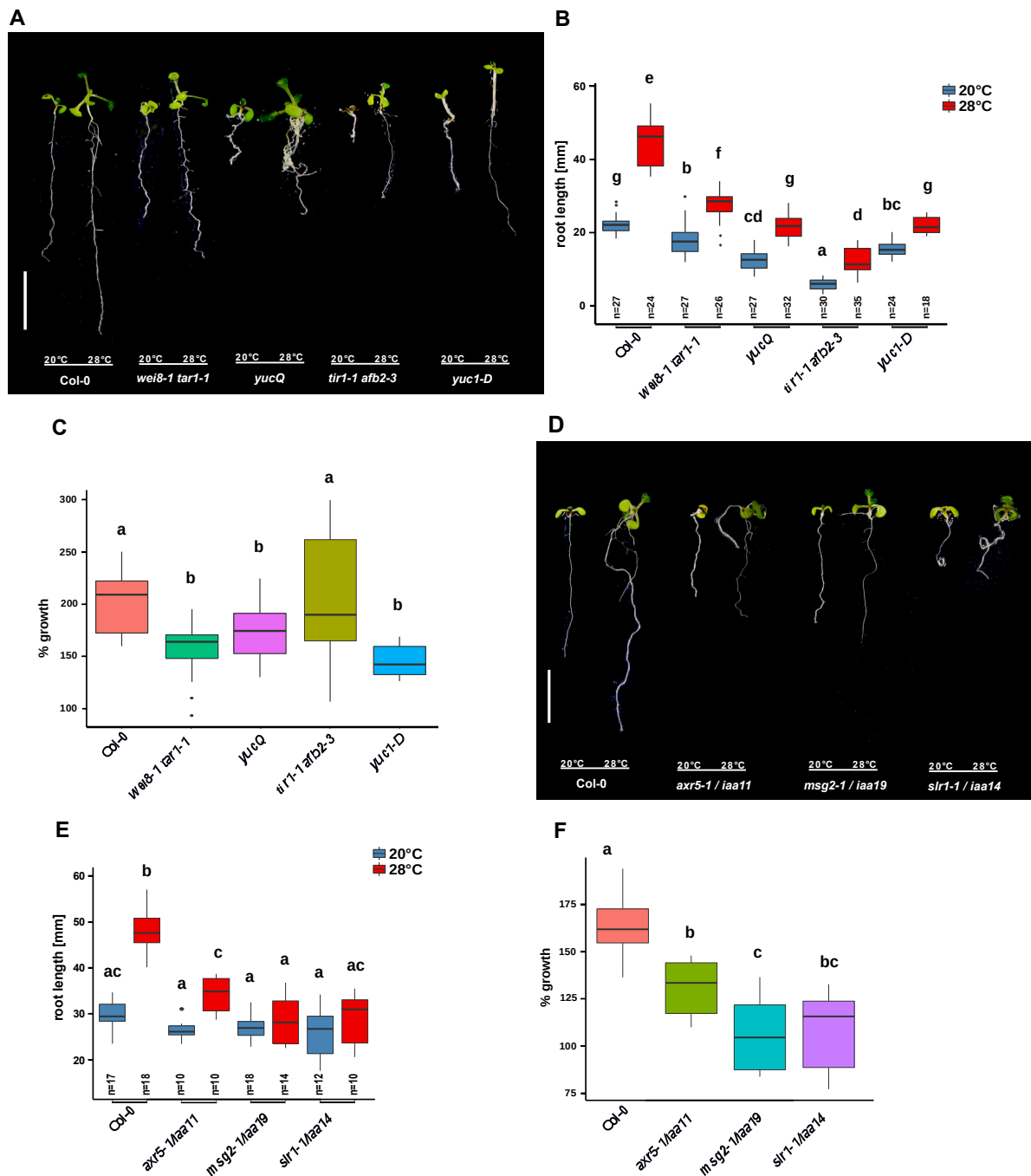
Figure 31. Impact of Auxin related genes on the temperature induced root growth. A,D Representative pictures of plants from corresponding TIRE assays (**B,E**). Scale bars: 10mm. **A-F** Box plots show relative (28°C/20°C in %; C,F) or absolute (**B,E**) root length of 7d-old wild-type plants and auxin related mutants (*wei8-1 tar1-1, yucQ, tir1-1 afb2-3, yuc1-D, axr5-1, msg2-1, slr1-1*) plants grown at 20°C or 28 °C under LD (16/8 h) and 90 μmol m^{-2} s^{-1} white fluorescent light. **B,C,E,F** Box plots show medians and interquartile ranges; outliers (greater than 1.52 interquartile range) are shown as black dots. **B,E** Different letters denote statistical differences at *p*< 0.05 as assessed by one-way ANOVA and Tukey's honestly significant difference (HSD) posthoc test. **C, F** Statistical differences were assessed by two-way ANOVA (*p*< 0.05) of the absolute data presented in Figure B,E. Different letters denote significant differences among all samples.

In summary, these findings suggest that auxin biosynthesis in the root is not only essential for root-specific development at ambient temperatures but also partially at higher temperatures. It is most likely that temperatures-induced root elongation is triggerd by a prolonged IAA biosynthesis due to the induction of *TAA1*, *TAR1* and *YUC3,5,7,8,9* genes encoding the indole-3-pyruvic acid (IPyA) pathway. But based on the observation that the auxin-deficient mutants showed only a partial reduction of temperature responses, it must it must be assumed that another still unknown factor are involved in the temperature-induced root growth are, therefore, required. The results of my pharmacological experiments also indicate that even very small increases in auxin level in the root tip (arround 0.01nM IAA) are sufficient to induce the temperature response in the root. Auxin levels above a these threshold result in inhibition of root elongation, an effect that seems to be pronounced at elevated temperatures.
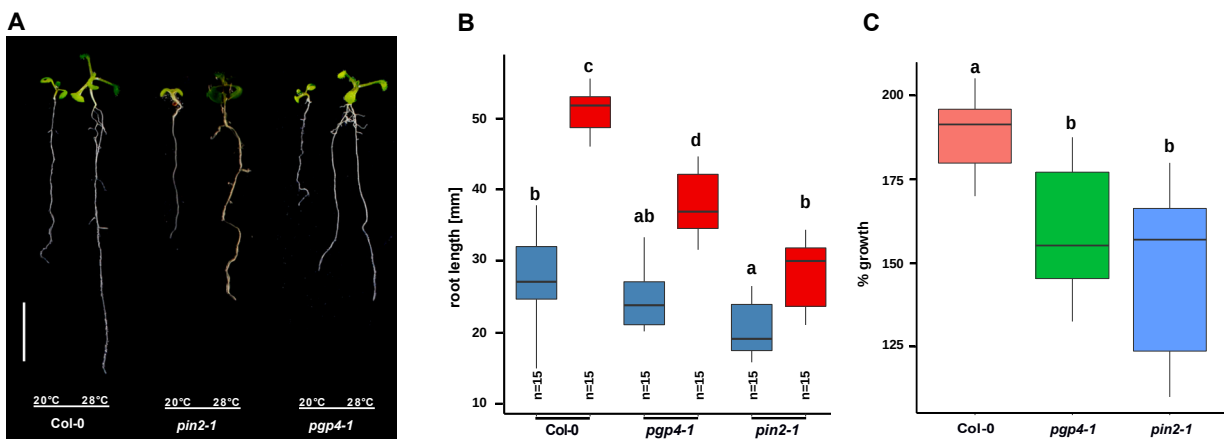
Figure 32. Impact of auxin transport related genes on the temperature induced root growth. A Representative pictures of plants from corresponding TIRE assay (**C**). Scale bars: 10mm. **A-C** Box plots show relative (28°C/20°C in %; **C**) or absolute (**B**) root length of 7d-old wild-type and auxin transport related mutant *(pgp4-1*, *pin2-1)* plants grown at 20°C or 28 °C under LD (16/8 h) and 90 µmol m^{-2}s^{-1} white fluorescent light. **B,C** Box plots show medians and interquartile ranges; outliers (greater than 1.52 interquartile range) are shown as black dots. **B** Different letters denote statistical differences at *p*< 0.05 as assessed by one-way ANOVA and Tukey's honestly significant difference (HSD) posthoc test. **C** Statistical differences were assessed by two-way ANOVA (*p*< 0.05) of the absolute data presented in Figure **B**. Different letters denote significant differences among all sample.

Carrier-driven auxin transport might be also important for maintaining the optimal auxin gradient (Rosquete et al., 2012). In this regard, I next explored root growth responses of auxin transport mutants. Among the eight polar localised PIN proteins in *A. thaliana*, loss-of-function mutants of *PIN2*, *PIN3*, *PIN4* and *PIN7* (*PIN-FORMED 2, 3, 4, 7, PINs*) genes were examined in terms of the temperature response in the root. It is known that these genes are involved in root elongation and in the regulation of auxin distribution (Kleine-Vehn and Friml, 2008, Krecek et al., 2009). According to Figures S12 and 32A, only *pin2-1* is mutated in a gene encoding a basipetal polar auxin transporter

(Luschnig et al., 1998, Müller et al., 1998), showed reduced temperature response in the root. While the root length of *pin2-1* mutants at 20°C showed a quite similar TIRE response to the wild-type, the root length at 28°C was significantly decreased. Similarly, another auxin transport mutant, *pgp4-1 (PHOSPHOGLYCOPROTEIN4)*, revealed decreased temperature-induced root growth (Figure 32A). PGPs also participate in auxin efflux from plant cells like PINs (Noh et al., 2001, Verrier et al., 2008), but in contrast to the PINs, their cellular localisation is mainly apolar (Geisler et al., 2005, Blakeslee et al., 2007, Wu et al., 2007). However, temperature phenotypes of both auxin transport mutants suggest that *PIN2* and *PGP4* are required for primary root elongation in warmth, possibly by promoting shootward auxin efflux in the outside cell layers as described by Hanzawa et al. (2013) for PIN2. Theassociated study showed that elevated temperature might modulate cellular auxin homeostasis by promoting SNX1 (SORTING NEXIN1)-dependent PIN2 targeting the plasma membrane. In this manner, roots can counterbalance the temperature-dependent increase of intracellular auxin concentration to an optimal level and thus promote primary root elongation. Unfortunately, I could not test a mutant line defective in *PIN1*, another important stele-localised auxin influx carrier involved. Thus, related experiments should be carried out in future.

Auxin seems to play a role in root development at elevated temperatures. The decreased TIRE-phenotype of some auxin signaling and biosynthesis mutants indicates that auxin might positively impact temperature-induced root growth. To further verify its involvement in the temperature response, I performed rescue experiments with selected biosynthesis mutants *wei8-4* and *yucQ* by applying of 0.01 nM IAA (=physiological concentration) to the medium to test if the treatment can restore the described defective phenotype. Indeed, all mutants can be rescued by treatment with low concentrations of IAA (Figure 33A-B).

Taken together, although not completely consistent, I found that several auxin mutants on all levels of auxin biology (biosynthesis, transport, signaling) displayed defects in temperature-induced root elongation. This indicates the necessity of a functioning auxin network for temperature-dependent root growth. However, except for *msg2-1* and *slr1-1,* all tested mutants still responded to various degrees to high temperature. Thus, additional factors seem to be involved in the process. Based on the results of the complementation experiment with low concentration of auxin, I conclude that parts of the tested auxin biosynthesis genes are linked to the temperature response in the root.
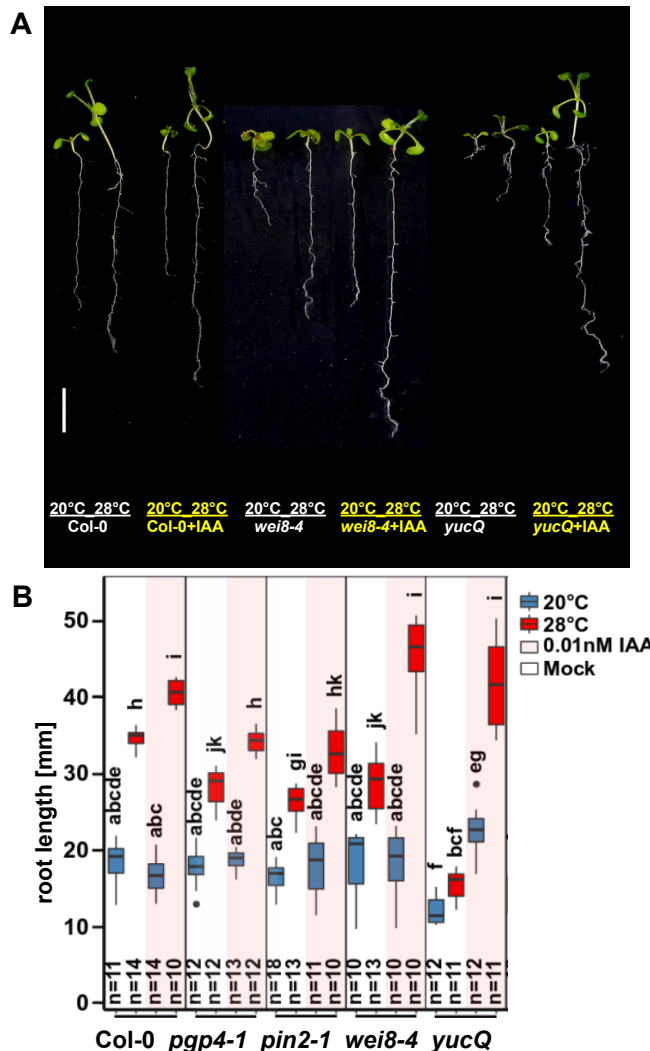
Figure 33. IAA-mediated rescue of temperature response in auxin-related mutants. A-B Root length of 7d-old wild type and auxin related mutant (*pgp4-1*, *pin2-1*, *wei8-4*, *yucQ*) plants grown at 20°C or 28 °C under LD (16/8 h) and 90 μmol m⁻²s⁻¹ white fluorescent light with or without 0.01NM IAA. Agar plates were additionally covered with yellow plastic plates. **A** Representative pictures of plants from corresponding TIRE assay **(B)** Scale bars: 10mm. **B** Box plots show medians and interquartile ranges; outliers (greater than 1.52 interquartile range) are shown as black dots. Different letters denote statistical differences at $p< 0.05$ as assessed by one-way ANOVA and Tukey's honestly significant difference (HSD) posthoc test. Different letters denote significant differences among all samples.

4.2.9 Elevated temperature can increase endogenous auxin production

Based on the results presented above, which indicate that the temperature response of primary roots can be enhanced by the application of a low concentration of exogenous auxin (Figure 26), I next investigated whether the endogenous auxin levels in the root apical meristem (RAM) of *A. thaliana* roots are also differentially modulated by elevated temperature. Therefore I used the *R2D2* fluorescent reporter line that expresses a Venus-tagged auxin degradable reporter protein (*DII:n3xVenus*) under control of an *RPS5A*

promoter along with an RFP-tagged undegradable protein (mDII:ntdTomato). The fluorescent reporters allow high-resolution visualization of changes in auxin distribution during root development (Liao et al. 2015). The fluorescence of DII correlates inversely with the endogenous levels of auxin (Brunoud et al. 2012, Liao et al., 2015), which permit monitoring the amount of free auxin indirectly. Comparing VENUS and tdTomato fluorescence in the *R2D2* line, the RAM showed reduced D2 fluorescence (Figure 34 A-B) at elevated temperatures, indicating higher nuclear auxin levels in cells of the RAM at 28°C. As predicted, the *R2D2*-derived auxin levels increase with rising temperatures, similar to the roots treated with exogenous Indole-3-Acetic Acid (IAA). This is in agreement with the pharmacological experiments (Figure 26) and provides additional correlative evidence for role of auxin in temperature responses in the roots.
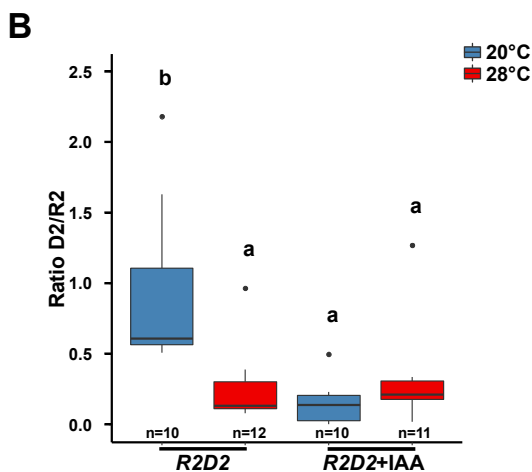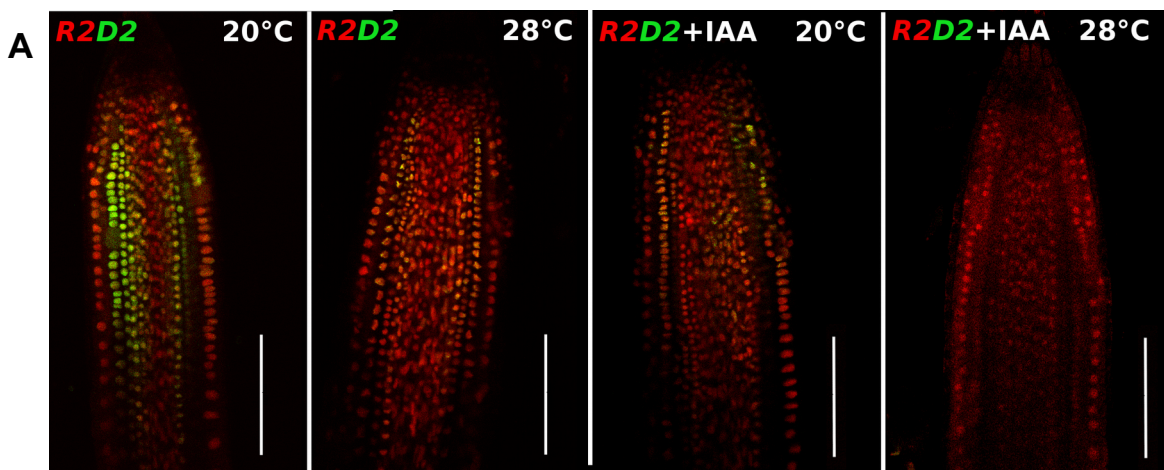
Figure 34. Temperature-mediated increase of endogenous auxin levels in the meristematic zone. **A** Merged confocal images of R2 (red) and D2 (green) expressing R2D2 marker and **B** quantification of D2/R2 ratio. Wild-type plants grown for 7d at 20 or 28 °C under LD (16/8 h)and 90 µmol m^{-2} s^{-1} white fluorescent light. Data collected 1h after dawn. Positive control plants were treated with 1mM IAA. Agar plates were additionally covered with yellow plastic plates. **A** Representative pictures of plants from corresponding TIRE assay. scale bars: 100µm . **B** Box plots show medians and interquartile ranges; outliers (greater than 1.52 interquartile range) are shown as black dots. Different letters denote statistical differences at $P < 0.05$ as assessed by one-way ANOVA and Tukey's honestly significant difference (HSD) posthoc test. Different letters denote significant differences among all samples.

4.2.10 IAA improves cell division in roots at elevated temperatures

For better understanding the specific roles of auxin in the temperature response of roots. allows visualization of changes in auxin distribution during development. First, I quantified

cell division and cell elongation in wild-type across the entire root zones using laser scanning microscopy. The roots of 7d-old Columbia seedlings were cultivated at 20°C or 28°C with or without 0.01 nM IAA. The data was collected and later processed in the same way as the experiments in Figure 20. Since the temperature-induced root elongation appeared to result from an alteration in cell proliferation rather than changes in cell expansion, I focusssed on the analysis of temperatur-induced changes in the meristematic zone (MZ). The results for the elongation zone (EZ) are attached in the Supplementary (Figure S13). As shown in Figure 35A, the MZ length was unaffected by auxin treatment as well as the cell number (Figure 35B). The length of the meristematic zone between 20°C and 28°Cwere not statistically different. The cell lengths have not been quantified at this point because, as explained above, cell elongation does not seem to play such a major role in this zone. Hence, it appears that the temperature-dependent meristem development, and thus, the cell division rates are independent of auxin. However, similar to the results of TIRE assays in Figure 20 I, J, the data of maturation zone (MaZ) contradict the observations in the MZ. Although the lengths of the MZ at both temperatures are almost as long as the meristem of plants grown on auxin supplemented medium, the cell number of the MaZ of these plants significantly increased if 28°C grown plants are treated with IAA (Figure 35C).

Accordingly, I analysed the cellular processes in the different root zones in the auxin biosynthesis mutants *wei8-1 tar1-1, yucQ, yuc1-D* (See Figure S14*).* Apart from the re- sults of cell analysis in the MZ and EZ, the cell number in the maturation zone (MaZ) was significantly decreased compared to the wild-type.

Taken together, these findings suggest that despite the lack of measurable morphological changes in the meristem of treated or untreated *A. thaliana* roots, the cell division rate, which determines the cell number, can be increased by adding 0.01 nM IAA at elevated temperatures.
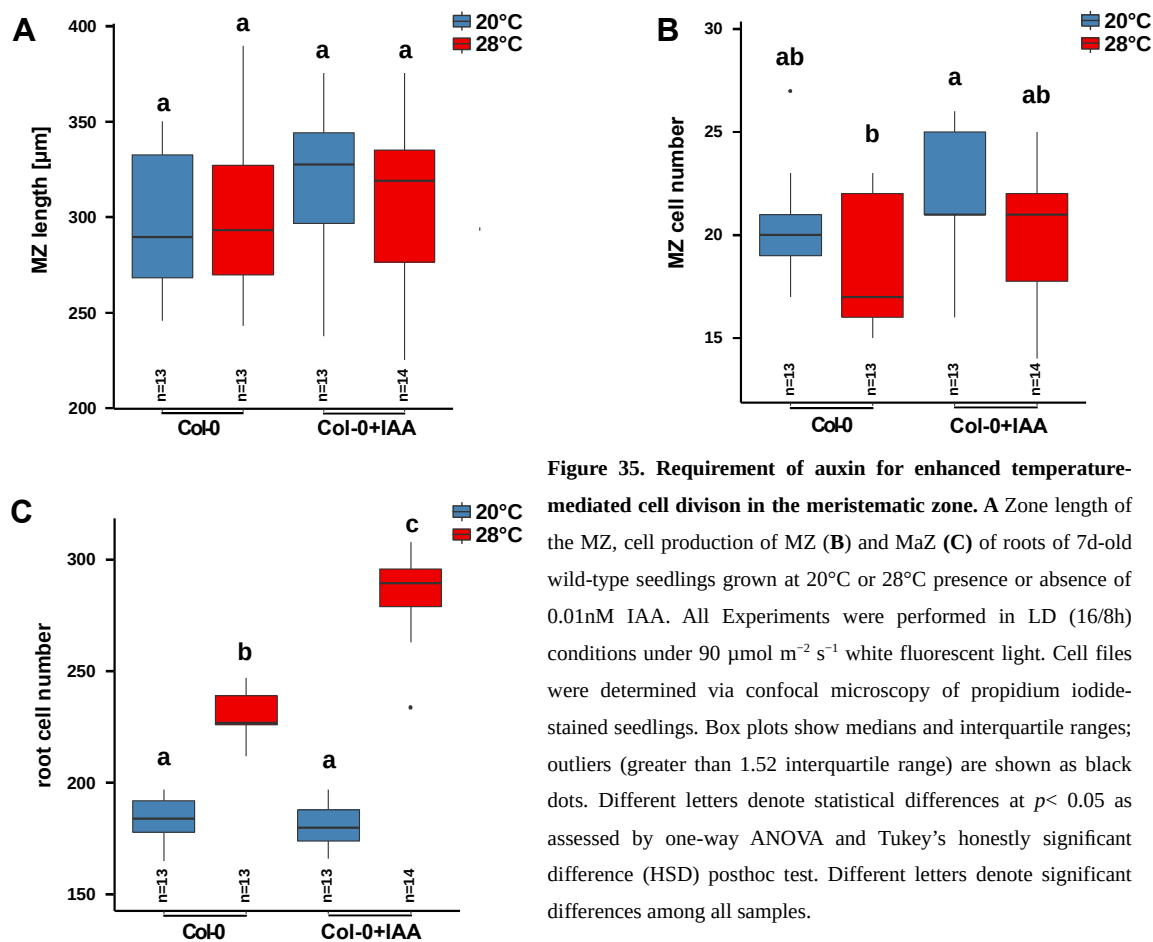
Figure 35. Requirement of auxin for enhanced temperature-mediated cell divison in the meristematic zone. A Zone length of the MZ, cell production of MZ (**B**) and MaZ (**C**) of roots of 7d-old wild-type seedlings grown at 20°C or 28°C presence or absence of 0.01nM IAA. All Experiments were performed in LD (16/8h) conditions under 90 µmol m^{-2} s^{-1} white fluorescent light. Cell files were determined via confocal microscopy of propidium iodide-stained seedlings. Box plots show medians and interquartile ranges; outliers (greater than 1.52 interquartile range) are shown as black dots. Different letters denote statistical differences at $p < 0.05$ as assessed by one-way ANOVA and Tukey's honestly significant difference (HSD) posthoc test. Different letters denote significant differences among all samples.

4.2.11 Effect of exogenous IAA application on S-phase entry of cells during the cell cycle

All previous data emerging from cell culture studies suggest that auxin acts directly or indirectly as a permissive signal for cells to enter the cell cycle (G1/S transition), likely through the activation of D-type cyclin and *cyclin-dependent kinase A,1* (*CDKA,1*) expression (Himanen et al., 2002, Perrot-Rechenmann, 2010). Likely, the temperature-induced alteration in the endogenous auxin concentration in the root could also modulate the basic cell cycle regulatory machinery to activate cell cycle entry. Thus, cells start earlier in the cell cycle stages at elevated temperatures. To test this hypothesis, I again used the dual-colour marker system "*Cytrap*". Roots of 7d-old *Cytrap* seedling were cultivated at 20°C or 28°C and were treated with (Figure 36C,D) or without (Figure 36A,B) 0.01 nM IAA. Indeed, when 0.01 nM IAA was added, the cells in S/G2-phase in the RAM at 28°C (Figure 36D) were significantly more than twice as many cells compared to the number of cells in S/G2-phase in RAM at 20°C and IAA treatment (Figure 36C,G). Although the number of cells in the MZ (See Figure 19C) was almost similar between 20°C and 28°C, the proportion of S-phase cells in the MZ of 7d-old

seedlings was more pronounced at 28°C at one hour after dawn. This observation suggests that auxin influenced the cell cycle at elevated temperatures.
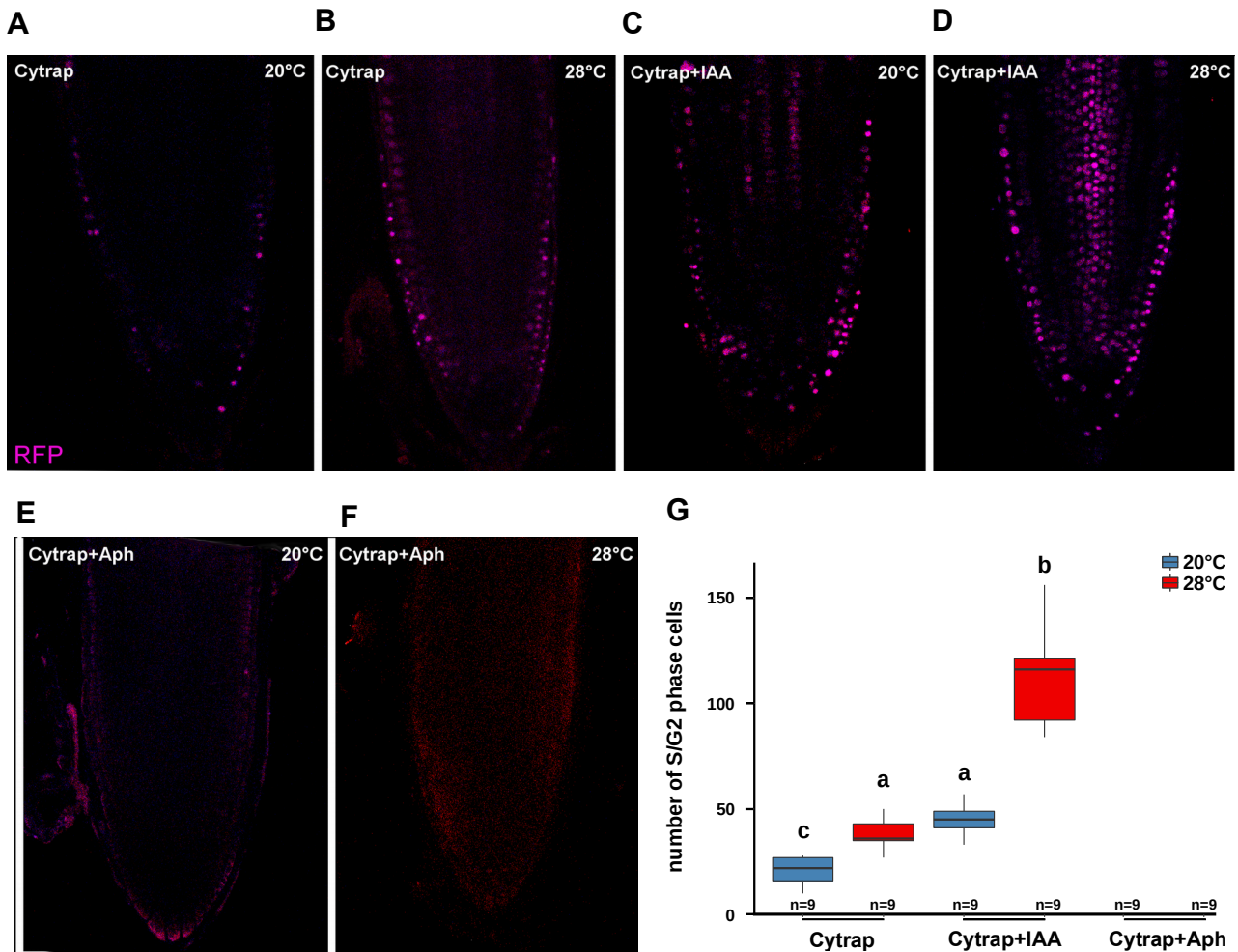
Figure 36. Auxin positively regulates temperature-Induced cell division. A-G Representative pictures of the RAM of *Cytrap* plants grown 7d at 20 °C (**A,C,D**) or 28 °C (**B,D,F**) under LD conditions (16/8 h) and 90 µmol m^{-2} s^{-1} white fluorescent light in either the absence (**A,B**) or presence of 0.01nM IAA (**C,D**). **E** Control of cell division by additionally adding aphidicolin (Aph) Agar plates were additionally covered with yellow plastic plates. **G** Quantification of measurements (1h after dawn). Plants Box plots show medians and interquartile ranges, outliers (greater than 1.52 interquartile range) are shown as black dots. Different letters denote statistical differences at $p < 0.05$ as assessed by one-way ANOVA and Tukey's honestly significant difference (HSD) posthoc test. Different letters denote significant differences among all samples.

4.2.12 Real-Time qRT-PCR measurements of tissues from EZ and MZ

To investigate the relationship between temperature responses in the meristematic zone (MZ) and the expression of cell cycle-related genes and cell expansion related genes, RT-qPCR were performed on MZ and elongation zone (EZ) tissues of 5 days old wild-type plants, grown at 20°C or 28°C. Related to the results of the root growth rate (Figure S15),

seedlings were dissected (See Figure 37A), 1h after dawn and 4h before the maximum growth rate was observed.

For validation of the histological identification of the isolated RNA samples, the transcriptional expression level of a temperature-responsive marker gene *HEAT SHOCK PROTEIN-70* (*HSP70*), an MZ-specific root zone marker gene *ROOT CLAVATA-HOMOLOG1* (*RCH1)*, and an EZ-specific root zone marker gene *XYLOGLUCAN ENDOTRANSGLUCOSYLASE/HYDROLASE 21* (*XTH21*) (Markakis et al., 2012) were analyzed. Gene expression level of *HSP70* increased significantly at 28°C compared to 20°C in all tissues, as described in literature (Lindquist and Craig, 1988, Vierling, 1991, Georgopoulos and Welch, 1993, Nover and Scharf, 1997) (Figure S15A). Furthermore, expression anlyses of the zone-specific marker genes revealed a high concordance between the RNA of the matched tissue samples and the corresponding root zones with little cross-contamination (Figure S15B). In summary, the positive quality control confirmed the suitability of representative samples for the transcriptional analysis.

As shown in Figure 37B, three D-type cyclins *CYCD3,1*, *CYCD1,1* and *CYCD6,1* which are key cell cycle regulators in the root elongation (De Veylder et al., 2002, Masubelele et al., 2005, Kono et al., 2006, Sozzani et al., 2006, Cruz-Ramirez et al. 2012), were significantly thermoresponsive in the MZ of the root tip, while the induction was absent in the samples of the EZ (Figure 37C). These results support the idea that increasing temperature affects the transcript abundance of cell cycle-related genes in the MZ by active promotion of transcription rates. However, data should be interpreted carefully as several other cell cycle stimulating genes, such as *E2Fb*, B-type cyclin *CycB1,1, RETINOBLASTOMA-RELATED* (*RBR) gene*, increased in the expression level at 28°C (Figure S15A-B). One reason for this inconclusiveness in the expresslevel of the cell cycle genes might be related to a wrong chosen time point for sampling. As shown in Figure S16, the growth rate starts to increase shortly before dusk, continues to rise during the night and peaks at mid-day. Thus, for future experiments, sampling time points should be adjusted toward dusk. Moreover, it was impossible to ascertain why RBR, which represses cell division (del Pozo et al., 2002, Wildwater et al., 2005), was normally expressed under elevated temperature.

Apart from that, it is surprising that all three temperature-inducible cell cycle genes *CYCD3,1*, *CYCD1,1* and *CYCD6,1* were associated with regulating the S-phase to the G-phase transition (Menges et al.,2005, 2006). However, no gene could be found, which plays a role in the G2-phase to M-phase transition. A reason could be that elevated temperatures speed up the M-phase (Rieder and Maiato, 2002). Consequently, the cells are more often in the S-phase than in the M-phase. This matches the contradictory results of the cell-cycle activation assay in root apices of 7d-old seedlings of a *CYCB1,1::GUS*

reporter line, cultivated at 20°C and 28°C. The β-Glucuronidase (GUS) protein is targeted for degradation in the M-phase, thereby allowing specific staining of G2/M cells.
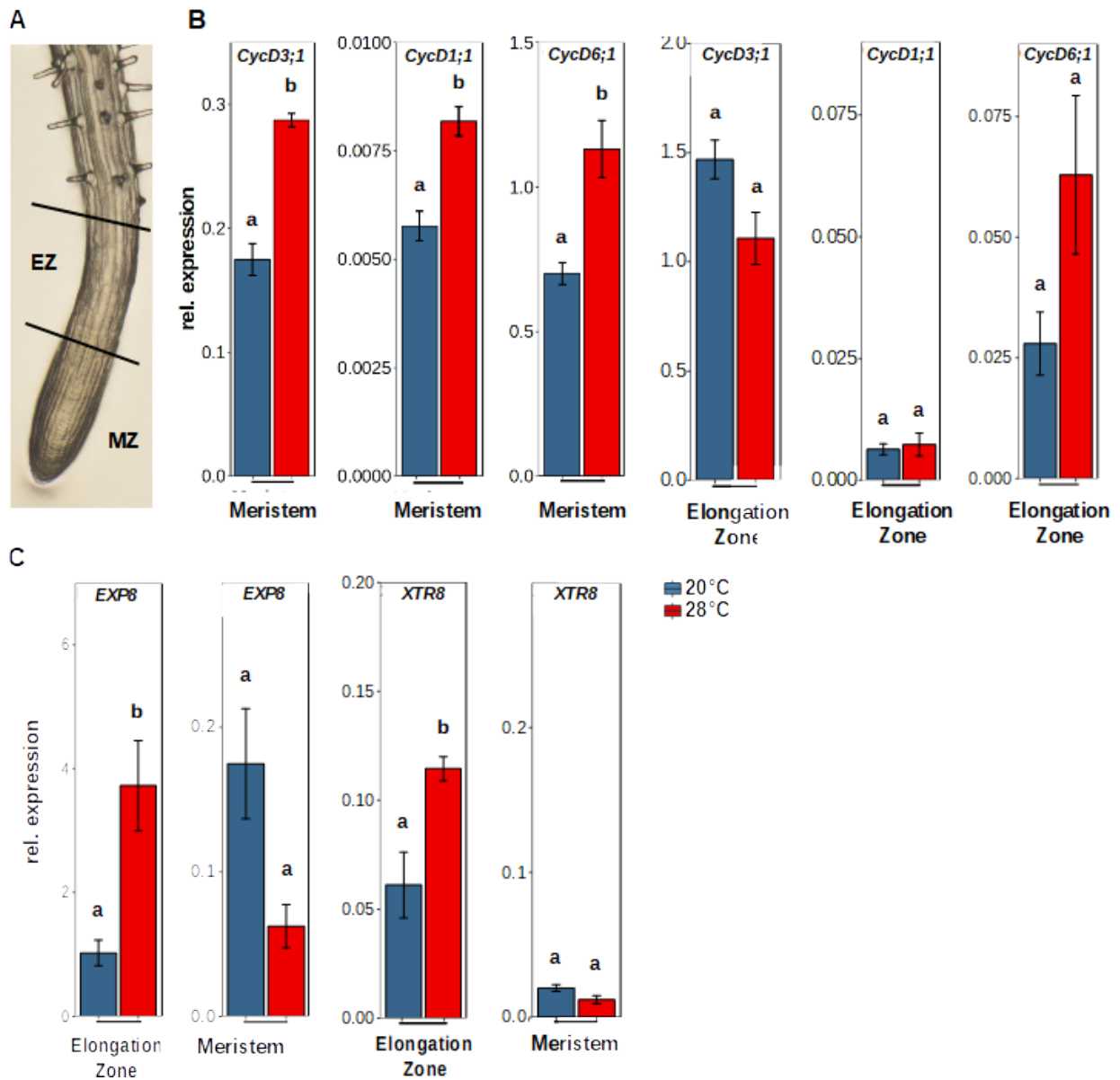
Figure 37. Organ-specific expression analysis of cell cycle and cell elongation-related genes. **A** Representative seedlings cultivated for 5d at 20°C or 28°C observed under an ordinary light microscope, Meristem and EZ were harvested separately at Zeitgeber time 1 (ZT1) for expression analysis. Reverse transcription quantitative PCR (RT-qPCR) expression of (**B**) cell cycle regulator genes, D-type cyclins *CYCD3;1*, *CYCD1;1* and *CYCD6;1* and (**C**) cell expansion genes, *EXP8, XTR8* were assessed in MZ and EZ samples. seedlings were grown in LD conditions (16/8h) under 90 μmol m^{-2} s^{-1} white fluorescent light. RT-qPCR analyses were performed on three   independent biological replicates. Bar plots show mean values, and error bars denote SE. Different letters denote statistical differences at *p*< 0.05 as assessed by one-way ANOVA and Tukey's HSD posthoc test.

Figure S17A-B showed the number of positively stained cells with *CYCB1,1::GUS* activities were not significantly different between 20 and 28°C. This discrepancy must be investigated further, perhaps by providing a time course with shorter intervals

between the measurements. By contrast, only two of all cell elongation promoting genes tested were temperature-responsive in the EZ, *XYLOGLUCAN ENDO-TRANSGLYCOSYLASE-RELATED8 / XYLOGLUCAN ENDO-TRANSGLYCOSYLASE-HYDROLASE31 (XTR8/XTH3*1*)*, and *EXPANSIN8 (EXP8)* (Figure 37C). Expansins and *XTH*s exist as a large gene family with distinct expression patterns and limitations to a single organ or cell type (Wu et al., 2001, Becnel et al., 2006). This could be why it is so difficult to identify candidate genes associated with temperature-induced cell elongation in my sample material. Nevertheless, among the tested cell elongation-related genes, *EXP8* showed a significant upregulatation at elevated temperatures in the elongation zone. (Figure 37C). Based on this result, it cannot be excluded at the moment that cell elongation proceses are also partially affected by elevated temperatures stimuli.

Taken together, the results of the expression analyses complemented the observations of the physiological assays. In contrast to the hypocotyl, both cell division and cell elongation may be involved in temperature-induced root elongation.

4.2.13 Expression analysis of genes related to auxin

Based on the results obtained so far, auxin is a potential positive regulator of temperature-induced root elongation, promoting cell division rather than cell elongation. Thus, auxin-related genes should show a higher expression level in tissue samples from root apical meristems (RAMs), which were exposed to elevated temperatures compared to corresponding tissue samples of plants cultivated at 20°C. To test this hypothesis, I assayed the expression of the auxin biosynthetic gene *YUCCA8* (*YUC8*), which is already known to integrate temperature into the auxin pathway in regulating *A. thaliana* hypocotyl growth (Sun et al. 2012). Indeed, the expression level of *YUC8* was significantly higher in meristem tissues at 28°C compared to 20°C (Figure 38).The early auxin-responsive IAA19 gene induced under elevated temperature in hypocotyls was also induced in RAMs of roots cultivated at warmth. (Figure 38). This might indicate an enhancement of auxin signaling in roots under elevated temperatures. It is also known that *small auxin up-regulated RNAs* (*SAUR*s) of the *small auxin up-regulated RNA 19* (*SAUR19*) subfamily positively regulate cell expansion to promote temperature-induced hypocotyl growth (Spartz et al., 2012, Spartz et al., 2014). While *SAUR19* is mostly active in the shoot, *small auxin up-regulated RNA 76* (*SAUR76*) was found to be involved in primary root growth (Figure 38).

Furthermore, auxin treatment could regulate *SAUR76* expression in roots (Markakis et al., 2013, Li et al., 2015). For this reason, I additionally investigated the

transcript level of *SAUR76*. As shown in Figure 38, all auxin-related genes were significantly upregulated at 28°C compared to 20°C. This might suggest that the thermoresponsive induction of auxin biosynthesis is most relevant in meristematic zone (MZ) rather than in elongation zone (EZ).

All in all, data indicate that elevated temperature might stimulate auxin biosynthesis in the root apical meristem (RAM) in a dose-dependent manner. Whether the increase in auxin level and cell production rate are somehow correlated, need to be addressed by others.
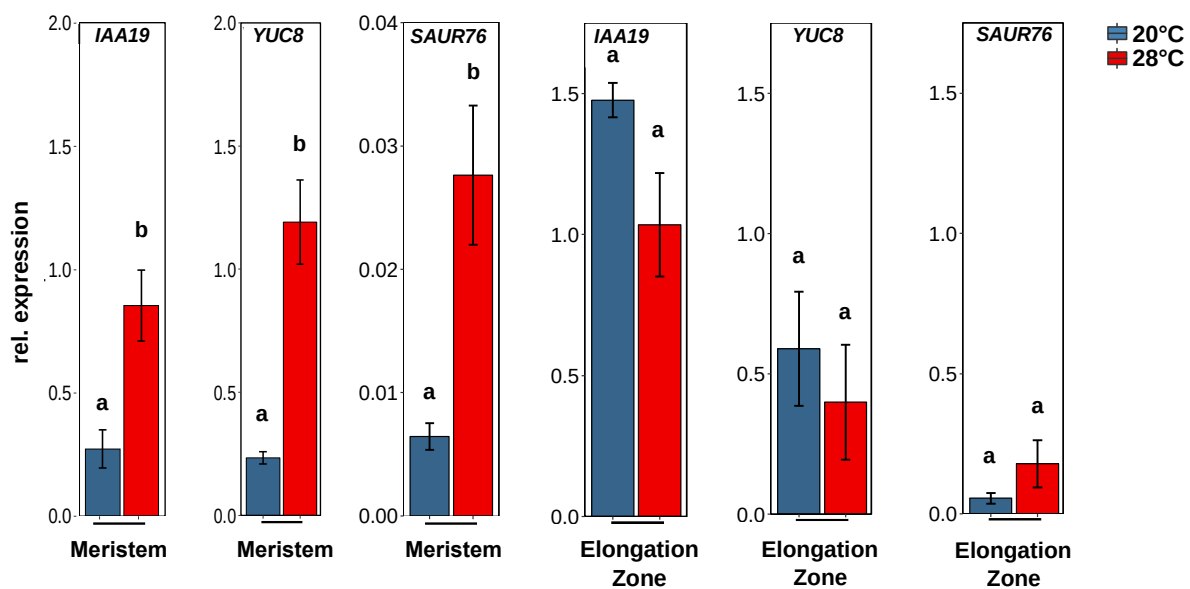
Figure 38. Organ-specific expression analysis of auxin-related and growth-related genes. Reverse transcription quantitative PCR (RT-qPCR) expression analysis of the auxin biosynthesis and response genes. MZ and EZ were harvested separately at Zeitgeber time 1 (ZT1) for expression analysis. Reverse transcription quantitative PCR (RT-qPCR) expression of auxin biosynthesis gene *YUC8* and a auxin response gene *IAA19* and *SAUR76* were assessed in MZ and EZ samples. seedlings were grown for 5d at 20°C or 28°C in LD conditions (16/8h) under 90 µmol m^{-2} s^{-1} white fluorescent light. RT-qPCR analyses were performed on three independent biological replicates. Bar plots show mean values, and error bars denote SE. Different letters denote statistical differences a*t* $p < 0.05$ as assessed by one-way ANOVA and Tukey's HSD posthoc test.

In summary, my data revealed that root growth in *A. thaliana* is a temperature-responsive process. Time-lapse experiments showed that the temperature-induced root response is restricted to a certain time window, in which the root is first capable of reacting to temperature changes. After an initially strong increase in root growth rate shortly after temperature exposure, stagnation could be observed due to an as yet unknown process. However, cell analysis revealed a large increase in the total cell number in the entire root at 28°C compared to 20°C. In contrast, the MZ and EZ cell number and length remained constant at both temperatures. Due to this observation, I suggested that cell division and

not cell elongation is clearly the major driver of temperature-induced root elongation (TIRE). Furthermore, I detected a higher number of cells containing EdU or the expression of the G2/S-phase marker and M-phase marker of *Cytrap* line at 28°C compared to 20°C, supporting the theory of a more active proliferating RAM at elevated temperatures, which produces more cells due to an accelerated cell cycle in a shorter time span.

Chapter I shows that the elongation response in roots is rather independent of shoot-derived signals. Work with mutants deficient in genes known from the shoot-thermomorphogenesis signaling pathway revealed that the temperature-induced root elongation might be also regulated by root-specific signaling pathways.

Martins et al. (2007) postulated that moderate heat stimulates the growth of Arabidopsis root in a BR-dependent manner. Based on my results from the TIRE assays with different BR signaling deficient mutants, I cannot confirm this claim. However, regarding my results genetic, biochemical and pharmacological experiments, I support the position of previous studies (Hanzawa et al., 2013, Wang et al., 2016, Yang et al., 2017, Feraru et al., 2019, Gaillochet et al., 2020) that the temperature-induced root response in *A. thaliana* is linked to an increasing auxin accumulation in the MZ. However, following a pharmacological approach, I was able to demonstrate that only low auxin levels of around 0.01nM can stimulate primary root elongation at elevated temperature, while concentrations above this threshold suppress the primary root growth significantly. Thus, maintaining the auxin concentration to an ideal range in the MZ is essential for optimal root growth and response to elevated temperatures. I suggest that plants at elevated temperatures attempt to compensate for the increase of auxin above the optimal level by an as yet unknown mechanism. Similar to Hanzawa et al. (2013), I could observe that the temperature-induced root elongation in *pin2* and *pgp4* mutants are reduced compared to the wild-type. This implicates that carrier-driven auxin transport is required for root elongation at elevated temperatures. I hypothesize that the shootward auxin transport of the auxin efflux carrier PIN-FORMED2 (PIN2) and P-GLYCOPROTEIN4 (PGP4) potentially help to keep the auxin concentration in the MZ to an optimal level and thus trigger temperature-induced root elongation.

5. Chapter III: Phenotyping and identification of QTLs for temperature-induced root architecture traits using wild barley introgression lines

In the first part of my work, I was investigating temperature-dependent regulation of plant growth and developmental responses (thermomorphogenesis) in *A. thaliana* as the most common eudicotyledons model plant species. In this context, the question arises whether these general processes observed in Arabidopsis can also be applied to monocots such

as barley. An alternative possibility is that barley has monocot-specific or barley-specific differences in response to warmth. However, relative to *A.thaliana*, little is known about crop responses to elevated temperatures. Therefore, I started to systematically profile morphological and physiological changes of barley plants grown under different temperatures by investigating a set of 48 wild barley introgression lines (ILs) from the S42IL population. These aforementioned data were used to perform quantitative trait locus (QTL) analysis for each growth-related trait to detect genomic regions influencing these traits of interest.

*Consid*ering a certain degree of redundancy among the original 73 wild barley ILs of the S42ILs library and concerning the presence of the individual introgressions, Honsdorf et al., 2015 selected these 47 essential ILs which still represent 87.3% of the wild barley genome, similar to the whole mapping population. Furthermore, this set has already been successfully used in other studies (Schmalenbach et al. 2011). In addition to the 47 ILs the line S42IL-176 (Schmalenbach et al.,2008) was also chosen for my analyses, because this IL revealed already remarkable trait increases in root length and root dry weight under normal conditions (Naz et al., 2014).

However, for a project of my scope and purposes, using this minimal set of 48 essential ILs, was a suitable choice (See Supplemental data Table S11). The fact that each ILs carry a single marker-defined chromosomal segment of the donor parent 'ISR42-8', whereas the rest of the genome is derived from the recurrent parent 'Scarlett' (the parent to which successive backcrosses are made in backcross breeding), substantially facilitate the access to information about the genomic regions that might be involved in the inheritance of the phenotypic differences between both parents. Subsequently, these data could provide the basis for further research in the future, such as candidate gene analyses which potentially allow the identification of conserved mechanisms between *A. thaliana* and barley (in case that the QTL regions are enriched for genes homologous to *A. thaliana* genes that are involved in ambient temperature signaling pathways).

Another benefit of this reduced population size was the possibility to use a special non-invasive, medium-throughput phenotyping method (GrowScreen-PaGe) (N_{MAX}=500), enabling semi-automatic measurements of the temperature-related phenotypic variation in root architecture traits and some shoot morphology traits of the different introgression lines grown on blue germination paper (Figure 39A). (Nagel et al. 2012, Jeudy et al. 2016, Atkinson et al. 2019). Consequently, access to specialized equipment was needed, which was realized by a collaboration with the Jülich Plant Phenotyping Center (JPPC, Forschungszentrum Jülich GmbH, Germany), enabling me to utilize their root phenotyping

facilities. 4d-old pre-germinated barley seedlings were grown for 12d under 16°C and in a second run under 24°C in long-day (LD) conditions (16h light, 8h dark) and light intensity of 470 µmol m^{-2} s^{-1}. The containers were covered with aluminum foil (Figure 39B). Repeated high-resolution images of the developing root systems on the germination paper were acquired every second day (six time points) using a mobile imaging box with fixed positions of cameras (Figure 39C). Data for each root trait (See Figure 40), except for the root dry weight (RDW) was collected for each time point and analysed automatically with the non-invasive root phenotyping system GrowScreen-PaGe (Gioia et al. 2016). Since the software was specifically designed for automatic root architecture analysis, shoot rela-ted traits were manually recorded only at day 12 (time point 6). In addition, shoot and root material of the different ILs were harvested separately on day 12 aftere treatment beginning to measure the shoot fresh weight (FWS), shoot dry weight (SDW), the root dry weight (RDW). Phenotypic data were collected from 340 individual plants (n≤7 per geno-type) for 25 morphological traits (Figure 40) and two different temperature conditions (16°C/24°C). To confirm the data from the Jülich phenotyping system, I repeated the experiment with a smaller number of genotypes and phenotypes under similar, but not identical, conditions in our own facilities at the Martin Luther University (MLU) in Halle (reach in phytotrons (Conviron Ataptis A1000, light intensity: 300 µmol m^{-2} s^{-1}). For replicates, data was captured and processed by hand. Details about the procedure are described in the "Materials and Methods" section.

5.1 Temperature responses in 'Scarlett' and 'ISR42-8'

The mapping population used is based on a cross between the cultivar 'Scarlett' and wild barley accession 'ISR42-8'. Therefore, I first focused on the phenotypic analysis of these two parental lines. Since a detailed discussion of all trait performances for each time point is beyond the context of this work, I only described the changes for the final time point 6 (12d after 4d pre-germination), shown in Figure 41 and 42, as exemplary. I chose this time point because data could be collected for all traits. However, the trend behavior of the roots at 24°C compared to 16°C at the other time points was almost similar (See Supplementary Figure S19).
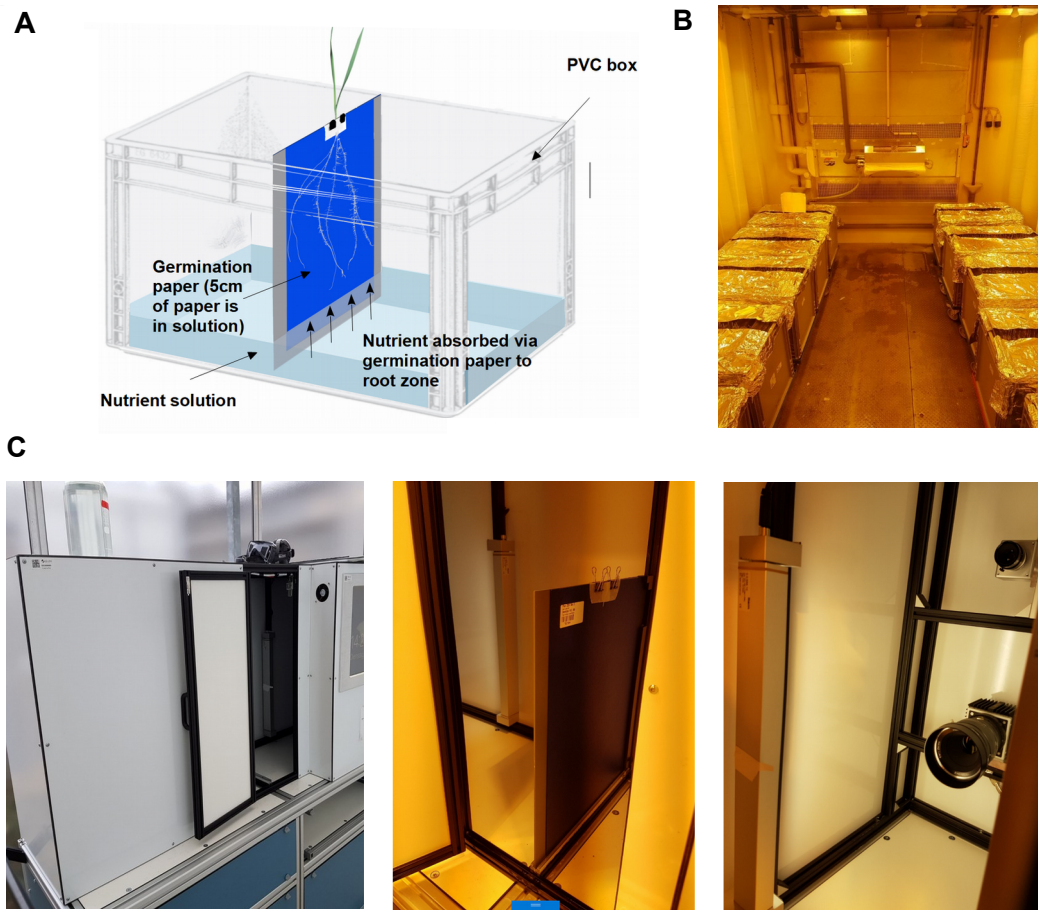
Figure 39. The GrowScreen-PaGe system for non-invasive and medium-throughput phenotyping of root systems. A Seedlings were grown on germination paper in a special cultivation system. **B** Plastic containers were covered with aluminium foil to simulate the dark environment of the roots. **C** Representative image of the imaging box from outside and insight.

5.1.1 Root growth related traits

The non-invasive, medium-throughput phenotyping setup used in this study has primarily been developed for root phenotyping. Thus the majority of the assessed traits are related to root growth and development. For almost all root traits (16) (Figure 40), and both parental lines, phenotypic values were increased at 24°C compared to 16°C (Figure 41, Supplementary Figure S18). The only exceptions were the ratio of root dry weight per total weight (RDW/TW) (See Supplementary Figure S18), number of seminal roots (NSR) and root angle related traits (root system angle left (RSAL), root system angle right (RSAR), root system angle left and right (RSALR) (Figure 41).

Generally, barley plants produced noticeable more lateral roots at these development stages which expanded more rapidly at elevated temperatures. Combined with a slightly increase in lateral root length, these growth parameters predominantly determine the

shape of barley roots. More interestingly, the length and number of seminal roots, as well as the root system depth (RSD) and width (RSW) changed comparatively less in response to elevated temperatures. While changes in lateral/fine roots are more evident at elevated temperatures, they may constitute a major part in the root adaptation process to higher temperatures.

A

B

Shoot traits	Short-form abbreviation	Unit	Trait description
Shootdryweight/ Totalrootweight	SDW/TRW	-	Ratio of shoot dry weight per total root weight
Freshweightshoot	FWS	g	Fresh weight of the shoot
Shootdryweight	SDW	g	Dry weight of the shoots
1stleafarea	1stLLA	cm²	Area of the 1st leaf
Length1stleafleafblade	1stLBL	cm	Length of the 1st leaf blade
Length2ndleafleafblade	2ndLBL	cm	Length of the 2nd leaf blade
Lengthleafsheath	1stLLS	cm	Length of the 1st leaf
Totallength1stleaf	1stLTL	cm	Total length of 1st leaf
Totallength2ndleaf	2ndLTL	cm	Total length of 2nd leaf

Root traits	Short-form abbreviation	Unit	Trait description
RootSystemWidthAngleLeft	RSAL	°	Angle between the outermost point from the left side to middle of the root system
RootSystemWidthAngle Right	RSAR	°	Angle between the outermost point from the right side to middle of the root system
RootSystemWidthAngle Left+Right	RSALR	°	Angle between the outermost point from the left side to the right side of the root system
NumberSeminalRoots	NSR	-	Number of all seminal roots
NumberLateralRoots	NLR	-	Number of all lateral roots
LengthSeminalRoots/ NumberSeminalRoots	LSR/NSR	cm	Ratio of the amount of all seminal roots per number of all seminal roots
LengthLateralRoots/ NumberLateralRoots	LLR/NLR	cm	Ratio of the amount of all lateral roots per number of all lateral roots
Rootdryweight	RDW	g	Dry weight of the roots
RootSystemDepth	RSD	cm	Maximum vertical depth of whole root system
RootSystemWidth	RSW	cm	Maximum horizontal width of whole root system
ConvexHullArea	CHA	cm²	Area of the convex hull that encompasses the whole root system
Root length density	RLD	-	Ratio of the length of lateral roots per length of seminal roots
Specific root length	SRL	m g⁻¹	Specific root length, Ratio of total root length per root dry mass
RootSystemDepth/ RootSystemWidth	RSD/RSW	-	Ratio of root system depth per root system width
Rootdryweight/ Totalrootweight	RDW/TW	-	Ratio of root dry weight per total root weight
Total root length	TRL	-	Sum of seminal and lateral roots

Figure 40. Measured and derived shoot and root system traits. A Schematic illustration of the observed root and shoot traits. **B** List of quantified traits, separated in root and shoot traits with trait description, information about the unit and abbreviation. While for all traits related to root growth data were collected for all six time points, except for RDW, RDW/TW, SRL. Data for the traits related to shoot exists only for the time point 6 (day 12 after treatment).

However, when comparing the performance of the parental lines to elevated temperature, two-factorial ANOVA revealed no significant differences among 'ISR42-8' and 'Scarlett'. Although no noteworthy differences in temperature response among the parental lines were found, the phenotype deviation (See histograms, Supplementary Figures S20, 21, 22, 23) for all root and shoot traits for time point 6 (12d after treatment beginning) at 24°C or 16°C, suggested that the introgressed regions of 'ISR42-8' in the 'Scarlett' background might broaden the gene pool and promote variations in the shoot and root response to elevated temperatures as well.

As expected, most of the ILs responded similarly to the parental lines at higher ambient temperatures, whereas in some ILs the *Hsp (H. spontaneum)* alleles seemed to affect crop trait performance at 24°C.

However, the histograms correspond to the time point 6, whereas for the other time points, similar behaviours at elevated temperatures could be observed for most of the root traits in 'ISR42-8' and 'Scarlett' (See Supplementary Figure S19). Elevated temperatures caused an increase in the trait performance, except for the root system angle related traits (RSAL, RSAR, RSALR) and the trait root system depth per root system width (RSD/RSW). Temperature effects at 24°C gradually increased, similar to the roots at 16°C, to a maximum from day 2 (time point 1) to day 8 (time point 4) and stagnated subsequently (length seminal roots per number seminal roots (LSR/NSR), length lateral roots per number lateral roots (LLR/NLR), convex hull area (CHA), root system width (RSW), root system depth (RSD)) or showed stable increase until the end of the experiment. (total root length (TRL), root length density (RLD)). In contrast, no stagnation could be measured at 16°C. In general, the differences between 24°C and 16°C became less pronounced over time.

5.1.2 Traits related to shoot growth

After 12d temperature treatment at 24°C, almost all nine shoot growth-related traits analyzed in this work were significantly positively affected by increased temperatures(Figure 42) compared to 16°C. Interestingly, these observations differed from the findings of other authors (Hemming et al. 2012, Kiss et al. 2017), who reported, for example a decrease in biomass (15°C vs. 25°C) throughout the plant development in long day (LD) conditions. Given that these studies focused on mature plants, ambient temperature likely deferentially affects early and late developmental stages, similar to *A. thaliana* (Ibañez et al., 2017). In general, among the two parents of the cross, the phenotypic evaluation

revealed largely similar temperature responses in all shoot growth associated traits (See Figure 42), except for the length of the first leaf sheath(1stLLS) (See Figure 42). However, the variation in 1stLLS between the parental lines could be explained by a different behaviour at 16°C.
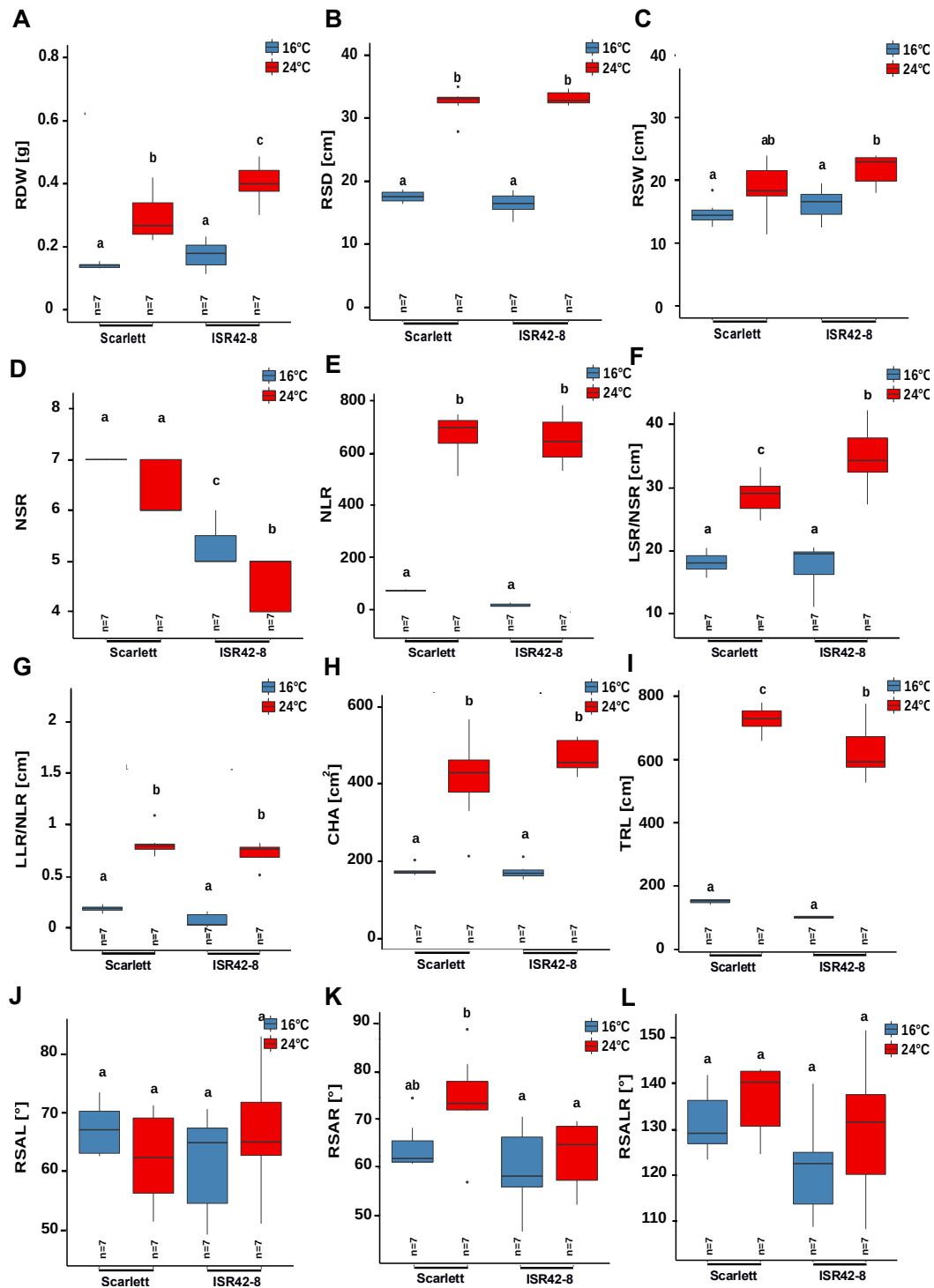
Figure 41. **Root growth responses to high ambient temperature of the parents of the S42IL population 'Scarlett' and 'ISR42-8'.** Box plots show medians and interquartile ranges of **A**) the dry weight (RDW), **B** root system depth (RSD), (**C**) root system width (RSW), (**D**) number of seminal roots (NSR) (**E**) number of lateral roots (NLR), (**F**) ratio of the length of the seminal roots and the number of seminal roots (LSR/NSR), (**G**) ratio of the length of the lateral roots and the number of lateral roots (LLR/NLR), (**H**) convex hull area (CHA), (**I**) ttotal root length (TRL), (**J**) root system

91

Figure 41 (Continued). angle left (RSAL), (**K**) root system angle right (RSAR), (**L**) the sum of the root system angle left and right (RSALR).The trait performance of 14d-old barley plants were quantified after 12 days at 24°C or 16°C. Letters denote statistical differences ($p < 0.05$) as assessed by one-way ANOVA and Tukey HSD. Outliers (greater than 1.5× interquartile range) are shown as black dots. Experiments were performed in LD (16/8h) conditions and light intensity of 470 µmol m^{-2} s^{-1}. The barley seedlings were pre-germinated for 4d at 16°C.
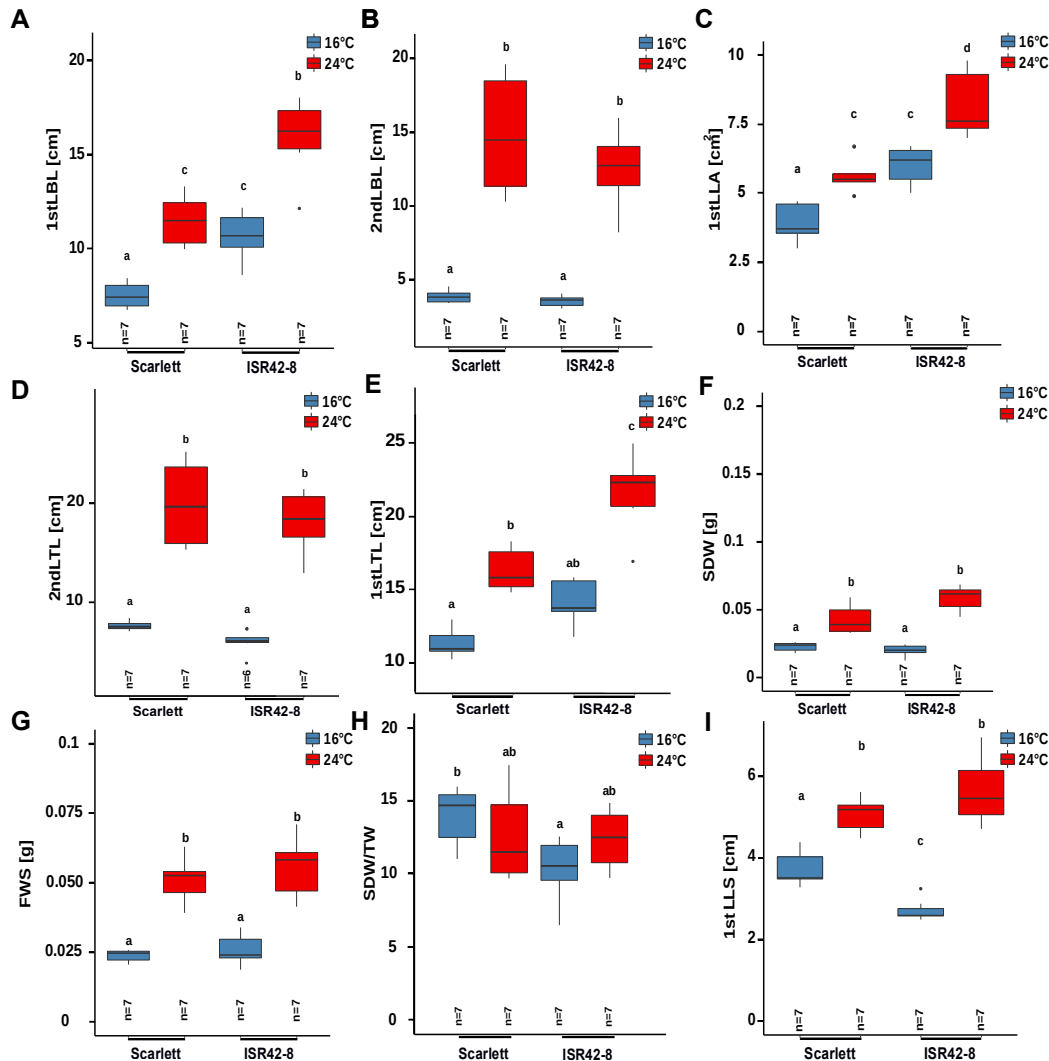
Figure 42. **Shoot growth responses to elevated ambient temperature of the parents of the S42IL population 'Scarlett' and 'ISR42-8'.** Box plots show medians and interquartile ranges of (**A**) length of the first leaf blade (1stLBL), (**B**) length of the second leaf blade (2ndLBL), (**C**) the area of the first leaf (1stLLA), (**D**) the total length of the second leaf (2ndLTL), (**E**) the total length of the first leaf (1stLTL), (**F**) the shoot dry weight (SDW), (**G**) the fresh weight of the shoot (FWS), (**H**) the ratio of the shoot dry weight and the total weight (SDW/TW) and (**I**) the length of the first leaf sheath (1stLTL). Letters denote statistical differences (p < 0.05) as assessed by one-way ANOVA and Tukey HSD. Outliers (greater than 1.5× interquartile range) are shown as black dots. The trait performance of 14d-old barley plants were quantified after 12 days at 24°C or 16°C. Letters denote statistical differences (p< 0.05) as assessed by one-way ANOVA and Tukey HSD. Outliers (greater than 1.5× interquartile range) are shown as black dots. Experiments were performed in LD (16/8h) conditions and light intensity of 470 µmol m^{-2} s^{-1}. The barley seedlings were pre-germinated for 4d at 16°C.

5.2 Trait performances and heritabilities of S42ILs

To assess which traits are particularly variable, the coefficient of variation (CV, standard deviation divided by mean x 100) was calculated. In general, all traits with low CVs (<10%) exhibit low variation between lines, indicating that these traits are not greatly affected by either genotype or treatment or a combination of both. Traits with ≥10% CV warrant further investigation as to the source of variation (e.g. G or E or GxE). Therefore, I primarily searched fo traits with CVs higher than 10% (Lamy et al. 2014) as this facilitates the marker-assisted search for genetic determinants involved in thermomorphogenesis.

Furthermore, high CVs (>50%, defined by King et al. (2015) for 'Scarlett' can cause a risk of low prediction accuracy for some traits. Thus, these traits are rather unfeasible for further analyses. This was not necessary in this case, as for all traits, CVs of 'Scarlett' were inferior (See Supplementary Table S11).

As expected, the phenotypic variation was increased in the S42ILs, quantified with the CV for all 25 traits compared to 'Scarlett' (See Supplementary Table S11). Although CV values ranged only between 20% and 30%, the distribution of CV clearly indicated the presence of phenotypic variability among the selected lines for the observed traits. This highlights the occurrence of diversity within the wild barley gene pool and this might increase the probability to detect genome regions associated with temperature-dependent phenotypes.

CVs lower than 10% for the S42ILs could be observed only for the trait root system depth (RSD) (8.44%) and the ratio of root dry weight per total weight (RDW/TW) (3.86%) at 42°C (See Table, Figure 43A). Using these phenotypic traits for further analysis to find novel regulators seems to be ineffective. More promising for the identification of molecular players involved in barley thermomorphogenesis are the traits with the highest CVs, such as the the total root length (TRL) (23.6%), the number of lateral roots (NLR) (23.72%), and root dry weight (RDW (28.34%). Some traits showed high CV values at 16°C and 24°C (e.g. NLR, root system width (RSW), root angle related traits, shoot dry weight (SDW), fresh weight shoot (FWS), area of the first leaf (1stLLA)) suggesting that these traits are generally highly variable and responsible for other factors independent of temperature treatment. As a result, it has been difficult to identify specific genes or gene regions associated with responses at elevated temperatures.

However, to determine the amount of the phenotypic variation in the given traits can be attributed to genetic variation, the broad-sense heritability (h^2) was estimated. A trait with a low heritability will present an ineffective selection response (Dudley and Moll 1969, Poehlman 1986, Piepho and Möhring 2007), High heritability is necessary for genetic investigations and provides confidence for trustable phenotype-genotype association

mapping. A heritability value >50 % is considered to be high and a value <10 % is considered to be low (Stanfield 1991).

For the QTL detection of the significant genotype x phenotype associations for every trait, I considered only traits with a heritability of h^2 > 10% (Hoffmann et al. 2012). As such, the specific root length (SRL), shoot dry weight (SDW), length of the leaf blade of the second leaf (2ndLBL), root length density (RLD), length of the first leaf sheath (1stLLS), root dry weight per total weight (RDW/TW), and shoot dry weight per total weight (SDW/TW) were excluded in QTL detection. Furthermore, the distributions of these phenotypic trait values in the IL population were skewed (left or right tail) and therefore not gaussian (Supplementary Figure S23-28). The linear regression residuals revealed a nonlinear pattern indicating that the data included outlying observations. This data was therefore subjected to log transformation to warrant the required normal distribution for subsequent analyses. The heritability for the other traits ranged from 14,9% to 75,9% (Figure 43A,B,C, Supplementary Figure S29) with the highest h^2 of the traits the number of seminal roots (NSR), the convex hull area (CHA), and the area of the first leaf (1stLLA).

A

		CHA	LLR/NLR	LSR/NSR	NLR	NSR	RDW	RSAL	RSALR	RSAR	RSD	RSW	TRL
CV	16°C	30.10	40.73	21.30	46.00	**10.27**	25.02	**15,39**	**13,15**	**15,78**	**13,33**	**19,96**	24,458
	24°C	22.95	21.23	**13.83**	23.72	**10.88**	28.34	**17,19**	**14,61**	**17,31**	**8,44**	**17,75**	23,609
h^2	ALL	65.73	14.98	36.07	14.92	62.21	42.68	31,34	41,08	31,70	43,45	54,35	35,491

B

		1stLBL	1stLLA	1stLTL	2ndLBL	2ndLTL	FWS	1stLLS	SDW
CV	16°C	**15,12**	27,07	**16,25**	19,93	**16,25**	26,54	25,44	27,22
	24°C	24,26	24,73	**19,72**	23,21	**19,21**	25,08	**16,33**	89,41
h^2	ALL	17,20	75,87	18,75	**1,06**	22,93	49,48	**7,95**	**5,93**

C

		RDW/TW	RLD	RSD/RSW	SDW/TW	SRL
CV	16°C	**13,16**	58,82	21,17	**13,79**	30,87
	24°C	**3,86**	27,29	23,06	27,14	25,53
h^2	ALL	**8,82**	**6,46**	25,44	**8,82**	**0,19**

Figure 43. Root trait performance of the 48 selected introgression lines to elevated ambient temperature and the underlying descriptive statistic. The phenotypic coefficient of variation (CV in %) and heritability (h^2 in %) estimates for selected root traits **(A)**, shoot traits **(B)**, specified root and shoot traits **(C).** Phenotypic coefficient of variation (CV in %) and heritability estimates (h^2 in %) for selected shoot phenotypes. The lowest CV values and h^2-values lower than 10% are in 'bold' . The CV were calculated by the methods suggested by Burton and De vane (1953) and Johnson et al., 1955a and 1955b. Definition and trait abbreviation are shown in Figure 40.

5.3 Statistical relationships among tested phenotypic traits

5.3.1 Correlation Networks (CorNet)

To account for biases due to different dynamic ranges in the respective trait data, multi-statistical techniques such as Pearson correlation matrix analysis (PCMA), principal component analysis (PCA) and hierarchical clustering analysis (HCA) were performed. At first step, correlograms (See Supplementary Figure S30) and trait correlation networks for both temperature treatments (16°C vs. 24°C) (See Figure 44A,B) according to the matrix of correlation coefficients were constructed for better visualization and interpretation of the relationships among the phenotypic trait. In general, most of the traits for both environments (16°Cvs. 24°C) correlated positively to one another. For both temperature conditions, each of the traits significantly correlated with more than one of the other qualitative traits tested (positiv or negative) (See Supplementary Figure S30A,B). The highest positive correlation represented by thicker edge connections between root traits at 16°C and 24°C conditions was found between the traits total root length (TRL), root dry weight (RDW), convex hull area (CHA), root system depth (RSD) (Figure 44A,B, lila nodes). These root growth related traits correlated not only with each other, but also with the shoot traits area of the first leaf (1stLLA), fresh weight shoot (FWS), shoot dry weight (SDW), which also correlated strongly among themselves (See Figure 44A,B, lila nodes). These results clearly support the assumption of a functional dependency between root and shoot at both temperature conditions. Interestingly, at 16°C conditions the root trait number lateral roots (NLR) was less correlated to the other shoot and root associated traits, while it changed at 24°C (Figure 44A). In contrast to 16°C, NLR, length of lateral roots per number of lateral roots (LLR/NLR) and root length density (RLD) were highly correlated with RDW, CHA, TRL, RSD and shoot traits 1stLLA, SDW and FWS (See Figure 44B, lila nodes). The impact of lateral root growth on the described root and shoot traits seemed to be larger at 24°C. Furthermore, while at 16°C the shoot traits length of the first leaf blade (1stLBL) and second leaf blade (2ndLBL) were highly positive-ly corrleated with the root traits TRL, RDW, RSD, CHA and length of seminal roots per number seminal roots (LSR/NSR), at 24°C conditions shoot traits related to shoot length (total length of the first (1stLTL) and second leaf (2ndLTL), 1stLBL, 2ndLBL, length of the first leaf sheath (1stLLS)) were highly correlated predominantly among each other (See Figure 44B, orange nodes, lila nodes with orange border). In constrast, shoot traits related to biomass production (SDW, FWS) and 1stLLA might be generally highly correlated with root traits RDW, CHA, TRL and RSD, regardless of the temperature treatment.

The highest negative correlation (>0.6) under both conditions was observed between the root system width (RSW) and root system depth per root system width (RSD/RSW) (See Figure 44A,B, red nodes). The root angle related traits (RSAL, RSAR, RSALR) were also slightly negatively correlated with almost all shoot and root related traits independent of the treatment conditions. In general, the root angle related traits (RSAL, RSAR, RSALR)

were only highly positively corrlated among themselves independent of the temperature treatment.

A possible explanation for these results may be the impact of the root angle on root distribution in different soil layers (Gioia et al., 2016). In this context, different studies of root traits in wheat, sorghum, maize, and rice (Manschadi et al. 2008, Mace et al. 2012, Christopher et al. 2013, Uga et al. 2013) noted a link between small angle and high root number as an indicator for deep rooting in the seedling stage. In gerneral, plants have higher water requirements in elevated temperature conditions due to increased water loss by evapotranspiration and decreased water uptake by the root. (Heckathorn et al., 2013).Thus the negative correlation between small angle and high root number which might be a precursor for increase total root length and root system depth seem to be particularly beneficial under elevated temperature conditions with evidence of water-rich soil layers (El Hassouni et al., 2018).

Another difference between both conditions could be found between the relation of shoot dry weight to total weight (SDW/TW) and root dry weight to total weight (RDW/TW). While at 24°C RDW/TW and SDW/TW were highly positively correlated (Figure 44B, green nodes), it was highly negatie at 16°C (Figure 44A, red nodes). Hence, some different temperature response mechanisms seem to be present at elevated temperatures compared to lower temperatures.
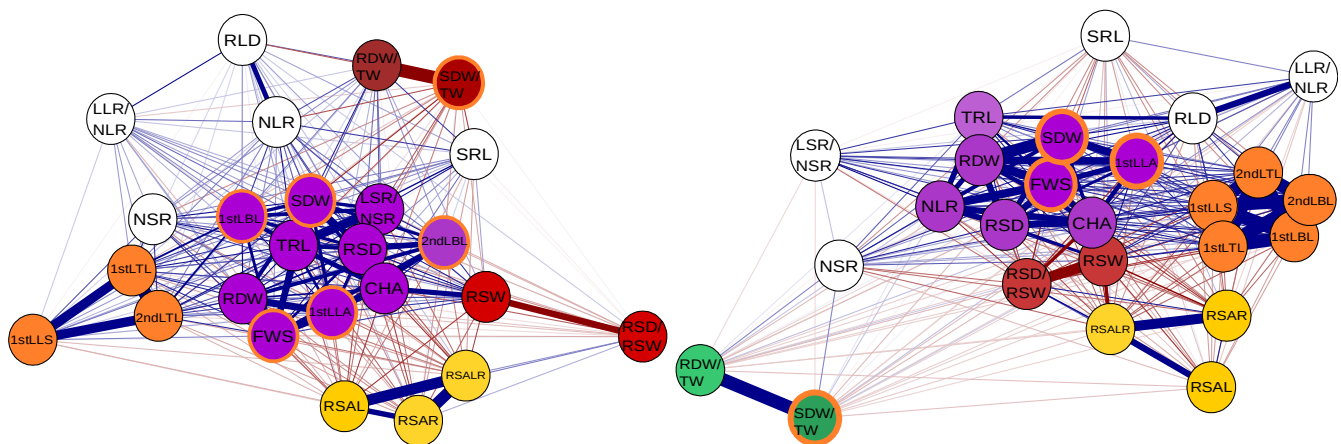
Figure 44. Correlation network for 25 traits. (A) 16°C treatment, **(B)** 24°C treatment. The Pearson correlation was used to estimate correlation coefficients. Spurious correlations were removed, while significant correlations were transformed into network form. Colored circles visualise groups. Lines in blue indicate positive correlations, lines in red indicate negative correlations. Thick lines, |r| > 0.6 (P < 0.01); thin lines, 0.5 < |r| < 0.6 (P < 0.05). All nodes with orange filling color or a orange border. Abbreviations: Figure abbreviation: area of the first leaf (1stLLA), convex hull area (CHA), number of seminal roots (NSR), root system width (RSW), fresh weight shoot (FWS), root system depth (RSD), root dry weight (RDW), root system angle left and right (RSALR), total weight (TW), length of the seminal roots per number of seminal roots (LSR/NSR), total root length (TRL), root system angle right (RSAR), root system angle left (RSAL), root system depth per root system width (RSD/RSW), total length of the first leaf (1stLTL), total length of the second leaf (2ndLTL), length of the first leaf blade (1stLBL), length of the lateral roots per number of lateral roots (LLR/NLR), number of lateral roots (NLR),

Figure 44 (Continued). shoot dry weight (SDW), root dry weight per total weight (RDW/TW), length of the first leaf sheath (1stLLS), root length density (RLD), shoot dry weight per total weight (SDW/TW), length of the second leaf blade (2ndLBL) and specific root length (SRL). Based on data collected from 4d-old pre-germinate ILs seedlings which grew for 12d at 16°C or 24°C in LD (16h/8h) and a light intensity of 470 μmol m^{-2} s^{-1}. Data shown are for 48 genotypes, with n>5 replicates, as means for the experiment in Jülich.

5.3.2 PCA and HCA

Constructed correlation networks provide an overview of the relations between the observed root and shoot traits, revealing groups of correlations that are of particular interest in explaining barley plant temperature responses. To better understand trait correlations and the interplay between leading variables, I then conducted Principal Component Analysis (PCA) and hierarchical clustering analysis (HCA).

The PCA revealed a total of 83.31% of the phenotypic variance in the first two dimensions. This finding showed that root and shoot variability cannot be fully reproduced if only a few root and shoot traits are measured. Most of the separation between treatments was achieved by the first principal component (labeled by PC1) (Figure 45). PC1 accounted for 72.01% of the total variance observed and has positive loadings of roughly equal size on all observed traits except for the root angle related traits (RSALR, RSAL, RSAR) with small positive loadings and number of seminal roots with small negative loadings. The second principal component (labeled of PC2) accounted for 13,01% of the total variance observed and was based primarily on the number of seminal roots (NSR), area of the first leaf (1stLLA) and root system width (RSW). PC2 has negative loadings for root angle related traits (RSALR, RSAL, RSAR) and the ratio of RSD/RSW. Examination of the first two PCA loadings revealed some of the strong correlations among traits in the dataset (Figure 45B) as seen previously in correlograms (Supplementary Figure S30).

The PCA score plot separates the genotypes into two groups along PC2 depending on temperature treatments. The left group contains the genotypes growing at 16°C, and on the right side, those growing at elevated temperature conditions. Thus, in this case PCA was also used as a quality control method to check the reliability of my experimental design. Based on the error lines, there were some outliers that do not cluster according to the temperature treatments (See Figure 45B, arrows).
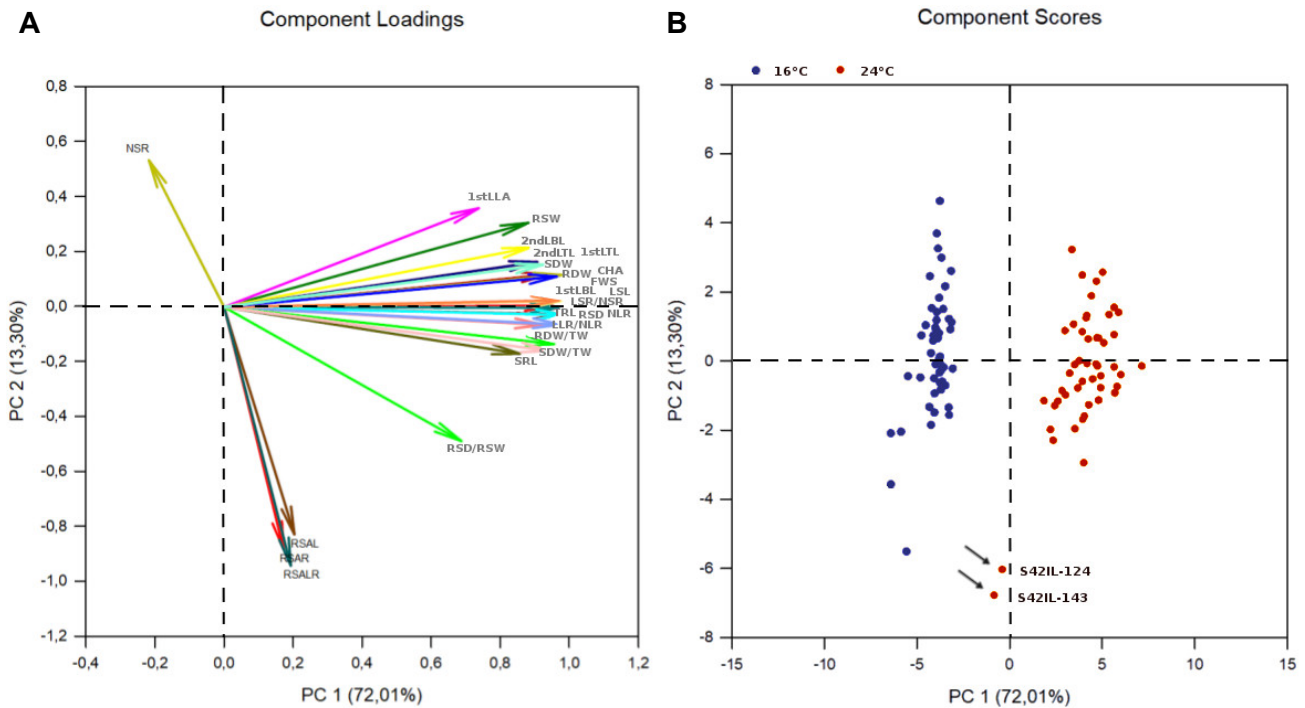
Figure 45. Principal component analysis (PCA) of the difference of all traits of the 48 barley genotypes under 16°C and 24°C. A showed the loading plot for all traits**.** Arrows indicate the loadings for each trait along the first two components, which comprise 85.31 of the total genetic variation for all traits. **B** represents the score plot of PCA expressed by first principle component (PC1) and second principle component (PC2) for classification of all selected ILs for all traits. Based on data collected from 4d-old pre-germinate ILs seedlings which grew for 12d at 16°C or 24°C in LD (16h/8h) and a light intensity of 470 µmol m^{-2} s^{-1}. The genotypes were clustered into two major groups with respect to the treatment response: low temperature barley genotypes (blue), high temperature barley genotypes (red). Arrows marked S42IL-124 and -143 as outliers showing a distinctive profile **A-B** Data shown are for 48 genotypes, with n>5 replicates, as means for the experiment in Jülich which were collected 12d after treatment beginning. PCA was performed using the software SigmaPlot ver. 13 (Systat Software Inc.) based on multiple group analysis, applying ANOVA test.

Cluster analysis confirmed that S42IL-124 und S42Il-143 were well distinguished from all the other ILs in elevated temperature conditions for both root and shoot traits(Figure 45B). Both lines are therefore probably very interesting from a genetic point of view. For the second component no grouping of the lines is visible, the distribution is rather gradual.

However, based on the HCA1 (Figure 46A) using all root traits, the genotypes can be divided into two highly differentiated groups according to their overall performance under the two different temperature treatments (16°C (group I) vs. 24°C (group II)). For the traits number of seminal roots (NSR), root system angle right (RSAR), root system angle left (RSAL), root system angle right and left (RSARL), the temperature effects of some lines seemed to fail to scale with temperature. Most z-scores for the genotypes for these traits diverged from the mean score of the parental line .(See Figure 46A,B, highlighted in black frame in each of the HCAs). As this is not restricted to 24°C, but is likewise evident for 16°C, it seems that these traits are regulated in a temperature-independent manner.

Accordingly, root traits clustered into three distinct groups (columns in Figure 46A groups III, IV, and V). Based on the trait differences, the trait number of seminal roots (NSR) (group III) formed a well- separate group, while the group IV includes the traits which were associated with the root shape (root system angle left (RSAL), root system angle right (RSAR), root system angle left and right (RSALR) and root system depth per root system width (RSD/RSW)). The group IV clustered together with group V containing the other root traits. Overall, most traits, as visualized by the z-score, seemed to be weak and rather similar to the recurrent parent 'Scarlett'.

Similar to the HCA1, the HCA2 (See Figure 46B) genotypes can be split into two highly differentiated groups. Group II represents all genotypes (12) grown under control conditions (16°C), while group I includes genotypes of the 24°C_dataset which clustered close together to genotypes of the 16°C-dataset. Thus, group I includes genotypes where treatments had partially only minor effects on the investigated shoot traits. For the following QTL analyses, I was therefore particularly more interested in group II containing more genotypes with high phenotypic divergence.

In terms of the observed shoot traits, cluster analysis divides the dataset into three distinct groups (Figure 46B, group III, IV, and V). Group III includes only the single trait larea of the first leaf (1stLLA) and was clearly separated from the other groups. Group IV contained only the trait shoot dry weight per total weight (SDW/TW) and clustered together with group V. The traits of group V were connected to biomass accumulation and plant height (See Figure 46B, group V) However, similar to the temperature effects observed for the root traits, the differential temperature responses for the shoot traits were rather weak among the ILs and compared to 'Scarlett' (Figure 46).

According to the PCA, in HCA3 (See Supplementary Figure S29) using all shoot and root traits, most of the traits clustered together, except for the number of seminal roots (NSR) and root angle related traits. The traits length of lateral roots per number of lateral roots (LLR/NLR), specific root length (SRL), root system depth per root system width (RSD/RSW) are also highly separated from the other traits.

Collectively, results showed that temperature impact on barley root and shoot growth was noticeable between clusters. Nevertheless, for these development stages and these populations the differences in trait performance between the ILs compared to 'Scarlett' were mild. Overall performance of the ILs indicated that the traits related to the root angle and the number of seminal roots (NSR) might be regulated independently of the temperature treatments. In contrast, results of the PCA and HCA3 revealed that some shoot traits (e.g. FWS with TRL) could be related to root traits through genetic correlation as described by Bouteille et al. (2012).
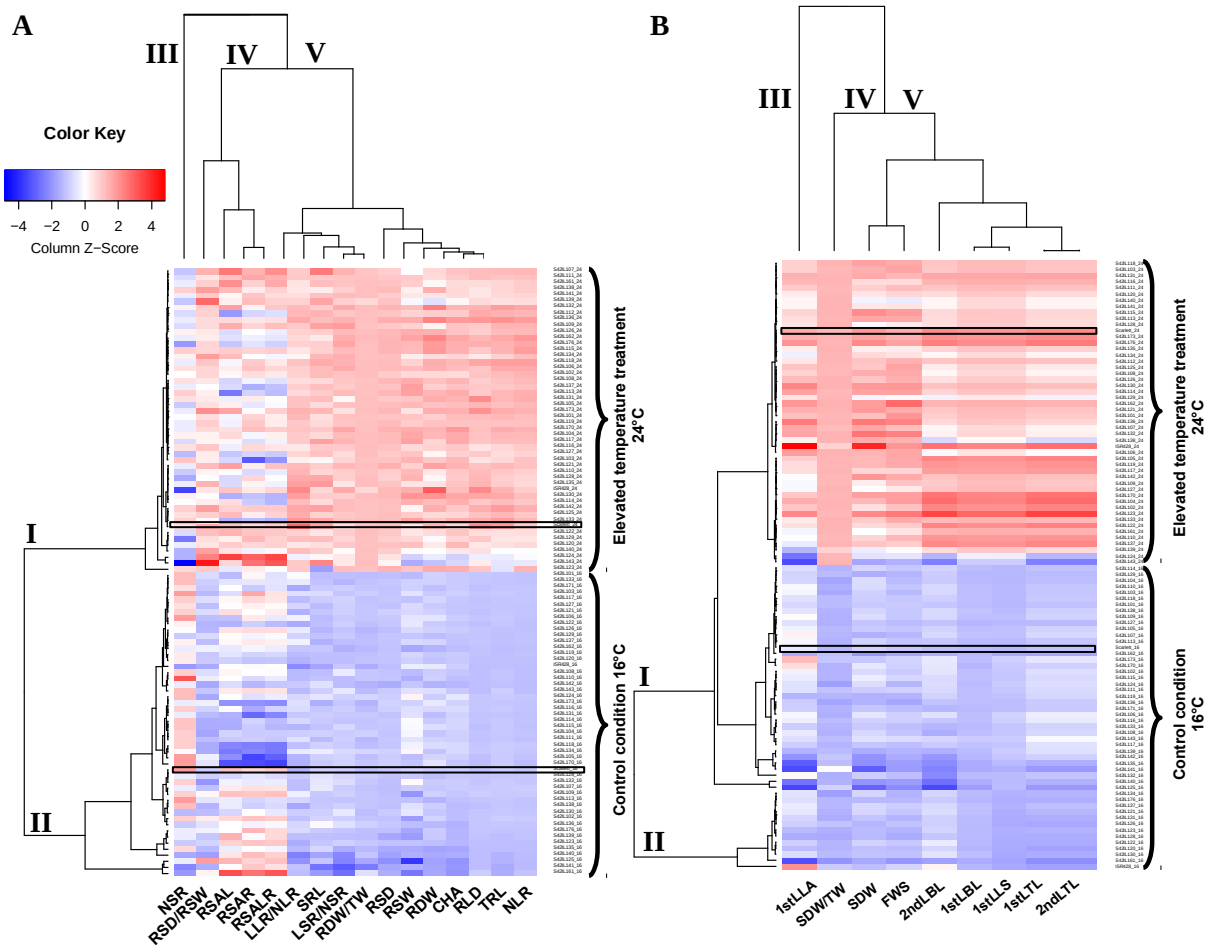
Figure 46. Heatmap and hierarchical clustering for all root and shoot traits in 48 ILs grown under 16°C and 24°C.
A showed the heatmap and hierarchical clustering for all root traits and (**B**) for all shoot traits. Data of each sample were standardised in order to have zero mean and unit variance. This scaled value, denoted as the column z-score, is plotted in red–blue colour scale with blue indicating low value and red indicating high value. Use Pearson distance for clustering. Figure abbreviation: area of the first leaf (1stLLA), convex hull area (CHA), number of seminal roots (NSR), root system width (RSW), fresh weight shoot (FWS), root system depth (RSD), root dry weight (RDW), root system angle leaft and right (RSALR), total weight (TW), length of the seminal roots per number of seminal roots (LSR/NSR), total root length (TRL), root system angle right (RSAR), root system angle left (RSAL), root system depth per root system width (RSD/RSW), total length of the first leaf (1stLTL), length of the first leaf blade (1stLBL), length of the lateral roots per number of lateral roots (LLR/NLR), number of lateral roots (NLR), shoot dry weight (SDW), root dry weight per total weight (RDW/TW), length of the first leaf sheath (1stLLS), root length density (RLD), shoot dry weight per total weight (SDW/TW), length of the second leaf blade (2ndLBL) and specific root length (SRL). Quantitative data used were collected 12d after treatment beginning in the experiment in Jülich. 4d -old pre-germinate ILs seedlings grew for 12d at 16°C or 24°C in LD (16h/8h) and a light intensity of 470 µmol m^{-2} s^{-1}. Parental line 'Scarlett' was marked with a black frame.

5.4 QTL detection based on the Dunnett test

To identify genomic regions involved in the inheritance of phenotypic differences, using introgression lines (ILs) libraries might be a good choice. Since, each ILs contains only one or few well-defined introgressions of a donor parent in an adapted, recurrent parent

background, thus any phenotypic differences between an IL and the recurrent parent can be attributed to a single specific genome segment from the donor parent. This can facilitate to narrowing down the genome search space in shorter time and is therefore also suitable to be used to identify Quantitative Trait Loci (QTLs). One of the objectives of this work was to perform a QTL analysis of various root and shoot related traits of selected ILs of the S42IL population at different temperature conditions (24°C vs. 16°C). With the help of Dr. Andreas Maurer, for detection of putative QTLs, a two-factorial mixed model ANOVA and, subsequently, a Dunnett test with the recurrent parent as a control were conducted with the phenotypic data collected 12d after treatment beginning (after 4d pre-germination at 16°C). Since traits with heritability below 10% are more strongly influenced by environmental factors with very little influence from genetic differences (Beaumont et al., 1997, Sapp et al., 2005), QTL detection was carried out for all traits except for length of the first leaf sheath (1stLLS), shoot dry weight (SDW), root dry weight per total weight (RDW/TW), shoot dry weight per total weight (SDW/TW), specific root length (SRL), root length density (RLD), leaf blade length of the second leaf (2ndLBL) showing trait heritabilities below 10%. However, in total the post-hoc Dunnett test revealed 346 significant line x phenotype trait associations across all traits ($p < 0.05$) for the control treatment and 322 for the elevated temperature treatment.152 of these associations identified in the 24°C dataset (8.71%) and 200 in the 16°C dataset (See Supplementary Table S12,13) (11.45%) were tested as highly significant ($p < 0.001$). As already mentioned in the temperature-induced root elongation (TIRE) assays using *A. thaliana*, since TIRE assays are difficult to interpret, if the plants show already phenotypic responses at the control treatment, I was particularly interested in lines that revealed an insignificant response to control temperature 16°C and a significant temperature reaction at 24°C. 150 line x phenotype associations of 322 putative associations across all traits could be found where the corresponding ILs fulfilled these criteria (~50%). Given that these ILs with - for these traits - significant differences to 'Scarlett' display overlapping wild barley introgressions, they would be ideal candidates for genetic mapping of the causative gene(s). In this case, the overlapping parts of the introgressions would define the target interval on the respective chromosome.

5.5 Location and distribution of QTLs

Next I surveyed the genomic locations of the introgressions of the respective introgression lines (ILs) (Supplementary Table S13). Therefore, I searched for ILs with overlapping or flanking introgression. To identify the physical position of the QTL intervals an existing and widely used barley 9k Infinium iSelect map were used. If these ILs showed

significant effects of the same direction, a single quantitative trait locus (QTL) was assumed to cause the effect. If ILs with flanking introgressions revealed nonsignificant effects or effects in the opposite direction, it was hypothesized that these flanking introgression regions covered adjacent loci. Thus, it was possible to further narrow down the regions of interest. However, ILs with overlapping introgressions, but non-ambiguous significant trait responses, were received. (Supplementary Tables S14A,B). In particular, these lines need to be re-examined. Furthermore, in this QTL analysis, I was specifically interested in identifying QTL hotspots (genomic locations enriched in QTLs) since it was speculated that these regions must be important for elevated temperature responses and thus may harbor genes associated with plant thermomorphogenesis. The QTL mapping results are in the Supplementary Tables S14A,B. They are sorted by trait and by the intensity of the effect compared to 'Scarlett'. Overall, 65 QTLs associated with the tested root traits and 57 QTLs which may regulate the given shoot traits, were identified. Here, QTL were identified for all traits except for RSD. For shoot (14) and root traits (18), the highest number of QTLs were located on chromosome 2H. Thus, genes located on chromosome 2H seem to be very important for regulation of temperature-induced root and shoot growth. In contrast, the lowest number of QTLs (5) affecting root growth responses were found on chromosome 7H and the lowest number of QTLs (2) may have an impact on phenotypic responses related to the shoot were detected on chromosome 4H. Among all QTLs, 11 were found where the corresponding ILs owned overlapping *Hsp* segments and showed statistically significant effects of the same direction (See Figure 47). 15 QTLs were found which were potentially associated with more than two traits (See Tables 15A-H), suggesting QTL pleiotropy (a QTL region affecting more than one trait). These QTL hotspots are distributed over all chromosomes. On chromosome 2H, I detected a large genomic region spanning over 18 cM (33.9-51.9) contains two QTLs only for the shoot traits length of the first leaf blade (1stLBL), total length of first leaf (1stLTL) and total length of second leaf (2ndLTL). The QTLs for these shoot traits were located close together indicating the importance of these regions for regulation of shoot growth in response to elevated temperatures. However, another major finding of this analysis was that several genomic 'hotspots' consist of colocalized QTL for multiple shoot and root traits. For instance QTRL.S42IL.2H, overlapped with Q1stLBL.S42IL.2Hg and QFWS.S42IL.2H on position 120.7-129.8cM (9.1cM), as well as QRDW.S42IL.6H colocalized with QRSD/RSW.S42IL.6H overlap with Q1stLBL.S42IL.6Ha, Q1stLLA.S42IL.6Ha, Q1stLTL.S42IL.6H and QFWS.S42IL.6Ha on position 38-46.7cM (8.7cM). These findings

indicated that specific loci can shape both shoot and root morphological traits, probably through tight linkage of several genes controlling individual traits or a single pleiotropic gene that controls several traits.

Other QTL that have specific effects on root or shoot morphological traits were also found. For example the QTLs QCHA.S42IL.2H, QLSR/NSR.S42IL.2H and QLLR/NLR.S42IL.2H were colocalized on chromosome 2H on position 0-7.8cM and were specifically contributed to the root traits convex hull area (CHA), length seminal roots per number seminal roots (LSR/NSR), Length lateral roots per number lateral roots (LLR/NLR). In contrast, the genome region on chromosome 7H on position 67.8-70.2cM are only contributed to the shoot traits 1stLTL and 2ndLTL. However, the QTLs with the strongest root growth effects were found for the traits total root length (TRL) (-67%) and LLR/NLR (-48%) and the QTLs with the lowest phenotypic variation to 'Scarlett' were detected for the trait number of seminal roots (NSR) (-8%) and root system angle left and right (~11%). Thus, the latter traits appear to be either influenced by fewer gene loci or, in general, there seems to be less variation between the two parents.

However, the QTLs with the strongest and the lowest effects in the shoot growth compared to 'Scarlett' were observed for the trait 2ndLTL (-43%/-15%) and 1stLBL (-42%/-15%). Accordingly, the major QTL associated with the strongest trait effect were QTRL.S42IL.2H/ QTRL.S42IL.4H (-67%), QLLR/NLR.S42IL.7Hc (-48%), Q1stLBL.S42IL.7Hb (-42%) and Q1stLBL.S42IL.6Hc/Q1stLBL.S42IL.6Ha (-35%). Generally, a large number of QTLs with a minor effect (<30%) compared to 'Scarlett' were found. Most of them owned genomic regions of 0.1-15cM, which will be helpful for fine mapping and identifying genes affecting the studied trait. Furthermore, many of the wild barley alleles seem to generally reduce the growth performance at elevated temperatures.

5.6 QTL validation

Results of the QTL analysis clearly showed that the non-invasive medium-throughput root phenotyping method using growth pouches can be used for my purposes to quantify phenotypic variation in shoot and root morphological traits from a set of 48 barley introgression lines of the population S42IL under elevated temperatures. However, due to the limited population sizes used in this QTL detection experiment can lead to underestimation of QTL number, overestimation of QTL effects, and failure to quantify QTL interactions. Thus, to assess if the results are reproducible I repeated the growth assay at first with a selected set of introgression lines (ILs) at the Martin-Luther-Universität Halle-Wittenberg (MLU) with slightly different conditions (growth cabinets with light intensities of max 300 µmol $m^{-2}s^{-1}$ and a different light spectrum), as it was not possible to

repeat the experiment in Jülich. At the MLU, at first only five ILs could be tested. Therefore, the lines S42IL-123, S42IL-109, S42IL-137 and S42IL-129 were chosen, due to their highly different trait performance compared to 'Scarlett' at 24°C in the experiment in Jülich. Figure 48 shows a scatter plot of all data mean values that were quantified for these lines for selected traits (See Figure 48).
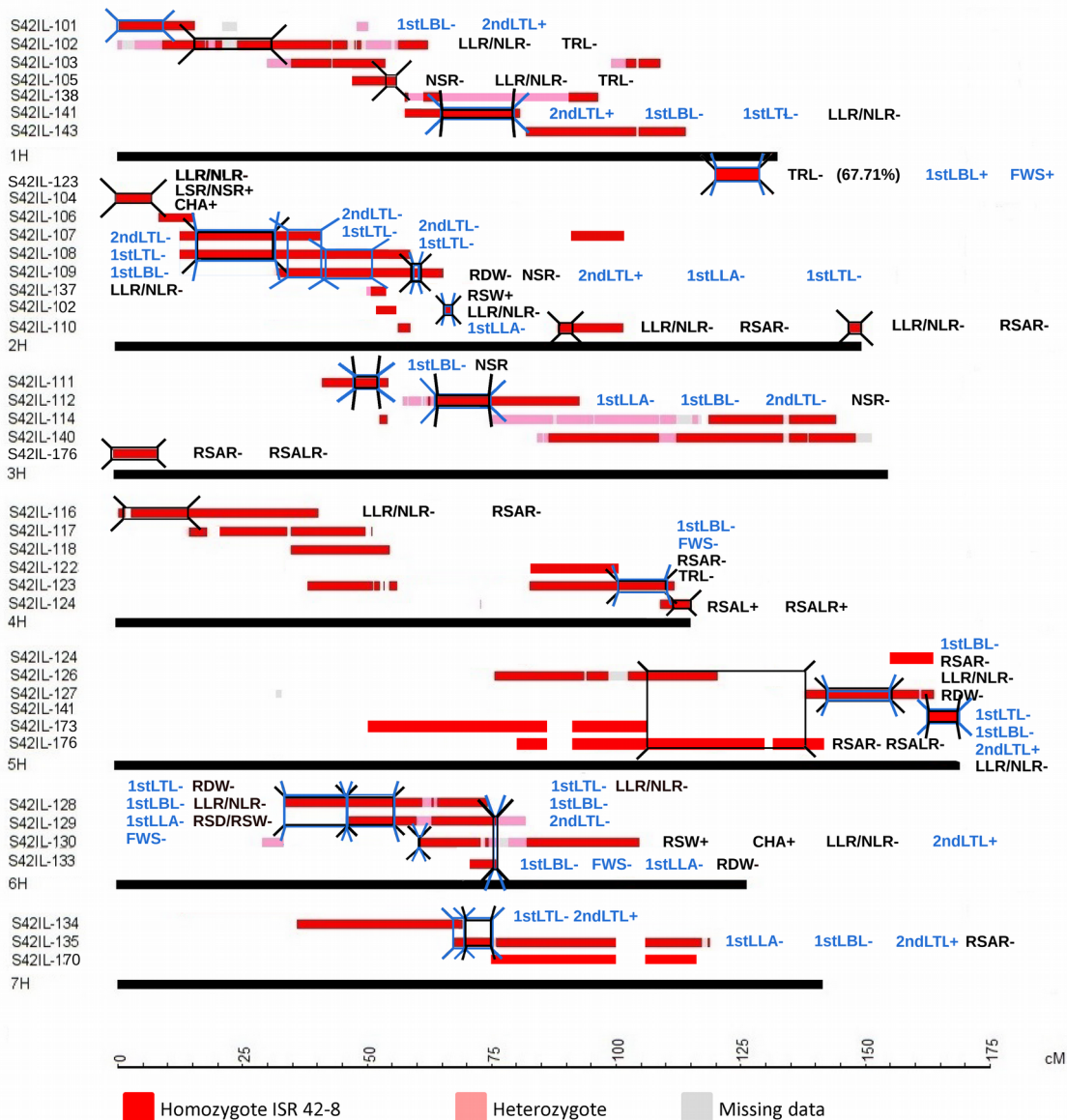
Figure 47. Genetic map with selected S42IL introgressions, QTL, are placed right to the S42ILs (left), indicated by trait abbreviations. Figure abbreviation: area of the first leaf (1stLLA), length of the first leaf blade (1stLBL),total length of the first leaf (1stLTL), total length of the second leaf (2ndLTL), convex hull area (CHA), number of seminal roots (NSR), root system width (RSW), fresh weight shoot (FWS), root dry weight (RDW), root system angle leaft and right (RSALR), length of the seminal roots per number of seminal roots (LSR/NSR), total root length (TRL), root system angle right (RSAR), root system angle left (RSAL), root system depth per root system width (RSD/RSW), total length of the first leaf (1stLTL), length of the first leaf blade(1stLBL), length of the lateral roots per number of lateral roots (LLR/NLR), number of lateral roots (NLR). The sign indicates an increasing (+) or decreasing (-) *Hsp* effect. Blue colored traits are shoot traits and black colored traits are root traits. The putative QTL region is marked with a frame.

Figure 47 (Continued). The map is based on the results (mean values) of QTL analysis using the data collected in Jülich. For the data collection 4d-old pre-germinate ILs seedlings grew for 12d at 16°C or 24°C in LD (16h/8h) and a light intensity of 470 µmol m^{-2} s^{-1}.

To ensure reproducibility and reliability of the results of the first phenotypic screen, only the values of those traits were considered, where the lines S42IL-123, S42IL-109, S42IL-137 and S42IL-129 showed significant differences to 'Scarlett' in the first QTL analysis. The correlation coefficient near 1 (R=0.89), based on Pearson correlation of all trait responses quantified at 16°C and 24°C of, revealed that certain similarities exist between the two repetitions. However, the increase in the fresh weight of the shoot (FWS) and reduction in the length of the first leaf blade (1stLBL) under elevated temperatures observed in the line S42IL-123 and the significant reduction in 1stLBL measured in the line S42IL-129 were not reproducible. Furthermore, some of the lines tested showed significant trait effects that they did not show in the first experiment in Jülich (See Supplementary Table 17,13,19). The difference in response may be due to changes in experimental conditions at MLU.
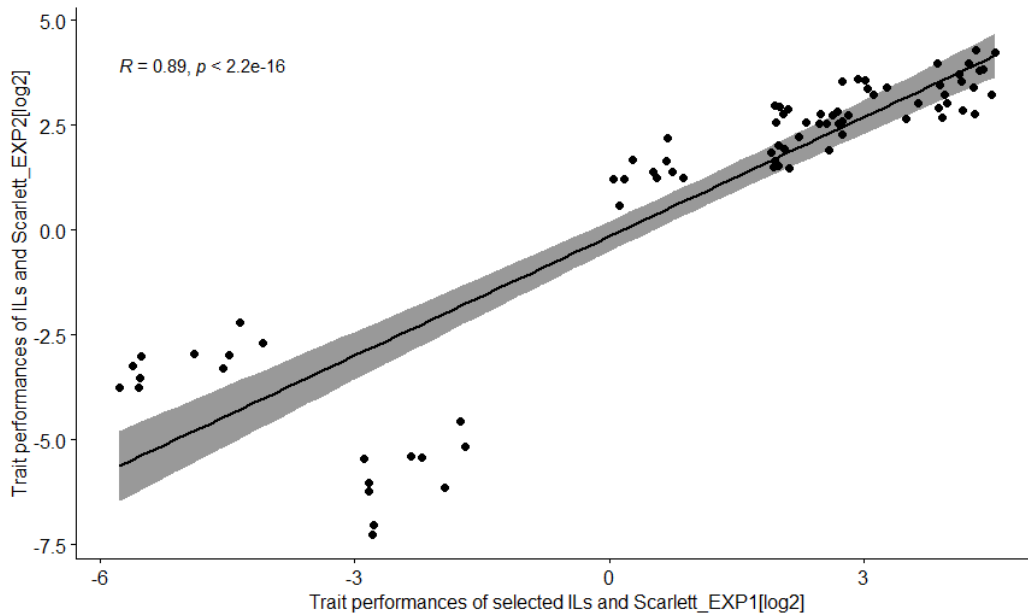
Figure 48. Cross-experiment comparison. Pearson's scatterplot with linear regression showing the correlation (and 95% confidence interval of the regression line= grey shape) between mean data (log2 transformed) collected in Jülich and Halle for the ILs S42IL-109, -123, -129, -137 and the parental line 'Scarlett' for the relevant traits with significant effects in the experiment in Jülich (number of seminal roots (NSR), total root length (TRL), root system depth per root system width (RSD/RSW), root system width (RSW), root dry weight (RDW), fresh weight of the shoot (FWS), total length of the first leaf (1stLTL), area of the first leaf (1stLLA), length of the first leaf blade(1stLBL). Correlation coefficient r is 0.89 with a significance level of $p< 2.2e^{-16}$.

However, some of the trait responses could be validated (See Supplementary Table 19). Finding significant effects in both phenotypic screens for some ILs and specific traits substantiates the assumption that genes in the corresponding QTL regions could be

associated with response to elevated temperature. The other putative QTL regions still need to be also confirmed.

Although in the corresponding association studies the size of the introgressed regions could be successfully reduced to an interval of arround 20 cM (around 40 Mb), the genomic regions of interest still contain hundreds of genes. Therefore, a speculation of candidate genes is not done at this point. Hence, in the future, fine-mapping of the validated QTL regions should be conducted to narrow down the target region under elevated temperatures to identifying promising candidate genes and pave the way for a better understanding of the molecular mechanisms underlying root elongation at elevated ambient temperatures in barley.

In summary, the present study was aimed to systematically profile root and shoot architecture traits in barley seedlings in response to elevated temperatures. The phenotypic evaluation has shown that barley root and shoot growth are both temperature sensitive. Generally, high temperature seems to affect growth in a positive manner. The development of the root angle, however, seems to be independent of the temperature treatment. By using a set of wild barley ILs population (S42ILs) for the phenotypic evaluation, I was able to perform QTL analyses with the phenotyped genotypes and get first access to the genetic basis of the underlying mechanisms of temperature responses in barley. A total of 112 putative QTL regions were identified in the present study, responsible for different root and shoot traits at elevated temperatures. The differences between the parental lines of an ILs population were mild, but more pronounced in the individuals of the ILs population. The next step is to fine map the region and narrow the chromosomal location harboring the QTL.

6. Discussion and outstanding questions

Long-term climate changes are expected to negatively affect our wild habitats and global agriculture. For example, Peng et al. (2004) projected that the crop yield would be reduced by 10% for each 1 °C increase in growing-season minimum temperature. That is a problem since elevated temperatures over a long period are supposed to be much more frequent in the coming decades and thus could threaten the global food supply. To reduce the impact of these changes, it is necessary to understand how plants respond to warmer temperatures. More accurate phenotypic data are required to improve the capacity of appropriate mathematical models to simulate climate change scenarios and better predict future phenological shifts in plants. Based on this knowledge, farmers can plan for sowing, protection, harvesting, and other field activities to avoid negative weather

effects and yield losses. Just as important for plant breeders, if not more so, is a solid knowledge about the molecular mechanisms underlying plant temperature responses to develop more resilient and efficient crops. The combination of genetic and phenotypic analyses could help us to project a species' full potential to adapt to elevated temperatures.

At the phenotypic level, shoot growth responses to higher ambient temperatures of at least the model species *A. thaliana* are generally well documented and functionally understood. In contrast, there are still many open questions at the molecular level. We have only begun to understand how plants sense temperature changes and translate this information into phenotypic features.

At the beginning of my thesis work, the Basic Helix-Loop-Helix (bHLH) transcription factor PHYTOCHROME INTERACTING FACTOR 4 (PIF4) was considered the central hub in regulating thermomorphogenesis (Koini et al., 2009). It turned out that PIF4 acts as a positive regulator in cell elongation, but also that its activity is regulated by various other environmental signals, including light, circadian clock, and phytohormones (gibberellic acid, brassinosteroid) on both transcriptional and post-translational levels. ELONGATED HYPOCOTYL 5 (HY5) and EARLY FLOWERING 3 (ELF3) were identified to act as negative regulators of PIF4. In addition, first studies had suggested that the red/far-red light receptor phytochrome B (phyB) could also integrate temperature signals in *A. thaliana* (Johansson et al., 2014, Legris et al., 2016). In 2017, two years after starting my work, Ibanez et al. (2017) highlighted the importance of brassinosteroids for temperature-induced hypocotyl growth in addition to auxin. It is not yet clear whether the same signaling pathways play a role in cultivated crop plants. The finding that H2A.Z-nucleosome-mediated temperature responses in the monocot model species *Brachypodium distachyon* are similar to those observed in the eudicot *A. thaliana* (Boden et al., 2013) suggests that at least some of the main molecular pathways underlying thermomorphogenesis are functionally conserved.

In recent years we have seen considerable progress in thermomorphogenesis. During my Ph.D. work, many new discoveries have been made across diverse areas of thermomorphogenesis. In general, most of these findings gained about thermomorphogenesis signaling originated from studies that mainly focussed on the model phenotype of temperature-induced hypocotyl elongation (TIHE). Other plant organs, such as cotyledons or roots, were rather neglected. Whether all above-ground organs are autonomously able to sense and respond to temperature stimuli or whether both processes might be spatially separated was unknown. Furthermore, hardly any research has been carried out on whether roots can sense temperature independent of the above-ground tissues. Although a few studies on root thermomorphogenesis have

meanwhile been published (Hanzawa et al. 2013, Heckathorn et al., 2013, Yang et al. 2016, Wang et al., 2016, Martins et al. 2017, Feraru et al., 2019, Luo et al. 2020, Kim et al. 2020, Gaillochet et al. 2020, Calleja-Cabrera et al. 2020, Lee et al. 2021, Parveen et al. 2021), there has so far been no answer to these questions.

In general, root phenotyping techniques, also for crops, have impressively evolved during the last decades. They can now be used to provide new insights in research directed towards the processes of temperature-induced root growth. For example, high resolution, live imaging of maize root tips provided evidence for root zone-specific temperature responses (Nagel et al. (2009). It was also already known that auxin could be involved in temperature-induced root growth. In this regard, Taiki Hanzawa et al. (2013) demonstrate that under high temperature, roots counterbalance the elevated level of intracellular auxin by promoting shoot-ward auxin efflux in a PIN-FORMED2 (PIN2)-dependent manner. Parallel to my investigations, several other groups have started research in this field and published first results, which support the involvement of various molecular pathways in the regulation of temperature responses in the root (Yang et al., 2016, Martins et al., 2017, Feraru et al., 2019, Gaichochet et al., 2020, Lee et al., 2021). The results of these studies, however, highlight the complexity of the mechanisms regulating root thermomorphogenesis.

The purpose behind my thesis was two-fold; The first and main objective was to investigate the mechanistic details of moderate temperature-induced shoot and root growth in the model plant *A. thaliana*. In a second part, a specific barley mapping population should be phenotypically characterized in response to elevated temperatures to gain first insights into the relationships between genetic constitution in monocot crop plants and temperature-induced phenotypic responses.

However, ambient temperatures affect all stages of plant development between germination and senescence (reviewed by Lippmann et al. 2019). While in *A. thaliana* the processes at the seedling stages are well described (See Ludwig et al. 2020), most of the studies on monocot crops, such as barley, investigated the morphology changes that happen during Seed germination (Purvis et al., 1934, Sudia et al., 1959, Sung et al., 2005, Hosseini et al., 2017) and reproductive growth (See review Jacott and Boden et al., 2020) at different temperatures, especially during flowering. In my work I have therefore focused on root and shoot responses to elevated temperatures at juvenile vegetative stages of barley plants, as less is known about the growth responses at this phase. The vegetative phase is defined as the period from Seed germination to the start of

flowering (in relation to barley the time of spikelet initiation in the main apex) (See thesis of Gomez-Macpherson et al., 1993). During the vegetative phase, plants are predominantly engaged in carbon capture through photosynthesis that will be needed as a resource for flowering and reproduction. In the vegetative growth stage, above-ground biomass accumulation is due to leaf and stem production. Thus, phenotypic changes in traits related to leaf shape and size are relevant parameters for this stage. As my main focus was on exploring temperature responses in barley roots, only few specific barley shoot traits were analyzed as well (See Figure 40). I will discuss some of these traits and the underlying mechanisms in the shoot, as also later for the root, here in detail and try to compare these processes between the two subjects of my studies, *A. thaliana* and barley. However, a comparison between both species is difficult, especially for the mechanistic parts, because the current knowledge has been acquired mainly by studies on *A. thaliana* and cannot be easily transferred to barley. On the other hand, there is a great lack of systematically generated data documenting and trying to explain growth responses in *A. thaliana* at elevated temperatures. Consequently, due to the fragmentary data situation, not for each of my investigated root and shoot traits in barley, experimentally validated results in *A. thaliana* could be found and discussed here. In this case, I will give some theoretical assumptions trying to close the gap between the visible morphology changes and the functional relevance for the observed model plant organisms in response to elevated temperatures. I have tried to summarize the results visually in Figure 50.

6.1 Physiological responses of barley and *A. thaliana* at elevated temperatures

6.1.1 Shoot traits

When young *A. thaliana* seedlings are grown at warmer temperatures, they show several morphological changes in the shoot, which have been well described. For example, to protect leaves from overheating and damaging: *A. thaliana* tends to elongate and stretch their hypocotyls away from heated soil (Gray et al., 1998), petioles lengthen (van Zanten et al., 2009), and leaves show upward leaf movement (hyponastic growth) (Patel & Franklin, 2009). These morphological adaptations all serve to enhance evaporative leaf cooling, and thus survival. In general, my phenotypic evaluation revealed that in some cases, barley and *A. thaliana* show similar effects in shoot and root growth at increased temperatures. However, as the following explanations show, the biological relevance of these temperature responses for the plant is likely to be species dependent.

This can be explained by the different anatomical characteristics of both plant species (e.g. homorhizic and allorhizic root systems).

- **Plant height**

I observed increased plant height at elevated temperatures in the 16d-old barley cultivars 'Scarlett' and 'ISR42-8' compared to the lower temperature. In contrast to *A. thaliana*, where plant height seems to have limited functional importance for the reproductive stage (Ibanez et al., 2017), increased plant height significantly affects the final grain yield in most cereal crops such as barley. This is because the stem of the cereal crop will be used as a reservoir for assimilates for grain development during the post-flowering period and thus plays also an important role in maintaining the rate of grain filling against post-flowering stresses like heat (Edmeades and Lafitte, 1993, as cited by Karuma et al., 2014; Sebetha et al., 2015). However, my measurements were taken on young barley plants (two-leaves stage, 16d after sawing). Campbel and Read (1968) and Begum et al. (2014) observed a shorter plant height at later development stages of wheat under higher temperatures. Similar responses were described by Rao and Wattal (1986), Hemming et al. (2012) and Dixon et al., (2019) in barley at later development stages and higher temperatures. The reduced plant height at later stages at elevated temperatures might be associated with the accelerated growth, earlier flowering and a higher number of ears per plant (Drebenstedt et al. 2020). At stages of floral development, the assimilates pre-stored in vegetative tissues are remobilized and transferred to the developing grains (Hemming et al., 2015). Thus, growing taller at later development stages to escape from a hot soil surface probably plays a minor role for an already high-growing plant-like barley. However, it seems relevant, if at all, only at the beginning of plant development when damaging young plant tissues by heat is likely lethal for the whole organism. For plants growing close to the ground, where the leaf cooling effect by wind or airflow is limited, already small differences in length, especially at earlier growth stages, may enable the seedling to escape elevated temperatures, which directly translates to a fitness advantage.

Besides directional growth away from the warm soil surface, in *A. thaliana*, an open rosette structure that promotes evaporative leaf cooling was observed (Crawford et al., 2012*)*. Although barley does not show a comparable rosette-like leaf formation, a more open plant architecture in barley could also be achieved by lengthening barley leaf sheaths or increasing internode length at elevated temperatures. Indeed, at the two-leaf stage, the first leaf sheath was significantly

increased at elevated temperatures before establishing the first visible internode. However, whether this phenotype is retained in later stages is unclear because my experiments were stopped after the two-leaves stage.

- **Leaf morphology changes**

Leaves are the main organ responsible for photosynthesis and thus important for the survival and growth of a plant. Elevated t*emperatures* also modulate *leaf* growth in *A. thaliana and* wheat. In the adult phases of vegetative development before undergoing a transition to reproductive growth, *A. thaliana* (Casal et al., 2013, Pantazopoulou et al., 2017) and wheat plants (Chakrabarti et al. 2013) showed reduced leaf area in response to elevated temperatures. For *A. thaliana*, it will be suggested that this morphology change could be a strategy to compensate for the temperature-induced increase in the rates of net photosynthesis, respiration, and metabolism and to balance it to the surrounding resources such as water, CO_2, and nutrient availability (reviewed by Lippmann et al., 2019). However, whether the decrease in leaf area in wheat also results in reduced photosynthesis rates in high temperatures is still elusive. In contrast, in the earlier vegetative stage of barley plants (two-leaves stage), a slight increase in leaf area at elevated temperature was measured (Figure 41), similar to Tamaki et al. (2001) in young wheat seedlings. Similar observations have been reported for *A. thaliana* and soybean seedlings (Alsajri et al., 2019; Vile et al., 2012). Thus, it seems that there are differences in temperature responses at the different plant growth stages.

The temperature-induced increase in leave (source) area during the seedling stage in barley, soybean and *A. thaliana* could be explained by higher demand for photo-assimilates in the rapidly growing roots (sink) (Hurewitz and Janes et al., 1983). As the leaf area increases, a greater photosynthetically active surface area becomes available. This is more important for plants in earlier developmental stages, where only few leaves are available to carry out photosynthesis. Highest light absorption may be achieved when the ground is completely covered with green leaves, and thus, a maximum of light can be absorbed (Goudriaan, 1995). There is little overlap between neighbouring leaves at the two-leaf stage in barley and *A. thaliana*, reducing light capture and photosynthetic interception activity. A higher investment of plants in maximization of their leaf area to allow greater access to light may still be beneficial for the plant at this stage.

In general, an increase in leaf area could be achieved by increasing the length or width of the leaves (Power et al., 1967, Bahmani et al., 2000 Evers et al., 2006). However, under my experimental setup, the width of young barley leaves did not change markedly under

elevated temperature conditions (data not shown). Although plants with wider leaves will accumulate leaf area more quickly (Gallagher, 1979), which are more likely to be an advantage for plant photosynthesis and resource capture (Forgiarini et al., 2015), wider leaves are considered a negative trait due to increased transpiration area and shading of the neighbouring leaves (Craw et al., 2004, Deák et al., 2011). Furthermore, Tozer et al. (2015) suggested that wider leaves in cereal crops reach critical lethal temperatures faster and experience leaf death earlier than narrower leaves.

Therefore, it was expected that in warmth, a narrower leaf form is generally more able to reduce water loss (Givnish & Vermeij, 1976, Givnish, 1979). Thus, barley seems to adapt to elevated temperatures by developing narrower and longer leaves, as I also observed in my experiments (See Figure 41)(reviewed Lippmann et al. 2019). Furthermore, as *A. thaliana* displayed a narrow leaf phenotype at elevated temperatures (Vile et al., 2012), this may be a generally conserved trait for temperature mitigation.

Furthermore, it seems that less branched veins as they are found in barley leaves, bring an evolutionary advantage in response to warmth. For example, measurements of convective heat transfer in *Phaseolus vulgaris* and spring barley indicated that uneven leaf surface with dichotomously branched veins can slow down the heat transfer to the outside of the leaf compared to more simply constructed barley leaves with linear, unbranched veins (Albrecht et al., 2019). Thus, it could be speculated that barley leaves are generally better adapted to elevated temperatures compared to eudicots such as *A. thaliana*. This could also be a reason why less temperature-induced morphology changes in barley leaves compared to *A. thaliana* at elevated temperatures were observable.

The temperature-induced hyperelongation of leaves of young barley plants were also reported earlier by Kirby et al. (1982), Natr and Natrova (1992), Bultynck et al. (2004). However, a similar response of *A. thaliana* leaves under elevated temperatures at this developmental stage could not be detected (Thingnaes et al., 2003). For barley, it appears to be an efficient strategy to maximizing leaf area for assimilate production while minimizing water loss.

Besides increasing leaf area, I measured a slightly enhanced biomass accumulation at elevated temperatures in the shoot at 16d after sowing in 'Scarlett' and 'ISR42-8'. Furthermore*, Alsajri et al*. (2019) also described an increase in plant height, leaf area, and dry weight during the seedling stage for soybean at elevated temperatures. Hence, the observation of increased shoot biomass could be a welcome carbon source for

accelerated root growth at elevated temperatures. However, nothing is known about equal measurements in young *A. thaliana* plants.

- **Leaf movement**

In *A. thaliana*, the elevated temperature has been shown to result in differential petiole growth-driven upward leaf movement (hyponastic growth) (van Zanten et al., 2009). It was proposed that this flexible and reversible temperature-induced nastic movement of leaves is used to position the photosynthesizing tissues away from heated soil. Although I did not examine leaf movement at elevated temperatures in barley, I will present some theoretical considerations concerning this issue in the following.

Since barley lacks crucial leaf structures such as petioles, this species is generally not able to perform a leaf movement equivalent to that in *A. thaliana*. While in *A. thaliana*, petioles flexibly connect the leaf blade to the stem, the sheath of barley plants wraps around the stem to which the leaf blade is adjacent. The ligular region between the blade and sheath consists of ligule and auricle (See Figure 49) and establishes the leaf angle. It is known that cereal crops like barley can adjust the ligular region in response to external stimuli. This could be beneficial for canopy photosynthesis or leaf cooling (See reviews by Trenbath and Angus, 1975, Ledent, 1974, McMillen and McClendon, 1979). However, fast, flexible and frequent adjustment of the leaf angle as observed in *A. thaliana* has not yet been described and would most likely be anatomically difficult to realize. Leaf cooling via changing leaf angle in barley seems to be rather a long-term response since changes appear to be non-elastic and irreversible. Generally, an optimal plant architecture in cereal crops with high photosynthetic efficiency will be achieved when upper leaves develop smaller leaf angles (resulting in more erect leaves), and lower leaves are standing in larger angles (Duncan, 1971, Long et al., 2006, Ku et al., 2010, Zhu et al., 2010). This ensures that, with a higher plant density, more sunlight still reaches the lower leaves, especially in the later vegetative stages (Li et al. 2020). Interestingly, the downward movement of barley leaves and thus the increase of the leaf angle may be faster at elevated temperatures (Ledent et al., 1975). It is conceivable that this process is supported by the considerable lengthening of the leaves and the accompanying weight that pulls the leaf downwards.
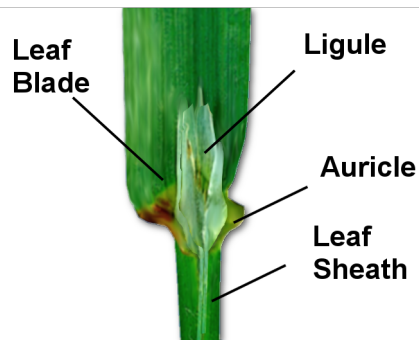
Figure 49. Illustration of barley leaf characteristics. Structure of a barley leaf, comprising the sheath and blade, the ligule and auricles.

Another possibility for leaf movement in barley is to avoid the heat load of leaves and reduce leaf transpiration (Lafitte, 2003), which is described in many important cereal crops, including sorghum, maize, rice and wheat reversible process of leaf rolling. Leaf rolling is the transverse rolling of the leaf lamina along the mid axis (Sarieva et al., 2010). Nevertheless, this specific phenotypic trait was also not part of my analysis.

To sum it up, the results of the shoot analysis in this work and observations from earlier studies suggest significant differences in morphological responses to elevated temperatures between *A. thaliana* and barley during the seedling stage, but also between the seedling stage and reproductive stages. Being only distantly related species, this was not surprising. Interestingly, there are also similarities between species during early juvenile development. Common to both *A. thaliana* and barley is their accelerated growth at elevated temperatures, which is partially driven by a faster metabolism through a higher assimilate supply. Improved assimilate production in *A. thaliana* and barley could result in better photosynthetic efficiency due to the leaf area expansion at elevated temperatures. However, further studies, specifically related to metabolism, photosynthetic rates, and transpiration in younger development stages, are required to to gain a better understanding of the underlying process.
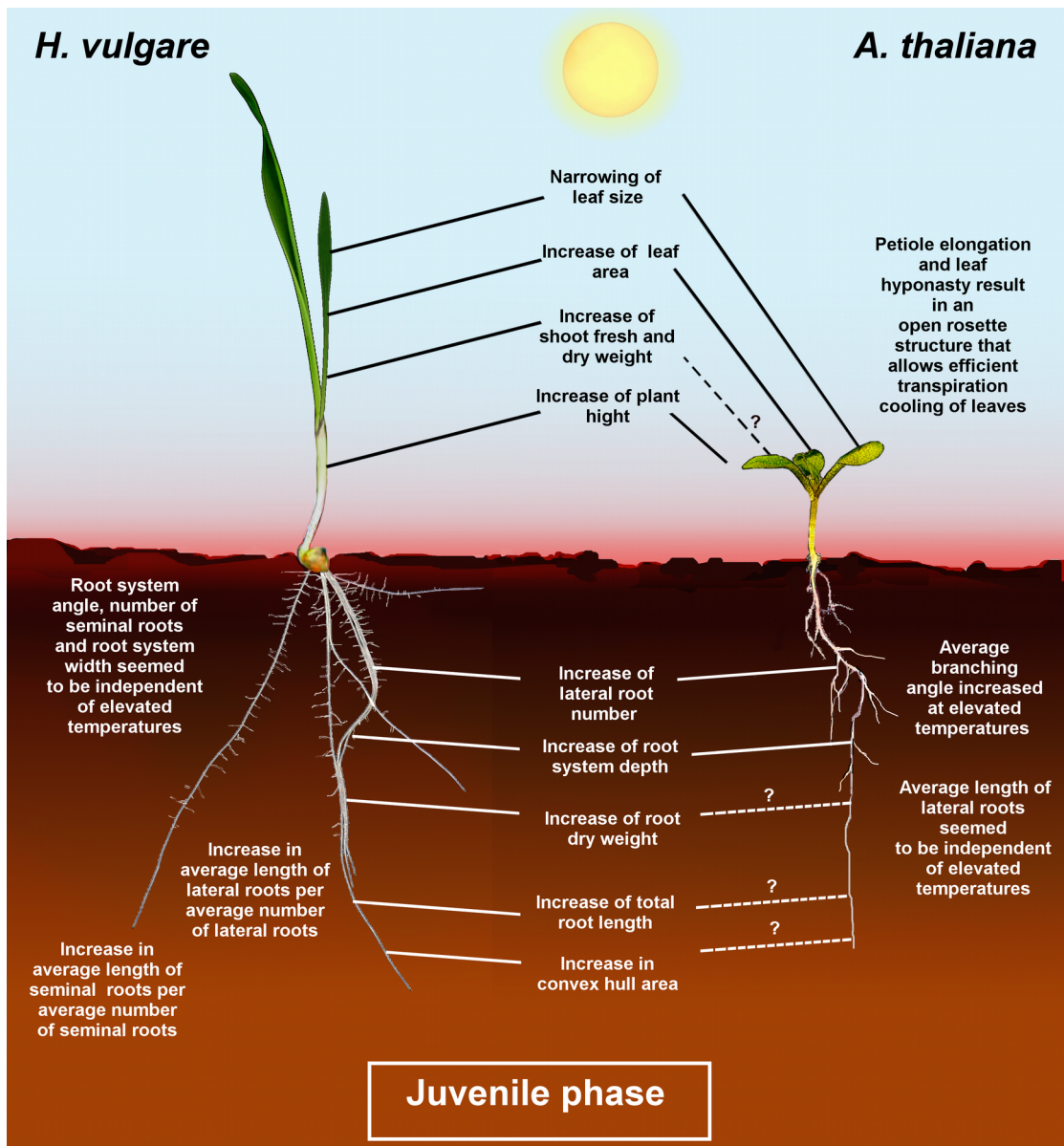
Figure 50. Comparison of selected growth morphology changes in root and shoot at elevated temperature in _A. thaliana_ and barley seedlings. On the left is an illustration of a representative barley plant and on the right is an _Arabidopsis thaliana_ plant in the juvenile phase. If no line is present, this is a species-specific barley or Arabidopsis phenotypic response. The solid lines indicate commonalities in phenotypic answers. Dashed lines with question marks present ambiguous specifications.

6.1.2 Below-ground changes

In contrast to the above-ground parts of the plants, we know much less about how the root system may respond to temperature changes, especially in monocots. Thus, I started Chapter III to systematically profile root architecture traits for a population (S42IL) consisting of genome-wide introgressions of the wild barley accession 'ISR42-8' into the 'Scarlett' background. To compare temperature responses in the root between barley and _A. thaliana_ is much more difficult than for the shoot due to the lack of published data about root thermomorphogenesis in both species. For some traits it was nevertheless tried.

Finally, I will provide some speculations in this section relating the relationships between structure and function of morphological changes observed in barley.

In the first temperature response experiments with 'Scarlett' and 'ISR42-8' in Jülich, I quantified 16 root traits at the seedling stage. I observed that the root angle between the two most outer seminal roots and the number of seminal roots were not affected by elevated temperatures in the investigated cultivars and the observed age. Similar to my experiments on barley, Nakamoto et al. (1991) observed that the seminal root angle in maize at root initiation was not significantly different between 18-32°C when the root grew under well-watered conditions as in my experimental conditions. In contrast, the initial angle was significantly smaller with reduced water content. Thus, Nakamoto et al. (1991) concluded that the soil water availability primarily affected the size of the root angle. Increased temperature, in turn, affects the water content in the ground and thus indirectly determines the root angle. It will be expected that at elevated temperatures and higher evaporation, the water use rate of the plants will be increase and the soil water reservoirs will depleted more rapidly. In general, a steeper seminal root angle in wheat and barley is often associated with a more compact root system and allocation of more roots to deeper soil layers, as observed at drought (Kirschner et al., 2021). In contrast, a higher root angle may enable the plant to penetrate a larger volume of soil and can therefore access nutrients over a larger area (Kirschner et al., 2021).

However, the number of seminal roots in barley and wheat appeared to play a minor role under well-watered conditions (Richards and Passioura, 1989). Hence, similar to the root angle, the temperature seems to have, if at all, only an indirect influence on the development of seminal roots by affecting the soil water content (Richards, 2008, Reynolds and Tuberosa, 2008). Furthermore, the number of seminal roots in barley and wheat seems to be largely under genetic control (Goss et al., 2010). In general, finding barley mutants affecting seminal root angle and number in barley seems like a challenging task. (Robinson et al., 2016).

- **Root system depth and width**

In accordance with the experimental findings of other groups, I could show that elevated ambient temperatures strongly affected root depth and root system width (See Figure 42, Macduff et al., 1986, Gladish et al., 1993, McMichael ·et al., 1998, Alvarez-Uria et al., 2007, Nagel et al., 2009, Yang et al., 2016, Martins et al., 2017, Bellstaedt et al., 2019, Luo et al., 2020). Root depth tends to increase with elevated temperatures until a species-specific threshold (Bellstaedt et al., 2019,

Nagel et al., 2009, Mcmichael and Burke, 1998, Glinski and Lepieck, 1990, Cooper, 1973, Pearson et al., 1970, Brar et al., 1970). The most common 'motivation' for roots to grow deeper at elevated temperatures is related to water availability. The increase in temperature is usually accompanied by a reductions in water availability (Nord and Lynch, 2009). Since the uppermost soil layers are highly affected by water losses (because they are closest to the sun), roots aspire to achieve deeper layers with higher soil water content.

However, I See this phenotype also at an optimal water supply in both *A. thaliana* and barley (See Figure 42). Thus, an alternative hypothesis for the temperature-induced hyperelongation of the root is based on the observation in *A. thaliana* that older roots suberize over time. Suberized roots of *A. thaliana* have more difficulties in water absorption than unsuberized roots (Taiz & Zeiger 2002). Roots increase apoplastic barriers and take up less water with age and exposure to dry soil (Steudle, 2000). The main zones of water uptake are young root tips (Sanderson, 1983, Haussling et al., 1988, Peterson et al., 1993; Varney et al., 1993, Kramer and Boyer, 1995). All roots, therefore, depend on being able to rejuvenate their base. Models show greater water uptake in *A. thaliana* when only small parts of the root system are unsuberized (e.g., when only root tips are unsuberized) because there is greater hydraulic conductance along the root axis compared to largely unsuberized root systems (Zwieniecki et al., 2003, Comas, 2013). Furthermore, it seems that the suberization rate in *A. thaliana* occurs faster at elevated temperatures (Kuhns et al., 1985). Accordingly, roots need to adjust their growth to maintain the life processes of the whole organ. It remains to be seen if this is the case; and, if so, whether it is conserved across species.

Likewise, increased root elongation observed in *A. thaliana* and barley in warmth could be considered an escape mechanism or, in general, to avoid root damaging (Gajghat et al., 2021). Accordingly, it might be assumed that enhanced root growth may allow protection of the root apical meristem bearing root stem cells from the superficial zone of the soil where the heat is more prominent. Generally, the existence of the above-ground parts of the plants depends on the health and functionality of the roots.

In contrast to the root system depth, which affects the vertical soil resource occupancy ability, the root system width, which is defined as the distance between the outermost lateral root tips (Colom et al., 2019), affects the plant horizontal soil resource occupancy ability (Belter and Cahill, 2015).

Similar to the depth, the root system width increased with elevated temperatures in the examined barley cultivars. Nothing has yet been described about the change in width in *A. thaliana*. Root width and root depth of Tiliaceae and Fabaceae species (eudicots)

(Luo et al., 2020) varied significantly in response to increased temperature, although the response of their above-ground shoot traits was very similar. This indicates that these traits are very susceptible to minor changes in the environment and experimental setups or that the temperature-induced growth changes are very species-specific. Accordingly, results of a recent phenotypic evaluation of thousands of plant species worldwide generally revealed a largely independent fine-root and shoot adjustment in many plant species (Carmona et al., 2021).

However, variations in width at elevated temperatures cannot be as massive as those in barley. While barley has an adventitious root system with seminal roots, the typical taproot system of eudicot plants has probably too few different root organs to vary in width (primary root, lateral root, root hairs).

The observation that root width in Scarlett' and 'ISR42-8' reached its plateau earlier (time point 3: 6d after treatment beginning) compared to the depth (See Supplementary Figure S19) may be related to the general limitation based on the size of the growing paper. The paper width was smaller than its depth. Therefore, it is exciting to investigate the changes that would occur under elevated temperatures if there were no limitations in width. However, at the earlier stages, before the root reached the outermost edges of the experimental system, the differences in root system depth between 16°C and 24°C compared to the root width were also higher. Thus, under my experimental setup, the adjustment of root system width seems to be rather independent of the temperature conditions. A maximization of the given root space of the barley plant already at lower temperatures for a faster response under unfavourable conditions is also conceivable.This raises the question of whether the large differences in root system depth between the temperature treatments become smaller under water-limiting conditions.

- **Root branching**

The length of the primary or seminal roots may be an important factor but are not the sole structures to characterize the three-dimensional underground space. Apart from the primary or seminal roots, there are second and third-degree branches (lateral roots, root hairs) to occupy the available space. My experiments showed that the number of lateral roots in the barley cultivars 'Scarlett' and 'ISR42-8' was also positively affected by moderate increases in temperature. The same was reported in winter wheat (*Triticum aestivum* L., cv. Newton) (Huang et al. 1991). The findings that in eudicots like *Brassica napus L.* and *A. thaliana*, the branching rate also significantly increased with rising temperatures (Nagel et al. (2009, Ibanez et al., 2017) indicate that this temperature

response may be highly conserved across species. Accordingly, at elevated temperatures, I could detect an increase in root length density (RLD) in 'Scarlett' and 'ISR42-8'. Increased lateral root number and density in warmth possibly allow plants higher access to water and nutrients (Huang et al., 1991, e Kroon et al., 2003). Increased lateral root number and density seem to be indirectly affected by elevated temperatures. Elevated temperatures reduced the water content (Liu and Huang, 2000) and root hydraulic conductivity (Morales et al., 2003), affecting nutrient acquisition. It is most likely that plants may compensate for these negative effects with altered lateral root emergence.

Generally, the increase in lateral root length and number in barley and lateral root number in *A. thaliana* and oilSeed rape could be explained by higher water and nutrient requirements due to the rapid vegetative growth and biomass accumulation in the shoot at elevated temperatures. Ludwig et al. (2020) postulated that temperature sensing in the roots could have derived from a drought sensing pathway, although the validity of this claim could not yet been experimentally verified.

Although my experimental setups were not limited by water availability, it seems to be a crucial trade-off component in this scenario because it is influenced by transpiration pull. Therefore it would be worthwhile to investigate how barley deals with the trade-offs involved with the increasing need to cool via transpiration along with limited water resources.

Although the relative length of lateral roots was slightly increased in 'Scarlett' and 'ISR42-8' at elevated temperatures, the differences are probably only of minor relevance for the overall root growth. In general, 'Scarlett' and 'ISR42-8' tended to produce more and shorter lateral roots at elevated temperatures, explaining the moderate increase in root dry weight. The more and shorter lateral root phenotypes go along with a higher potential for a stronger allocation to deep roots rather than to laterals. Whether lateral root elongation in the seedling stage of barley will be actively inhibited at elevated temperatures to promote the seminal root growth cannot be clarified in this thesis.

It has also been shown that elongation of the lateral roots in *A. thaliana* requires increased photoassimilates from the shoot (Amsbury et al., 2019). If this is also the case in barley, it is likely that plants at the two-leaf stage cannot be produce photoassimilates in sufficient amounts which results in shorter lateral roots. Therefore, the question arises of how the length of the lateral roots will change when more leaves are developed. In general, root growth traits at the early seedling stage are not always correlated with the adult root system, as demonstrated for other species like wheat (Watt et al., 2013).

Besides the regular functions, which are also part of the primary root, they help optimize root functions and are responsible for fine-tuning. Therefore, a higher

number of lateral roots also implies a higher number of meristematic tissues. The results of Hanzawa et al. (2013) and my experiments on *A. thaliana* showed that the root apical meristem is especially responsible for elevated temperatures. Whether elevated temperatures may have similar effects on the root apical meristem in barley roots is currently not known. Nonetheless, based on the observations in *A. thaliana*, it can be speculated that the sensor for root temperature perception in *A. thaliana*, if it exists, is located in these special tissues. Following this assumption, more meristematic tissues of lateral roots observed in *A. thaliana* may serve as another opportunity for roots to perceive temperature differences in different soil layers and directions. Thus, with more root tips, the root system can answer more quickly to environmental changes. This could also explain why the effect of elevated temperatures on the growth and development of lateral roots was more pronounced than on seminal roots with no branching.

Epidermal cells of both primary and lateral roots also produce root hairs (root hair cells). An increase in root hairs will further enhance root surface area, which in turn will facilitate water and nutrient uptake (Pregitzer et al., 2000). Although root hair development at elevated temperatures was not part of my research, the results of previous studies in *A. thaliana* and soybean suggest that they are also important structures for short-term adaptation to high temperatures (Tanaka et al., 2014, Valdés-López et al., 2016). Furthermore, transcriptome analysis of root hair mutants highlighted a potential role of root hairs as sensors of environmental conditions such as heat in barley. However, it is also possible that root hair production is indirectly influenced by temperatures, for example, through temperature-induced decreases in water availability. How roots perceive increased temperatures is currently not known. According to the results of my dissection experiments in *A. thaliana*, the root may perceive temperatures separately and independently from the shoot. Whether every root cell can perceive temperature changes or whether the perception is limited to a certain part of the root, such as the meristem or root hairs, must be clarified. The meristem and the root cap are the first part of the root to reach the new soil region. This tissue could, therefore, be the major candidate region for sensing temperature changes.

- **Complex root architecture traits**

The root system is a complex three-dimensional structure that cannot be described by selected singular phenotypes (Nagel et al., 2009). Thus, I also measured complex traits such as convex hull area (CHA), specific root length (SRL), the ratio of root system depth and root system width (RSD/RSW) to understand functional relationships between specific

traits. The CHA is the smallest area that encloses the whole root system (Nagel et al., 2009) and is thus automatically determined by the root depth and width. Plants with a higher CHA (and thereby branching) could have greater access to nutrients and water and are better adapted to severe environmental conditions such as elevated temperature. Furthermore, a larger CHA improves soil exploration by roots and may allow the plant to have a functional benefit over, for example, neighbouring plants. The CHA of 'Scarlett' and 'ISR42-8' also increased with elevated temperatures.

Like the root system angle (RSA), the RSD/RSW of the different cultivars was almost the same at both temperature treatments and all six time points. Therefore, if the length to width ratio remains the same, it simply means that roots grow faster at high temperatures. Based on this observation, it can not be excluded that the strong increase in the overall size of the barley plants (length and width) at elevated temperatures compared to lower temperatures was only a result of altered metabolism or other passive, thermodynamic changes on the molecular level (e.g. chemical cross-links). Therefore, using the trait RSD/RSW to identify novel factors of themomorphogenesis signaling in barley does not seem promising.

The specific root length (SRL) was another complex soil-resource exploitation trait (Tardy et al., 2017) of my phenotypic analysis. SRL was defined according to Nagel et al. (2009) as the ratio of total root length to root dry weight. It would be expected that plants with a higher SRL produce more root length for a given dry-mass investment and are generally considered to have higher rates of nutrient and water uptake (per dry mass)(Ostonen et al., 2007). The root of high SRL plants has a shorter root lifespan than that of low-SRL plants. In general, the TRL and RDW in 'Scarlett' and 'ISR42-8' increased significantly at elevated temperature compared to lower temperature at 12d after temperature treatment began. However, the increase in RDW at 24°C is not very large compared to 16°C. Thus, I measured a slight increase at elevated temperatures for SRL (with a difference of around 30% between the mean values at 16°C and 24°C) in both cultivars 'Scarlett' and 'ISR42-8', which is probably negligible. Overall, the values for SRL at 24°C compared to 16°C are relatively low. Several studies (Eissenstat, 1992, Comas et al., 2000) have concluded that the traits of relatively low SRL and high lateral roots density (LRD), which I also observed, indicate that fine roots adapt to resource-poor environments by reducing absorptive capacities. Under optimal water and nutrient supply, I saw a similar response in 'Scarlett' and 'ISR42-8'. This observation could suggest that plants at elevated temperatures enjoy a strategy in which more carbon is invested in building a dense root system of relatively short lateral roots along the main axis, and thus potentially less carbon is invested in absorption. A higher number of short lateral roots not only ensures better anchoring but could potentially also regulate and balance excessive

nutrient and water uptake and consumption caused by the temperature-induced acceleration of metabolic processes. Generally, a short and dense lateral root system, such as in maize, reduced absorption capacity (Zhan et al., 2015, Passot et al., 2016). The root could use the existing resources more efficiently and longer by actively reducing the water- and nutrient uptake by decreasing lateral root elongation.

It is also most likely that young barley plants use the advantages of optimal environmental conditions (no limitation in water and nutrients, temperature-induced acceleration of particles such as ions) to establish faster structural tissues/organs, which could bring a survival benefit for later development stages. It would be interesting to See whether the lateral root length at elevated temperatures will be further increased at later development stages. However, experimental data about temperature-induced changes in specific root length in *A. thaliana* are not yet available.

In summary, elevated temperatures induce numerous morphological changes in young barley roots on a macroscopic level, which could be positive for present and future survival and underground competition for water and nutrients (e.g., increased root length and lateral root number, faster root elongation rate). Generally, my explanations above also revealed that we have very little knowledge about temperature responses in the root also in the model plant *A. thaliana.* Therefore, to compare these two species, especially root morphology changes to elevated temperatures in *A. thaliana* must be studied in more detail.

However, some similarities between *A. thaliana* and barley were found n turn of their root elongation in the depth, width and lateral root developing in response to elevated temperatures (Rellán-Álvarez et al., 2015) (Figure 50). Compared to monocots, it may be reasonable to assume that eudicot plants, due to their allorhizic root system architecture, have a more limited scope in modifying their root growth at elevated temperatures. Thus, monocots may have more variability and flexibility to react to short-term changes in the surrounding environments. However, this hypothesis needs to be addressed and validated by further studies. Generally, to better understand root functional traits and how traits are related to whole plant strategies, further studies on A. *thaliana* and barley with more time points are needed. Thermal imaging could be a useful approach to determine if and where cooling processes in the root take place. Furthermore, aspects like different soil structures, minimum spatial limitations, competitions for resources with other plants that may contribute to final plant performance must be considered too. Thus, validations of plants growing under complete field conditions are desired.

6.1.3 Conceptual comparison of temperature responses in shoot and root

To better understand the macro-scale patterns of the observed phenotypic responses in more detail, I also investigated micromorphological changes at the cellular level. According to published studies, I am focussing on the model phenotypes temperature-induced hypocotyl and root elongation. Obviously, temperature-induced hyperelongation of roots and shoots can only be caused by modifications in cell length or cell number or a combination thereof. To assess the impact of each of these modifications, I quantified cell length and cell number in different root zones and the entire hypocotyl of *A. thaliana* for temperature-induced phenotypic differences. I performed these tedious and elaborate cellular studies exclusively in *A. thaliana* because the model plant was easier to handle and to analyze. I found that hyperelongation of the root is primarily caused by an increase in the cell production rate and not by an increase in cell expansion (Figure 51). Although the length of meristematic zones (MZ) and elongation zone (EZ) was only slightly negatively affected by elevated temperatures (Yang et al., 2016, Martins et al., 2017, Feraru et al., 2019, Gaillochet et al., 2020), the maturation zone (MaZ) showed a significant increase in cell numbers (Figure 20C,D), which indicated an acceleration of cell production rate at higher temperatures. This is consistent with observations in maize, where temperature increase may positively affect the elongation and cell division rate in seminal roots (Nagel et al. 2009). This was also supported by my expression data results, where I observed a significant increase in expression of cell cycle regulatory genes *CYCD3;1, CYCD6;1, CYCD1;1* in the MZ at elevated temperatures compared to the control. In support of Yang et al. (2016), I found that the rate of cell production in the meristem is not determined by an increase in cell number of dividing cells (e.g., more dividing cells in the MZ), but rather via their rate of cell division. At high temperature, the root meristem produced cells more rapidly, but the newly proliferated cells elongated in a temperature-independent manner.

Different patterns in cell growth and proliferation were observed for the shoot at elevated temperatures. In the hypocotyl of young Arabidopsis seedlings, cell elongation seems to play the dominating role (Ibanez et al. 2017, Bellstaedt et al., 2019) in temperature-induced hyperelongation. Why root and shoot seem to follow such different strategies in regulating their growth rate is not known. In general, plants have only a limited repertoire to change their shape at the cellular level - for example, faster or slower division, elongation in one or more directions, or thickening or thinning of cell walls. These responses must be integrated with various environmental changes and potentially concurrent stimuli that can elicit contrasting responses. Thus, it might be expected that the environmental factors that affect shoots and roots differ due to the location of the

corresponding tissues in the plant. The shoot is mainly surrounded by air and grows primarily in the light, while the underground tissues of the plant are covered by soil and grow predominantly in the dark. Due to the strength of the soil, the root system is constantly exposed to a certain mechanical force. It seems that there are different selection pressures on the cellular programs of the different tissues to elevated temperatures. Accordingly, an increase in shoot length may be, in general, largely dependent on cell elongation (Voesenek et al., 1990). It could be expected that temperature-induced hyperelongation of the stem with longer and narrower cells may be associated with lower resistance to mechanical forces such a wind. Thus stems with this phenotype could break through more easily. However, reduced stiffness may impart more flexibility and may be accompanied by a higher load avoidance (bending in the wind) rather than load tolerance (absorbing the loading force) (Telewski, 1995, Puijalon et al., 2008, 2011, Huber et al. 2013). It is also interesting to know how the stem diameter changes under elevated temperatures. An increase in diameter growth of the stem could also provide additional stability and take over a storage function for the number of resources supplied per unit cross-section to developing leaves. The data of Lee et al. (2021) showed that the hypocotyl diameter in *A. thaliana* was increased at elevated temperatures indicating that high ambient temperature promotes the thickness as well as elongation of hypocotyl. Ohtaka et al. (2020) also observed increased stem length and thickness in the shoot of Tomato (*Solanum lycopersicum*) seedlings at elevated temperatures. In contrast to the hypocotyls, the root may invest more energy in cell division. A higher number of cells implies more cell walls that are lying against each other. More cell walls increase physical strength (e.g., force to fracture) and therefore confer higher resistance to increased soil pressure (Onoda et al., 2017). Furthermore, a higher cell number due to an increase in cell production rate goes along with a higher amount of cells, which could differentiate in more specialized root structures, such as root hairs. More cells in the primary roots (~320 cells) compared to hypocotyls (~27 cells) of 7d-old *A. thaliana* plants could give their roots more flexibility in shaping the overall root morphology (See Supplementary Figure S2C). The root system may be, thus, more responsive to short-term changes in the environment or may compensate for potential losses resulting from elevated temperature-provoked apoptotic cell death. In this regard, Yang et al. (2016) See in the slight changes in the meristematic zone an indication of compensatory mechanisms to counteract the cost-intensive increase in the cell production rate at elevated temperatures. However, this is purely speculative at this point and requires further investigations. In this context, It has also been shown that in the embryo

of *A. thaliana* the majority of the cells for the hypocotyls are already established. Thus, cell elongation has a greater effect in the hypocotyl than cell division. In the root, it is exactly the other way around.

In conclusion, differences in cell length and number of *A. thaliana* roots and shoots at elevated temperatures suggest tissue- specific coping strategies. The specific program of cell adjustment shown by root and shoot may have an impact on their stiffness. An optimal stiffness of the plant in turn influences their ability to withstand external forces such as wind or soil strength. How individual plant organs regulate their stiffness at elevated temperatures on cellular level is poorly investigated, but fundamental to understanding how plants control their shape in response to warmth. Therefore, further research on this topic would be highly desirable.

6.2 Molecular signaling

Based on the different morphological changes observed on the tissue and cellular level, it may be assumed that root and shoot may also differ in their molecular regulation underlying temperature-induced phenotypic differences (Bellstädt et al., 2019). Indeed, this hypothesis was supported by the results of my detached organ experiments and transcriptome analysis of the different plant tissues exposed to elevated temperatures (See Chapter I). On the one hand, these experiments show that temperature-induced root elongation runs partially independent of the shoot and may be based, similar to the cotyledons and the shoot, on tissue-specific transcriptional activation of genes. On the other hand, it demonstrated that roots could partially sense temperature autonomously. Together, these data support the idea that thermo-regulation of root and shoot growth could be based on at least partially different signaling pathways (See the model, Figure 51).

Fortunately, research progress over the last years has constantly improved our knowledge about the molecular and genetic control of shoot thermomorphogenesis. Although first studies have been published in the recent past on root thermomorphogenesis, its mechanistic understanding is poor at best. Another important question is how the interactions between the different plant structures are regulated, if at all?

My results of the genetic, transcriptomic, physiological, and pharmacological experiments showed that the transcriptome responses to elevated temperatures in different parts of the plant (cotyledons, hypocotyls, and roots) were partially organ-specific. Thus, shoot thermomorphogenesis may involve both autonomous and organ-interdependent temperature sensing and signaling. Hypocotyl cell elongation requires temperature sensing in the cotyledons (Bellstaedt et al., 2019). The derepression of PHYTOCHROME INTERACTING FACTOR4 (PIF4) induces the production of auxin in the epidermis of

cotyledons (Tao et al., 2008, Procko et al., 2014, Procko et al., 2016, Bellstaedt et al. 2019, Kim et al. 2020), which then serves as a mobile long-distance signal promoting brassinosteroids (BR) biosynthesis and signaling in the hypocotyl. The presence of BR-activated BRASSINAZOLE RESISTANT1 (BZR1) inhypocotyl cells subsequently controls the transcriptional activity of growth-promoting genes, resulting in cell elongation (See Figure 51A). However, the cotyledon-derived auxin signal seems to be gated in hypocotyls by a second permissive yet unknown thermosensor that determines the capacity to induce cell elongation. Changes in the chromatin structure could constitute one possible candidate for a permissive temperature sensor acting downstream or in concert with gating BZR1 function in the hypocotyl (van der Woude et al. 2019). Thermomorphogenesis has been shown to require chromatin remodelling that involves histone deacetylation (Tasset et al., 2018) and the eviction of the H2A histone variants H2A.Z (Kumar and Wigge, 2010). However, at this stage, the origin of the permissive temperature sensing mechanism remains elusive and needs further investigation.
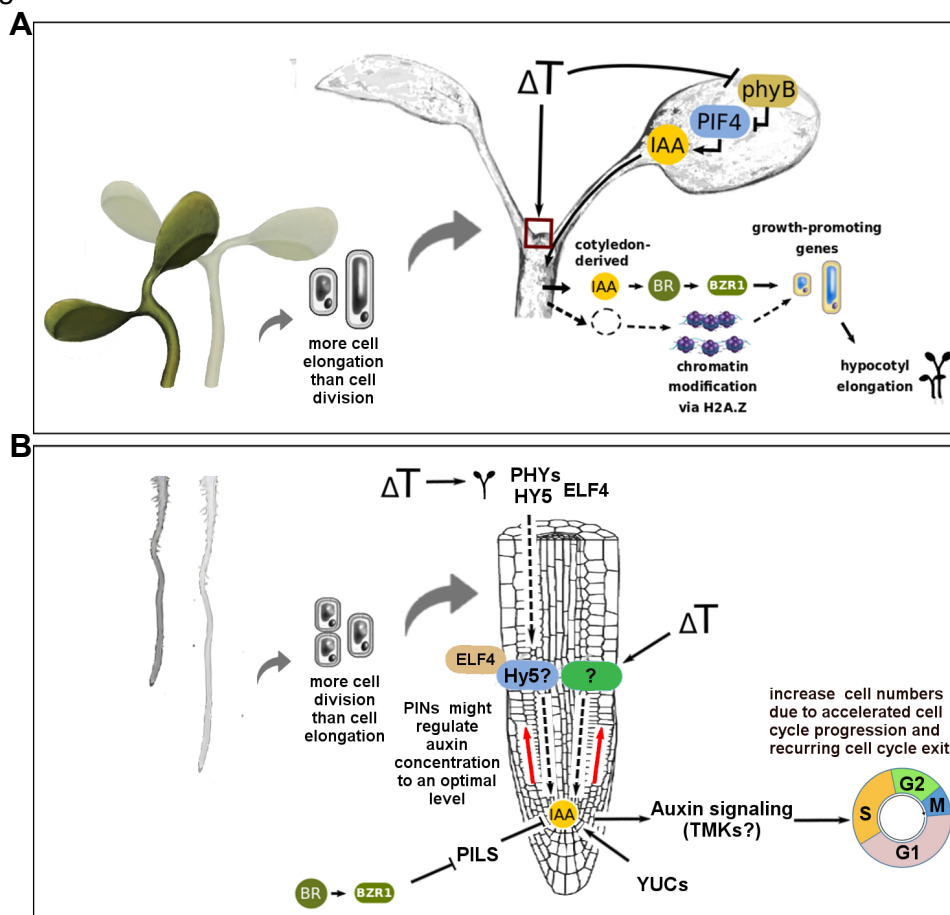
Figure 51. Model of spatial sensing and signaling specificities in seedling thermomorphogenesis in shoot and root. A Experiments have shown that temperature-induced hypocotyl elongation is rather determined by increased cell length. However, the induction of cell elongation in hypocotyls requires temperature sensing in cotyledons, followed by the

Figure 51 (Continued). generation of a mobile auxin signal. Subsequently, auxin travels to the hypocotyl, which triggers local brassinosteroid induced cell elongation in seedling stems, which depends upon a distinct, permissive temperature sensor in the hypocotyl. **B** In contrast to the shoot, the increase in root length is caused by a higher cell division rate. The temperature-induced acceleration of cell division in roots seemed to be regulated by locally expressed and shoot-derived signals. Thus, besides the temperature sensing and signaling in the shoot, which influences temperature responses in the root. It is most likely that roots can also partially sense and respond to elevated temperature autonomously. Although I could not show this, several studies (Gaillochet et al. 2020, Lee et al. 2021) postulated the hypothesis that roots integrate regulatory signals coming from the shoot through the activity of phytochromes, HY5 or other still unknown genes. ELF4 could be another potential candidate that delivers temperature information from shoots to roots and helpes to initiate temperature-induced root elongation (Chen et al. 2020). Gaillochet et al. 2020 speculated that these signals promote local HY5 rescue and induced de novo auxin biosynthesis. Furthermore, he postulated that auxin promotes temperature responses in the root in a TMK-dependent manner. My experiments also indicated a temperature-induced increase in auxin level in the meristematic zone (possibly synthesized by members of the YUCCA (YUC) family). I supposed that these local increases in auxin concentration could act as a permissive signal for cells to accelerate the cell cycle. Furthermore, Lin Sun et al. 2020 suggested that BR signaling transcriptionally and post-translationally represses the accumulation of PILS proteins at the endoplasmic reticulum, and thus increasing nuclear abundance and signaling of auxin in the root at elevated temperatures. Further regulating function may be exerted by the activity of the PINs, which maintains the endogenous auxin concentration to an optimal level via their shootward transport.

Furthermore, in the meantime, other sensing mechanisms were discovered, for example, reshaping of the mRNA stem-loop structure by elevated temperatures, which may facilitate translation initiation of thermo-responsive genes such as PIF7 (Chung et al., 2020). Moreover, Silva et al. (2020) have suggested that high temperatures directly repress the evening complex ability to bind DNA. Thus, upon a high-temperature stimulus, the evening complex releases the repression of PIF4 (Nusinow et al., 2011). Furthermore, Jung et al. (2020) demonstrated that phase separation of EARLY FLOWERING3 (ELF3), a component of the evening complex, acts as a thermosensor. EARLY FLOWERING 4 (ELF4) is also temperature-sensitive and should be considered in this context, too. It was shown that the movement of ELF4 through the vascular system permits the shoot clock to coordinate the root clock (Chen et al 2019). The putative CDC-Like Kinase (CLK) involvement as a potential thermosensor in human cells (Lin et al., 2020) is currently under debate. This may sense temperature changes via a mechanism, which is yet unknown in plants, that leads to alternative splicing and plant acclimation to a wide range of temperatures (Haltenhof et al., 2020). Thus, there is a range of potential mechanisms and specific molecular candidates for the above described unknown permissive thermosensor in hypocotyls (reviewed in Hayes et al., 2020), which may act downstream or in concert with BZR1 to gate its function in the hypocotyl. Well-thought-out experiments are needed to disentangle the complex interplay between the various potential candidates for thermal sensors and their hierarchies.

However, *PIF4* is most strongly expressed in the vascular tissues of the leaves, but to regulate hypocotyl elongation during thermomorphogenesis requires its expression or presence in the epidermis (Kim et al., 2020). The regulation of the spatiotemporal

expression of *PIF4* in response to temperature is not fully understood. Endo et al. (2005) also showed that cotyledons are the major site of phytochrome B (phyB9-mediated red light perception to regulate seedling de-etiolation. Whether cotyledon-localized phyB is necessary for temperature-induced hypocotyl elongation or mesophyll-specific phyB in the hypocotyl, similar to the phyA in light perception (Sankalpi et al., 2009), is required, remains to be seen. Again, these questions highlight the need for cell- or at least tissue-specific analyses. Cotyledon-to-petiole micrografting with different combinations of known major players of shoot thermomorphogenesis (e.g. PIF4, phyB, ELF3/ELF4) might be a promising approach (Bartusch et al., 2020). Developing tissue- or cell-type-specific transgenic reporter lines crossed into various thermomorphogenesis mutants combined with time-lapse imaging of temperature responses in the shoot by confocal laser scanning microscopy (CLSM) (Sawchuk et al., 2007) could be another experiment for future study to better understand the spatio-temporal thermomorphogenesis signaling in the shoot.

Although my transcriptomic data and detached organ experiments indicate a certain root-specificity in gene regulation under elevated temperatures, the involvement of shoot thermomorphogenesis regulators HY5, Phys, and PIFs as binding factors between root and shoot temperature response is being promoted by other groups (Gaillochet et al. 2020, Burko et al. 2020, Lee et al. 2021). Neither the *pifQ* mutant, which lacks the major central players in hypocotyl thermomorphogensis, the PIF-family members, PIF1, PIF3, PIF4, and PIF5, nor the mutant of the PIF4 negative regulator HY5 or the phytochrome thermosensory mutants *phyABCDE*, which display a constitutive warm temperature response in the hypocotyls (Legris et al. 2016), showed apparent defects in root thermo-response under my experimental conditions (Figure 25D). These observations contradict the findings of Gaillochet et al. (2020). In contrast, the thermo-responses in the shoot mutants *hy5-221*, *phyAB*, *35S:PIF4* responded slightly, but are significantly hyperelongated compared to the wild-type. Thus, Gaillochet et al. (2020) support a model where PIF4 acts downstream of the phytochromes and functionally converges with HY5 to regulate root thermomorphogenesis. Moreover, a group of researchers hypothesized that roots integrate regulatory signals coming from the shoot through the activity of phytochromes and HY5. Potentially, these signals promote local HY5 rescue and induce *de novo* auxin biosynthesis. However, the results of Lee et al. (2021) indicate that *HY5* gene expression and protein stability are both stimulated by elevated temperatures in a root-specific manner. In contrast, the PIF4-SPA module only may play a central role in hypocotyl elongation at elevated temperatures (Lee et al., 2021).

Based on these results, TIHE and TIRE seem to be regulated by distinct tissue-specific signaling mechanisms that may nevertheless contain common modules (See Figure 51B). Results of root detachment experiments with *hy5* and other *pif* mutants combined with different temperature treatments would potentially deliver the missing answers. However, as mechanical detachment of the plant is a highly invasive approach, the combined effects of the wounding response and the loss of all mobile signals make specific effects probably difficult to detect. Reciprocal root-shoot grafting experiments with various mutant/wild-type combinations of common thermomorphogenesis genes (e.g., *hy5-51*/Col0, *phyB-9*/Col-0, *phyABCDE*/Ler-0, *pifQ*/Col0-0, *elf3-1*/Col-0) at elevated temperatures would achieve the same effect with regenerated seedlings long after wounding. Furthermore, this approach may uncover interacting effects in temperature-responsive root-shoot/shoot-root signaling and communication. Although, as described in detail above, roots seem to have partially distinct signaling pathways regulating temperature response (See Figure 51), there might be nevertheless feedback effects that influence shoot or root growth, respectively (e.g., Vapaavuori et al., 1992, Al-Rawahy et al., 2019, Lam et al., 2020). However, evidence of direct signaling is currently lacking. Thus, investigating the interaction processes between aerial and underground organs at elevated temperatures is crucial to understanding thermoregulation at the whole-plant level. The following questions still need to be answered: How do roots and shoots communicate through elevated temperatures? (How) do roots sense shoot-experienced temperature changes and vice versa? Do shoot-derived mobile signals exist that initiate temperature-responsive root growth? However, the finding that HY5, which seems to be a master regulator of shoot and root photomorphogenesis (Zhang et al. 2019), also might play a role in root thermomorphogenesis, indicating that some molecular components nevertheless overlap between both tissues. Although mutant screens with phytochromes and cryptochrome mutants (See Supplementary Figure S23) failed to show any TIRE effects, other known photoreceptors like phot1, ultraviolet-B (UV-B) photoreceptor UVR8, circadian clock photoreceptor ZEITLUPE (ZTL) should be included in future tests for potential roles in TIRE.

However, in general further studies are required to understand if any other factors exist which also regulate temperature responses primarily in the root or together with HY5. Future mutagenesis screens associated with this temperature-induced root elongation in *A. thaliana* could aim to discover new players.

Another pivotal step in the research of root thermomorphogenesis will be to resolve how high temperature is perceived in the root. Do root-specific temperature sensors exist? To answer this question, it might be helpful to find out if the root and shoot have different temperature optima. Differences would support the theory that the root must perceive

temperature independently from the shoot. Investigation of organ-specific impact of different temperature regimes seems to be very difficult. A direct effect of root medium temperature on shoot growing points could not be ruled out under my experimental setup for TIRE-assays in *A. thaliana*. So there is a need for optimization of parameters. Another problem to investigate the impact of temperature only on root growth are the existing interaction processes with the shoot that corrupt the root responses. Hence, this topic represents a promising research area with high potential for future discoveries.

6.2.1 The role of Auxin and BR in root thermomorphogenesis

Beside the involvement of the HY5-PIF module, the requirement of another important signal, the phytohormone auxin, is currently discussed. Previous studies have shown that auxin transport and signaling together with brassinosteroids (BRs) regulate temperature-induced hypocotyl elongation. Auxin might likewise be involved in root thermomorphogenesis. However, while several studies suggest that elevated temperatures also affect root growth in an auxin-dependent manner (Hanzawa et al., 2013, Wang et al., 2016, Fei et al., 2017), Martins et al. (2017) claimed that under the conditions used in their experiments (no sugar, 15d old plants) - auxin signaling played a minor role in temperature-induced root elongation. Nevertheless, the decreased root elongation of the auxin signaling mutants *axr5-1/iaa1*, *msg2-1/iaa19*, and *slr1-1/iaa14*, of the auxin biosynthesis mutant *yucQ* and the auxin transport mutants *pin2* and *pgp4* at elevated temperatures compared to the control observed in my TIRE assays (See Chapter II), indicate that auxin might be involved in the temperature response in the root. Although this conclusion was in line with the observed reduction of the D2 fluorescence signal in the root tip of an *R2D2* fluorescent auxin reporter line cultivated at 28°C, this result should be viewed with caution. In a recent study, Feraru et al. (2019) could that both the auxin-sensitive D2 as well as its insensitive counterpart R2 were sensitive to heat. Thus, this fluorescent auxin reporter line is less suitable for use in an experiment with temperature treatments. However, the synthetic auxin response reporter *DR5::GFP* and *DR5::RFP* in Arabidopsis roots showed similar patterns (Feraru et al. 2019). Furthermore, Gaillochet et al. (2020) could show that the transmembrane kinases TMK1/4, which are involved in TRANSPORT INHIBITOR RESPONSE1 (TIR1)/ Auxin F-Box Signaling (AFB) independent auxin perception and signaling (Cao et al., 2019, Xu et al., 2014), may be required for root thermomorphogenesis. The inhibition of root elongation at elevated temperature in my work through the external addition of BR and auxin inhibitors to growth media, as well as

the promoting root growth effect observed when BR and auxin are added in physiological (=low) concentrations, strongly suggests a significant role of these phytohormones in root thermomorphogenesis. However, BR mutants, which showed a strong temperature phenotype in the hypocotyls, did not deviate from the wild-type in TIRE assays, meaning that here genetics contradicts the pharmacological approach. The TIRE effects of other tested *A. thaliana* mutants defective in genes important for biosynthesis or signaling of five additional plant hormones were also inconclusive. In general, working with hormone mutants in the root is more challenging than in hypocotyls. The explanation may have to do with the general essential role of hormones in the regulation of root growth where they act in much smaller concentrations than in the shoot. As a result, both pharmacological inhibitors and mutations of important genes in the hormone pathways often result in strong root growth defects already at control conditions (in my case 20°C). This makes it difficult to identify conditional and temperature-specific effects among the extensive pleiotropic effects. However, the absence of any phenotypic abnormalities of the selected BR mutants in the corresponding TIRE-assays argue rather against the assumption that BRs might play an important role in root thermomerphogenesis. Instead, I assume that BRs, besides other hormones, fulfill a subordinate regulatory function in the complex processes underlying temperature-induced root growth. The discrepancy between the data of my pharmacological and genetic experiments and could not yet be conclusively clarified. However, Lin Sun et al. (2020) suggested BR signaling transcriptionally and post-translationally represses the accumulation of PIN-LIKES (PILS) proteins at the endoplasmic reticulum, by increasing nuclear abundance and signaling of auxin in the root. Nonetheless, based on my results, I support the hypothesize of previous studies (Hanzawa et al., 2013, Wang et al., 2016) that temperature-induced primary root elongation is linked to the increased synthesis of the phytohormone auxin (See Figure 50).

6.3.2 Accelerated cell cycle progression drives temperature-mediated root elongation

While my results in in the first part of Chapter II support the conclusion that the function of auxin signaling, biosynthesis, and transport during root thermomorphogenesis my be sufficient, the second part depicts the specific role of auxin in temperature-induced root elongation. As already mentioned, temperature-induced shoot elongation is determined by increased cell length in an auxin-dependent manner. In contrast, increases in the primary root length are more likely caused by a higher cell production rate in the root apical meristem.

Auxins were shown to play important roles in the induction of cell division and the control of cell cycle progression in the root (Perrot-Rechenmann et al., 2010). I therefore asked whether auxin can directly or indirectly increase mitotic activity in the root apical meristem at elevated temperatures by modulating cell cycle entry. Indeed, the external addition of a low concentration of IAA to the growth media combined with elevated temperature exposure increased the total cell number of 7d-old *A. thaliana* seedlings beyond its normal level (See Figure 35). Furthermore, the quantification of the number of cells in the S/G2-phases based on *Cytrap* reporter lines indicated that auxin can increase the number of cells in the S-phase in the meristematic zone of temperature-induced roots (Figure 37), while cells in the G2 phase (c-17 positive cells) could barely be identified. To exclude singular effects on the S-phase which may be buffered in later cell cycle stages, future experiments should also quantify the amount of cells in the M-phase, for example by DAPI staining to visualize cells undergoing cytokinesis. Likewise, promotion of mitotic activity by a temperature-dependent increase of auxin levels, which would ultimately result in more root cells in total needs to be tested. This could be achieved by light sheet based fluorescence microscopy for live imaging of roots of the *Cytrap* line at different temperature conditions (Berthet et al. 2016) and over a longer time scale. However, cell cycle entering might be accelerated, which then caused more cell division at the meristem and pushed consequently more cells over the transitions zone in the maturation zone and lead to the longer root phenotype.

Accordingly, expression analysis indicated that D-type cyclins *CYCD3;1, CYCD6;1, CYCD1;1* play a role in temperature induced root growth. It was shown that overexpression of *CYCD* genes promoted G1/S phase transition in *A. thaliana* ((Resnitzky et. al., 1994, Liu et al., 1995, Montalto et al., 2020) and therefore can regulate the timing of the cell division processes. I expect that the upregulation of *CYCD3;1, CYCD6;1, CYCD1;1* genes at elevated temperatures will accelerate the cell cycle of meristematic cells. To test this hypothesis TIRE assays with corresponding loss of function mutants of these D-type cyclins *CYCD3;1, CYCD6;1, CYCD1;1* should be conducted. If these genes play an important role in temperature-induced root elongation, the root should be shorter. A big advantage is that mutants of these genes already exist and are published (Masubelele et al., 2005, Yu et al 2017, Jones et al., 2017). Since the cell cycle delay could only be shown for the *cycd1;1* mutant (Kleinboelting et al., 2012), this line should be prioritized. Interestingly, experiments of Wang et al. (2016) showed that a low auxin dose is able to induce the expression of *CYCD1;1* (0.05 nM IAA) in roots. These result could indicate a link between temperature-induced auxin increase and the

accelerated cell cycle at elevated temperatures. Thus, I proposed that increased auxin levels at elevated temperatures induce the expression of cell cycle genes such as *CYCD1;1* that promote primary root growth through accelerating the entry into both S-phase and mitosis. However, to address this issue more clearly, more auxin-related and temperature-sensitive mutants associated with primary root elongation have to be found and analysed .

Beside the observation of an increase of the auxin level in the root apical meristem and the acceleration of the cell cycle in the meristematic cells at elevated temperatures, analysis revealed that the auxin transporter PIN-FORMED2 (PIN2) are required as well for TIRE-response. Presumably, the specific pattern of PIN2 localization is required to maintain the auxin maximum in the root tip (Sabatini et al., 1999, Friml et al., 2004). To test this hypothesis,in a next step the distribution of PIN2 in the plasma membrane of *A. thaliana* root cells should be investigated, potentially by live-imaging of a functional PIN2-GFP fusion protein. It is supposed that shoot-derived auxin and its downward transport is the main source for auxin-mediated root growth and development. (Morffy et al., 2018). However, the finding that roots which are separated from the shoot are able to show temperature-induced root elongation (Figure 2), indicate that locally generated sources of auxin in the root could be accountable for the temperature response. This hypothesis was supported by the observation that plants with naphthylphtalamic acid (NPA)-patches on the hypocotyls still showed temperature-induced root elongation. However, further studies are required that can reveal the origin of the auxin increase in the root meristem.

In conclusion, it is likely that multiple changes in auxin transport and metabolism occur during temperature-induced primary root elongation, the first of which may be a temporal increase in the auxin level from a possibly root specific source in the root tip. Secondly, any auxin transport components such as PIN2 regulate the auxin concentration in the root tip to an optimal level at elevated temperature. Either this is done by relocalization of Auxin in the root to the RAM or shoot-ward transport mediated by PIN2 or both. Finally, it is most likely that Auxin directly stimulates S/G1 and maybe also G2/M specific events in the meristematic cells, as reflected by activation of CyclinD specific genes which result in an accelerated cell cycle (See Figure 53).

6.4 QTL analysis

As described above elevated temperature impacts root and shoot growth of many plants species including agricultural crops such as barley. The current knowledge on the molecular processes behind the common temperature phenotypes (predominantly

temperature-induced hypocotyl and root elongation) based primarily on investigations of the model organism *A. thaliana*. A future goal of thermomorphogenesus researchers is to transfer the knowledge about the functional genes in *A. thaliana* to crops of agronomic importance. Thus, finally we are able to develop thermotolerant plants and protect crop production against global warming. The present study in Chapter III is one of the first efforts in this direction. However, because of the evolutionary distance of the two species and the large size and the complexity of the barley genome (appr. 40x larger than the *A. thaliana* genome with approximately 84% of the genome being comprised of mobile elements or other repeated structures (The International Barley Genome Sequencing Consortium. 2012) a 1:1 assignment of functional orthologs or homologs of *A. thaliana* thermomorphogenesis genes in barley is often impossible because members of gene families tend to cluster by species and not by genes. Furthermore, due to the lack of mutant lines for putative candidate genes in barley the direct investigations of their function is not straight-forward. Thus, I followed a forward genetic approach by performing quantitative trait locus (QTL) analyses using a barley introgression line population based on the parents 'Scarlett' and 'ISR42-8'. Association mapping revealed novel genomic regions and hotspots controlling temperature-sensitive root or shoot growth traits or both together in barley (See Figure 47). In terms of identifying candidate genes, most of these regions are much too large to pinpoint single candidates. Hence, future studies need to narrow down the introgression regions by repeated back-crossing to identify promising candidates for these QTLs (Grando et al., 1995). Overall, 65 QTLs associated with the 11 tested root traits and 57 QTLs associated with the 5 investigated shoot traits (See Figure 52A,B) Two QTLs on position 107.63-108.71 cM on chromosome 2H and between 24.17 to 40.51 cM on chromosome overlapped with genome regions detected in study from Naz et al. (2014), who investigated root architecture traits in the same introgression population in response to drought stress. While in my analysis these QTL regions were responsible for temperature-induced changes in total root growth and root dry weight at elevated temperatures, in the study from Naz et al. (2014) they were specifically associated with changes in root length, root dry weight, and root volume at drought stress conditions. This observation could support the theory of Ludwig et al. (2020), who proposed that temperature sensing and drought sensing in the roots could be regulated by parts of the same pathway. However, Hoffmann et al. (2012) also detect these two specific QTL regions potentially containing genes regulating root dry weight under nutrient deficiency. The overlaps between the QTL analyses of this three independent studies investigating root growth in response to different types of abiotic

stress,suggest the presence of stress response master regulators that should be followed up in future studies. However, several other QTLs detected in my QTL analyses were specifically associated with root temperature responses.

In contrast, among the 57 putative QTLs associated with different shoot related responses at elevated temperatures, 32 QTL positions found were previously reported in the literature related to grain threshability and other agronomic traits under control condition, hydroponic nitrogen (N) supplies. N stress, drought stress (Supplementary Table S20). Interestingly, although the flowering development stages were not part of my phenotypic investigations in barley, co-localization with flowering time-related genes including photoperiodic- and circadian clock-related genes, which are known from other studies (See Song et al., 2010) was observed for some of my detected QTL regions (See Supplementary Table S20). This may refer to pleiotropic effects of these genes or genetic linkage of flowering time-related genes and temperature-sensitive shoot regulated genes. This was also suggested by Abdel-Ghani et al. (2019) based on a genome-wide association study of a spring barley collection under variable water availability. Thus, photoperiod and clock pathway homologs in barley, such as *Ppd-H1, HvCO1, HvCO2, HvFT4,* and *HvCEN* (See Supplementary Table S20) are positional candidates for some QTLs (See Supplementary Table S20) associated with the shoot trait total length of the second leaf (2ndLTL) (which is in this case equal to the final shoot length). Conducting further studies on these QTL regions to verify their precise position seem to be a good choice, because the associated trait 2ndLTL is the only one which were positively affected by elevated temperature in my QTL study, similar to the temperature- induced shoot elongation observed in *A. thaliana* (Gray et al., 1998).

In contrast, most of the *Hsp* alleles in the *Scarlett* background reduced plant performance at elevated temperatures, especially in roots. Other studies have supposed that exotic introgression in a locally adapted line can reduce fitness (outbreeding depression) (Lynch 1991, Edmands 1999) and explained this with the breaking-up of co-adapted genes or introgression of non-locally adapted gene variants. These examples underscore that increase in heterozygosity due to outbreeding can also be detrimental to fitness (Moehring et al 2011). Furthermore, most identified loci are minor effect QTLs, indicating that the vast majority of phenotypic variation is explained by QTLs with smaller effects. In recent years, more attention has been given to QTLs with relatively small effects. It was shown that minor effect QTLs also make important contributions for example to flowering time regulation in barley. (Chen et al 2015) In this regard, genes located in the detected regions may be particularly important for regulating plant growth at elevated temperatures.
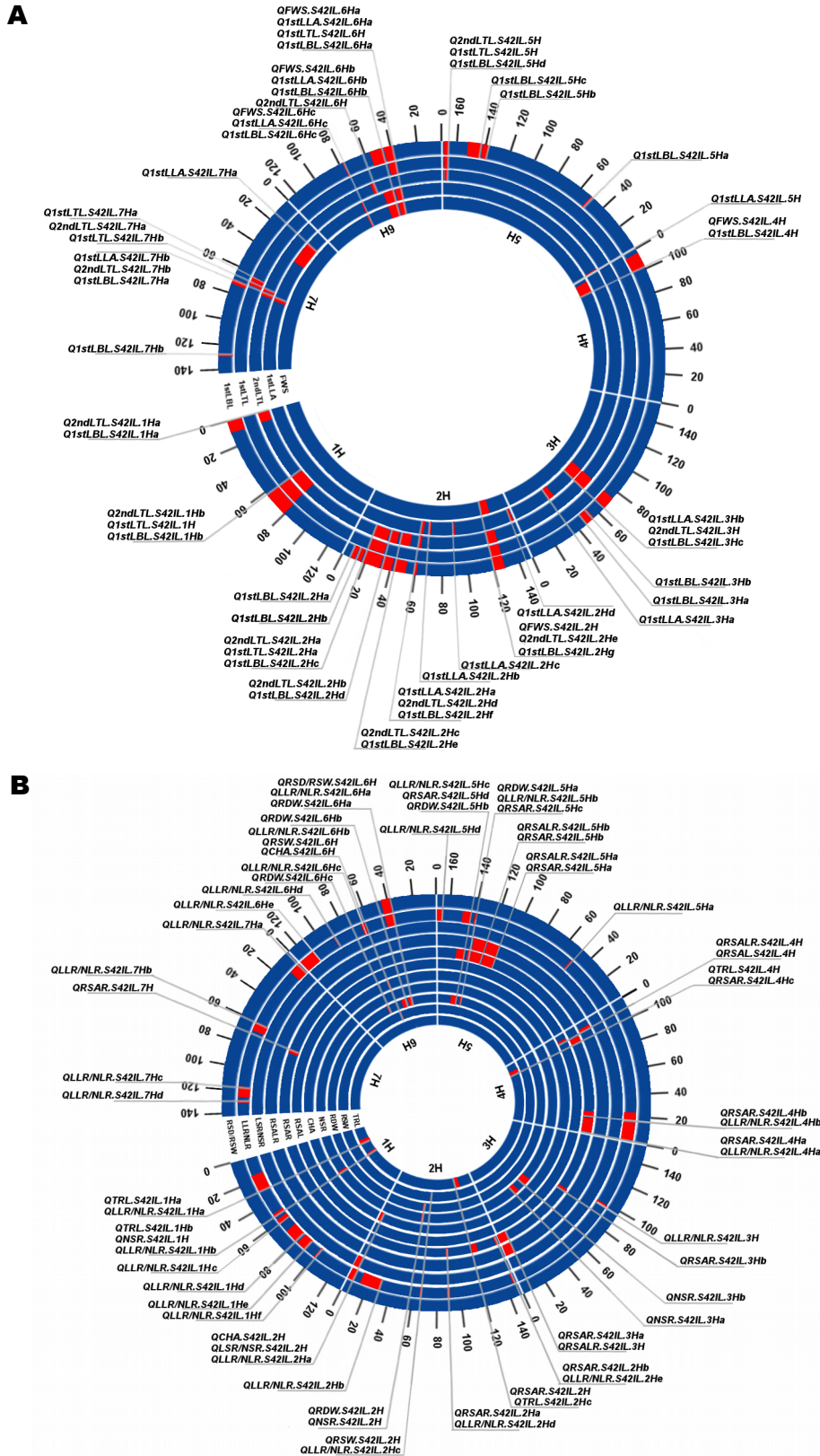
Figure 52. Genetic mapping of all putative QTLs for selected phenotypic traits. Circos plot indicating QTLs (red bars) involved associated with the selected root traits (total root length (TRL), root system width (RSW), root dry weight (RDW), number of seminal roots (NSR), convex hull area (CHA), root system angle left (RSAL), root system angle right (RSAR), root system angle left and right (RSALR), length of seminal roots per number of seminal roots (LSR/NSR), length of lateral

Figure 52 (Continued). roots per number of lateral roots (LLR/NLR), root systrem depth per root system width (RSD/RSW)) (**A**) and shoot traits (fresh weight shoot (FWS), area of the first leaf (1stLLA), total length of the second leaf (2ndLTL), total length of the first leaf (1stLTL), length of the first leaf blade (1stLBL)) (**B**) on all seven barley chromosoms. The plot was created using the location data of all puative QTLs found in the first QTL analysis (See Supplementary Table S14). Experiments were performed in LD (16/8h) conditions and light intensity of 470 µmol m^{-2} s^{-1} in Jülich.. For the data collection 48 4d-old pre-germinate ILs seedlings of the S42IL population grew for 12d at 16°C or 24°C in LD (16h/8h) and a light intensity of 470 µmol m^{-2} s^{-1}.

In contrast, I also found strong QTL effects for total root length and root dry weight on chromosome 2H between 59.5-60.8 cM and between 120.7 to 129.8 cM, respectively. In addition to these either root- or shoot-specific QTLs, some QTLs were associated with both root and shoot traits simultaneously, indicating pleiotropic effects of these QTLs. Accordingly, my correlation analysis revealed a highly significant positive correlation between the different root and shoot traits at elevated temperatures (e.g., root dry weight and total length of the second leaf (2ndLTL).The extent to which individual genes simultaneously control root and shoot traits at elevated temperatures in barley remains to be seen. From the *A. thaliana* model system, several mobile regulators have been described that control traits in shoots and roots. For example, Chen et al. 2019 showed that ELF4 delivers circadian temperature information from shoots to roots in *A. thaliana.* Similar mechanisms could be involved in the causal genes underlying the pleiotropic QTLs in barley and have to be investigated by others in the future.

7. Conclusion

The aim of my work was to shed light on the genetic mechanisms of temperature root and shoot responses by using a) the established model plant *A. thaliana* and b) initiating first genetic and phenotypic approaches in the monocot barley. Although significant progress has been made to identify the molecular mechanisms of temperature response in the hypocotyls of the model organism, less was known about how these regulators function in a tissue-specific manner during thermomorphogenesis and how temperature signals are communicated between organs. My results postulate a physiological model describing temperature-induced elongation of seedling organs as a result of distinct processes in thermosensing, signaling, and elongation growth, which, in some cases, are spatially separated (Bellstaedt et al. 2019). Together these findings provide a new view to investigate the regulation processes of plant thermomorphogenesis and highlight the general importance for future studies to analyse such signaling and regulatory pathways in a spatiotemporal and tissue-specific context. Moreover, it seems that the root is able to autonomously sense and respond to temperature through partially distinct molecular pathways. The presented data suggest that plants used root-specific regulators to promote temperature-induced root elongation. This assumtion was supported recently by

other studies (Hanzawa et al., 2013, Wang et al., 2016, Yang et al., 2017, Feraru et al., 2019, Gaillochet et al., 2020, Lee et al. 2021). Although I could not See this in my own TIRE-assays, Lee et al. (2021) demonstrated that HY5 as a major playor might regulate temperature responses in the root in a tissue-specific manner. Their data also indicate that HY5 might regulate root thermomorphogenesis by controlling the brassinosteroids (BR) signaling pathway. However, my results of the pharmacolgical experiments with BR biosynthsis inhibitors and of the phenotypic analysis of primary root length using different hormone biosynthsis and signaling mutants indicate that BR plays a minor role in root thermormophogenesis. In contrast, molecular and cellular analyses revealed that an increase of phytohormone Auxin at elevated temperatures in the root apical meristem (RAM) might stimulate temperature-induce primary root elongation. However, compared to the shoot extremly low concentrations of auxin promote elongation and high concentrations inhibit it. Although PIN-FORMED2 (PIN2) might be involved in primary root elongation at elevated temperatures, their exact function still needs to be clarified. It is most likely that the optimal concentration of Auxin in the RAM at elevated temperature might be regulated among other things by the enhanced shootward auxin transport of PIN2.

In general, warm-induced root elongation might be primarily driven by cell divison and not cell elongation such as in temperature-induced hypocotyls elongation. I speculated in turn that auxin might directly affects the cell cycle progression in the root tip by increase the expression level of *CYCD* to activate CDKA which regulate cell entry into both S-and M-phases. However, the link between accelerated cell division and auxin remains to be confirmed by others. Although auxin is sufficient to promote primary root elongation at elevated temperatures in *A. thaliana*, the response level of the hormon mutants in my TIRE assays revealed that auxin signaling and biosynthesis alone is not enough to initiate temperature-induced root elongation. Therefore, additional mechanisms are required in this process. Other thermomorphogenesis players TOC1, HMR, BBX18/23, TCP, FCA working in concert with PIF4 during Arabidopsis hypocotyl elongation, must be analysed for their involevement in temperature-induced root elongation. Thus, continual and further elucidation of the mechanisms allows not only better understanding of the underlying responses but also may help plant breeders for developing varieties suitable for different temperatures in turms of global warming.

Although the 1:1 transfer of the molecular pathways that are known to regulate thermomorphogenesis from well-studied species, such as *A. thaliana*, to other, less well characterized species such as barley, is not possible. The Knowledge about root

thermomorphogenesis will help to identify candidate genes. The large genome size and high abundance of repetitive elements may additionally hamper the progress in identification of temperatur-related regulators. With the present QTL analyses of an barley introgression line poulation, genome regions of interests associated with common temperatur-sensitive root and shoot growth traits could be narrowed down. While most of these QTL regions will remain inaccessible for experimental investigation, some of the major QTLs can be used for fine mapping and cloning of the causal genes and subsequent analyses of the underlying molecular mechanisms in root and shoot at elevated temperatures in barley.

However, although many questions remain unanswered and need to be adressed in the future, my data advances new knowledge of how plants regulated by the plant in response to elevated temperature, and may be helpful in understanding plant adaptations to warmth.

References

Abdel-Ghani, A.H., Sharma, R., Wabila, C. *et al.* (2019). Genome-wide association mapping in a diverse spring barley collection reveals the presence of QTL hotspots and candidate genes for root and shoot architecture traits at seedling stage. *BMC Plant Biol, 19*, 216.

Abts, W., Vandenbussche, B., De Proft, M. P., and Van de Poel, B. (2017). The role of auxin-ethylene crosstalk in orchestrating primary root elongation in sugar beet. *Front. Plant Sci., 8,* 444.

Adamowski, M., Friml, J. (2015). PIN-dependent auxin transport: Action, regulation, and evolution. *Plant Cell*, *27,* 20-2.

Adu, M.O., Chatot, A., Wiesel, L., Bennett, M.J., Broadley, M.R., White, P.J., Dupuy, L.X. (2014). A scanner system for high-resolution quantification of variation in root growth dynamics of Brassica. *Journal of Experimental Botany, 65,* 2039-2048.

Aki, S. S. and Umeda, M. (2016). Cytrap marker systems for in vivo visualization of cell cycle progression in Arabidopsis. *Methods Mol. Biol., 1370,* 51-57.

Al-Rawahy, M.S., Al-Rawahy, S.A., Al-Mulla, Y.A., Nadaf, S.K. (2019). Effect of cooling root-zone temperature on growth, yield and nutrient uptake in cucumber grown in hydroponic system during summer season in cooled greenhouse. *Journal of Agricultural Science, 11,* 47-60.

Alarcón, MV., Salguero J. (2017). Transition zone cells reach G2 phase before initiating elongation in maize root apex. *Biology Open, 6,* 909-913.

Albrecht, H., Fiorani, F., Pieruschka, R., Müller-Linow, M., Jedmowski, C., Schreiber, L., Schurr, U., Rascher, U. (2020).Quantitative Estimation of Leaf Heat Transfer Coefficients by Active Thermography at Varying Boundary Layer Conditions. Frontiers. In *Plant Science,10*.1684

Alsajri, F.A., Singh, B., Wijewardana, C., Irby, J.T. (2019). Gao, W., Reddy, K.R. Evaluating Soybean Cultivars for Low- and High-Temperature Tolerance During the seedling Growth Stage. *Agronomy, 9*, 13.

Amsbury, S., Benitez-Alfonso, Y. (2019). Tightening the pores to unload the phloem. *Nat. Plants, 5*, 561562

Andronis, C., Barak, S., Knowles, S.M., Sugano, S., Tobin, E.M. (2008). The clock protein CCA1 and the bZIP transcription factor HY5 physically interact to regulate gene expression in Arabidopsis. *Mol. Plant,* 1*,* 58-67.

Ang, L.H., Chattopadhyay, S., Wei, N., Oyama, T., Okada, K., Batschauer, A., Deng, X.W. (1998). Molecular interaction between COP1 and HY5 defines a regulatory switch for light control of Arabidopsis development. *Mol. Cell, 1,* 213-222.

Atkinson, J., Pound, M., Bennett, M., Wells, D. (2019). Uncovering the hidden half of plants using new advances in root phenotyping. Curr. Opin. Biotechnol. *55*,1-8.

Arifuzzaman, M., Sayed, MA., Muzammil S., Pillen, K., Schumann, H., Naz, AA., Léon, J. (2014). Detection and validation of novel QTL for shoot and root traits in barley (*Hordeum vulgare* L.). *Mol. Breed., 34,*1373-1387.

Arifuzzaman, M., Günal, S., Bungartz, A., Muzammil, S., Afsharyan, N.P., Léon, J., Naz, A.A. (2017). Correction: Genetic Mapping Reveals Broader Role of *Vrn-H3* Gene in Root and Shoot Development beyond Heading in Barley. *PLOS ONE, 12,* e0177612.

Arndt, D. (2015). Climate change rule of thumb: cold 'things' warming faster than warm 'things. Washington, DC: National Oceanographic and Atmospheric Administration. https://www.climate.gov/news-features/blogs/beyond-data/climatechange-rule-thumb-cold-things-warming-faster-warm-things.

Arndt, C. H. (1937). Water absorption in the cotton plant as affected by soil and water temperatures. *Plant physiology, 2,* 703-720.

Atkin, O.K., Loveys, B.R., Atkinson, L.J., Pons, T.L. (2006). Phenotypic plasticity and growth temperature: understanding interspecific variablility. *J. Exp. Bot.* 57*,* 267-281.

Atkinson, J.A., Wingen, L.U., Griffiths, M., Pound, M.P., Gaju, O., Foulkes, M.J., LeGouis, J., Griffiths, S., Bennett, M.J., King, J., Wells, D.M. (2015). Phenotyping pipeline reveals major seedling root growth QTL in hexaploid wheat. *Journal of Experimental Botany, 66,* 2283-2292.

Atkinson, J. A., Pound, M. P., Bennett, M. J., & Wells, D. M. (2019). Uncovering the hidden half of plants using new advances in root phenotyping. *Current Opinion in Biotechnology, 55,* 1-8.

Belkhadir, Y., Durbak, A., Wierzba, M., Schmitz, RJ., Aguirre, A., Michel, R., Rowe, S., Fujioka, S., Tax, FE. (2010). Intragenic suppression of a trafficking-defective brassinosteroid receptor mutant in Arabidopsis. Genetics *185,* 1283-1296.

Bai, M. Y., Shang, J. X., Oh, E., Fan, M., Bai, Y., Zentella, R., et al. (2012). Brassinosteroid, gibberellin and phytochrome impinge on a common transcription module in Arabidopsis. *Nat. Cell Biol., 14,* 810–817.

Balasubramanian, S., Sureshkumar, S., Lempe, J., Weigel, D. (2006). Potent induction of *Arabidopsis thaliana* flowering by elevated growth temperature. *PLoS Genetics, 2,*106.

Bargmann, BOR, Birnbaum, KD. (2009). Positive fluorescent selection permits precise, rapid, and in-depth overexpression analysis in plant protoplasts. *Plant Physiol., 149,*1231-9.

Baum, S. & T., Nhat, P., Silk, W. (2000). Effects of salinity on xylem structure and water use in growing leaves of sorghum. *New Phytologist., 146,* 119-127.

Becnel, J., Natarajan, M., Kipp, A., Braam, J. (2006). Developmental expression patterns of Arabidopsis *XTH* genes reported by transgenes and Genevestigator. *Plant Mol. Biol., 61,* 451-467.

Beemster, G. T., & Baskin, T. I. (1998). Analysis of cell division and elongation underlying the developmental acceleration of root growth in Arabidopsis thaliana. *Plant physiology, 116,* 1515–1526.

Bellstaedt, J., Trenner, J., Lippmann, R., Poeschl, Y., Zhang, X., Friml,. J, Quint, M., Delker, C. (2019). A mobile auxin signal connects temperature sensing in cotyledons with growth responses in hypocotyls. *Plant Physiol., 180,* 757-766.

Belter, P. R., Cahill, J. F., J. (2015). Disentangling root system responses to neighbours: identification of novel root behavioural strategies. *AoB Plants*, *7,* plv059.

Benfey, P. N. (2002). Auxin action: slogging out of the swamp. *Curr. Biol.*, *12,* 389-390. Bengough, G., Gordon, D.C., Al-Menaie, H., Ellis, R.P. ,Allan, D., Keith, R., Thomas, W.T.B, Forster, B.P. (2004). Gel observation chamber for rapid screening of root traits in cereal seedlings. *Plant and Soil, 262,* 63-70.

Berriri, S., Gangappa, S.N., Kumar, S.V. (2016). SWR1 chromatin-remodeling complex subunits and H2A.Z have non-overlapping functions in immunity and gene regulation in Arabidopsis. *Mol. Plant, 9,* 1051-1065.

Björk, R.G., Majdi, H., Klemedtsson, L., Lewis-Jonsson, L., Molau, U. (2007). Long-term warming effects on root morphology, root mass distribution, and microbial activity in two dry tundra plant communities in northern Sweden. *New Phytologist*, *176,* 862-873.

Blakeslee, J., Bandyopadhyay, A., Lee, O.R., Mravec, J., Titapiwatanakun, B., Sauer, M., Makam, S.N., Cheng, Y., Bouchard, R., Adamec, J., Geisler, M., Nagashima, A., Sakai, T., Martinoia, E., Friml, J., Peer, W.A., Murphy, A.S. (2007). Interactions among PIN-FOR-MED and P-Glycoprotein auxin transporters in Arabidopsis. *Plant Cell, 19,* 131-47.

Blilou, I., Xu, J., Wildwater, M., Willemsen, V., Paponov, I., Friml, J.,et al. (2005). The PIN auxin efflux facilitator network controls growth and patterning in Arabidopsis roots. *Nature, 433,* 39–44.

Boden, S.A., Kavanová, M., Finnegan, E.J., Wigge, P.A. (2013). Thermal stress effects on grain yield in *Brachypodium distachyon* occur via H2A.Z-nucleosomes. *Genome Biol., 14,* 65.

Bahmani, I., Hazard, L., Varlet-Grancher, C., Betin, M., Lemaire, G., Mattew, C., Thom, E.R. (2000). Differences in tillering of long- and short-leaved perennial ryegrass genetic lines under full light and shade treatments. *Crop Science*, *40,* 1095–1102.

Beaumont, C., Millet, N., Le Bihan-Duval, E., Kipi, Dupuy, A., V. (1997). Genetic parameters of survival to the different stages of embryonic death in laying hens. Poult. Sci., *76 ,* 1193-1196.

Bojar, D. , Martinez, J. , Santiago, J. , Rybin, V. , Bayliss, R. , Hothorn, M. (2014). Crystal structures of the phosphorylated BRI1 kinase domain and implications for brassinosteroid signal initiation. *Plant J., 78,* 31-43.

Bouteillé M, Rolland G, Balsera C, Loudet O, Muller B. (2012). Disentangling the intertwined genetic bases of root and shoot growth in Arabidopsis. *PLoS ONE, 7.*

Box, J.E., Ramsuer, E.L. (1993). Mini rhizotron wheat root data: comparisons to soil core root data. *Agronomy Journal, 85,* 1058-1060.

Brar, G.S., Gomez, J.F., McMichael, B.L., Matches, A.G., Tailor, H.M. (1991). Germination of twenty forage legumes as influenced by temperature. *Agron. J., 83,* 173-175.

Bingham, I. (2001). Soil-root-canopy Interactions. *Ann. Appl. Biol.*, *138*, 243-251.

Brunoud, G., Wells, DM. Oliva, M., Larrieu, A., Mirabet, V., Burrow, AH., Beeckman, T., Kepinski, S., Traas, J., Bennett, M.J., Vernoux, T. (2012). A novel sensor to map auxin response and distribution at high spatio-temporal resolution. *Nature, 482,* 103-106.

Bultynck L., Ter Steege M.W., Schortemeyer M., Poot P., Lambers H. (2004). From individual leaf elongation to whole shoot leaf area expansion: a comparison of three Aegilops and two Triticum species. Annals of Botany *94,* 99-108.

Burgess, A. J., Retkute, R., Preston, S. P., Jensen, O. E., Pound, M. P., Pridmore, T. P., et al. (2016). The 4-dimensional plant: effects of wind-induced canopy movement on light fluctuations and photosynthesis. *Front. Plant Sci., 7,* 1392.

Burko, Y., Gaillochet, C., Seluzicki, A., Chory, J. & Busch, W. Local HY5 activity mediates hypocotyl growth and shoot-to-root communication.(2020). *Plant Commun., 1,* 100078.

Burton G.W. and Devane E.M. (1953) Estimating heritability in tall fescue (*Festuca arundinacea*) from replicated clonal material. *Agronomy Journal*, 45, 478-481.

Calleja-Cabrera, J., Boter, M., Oñate-Sánchez, L., & Pernas, M. (2020). Root Growth Adaptation to Climate Change in Crops. *Frontiers in plant science, 11,* 544.

Calixto, C.P.G., Waugh, R. & Brown, J.W.S. Evolutionary Relationships Among Barley and Arabidopsis Core Circadian Clock and Clock-Associated Genes. (2015). J. Mol. Evol. *80,* 108-119.

Camut, L., Regnault, T., Sirlin-Josserand, M., Sakvarelidze-Achard, L., Carrera, E., Zumsteg, J., et al. (2019). Root-derived GA12 contributes to temperatureinduced shoot growth in Arabidopsis. *Nat. Plants*, *5,* 1216-1221.

Canamero, R.C., Bakrim, N., Bouly, J.P., Garay, A., Dudkin, E.E., Habricot, Y., Ahmad, M. (2006). Cryptochrome photoreceptors cry1 and cry2 antagonistically regulate primary root elongation in *Arabidopsis thaliana*. *Planta, 224*, 995-1003.

Cano-Delgado, A., Yin, Y., Yu, C., Vafeados, D., Mora-Garcia, S., Cheng, J. C., Nam, K. H., Li, J. Chory, J. (2004). BRL1 and BRL3 are novel brassinosteroid receptors that function in vascular differentiation in Arabidopsis. *Development*,*131*, 5341-5351.

Cao, M., Chen, R., Li, P., Yu, Y., Zheng, R., Ge, D., Zheng, W., Wang, X., Gu, Y., Gelova, Z., Friml, J., Zhang, H., Liu, R., He, J. and Xu, T. (2019). TMK1-mediated auxin signaling regulates differential growth of the apical hook. *Nature, 568*, 240-243.

Casal, J.J., Balasubramanian, S. (2019). Thermomorphogenesis. *Annu. Rev. Plant Biol.,* 70, 321-346.

Castillon, A., Shen, H., and Huq, E. (2007). Phytochrome interacting factors: central players in phytochrome-mediated light signaling networks. *Trends Plant Sci., 12,* 514-521.

Chakrabarti, B., Singh, S.D., Kumar, V. *et al.* Growth and yield response of wheat and chickpea crops under high temperature.(2013). *Ind. J .Plant Physiol., 18*, 7-14 .

Chaiwanon, J., Wang, Z.Y. (2015). Spatiotemporal brassinosteroid signaling and antagonism with auxin pattern stem cell dynamics in Arabidopsis roots. *Curr. Biol., 25,* 1031-1042.

Chen, Q., Dai, X., De-Paoli, H., Cheng, Y., Takebayashi, Y., Kasahara, H., Kamiya, Y., Zhao Y. (2014). Auxin overproduction in shoots cannot rescue auxin deficiencies in Arabidopsis roots. *Plant and Cell Physiol.*, *55,* 1072-1079.

Chen, W.W., Takahashi, N., Hirata, Y., Ronald, J., Porco, S., Davis, S.J., Nusinow, D.A., Kay, S.A., and Mas, P. (2020). A mobile ELF4 delivers circadian temperature information from shoots to roots. *Nature Plants*, *6,* 416-426.

Choudhary, S.P., Yu, J.Q., Yamaguchi-Shinozaki, K., Shinozaki, K., Tran, L. S. P. (2012). Benefits of brassinosteroid crosstalk. *Trends Plant Sci., 17,* 594-605.

Christopher, J., Christopher, M., Jennings, R., Jones, S., Fletcher, S., Borrell, A., Manschadi, A.M., Jordan, D., Mace, E., Hammer, G. (2013). QTL for root angle and number in a population developed from bread wheats (Triticum aestivum) with contrasting adaptation to water-limited environments. *Theoretical and Applied Genetics, 126*, 1563-1574.

Chung, B.Y.W., Balcerowicz, M., Di Antonio, M., Jaeger, K.E., Geng, F., Franaszek, K., Morriott, P., Brierley, I., Firth, A.E., Wigge, P.A. (2020). An RNA thermoswitch regulates daytime growth in Arabidopsis. *Nat. Plants*, *6*, 522-532.

Clark, R.T., McCurdy, R.B., Jung, J.K., Shaff, J.E., McCouch, S.R., Aneshansley, D.J., Kochian, L.V. (2011). Three-dimensional root phenotyping with a novelimaging and software platform. *Plant Physiology*, *156*, 455-465.

Coleman-Derr, D., Zilberman, D. (2012). Deposition of Histone Variant H2A.Z within Gene Bodies Regulates Responsive Genes. *PLoS Genet, 8*, 1002988.

Colom, S. M., and Baucom, R. S. (2020). Belowground competition can influence the evolution of root traits. *Am. Nat., 195*, 577-590.

Comadran, J., Kilian, B., Russell, J., Ramsay, L., Stein, N., Ganal, M., Shaw, P., Bayer, M., Thomas, W., Marshall, D., Hedley, P., Tondelli, A., Pecchioni, N., Francia, E., Korzun, V., Walther, A., Waugh, R. (2012). Natural variation in a homolog of Antirrhinum CENTRORADIALIS contributed to spring growth habit and environmental adaptation in cultivated barley. *Nat. Genet.*, *44*, 1388.

Comas, L. H., Bouma, T. J., and Eissenstat, D. M. (2002). Linking root traits to potential growth rate in six temperate tree species. *Oecologia, 132*, 34-43.

Comas, L. H., Mueller, K. E., Taylor, L. L., Midford, P. E., Callahan, H. S., and Beerling, D. J. (2012). Evolutionary patterns and biogeochemical significance of angiosperm root traits. *Int. J. Plant Sci.*, *173*, 584-595.

Cooper, A.J. (1973). Influence of rooting-medium temperature on growth of *Lycopersicon esculentum. Annals of Applied Biology*, *74,* 379-385.

Correll, M.J., Kiss, J.Z. (2005). The roles of phytochromes in elongation and gravitropism of roots. *Plant Cell Physiol.*, *46*, 317-323.

Cortijo, S., Charoensawan, V., Brestovitsky, A., Buning, R., Ravarani C, Rhodes D, van Noort J, Jaeger KE, Wigge P.A. (2017).Transcriptional regulation of the ambient

temperature response by H2A.Z-nucleosomes and HSF1 transcription factors in Arabidopsis. *Mol. Plant,* 10, 1258-1273.

Craw, D., Wilson, N. and Ashley, P.M. (2004) Investigation of physiological responses and leaf morphological traits of wheat genotypes with contrasting drought stress tolerance. *Appl. Earth Sci. Imm. Trans., 113*, B3-B10.

Crawford, A.J., McLachlan, D.H., Hetherington, A.M., Franklin KA. (2012). High temperature exposure increases plant cooling capacity. *Curr. Biol., 22*, R396-R397.

Cruz-Ramírez, A., Díaz-Triviño, S., Blilou, I., Grieneisen, V. A., Sozzani, R., Zamioudis, C., Miskolczi, P., Nieuwland, J., Benjamins, R., Dhonukshe, P., Caballero-Pérez, J., Horvath, B., Long, Y., Mähönen, A. P., Zhang, H., Xu, J., Murray, J. A., Benfey, P. N., Bako, L., Marée, A. F. M., Scheres, B. (2012). A bistable circuit involving SCARECROW-RETINOBLASTOMA integrates cues to inform asymmetric stem cell division. *Cell, 150,*1002-1015.

Cuadrado, A., Navarrete, M.H.,Canovas, J.L. (1989). Exponential pattern of cell age distribution in dividing cells of plant meristems. *Cell Biololy International Reports, 13*, 283-289.

Czechowski, T., Stitt, M., Altmann, T., Udvardi, M.K., Scheible, W.R. (2005). Genome-wide identification and testing of superior reference genes for transcript normalization in Arabidopsis. *Plant Physiol., 139,* 5-17.

David, K.M., Couch, D., Braun, N., Brown, S., Grosclaude, J., Perrot-Rechenmann, C. (2007). The auxin-binding protein 1 is essential for the control of cell cycle. *Plant J., 50,*197-206

Davies, K., Evans, A., Oxley, S. (2007). Impact of climate change in Scotland on crop pests, weeds and diseases. Technical note *605*. The Scottish Agricultural College, Edinburgh.

Deal, R.B., Topp, C.N., McKinney, E.C., Meagher, R.B. (2007). Repression of flowering in Arabidopsis requires activation of *FLOWERING LOCUS C* expression by the histone variant H2A.Z. *Plant Cell*, *19*, 74-83.

Deák, C., Jäger, K., Fábián, A., Nagy, V., Albert, Z., Miskó, A., Barnabás, B. et al. (2011). Investigation of physiological responses and leaf morphological traits of wheat genotypes with contrasting drought stress tolerance. *Acta Biologica Szegediensis*, *55*, 69-71.

De Veylder, L., Beeckman, T., Beemster, G.T., de Almeida Engler, J., Ormenese, S., Maes, S., Naudts, M., Van Der Schueren, E., Jacqmard, A., Engler, G. and Inze, D. (2002). Control of proliferation, endoreduplication and differentiation by the Arabidopsis E2Fa-DPa transcription factor. *EMBO J.*, *21,* 1360-1368.

de Lucas, M., Davière, J.M. Rodríguez-Falcón, M., Pontin, M., Iglesias-Pedraz, J.M., Lorrain, S., Fankhauser, C., Blázquez, M.A., Titarenko, E., Prat, S. (2008). A molecular framework for light and gibberellin control of cell elongation. *Nature*, *451,* 480-484.

Dello Ioio R, Scaglia Linhares F, Scacchi E, Casamitjana-Martinez E, Heidstra R, et al. (2007). Cytokinins determine Arabidopsis root-meristem size by controlling cell differentiation. *Current Biology*, *17,* 678-682.

del Pozo, J.C., Boniotti, M.B., Gutierrez, C. (2002). Arabidopsis *E2Fc* functions in cell division and is degraded by the ubiquitin-SCF(AtSKP2) pathway in response to light. Plant Cell *14,* 3057-3071.

Delker, C., Sonntag, L., James, G.V., Janitza,. P, Ibañez, C., Ziermann, H., Peterson, T., Denk, K., Mull, S., Ziegler, J., Davis, S.J., Schneeberger, K., Quint, M. (2014). The DET1-COP1-HY5 pathway constitutes a multipurpose signaling module regulating plant photo-morphogenesis and thermomorphogenesis. *Cell Rep.*, *9,* 1983-1989.
Delker, C., van Zanten, M., Quint, M. (2017). Thermosensing enlightened. *Trends Plant Sci., 22,* 185-187.

De Smet, I. (2012). Lateral root initiation: one step at a time. *New Phytologist ,193*, 867-873.

Draeger, T., Moore, G. (2017). Short periods of high temperature during meiosis prevent normal meiotic progression and reduce grain number in hexaploid wheat (*Triticum aestivum L.*). *Theoretical and Applied Genetics, 130*, 1785-1800.

Drebenstedt, I., Schmid, I., Poll, C., Marhan, S., Kahle, R., Kandeler, E., Högy, P. (2020). Effects of soil warming and altered precipitation patterns on photosynthesis, biomass production and yield of barley. *Journal of Applied Botany and Food Quality*, *93*, 44-53.

do Rosário, G.O., Van Noordwijk, M. ,Gaze, S.R.,, Brouwer, G., Bona, S., Mosca, G., Hairiah, K. (2000). Auger sampling, in growth cores and pinboard methods. In: Root methods: A Handbook. Eds. A. L. Smit, A. G. Bengough, C. Engels, M. van Noordwijk, S. Pellerin and S. C. van de Geijn. pp. 175–210. Springer-Verlag, Berlin.

Downie, H., Holden, N., Otten, W., Spiers, A.J., Valentine, T.A., Dupuy, L.X. (2012). Transparent soil for imaging the rhizosphere. *PLoS One, 7,* e44276.

Duncan, W.G. (1971) Leaf angle, leaf area and canopy photosynthesis. *Crop Sci.,11*, 482-485

Edgar, R., Domrachev, M., Lash, A.E. (2002). Gene Expression Omnibus: NCBI gene expression and hybridization array data repository. *Nucleic Acids Res.*, *30*, 207-210.

Edmands, S., (1999). Heterosis and outbreeding depression in interpopulation crosses spanning a wide range of divergence. *Evolution*, *53*, 1757-1768.

Edwards, K.D., Akman, O.E., Knox, K., Lumsden, P.J., Thomson, A.W., Brown, P.E., Pokhilko, A., Kozma-Bognár, L., Nagy, F., Rand, D.A., Millar, A.J. (2010). Quantitative analysis of regulatory flexibility under changing environmental conditions. *Mol. Syst. Biol.*, *6,* 424.

Eissenstat, D.M. (1992). Costs and benefits of constructing roots of small diameter. *J. Plant Nutr.*, *15*, 763-782.

Ejaz, M., von Korff, M. (2017). The Genetic Control of Reproductive Development under High Ambient Temperature, Plant Physiology ,*173*, 294-306.

El Hassouni, K., Alahmad, S., Belkadi, B., Filali-Maltouf, A., Hickey, L. T., and Bassi, F. M. (2018). Root system architecture and its association with yield under different water regimes in durum wheat. *Crop Sci., 58*, 2331-2346.

Endo, M., Nakamura, S., Araki, T., Mochizuki, N., Nagatani, A. (2005). Phytochrome B in the mesophyll delays flowering by suppressing *FLOWERING LOCUS T* expression in Arabidopsis vascular bundles. *Plant Cell*., *17,* 1941-1952.

Erwin, J.E., Heins, R.D., Karlsson, M.G. (1989). Thermomorphogenesis in Lilium longiflorum. *Thunb. Amer. J. Bot., 76,*47-52.

Evers, J.B., Vos, J., Andrieu, B., Struik, P.C. (2006). Cessation of tillering in spring wheat in relation to light interception and red: far red ratio. *Annals of Botany*, *97*, 649-658.

Feng, S., Martinez, C., Gusmaroli, G., Wang, Y., Zhou, J., Wang, F., Chen, L., Yu, L., Iglesias-Pedraz, J.M., Kircher, S., Schafer, E., Fu, X., Fan, L.M., Deng, X.W. (2008). Coordinated regulation of *Arabidopsis thaliana* development by light and gibberellins. *Nature, 451,* 475-479.

Fei, Q., Wei, S., Zhou, Z., Gao, H., Li, X. (2017). Adaptation of root growth to increased ambient temperature requires auxin and ethylene coordination in Arabidopsis. *Plant cell reports*, *36*, 1507-1518.

Fei, Q., Liang, L., Li, F., Zhang, L., Li, Y., Guo, Y., Wu, L., Meng, X., Gao H., Li, X. (2019). Transcriptome profiling and phytohormone responses of Arabidopsis roots to different ambient temperatures, *Journal of Plant Interactions*, *14*, 314-323,

Fei, Q., Li, J., Luo, Y.，Kun, Ma., Niu, B., Mu, C.H., Gao, H.，Li, X. (2018). Plant molecular responses to the elevated ambient temperatures expected under global climate change. *Plant signaling & Behavior*, *13*, 1414123.

Feng, J., Ma, L. A. (2017). Method for Characterizing Embryogenesis in *Arabidopsis*. *J. Vis. Exp.* 126, e55969

Feraru, E., Feraru, M.I., Barbez, E., Waidmann, S., Sun, L., Gaidora, A., Kleine-Vehn, J. (2019). PILS6 is a temperature-sensitive regulator of nuclear auxin input and organ growth in *Arabidopsis thaliana*. *Proc. Natl. Acad. Sci. USA, 116*, 3893-3898.

Ferreira, P.C., Hemerly, A.S., Engler, J.D., van Montagu, M., Engler, G., Inzé, D. (1994) Developmental expression of the Arabidopsis cyclin gene cyc1. *At. Plant Cell*, *6*,1763-1774.

Fiorani, F., Schurr, U. (2013). Future scenarios for plant phenotyping. *Annu. Rev. Plant Biol.*, *64*, 267-291.

Fleming M., McCormack, M. (2012). Effect of Ambient Air Temperature on Leaf Size in Raphanus sativus. Pepperdine University, Featured Research. Paper 50. https://digital-commons.pepperdine.edu/sturesearch/50

Forgiarini, C. , Souza, A. F. , Longhi, S. J. , Oliveira, J. M. (2015). In the lack of extreme pioneers: Trait relationships and ecological strategies of 66 subtropical tree species. *Journal of Plant Ecology, 8*, 359-367.

Francis, D., Barlow, P.W. (1988). Temperature and the cell cycle. Symp. Soc. Exp. Biol. *42*, 181-202.

Franklin, K.A., Wigge, P.A. (2014). Temperature and Plant Development. *John Wiley and Sons Inc. Oxford. UK., 243*.

Franklin K.,A., Lee, S.H., Patel, D., Kumar, S.V., Spartz A.K., Gu, C., Ye, S., Yu, P., Breen, G., Cohen, J.D., Wigge, P.A., Gray, W.M. (2011). Phytochrome-interacting factor 4 (PIF4) regulates auxin biosynthesis at high temperature. *Proc. Natl. Acad. Sci. USA, 108*, 20231-20235.

Friml, J., Benková, E., Blilou, I., Wisniewska, J., Hamann, T., Ljung, K., Woody, S., Sandberg, G., Scheres, B., Jürgens, G. ,Palme, K. (2002) AtPIN4 mediates sink-driven auxin gradients and root patterning in Arabidopsis. *Cell*, *108*, 661-673.

Friml, J., Vieten, A., Sauer, M., Weijers, D., Schwarz, H., Hamann, T., Offringa, R., Jürgens, G. (2003). Efflux-dependent auxin gradients establish the apical-basal axis of Arabidopsis. *Nature*, *426*, 147-153.

Friml, J., Yang, X., Michniewicz, M., Weijers, D., Quint, A., Tietz, O., Benjamins, R., Ouwerkerk, P.B.F, Ljung, K., Sandberg, G., et al. (2004). A PINOID-dependent binary switch in apical-basal PIN polar targeting directs auxin efflux. *Science, 306,* 862-865

Fujii, Y., Tanaka, H., Konno, N., Ogasawara, Y., Hamashima, N., Tamura, S., Hasegawa, S., Hayasaki, Y., Okajima, K., Kodama, Y. (2017). Phototropin perceives temperature based on the lifetime of its photoactivated state. *Proc. Natl. Acad. Sci. USA*, *114,* 9206-9211.

Gaillochet,C., Burko, Y., Platre, M.P., Zhang, L., Simura, J., Kumar, V., Ljung, K., Chory, J., Busch, W. (2020). Shoot and root thermomorphogenesis are linked by a developmental trade-off *bioRxiv.*

Gallagher, J.N. (1979). Field studies of cereal leaf growth: 1. initiation and expansion in relation to température and ontogeny. *Journal of Experimental Botany*, *30.* 625-636.

Gampala, S. S., Kim, T. W., He, J. X., Tang, W., Deng, Z., Bai, M. Y., Guan, S., Lalonde, S., Sun, Y., Gendron, J. M., Chen, H., Shibagaki, N., Ferl, R.J., Ehrhardt, D., Chong, K., Burlingame, A.L., Wang, Z.Y. (2007). An essential role for 14-3-3 proteins in brassinosteroid signal transduction in Arabidopsis. *Dev. Cell, 13*, 177-189 .

Gangappa, S.N., Botto, J.F. (2014). The BBX family of plant transcription factors. *Trends in Plant Science, 19*, 60-470.

Gangappa, S.N., Botto, J.F. (2016). The multifaceted roles of HY5 in plant growth and development. *Mol. Plant*, *9,* 1353-1365.

Gangappa, S.N., Kumar, S.V. (2017). DET1 and HY5 control PIF4-mediated thermosensory elongation growth through distinct mechanisms. *Cell Rep.*, *18*, 344-351.

Gangappa, S.N., Berriri, S., Kumar, S.V. (2017). PIF4 coordinates thermosensory growth and immunity in Arabidopsis. *Curr. Biol.*, *27*, 243-249.

Gates, D.M., Alderfer, R., Taylor, E. (1968). Leaf temperatures of desert plants. *Science.,* 15, 994-995.

Gavito, M. E., Curtis, P.S., Mikkelsen, T. N., Jakobsen, I. (2001). Interactive effects of soil temperature, atmospheric carbon dioxide and soil N on root development, biomass and

nutrient uptake of winter wheat during vegetative growth, *Journal of Experimental Botany, 52(362),* 1913-1923.

Geisler, M., Blakeslee, J.J., Bouchard, R., Lee, O.R., Vincenzetti, V., Bandyopadhyay, A., Titapiwatanakun, B., Peer, W.A., Bailly, A., Richards, E.L., Ejendal, K.F.K., Smith, A.P., Baroux, C., Grossniklaus,U., Müller, Hrycyna, C.A., Dudler, R., Murphy, A.S., Martinoia, E. (2005). Cellular efflux of auxin catalyzed by the Arabidopsis MDR/PGP transporter AtPGP1. *Plant J., 44,* 179-194.

Georgopoulos, C., Welch, W.J. (1993). Role of the major heat shock proteins as molecular chaperones. *Annu. Rev. Cell Biol., 9,* 601-634.

Gillman, J.D., Biever, J.J., Ye, S., Spollen, W.G., Givan, S.A., Lyu, Z., Joshi, T., Smith, J.R., Fritschi, F.B. (2019). A Seed germination transcriptomic study contrasting two soybean genotypes that differ in terms of their tolerance to the deleterious impacts of elevated temperatures during Seed fill. *BMC Research Notes, 12*, 522.

Gioia, T., Galinski, A., Lenz, H., Müller, C., Lentz, J., Heinz, K., Briese, C., Putz, A., Fiorani, F., Watt, M., Schurr, U., Nagel, K.A. (2016). GrowScreen-PaGe, a non-invasive, medium-throughput phenotyping system based on germination paper to quantify crop phenotypic diversity and plasticity of root traits under varying nutrient supply. *Funct. Plant Biol., 44*, 76-93.

Givnish, T. J. (1979). On the adaptive significance of compound leaves, with particular reference to tropical trees. In:Tropical Trees as Living System (Tomlinson, P. B. & Zimmermann, M. H., eds) pp. 351-380. Cambridge: Cambridge University Press.

Givnish, T. J. &Vermeij, G. A. (1976). Sizes and shapes of liane leaves. *Am. Nat., 110*, 743-776.

Glinski, J., Lipiec, J. (1990). Soil physical conditions and plant roots. CRC Press. *Boca Raton, FL.*

GOMEZ-MACPHERSON, H. A. (1993). Variation in phenology and its influence on growth, development and yield of dryland wheat . Ph.D. Thesis. *Australian National University, Canberra Australia,*

González-García, M.P., Vilarrasa-Blasi, J., Zhiponova, M., Divol, F., Mora-García, S., Russinova, E., Caño-Delgado, AI. (2011). Brassinosteroids control meristem size by promoting cell cycle progression in Arabidopsis roots. *Development., 138*, 849-59.

Goudriaan, J. (1995). Optimization of nitrogen distribution and of leaf area index for maximum canopy assimilation rate. In Thiyagarajan, T.M., ten Berge, H.F.M. and Wopereis, M. C.S., nitrogen management studies in irrigated rice. *SARP Research Proceedings-May.,* 85-97.

Gould, P.D., Locke, J.C., Larue, C., Southern, M.M., Davis, S.J., Hanano, S., Moyle, R., Milich, R., Putterill, J., Millar, A.J., Hall, A. (2006). The molecular basis of temperature compensation in the Arabidopsis circadian clock. *Plant Cell, 18,* 1177-1187.

Grando, M.S., De Micheli, L., Biasetto, L.,Scienza, A. (1995). RAPD markers in wild and cultivated Vitis vinifera. *Vitis, 34*, 37-39.

Gray, W.M., Östin, A., Sandberg, G., Romano, C.P., Estelle, M. (1998). High temperature promotes auxin-mediated hypocotyl elongation in Arabidopsis. *Proc. Natl. Acad. Sci. USA*, *95*, 7197-7202.

Gregory, P. J. (1986). Response to temperature in a stand of Pearl Millet (Pennisetum typhoides S. & H.). VIII. Root growth. *J. Exp. Bot., 37,* 379-388.

Gregory, F. G. (1928). Studies in the energy relations of plants. II. The effect of temperature on increase in area of leaf surface and in dry weight of *Cucumis tativus*. Part I. The effect of temperature on the increase in area of leaf surface. *Ann. Bot.*, *42*, 460-507

Grieneisen, V.A.,Xu, J., Marée, A.F.M, Hogeweg, P., Scheres, B. (2007). Auxin transport is sufficient to generate a maximum and gradient guiding root growth. *Nature, 449*,1008-1013

Guan, Y. F., Li, G. R., Wang, R. J., Yi, Y. T., Yang, L., Jiang, D., Zhang, X. P., & Peng, Y. (2012). Application of next-generation sequencing in clinical oncology to advance personalized treatment of cancer. *Chinese journal of cancer*, *31,* 463-470.

Guo, Z., Fujioka, S., Blancaflor, E.B., Miao, S., Gou, X., Li, J. (2010). TCP1 modulates brassinosteroid biosynthesis by regulating the expression of the key biosynthetic gene *DWARF4* in *Arabidopsis thaliana. Plant Cell*, *22*, 1161-1173.

Hacham, Y., Holland, N., Butterfield, C., Ubeda-Tomas, S., Bennett, M.J., Chory, J., Savaldi-Goldstein, S. (2011). Brassinosteroid perception in the epidermis controls root meristem size. Development *138,* 839-48.

Haltenhof, T., Kotte, A., De Bortoli, F., Schiefer, S., Meinke, S., Emmerichs, A.K., Petermann, K.K., Timmermann, B., Imhof, P., Franz, A., Loll, B., Wahl, M.C., Preußner, M., Heyd, F. A. (2020). Conserved Kinase-Based Body-Temperature Sensor Globally Controls Alternative Splicing and Gene Expression. *Mol. Cell*, *78,* 57-69.

Hanzawa, Y., Money, T., Bradley, D. (2005). A single amino acid converts a repressor to an activator of flowering. *Proc. Natl. Acad. Sci. USA,102*, 7748-7753.

Hanzawa, T., Shibasaki, K., Numata, T., Kawamura, Y., Gaude, T., Rahman, A. (2013). Cellular auxin homeostasis under high temperature is regulated through a SORTING NEXIN1–dependent endosomal trafficking pathway. *Plant Cell*, *25,* 3424-33.

Haussling, M., Jorns, C. A., Lehmbecker, G., Hechtbuchholz, C., and Marschner, H. (1988). Ion and water uptake in relation to root development in Norway spruce (*Picea abies* (L.) Karst.). *J. Plant Physiol.*, *133*, 486-491.

Hayashi, K. (2012). The interaction and integration of auxin signaling components. Plant Cell Physiol., *53*, 965-75.

Hayes, S., Sharma, A., Fraser, D.P., Trevisan, M., Cragg-Barber, C.K., Tavridou E, Fankhauser C, Jenkins GI, Franklin, K.A. (2017). UV-B perceived by the UVR8 photoreceptor inhibits plant thermomorphogenesis. *Curr. Biol.*, *27*, 120-127.

He, S.B., Wang, W.X., Zhang, J.Y., Xu, F., Lian, H.L., Li, L., Yang, H.Q. (2015). The CNT1 domain of Arabidopsis CRY1 alone is sufficient to mediate blue light inhibition of hypocotyl elongation. *Mol. Plant*, *8*, 822-825.

Heckathorn, S.A., Giri, A., Mishra, S., Bista,. D (2013). Heat stress and roots. In: Climate Change and Plant Abiotic Stress Tolerance. (eds. Tuteja N, Gill SS). Wiley-VCH Verlag GmbH & Co. Weinheim, Germany, 109-136.

Heckathorn, S. A., Poeller, G. J., Coleman, J. S., and Hallberg, R. L. (1996). Nitrogen availability alters patterns of accumulation of heat stress-induced proteins in plants. *Oecologia, 105*, 413-418.

Hellmann, H., Estelle, M. (2002). Plant development: regulation by protein degradation. *Science*, *297,* 793-797.

Hemming, M.N., Walford, S.A., Fieg, S., Dennis, E.S., Trevaskis, B. (2012). Identification of high-temperature-responsive genes in cereals. *Plant Physiology*,*158*, 1439–1450.

Himanen, K., Boucheron, E., Vanneste, S., Engler, J.D.A., Inzé, D., Beeckman, T. (2002). Auxin-mediated cell cycle activation during early lateral root initiation. *Plant Cell*, *14*, 2339-2351.

Hoffmann, A., Maurer, A., Pillen, K. (2012). Detection of nitrogen deficiency QTL in juvenile wild barley introgression lines growing in a hydroponic system. *BMC Genet., 13*, 88.

Holm, M., Ma, L.G., Qu, L.J., Deng, X.W. (2002). Two interacting bZIP proteins are direct targets of COP1-mediated control of light-dependent gene expression in Arabidopsis. *Genes Dev., 16*, 1247-1259.

Honsdorf, N., March, T.J., Berger, B., Tester, M., Pillen, K. (2014a). medium-throughput phenotyping to detect drought tolerance QTL in wild barley introgression lines. *PLoS ONE, 9*, 97047.

Honsdorf, N., March, T.J., Berger, B., Tester, M., Pillen, K. (2014b). Evaluation of juvenile drought stress tolerance and genotyping by sequencing with wild barley introgression lines. *Mol. Breed., 34*, 1475-1495.

Honsdorf, N., March, T.J., Pillen, K. (2017). QTL controlling grain filling under terminal drought stress in a set of wild barley introgression lines. *PLoS ONE, 12*, e0185983.
Huang B. R., Taylor H. M., McMichael B. L. (1991). Growth and development of seminal and crown roots of wheat seedlings as affected by temperature. *Environ. Exp. Bot.*, *31* 471-477.

Hu, W., Franklin, K.A., Sharrock, R.A., Jones, M..A, Harmer, S.L., Lagarias, J.C. (2013). Unanticipated regulatory roles for Arabidopsis phytochromes revealed by null mutant analysis. Proc. *Natl. Acad. Sci. USA, 110*, 1542-1547.

Hu, W., Figueroa-Balderas, R., Chi-Ham, C., & Lagarias, J. C. (2020). Regulation of monocot and dicot plant development with constitutively active alleles of phytochrome B. *Plant direct*, *4*, e00210.
Hund, A., Trachsel, S., Stamp, P. (2009). Growth of axile and lateral roots of maize. *In* Development of a phenotying platform. *Plant and Soil, 325*, 335-349.

Herud-Sikimić, O., Stiel, A.C., Kolb, M., Shanmugaratnam, S., Berendzen, K.W., Feldhaus, C., Höcker, B., Jürgens, G. A. (2021). biosensor for the direct visualization of auxin. *Nature*, *592*, 768-772.

Hurewitz, J.,Janes, H. W. (1983). Effect of altering the rootzone temperature on growth, translocation, carbon exchange rate, and leaf starch accumulation in the tomato. *Plant Physiol*. *73*, 46-50.

Ibañez, C., Poeschl, Y., Peterson, T., Bellstädt, J., Denk, K., Gogol-Döring, A., Quint, M., Delker, C. (2017). Ambient temperature and genotype differentially affect developmental and phenotypic plasticity in *Arabidopsis thaliana*. *BMC Plant Biol.*, *17*, 114.

Ibañez, C., Delker, C., Martinez, C., Bürstenbinder, K., Janitza, P., Lippmann, R., Ludwig, W., Sun, H., James, G.V., Klecker, M., Grossjohann, A., Schneeberger, K., Prat, S., Quint, M. (2018). Brassinosteroids dominate hormonal regulation of plant thermomorphogenesis via *BZR1*. *Curr Biol.*, *28,* 303-310.

Iqbal, A., Wang, T., Wu, G., Tang, W., Zhu, C., Wang, D., Li, Y., Wang, H. (2017). Physiological and transcriptome analysis of heteromorphic leaves and hydrophilic roots in response to soil drying in desert *Populus euphratica*. *Sci. Rep., 7,*12188.

Ioio, R. D., Nakamura, K., Moubayidin, L., Perilli, S., Taniguchi, M., Morita, M. T., Aoyama, T., Costantino, P., Sabatini, S.(2008). A genetic framework for the control of cell division and differentiation in the root meristem. *Science*, *322*, 1380-1384.

IPCC, (2014). Climate Change 2014: Synthesis Report. Contribution of Working Groups I, II and III to the Fifth Assessment Report of the Intergovernmental Panel on Climate Change [Core Writing Team, R.K. Pachauri and L.A. Meyer (eds.)]. IPCC,. Geneva. Switzerland, 151.

Iyer-Pascuzzi, A.S., Symonova, O., Mileyko, Y., Hao, Y., Belcher, H., Harer, J., Weitz, J.S., Benfey, P.N. (2010). Imaging and analysis platform for automatic phenotyping and trait ranking of plant root systems. *Plant Physiology*, *152,* 1148-1157.

Jacott CN, Boden SA. 2020. Feeling the heat: developmental and molecular responses of wheat and barley to high ambient temperatures. *Journal of Experimental Botany*, *71*, 5740-5751.

Janda, M., Lamparová, L., Zubíková, A., Burketová, L., Martinec, J., Krčková, Z. (2019). Temporary heat stress suppresses PAMP-triggered immunity and resistance to bacteria in *Arabidopsis thaliana*. *Molecular Plant Pathology*, *20*, 1005-1012.

Jeudy, C., Adrian, M., Baussard, C. *et al.* (2016). RhizoTubes as a new tool for high throughput imaging of plant root development and architecture: test, comparison with pot grown plants and validation. *Plant Methods*, *12***,** 31.

Jin, Z., Qiao, Y., Wang, Y., Fang, Y., Yi, W. (2011). A new parameterization of spectral and broadband ocean surface albedo. *Opt. Express*, *19*, 26429-26443.

Johansson, H., Jones, H., Foreman, J. *et al.* (2014). Arabidopsis cell expansion is controlled by a photothermal switch. *Nat. Commun.*, *5***,** 4848.

Johnson, H.W., Robinson, H.F., Comstock, R.G. (1955b). Estimates of genetic and environmental variability in soybean. *Agronomy Journal, 47,* 314-318.

Johnson, H.W., Robinson, H.F, Comstock, R.E. (1955a). Estimates of genetic and environmental variability in soybeans. *Agronomy Journal*, *47,* 314-318.

Jones, J.B. (1982). Hydroponics: its history and use in plant nutrition studies. *Journal of Plant Nutrition, 5,* 1003-1030.

Jones, R. A., Forero-Vargas, M., Withers, S.P., Smith, R.S., Traas, J., Dewitte, W., Murray, J.A.H. (2017). Cell-size dependent progression of the cell cycle creates homeostasis and flexibility of plant cell size. Nat Commun. *8,* 15060.

Jung, J.H., Domijan, M., Klose, C., Biswas, S., Ezer, D., Gao, M., Khattak, A.K., Box, M.S., Charoensawan, V., Cortijo, S., Kumar, M., Grant, A., Locke, J.C., Schäfer, E., Jaeger, K.E., Wigge, P.A. (2016). Phytochromes function as thermosensors in Arabidopsis. Science *354*: 886-889.

Jung, J.H., Barbosa, A.D., Hutin, S. *et al.*(2020). A prion-like domain in ELF3 functions as a thermosensor in Arabidopsis. *Nature, 585***,** 256-260.

Jurado, S., Trivino, S.D., Abraham, Z., Manzano, C., Gutierrez, C., Del Pozo, C. (2008). SKP2A protein, an F-box that regulates cell division, is degraded via the ubiquitin pathway. *Plant Signal Behav.*, *3*, 810-812 .

Kamińska, M., Gołębiewski, M., Tretyn, A., Trejgell, A. (2018). Efficient long-term conservation of *Taraxacum pieninicum* synthetic Seeds in slow growth conditions. *Plant Cell Tissue Organ Cult., 132,* 469-478.

Karuma, A., Mtakwa, P., Amuri, N., Gachene, C.K., & Gicheru, P. (2014). Enhancing Soil Water Content for Increased Food Production in Semi-Arid Areas of Kenya. *Journal of Agricultural Science, 6,* 125-134.

Keuskamp, D.H., Sasidharan, R., Vos, I., Peeters, A.J.M, Voesenek, L.A.C.J, Pierik, R. (2011). Blue-light-mediated shade avoidance requires combined auxin and brassinosteroid action in Arabidopsis seedlings. *Plant J.*, *67*, 208-217.

Kim, S., Xing, E.P. (2009). Statistical Estimation of Correlated Genome Associations to a Quantitative Trait Network. *PLoS Genet.*, *5,* 1000587.

Kim, T.W., Guan, S., Sun, Y., Deng, Z, Tang, W., Shang, J.X., Sun, Y., Burlingame, A.L., Wang, Z.Y. (2009). Brassinosteroid signal transduction from cell-surface receptor kinases to nuclear transcription factors. *Nature Cell Biology*, *11*, 1254-1260.

Kim, S.-C., Guo, L., & Wang, X. (2020). Nuclear moonlighting of cytosolic glyceraldehyde-3-phosphate dehydrogenase regulates Arabidopsis response to heat stress. Nature Communications *11,* 3439.

Kirby, E.J.M., Appeyard, M., Fellowes, G. (1982). Effect of sowing date on the temperature response of leaf emergence and leaf size in barley. Plant, *Cell and Environment*, *5*, 477-484.

Kirschner, G.K. et al. (2021). ENHANCED GRAVITROPISM 2 encodes a STERILE ALPHA MOTIF-containing protein that controls root growth angle in barley and wheat. *PNAS, 118,* e2101526118*.*
Kleine-Vehn, J., Friml, J. (2008). Polar targeting and endocytic recycling in auxin-dependent plant development, *Annu. Rev. Cell Dev. Biol., 24,* 447-473.

Klose, C., Venezia, F., Hussong, A., Kircher, S., Schäfer, E., Fleck, C. (2015). Systematic analysis of how phytochrome B dimerization determines its specificity. *Nat. Plants*, *1,* 15090.

Koini, M.A., Alvey, L., Allen, T., Tilley, C.A., Harberd, N.P., Whitelam, G.C., Franklin, K.A. (2009). High temperature-mediated adaptations in plant architecture require the bHLH transcription factor PIF4. *Curr. Biol.*, *19,* 408-413.

Kondo, M., Okamura, T. (1931). Growth response of rice plant to water temperature. *Agric. Hortic.,* 6, 517-530.

Kong, X., Liu, G., Liu, J., Ding, Z. (2018). The root transition zone: A hot spot for signal crosstalk. *Trends Plant Sci., 23,* 403-409.

Kong, X., Zhang, M., De Smet, I., Ding, Z. (2014). Designer crops: optimal root system architecture for nutrient acquisition. *Trends in Biotechnology, 32*, 597-598

Kono, A., Ohno, R., Umeda-Hara, C., Uchimiya, H., Umeda, M. (2006) A distinct type of cyclin D, *CYCD4,2*, involved in the activation of cell division in Arabidopsis, *Plant Cell Rep., 25*, 540-545.

Kostaki, K.-I., Coupel-Ledru, A., Bonnell, V. C., Gustavsson, M., Sun, P., McLaughlin, F. J., Franklin, K. A. (2020). Guard cells integrate light and temperature signals to control stomatal aperture. *Plant Physiol.*, *182*, 1404-1419.

Kotogány, E., Dudits, D., Horváth, G.V., Ayaydin, F. (2010). A rapid and robust assay for detection of S-phase cell cycle progression in plant cells and tissues by using ethynyl deoxyuridine. *Plant Methods*, *6*, 5.

Kramer, P. J., and Boyer, J. S. (1995). Water Relations of Plants and Soils. San Diego: Academic Press.

Krecek, P., Skupa, P., Libus, J., Naramoto, S., Tejos, R., Friml, J., Zazímalová, E. (2009). The PIN-FORMED (PIN) protein family of auxin transporters, *Genome Biol.*, *10*, 249.

Krishnan, P., Ramakrishnan, B,, Raja Reddy, K.,, Reddy, V.R. (2011). High-temperature effects on rice growth, yield, and grain quality. *Adv. Agron.*, *111,* 87-206.

Kuhns, M. R., Garrett, H. E., Teskey, R. O., Hinckley, T. M. (1985). Root Growth of Black Walnut Trees Related to Soil Temperature, Soil Water Potential, and Leaf Water Potential, *Forest Science, 31*, 617-629

Ku, L.X., Zhao, W.M., Zhang, J., Wu, L.C., Wang, C.L., Wang, P.A., Zhang, W.Q., Chen, Y.H. (2010). Quantitative trait loci mapping of leaf angle and leaf orientation value in maize (*Zea mays L.*). *Theor. Appl. Genet.*, *121,* 951-959

Kumar, S.V., Wigge, P.A. (2010). H2A.Z-containing nucleosomes mediate the thermosensory response in Arabidopsis. *Cell*, *140,* 136-147.
Lafitte, R.A., Blum, A., Atlin, G. (2003). Using secondary traits to help identify drought-tolerant genotypes. In: Fischer, K.S., Lafitte, R., Fukai, S., Atlin, G., Hardy, B. (Eds.), Breeding Rice for Drought-Prone Environments. IRRI, Los Banos, pp. 37-48.

Lahiri, K., Vallone, D., Gondi, S.B., Santoriello, C., Dickmeis, T., Foulkes, N.S. (2005). Temperature regulates transcription in the zebrafish circadian clock. *PLoS Biol., 3,* 351.

Lam, V.P., Kim, S.J., Bok, G.J., Lee, J.W., Park, J.S. (2020). The effects of root temperature on growth, physiology, and accumulation of bioactive compounds of *Agastache rugosa. Agriculture*, *10*, 162.

Laplaze, L., Benkova, E., Casimiro, I., Maes, L., Vanneste, S., Swarup, R., Weijers, D., Calvo, V., Parizot, B., Herrera-Rodriguez, M.B., Offringa, R., Graham, N., Doumas, P., Friml, J., Bogusz, D., Beeckman, T., Bennett, M. (2007). Cytokinins act directly on lateral root founder cells to inhibit root initiation. *Plant Cell*, *19*, 3889-3900.

Ledent, J.F., 1974. Contribution a l'etude des relations entre l'epi et les parties sommitales de la plante chez le froment d'hiver (*Triticum aestivum L*.). *Rev. Agric.*, *27*, 1407-1420.

Lee, H.J., Jung, J.H., Cortés, L., lorca, L., Kim, S.G., Lee, S., Baldwin, I.T., Park, C.M. (2014). FCA mediates thermal adaptation of stem growth by attenuating auxin action in Arabidopsis. *Nat. Commun., 5,* 5473.

Lee, J.K., Woo, S.Y., Kwak, M.J., Park, S.H., Kim, H.D., Lim, Y.J., Park, J.H., Lee, K.A. (2020). Effects of Elevated Temperature and Ozone in *Brassica juncea* L.: Growth, Physiology, and ROS Accumulation. *Forests, 11,* 68.

Lee, S., Wang, W. & Huq, E.(2021). Spatial regulation of thermomorphogenesis by HY5 and PIF4 in Arabidopsis. Nat. Commun. *12***,** 3656.

Legris, M., Klose, C., Burgie, E.S., Rojas, C.C., Neme, M., Hiltbrunner, A., Wigge, P.A., Schäfer, E., Vierstra, R.D., Casal, J.J. (2016). Phytochrome B integrates light and temperature signals in Arabidopsis. *Science*, *354*, 897-900.

Leigh, A., Sevanto, S., Ball, M. C., Close, J. D., Ellsworth, D. S., Knight, C. A., Nicotra, A. B., and Vogel, S. (2012). Do thick leaves avoid thermal damage in critically low wind speeds? *New Phytologist*, *194*, 477-487.

Leigh, A., Sevanto, S., Close, J. D.,Nicotra, A. B. (2017). The influence of leaf size and shape on leaf thermal dynamics: does theory hold up under natural conditions? *Plant, cell & environment, 40*, 237-248.

Leivar, P., Monte, E., Oka, Y., Liu, T., Carle, C., Castillon, A., Huq, E., Quail, P.H. (2008). Multiple phytochrome-interacting bHLH transcription factors repress premature seedling photomorphogenesis in darkness. *Curr. Biol.*, *18*, 1815-1823.

Le Marié, C., Kirchgessner, N., Marschall, D., Walter, A., Hund, A. (2014). Rhizoslides: paper-based growth system for non-destructive, high throughput phenotyping of root development by means of image analysis. *Plant Methods*, *10*, 13.

Lewis, D.R., Negi, S., Sukumar, P., Muday, G.K. (2011). Ethylene inhibits lateral root development, increases IAA transport and expression of PIN3 and PIN7 auxin efflux carriers. *Development*, *138,* 3485-3495.
Li, B., Pattenden, S.G, Lee, D., Gutierrez, J., Chen, J., Seidel, C., Gerton, J., Workman, J.L. (2005). Preferential occupancy of histone variant H2AZ at inactive promoters influences local histone modifications and chromatin remodeling. *Proc. Natl. Acad. Sci. USA*, *102*, 18385-18390.

Li, Q.F., Wang, C., Jiang, L., Li, S., Sun, S.S., He, J.X. (2012). An interaction between BZR1 and DELLAs mediates direct signaling crosstalk between brassinosteroids and gibberellins in Arabidopsis. *Science signaling, 5,* 72.

Li, Z.G., Chen, H.W., Li, Q.T., Tao, J.J., Bian, X.H., Ma B.,, Zhang, W.K., Chen, S.Y., Zhang, J.S. (2015). Three SAUR proteins SAUR76, SAUR77 and SAUR78 promote plant growth in Arabidopsis. *Scientific Reports*, *5*, 12477.
Li, G.J., Zhu, C.H., Gan, L.J., Ng, D., Xia, K. (2015). GA3 enhances root responsiveness to exogenous IAA by modulating auxin transport and signaling in Arabidopsis. *Plant Cell Rep., 34*, 483-494.

Li, Z., Zhang, Q., Li, J. et al. (2020). Solar-induced chlorophyll fluorescence and its link to canopy photosynthesis in maize from continuous ground measurements. *Remote Sens. Environ., 236*,11420.

Liao, C.Y., Smet, W., Brunoud, G., Yoshida, S., Vernoux, T., Weijers, D. (2015). Reporters for sensitive and quantitative measurement of auxin response. *Nat. Methods, 12*, 207-210.

Liao, C.-Y., Smet, W., Brunoud, G., Yoshida, S., Vernoux, T., & Weijers, D. (2015). Reporters for sensitive and quantitative measurement of auxin response. *Nature Methods, 12*, 207–210.

Lilley, J.L., Gee, C.W., Sairanen, I., Ljung, K., Nemhauser, J.L. (2012). An endogenous carbon- sensing pathway triggers increased auxin flux and hypocotyl elongation. *Plant Physiol.*, *160,* 2261-70.

Lin, Z., Yin, K., Zhu, D., Chen, Z., Gu, H., Qu, L.-J. (2007). AtCDC5 regulates the G2 to M transition of the cell cycle and is critical for the function of Arabidopsis shoot apical meristem. *Cell Res.*, *17*, 815-828.

Lin, J., Xu, Y., Zhu, Z. (2020.) Emerging Plant Thermosensors: From RNA to Protein. *Trends in Plant Science*, *25*, 1187-1189.

Lincoln, C., Britton, J.H., Estelle, M. (1990). Growth and development of the *axr1* mutants of Arabidopsis. *Plant Cell, 2*, 1071-1080.

Lindquist, S., Craig, E.A. (1988). The heat-shock proteins. *Annu. Rev. Genet., 22,* 631-677.

Lippmann, R., Babben, S., Menger, A., Delker, C., and Quint, M. (2019). Development of wild and cultivated plants under global warming conditions. *Curr. Biol., 29*, 1326-1338.

Liu, Y., Schieving, F., Stuefer, J.F., Anten, N.P.R. (2007). The effects of mechanical stress and spectral shading on the growth and allocation of ten genotypes of a stoloniferous plant. *Ann. Bot., 99*,121-130.

Liu JJ, Chao JR, Jiang MC, Ng SY, Yen JJ, Yang-Yen HF (1995) Ras transformation results in an elevated level of cyclin D1 and acceleration of G1 progression in NIH 3T3 cells. Mol. *Cell Biol., 15*, 3654-3663

Lohraseb, I., Collins, N.C., Parent, B. (2017). Diverging temperature responses of CO2 assimilation and plant development explain the overall effect of temperature on biomass accumulation in wheat leaves and grains. *AoB Plants, 9*, plw092.

Lopez-Saez, J.F., Gimenez-Martin, G., Gonzales-Fernandez, A. (1966). Duration of the cell division cycle and its dependence on temperature. *Z. Zellforsch*. *75*, 591-600.

Long, S.P., Zhu, X.G., Naidu, S.L., Ort, D.R. (2006) Can improvement in photosynthesis increase crop yields? *Plant Cell Environ., 29*, 315-330.

Loomis, W. E. (1965).Absorption of Radiant Energy by Leaves. *Ecology, 46*,14-17,

Los, D.A., Murata, N. (2004). Membrane fluidity and its roles in the perception of environmental signals. *Biochim. Biophys. Acta*, *1666*, 142-157.

Luo, H., Xu, H., Chu, C., He, F., Fang, S. (2020). High temperature can change root system architecture and intensify root interactions of plant seedlings. *Frontiers in Plant Science, 11*, 160.

Luschnig, C., Gaxiola, R.A., Grisafi, P., Fink, G.R. (1998). EIR1, a root-specific protein involved in auxin transport, is required for gravitropism in *Arabidopsis thaliana*. *Genes Dev., 12, 2175-87.*

Lutz, U., Pose, D., Pfeifer, M., Gundlach, H., Hagmann, J., Wang, C., Weigel, D., Mayer, K.F., Schmid M, Schwechheimer, C. (2015). Modulation of ambient Temperature-Dependent flowering in *Arabidopsis thaliana* by natural variation of *FLOWERING LOCUS M*. *PLoS Genetics, 11,* 1005588.

Lynch, JP. (2018). Rightsizing root phenotypes for drought resistance. *J. Exp. Bot.*, *69*, 3279-3292.

Lynch, M. (1991). The genetic interpretation of inbreeding depression and outbreeding depression. *Evolution*, *45*, 622–629

Ma, D., Li, X., Guo, Y., Chu, J., Fang, S., Yan, C., Noel, J.P., Liu, H. (2016). Cryptochrome 1 interacts with *PIF4* to regulate high temperature-mediated hypocotyl elongation in response to blue light. *Proc. Natl. Acad. Sci. USA, 113*, 224-229.

Mace, E.S., Singh, V., Van Oosterom, E.J., Hammer, G.L., Hunt, C.H., Jordan, D.R. (2012). QTL for nodal root angle in sorghum (Sorghum bicolor L. Moench) co-locate with QTL for traits associated with drought adaptation. *Theoretical and Applied Genetics, 124,* 97-109.

Maloof, J.N. (2015). Shade avoidance components and pathways in adult plants revealed by phenotypic profiling. PLoS Genet. *11*, 1004953.

Mambro, R. Di., Sabatini. S. (2018). Developmental Analysis of Arabidopsis Root Meristem. *Methods Mol. Biol*., *1761* 33-45

Mano, Y., Nemoto, K. (2012). The pathway of auxin biosynthesis in plants, *J. Exp. Bot., 63*, 2853-2872.

Manschadi, A.M., Hammer, G.L., Christopher, J.T., de Voil, P. (2008). Genotypic variation in seedling root architectural traits and implications for drought adaptation in wheat (Triticum aestivum L.). *Plant Soil, 303*, 115-129

March-Diaz, R., Garcia-Dominguez, M., Lozano-Juste, J., Leon, J., Florencio, F.J., and Reyes, J.C. (2008). Histone H2A.Z and homologues of components of the SWR1 complex are required to control immunity in Arabidopsis. *Plant J.*, *53*, 475-487.

Markakis, M. N., Boron, A. K., Van Loock, B., Saini, K., Cirera, S., Verbelen, J. P., Vissenberg, K. (2013). Characterization of a small *auxin-up RNA (SAUR)-like* gene involved in *Arabidopsis thaliana* development. *PLoS ONE, 8*, 11 .

Martins, S., Montiel-Jorda, A., Cayrel, A., Huguet, S., Roux, C.P., Ljung, K., Vert, G. (2017). Brassinosteroid signaling-dependent root responses to prolonged elevated ambient temperature. *Nature communications*, *8*, 309.

Martínez, C., Espinosa-Ruíz, A., de Lucas, M., Bernardo-García, S., Franco-Zorrilla, J.M., Prat, S. (2018). PIF4-induced BR synthesis is critical to diurnal and thermomorphogenic growth. *EMBO J.*, *37*, 99552.

Marquès-Bueno, M.D.M., Morao, A.K., Cayrel, A., Platre, M.P., Barberon, M., Caillieux, E., Colot, V., Jaillais, Y., Roudier F, Vert G. (2016). A versatile Multisite Gateway-compatible promoter and transgenic line collection for cell type-specific functional genomics in Arabidopsis*. Plant J.*, *85*, 320-333.

Masubelele, N.H., Dewitte, W., Menges, M., Maughan, S., Collins C, Huntley R, Nieuwland, J., Scofield, S., Murray, JA. (2005). D-type cyclins activate division in the root apex to promote Seed germination in Arabidopsis, *Proc. Natl Acad. Sci. USA, 02*, 15694-15699.

Matyszczak, I., Tominska, M., Zakhrabekova, S., Docktor, C., Hansson, M. (2020). Analysis of early-flowering genes at barley chromosome 2H expands the repertoire of mutant alleles at the *Mat-c* locus. *Plant Cell Rep., 39***,** 47-61.

McMichael, B.L., Taylor, H.M., (1987). Applications and limitations of rhizotrons and minirhizotrons. In: Taylor, H.M. (Ed.), Minirhizotron Observation Tubes: Methods and Applications for Measuring Rhizosphere Dynamics. ASA, CSSA, SSA, Madison, WI, 14.

McMichael, B.L., Burke, J.J., (1999). Temperature effects on root growth. In: Eshel, Y., Kafkafi, U., Waisel, Y. (Eds.), Plant Roots: the Hidden Half. Marcel Dekker, New York, NY.

McMichael, B., Burke, J. (1998). Soil Temperature and Root Growth. *Hortscience, 33*, 947-951.

McMillen, G.G., McClendon, J.H. (1983). Dependence of photosynthetic rates on leaf density thickness in deciduous woody plants grown in sun and shade. *Plant Physiology, 72*, 674-678.

McSteen, P. (2010). Auxin and monocot development. Cold Spring Harb. Perspect. *Biol., 2*, a001479.

Mi, H., Huang, X., Muruganujan, A., Tang, H., Mills, C., Kang, D., Thomas, P.D. (2017). PANTHER version 11: Expanded annotation data from Gene Ontology and Reactome pathways, and data analysis tool enhancements. *Nucleic Acids Res.* 45, 183-189.

Michaud, O., Fiorucci, A.S., Xenarios, I., Fankhauser, C. (2017). Local auxin production underlies a spatially restricted neighbor-detection response in Arabidopsis. *Proc. Natl. Acad. Sci. USA, 114*, 7444-7449.

Misra, R. K. (1999). Root and shoot elongation of rhizotron-grown seedlings of *Eucalyptus nitens* and *Eucalyptus globulus* in relation to temperature. *Plant Soil*, *206*, 37-46.

Mizuno, T., Nomoto, Y., Oka, H., Kitayama, M., Takeuchi, A., Tsubouchi, M. and Yamashino, T. (2014). Ambient temperature signal feeds into the circadian clock transcriptional circuitry through the EC night-time repressor in *Arabidopsis thaliana*. *Plant Cell Physiol.*, *55*, 958-976.

Mo, M., Yokawa, K., Wan, Y., Baluška, F., Mo, M., Yokawa, K., Wan, Y., Baluška, F. (2015). How and why do root apices sense light under the soil surface? *Front Plant Sci.*, *6*, 775.

Mo, M., Yokawa, K., Montgomery, B.L. (2016). Spatiotemporal phytochrome signaling during photomorphogenesis: From physiology to molecular mechanisms and back. *Front Plant Sci., 7*, 480.

Mockaitis, K., Estelle, M. (2008). Auxin receptors and plant development: a new signaling paradigm. *Annu. Rev. Cell Dev. Biol.*, 24, 55-80.

Moehring, A. J. (2011). Heterozygosity and its unexpected correlations with hybrid sterility. *Evolution., 65*, 2621-2630.

Nicholas, J., Morffy, Lucia, C., Strader. (2018). Auxin Biosynthesis and Transport in the Root Meristem. *Developmental Cell, 47*, 262-264.

Montalto, F.I., De Amicis, F. (2020). Cyclin D1 in Cancer: A Molecular Connection for Cell Cycle Control, Adhesion and Invasion in Tumor and Stroma. Cells, *9*, 2648.

Muto, H., Watahiki, M.K., Nakamoto, D., Kinjo, M., Yamamoto, K.T. (2007). Specificity and similarity of functions of the Aux/IAA genes in auxin signaling of Arabidopsis revealed by promoter-exchange experiments between *MSG2/IAA19*, *AXR2/IAA3* and *SLR/IAA14*, *Plant Physiol.,* 144, 187-196.

Müller, L.M., Mombaerts, L., Pankin, A., Davis, S.J., Webb, A.A.R., Goncalves, J., von Korff., M. (2020). Differential Effects of Day/Night Cues and the Circadian Clock on the Barley Transcriptome, *Plant Physiol.*, *183*, 765-779

Müller, A., Guan, C., Gälweiler, L., Tänzler, P., Huijser, P., Marchant, A., Parry, G., Bennett, M., Wisman, E., Palme, K. (1998). *AtPIN2* defines a locus of Arabidopsis for root gravitropism control. EMBO J. *17*, 6903-6911.

Müssig, C., Shin, G.H., Altmann, T. (2003). Brassinosteroids promote root growth in Arabidopsis. *Plant Physiol.*, *133*, 1-11.

Nagatani, A. (2015). Spatial regulation of the gene expression response to shade in Arabidopsis seedlings. *Plant Cell Physiol*., *56*, 1306-1319.

Nagel, K., Kastenholz, B., Jahnke, S., van Dusschoten, D., Aach,. T, Muhlich, M., Truhn, D., Scharr, H., Terjung, S., Walter, A., Schurr, U. (2009). Temperatureresponses of roots: impact on growth, root system archetecture andimplications for phenotyping. *Functional Plant Biology*, *36*, 947-959.

Nagel, K., Putz, A., Gilmer, F., Heinz, K., Fischbach, A., Pfeifer, J., Faget, M., Blossfeld, S., Ernst, M., Dimaki, C., Kastenholz, B., Kleinert, A.-K., Galinski, A., Scharr, H., Fiorani, F., Schurr, U. (2012). GROWSCREEN-Rhizo is a novel phenotyping robot enabling

simultaneous measurements of root and shoot growth for plants grown in soil-rhizotrons. *Functional plant biology*, *39***,** 891-904.

Natr, L., Natrova, Z. (1992). Characteristics of leaf growth in 6 varieties of spring wheat cultivated under constant conditions. *Rostlinná Výroba*, *38*, 247–251.

Naz, A.A., Ehl, A., Pillen, K., Léon, J. (2012). Validation for root-related quantitative trait locus effects of wild origin in the cultivated background of barley (*Hordeum vulgare* L.). *Plant Breed.*, 131, 392-398.

Naz, A.A., Arifuzzaman, M., Muzammil, S., Pillen, K., Léon, J. (2014). Wild barley introgression lines revealed novel QTL alleles for root and related shoot traits in the culti-vated barley (*Hordeum vulgare L.*). *BMC genetics*, *15*, 107.

Nehe, A.S., Foulkes, M.J., Ozturk, I., Rasheed, A., York, L., et al. (2021). Root and canopy traits and adaptability genes explain drought tolerance responses in winter wheat. *PLOS ONE, 16*, e0242472.

Nicole, F., Dahlgren, J.P, Vivat, .A., Till-Bottraud, I., Ehrlen. J. (2011). Interdependent effects of habitat quality and climate on population growth of an endangered plant. *Journal of Ecology, 99*, 1211-1218.

Nito, K., Kajiyama, T., Unten-Kobayashi, J., Fujii, A., Mochizuki, N., Kambara, H., Nagatani, A. (2015). Spatial regulation of the gene expression response to shade in Arabidopsis seedlings. *Plant Cell Physiol., 5*, 1036-1319.

Nielsen, K.F. (1974). Roots and root temperatures. In: E.W Carson (ed.) The Plant Root Environment, Univ. Press, Virginia, 293-333.

Nieto, C., López-Salmerón, V., Davière, J.-M., and Prat, S. (2014). *ELF3-PIF4* Interaction Regulates Plant Growth Independently of the Evening Complex. *Curr. Biol., 25*, 187-193.

Nievola, C.C., Carvalho, C.P., Carvalho, V., Rodrigues, E. (2017). Rapid responses of plants to temperature changes. *Temperature, 4*, 371-405.

Noguchi, T., Fujioka, S., Choe, S., Takatsuto, S., Yoshida, S., Yuan, H., Feldmann, K.A., Tax, F.E. (1999). Brassinosteroid-insensitive dwarf mutants of Arabidopsis accumulate brassinosteroids. *Plant Physiol.*, *121*, 743-752.

Noh, B., Murphy, A.S., Spalding, E.P. (2001). Multidrug resistance-like genes of Arabidopsis required for auxin transport and auxin-mediated development. *The Plant Cell*, *13*, 2441-2454.

Nomoto, Y., Kubozono, S., Yamashino, T., Nakamichi, N., and Mizuno, T. (2012). Circadian clock- and PIF4-controlled plant growth: a coincidence mechanism directly integrates a hormone signaling network into the photoperiodic control of flowering time in *Arabidopsis thaliana*. *Plant and Cell Physiology*, *48*, 925-937.

Nord, E. A., Lynch, J. P. (2009). Plant phenology: a critical controller of soil resource acquisition. *J. Exp. Bot.*, *60*, 1927-1937.

Nover, L., Scharf, KD. (1997). Heat stress proteins and transcription factors. *CMLS Cell Mol Life Sci.*, *53*, 80-103.

Nozue, K., Covington, M.F., Duek, P.D., Lorrain, S., Fankhauser, C., Harmer, S.L., Maloof, J.N. (2007). Rhythmic growth explained by coincidence between internal and external cues. *Nature*, *448*, 358-361.

Nozue, K., Tat, A.V., Kumar Devisetty, U., Robinson, M., Mumbach, M.R., Ichihashi, Y., Lekkala, S., Maloof, J. N. (2015). Shade avoidance components and pathways in adult plants revealed by phenotypic profiling. *PLoS Genet.*, 4, 1004953.

Nultsch, W. (2001). Allgemeine Botanik. Thieme. Raven et al. 2000: Biologie der Pflanzen. Spektrum.

Oh, M.H. , Wang, X. , Kota, U. , Goshe, M.B. , Clouse, S.D. , Huber, S.C. (2009). Tyrosine phosphorylation of the BRI1 receptor kinase emerges as a component of brassinosteroid signaling in Arabidopsis. *Proc. Natl. Acad. Sci. USA, 106*, 658-663.

Oh, E., Zhu, J.Y., Wang, Z.Y. (2012). Interaction between *BZR1* and *PIF4* integrates brassinosteroid and environmental responses. *Nat. Cell Biol.*, *14*, 802-809.

Oh, E., Zhu, J.Y., Bai, M.Y., Arenhart, R.A., Sun, Y., Wang, Z.Y. (2014). Cell elongation is regulated through a central circuit of interacting transcription factors in the Arabidopsis hypocotyl. *ELife*, *3*, 03031.

Oh, E., Zhu, J.Y., Ryu, H., Hwang, I., Wang, Z.Y. (2014). *TOPLESS* mediates brassinosteroid-induced transcriptional repression through interaction with BZR1. *Nat. Commun.*, *5*, 4140.

Onoda, Y. et al. Physiological and structural tradeoffs underlying the leaf economics spectrum. (2017). *N. Phytol.,* 214, 1447-1463.

Osada, A., Sasiprada, V., Rahong, M., Dhammanuvong, S., Chakrabandhu, M. (1973). Abnormal occurrence of empty grains of indica rice plants in the dry, hot season in Thailand. *Proc. Crop. Sci. Jpn., 42.* 103-109.

Ostonen, I, Püttsepp, U., Biel, C. et al. (2007). Specific root length as indicator of environmental change. *Plant Biosystems., 141*, 426-44.

Oyama, T., Shimura, Y., Okada, K. (1997). The Arabidopsis *HY5* gene encodes a bZIP protein that regulates stimulus-induced development of root and hypocotyl. *Genes Dev.*,*11*, 2983-2995.

Pahlavanian, A.M. , Silk, W.K. (1988). Effect of temperature on spatial and temporal aspects of growth in the primary maize root. *Plant Physiology*, *87*, 529-532.

Pantazopoulou, C.K., Bongers, F.J., Küpers, J.J., Reinen, E., Das, D., Evers, J.B., Anten, N.P.R, Pierik, R. (2017). Neighbor detection at the leaf tip adaptively regulates upward leaf movement through spatial auxin dynamics. *Proc. Natl. Acad. Sci. USA, 114*, 7450-7455.

Park, S.J., Jiang, K., Schatz, M.C., Lippman, Z.B. (2012). Rate of meristem maturation determines inflorescence architecture in tomato. *Proc. Natl. Acad. Sci. USA*, *10*, 639-644.

Parry, G., Calderon-Villalobos, L.I., Prigge, M., Peret, B., Dharmasiri, S., Itoh, H., Lechner, E., Gray, W.M., Bennett, M., Estelle, M. (2009). Complex regulation of the TIR1/AFB family of auxin receptors. *Proc. Natl. Acad. Sci. USA, 106*, 22540-22545.

Parveen, S., Rahman, A. (2021). Actin Isovariant ACT7 Modulates Root Thermomorphogenesis by Altering Intracellular Auxin Homeostasis. *International journal of molecular sciences*, *22*, 7749.

Passot, S., Gnacko, F., Moukouanga, D., Lucas, M., Guyomarch, S., Ortega, B.M., Atkinson, J.A., Belko, M.N., Bennett, M.J., Gantet, P., et al. (2016) Characterization of pearl millet root architecture and anatomy reveals three types of lateral roots. *Front Plant Sci., 7*, 829.

Patel, D., Franklin, K.A. (2009). Temperature-regulation of plant architecture. *Plant Signaling & Behavior, 4,* 577-579.

Patil, R. H., Laegdsmand, M., Olesen, J. E., Porter, J. R. (2010). Effect of soil warming and rainfall patterns on soil N cycling in Northern Europe, *Agr. Ecosyst. Environ.,139*, 195-205.

Pearson. R.W, Ratliff, L.F, Taylor, H.M (1970). Effects of soil temperature, strength, and pH on cotton seedling root elongation. *Agron. J.*, *62*, 243-246.

Peterson, C. A., Murrmann, M., and Steudle, E. (1993). Location of the major barriers to water and ion movement in young roots of *Zea mays L. Planta, 190*, 127-136.

Peleman, J. D. ,van der oort, J.R. (2003). Breeding by design. *Trends in Plant Science,* 8, 330334.

Peng, B., Wang, L., Fan, C., Jiang, G., Luo, L., Li ,Y., He, Y. (2014). Comparative mapping of chalkiness components in rice using five populations across two environments. *BMC Genet., 15*, 49.

Petrasek, J., Mravec, J., Bouchard, R., Blakeslee, J.J., Abas, M., Seifertova, D., Wisniewska, J., Tadele, Z., Kubes, M., Covanova, M., Dhonukshe, P., Skupa, P., Benkova, E., Perry, L., Krecek, P., Lee, O.R., Fink, G.R., Geisler, M., Murphy, A.S., Luschnig, C., Zazimalova, E., Friml, J. (2006). PIN proteins perform a rate-limiting function in cellular auxin eflux. *Science, 312*, 914-918.

Perrot-Rechenmann, C. (2010). Cellular responses to auxin: division versus expansion. Cold Spring Harb. Perspect. Biol. *2*, a001446.

Pieper, R., Tome, F., Pankin, A., von Korff Schmising, M. (2021). *FLOWERING LOCUS T4* delays flowering and decreases fertility in barley. *Journal of Experimental Botany*, *72*, 107-121.

Plieth, C. (1999). Temperature sensing by plants: calcium-permeable channels as primary sensors -a model. *J. Membr. Biol.*, *172*, 121-127.

Power, J.F., Willis, W.O., Grunes, D.L. and Reichman, G.A. (1967), Effect of Soil Temperature, Phosphorus, and Plant Age on Growth Analysis of Barley. *Agron. J.*, *59*, 231-234.

Prerostova, S., Dobrev, P.I., Kramna, B., Gaudinova, A., Knirsch, V., Spichal, L., Zatloukal, M., Vankova, R. (2020). Heat Acclimation and Inhibition of Cytokinin Degradation Positively Affect Heat Stress Tolerance of Arabidopsis, *Front. in Plant Science, 11*, 87.

Pregitzer, K.S., King, J.S., Burton, A.J. and Brown, S.E. (2000). Responses of tree fine roots to temperature. *New Phytologist, 147*, 105-115.

Pregitzer K. S., Zak D. R., Maziasz J., DeForest J., Curtis P. S., Lussenhop J. (2000). Interactive effects of atmospheric CO2 and soil-N availability on fine roots of Populus tremuloides. *Ecol. Appl., 10*, 18-33.

Price, A.L., Patterson, N.J., Plenge, R.M., Weinblatt, M.E., Shadick, N.A., Reich, D. (2006). Principal components analysis corrects for stratification in genome-wide association studies. *Nat. Genet., 38*, 904-909.

Procko, C., Crenshaw, C.M., Ljung, K., Noel, J.P., Chory, J. (2014). Cotyledon-generated auxin is required for shade-induced hypocotyl growth in Brassica rapa. *Plant Physiol., 165*, 1285-1301.

Procko, C., Burko, Y., Jaillais, Y., Ljung, K., Long, J.A., Chory, J. (2016).The epidermis coordinates auxin-induced stem growth in response to shade. *Genes Dev.*, 30: 1529-1541.

Proveniers, M.C., Van Zanten, M. (2013). High temperature acclimation through *PIF4* signaling.*Trends Plant Sci.*, *18*, 59-64.

Purvis, ON . (1934). An analysis of the influence of temperature during germination on the subsequent development of certain winter cereals and its relation to the effect of length of day. *Annals of Botany*, *48*, 919-957.

Qin, H., He, L., Huang, R. (2019) The Coordination of Ethylene and Other Hormones in Primary Root Development. *Front. Plant Sci.*, *10*, 874.

Quint, M., Barkawi, L.S., Fan, K.T., Cohen, J.D., Gray, W.M. (2009). Arabidopsis *IAR4* modulates auxin response by regulating auxin homeostasis. *Plant Physiol.*, 150, 748-758.

Quint, M., Delker C., Franklin, K.A., Wigge, P.A., Halliday, K.J., van Zanten, M. (2016). Molecular and genetic control of plant thermomorphogenesis. *Nat. Plants*, *2*, 15190.

Ratcliffe, O.J., Amaya, I., Vincent, C.A., Rothstein, S., Carpenter, R., Coen, E.S., Bradley, D.J .(1998). A common mechanism controls the life cycle and architecture of plants. *Development*, *125*, 1609-1615.

Rayle, D.L., Evans, M.L., Hertel, R. (1970). Action of auxin on cell elongation. *Proc. Natl. Acad. Sci. USA*, *65*, 184-91.

R Development Core Team. (2018). R: A language and environment for statistical computing. R Foundation for Statistical Computing, Vienna, Austria.
Rellán-Álvarez, R., Lobet, G., and Dinneny, J. R. (2016). Environmental control of root system biology. *Annu. Rev. Plant Biol.*, *67*, 1-26.

Resnitzky, D., Gossen, M., Bujard, H., Reed, S.I.(1994). Acceleration of the G1/S phase transition by expression of cyclins D1 and E with an inducible system. *Mol. Cell Biol., 14*, 1669-1679.

Reuscher, S., Kolter, A., Hoffmann, A., Pillen, K., Krämer, U. (2016). Quantitative trait loci and inter-organ partitioning for essential metal and toxic analogue accumulation in barley. *PLoS ONE*, *11*, 0153392.

Richards, R.A., López-Castañeda, C., Gomez-Macpherson, H. *et al.* (1993) Improving the efficiency of water use by plant breeding and molecular biology. *Irrig. Sci.*, *14*, 93-104.

Rickels, W., Klepper, G., Dovern, J., Betz, G., Brachatzek, N., Cacean, S., Güssow, K.J.H., Hiller, S., Hoose, C., Leisner, T., Oschlies, A., Platt, U., Proelß, A., Renn, O., Schäfer, S., Zürn, M. (2011). Gezielte Eingriffe in das Klima? Eine Bestandsaufnahme der Debatte zu Climate Engineering. *Sondierungsstudie für das Bundesministerium für Bildung und Forschung*, Kiel.

Rieder, C.L., Maiato, H. (2004). Stuck in division or passing through: what happens when cells cannot satisfy the spindle assembly checkpoint. *Dev. Cell*, *7*, 637-651.

Ruelland E, Zachowski A. (2010). How plants sense temperature. *Environ. Exp. Bot.*, 69, 225-232.

Sabatini S., Beis D., Wolkenfelt H., Murfett J., Guilfoyle T., Malamy J., Benfey P., Leyser O., Bechtold N., Weisbeek P., Scheres B. (1999). An auxin-dependent distal organizer of pattern and polarity in the Arabidopsis root. *Cell*, *99*, 463-472.

Sakamoto, M., Mayuka, U., Kengo, M. Takahiro, S. (2016). Effect of root-zone temperature on the growth and fruit quality of hydroponically grown strawberry plants *J. Agr. Sci.*, *8*, 122-131.

Sakata, T., Yagihashi, N., Higashitani, A. (2010). Tissue-specific auxin signaling in response to temperature fluctuation. *Plant Signal. Behav.*, *5*, 1510-1512.

Salisbury, F.J., Hall, A., Grierson, C.S., Halliday, K.J. (2007). Phytochrome coordinates Arabidopsis shoot and root development. *Plant J., 50*, 429-438.

Sanderson, J. (1983). Water-uptake by different regions of the barley root - pathways of radial flow in relation to development of the endodermis. *J. Exp. Bot.*, *34*, 240-253.

Sapp, R.L., Rekaya, R.,Misztal, I., Wing, T. (2005). Longitudinal multiple-trait versus cumulative single-trait analysis of male and female fertility and hatchability in chickens. *Poult. Sci.*, *84* , 1010-1014.

Sarieva, G.E., Kenzhebaeva, S.S. & Lichtenthaler, H.K. (2010). Adaptation potential of photosynthesis in wheat cultivars with a capability of leaf rolling under high temperature conditions. *Russ. J. Plant Physiol.*, *57*, 28-36.

SAS Institute. (2008). The SAS Enterprise guide for Windows, release 4.2. SAS Institute, Cary, NC.

Sassi, M., Lu, Y.F., Zhang, Y.H., Wang, J., Dhonukshe, P., Blilou, I., Dai, M.Q., Li, J., Gong, X.M., Jaillais, Y., Yu, X.H., Traas, J., Ruberti, I., Wang, H.Y., Scheres, B., Vernoux, T., Xu, J. (2012). *COP1* mediates the coordination of root and shoot growth by light through modulation of PIN1- and PIN2-dependent auxin transport in Arabidopsis. *Development*, *139*, 3402–3412.

Sawchuk M.G., Head P., Donner T.J., Scarpella E. (2007). Timelapse imaging of Arabidopsis leaf development shows dynamic patterns of procambium formation. *New Phytol.*, *176*, 560–571.

Schmalenbach, I., Pillen, K. (2009). Detection and verification of malting quality QTLs using wild barley introgression lines. *Theor. Appl. Genet*., *118*, 1411-1427.

Schmalenbach, I., Körber, N., Pillen, K. (2008). Selecting a set of wild barley introgression lines and verification of QTL effects for resistance to powdery mildew and leaf rust. *Theor. Appl. Genet., 117*, 1093-1106.

Schmalenbach, I., Léon, J., Pillen, K. (2009). Identification and verification of QTLs for agronomic traits using wild barley introgression lines. *Theor. Appl. Genet.*, *118*, 483-497.

Schmalenbach, I., March, T.J., Bringezu, T., Waugh, R., Pillen, K. (2011). High-resolution genotyping of wild barley introgression lines and fine-mapping of the threshability locus *thresh-1* using the Illumina GoldenGate assay. *G3: Genes Genom Genet., 1*, 187-196.

Schnaithmann, F., Pillen, K. (2013). Detection of exotic QTLs controlling nitrogen stress tolerance among wild barley introgression lines. *Euphytica*, *189*, 67-88.

Schmalenbach, I., Léon, J., Pillen, K. (2009). Identification and verification of QTLs for agronomic traits using wild barley introgression lines. *Theor. Appl. Genet., 11*, 483-497.

Schroda, M., Hemme, D., Mühlhaus, T. (2015). The Chlamydomonas eat stress response. *Plant J.,* 82, 66-480.

Sebetha, E. (2015). The Effect of Maize Legume Cropping System and Nitrogen Fertilization on Yield, Soil Organic Carbon and Soil Moisture. Doctor of Philosophy Thesis. University of KwaZulu-Natal.

Seiler, G.J. (1998). Seed maturity, storage time and temperature, and media treatment effects on germination of two wild sunflowers. *Agron J.*, 90, 221-226.

Silva, C.S., Nayak, A., Lai, X., Hutin, S., Hugouvieux, V., Jung, J.H., Lopez-Vidriero, I., Franco-Zorrilla, J.M., Panigrahi, K.C.S, Nanao, M.H., Wigge, P.A., Zubieta, C. (2020). Molecular mechanisms of Evening Complex activity in Arabidopsis. *Proceedings of the National Academy of Sciences*, *USA, 117*, 6901-6909.

Silva-Navas, J., Moreno-Risueno, M.A., Manzano, C., Pallero-Baena, M., Navarro-Neila, S., Téllez-Robledo, B., Garcia-Mina, J.M., Baigorri, R., Gallego, F.J., del Pozo, J.C. (2015). D-Root: a system for cultivating plants with the roots in darkness or under different light conditions. *Plant J.*, *84*, 244-255.

Simon, R., Coupland, G. (1996). Arabidopsis genes that regulate flowering time in response to day-length. Semin. Cell Dev. Biol. *7*, 419-425.

Simonini, S., Bemer, M., Bencivenga, S., Gagliardini, V., Pires, N.D., Desvoyes, B., van der Graaff, E., Gutierrez, C., Grossniklaus, U., (2021). The Polycomb group protein ME-DEA controls cell proliferation and embryonic patterning in Arabidopsis, *Developmental Cell, 13*, 1945-1960.e7.

Smit, A.L., Bengough, A.G., Engels, C., van Noordwijk, M., Pellerin, S., van deGeijn, S.C. (2013). Root methods: a Handbook. Springer Science & Business Media.

Smith, S., De Smet, I. (2012). Root system architecture: insights from Arabidopsis and cereal crops. *Philosophical Transactions of the Royal Society B: Biological Sciences*, *367*, 1441-1452.

Soleimani, B., Sammler, R., Backhaus, A., Beschow, H., Schumann, E., Mock, H.P., von Wirén, N., Seiffert U., Pillen, K. (2017). Genetic regulation of growth and nutrient content under phosphorus deficiency in the wild barley introgression library *S42IL*. *Plant Breed.*, *36*, 892-907.

Somers, D.E., Kim, W.Y., Geng, R. (2004). The F-box protein ZEITLUPE confers dosage-dependent control on the circadian clock, photomorphogenesis, and flowering time. *Plant Cell*, *16,* 769–782.

Song, Y. H., Ito, S., & Imaizumi, T. (2010). Similarities in the circadian clock and photoperiodism in plants. *Current opinion in plant biology*, *13*, 594-603.

Sozzani, R., Maggio, C., Varotto, S., Canova, S., Bergounioux, C., Albani, D., Cella, R. (2006). Interplay between Arabidopsis activating factors E2Fb and E2Fa in cell cycle progression and development, *Plant Physiol.*, *140*, 1355-1366.

Spartz, A.K., Lee, S.H., Wenger, J.P., Gonzalez, N., Itoh H, Inzé D, Peer WA, Murphy AS, Overvoorde PJ, Gray WM (2012). The *SAUR19* subfamily of *SMALL AUXIN UP RNA* genes promote cell expansion. *Plant J., 70*, 978-990.

Spartz, A.K., Ren, H., Park, M.Y., Grandt, K.N., Lee, S.H., Murphy, A.S., Sussman, M.R., Overvoorde, P.J., Gray, W.M. (2014). SAUR Inhibition of PP2C–D Phosphatases Activates Plasma Membrane H+-ATPases to Promote Cell Expansion in Arabidopsis. *Plant Cell.*, 26, 2129-2142.

Srinivasan, V., Kumar, P., Long, S.P. (2017). Decreasing, not increasing, leaf area will raise crop yields under global atmospheric change. *Glob. Chang. Biol*., *23*, 1626-1635

Stavang, J.A., Gallego-Bartolomé, J., Gómez, M.D., Yoshida, S., Asami, T., Olsen, J.E., García-Martínez, J.L., Alabadí, D., Blázquez, M.A. (2009). Hormonal regulation of temperature-induced growth in Arabidopsis. *Plant J.*, *60*, 589-601.

Steinhorst, L., Kudla, J. (2014). signaling in cells and organisms – calcium holds the line. *Current Opinion in Plant Biology, 2*, 14-21.

Stepanova, A.N., Robertson-Hoyt, J., Yun, J., Benavente, L.M., Xie, D.Y., Dolezal, K., Schlereth, A., Jürgens, G., Alonso, J.M. (2008). TAA1-mediated auxin biosynthesis is essential for hormone crosstalk and plant development. *Cell, 133*, 177-191.

Su, Y.S., Lagarias, J.C. (2007). Light-independent phytochrome signaling mediated by dominant GAF domain tyrosine mutants of Arabidopsis phytochromes in transgenic plants. *Plant Cell*, *19*, 2124-2139.

Sun, L., Feraru, E., Mugurel I. Feraru, Waidmann, S., Wang, W., Passaia, G., Wang, Z.Y., Wabnik, K., Kleine-Vehn, J. (2020). PIN-LIKES Coordinate Brassinosteroid Signaling with Nuclear Auxin Input in *Arabidopsis thaliana. Current Biology, 30*, 1579-1588.e6.

Sun, Y., Fan, X.Y., Cao, D.M., Tang, W., He, K., Zhu, J.Y., He, J.X., Bai, M.Y., Zhu, S., Oh, E., Patil, S., Kim, T.W., Ji, H., Wong W. H., Rhee, S.Y., Wang, Z.Y. (2010). Integration of brassinosteroid signal transduction with the transcription network for plant growth regulation in Arabidopsis. *Developmental Cell*, *19*, 765–777.

Sun, J., Qi, L., Li, Y., Chu, J., Li, C. (2012). PIF4–mediated activation of *YUCCA8* expression integrates temperature into the auxin pathway in regulating Arabidopsis hypocotyl growth. *PloS Genetics*, *8*, 1002594.

Sun, H.W., Tao, J.Y., Liu, S.J., Huang, S.J., Chen, S., Xie, X.N., Yoneyama, K., Zhang, Y.L., Xu, G.H. (2014). Strigolactones are involved in phosphate- and nitrate-deficiency-induced root development and auxin transport in rice. *J. Exp. Bot.*, *65*, 6735-6746.

Sun, C. , Yan, K. , Han, J.T. , Tao, L. , Lv, M.H. , Shi, T. , He, Y.X. , Wierzba, M. , Tax, F.E. , Li, J. (2017). Scanning for new *BRI1* mutations via TILLING Analysis. *Plant Physiol.*, *174*, 1881-1896.

Sun, Q.H, Miao, C.Y., Hanel, M., Borthwick, A.G.L., Duan, Q.Y., Ji, D.Y. Li, H. (2019). Global heat stress on health, wildfires, and agricultural crops under different levels of climate warming. *Environ. Int.*, *128*, 125-136.

Sun, L., Feraru, E., Feraru, M.I., Waidmann, S., Wang, W., Passaia, G., Wang, Z.Y., Wabnik, K., Kleine-Vehn, J. (2020). PIN-LIKES Coordinate Brassinosteroid signaling with Nuclear Auxin Input in *Arabidopsis thaliana*. *Curr Biol.*, *30*, 1579-1588.

Sura, W., Kabza, M., Karlowski, W.M., Bieluszewski, T., Kus-Slowinska, M., Pawełoszek, Ł., Sadowski, J., Ziolkowski, P.A. (2017). Dual role of the histone variant H2A.Z in transcriptional regulation of stress-response genes. *Plant Cell*, *29*, 791-807.

Sureshkumar, S., Dent, C., Seleznev, A., Tasset, C., Balasubramanian, S. (2016). Nonsense-mediated mRNA decay modulates FLM-dependent thermosensory flowering response in Arabidopsis. *Nature Plants*, *2*, 16055.

Sweere, U. (2001). Interaction of the response regulator ARR4 with phytochrome B in modulating red light signaling. *Science*, *294*, 1108-1111.

Taiz L, Zeiger E (2002) Plant physiology. Ed. 3. Sinauer Associates, Inc., Sunderland

Talanova, V.V., Alkimova T.,V., Titov, A.F. (2003). Effect of whole plant and local heating on the ABA content in cucumber seedling leaves and roots and on their heat tolerance. *Rus. J. Plant Physiol., 50*, 90-94.

Tamaki, M., Imai, K., & Dale, N.M. (1998). The Effect of Day to Night Temperature Variation on Leaf Development in Wheat. *Plant Production Science, 1*, 254-257.

Tanaka N., Kato M., Tomioka R., Kurata R., Fukao Y., Aoyama T., et al. (2014). Characteristics of a root hair-less line of *Arabidopsis thaliana* under physiological stresses. *J. Exp. Bot.*, *65*, 1497-1512

Tang, W., Kim TW, Oses-Prieto JA, Sun Y, Deng Z, Zhu S, Wang R, Burlingame AL, Wang Z.Y. (2008). BSKs mediate signal transduction from the receptor kinase BRI1 in Arabidopsis. *Science*, *321*, 557-560.

Tang W., Yuan M., Wang R., Yang Y., Wang C., Oses-Prieto J. A., Kim T. W., Zhou H. W., Deng Z., Gampala S. S., et al. (2011). PP2A activates brassinosteroid-responsive gene expression and plant growth by dephosphorylating BZR1. *Nat. Cell Biol., 13*, 124-131. Tao, Y., Ferrer, J.L., Ljung, K., Pojer, F., Hong, F., Long, J.A., Li, L., Moreno, J.E., Bowman, M.E., Ivans, L.J. (2008). Rapid synthesis of auxin via a new tryptophan-dependent pathway is required for shade avoidance in plants. *Cell, 133*, 164-176.

Tardieu, F., Granier, C. (2000). Quantitative analysis of cell division in leaves: methods, developmental patterns and effects of environmental conditions. *Plant Molecular Biology, 43*, 555-567.

Tardieu, F., Granier, C., and Muller, B. (1999). Modelling leaf expansion in a fluctuating environment: are changes in specific leaf area a consequence of changes in expansion rate. *New Phytol., 143*, 33-43.

Tardy, F., Damour, G., Dorel, M., & Moreau, D. (2017). Trait-based characterisation of soil exploitation strategies of banana, weeds and cover plant species. *PloS one, 12*, e0173066.

Tasset, C., Singh Yadav, A., Sureshkumar, S., Singh, R., van der Woude, L., Nekrasov, M., Tremethick, D., van Zanten, M., Balasubramanian, S. (2018). POWERDRESS-mediated histone deacetylation is essential for thermomorphogenesis in *Arabidopsis thaliana*. *PLoS Genet., 14,* 1007280.

Telewski, F.W. (1995). Wind induced physiological and developmental responses in trees. In: Wind and trees, Coutts, M.P., Grace, J. (eds). Cambridge University Press, pp237-263

Thines, B., Harmon, F.G. (2010). Ambient temperature response establishes ELF3 as a required component of the core Arabidopsis circadian clock. *Proceedings of the National Academy of Sciences, USA, 107*, 3257-3262.

Thingnaes, E., Torre, S., Ernstsen, A., Moe, R. (2003). Day and night temperature responses in Arabidopsis: effects on gibberellin and auxin content, cell size, morphology and flowering time. *Ann Bot., 2*, 601-12.

Thuzar, M., Puteh, A.B., Abdullah, N.A.P, Lassim Mohd, M.B., Kamaruzaman, J. (2010). The effects of temperature stress on the quality and yield of soybean [(*Glycine max L.*) Merrill.]. *Journal of Agricultural Science*, 2, 172-179.

Tian, L., Fong, M.P., Wang, J.J., Wei, N.E., Jiang, H., Doerge, R.W., Chen, Z.J. (2005). Reversible histone acetylation and deacetylation mediate genome-wide, promoter-dependent and locus-specific changes in gene expression during plant development. *Genetics*, *169*, 337-345.

Tian, H., De Smet, I., Ding, Z. (2014). Shaping a root system: regulating lateral versus primary root growth. *Trends in Plant Science, 19*, 426-431.

Tozer, W. C., Rice, B., and Westoby, M. (2015). Evolutionary divergence of leaf width and its correlates. *Am. J. Bot., 102*, 367-378.

Trachsel, S., Kaeppler, S.M., Brown, K.M., Lynch, J.P. (2011). Shovelomics: high throughput phenotyping of maize (*Zea mays L.*) root architecturein the field. *Plant and Soil*, 341, 75-87.

Trenbath, B.R., Angus, J.F.(1975). Leaf inclination and crop production. *Field Crop Abstr., 28* , 231-244.

Tsukaya, H. (2002). Leaf development. In: Somerville CR, Meyerowitz EM (eds) The Arabidopsis book. *American Society of Plant Biologists, Rockville, MD*.

Tuberosa, R., Sanguineti, M.C., Landi, P., Giuliani, M.M., Salvi, S., Conti, S. (2002). Identification of QTLs for root characteristics in maize grown in hydroponics and analysis of their overlap with QTLs for grain yield in the field at two water regimes. *Plant Molecular Biology, 48*, 697-712.

Ubeda-Tomás, S., Beemster, G.T.S. and Bennett, M.J. (2012). Hormonal regulation of root growth: integrating local activities into global behavior. *Trends Plant Sci., 17*, 326-331.

Uga, Y., Sugimoto, K., Ogawa, S. et al. (2013). Control of root system architecture by *DEEPER ROOTING 1* increases rice yield under drought conditions. *Nat. Genet., 45*, 1097-1102.

Valdés-López O., Batek J., Gomez-Hernandez N., Nguyen C. T., Isidra-Arellano M. C., Zhang N., et al. (2016). Soybean roots grown under heat stress show global changes in their transcriptional and proteomic profiles. *Front. Plant Sci., 7*, 517.

van der Woude, L.C., Perrella, G., Snoek, B.L., Van Hoogdalem, M., Novak, O., Van Verk, M.C., Van Kooten, H.N., Zorn, L.E., Tonckens, R., Dongus, J.A., Praat, M., Stouten, E.A., Proveniers, M.C.G., Vellutini, E., Patitaki, E. Shapulatov, U., Kohlen, W., Balasubramanian, S., Ljung, K., Van der Krol, A.R., Smeekens. S., Kaiserli, E. and Van Zanten, M. (2019). *HISTONE DEACETYLASE 9* stimulates auxin-dependent thermomorphogenesis in *Arabidopsis thaliana* by mediating *H2A.Z* depletion. *Proceedings of the National Academy of Sciences USA*, *116*, 25343-25354.

van Zanten, M., Voesenek, L.A.C.J, Peeters, A.J.M., Millenaar, F.F. (2009). Hormone- and light-mediated regulation of heat-induced differential petiole growth in *Arabidopsis thaliana*. *Plant Physiol., 151*, 1446-1458.

Van Zanten M, Bours R, Pons TL, Proveniers MCG. (2013). Plant acclimation and adaptation to warm environments. In: Temperature and Plant Development (Ed. Franklin KA & Wigge PA), Wiley-Blackwell publishers. pp. 49-68.

Vapaavuori, E.M., Rikala, R., Ryyppö, A. (1992). Effects of root temperature on growth and photosynthesis in conifer seedlings during shoot elongation. *Tree Physiology, 10*, 217-230.

Varney, G. T., McCully, M. E., and Canny, M. J. (1993). Sites of entry of water into the symplast of maize roots. *New Phytol.*, *125*, 733-741.

Vepraskas, M.J., Hoyt, G.D. (1988). Comparison of the trench-pro file and coremethods for evaluating root distributions in tillage studies. *Agronomy Journal, 80*, 166-172.

Verrier, P.J., Bird, D., Burla, B., Dassa, E., Forestier, C., Geisler, M., Klein, M., Kolukisaoglu, U., Lee, Y., Martinoia, E., Murphy, A., Rea, P .A., Samuels, L., Schulz, B., Spalding, E. J., Yazaki, K., Theodoulou, F. L. (2008). Plant ABC proteins: a unified nomenclature and updated inventory. *Trends in Plant Science, 13*, 151-159.

Vierling, E. (1991). The roles of heat shock proteins in plants. Annu. Rev. Plant Physiol. Plant Mol. Biol. *42*, 579-620.

Vigh, L., Nakamoto, H., Landry, J., Gomez-Munoz, A., Harwood, J. L., Horvath, I. (2007). Membrane regulation of the stress response from prokaryotic models to mammalian cells. *Ann. N. Y. Acad. Sci.*, *1113*, 40-51.

Vile D, Pervent M, Belluau M, Vasseur F, Bresson J, Muller B, Granier C, Simonneau T. (2012). Arabidopsis growth under prolonged high temperature and water deficit: independent or interactive effects? *Plant Cell Environ.*, *35*, 702-18.

Voesenek LACJ, Banga M, Thier RH, Mudde CM, Harren FJM, Barendse GWM, Blom CWPM. (1993). Submergence-induced ethylene synthesis entrapment, and growth in two plant species with contrasting Flooding resistances. *Plant Physiol.*, *103*, 783-791.

von Korff, M., Wang, H., Léon, J., Pillen, K. (2004). Development of candidate introgression lines using an exotic barley accession (*Hordeum vulgare* ssp. *spontaneum*) as donor. *Theor. Appl. Genet.*, *109*, 1736-1745.

Vu, L.D., Gevaert, K., De Smet, I. (2019). Feeling the heat: Searching for plant thermosensors. *Trends Plant Sci.*, *24*, 210-219.

Vu, L. D., Xu, X., Gevaert, K., and De Smet, I. (2019). Developmental plasticity at high temperature. *Plant Physiol.*, *181*, 399-411.

Wahid, A., Gelani, S., Ashraf, M., Foolad, M. (2007). Heat tolerance in plants: an overview. *Environ. Exp. Bot., 61*, 199-223.

Wang, Z.Y., Nakano, T., Gendron, J., He, J., Chen, M., Vafeados, D., Yang, Y., Fujioka, S., Yoshida, S., Asami, T., Chory, J. (2002). Nuclear-localized BZR1 mediates brassinosteroid-induced growth and feedback suppression of brassinosteroid biosynthesis. *Dev. Cell, 2*, 505-513.

Wan, Y., Jasik, J., Wang, L., Hao, H., Volkmann, D., Menzel, D., et al. (2012). The signal transducer NPH3 integrates the phototropin1 photosensor with PIN2-based polar auxin transport in Arabidopsis root phototropism. *Plant Cell*, *24*, 551-565.

Wang, X. , Goshe, M.B. , Soderblom, E.J. , Phinney, B.S. , Kuchar, J.A. , Li, J. , Asami, T. , Yoshida, S. , Huber, S.C. , Clouse, S.D. (2005). Identification and functional analysis of in vivo phosphorylation sites of the Arabidopsis BRASSINOSTEROID-INSENSITIVE1 receptor kinase. *Plant Cell*, *17*, 1685-1703.

Wang, Z.Y., Bai, M.Y., Oh, E., Zhu, J.Y. (2012). Brassinosteroid signaling network and regulation of photomorphogenesis. *Annual Review of Genetics*, *46*, 701-724.

Wang, Z., Chen, F., Li, X. et al. (2016). Arabidopsis Seed germination speed is controlled by SNL histone deacetylase-binding factor-mediated regulation of AUX1. *Nat. Commun., 7*, 13412.

Wang, R., Zhang, Y., Kieffer, M., Yu, H., Kepinski, S., Estelle, M. (2016). HSP90 regulates temperaturedependent seedling growth in Arabidopsis by stabilizing the auxin co-receptor F-box protein TIR1. *Nature communications*, *7*, 10269.

Wasson, A.P., Rebetzke, G.J., Kirkegaard, J.A., Christopher, J., Richards, R.A., Watt, M. (2014). Soil coringat multiple field environment scan directly quantify variation in deep root traits to select wheat genotypes for breeding. *Journal of Experimental Botany*, *65*, 6231-6249.

Watt,M., Moosavi,S., Cunningham, S.C. ,Kirkegaard, J.A., Rebetzke, G.J., Richards, R.A. (2013). A rapid, controlled-environment seedling root screen for wheat correlates well with

rooting depths at vegetative, but not reproductive, stages at two field sites. *Annals of Botany, 112*, 447-455.

Wei, Q., Zhou, W., Hu, G., Wei, J., Yang, H., Huang, J. (2008). Heterotrimeric G-protein is involved in phytochrome A-mediated cell death of Arabidopsis hypocotyls. *Cell Res., 18*, 949-960.

Wigge, P.A. (2017). Transcriptional regulation of the ambient temperature response by H2A.Z nucleosomes and HSF1 transcription factors in Arabidopsis. *Molecular Plant*, *10*, 1258-1273.

Wildwater, M., Campilho, A., Perez-Perez, J.M., Heidstra, R., Blilou, I., Korthout, H., Chatterjee, J., Mariconti, L., Gruissem, W., Scheres, B. (2005). The RETINOBLASTOMA-RELATED gene regulates stem cell maintenance in Arabidopsis roots. *Cell*, *123*, 1337-1349.

Wu, G., Lewis, D.R. and Spalding, E.P. (2007). Mutations in Arabidopsis multidrug resistance-like ABC transporters separate the roles of acropetal and basipetal auxin transport in lateral root development. *Plant Cell*, *19*, 1826-1837.

Xiang, D.B., Zhao, G., Wan, Y., Tan, M.L., Song, C., Song, Y. (2016). Effect of planting density on lodging-related morphology, lodging rate, and yield of tartary buckwheat (*Fagopyrum tataricum*) *Plant Prod Sci.*, *19*, 479-488.

Xu, W.F., Jia, L.G., Shi, W.M., Liang, J.S., Zhou, F., Li, Q.F., Zhang, J.H. (2013). Abscisic acid accumulation modulates auxin transport in the root tip to enhance proton secretion for maintaining root growth under moderate water stress. *New Phytol.*, *197*, 139-150.

Xu, T., Dai, N., Chen, J., Nagawa, S., Cao, M., Li, H., Zhou, Z., Chen, Z., De Rycke, R. Rakusova, H., Wang, W., Jones, A.M., Friml, J., Patterson, S.E., Bleecker, A.B. and Yang, Z. (2014). Cell surface ABP1-TMK auxin-sensing complex activates ROP GTPase signaling. *Science, 343*, 1025-1028.

Yang, X., Dong, G., Palaniappan, K., Mi, G., Baskin, T. I. (2017). Temperature compensated cell production rate and elongation zone length in the root of *Arabidopsis thaliana*: temperature compensation in root growth. *Plant, Cell & Environment.*, *40*, 264-276.

Yang, H., Waugh, D.W.,, Orbe, C.,Patra, P., Jöckel, P., Lamarque, J.F., Tilmes, S., Kinnison, D., Elkins, J., Dlugokencky, E. (2019). Evaluating simulations of interhemispheric transport: Interhemispheric exchange time versus SF6 age. *Geophys. Res. Lett., 46*, 1113-1120.

Yin, K., Ueda, M., Takagi, H., Kajihara, T, Aki, S.S., Nobusawa, T., Umeda-Hara, C., Umeda, M. (2014). A dual-color marker system for in vivo visualization of cell cycle pro-gression in Arabidopsis. Plant J. *80*, 541-552.

Yin, Y., Wang, Z.Y., Mora-Garcia, S., Li, J., Yoshida, S., Asami, T., Chory, J. (2002). *BES1* accumulates in the nucleus in response to brassinosteroids to regulate gene expression and promote stem elongation. *Cell*, *109*, 181-191.

Yin, Y., Vafeados, D., Tao, Y., Yoshida, S., Asami, T., Chory, J. (2005). A new class of transcription factors mediates brassinosteroid-regulated gene expression in Arabidopsis. *Cell*, *120*, 249-259.
Yoshida, S. (1978). Tropical climate and its influence on rice. IRRI research paper series 20. International Rice Research Institute, Los Banos.

Yu, Q., Li, P., Liang, N., Wang, H., Xu, M., & Wu, S. (2017). Cell-Fate Specification in Arabidopsis Roots Requires Coordinative Action of Lineage Instruction and Positional Reprogramming. *Plant Physiol. 175*, 816-827*.*

Yunbi, Xu. (2010). Molecular Plant Breeding. CAB International. London UK.

Zhan, A., Schneider, H., and Lynch, J. P. (2015). Reduced lateral root branching density improves drought tolerance in maize. *Plant Physiol., 168*, 1603-1615.

Zhang, J., Nodzyński, T., Pencík, A., Rolcík, J., Friml, J. (2010). PIN phosphorylation is sufficient to mediate PIN polarity and direct auxin transport. *Proc. Natl. Acad. Sci. USA*, *107*, 918-922.

Zhang, Y., Wang, C., Xu, H., Shi, X., Zhen, W., Hu, Z., Huang, J., Zheng, Y., Huang, P., Zhang, K. X., Xiao, X., Hao, X., Wang, X., Zhou, C., Wang, G., Li, C., & Zheng, L. (2019). HY5 Contributes to Light-Regulated Root System Architecture Under a Root-Covered Culture System. *Frontiers in plant science*, *10,* 1490.

Zhao, Y., Christensen, S.K., Fankhauser, C., Cashman, J.R., Cohen, J.D., Weigel, D., Chory, J. (2001). A role for flavin monooxygenase-like enzymes in auxin biosynthesis. *Science*, *291*, 306-309.

Zhao, C., Liu, B., Piao, S., Wang, X., Lobell, D.B.,Huang, Y., Huang, M.,Yao, Y., Bassu, S., Ciais, P., Durand, J.-L., Elliott, J., Ewert, F., Janssens, I.A., Li, T., Lin, E., Liu, Q., Martre, P., Müller, C., Peng, S., Peñuelas, J., Ruane, A.C., Wallach, D., Wang, T., Wu, D., Liu, Z., Zhu, Y., Zhu, Z., Asseng, S. (2017). Temperature increase reduces global yields of major crops in four independent estimates. *Proc. Natl. Acad. Sci.*, *114*, 9326-9331.

Zheng, X.H., Miller, N.D., Lewis, D.R., Christians, M.J., Lee, K.H., Muday, G.K., Spalding, E.P., Vierstra, R.D. (2011). AUXIN UP-REGULATED F-BOX PROTEIN1 regulates the cross talk between auxin transport and cytokinin signaling during plant root growth. *Plant Physiol.*, *156*, 1878-1893.

Zheng, Z., Guo, Y., Novák, O., Chen, W., Ljung, K., Noel, J.P., Chory, J. (2016). Local auxin metabolism regulates environment-induced hypocotyl elongation. *Nat. Plants*, *2*, 16025

Zhou Y., Xun, Q., Zhang, D., Lv, M., Ou, Y., Li, J. (2019). TCP transcription factors associate with PHYTOCHROME INTERACTING FACTOR 4 and CRYPTOCHROME 1 to regulate thermomorphogenesis in *Arabidopsis thaliana*. *Science*, *15*, 600-610.

Zhu, J., Kaeppler, S.M., Lynch, J.P. (2005). Mapping of QTLs for lateral root branching and length in maize (*Zea mays L.*) under differential phosphorus supply. *Theoretial and Applied Genetics*, *111*, 688-695.

Zhu, J., Bailly, A., Zwiewka, M., Sovero, V., Di, Donato, M., Ge, P., Oehri, J., Aryal, B., Hao, P., Linnert, M., Burgardt , N., Lucke, C., Weiwad, M., Michel, M., Weiergraber, O.H., Pollmann, S., Azzarello, E., Mancuso, S., Ferro, N., Fukao, Y., Hoffmann, C., Wedlich-Soldner, R., Friml, J., Thomas, C., Geisler, M. (2016). TWISTED DWARF1

mediates the action of auxin transport inhibitors on actin cytoskeleton dynamics. *Plant Cell, 28*. 930-948.

Zhu, J., Zhang, K.X., Wang, W.S., Gong, W., Liu, W.C., Chen, H.G., Xu, H.H., Lu, Y.T. (2018). Low temperature inhibits root growth by reducing auxin accumulation via *ARR1/12*. *Plant Cell Physiol.*, *56*, 727-736.

Zhu, X.G., Long, S.P., Ort, D.R. (2010). Improving photosynthetic efficiency for greater yield*. Annu. Rev. *Plant Biol*., *61, 235-261*

Zourelidou, M., Müller, I., Willige, B.C., Nill, C., Jikumaru, Y., Li, H., Schwechheimer, C. (2009). The polarly localized D6 PROTEIN KINASE is required for efficient auxin transport in *Arabidopsis thaliana*. *Development*,*136*, 627-636.

Zwieniecki, M. A., Thompson, M. V., and Holbrook, N. M. (2003). Understanding the hydraulics of porous pipes: tradeoffs between water uptake and root length utilization. *J. Plant Growth Regul.*, *21*, 315-323.

Appendix

List of Figures

List of abbreviations

A. thaliana   Arabidopsis thaliana

ABA   Abscisic acid

AFB2	AUXIN SIGNALING F-BOX2
AFB2	AUXIN SIGNALING F-BOX3
AHKs	ARABIDOPSIS HISTIDINE KINASES
AHPs	ARABIDOPSIS HISTIDINE PHOSPHOTRANSFER PROTEINS
ANOVA	Analysis of variance
ARF	AUXIN RESPONSE FACTOR
ARR1	ARABIDOPSIS RESPONSE REGULATORS1
ARR12	ARABIDOPSIS RESPONSE REGULATORS12
ATS	Arabidopsis thaliana solutions
Aux/IAA	Auxin/Indole-3-acetic acid
AVDT	Annual average daytime temperatures
bHLH	basic helix-loop-helix
BIN2	BRASSINOSTEROID-INSENSITIVE2
BRI1	BRASSINOSTEROID-INSENSITIVE1
BSU1	BRI1-SUPPRESSOR1
BSL1	BSU1-LIKE
BSK1	BRI1-SUPPRESSOR KINASE1
BZR1	BRASSINOZOLE-Resistant 1
BES1	BRI1-EMS-SUPPRESSOR1
BRs	Brassinosteroids
CCA1	CIRCADIAN CLOCK-ASSOCIATED1
CK	Cytokinin
CPD	CONSTITUTIVE PHOTOMORPHOGENESIS AND DWARFISM
Col-0	Columbia-0
COP1	CONSTITUTIVE PHOTOMORPHOGENIC1
CREs	CIS-REGULATIRY ELEMENTS
CRY1	CRYPTOCHROME1
CRY2	CRYPTOCHROME2
CTR1	CONSTITUTIVE TRIPLE RESPONSE
CYCD	D-type cyclins
DET1	DE-ETIOLATED1
DEGs	Differentially expressed genes
DNA	Deoxyribonucleic acid
DP	Donor Plant
DWF4	DWARF4
DWF7	DWARF7
ELF3	EARLY FLOWERING3

ELF4	EARLY FLOWERING4
HY5	ELONGATED HYPOCOTYL 5
EC	Evening complexes
EIN3	ETHYLENE INSENSITIVE3
Enk-1	Enkeim-1
Epi-BL	Epi-brassinolide
ETR1	ETHYLENE RECEPTOR1
ET	Ethylene
EXP8	EXPANSIN8
EZ	Elongation zone
GA	Gibberellin
GA3OX2	GIBBERELLIN 3-OXIDASE 2
GA2OX1	GIBBERELLIN 2-OXIDASE1
GA2OX4	GIBBERELLIN 2-OXIDASE4
GO	Gene ontology
GFP	Green fluorescent proteins
GUS	Beta-glucuronidase
HDA9	HISTONE DEACETYLASE9
HCA	Hierarchical clustering analysis
IAA	INDOLE-3-ACETIC ACID
IL	Introgression line
JA	Jasmonate
LD	Long-day
Ler-0	Landsberg erecta
LHY	LATE ELONGATED HYPOCOTYL
L-Kyn	L-kynurenin
MaZ	Maturation zone
MDS	Multidimensional scaling
MSG2	MASSUGU2
MZ	Meristematic zone
NPA	1-N-naphthylphthalamic acid
PCA	Principal component analysis
PIN	PIN-FORMED
PILS6	PIN-LIKES6
phys	Phytochromes

PGP4	PHOSPHOGLYCOPROTEIN4
PIFs	PHYTOCHROME INTERACTING FACTORs
PIF4	PHYTOCHROME INTERACTING FACTOR4
pifQ	pif quadruple
PRR1	PSEUDO-RESPONSE REGULATOR1
QC	Quiescent center
QTL	Quantitative Trait Locus
qPCR	quantitative polymerase chain reaction
RAM	Root apical meristem
RBR	RETINOBLASTOMA-RELATED
RFP	Red fluorescent protein
RP	Recipient plant
RNA	Ribonucleic acid
SAM	Shoot apical meristem
SAURs	SMALL AUXIN UP RNAs
SLR1	SOLITARY-ROOT1
SNP	Single nucleotide polymorphism
SPA1	SUPRESSOR OF PHYA
TAA1	TRYPTOPHAN AMINOTRANSFERASE OF ARABIDOPSIS1
TAR1	TRYPTOPHAN AMINOTRANSFERASE RELATED1
TIHE	Temperature-induced hypocotyl elongation
TIRE	Temperature-induced root elongation
TIR1	TRANSPORT INHIBITOR RESPONSE1
TIR3	TRANSPORT INHIBITOR RESPONSE3
TMKs	TRANSMEMBRANE KINASEs
TOC1	TIMING OF CAB EXPRESSION1
TZ	Transition zone
UVR8	UVB-RESISTANCE8
WEI8	WEAK ETHYLENE INSENSITIVE8
XTR8	XYLOGLUCAN ENDO-TRANSGLYCOSYLASE-RELATED8
XTH31	XYLOGLUCAN ENDO-TRANSGLYCOSYLASE-HYDROLASE31
Yuc	Yuccasin
YUC	YUCCAs
ZEITLUPE	ZTL
Zeitgeber	ZT

Supplementary Figures

Table S10: Oligonucleotide primers used in qPCR analyses

Gene name	NCBI accession number	Forward prime (5'→ 3')	Reverse prime (5'→ 3')
YUC8	AT4G28720	CGACTGCTCGGTTCGATGA	TTACTTCCCTCGGCATCACG
SAUR19	AT5G18010	CTTCAAGAGCTTCATAATAATTCAAACTT	GAAGGAAAAAATGTTGGATCATCTT
SAUR20	AT5G18020	AACTTGAATCTTTTCATACATCTTCAGAAGA	TAACTAGGAAGAAAAATGTTGGCTCATC
IAA19	AT3G15540	GGTGACAACTGCGAATACGTTACCA	CCCGGTAGCATCCGATCTTTTCA
PIF4	AT2G43010	AGATGCAGCCGATGGAGATG	GCTCACCAACCTAGTGGTCC
CYCD3;1	AT4G34160	CGTTCGTAGACCACATTATCAGGAG	CGGAGATTACAGAGAGGAGGAGAC
CYCD1;1	AT1G70210	ACTCGCACTCGCACTGACC	CAAGTGATGAGGGAGGGTAGAGG
CYCD6;1	AT4G03270	GCGCTCTGTTACTCCTTTCTCC	CGCCTGCAATCACCGATGG
CYCD4;2	AT5G10440	CCTAGTGAAAAGCTTGGACTG	TTAGCCTCAAACACGAACATG
CYCB1;1	AT4G37490	ACTCGCACTCGCACTGACC	GAGCCGAGAGCACAGAAGAAAG
EXP8	AT2G40610	GTTCCTGTCTCTTTCCGAAGAG	TACGTCTCCTGCTCCTCCTA
EXP18	AT1G62980	AACATGAACGCACGTC	ATAGTGTTTCTCACGTT
XTH21	AT2G18800	GGGTGTGGCTTATCCAAAGA	GGTCCCTGTGACCAGTTTGT
XTH19	AT4G30290	TGCAGCTAAATGATTGATTCTTTGAT	CCATTGAGTTACAAAGACAACGCAA
RCH1	AT5G48940	AGAGAACGTGCCAAAGATGA	CGCAGAGAAACTCGTGCTAC
XTR8	AT3G44990	ACATACATGAATAATTGGAGGTCTTG	CTTTTCTTTTTAATCTCAAATCATAGAGG
RBR1	AT3G12280	CTCATAAGTCGCCTGCTGCTAAG	TTGCTGTGCTCACTGGTGTTG
E2FB	AT5G22220	CCGATGAAAGAGGAAAGCACCG	CGCCTACCTCTGATCGAAACC
UBQ10	AT4G05320	TGCTGCCCAACATCAGGTT	TGCGCTGCCAGATAATACACTATT
PP2A	AT1G13320	AGACAACGTTCACTCAATCGGTG	CATTCAGGACCAAACTCTTCAGC
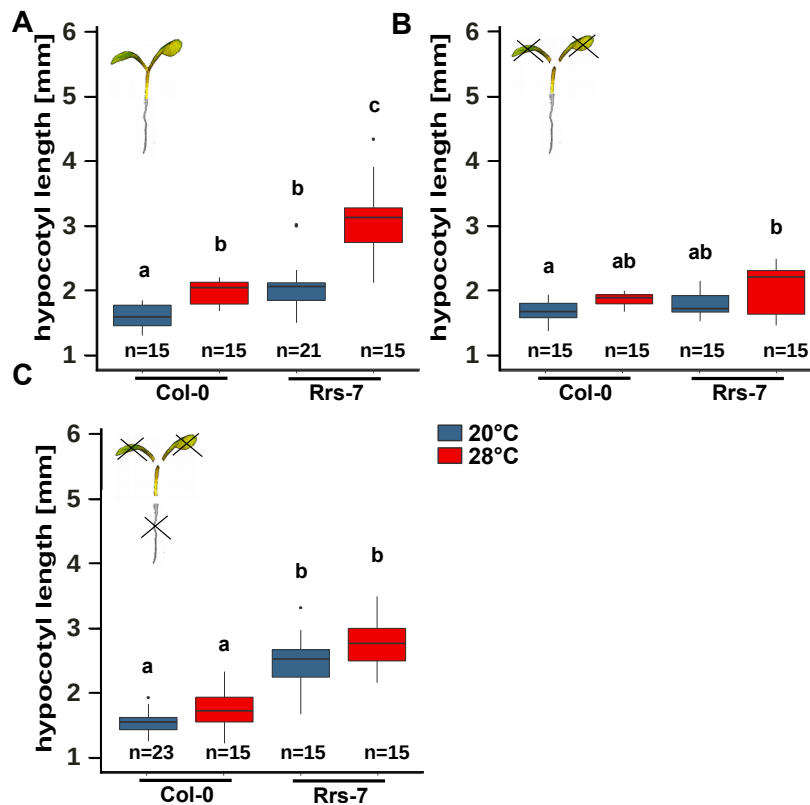
Figure S1. Elongation responses of detached seedling organs. A-C petioles and cotyledons or whole shoots were removed from 4d-old seedlings grown at 20°C. Subsequently, detached organs were placed on growth medium and cultivated for an additional 4 d at 20°C or 28°C. **A** TIHE of hypocotyls with root and with cotyledons. **B** TIHE of hypocotyls with root and without cotyledons. **C** TIHE of hypocotyls without root and without cotyledons. Experiments were performed in LD (16/8 h) conditions under 90 µmol m^{-2} s^{-1} white fluorescent light. Box plots show medians and interquartile ranges of total organ lengths; outliers (greater than 1.5× interquartile range) are shown as black dots. Different letters denote statistical differences at $p < 0.05$ as assessed by one-way ANOVA and Tukey's honestly significant difference (HSD) posthoc test. (modified from Bellstaedt et al. ,2019)
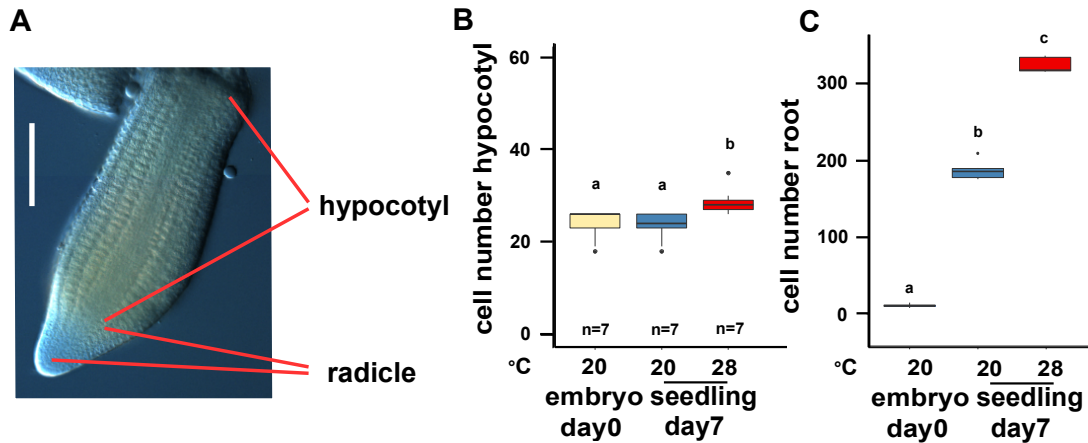
Figure S2. High capacity for cell elongation in the hypocotyl and cell division in the roots. A Representative picture of a isolated and cleared embryo in maturation stage. Isolation procedure was used **according to** Feng et al. 2017 **C,B** Cell number of hypocotyls (**B**) and radicles (**C**) of mature embryos (0d) compared to the cell number of hypocotyls (**B**) and roots (**C**) of 7d-old seedlings grown at 28°C, respectively LD (16/8 h), 90 µmol m^{-2} s^{-1}.Box plots show medians and interquartile ranges of total organ lengths; outliers (greater than 1.5× interquartile range) are shown as black dots. Different letters denote statistical differences at $p < 0.05$ as assessed by one-way ANOVA and Tukey's honestly significant difference (HSD) posthoc test. The experiment was repeated once with similar results.
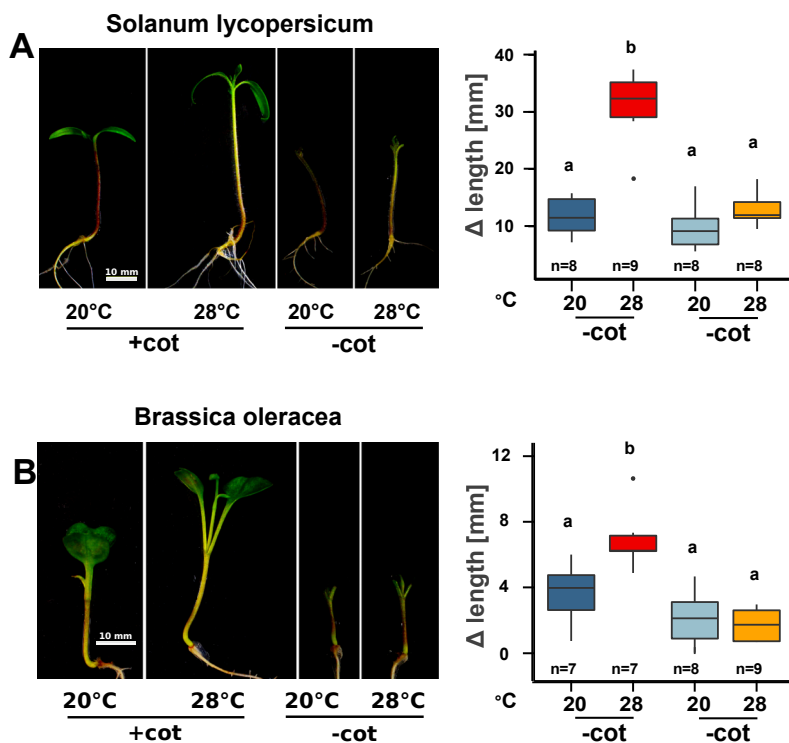
Figure S3. The effect of cotyledon removal in other flowering plant species. Representative pictures of temperature-induced changes in hypocotyl lengths of 11d-old tomato (**A**) and cabbage (**B**) seedlings. Plants were initially grown for 8d at 20°C. Cotyledons were detached or seedlings remained intact prior to the shift to 28°C for an additional 3d. Corresponding Δlength was calculated as the hypocotyl length on day 11 minus the length prior to shift. Experiments were performed in LD conditions (16/8 h) under 90 µmol m^{-2} s^{-1} white fluorescent light. Control plants in all experiments were treated similarly but were grown at 20°C for the whole time instead of shifting to 28°C. Box plots show medians and interquartile ranges of total organ lengths; outliers (greater than 1.5× interquartile range) are shown as black dots. Different letters denote statistical differences at $p < 0.05$ as assessed by one-way ANOVA and Tukey's honestly significant difference (HSD) posthoc test. Experiments were repeated once with similar result.
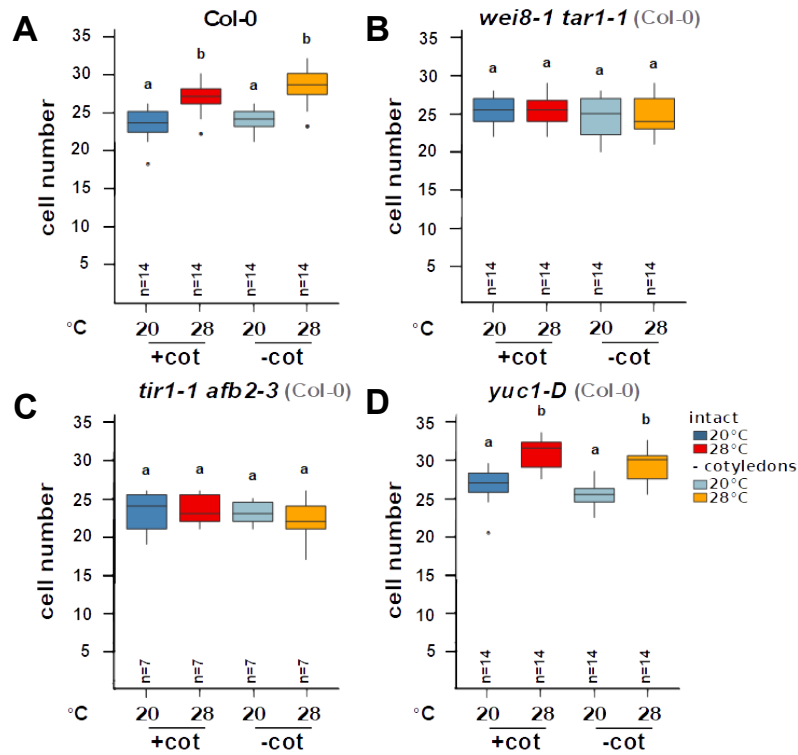
Figure S4. Temperature-induced cell division in auxin mutants. Wild-type (Col-0) and *wei8-1tar1-1*, *tir1-1afb2-3*, *yuc1-D* mutant seedlings were initially grown in LD (16/8 h) under 90 µmol m^{-2} sec^{-1} white fluorescent light at 20°C for 4d. Petioles and cotyledons were removed or seedlings were left intact prior to a shift to 28°C for additional 3d. Control plants were treated similarly but grown at 20°C. Number of consecutive hypocotyl cortex cell files were determined via microscopy after propidium iodide staining. Box plots show medians and interquartile ranges (IQR), outliers (> 1.5 x IQR) are shown as black dots. Different letters denote statistical differences at *p*< 0.05 as assessed by one-way ANOVA and Tukey HSD post hoc test. Experiments were repeated once with similar results, except for *tir1-1 afb2-3*. (modified from Bellstaedt et al., 2019)
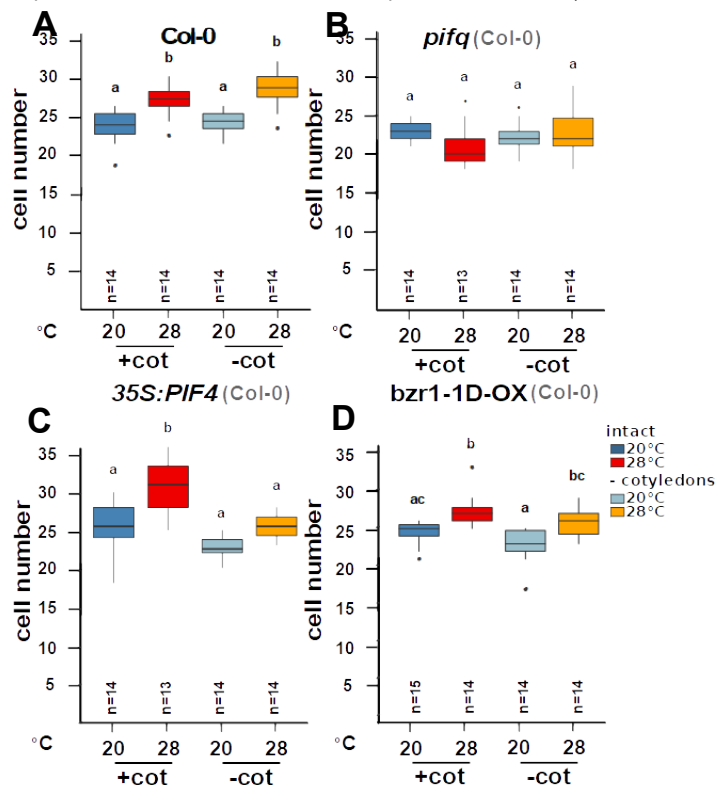
Figure S5. Temperature-induced cell division in mutants of thermomorphogenesis regulators. A-D Effects of cotyledon detachment on hypocotyl cell number in one consecutive cortex cell file of Col-0 (**A**), *pifq* (**B**), *35S:pIF4* (**C**) and *bzr1-1D-OX* (**D**).

Figure S5 (Continued). Seedlings were grown at 20°C for 4d. petioles and cotyledons were removed or seedlings were left intact prior to a shift to 28°C for an additional 3d. Experiments were performed in LD conditions (16/8 h) under 90 µmol m^{-2} s^{-1} white fluorescent light. Control plants in all experiments were treated similarly but were grown at 20°C for the whole time instead of shifting to 28°C. Box plots show medians and interquartile ranges; outliers (greater than 1.5× interquartile range) are shown as black dots. Different letters denote statistical differences at $p< 0.05$ as assessed by one-way ANOVA and Tukey's HSD posthoc test. (modified from Bellstaedt et al., 2019)

Figure S6. Temperature-induced cell division in photomorphogenesis mutants. A-C Effects of cotyledon detachment on hypocotyl cell number in one consecutive cortex cell file of Ler-0 (**A**), *YHB* (**B**) and *phyABCDE* (**C**). Seedlings were initially grown in LD (16/8 h) under 90 µmol m^{-2} sec^{-1} white uorescent light at 20°C for 4d. petioles and cotyledons were removed or seedlings were left intact prior to a shift to 28°C for additional 3d. Control plants were treated similarly but grown at 20°C.Number of consecutive hypocotyl cortex cell files were determined via microscopy after propidium iodide staining. Box plots show medians and interquartile ranges (IQR), outliers (> 1.5 x IQR) are shown as black dots. Different letters denote statistical di erences at $p< 0.05$ as assessed by one-way ANOVA and Tukey HSD post hoc test. Experiments were repeated with similar results. (modified from Bellstaedt et al., 2019).
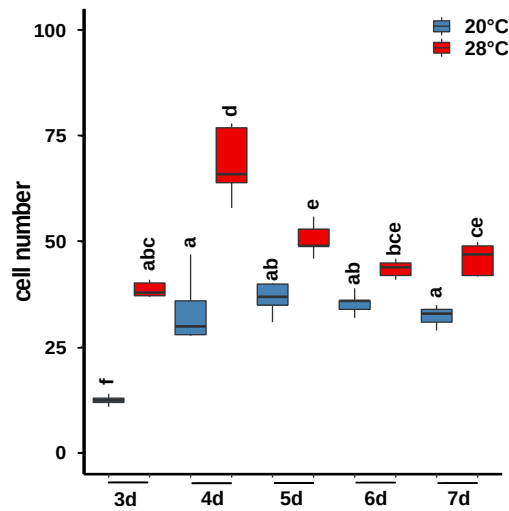
Figure S7. Relative increase in cell number in the maturation zone (MaZ) compared to the previous days at the different temperatures. Roots were cultivated at 28°C or 20°C at constant temperatures . The cells of the MaZ of a consecutive cell file were countered after 2, 3, 4, 5, 6, 7d (number of cells in the MaZ at day3 – number of cells in the MaZ at day2 etc..). The experiments were performed in LD (16/8 h) conditions under 90 µmol m^{-2} s^{-1} white fluorescent light and constant temperatures. Box plots show medians and interquartile ranges of total organ lengths; outliers (greater than 1.53 interquartile range) are shown as black dots. Different letters denote statistical differences at $p < 0.05$ as assessed by one-way ANOVA and Tukey's honestly significant difference (HSD) posthoc test.
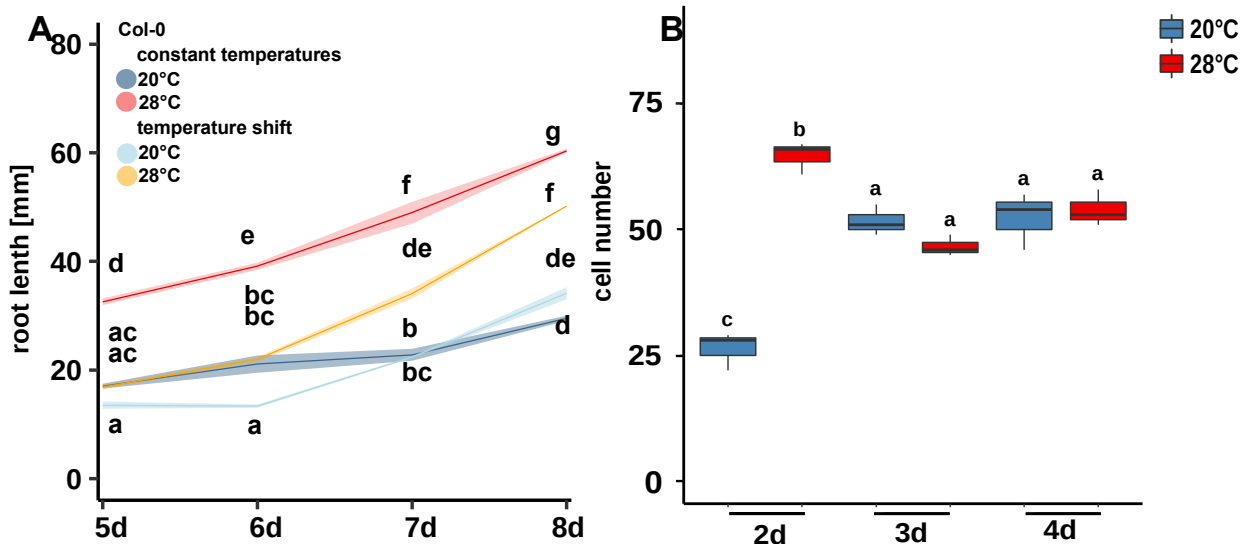
Figure S8. Increase in root length and cell number under shift conditions. A Root elongation under constant temperatures and temperature shift conditions, monitored over a time scale of 4d. The first time point for quantification was taken 24h after the shift to the higher temperature (day 5). Roots under constant temperature conditions were cultivated at 28°C or 20°C at constant temperature. Root under temperature shift conditions were cultivated 4d at 20°C and half of them were shifted to 28°C for further 4d. The control plants grew further at 20°C conditions. **B** Relative increase in number of cells in the MaZ per day of roots cultivated under temperature shift conditions (number of cells in the MaZ at day2 – number of cells in the MaZ at day 1 etc.) . The cells of the MaZ of a consecutive cell file were countered after 1,2,3,4d after the shift. The experiments were performed in LD (16/8 h) conditions under 90 µmol m^{-2} s^{-1} white fluorescent light and constant temperatures. Bold lines in ribbon plots show mean lengths of individual roots. The shadowed ribbon denotes the SEM. Box plots show medians and interquartile ranges of total organ lengths; outliers (greater than 1.53 interquartile range) are shown as black dots. Different letters denote statistical differences at $p < 0.05$ as assessed by one-way ANOVA and Tukey's honestly significant difference (HSD) posthoc test.
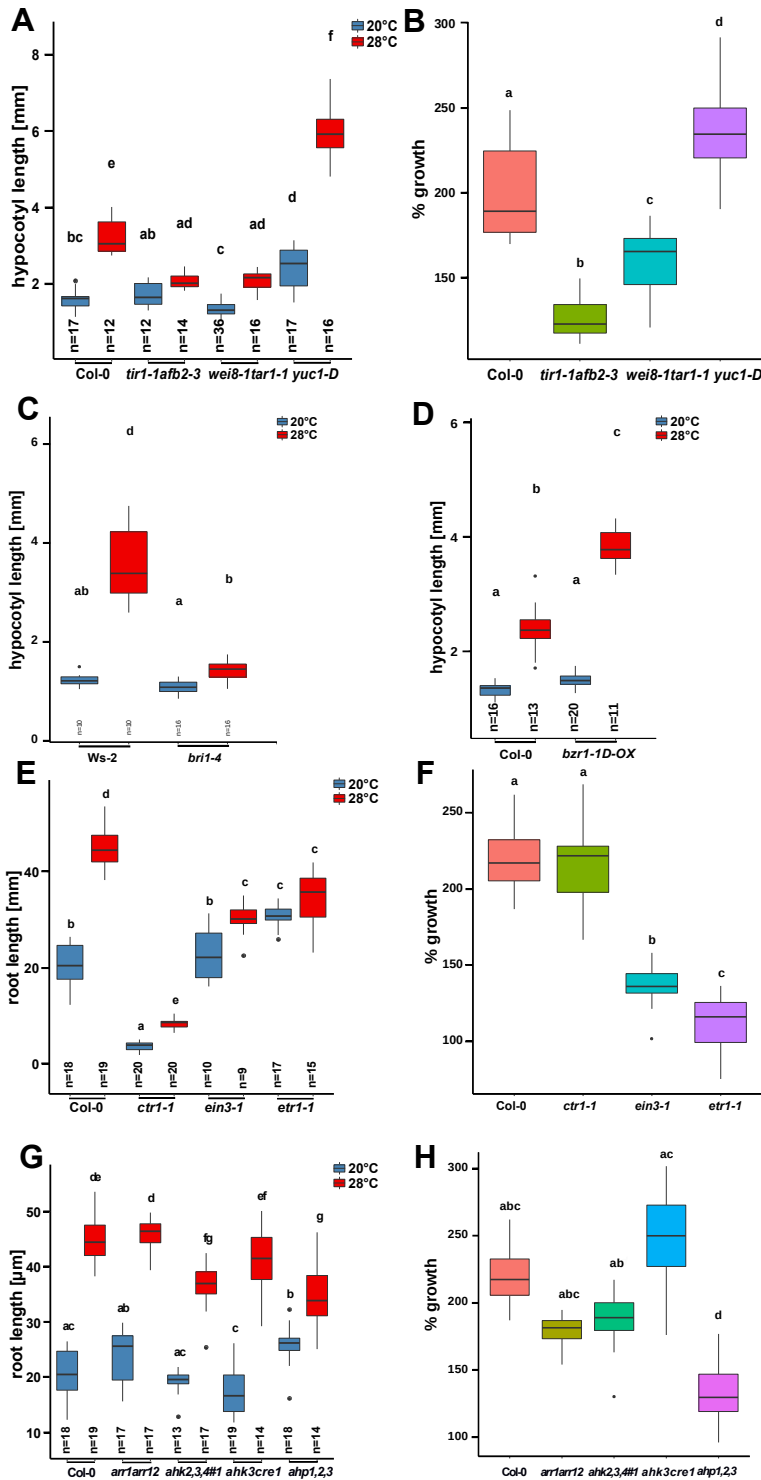
Figure S9. Impact of auxin, BR, ethylene and cytolkinin related genes on temperature induced hypocotyl or root growth. **A-D** hypocotyl length of auxin related (**A-B**) or BR related (**C-D**) mutant plants. **E-J** root length of ethylene related (**E-F**), cytokinin related (**G-H**) and jasmonate related (**I-J**) mutant plants. **A-H** Seedlings were grown under LD conditions (16/8 h) and 90 µmol m^{-2} s^{-1} white fluorescent light at 20◦C or 28°C for 7d . Box plots show medians and interquartile ranges; outliers (greater than 1.53 interquartile range) are shown as black dots. **A,C,D,E,G,H** Different letters denote statistical differences at $p < 0.05$ as assessed by one-way ANOVA and Tukey's honestly significant difference (HSD) posthoc test. **B,F,H,J** Statistical differences were assessed by two-way ANOVA ($p < 0.05$) of the absolute data presented in Figure **A,E,G,I**. Different letters denote significant differences among all samples; asterisks highlight significant differences to the wild-type response.

186
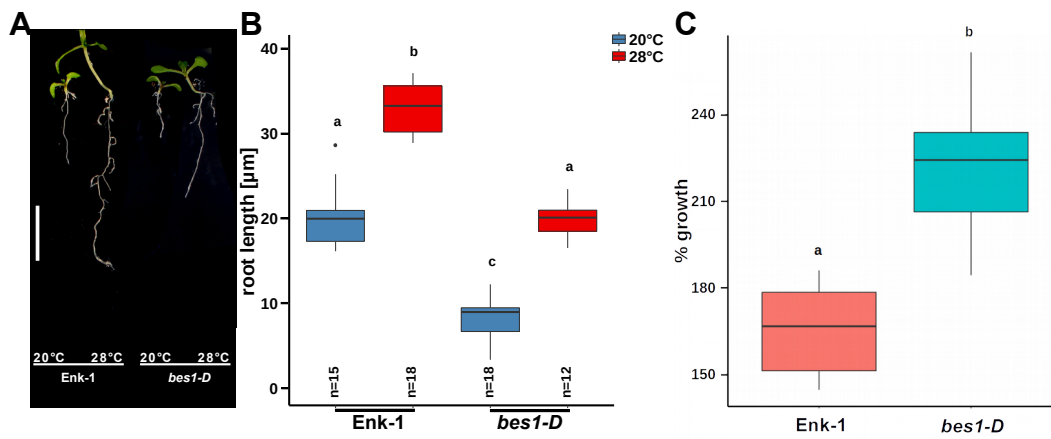
Figure S10. Impact of BES1 gene on the temperature induced root growth. **A-C** Root length of 7d-old wild type plants and *bes1-D* grown at 20 or 28 °C under LD (16/8h) and 90 µmol m^{-2} s^{-1} white fluorescent light. **A** Representative picture of plants from corresponding TIRE-assay. scale bars: 10mm. Box plots show medians and interquartile ranges; outliers (greater than 1.53 interquartile range) are shown as black dots. **B** Different letters denote statistical differences at $p< 0.05$ as assessed by one-way ANOVA and Tukey's honestly significant difference (HSD) posthoc test. **C** Statistical differences were assessed by two-way ANOVA ($p < 0.05$) of the absolute data presented in Figure **B** (left) Different letters denote significant differences among all samples; asterisks highlight significant differences to the wild-type response.
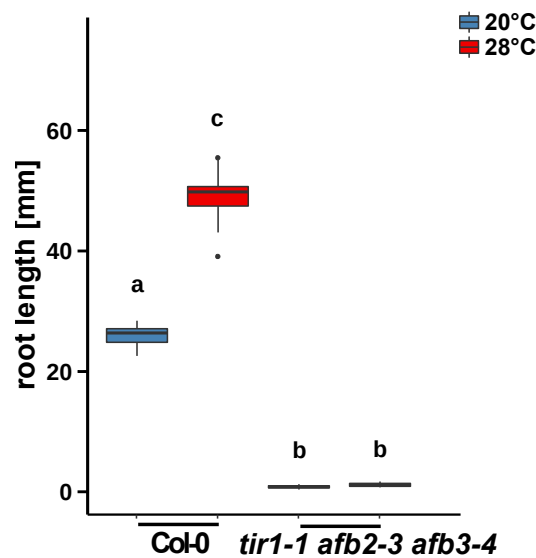
Figure S11. Impact of TIR1, AFB2, AFB3 genes on the temperature induced root growth. Root length of 7d-old wild type plants and *tir1-1 afb2-3 afb3-4* mutant line grown at 20 or 28 °C under LD (16/8 h) and 90 µmol m^{-2} s^{-1} white fluorescent light. Box plots show medians and interquartile ranges; outliers (greater than 1.53 interquartile range) are shown as black dots. Different letters denote statistical differences at $p< 0.05$ as assessed by one-way ANOVA and Tukey's honestly significant difference (HSD) posthoc test.. Different letters denote significant differences among all samples; asterisks highlight significant differences to the wild-type response.
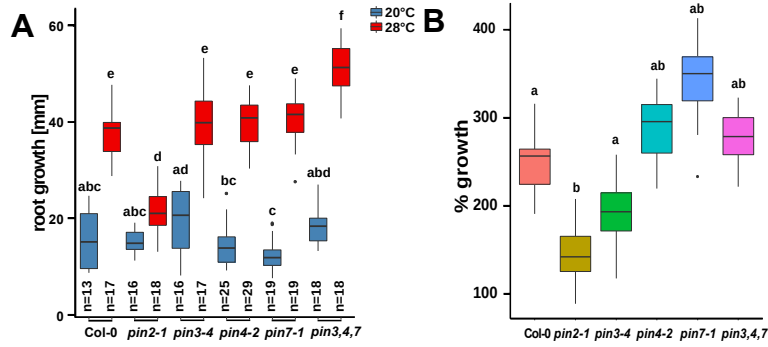
Figure S12 Impact of slected PIN genes on the temperature induced root growth. **A** root length of 7d-old wild type and auxin related mutant plants grown constantly at 20 or 28 °C under LD (16/8 h)and 90 μmol m⁻² s⁻¹ white fluorescent light. **A, B** Box plots show medians and interquartile ranges; outliers (greater than 1.52 interquartile range) are shown as black dots. Different letters denote statistical differences at *p*< 0.05 as assessed by one-way ANOVA and Tukey's honestly significant difference (HSD) posthoc test. **B** Statistical differences were assessed by two-way ANOVA *(p< 0.05)* of the absolute data presented in Figure **A**. Different letters denote significant differences among all samples; asterisks highlight significant differences to the wild type response.
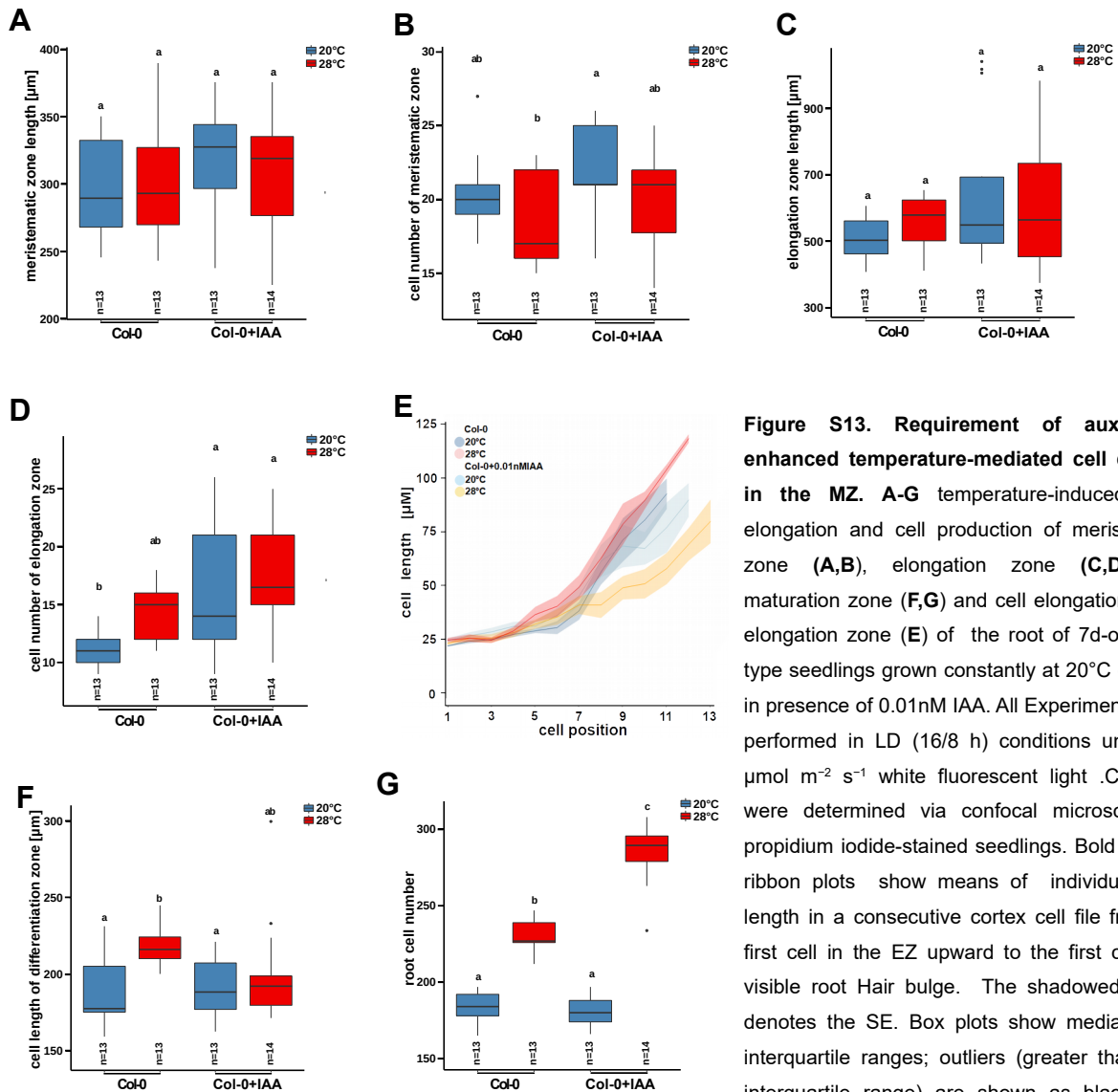
Figure S13. Requirement of auxin for enhanced temperature-mediated cell divison in the MZ. A-G temperature-induced zone elongation and cell production of meristematic zone **(A,B)**, elongation zone **(C,D)** and maturation zone (**F,G**) and cell elongation in the elongation zone (**E**) of the root of 7d-old wild type seedlings grown constantly at 20°C or 28°C in presence of 0.01nM IAA. All Experiments were performed in LD (16/8 h) conditions under 90 μmol m⁻² s⁻¹ white fluorescent light .Cell files were determined via confocal microscopy of propidium iodide-stained seedlings. Bold lines in ribbon plots show means of individual cells length in a consecutive cortex cell file from the first cell in the EZ upward to the first cell with visible root Hair bulge. The shadowed ribbon denotes the SE. Box plots show medians and interquartile ranges; outliers (greater than 1.53 interquartile range) are shown as black dots. Different letters denote statistical differences at
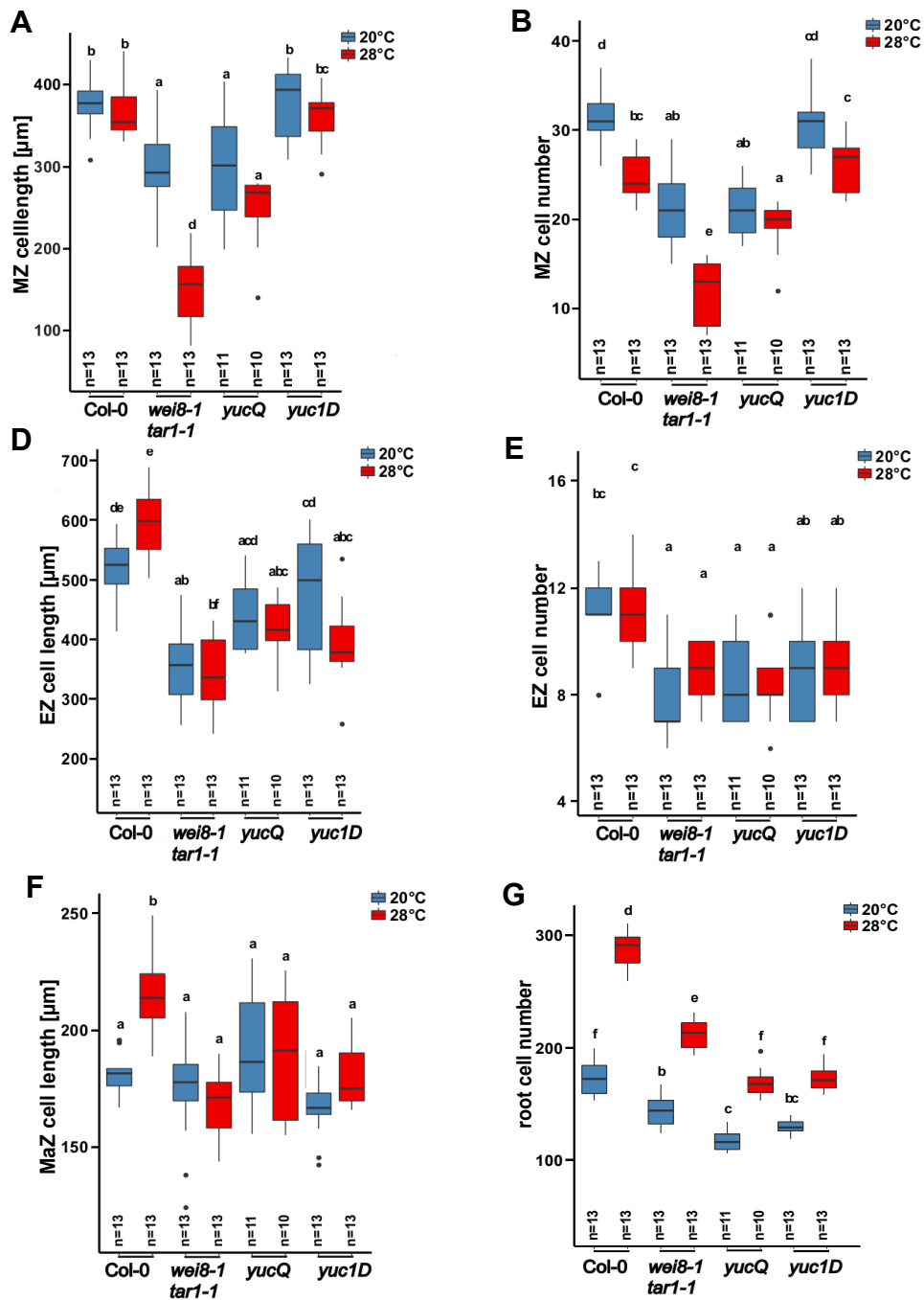
Figure S14. Requirement of auxin for cell divison in temperature induced root growth. **A-F** temperature- induced cell elongation, cell production of meristematic zone **(A,B)**, elongation zone **(C,D)** and cell elongation of the cells in the maturation zone **(F)** of the root of 7d-old auxin related mutant seedlings *wei8-1 tar1-1*, *yucQ*, *yuc1D* and wild type Col-0. **G** Boxplots show the cell number of the entire root of the mutant lines at 20°C or 28°C. All plants grew constantly at 20°C or 28°C. All Experiments were performed in LD (16/8h) conditions under 90 µmol m^{-2} s^{-1} white fluorescent light. Cell files were determined via confocal microscopy of propidium iodide-stained seedlings. Box plots show medians and interquartile ranges; outliers (greater than 1.53 interquartile range) are shown as black dots. Different letters denote statistical differences at *P*< 0.05 as assessed by one-way ANOVA and Tukey's honestly significant difference (HSD) posthoc test. Different letters denote significant differences among all samples; asterisks highlight significant differences to the wild-type response.

189
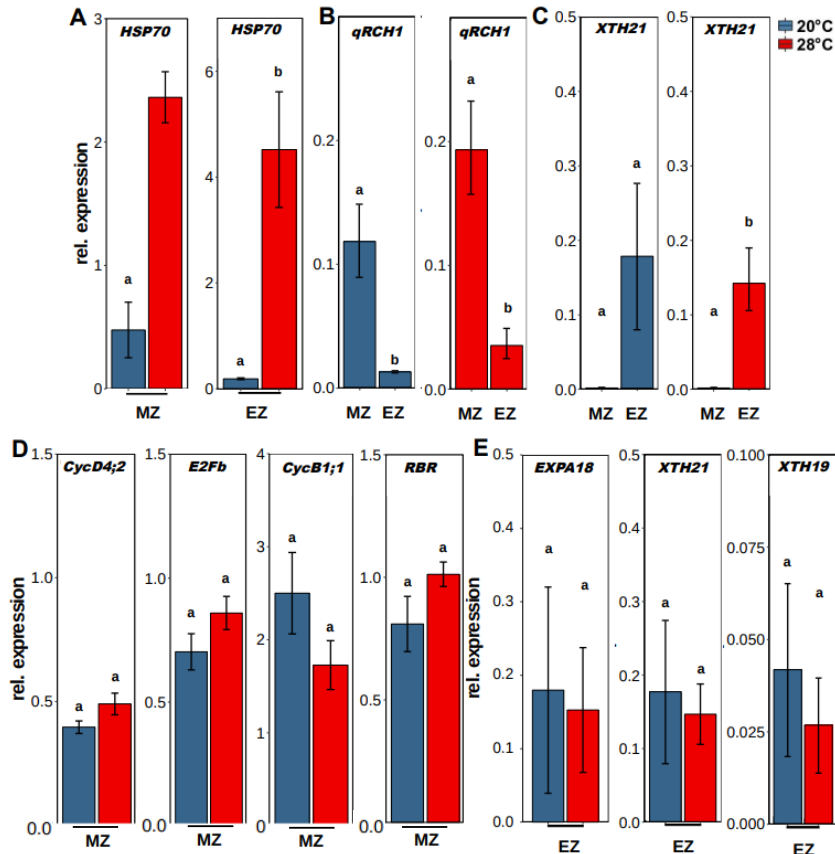
Figure S15. RNA quality control and organ-specific expression analysis of cell cycle and cell elongation related genes. **A-E** Meristem and EZ were harvested seprately at zeitgeber time 1 (ZT1) for expression analysis . Graphs showing the reverse transcription quantitative PCR (RT-qPCR) expression of a temperature responsive marker gene *HSP70* **(A)**, a meristematic zone (MZ) specific marker gene *qRCH1* **(B)** and an elongation zone (EZ) marker gene *XTH21*, **(C)**, cell cycle regulator genes, as D-type cyclins *CYCD4;2*, a transcription factor *E2Fb*, G2-to-M phase-specific gene *CycB1;1* and a cell cycle repressor RBR **(D)** and cell expansion genes, *EXPA18, XTH21, XTH19* in MZ and/or EZ samples of Col-0 seedlings. Before harvesting, seedlings have been grown for 5d constantly at 20°C or 28°C in LD conditions (16/8 h) under 90 μmol m^{-2} s^{-1} white fluorescent light. RT-qPCR analyses were performed on three independent biological replicates. Bar plots show mean values, and error bars denote se. Different letters denote statistical differences at $p < 0.05$ as assessed by one-way ANOVA and Tukey's HSD posthoc test.
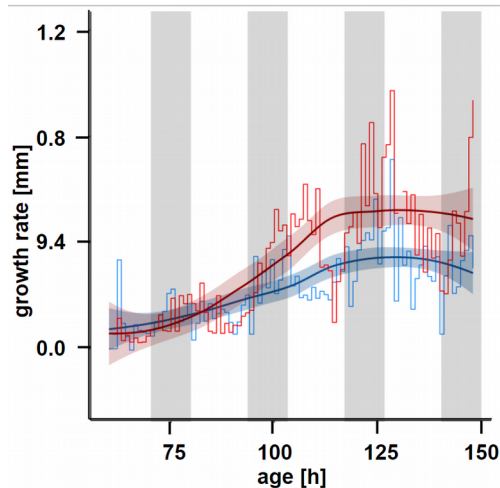
Figure S16. Effect of temperature (°C) and exposure time (h) combined with light and dark periods on the root elongation rate (mm/h) in *Arabidopsis*. Step plots represent the root elongation rate of Col-0 seedling (mm/h) which

Figure S16 (Continued). grown constantly in standard LD conditions (16/8 h) under 90 µmol m^{-2} s^{-1} white fluorescent light at 20°C (blue line) or 28°C(red line). The length of the roots were measured every hour for 6d. Root elongation rate was calculated as the length of root divided by the duration of growth (mm/h). Root length monitoring starts 48h after sawing where the root was clearly visible. The red (28°C) and blue (20°C) almost diagonal lines are the regression lines of the corresponding growth rate curves. Vertical gray bars represent the dark periods and the wight bars indicate the light periods. Root elongation rate was computed as mean moving average of individual curves (red line n$_{root}$=17; blue line n$_{root}$=17). The shadow ribbons represent the standrd error of each mean
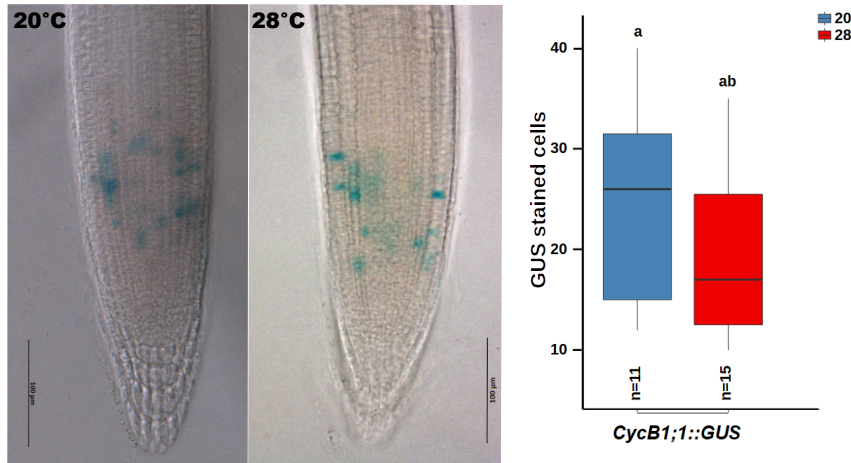
Figure S17. Effect of elevated temperature on the capacity for cell division in the primary root meristem. Expression of the *CycB1::GUS* reporter in the meristem of the primary root. Plants were mounted in a chloral hydrate solution (8:3:1 mixture of chloral hydrate:water:glycerol) (Mambro et al. 2018). One representative sample for each temperature is shown. Scale bars = 100µm. Seedlings were grown under long-day conditions (16/8h) and 90 µmol m^{-2} s^{-1} white fluorescent light at 20°C or 28°C for 7d. Box plots show medians and interquartile ranges; outliers (greater than 1.53 interquartile range) are shown as black dots. Different letters denote statistical differences at *p*< 0.05 as assessed by one-way ANOVA and Tukey's honestly significant difference (HSD) posthoc test.
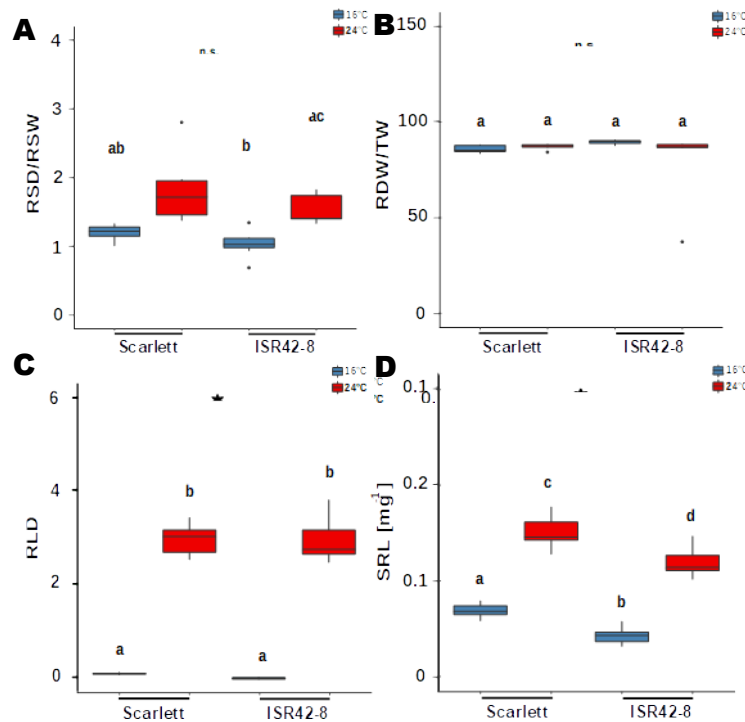
Figure S18. Root growth responses to high ambient temperature of the parents of the population S42IL, 'Scarlett' and 'SR42-8'. Box plots show medians and interquartile ranges of **(A)** the ration of the root system width and root system
Figure S18 (Continued). depth (RSW/RSD), **(B)** the ratio of the root dray weight and total weight (RDW/TW), **(C)** the root length density (RLD), **(D)** the specific root length (SRL). Box plots show means of the measurement data of time point 6

191

(12d after temperature reatment at 16°C or 24°C). Experiments were performed in LD (16/8h) conditions and light intensity of 470 μmol m^{-2} s^{-1}. Letters denote statistical differences ($p < 0.05$) as assessed by one-way ANOVA and Tukey HSD. Outliers (greater than 1.5× interquartile range) are shown as black dots.

Table S11. Selected S42IL introgression lines

Genotype	Species
Scarlett	*Hordeum vulgare*
ISR42-8	*Hordeum spontaneum*
S42IL-101	*Hordeum vulgare*
S42IL-102	*Hordeum vulgare*
S42IL-103	*Hordeum vulgare*
S42IL-104	*Hordeum vulgare*
S42IL-105	*Hordeum vulgare*
S42IL-106	*Hordeum vulgare*
S42IL-107	*Hordeum vulgare*
S42IL-108	*Hordeum vulgare*
S42IL-109	*Hordeum vulgare*
S42IL-110	*Hordeum vulgare*
S42IL-111	*Hordeum vulgare*
S42IL-112	*Hordeum vulgare*
S42IL-113	*Hordeum vulgare*
S42IL-114	*Hordeum vulgare*
S42IL-115	*Hordeum vulgare*
S42IL-116	*Hordeum vulgare*
S42IL-117	*Hordeum vulgare*
S42IL-118	*Hordeum vulgare*
S42IL-119	*Hordeum vulgare*
S42IL-120	*Hordeum vulgare*
S42IL-121	*Hordeum vulgare*
S42IL-122	*Hordeum vulgare*
S42IL-123	*Hordeum vulgare*
S42IL-124	*Hordeum vulgare*
S42IL-125	*Hordeum vulgare*
S42IL-126	*Hordeum vulgare*
S42IL-127	*Hordeum vulgare*
S42IL-128	*Hordeum vulgare*
S42IL-129	*Hordeum vulgare*
S42IL-130	*Hordeum vulgare*
S42IL-131	*Hordeum vulgare*
S42IL-132	*Hordeum vulgare*
S42IL-133	*Hordeum vulgare*
S42IL-134	*Hordeum vulgare*
S42IL-135	*Hordeum vulgare*
S42IL-136	*Hordeum vulgare*
S42IL-137	*Hordeum vulgare*
S42IL-138	*Hordeum vulgare*
S42IL-139	*Hordeum vulgare*
S42IL-140	*Hordeum vulgare*
S42IL-141	*Hordeum vulgare*
S42IL-142	*Hordeum vulgare*
S42IL-143	*Hordeum vulgare*
S42IL-161	*Hordeum vulgare*
S42IL-162	*Hordeum vulgare*
S42IL-170	*Hordeum vulgare*
S42IL-173	*Hordeum vulgare*
S42IL-176	*Hordeum vulgare*

Figure S19. Comparison of root trait data of all time points for 'Scarlett' and 'ISR42-8'. A-M temperature-induced total root elongation (TRL) (**A**), maximum depth penetration (RSD) (**B**), maximum horizontal expansion (RSW) (**C**), enlargement of the minimum area (CHA) (**D**) relative lateral root elongation (LLR/NLR) (**E**), lateral root emergence (NLR) (**F**), root length density distribution (RLD) (**G**), relative seminal root elongation (LSR/NSR) (**H**), seminal root emergance (NSR) (**I**) root system angle formation left (RSAL) (**J**), right (RSAR) (**K**), total RSALR) (**L**)

Figure S19 *(Continued).*), changes in the ratio of root system depth per root system width (RSD/RSW) (**M**) from day 1 to day 12 after treatment (16°C vs. 24°C, after 4d pre-germination at 16°C) of Scarlett and ISR42-8. Bold lines in ribbon plots show means of the measurment data. Experiments were performed in LD (16/8h) conditions and light intensity of 470 µmol m^{-2} s^{-1}. The shadow ribbon denotes the SE, n>7. Barley seedlings were pre-germinated at 16°C or 24°C.
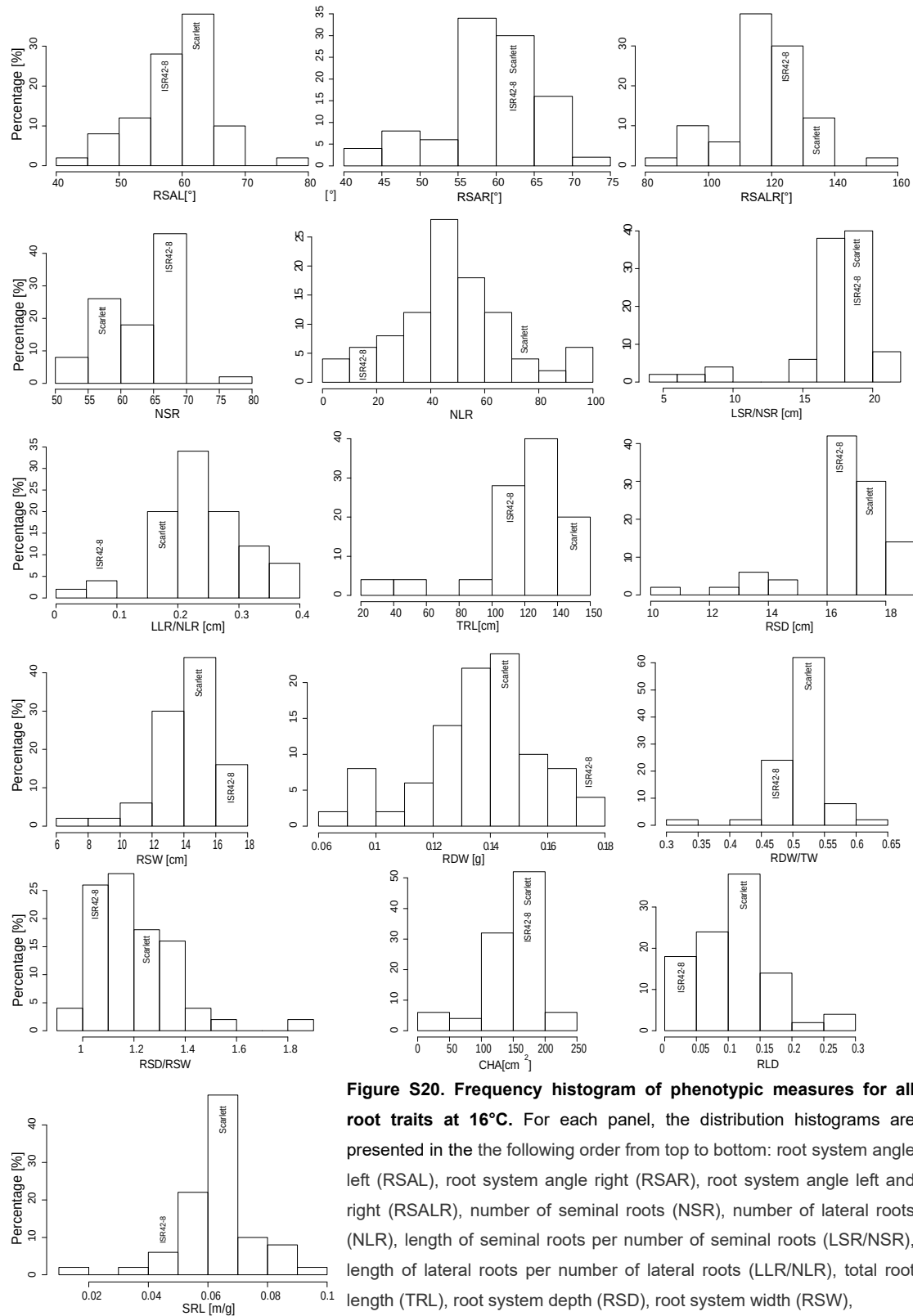
Figure S20. Frequency histogram of phenotypic measures for all root traits at 16°C. For each panel, the distribution histograms are presented in the the following order from top to bottom: root system angle left (RSAL), root system angle right (RSAR), root system angle left and right (RSALR), number of seminal roots (NSR), number of lateral roots (NLR), length of seminal roots per number of seminal roots (LSR/NSR), length of lateral roots per number of lateral roots (LLR/NLR), total root length (TRL), root system depth (RSD), root system width (RSW),

194

Figure S21. Frequency histogram of phenotypic measures for all shoot traits at 16°C. For each panel, the distribution histograms are presented in the the following order from top to bottom: total length of the first leaf (1stLTL), total length of the second leaf (2ndLTL), length of the first leaf sheath (1stLLS), length of the first leaf blade (1stLBL), length of the second leaf blade (2ndLBL), area of the first leaf (1stLLA), shoot dry weight (SDW), shoot dry weight per total weight (SDW/TW), fresh weight of the shoot (FWS). Most of the 48 introgression lines responded similar to the phenotype of the parental lines (labeled). For creating histograms all measurment values for each trait were used. The data were collected 12d after treatment beginning. The histogram plots were produced in R using the hist(x) function. Experiments were performed in LD (16/8h) conditions and light intensity of 470 μmol m^{-2} s^{-1}. The barley seedlings were pre-germinated for 4d at 16°C. Pre-germinated plants grew 12d at 16°C.
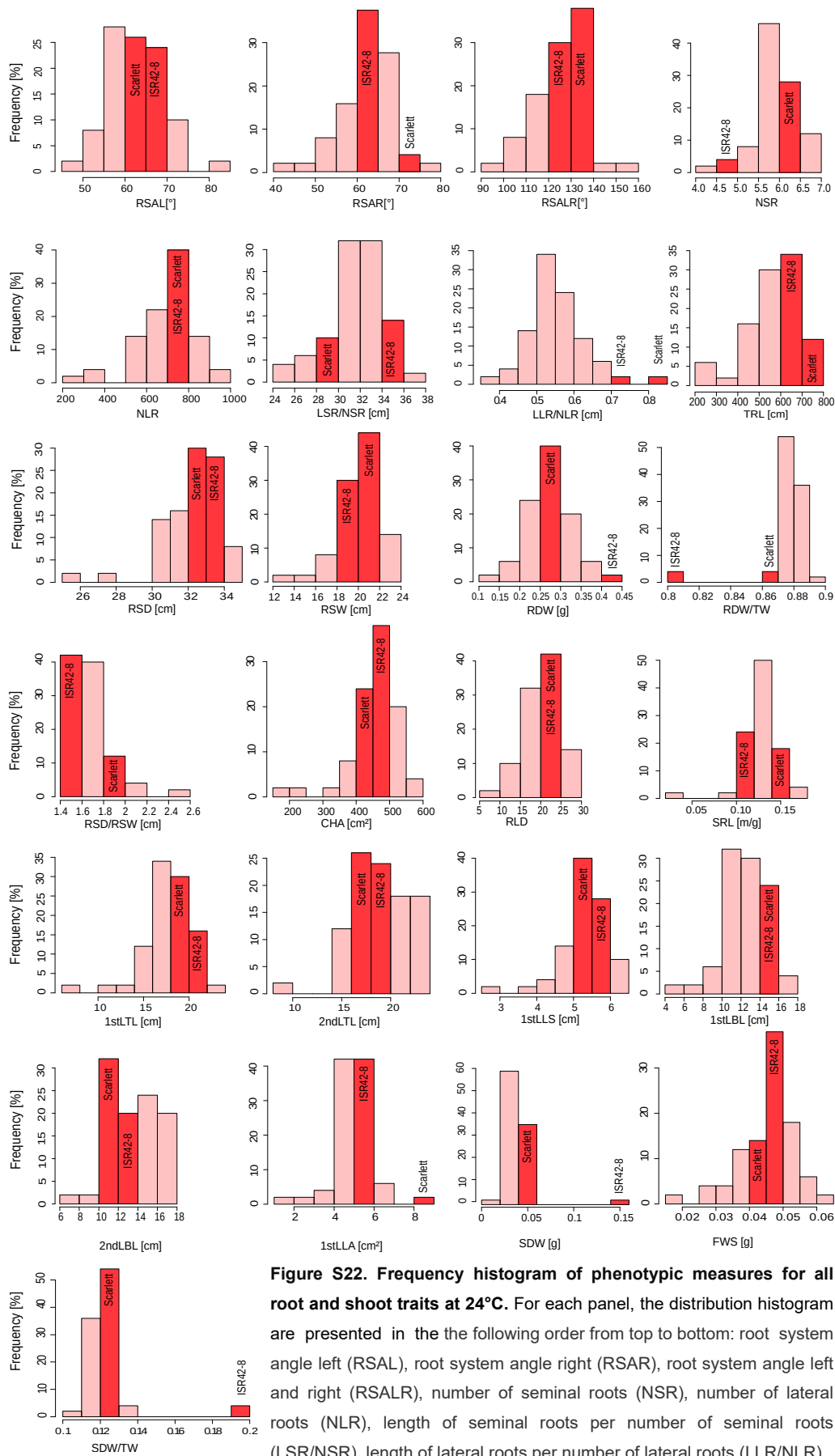
Figure S22. Frequency histogram of phenotypic measures for all root and shoot traits at 24°C. For each panel, the distribution histogram are presented in the the following order from top to bottom: root system angle left (RSAL), root system angle right (RSAR), root system angle left and right (RSALR), number of seminal roots (NSR), number of lateral roots (NLR), length of seminal roots per number of seminal roots (LSR/NSR), length of lateral roots per number of lateral roots (LLR/NLR),

196

Figure S22 (Continued). total root length (TRL), root system depth (RSD), root system width (RSW), root dry weight (RDW), root dry weight per total weight (RDW/TW), root system depth per root system width (RSD/RSW), convex hull area (CHA), root length density (RLD), specific root length (SRL), total length of the first leaf (1stLTL), total length of the second leaf (2ndLTL), length of the first leaf sheath (1stLLS), length of the first leaf blade (1stLBL), length of the second leaf blade (2ndLBL), area of the first leaf (1stLLA), shoot dry weight (SDW), fresh weight of the shoot (FWS), shoot dry weight per total weight (SDW/TW). Most of the 48 introgression lines responded similar to the phenotype of the parental lines (labeled and colored in dark red). For creating histogramts all measurment values for each trait were used. The data were collected 12d after treatment beginning. The histogram plots were produced in R using the hist(x) function. Experiments were performed in LD (16/8h) conditions and light intensity of 470 µmol m^{-2} s^{-1}. The barley seedlings were pre-germinated for 4d at 16°C. Pre-germinated plants grew 12d at 24°C.

Table S11: Descriptive statistics for S42ILs

Variable [a]	Treatment [b]	N [c]	Mean [d]	Min. [e]	Max. [e]	SD [f]	CV [g]	h² [h]
RSAL	16(S42ILs)	339	59,1647	35,3840	87,8860	9,1080	15,3944	31,3384
	24(S42Ils)	333	62,5291	34,2270	89,9360	10,7498	17,1917	
	16(Scarlett)	7	67,0704	62,5570	73,4230	4,6304	6,9038	
	24(Scarlett)	7	62,1947	51,3460	71,2050	8,3228	13,3818	
RSAR	16(S42ILs)	339	58,9438	32,5430	86,0750	9,3034	15,7835	31,6999
	24(S42Ils)	333	62,6939	29,4550	89,8370	10,8525	17,3102	
	16(Scarlett)	7	64,4687	60,8800	74,5890	63,0230	5,1571	
	24(Scarlett)	7	74,1711	57,1250	88,8160	9,7434	6,1571	
RSALR	16(S42ILs)	339	118,1085	75,3410	161,9960	15,5269	13,1463	41,0846
	24(S42Ils)	333	125,2230	66,8800	165,9420	18,2998	14,6137	
	16(Scarlett)	7	131,5391	123,4370	141,7620	6,7077	5,0994	
	24(Scarlett)	7	136,3659	124,6730	143,0920	8,2678	6,0630	
NSR	16(S42ILs)	339	6,3274	5,0000	8,0000	0,6497	10,2673	62,2061
	24(S42Ils)	333	5,9882	4,0000	7,0000	0,6516	10,8821	
	16(Scarlett)	7	7,0000	7,0000	7,0000	0,0000	0,0000	
	24(Scarlett)	7	6,4286	6,0000	7,0000	0,5345	8,3148	
NLR	16(S42ILs)	339	48,3510	1,0000	127,0000	22,2406	45,9981	14,9187
	24(S42Ils)	333	699,2324	203,0000	1098,0000	165,8921	23,7249	
	16(Scarlett)	7	74,4286	71,0000	79,0000	2,9358	3,9445	
	24(Scarlett)	7	669,1429	513,0000	749,0000	85,8631	12,8318	
LSR/NSR	16(S42ILs)	339	17,1617	3,4402	24,1900	3,6556	21,3011	36,0742
	24(S42Ils)	333	31,6467	15,6053	42,7273	4,3764	13,8288	
	16(Scarlett)	7	18,1166	15,7157	20,4466	1,6154	8,9170	
	24(Scarlett)	7	28,7061	24,7773	33,2495	2,8504	9,9297	
LLR/NLR	16(S42ILs)	339	0,2408	0,0074	0,7709	0,0981	40,7317	14,9759
	24(S42Ils)	333	0,5565	0,2746	1,0958	0,1182	21,2305	
	16(Scarlett)	7	0,1910	0,1436	0,2341	0,0288	15,0685	
	24(Scarlett)	7	0,8220	0,6983	1,0958	0,1287	15,6593	

Figure S22 (Continued). For creating histograms all measurment values for each trait were used. The histogram plots were produced in R using the hist(x) function. Experiments were performed in LD (16/8h) conditions and light intensity of 470 µmol m⁻² s⁻¹. The barley seedlings were pre-germinated for 4d at 16°C . The data were collected 12d after treatment beginning.

TRL	16(S42ILs)	339	119,5322	17,9070	168,4630	29,2355	24,4583	
	24(S42lls)	333	569,2069	181,4000	848,6270	134,3847	23,6091	35,4911
	16(Scarlett)	7	150,3966	140,4870	156,8360	6,9787	4,6402	
	24(Scarlett)	7	725,7459	657,6290	695,2830	41,9963	5,7866	
RDW	16(S42ILs)	339	0,1364	0,0211	0,2333	0,0341	25,0232	
	24(S42lls)	333	0,2703	0,0220	0,4863	0,0766	28,3388	42,6775
	16(Scarlett)	7	0,1403	0,1313	0,1541	0,0079	5,6172	
	24(Scarlett)	7	0,2951	0,2209	0,4199	0,0782	26,4933	
RSD	16(S42ILs)	339	16,6364	8,0740	21,7050	2,2172	13,3273	
	24(S42lls)	333	32,2462	18,2140	35,4690	2,7226	8,4433	43,4466
	16(Scarlett)	7	17,5599	16,4210	18,6860	0,8915	5,0767	
	24(Scarlett)	7	32,5260	27,9410	35,0550	2,2193	6,8230	
RSW	16(S42ILs)	339	14,3795	4,0590	21,8890	2,8704	19,9618	
	24(S42lls)	333	20,0996	4,2290	23,9700	3,5684	17,7536	54,3485
	16(Scarlett)	7	14,7386	12,5610	18,4650	1,9406	13,1668	
	24(Scarlett)	7	18,8213	11,3800	23,9630	4,3277	22,9935	
CHA	16(S42ILs)	339	148,4555	0,9330	248,8510	44,6815	30,0975	
	24(S42lls)	333	454,1976	11,8060	654,4740	104,2388	22,9501	65,7261
	16(Scarlett)	7	174,9151	164,2930	203,3320	13,1952	7,5438	
	24(Scarlett)	7	413,1751	213,9310	567,1970	113,2951	27,4206	
RLD	16(S42ILs)	339	0,1095	0,0014	0,3732	0,0644	58,8164	
	24(S42lls)	333	2,0549	0,6915	3,8179	0,5608	27,2896	6,4597
	16(Scarlett)	7	0,1123	0,0917	0,1405	0,0167	14,9151	
	24(Scarlett)	7	2,9672	2,5476	3,4383	0,3328	11,2174	
SRL	16(S42ILs)	339	0,0634	0,0101	0,1999	0,0196	30,8661	
	24(S42lls)	333	0,1288	0,1095	0,1406	0,0329	25,5319	0,1865
	16(Scarlett)	7	0,1295	0,0646	0,0752	0,0329	25,4328	
	24(Scarlett)	7	0,1508	0,1277	0,1763	0,0174	11,5634	

RSD/RSW	16(S42ILs)	339	1,1952	0,6104	2,8165	0,2531	21,1739	25,4373
	24(S42Ils)	333	1,6632	0,9845	4,6699	0,3835	23,0589	
	16(Scarlett)	7	1,2029	1,0120	1,3287	0,1089	9,0529	
	24(Scarlett)	7	1,8196	1,3798	2,8106	0,4981	27,3716	
RDW/TW	16(S42ILs)	339	0,5117	0,1399	0,7860	0,0673	13,1550	8,8204
	24(S42Ils)	333	0,8755	0,3760	0,9205	0,0338	3,8603	
	16(Scarlett)	7	0,5099	0,4351	0,5396	0,0353	6,9244	
	24(Scarlett)	7	0,8723	0,8447	0,8838	0,0136	1,5561	
SDW/TW	16(S42ILs)	339	0,4883	0,2140	0,8601	0,0673	13,7876	8,8204
	24(S42Ils)	333	0,1245	0,0795	0,6240	0,0338	27,1368	
	16(Scarlett)	7	0,4901	0,4604	0,5649	0,0353	7,2033	
	24(Scarlett)	7	0,1277	0,1162	0,1553	0,0136	10,6315	
1stLBL	16(S42ILs)	339	3,8161	5,2423	5,2423	0,5771	15,1218	17,2039
	24(S42Ils)	333	12,5419	4,0000	21,5918	3,0430	24,2629	
	16(Scarlett)	7	3,8665	3,4315	4,5558	0,4280	11,0688	
	24(Scarlett)	7	14,8754	10,3000	19,6238	3,9919	26,8354	
2ndLBL	16(S42ILs)	339	7,8599	12,1647	12,1647	1,5668	19,9345	1,0591
	24(S42Ils)	333	13,5548	22,2573	3,1586	3,1463	23,2117	
	16(Scarlett)	7	7,5061	6,7353	8,4215	0,6704	8,9309	
	24(Scarlett)	7	11,3227	10,0000	12,9439	1,1560	10,2094	
LLS	16(S42ILs)	339	3,8214	1,2924	7,5706	0,9720	25,4363	7,9479
	24(S42Ils)	333	5,2872	2,0000	7,7460	0,8635	16,3329	
	16(Scarlett)	339	3,7364	3,2770	4,3767	0,4080	10,9188	
	24(Scarlett)	333	5,0441	4,4774	5,6054	0,4297	8,5181	
1stLTL	16(S42ILs)	339	7,6375	4,4394	11,1282	1,2412	16,2508	18,7499
	24(S42Ils)	333	17,8290	6,6000	28,2662	3,5154	19,7172	
	16(Scarlett)	7	7,6029	7,0603	8,3473	0,4531	5,9597	
	24(Scarlett)	7	19,9195	15,3396	25,2292	4,2989	21,5813	

2ndLTL	16(S42ILs)	339	7,6375	4,4394	11,1282	1,2412	16,2508	22,9267
	24(S42Ils)	333	18,8530	8,2791	28,9000	3,6221	19,2123	
	16(Scarlett)	7	7,6029	7,0603	8,3473	0,4531	5,9597	
	24(Scarlett)	7	16,3668	14,8255	18,3129	1,4372	8,7809	
1stLA	16(S42ILs)	339	3,6322	0,8000	3,0000	0,9834	27,0731	75,8665
	24(S42Ils)	333	4,9600	1,0000	9,8000	1,2264	24,7263	
	16(Scarlett)	7	3,9571	3,0000	4,7000	0,6729	17,0059	
	24(Scarlett)	7	5,6143	4,9000	6,7000	0,5490	9,7791	
FWS	16(S42ILs)	339	0,0195	0,0049	0,0329	0,0052	26,5448	49,4848
	24(S42Ils)	333	0,0458	0,0064	0,0741	0,0115	25,0777	
	16(Scarlett)	7	0,0219	0,0187	0,0239	0,0021	9,4395	
	24(Scarlett)	7	0,0489	0,0373	0,0610	0,0080	16,2969	
SDW	16(S42ILs)	339	0,0207	0,0020	0,0342	0,0056	27,2233	5,9315
	24(S42Ils)	333	0,0391	0,0104	0,6550	0,0350	89,4129	
	16(Scarlett)	7	0,0229	0,0181	0,0262	0,0032	13,9105	
	24(Scarlett)	7	0,0428	0,0330	0,0592	0,0103	23,9633	

[a] **Trait abbreviations are given in Table 1**
[b] **both treatments 16°C and 24°C, across all lines and Scarlett**
[c] **Number of observations**
[d] **Average trait performance**
[e] **Minmum and maximum trait performance**
[f] **Standard deviation**
[g] **Coefficient of variation (in %)**
[h] **Heritability (in %)**
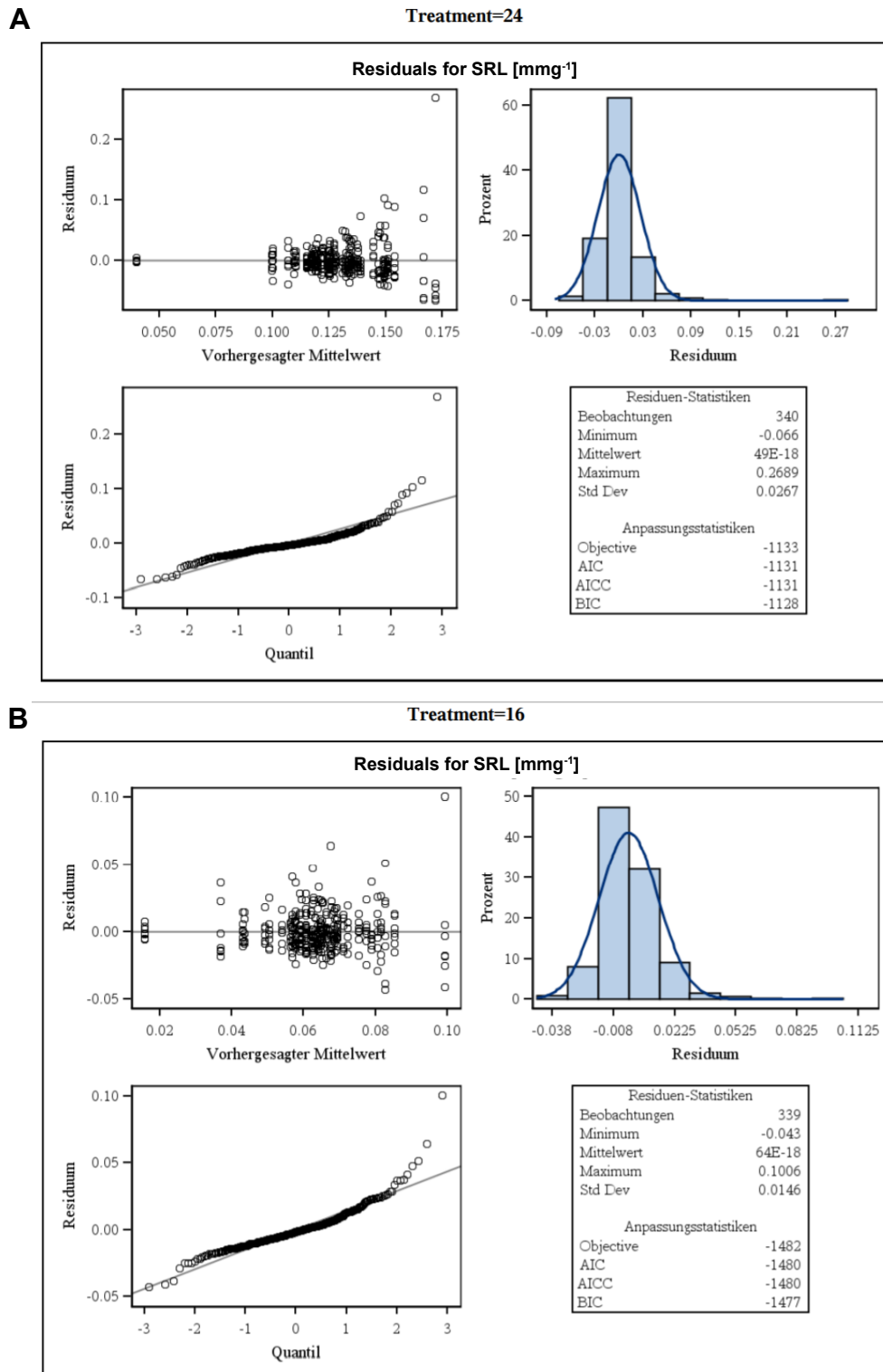
Figure S23. Residual analysis for the trait specific root length (SRL) for Dataset_16°C and Dataset_24°C. Residual analysis results of SRL for Dataset_24°C is shown in **A** and for Dataset_16°C in **B**. The analysis is based on marginal studentized residuals. All model fittings were implemented using SAS pROC MIXED. The data were collected 12d after treatment beginning. Experiments were performed in LD (16/8h) conditions and light intensity of 470 μmol m^{-2} s^{-1}. The barley seedlings were pre-germinated for 4d at 16°C.

Treatment=24

Residuals for RSD/RSW
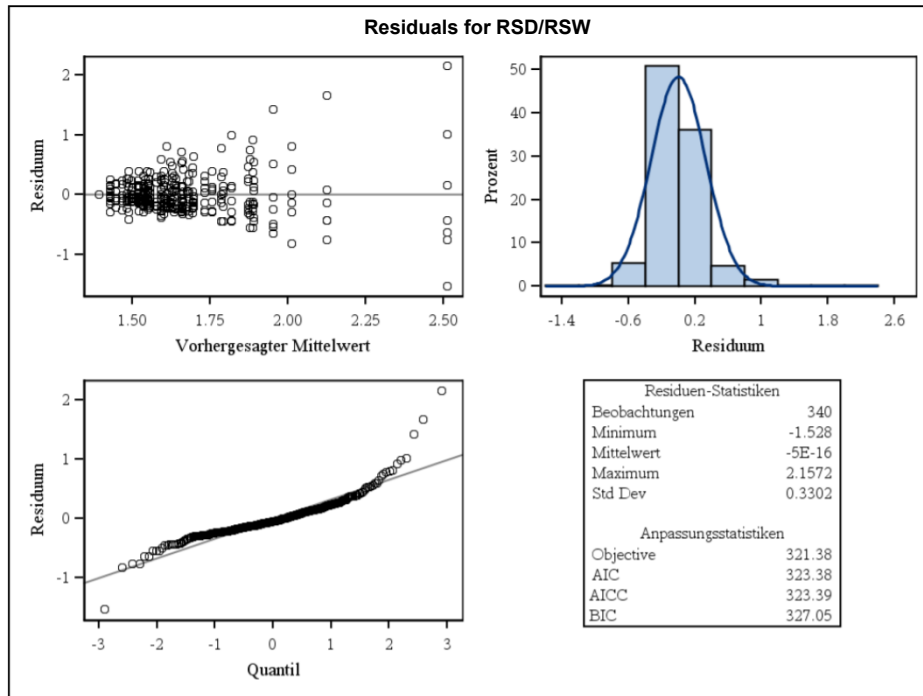
Figure S24. Residual analysis for the trait system depth per root system width (RSD/RSW) for Dataset_24°C. The analysis is based on marginal studentized residuals. All model fittings were implemented using SAS pROC MIXED. The data were collected 12d after treatment beginning. Experiments were performed in LD (16/8h) conditions and light intensity off 470 µmol m^{-2} s^{-1}. The barley seedlings were pre-germinated for 4d at 16°C.

Treatment=24

Residuals for RDW/TW
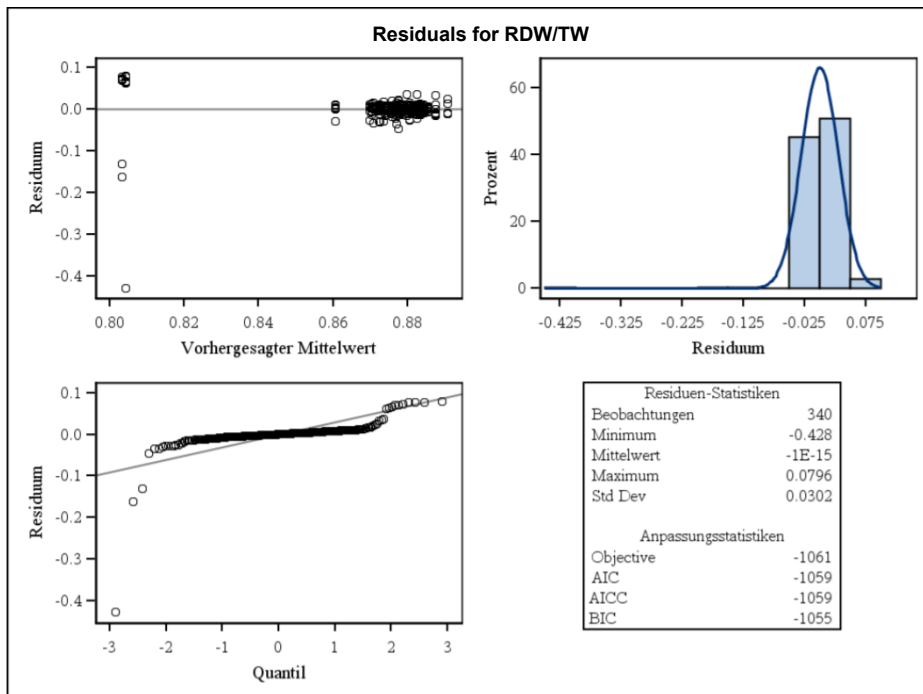
Figure S25. Residual analysis for the trait root dry weight per total weight (RDW/TW) for Dataset_24°C. The analysis is based on marginal studentized residuals. All model fittings were implemented using SAS pROC MIXED. The data were collected 12d after treatment beginning. Experiments were performed in LD (16/8h) conditions and light intensity of 470 µmol m^{-2} s^{-1}. The barley seedlings were pre-germinated for 4d at 16°C.

203

Residuals for SDW
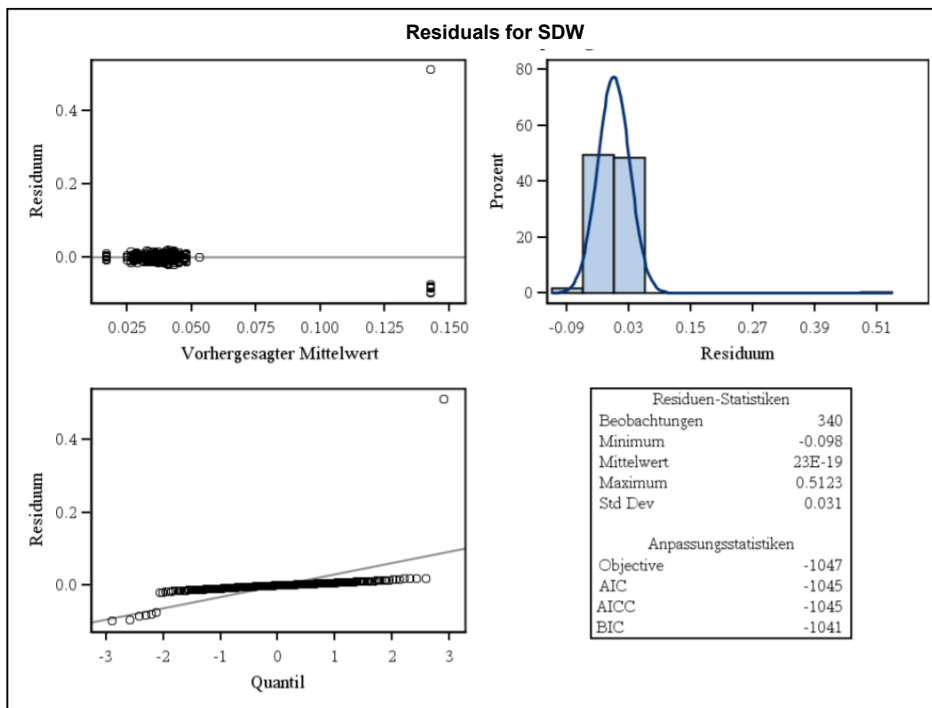
Figure S26. Residual analysis for the trait shoot dry weight (SDW) for Dataset_24°C. The analysis is based on marginal studentized residuals. All model fittings were implemented using SAS pROC MIXED. The data were collected 12d after treatment beginning. Experiments were performed in LD (16/8h) conditions and light intensity of 470 µmol m^{-2} s^{-1}. The barley seedlings were pre-germinated for 4d at 16°C.

Residuals for SDW/TW
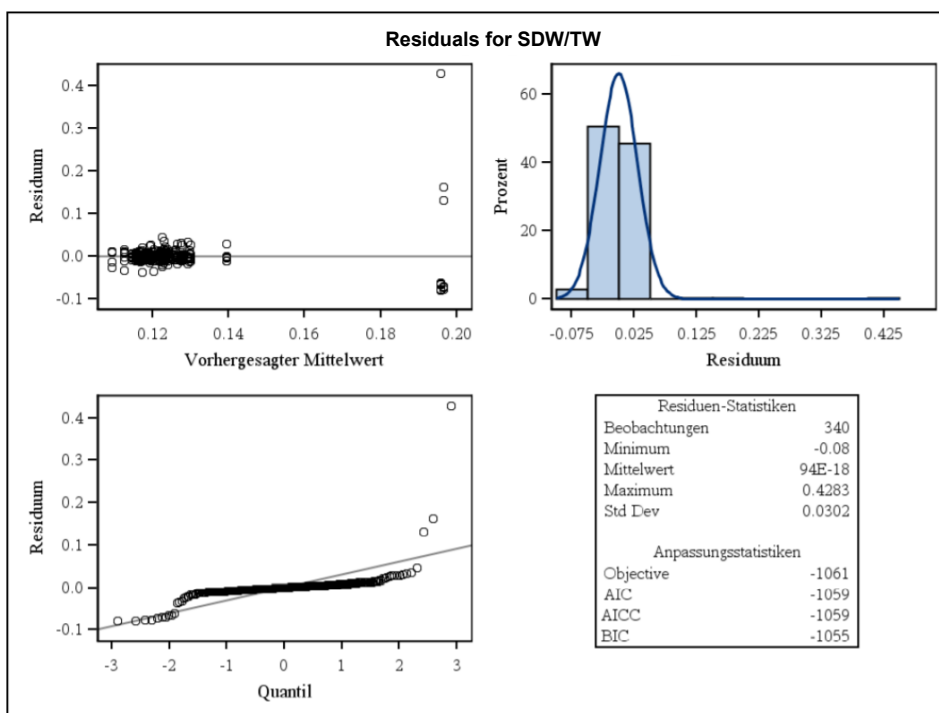
Figure S27. Residual analysis for the traits shoot dry weight per total weight (SDW/TW) for Dataset_24°C. The analysis is based on marginal studentized residuals. All model fittings were implemented using SAS pROC MIXED. The data

were collected 12d after treatment beginning. Experiments were performed in LD (16/8h) conditions and light intensity of 470 µmol m^{-2} s^{-1}. The barley seedlings were pre-germinated for 4d at 16°C.
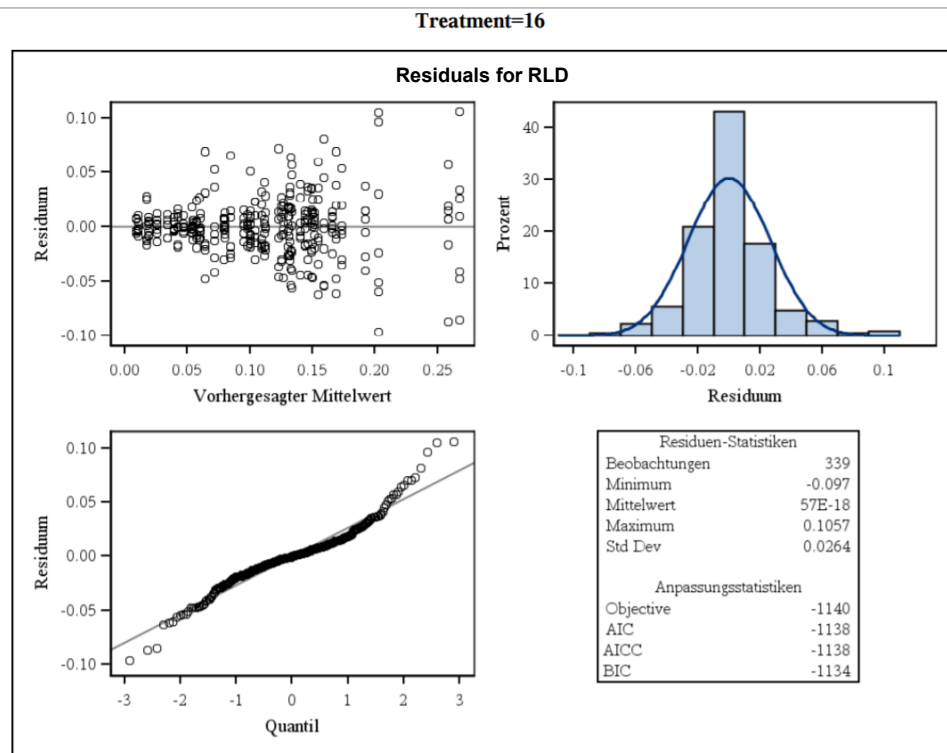
Figure S28. Residual analysis for the traits RLD for Dataset_ 16°C. The analysis is based on marginal studentized residuals. All model fittings were implemented using SAS pROC MIXED. The data were collected 12d after treatment beginning. Experiments were performed in LD (16/8h) conditions and light intensity of 470 µmol m^{-2} s^{-1}. The barley seedlings were pre-germinated for 4d at 16°C.
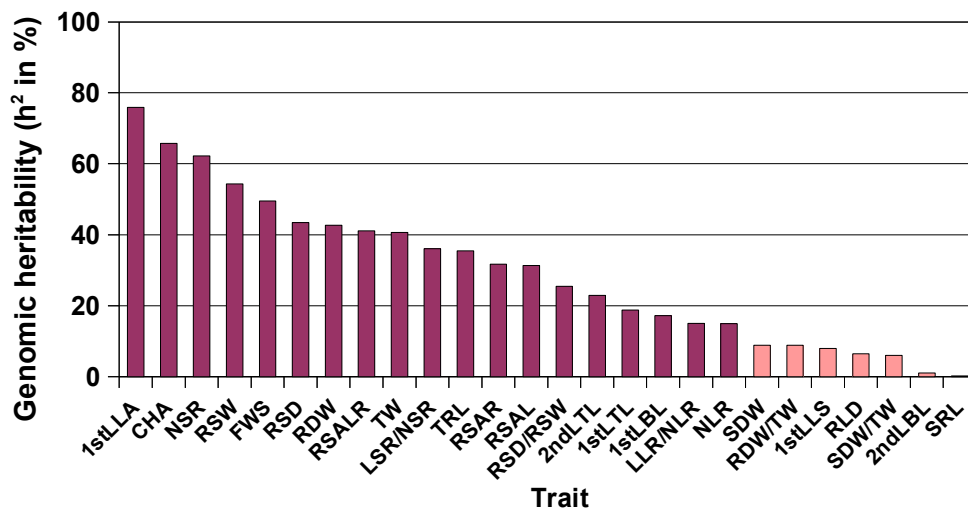
Figure S29. Distribution of heritability estimates for all traits tested. The traits SDW, RDW/TW, LLS, RLD, SDW, 2ndLBL, SRL showed a genetic heritability below 10%. Figure abbreviation: area of the first leaf (1stLLA), convex hull area (CHA), number of seminal roots (NSR), root system width (RSW), fresh weight shoot (FWS), root system depth (RSD), root dry weight (RDW), root system angle leaft and right (RSALR), total weight (TW), length of the seminal roots per number of seminal roots (LSR/NSR), total root length (TRL), root system angle right (RSAR), root system angle left (RSAL), root sys-tem depth per root system width (RSD/RSW), total length of the first leaf (1stLTL), length of the first leaf blade (1stLBL), length of the lateral roots per number of lateral roots (LLR/NLR), number of lateral roots (NLR), shoot dry **Figure S29 (Con-**

tinued). weight (SDW), root dry weight per total weight (RDW/TW), length of the first leaf sheath (1stLLS), root length density (RLD), shoot dry weight per total weight (SDW/TW), length of the second leaf blade (2ndLBL) and specific root length (SRL). These bar plots were created in R using quantification data of the experiments in Jülich and the ggplot2 library For the data collection 4d-old pre-germinate ILs seedlings grew for 12d at 16°C or 24°C in LD (16h/8h) and a light intensity of 470 µmol m^{-2} s^{-1}.
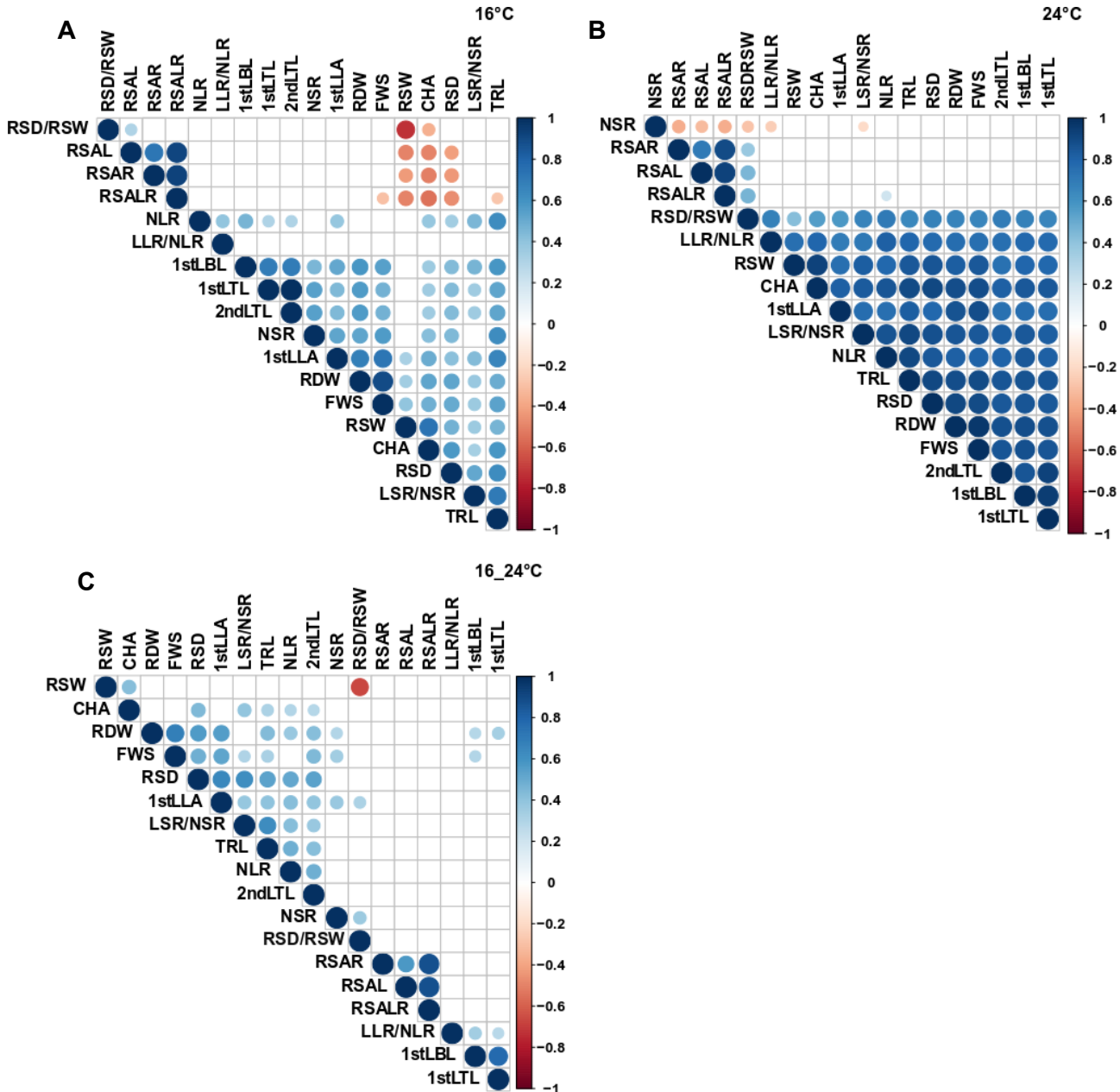
Figure S30. Correlogram representing Pearson's correlation coefficient rank between and among the root and shoot traits and temperature treatment abundances. All parameters were LOG10 transformed before statistical analysis. The different correlograms show the results of the pearson correlation analysis for **A)** the 16°C environment, **B)** the 24°C treatment and **C)** the relative temperature responses of the means of the quantitative data collected 12d after treatment beginning in the experiment in Jülich. 4d-old pre-germinate ILs seedlings grew for 12d at 16°C or 24°C in LD (16h/8h) and a light intensity of 470 µmol m^{-2} s^{-1}. Positive correlations are displayed in blue and negative correlations in red. Color intensity and the size of the circles are proportional to the correlation coefficients. On the right-side of he correlogram, the legend color shows the correlation coefficients and the corresponding colors. Data were collected 12d after treatment beginning.
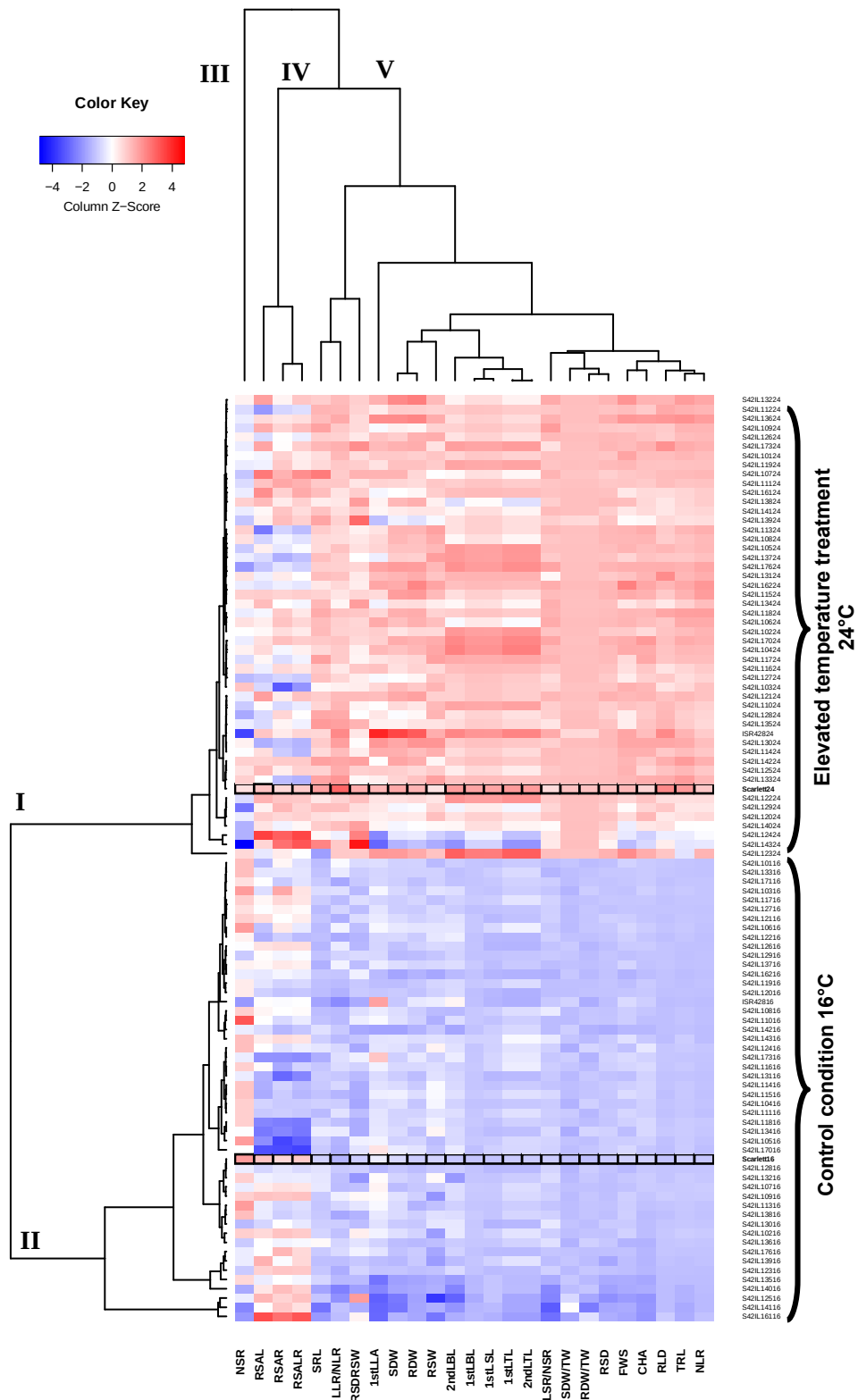
Figure S29.Heatmap and hierarchical clustering for the temperature responses of the 48 ILS for all traits. Data of each sample were standardised in order to have zero mean and unit variance. This scaled value, denoted as the column Z-score, is plotted in red–blue colour scale with blue indicating low value and red indicating high value. Use pearson distance for clustering. For the hierarchical clustering analysis the means of the quantitative data collected 12d after treatment beginning in the experiment in Jülich were used. 4d-old pre-germinate ILs seedlings grew for 12d at 16°C or 24°C in LD (16h/8h) and a light intensity of 470 µmol m⁻² s⁻¹. The temperature responses of parental line 'Scarlett' was marked with a black frame.
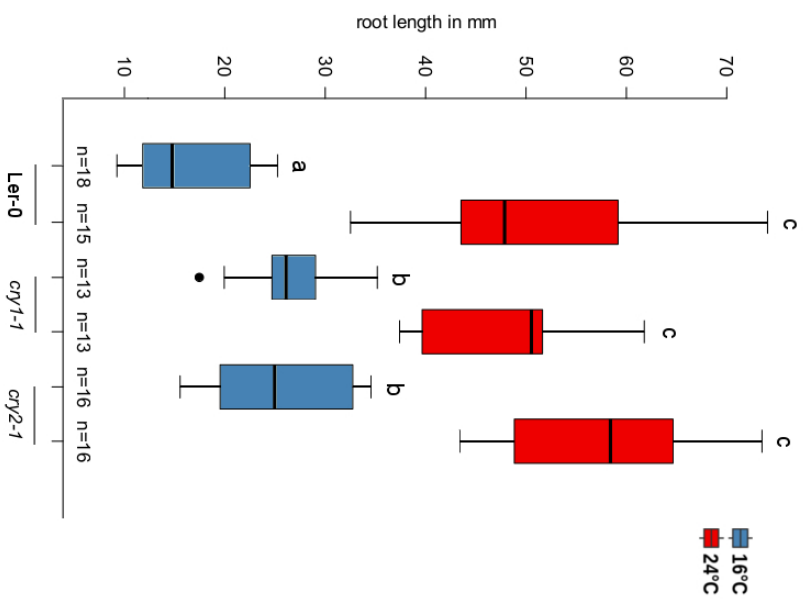
Figure S30. Impact of cryptochrome genes on the temperature induced root growth. Box plots show the absolute root length of 7d-old wild-type plants and cry1-1 and cry2-1 mutants. plants grown at 20°C or 28°C under LD (16/8 h) and 90 µmol m−2 s−1 white fluorescent light. Box plot show medians and interquartile ranges; outliers (greater than 1.52 interquartile range) are shown as black dots. Different letters denote statisticaldifferences at p< 0.05 as assessed by one-way ANOVA and Tukey's honestly significant difference (HSD) posthoc test. Experiments were repeated with similar results.

Table S12. S42ILs showing significant effects (*p*<0.05) for the observed root traits and shoot traits at 16°C

trait	Treatment	Effect	Genotype	Parent	Estimate	StdErr	DF	tValue	Probt	Adjustment	Adjp	LSMeans_genotype	LSMeans_Scarlett	RP_PCT	significance
RSAL	16	Genotype	S42IL-101	Scarlett	-13,1700	3,8731	289	-3,40	0,0008	Dunnett	0,0245	53,9004	67,0704	-19,6361	p <0.001
	16	Genotype	S42IL-105	Scarlett	-17,7709	3,8731	289	-4,59	0,0000	Dunnett	0,0003	49,2996	67,0704	-26,4958	p <0.001
	16	Genotype	S42IL-106	Scarlett	-13,4301	3,8731	289	-3,47	0,0006	Dunnett	0,0199	53,6403	67,0704	-20,0239	p <0.001
	16	Genotype	S42IL-113	Scarlett	-14,5013	4,0312	289	-3,60	0,0004	Dunnett	0,0130	52,5692	67,0704	-21,6209	p <0.001
	16	Genotype	S42IL-114	Scarlett	-14,7388	4,0312	289	-3,66	0,0003	Dunnett	0,0107	52,3317	67,0704	-21,9751	p <0.001
	16	Genotype	S42IL-117	Scarlett	-18,6669	3,8731	289	-4,82	0,0000	Dunnett	0,0001	48,4036	67,0704	-27,8317	p <0.001
	16	Genotype	S42IL-121	Scarlett	-14,1913	3,8731	289	-3,66	0,0003	Dunnett	0,0104	52,8791	67,0704	-21,1588	p <0.001
	16	Genotype	S42IL-130	Scarlett	-14,1904	3,8731	289	-3,66	0,0003	Dunnett	0,0104	52,8800	67,0704	-21,1575	p <0.001
	16	Genotype	S42IL-133	Scarlett	-19,8787	3,8731	289	-5,13	0,0000	Dunnett	0,0000	47,1917	67,0704	-29,6386	p <0.001
	16	Genotype	S42IL-162	Scarlett	-24,0764	4,0312	289	-5,97	0,0000	Dunnett	0,0000	42,9940	67,0704	-35,8972	p <0.001
	16	Genotype	S42IL-173	Scarlett	-17,2917	3,8731	289	-4,46	0,0000	Dunnett	0,0005	49,7787	67,0704	-25,7814	p <0.001
	16	Genotype	S42IL-104	Scarlett	-10,6809	3,8731	289	-2,76	0,0062	Dunnett	0,1422	56,3896	67,0704	-15,9248	p <0.01
	16	Genotype	S42IL-111	Scarlett	-11,7097	3,8731	289	-3,02	0,0027	Dunnett	0,0729	55,3607	67,0704	-17,4588	p <0.01
	16	Genotype	S42IL-119	Scarlett	-10,9769	4,0312	289	-2,72	0,0069	Dunnett	0,1542	56,0935	67,0704	-16,3663	p <0.01
	16	Genotype	S42IL-127	Scarlett	-10,4724	3,8731	289	-2,70	0,0073	Dunnett	0,1611	56,5980	67,0704	-15,6141	p <0.01
	16	Genotype	S42IL-129	Scarlett	-10,4601	3,8731	289	-2,70	0,0073	Dunnett	0,1623	56,6103	67,0704	-15,5958	p <0.01
	16	Genotype	S42IL-143	Scarlett	11,9809	3,8731	289	3,09	0,0022	Dunnett	0,0603	79,0513	67,0704	17,8631	p <0.01
	16	Genotype	S42IL-103	Scarlett	-9,6561	3,8731	289	-2,49	0,0132	Dunnett	0,2544	57,4143	67,0704	-14,3970	p <0.05
	16	Genotype	S42IL-112	Scarlett	-8,1693	4,0312	289	-2,03	0,0436	Dunnett	0,5743	58,9012	67,0704	-12,1801	p <0.05
	16	Genotype	S42IL-118	Scarlett	-8,9888	4,0312	289	-2,23	0,0265	Dunnett	0,4172	58,0817	67,0704	-13,4020	p <0.05
	16	Genotype	S42IL-131	Scarlett	-7,6270	3,8731	289	-1,97	0,0499	Dunnett	0,6216	59,4434	67,0704	-11,3716	p <0.05
	16	Genotype	S42IL-132	Scarlett	-8,8853	3,8731	289	-2,29	0,0225	Dunnett	0,3727	58,1851	67,0704	-13,2477	p <0.05
	16	Genotype	S42IL-134	Scarlett	-8,1504	4,0312	289	-2,02	0,0441	Dunnett	0,5781	58,9200	67,0704	-12,1520	p <0.05
	16	Genotype	S42IL-137	Scarlett	-8,1909	3,8731	289	-2,11	0,0353	Dunnett	0,5034	58,8796	67,0704	-12,2123	p <0.05
	16	Genotype	S42IL-141	Scarlett	-9,8040	3,8731	289	-2,53	0,0119	Dunnett	0,2351	57,2664	67,0704	-14,6175	p <0.05
	16	Genotype	S42IL-161	Scarlett	-8,5279	3,8731	289	-2,20	0,0285	Dunnett	0,4374	58,5426	67,0704	-12,7148	p <0.05
RSAR	16	Genotype	S42IL-105	Scarlett	-22,7217	3,6726	289	-6,19	0,0000	Dunnett	0,0000	41,7470	64,4687	-35,2446	p <0.001
	16	Genotype	S42IL-115	Scarlett	-12,6287	3,6726	289	-3,44	0,0007	Dunnett	0,0218	51,8400	64,4687	-19,5889	p <0.001
	16	Genotype	S42IL-117	Scarlett	-17,0199	3,6726	289	-4,63	0,0000	Dunnett	0,0002	47,4489	64,4687	-26,4002	p <0.001
	16	Genotype	S42IL-130	Scarlett	-19,1887	3,6726	289	-5,22	0,0000	Dunnett	0,0000	45,2800	64,4687	-29,7644	p <0.001
	16	Genotype	S42IL-133	Scarlett	-16,1499	3,6726	289	-4,40	0,0000	Dunnett	0,0007	48,3189	64,4687	-25,0507	p <0.001
	16	Genotype	S42IL-162	Scarlett	-22,1862	3,8226	289	-5,80	0,0000	Dunnett	0,0000	42,2825	64,4687	-34,4139	p <0.001
	16	Genotype	S42IL-173	Scarlett	-14,9924	3,6726	289	-4,08	0,0001	Dunnett	0,0023	49,4763	64,4687	-23,2554	p <0.001
	16	Genotype	S42IL-119	Scarlett	-9,9887	3,8226	289	-2,61	0,0094	Dunnett	0,1975	54,4800	64,4687	-15,4939	p <0.01
	16	Genotype	S42IL-141	Scarlett	-11,2829	3,6726	289	-3,07	0,0023	Dunnett	0,0639	53,1859	64,4687	-17,5013	p <0.01
	16	Genotype	S42IL-143	Scarlett	10,5169	3,6726	289	2,86	0,0045	Dunnett	0,1100	74,9856	64,4687	16,3131	p <0.01
	16	Genotype	S42IL-104	Scarlett	-9,3527	3,6726	289	-2,55	0,0114	Dunnett	0,2277	55,1160	64,4687	-14,5074	p <0.05
	16	Genotype	S42IL-111	Scarlett	-9,0409	3,6726	289	-2,46	0,0144	Dunnett	0,2711	55,4279	64,4687	-14,0236	p <0.05
	16	Genotype	S42IL-112	Scarlett	-8,2735	3,8226	289	-2,16	0,0313	Dunnett	0,4653	56,1952	64,4687	-12,8334	p <0.05
	16	Genotype	S42IL-113	Scarlett	-8,3875	3,8226	289	-2,19	0,0290	Dunnett	0,4430	56,0812	64,4687	-13,0103	p <0.05
	16	Genotype	S42IL-114	Scarlett	-9,2297	3,8226	289	-2,41	0,0164	Dunnett	0,2976	55,2390	64,4687	-14,3166	p <0.05
	16	Genotype	S42IL-118	Scarlett	-8,5235	3,8226	289	-2,23	0,0265	Dunnett	0,4172	55,9452	64,4687	-13,2212	p <0.05
	16	Genotype	S42IL-121	Scarlett	-8,9110	3,6726	289	-2,43	0,0159	Dunnett	0,2908	55,5577	64,4687	-13,8222	p <0.05
	16	Genotype	S42IL-137	Scarlett	-8,9256	3,6726	289	-2,43	0,0157	Dunnett	0,2885	55,5431	64,4687	-13,8448	p <0.05
	16	Genotype	S42IL-170	Scarlett	-9,3721	3,6726	289	-2,55	0,0112	Dunnett	0,2252	55,0966	64,4687	-14,5375	p <0.05

RSALR	16	Genotype	S42IL-104	Scarlett	-20,0336	5,5122	289	-3,63	0,0003	Dunnett	0,0115	111,5056	131,5391	-15,2301	p <0.001
	16	Genotype	S42IL-105	Scarlett	-40,4926	5,5122	289	-7,35	0,0000	Dunnett	0,0000	91,0466	131,5391	-30,7837	p <0.001
	16	Genotype	S42IL-111	Scarlett	-20,7506	5,5122	289	-3,76	0,0002	Dunnett	0,0074	110,7886	131,5391	-15,7752	p <0.001
	16	Genotype	S42IL-113	Scarlett	-22,8888	5,7372	289	-3,99	0,0001	Dunnett	0,0033	108,6503	131,5391	-17,4008	p <0.001
	16	Genotype	S42IL-114	Scarlett	-23,9685	5,7372	289	-4,18	0,0000	Dunnett	0,0016	107,5707	131,5391	-18,2216	p <0.001
	16	Genotype	S42IL-115	Scarlett	-18,4040	5,5122	289	-3,34	0,0010	Dunnett	0,0296	113,1351	131,5391	-13,9913	p <0.001
	16	Genotype	S42IL-117	Scarlett	-35,6867	5,5122	289	-6,47	0,0000	Dunnett	0,0000	95,8524	131,5391	-27,1301	p <0.001
	16	Genotype	S42IL-119	Scarlett	-20,9656	5,7372	289	-3,65	0,0003	Dunnett	0,0108	110,5735	131,5391	-15,9387	p <0.001
	16	Genotype	S42IL-121	Scarlett	-23,1023	5,5122	289	-4,19	0,0000	Dunnett	0,0015	108,4369	131,5391	-17,5631	p <0.001
	16	Genotype	S42IL-130	Scarlett	-33,3791	5,5122	289	-6,06	0,0000	Dunnett	0,0000	98,1600	131,5391	-25,3758	p <0.001
	16	Genotype	S42IL-133	Scarlett	-36,0286	5,5122	289	-6,54	0,0000	Dunnett	0,0000	95,5106	131,5391	-27,3900	p <0.001
	16	Genotype	S42IL-141	Scarlett	-21,0869	5,5122	289	-3,83	0,0002	Dunnett	0,0059	110,4523	131,5391	-16,0309	p <0.001
	16	Genotype	S42IL-143	Scarlett	22,4977	5,5122	289	4,08	0,0001	Dunnett	0,0023	154,0369	131,5391	17,1034	p <0.001
	16	Genotype	S42IL-162	Scarlett	-46,2626	5,7372	289	-8,06	0,0000	Dunnett	0,0000	85,2765	131,5391	-35,1702	p <0.001
	16	Genotype	S42IL-173	Scarlett	-32,2841	5,5122	289	-5,86	0,0000	Dunnett	0,0000	99,2550	131,5391	-24,5434	p <0.001
	16	Genotype	S42IL-101	Scarlett	-16,1253	5,5122	289	-2,93	0,0037	Dunnett	0,0942	115,4139	131,5391	-12,2589	p <0.01
	16	Genotype	S42IL-106	Scarlett	-14,6114	5,5122	289	-2,65	0,0085	Dunnett	0,1817	116,9277	131,5391	-11,1080	p <0.01
	16	Genotype	S42IL-112	Scarlett	-16,4428	5,7372	289	-2,87	0,0045	Dunnett	0,1094	115,0963	131,5391	-12,5003	p <0.01
	16	Genotype	S42IL-118	Scarlett	-17,5123	5,7372	289	-3,05	0,0025	Dunnett	0,0674	114,0268	131,5391	-13,3134	p <0.01
	16	Genotype	S42IL-127	Scarlett	-17,0540	5,5122	289	-3,09	0,0022	Dunnett	0,0602	114,4851	131,5391	-12,9650	p <0.01
	16	Genotype	S42IL-129	Scarlett	-14,5684	5,5122	289	-2,64	0,0087	Dunnett	0,1849	116,9707	131,5391	-11,0754	p <0.01
	16	Genotype	S42IL-132	Scarlett	-15,2689	5,5122	289	-2,77	0,0060	Dunnett	0,1381	116,2703	131,5391	-11,6078	p <0.01
	16	Genotype	S42IL-137	Scarlett	-17,1164	5,5122	289	-3,11	0,0021	Dunnett	0,0583	114,4227	131,5391	-13,0124	p <0.01
	16	Genotype	S42IL-170	Scarlett	-15,6384	5,5122	289	-2,84	0,0049	Dunnett	0,1175	115,9007	131,5391	-11,8888	p <0.01
	16	Genotype	S42IL-110	Scarlett	-13,9547	6,0383	289	-2,31	0,0215	Dunnett	0,3615	117,5844	131,5391	-10,6088	p <0.05
	16	Genotype	S42IL-123	Scarlett	-13,3987	5,5122	289	-2,43	0,0157	Dunnett	0,2883	118,1404	131,5391	-10,1861	p <0.05
	16	Genotype	S42IL-128	Scarlett	-10,9323	5,5122	289	-1,98	0,0483	Dunnett	0,6099	120,6069	131,5391	-8,3111	p <0.05
	16	Genotype	S42IL-131	Scarlett	-13,7379	5,5122	289	-2,49	0,0133	Dunnett	0,2549	117,8013	131,5391	-10,4439	p <0.05
	16	Genotype	S42IL-134	Scarlett	-12,0595	5,7372	289	-2,10	0,0364	Dunnett	0,5135	119,4797	131,5391	-9,1680	p <0.05
	16	Genotype	S42IL-135	Scarlett	-11,4033	5,5122	289	-2,07	0,0395	Dunnett	0,5400	120,1359	131,5391	-8,6691	p <0.05
	16	Genotype	S42IL-161	Scarlett	-13,5543	5,5122	289	-2,46	0,0145	Dunnett	0,2726	117,9849	131,5391	-10,3044	p <0.05
NSR	16	Genotype	S42IL-107	Scarlett	-1,0000	0,2348	289	-4,2596	2,77E-05	Dunnett	0,0011	6,0000	7,0000	-14,2857	p <0.001
	16	Genotype	S42IL-122	Scarlett	-1,2857	0,2348	289	-5,4766	9,43E-08	Dunnett	4E-06	5,7143	7,0000	-18,3673	p <0.001
	16	Genotype	S42IL-124	Scarlett	-1,0000	0,2572	289	-3,8885	0,00013	Dunnett	0,0047	6,0000	7,0000	-14,2857	p <0.001
	16	Genotype	S42IL-125	Scarlett	-0,8571	0,2348	289	-3,6511	0,00031	Dunnett	0,0109	6,1429	7,0000	-12,2449	p <0.001
	16	Genotype	S42IL-127	Scarlett	-1,0000	0,2348	289	-4,2596	2,77E-05	Dunnett	0,0011	6,0000	7,0000	-14,2857	p <0.001
	16	Genotype	S42IL-128	Scarlett	-1,2857	0,2348	289	-5,4766	9,43E-08	Dunnett	4E-06	5,7143	7,0000	-18,3673	p <0.001
	16	Genotype	S42IL-129	Scarlett	-1,4286	0,2348	289	-6,0852	3,69E-09	Dunnett	2E-07	5,5714	7,0000	-20,4082	p <0.001
	16	Genotype	S42IL-130	Scarlett	-1,0000	0,2348	289	-4,2596	2,77E-05	Dunnett	0,0011	6,0000	7,0000	-14,2857	p <0.001
	16	Genotype	S42IL-133	Scarlett	-0,8571	0,2348	289	-3,6511	0,00031	Dunnett	0,0109	6,1429	7,0000	-12,2449	p <0.001
	16	Genotype	S42IL-135	Scarlett	-1,2857	0,2348	289	-5,4766	9,43E-08	Dunnett	4E-06	5,7143	7,0000	-18,3673	p <0.001
	16	Genotype	S42IL-138	Scarlett	-1,0000	0,2348	289	-4,2596	2,77E-05	Dunnett	0,0011	6,0000	7,0000	-14,2857	p <0.001
	16	Genotype	S42IL-139	Scarlett	-1,5714	0,2348	289	-6,6937	1,13E-10	Dunnett	5E-09	5,4286	7,0000	-22,4490	p <0.001
	16	Genotype	S42IL-140	Scarlett	-1,8571	0,2348	289	-7,9107	5,48E-14	Dunnett	1E-12	5,1429	7,0000	-26,5306	p <0.001
	16	Genotype	S42IL-141	Scarlett	-1,0000	0,2348	289	-4,2596	2,77E-05	Dunnett	0,0011	6,0000	7,0000	-14,2857	p <0.001
	16	Genotype	S42IL-143	Scarlett	-1,7143	0,2348	289	-7,3022	2,76E-12	Dunnett	1E-12	5,2857	7,0000	-24,4898	p <0.001
	16	Genotype	S42IL-161	Scarlett	-1,0000	0,2348	289	-4,2596	2,77E-05	Dunnett	0,0011	6,0000	7,0000	-14,2857	p <0.001

	16	Genotype	S42IL-173	Scarlett	-1,0000	0,2348	289	-4,2596	2,77E-05	Dunnett	0,0011	6,0000	7,0000	-14,2857	p <0.001
	16	Genotype	S42IL-176	Scarlett	-1,0000	0,2348	289	-4,2596	2,77E-05	Dunnett	0,0011	6,0000	7,0000	-14,2857	p <0.001
	16	Genotype	S42IL-118	Scarlett	-0,6667	0,2443	289	-2,7283	0,00676	Dunnett	0,1523	6,3333	7,0000	-9,5238	p <0.01
	16	Genotype	S42IL-119	Scarlett	-0,6667	0,2443	289	-2,7283	0,00676	Dunnett	0,1523	6,3333	7,0000	-9,5238	p <0.01
	16	Genotype	S42IL-121	Scarlett	-0,7143	0,2348	289	-3,0426	0,00256	Dunnett	0,0692	6,2857	7,0000	-10,2041	p <0.01
	16	Genotype	S42IL-136	Scarlett	-0,7143	0,2348	289	-3,0426	0,00256	Dunnett	0,0692	6,2857	7,0000	-10,2041	p <0.01
	16	Genotype	S42IL-110	Scarlett	0,6000	0,2572	289	2,33308	0,02033	Dunnett	0,3472	7,6000	7,0000	8,5714	p <0.05
	16	Genotype	S42IL-126	Scarlett	-0,5714	0,2348	289	-2,4341	0,01554	Dunnett	0,2864	6,4286	7,0000	-8,1633	p <0.05
	16	Genotype	S42IL-134	Scarlett	-0,5000	0,2443	289	-2,0463	0,04164	Dunnett	0,5582	6,5000	7,0000	-7,1429	p <0.05
	16	Genotype	S42IL-170	Scarlett	-0,5714	0,2348	289	-2,4341	0,01554	Dunnett	0,2864	6,4286	7,0000	-8,1633	p <0.05
NLR	16	Genotype	S42IL-101	Scarlett	-25,5714	4,6435	289	-5,5069	8,07E-08	Dunnett	4E-06	48,8571	74,4286	-34,3570	p <0.001
	16	Genotype	S42IL-102	Scarlett	18,0000	4,6435	289	3,87636	0,00013	Dunnett	0,0049	92,4286	74,4286	24,1843	p <0.001
	16	Genotype	S42IL-104	Scarlett	-23,5714	4,6435	289	-5,0762	6,91E-07	Dunnett	3E-05	50,8571	74,4286	-31,6699	p <0.001
	16	Genotype	S42IL-105	Scarlett	-26,1429	4,6435	289	-5,6299	4,27E-08	Dunnett	2E-06	48,2857	74,4286	-35,1248	p <0.001
	16	Genotype	S42IL-106	Scarlett	-30,7143	4,6435	289	-6,6144	1,8E-10	Dunnett	8E-09	43,7143	74,4286	-41,2668	p <0.001
	16	Genotype	S42IL-107	Scarlett	24,7143	4,6435	289	5,3223	2,06E-07	Dunnett	1E-05	99,1429	74,4286	33,2054	p <0.001
	16	Genotype	S42IL-108	Scarlett	-40,0000	4,6435	289	-8,6141	4,66E-16	Dunnett	1E-12	34,4286	74,4286	-53,7428	p <0.001
	16	Genotype	S42IL-109	Scarlett	18,1429	4,6435	289	3,90712	0,00012	Dunnett	0,0044	92,5714	74,4286	24,3762	p <0.001
	16	Genotype	S42IL-110	Scarlett	-40,0286	5,0867	289	-7,8692	7,2E-14	Dunnett	1E-12	34,4000	74,4286	-53,7812	p <0.001
	16	Genotype	S42IL-111	Scarlett	-35,5714	4,6435	289	-7,6604	2,81E-13	Dunnett	1E-12	38,8571	74,4286	-47,7927	p <0.001
	16	Genotype	S42IL-112	Scarlett	-22,9286	4,8331	289	-4,744	3,3E-06	Dunnett	0,0001	51,5000	74,4286	-30,8061	p <0.001
	16	Genotype	S42IL-113	Scarlett	-28,9286	4,8331	289	-5,9855	6,38E-09	Dunnett	3E-07	45,5000	74,4286	-38,8676	p <0.001
	16	Genotype	S42IL-114	Scarlett	-32,9286	4,8331	289	-6,8131	5,55E-11	Dunnett	2E-09	41,5000	74,4286	-44,2418	p <0.001
	16	Genotype	S42IL-115	Scarlett	-22,0000	4,6435	289	-4,7378	3,39E-06	Dunnett	0,0002	52,4286	74,4286	-29,5585	p <0.001
	16	Genotype	S42IL-118	Scarlett	-24,4286	4,8331	289	-5,0544	7,67E-07	Dunnett	4E-05	50,0000	74,4286	-32,8215	p <0.001
	16	Genotype	S42IL-119	Scarlett	-38,4286	4,8331	289	-7,9511	4,2E-14	Dunnett	1E-12	36,0000	74,4286	-51,6315	p <0.001
	16	Genotype	S42IL-120	Scarlett	-19,4286	4,6435	289	-4,184	3,8E-05	Dunnett	0,0015	55,0000	74,4286	-26,1036	p <0.001
	16	Genotype	S42IL-121	Scarlett	-35,8571	4,6435	289	-7,722	1,89E-13	Dunnett	1E-12	38,5714	74,4286	-48,1766	p <0.001
	16	Genotype	S42IL-122	Scarlett	-48,0000	4,6435	289	-10,337	1,61E-21	Dunnett	1E-12	26,4286	74,4286	-64,4914	p <0.001
	16	Genotype	S42IL-124	Scarlett	-68,8286	5,0867	289	-13,531	1,2E-32	Dunnett	1E-12	5,6000	74,4286	-92,4760	p <0.001
	16	Genotype	S42IL-125	Scarlett	-33,8571	4,6435	289	-7,2912	3E-12	Dunnett	1E-12	40,5714	74,4286	-45,4894	p <0.001
	16	Genotype	S42IL-126	Scarlett	-21,1429	4,6435	289	-4,5532	7,8E-06	Dunnett	0,0003	53,2857	74,4286	-28,4069	p <0.001
	16	Genotype	S42IL-128	Scarlett	-26,4286	4,6435	289	-5,6915	3,09E-08	Dunnett	1E-06	48,0000	74,4286	-35,5086	p <0.001
	16	Genotype	S42IL-130	Scarlett	-32,8571	4,6435	289	-7,0759	1,13E-11	Dunnett	1E-12	41,5714	74,4286	-44,1459	p <0.001
	16	Genotype	S42IL-132	Scarlett	-28,7143	4,6435	289	-6,1837	2,13E-09	Dunnett	1E-07	45,7143	74,4286	-38,5797	p <0.001
	16	Genotype	S42IL-134	Scarlett	-56,2619	4,8331	289	-11,641	6,11E-26	Dunnett	1E-12	18,1667	74,4286	-75,5918	p <0.001
	16	Genotype	S42IL-136	Scarlett	-30,4286	4,6435	289	-6,5529	2,58E-10	Dunnett	1E-08	44,0000	74,4286	-40,8829	p <0.001
	16	Genotype	S42IL-137	Scarlett	-31,0000	4,6435	289	-6,6759	1,25E-10	Dunnett	5E-09	43,4286	74,4286	-41,6507	p <0.001
	16	Genotype	S42IL-138	Scarlett	-30,2857	4,6435	289	-6,5221	3,09E-10	Dunnett	1E-08	44,1429	74,4286	-40,6910	p <0.001
	16	Genotype	S42IL-139	Scarlett	-61,0000	4,6435	289	-13,137	3,16E-31	Dunnett	1E-12	13,4286	74,4286	-81,9578	p <0.001
	16	Genotype	S42IL-140	Scarlett	-72,5714	4,6435	289	-15,628	2,5E-40	Dunnett	1E-12	1,8571	74,4286	-97,5048	p <0.001
	16	Genotype	S42IL-141	Scarlett	-52,0000	4,6435	289	-11,198	2E-24	Dunnett	1E-12	22,4286	74,4286	-69,8656	p <0.001
	16	Genotype	S42IL-142	Scarlett	-54,1429	4,6435	289	-11,66	5,25E-26	Dunnett	1E-12	20,2857	74,4286	-72,7447	p <0.001
	16	Genotype	S42IL-143	Scarlett	-31,4286	4,6435	289	-6,7682	7,25E-11	Dunnett	3E-09	43,0000	74,4286	-42,2265	p <0.001
	16	Genotype	S42IL-161	Scarlett	-36,8571	4,6435	289	-7,9373	4,6E-14	Dunnett	1E-12	37,5714	74,4286	-49,5202	p <0.001
	16	Genotype	S42IL-162	Scarlett	-48,9286	4,8331	289	-10,124	8,13E-21	Dunnett	1E-12	25,5000	74,4286	-65,7390	p <0.001
	16	Genotype	S42IL-170	Scarlett	-15,5714	4,6435	289	-3,3534	0,0009	Dunnett	0,0283	58,8571	74,4286	-20,9213	p <0.001
	16	Genotype	S42IL-173	Scarlett	-16,8571	4,6435	289	-3,6302	0,00033	Dunnett	0,0117	57,5714	74,4286	-22,6488	p <0.001
	16	Genotype	S42IL-176	Scarlett	-21,0000	4,6435	289	-4,5224	8,93E-06	Dunnett	0,0004	53,4286	74,4286	-28,2150	p <0.001
	16	Genotype	S42IL-103	Scarlett	-14,7143	4,6435	289	-3,1688	0,0017	Dunnett	0,0488	59,7143	74,4286	-19,7697	p <0.01
	16	Genotype	S42IL-116	Scarlett	-13,8571	4,6435	289	-2,9842	0,00309	Dunnett	0,0809	60,5714	74,4286	-18,6180	p <0.01

	16	Genotype	S42IL-127	Scarlett	-13,0000	4,6435	289	-2,7996	0,00546	Dunnett	0,1287	61,4286	74,4286	-17,4664	p <0.01
	16	Genotype	S42IL-135	Scarlett	-14,0000	4,6435	289	-3,0149	0,0028	Dunnett	0,0745	60,4286	74,4286	-18,8100	p <0.01
	16	Genotype	S42IL-129	Scarlett	-9,5714	4,6435	289	-2,0612	0,04017	Dunnett	0,5461	64,8571	74,4286	-12,8599	p <0.05
LSR/NSR	16	Genotype	S42IL-108	Scarlett	3,7460	0,9081	289	4,12516	4,85E-05	Dunnett	0,0019	21,8626	18,1166	20,6770	p <0.001
	16	Genotype	S42IL-124	Scarlett	-8,9182	0,9948	289	-8,9653	4E-17	Dunnett	1E-12	9,1984	18,1166	-49,2269	p <0.001
	16	Genotype	S42IL-129	Scarlett	3,4378	0,9081	289	3,78576	0,00019	Dunnett	0,0068	21,5544	18,1166	18,9758	p <0.001
	16	Genotype	S42IL-134	Scarlett	-4,0321	0,9452	289	-4,2661	2,7E-05	Dunnett	0,0011	14,0845	18,1166	-22,2564	p <0.001
	16	Genotype	S42IL-139	Scarlett	-8,4873	0,9081	289	-9,3464	2,57E-18	Dunnett	1E-12	9,6293	18,1166	-46,8482	p <0.001
	16	Genotype	S42IL-140	Scarlett	-13,9103	0,9081	289	-15,318	3,48E-39	Dunnett	1E-12	4,2063	18,1166	-76,7820	p <0.001
	16	Genotype	S42IL-142	Scarlett	3,3394	0,9081	289	3,67749	0,00028	Dunnett	0,0099	21,4560	18,1166	18,4331	p <0.001
	16	Genotype	S42IL-143	Scarlett	-11,3967	0,9081	289	-12,55	3,92E-29	Dunnett	1E-12	6,7199	18,1166	-62,9076	p <0.001
	16	Genotype	S42IL-161	Scarlett	-3,4887	0,9081	289	-3,8418	0,00015	Dunnett	0,0056	14,6279	18,1166	-19,2569	p <0.001
	16	Genotype	S42IL-132	Scarlett	-2,8627	0,9081	289	-3,1525	0,00179	Dunnett	0,0511	15,2539	18,1166	-15,8015	p <0.01
	16	Genotype	S42IL-135	Scarlett	2,4510	0,9081	289	2,69914	0,00736	Dunnett	0,1629	20,5676	18,1166	13,5292	p <0.01
	16	Genotype	S42IL-110	Scarlett	-2,0076	0,9948	289	-2,0182	0,04449	Dunnett	0,5811	16,1090	18,1166	-11,0816	p <0.05
	16	Genotype	S42IL-131	Scarlett	1,8646	0,9081	289	2,05335	0,04094	Dunnett	0,5524	19,9812	18,1166	10,2922	p <0.05
	16	Genotype	S42IL-136	Scarlett	-1,9201	0,9081	289	-2,1145	0,03533	Dunnett	0,5037	16,1965	18,1166	-10,5987	p <0.05
	16	Genotype	S42IL-138	Scarlett	-1,8558	0,9081	289	-2,0437	0,04189	Dunnett	0,5603	16,2608	18,1166	-10,2437	p <0.05
	16	Genotype	S42IL-141	Scarlett	-2,0791	0,9081	289	-2,2896	0,02277	Dunnett	0,3757	16,0375	18,1166	-11,4764	p <0.05
LLR/NLR	16	Genotype	S42IL-101	Scarlett	0,1918	0,0374	289	5,12525	5,45E-07	Dunnett	3E-05	0,3827	0,1910	100,4201	p <0.001
	16	Genotype	S42IL-106	Scarlett	0,2030	0,0374	289	5,42508	1,23E-07	Dunnett	6E-06	0,3939	0,1910	106,2948	p <0.001
	16	Genotype	S42IL-109	Scarlett	0,1602	0,0374	289	4,28081	2,54E-05	Dunnett	0,0011	0,3511	0,1910	83,8748	p <0.001
	16	Genotype	S42IL-111	Scarlett	0,1250	0,0374	289	3,34207	0,00094	Dunnett	0,0293	0,3160	0,1910	65,4819	p <0.001
	16	Genotype	S42IL-125	Scarlett	0,1500	0,0374	289	4,00808	7,8E-05	Dunnett	0,003	0,3409	0,1910	78,5311	p <0.001
	16	Genotype	S42IL-132	Scarlett	0,1468	0,0374	289	3,923	0,00011	Dunnett	0,0042	0,3377	0,1910	76,8642	p <0.001
	16	Genotype	S42IL-133	Scarlett	0,1485	0,0374	289	3,96951	9,09E-05	Dunnett	0,0035	0,3395	0,1910	77,7754	p <0.001
	16	Genotype	S42IL-136	Scarlett	0,1680	0,0374	289	4,49106	1E-05	Dunnett	0,0004	0,3590	0,1910	87,9942	p <0.001
	16	Genotype	S42IL-139	Scarlett	-0,1453	0,0374	289	-3,8828	0,00013	Dunnett	0,0048	0,0457	0,1910	-76,0758	p <0.001
	16	Genotype	S42IL-103	Scarlett	0,1164	0,0374	289	3,11189	0,00204	Dunnett	0,0573	0,3074	0,1910	60,9718	p <0.01
	16	Genotype	S42IL-115	Scarlett	0,1072	0,0374	289	2,86447	0,00448	Dunnett	0,1098	0,2981	0,1910	56,1240	p <0.01
	16	Genotype	S42IL-173	Scarlett	0,1160	0,0374	289	3,10131	0,00212	Dunnett	0,059	0,3070	0,1910	60,7646	p <0.01
	16	Genotype	S42IL-176	Scarlett	0,1018	0,0374	289	2,72037	0,00692	Dunnett	0,1551	0,2927	0,1910	53,3007	p <0.01
	16	Genotype	S42IL-112	Scarlett	0,0906	0,0389	289	2,32672	0,02067	Dunnett	0,3513	0,2816	0,1910	47,4494	p <0.05
	16	Genotype	S42IL-113	Scarlett	0,0957	0,0389	289	2,45766	0,01457	Dunnett	0,2733	0,2867	0,1910	50,1196	p <0.05
	16	Genotype	S42IL-123	Scarlett	0,0961	0,0374	289	2,56738	0,01075	Dunnett	0,2179	0,2870	0,1910	50,3031	p <0.05
	16	Genotype	S42IL-124	Scarlett	-0,0958	0,0410	289	-2,3362	0,02017	Dunnett	0,3452	0,0952	0,1910	-50,1417	p <0.05
	16	Genotype	S42IL-126	Scarlett	0,0891	0,0374	289	2,38212	0,01786	Dunnett	0,3167	0,2801	0,1910	46,6733	p <0.05
	16	Genotype	S42IL-128	Scarlett	0,0840	0,0374	289	2,24602	0,02546	Dunnett	0,4057	0,2750	0,1910	44,0066	p <0.05
	16	Genotype	S42IL-135	Scarlett	0,0900	0,0374	289	2,40553	0,01678	Dunnett	0,3028	0,2810	0,1910	47,1320	p <0.05

TRL	16	Genotype	S42IL-101	Scarlett	-29,8350	5,1056	289	-5,8436	1,38E-08	Dunnett	7E-07	120,5616	150,3966	-19,8376	p <0.001
	16	Genotype	S42IL-104	Scarlett	-20,1747	5,1056	289	-3,9515	9,77E-05	Dunnett	0,0038	130,2219	150,3966	-13,4143	p <0.001
	16	Genotype	S42IL-108	Scarlett	-30,2634	5,1056	289	-5,9275	8,75E-09	Dunnett	4E-07	120,1331	150,3966	-20,1224	p <0.001
	16	Genotype	S42IL-110	Scarlett	-31,3250	5,5929	289	-5,6008	5E-08	Dunnett	2E-06	119,0716	150,3966	-20,8282	p <0.001
	16	Genotype	S42IL-111	Scarlett	-21,2866	5,1056	289	-4,1693	4E-05	Dunnett	0,0016	129,1100	150,3966	-14,1536	p <0.001
	16	Genotype	S42IL-112	Scarlett	-20,5969	5,3141	289	-3,8759	0,00013	Dunnett	0,005	129,7997	150,3966	-13,6951	p <0.001
	16	Genotype	S42IL-116	Scarlett	-25,9544	5,1056	289	-5,0835	6,67E-07	Dunnett	3E-05	124,4421	150,3966	-17,2573	p <0.001
	16	Genotype	S42IL-118	Scarlett	-49,0569	5,3141	289	-9,2315	5,89E-18	Dunnett	1E-12	101,3397	150,3966	-32,6184	p <0.001
	16	Genotype	S42IL-119	Scarlett	-40,9854	5,3141	289	-7,7126	2E-13	Dunnett	1E-12	109,4112	150,3966	-27,2516	p <0.001
	16	Genotype	S42IL-120	Scarlett	-21,9106	5,1056	289	-4,2915	2,42E-05	Dunnett	0,001	128,4860	150,3966	-14,5685	p <0.001
	16	Genotype	S42IL-121	Scarlett	-26,8916	5,1056	289	-5,2671	2,71E-07	Dunnett	1E-05	123,5050	150,3966	-17,8804	p <0.001
	16	Genotype	S42IL-122	Scarlett	-45,9551	5,1056	289	-9,0009	3,07E-17	Dunnett	1E-12	104,4414	150,3966	-30,5560	p <0.001
	16	Genotype	S42IL-124	Scarlett	-95,5034	5,5929	289	-17,076	1,1E-45	Dunnett	1E-12	54,8932	150,3966	-63,5010	p <0.001
	16	Genotype	S42IL-125	Scarlett	-41,4529	5,1056	289	-8,1191	1,37E-14	Dunnett	1E-12	108,9437	150,3966	-27,5624	p <0.001
	16	Genotype	S42IL-126	Scarlett	-30,6206	5,1056	289	-5,9974	6E-09	Dunnett	3E-07	119,7760	150,3966	-20,3599	p <0.001
	16	Genotype	S42IL-127	Scarlett	-24,4221	5,1056	289	-4,7834	2,75E-06	Dunnett	0,0001	125,9744	150,3966	-16,2385	p <0.001
	16	Genotype	S42IL-128	Scarlett	-45,6254	5,1056	289	-8,9363	4,86E-17	Dunnett	1E-12	104,7711	150,3966	-30,3367	p <0.001
	16	Genotype	S42IL-129	Scarlett	-18,0581	5,1056	289	-3,5369	0,00047	Dunnett	0,0159	132,3384	150,3966	-12,0070	p <0.001
	16	Genotype	S42IL-130	Scarlett	-33,9856	5,1056	289	-6,6565	1,41E-10	Dunnett	6E-09	116,4110	150,3966	-22,5973	p <0.001
	16	Genotype	S42IL-132	Scarlett	-34,4490	5,1056	289	-6,7473	8,22E-11	Dunnett	3E-09	115,9476	150,3966	-22,9054	p <0.001
	16	Genotype	S42IL-134	Scarlett	-55,7217	5,3141	289	-10,486	5,18E-22	Dunnett	1E-12	94,6748	150,3966	-37,0499	p <0.001
	16	Genotype	S42IL-135	Scarlett	-18,1219	5,1056	289	-3,5494	0,00045	Dunnett	0,0153	132,2747	150,3966	-12,0494	p <0.001
	16	Genotype	S42IL-136	Scarlett	-41,9927	5,1056	289	-8,2248	6,72E-15	Dunnett	1E-12	108,4039	150,3966	-27,9213	p <0.001
	16	Genotype	S42IL-137	Scarlett	-21,1287	5,1056	289	-4,1383	4,59E-05	Dunnett	0,0018	129,2679	150,3966	-14,0487	p <0.001
	16	Genotype	S42IL-138	Scarlett	-49,5436	5,1056	289	-9,7038	1,87E-19	Dunnett	1E-12	100,8530	150,3966	-32,9420	p <0.001
	16	Genotype	S42IL-139	Scarlett	-96,0826	5,1056	289	-18,819	4E-52	Dunnett	1E-12	54,3140	150,3966	-63,8861	p <0.001
	16	Genotype	S42IL-140	Scarlett	-128,6546	5,1056	289	-25,199	6,51E-75	Dunnett	1E-12	21,7420	150,3966	-85,5436	p <0.001
	16	Genotype	S42IL-141	Scarlett	-42,8553	5,1056	289	-8,3938	2,13E-15	Dunnett	1E-12	107,5413	150,3966	-28,4949	p <0.001
	16	Genotype	S42IL-143	Scarlett	-114,3347	5,1056	289	-22,394	4,2E-65	Dunnett	1E-12	36,0619	150,3966	-76,0222	p <0.001
	16	Genotype	S42IL-161	Scarlett	-55,2587	5,1056	289	-10,823	3,83E-23	Dunnett	1E-12	95,1379	150,3966	-36,7420	p <0.001
	16	Genotype	S42IL-170	Scarlett	-29,2334	5,1056	289	-5,7258	2,58E-08	Dunnett	1E-06	121,1631	150,3966	-19,4376	p <0.001
	16	Genotype	S42IL-173	Scarlett	-28,9321	5,1056	289	-5,6667	3,52E-08	Dunnett	2E-06	121,4644	150,3966	-19,2372	p <0.001
	16	Genotype	S42IL-176	Scarlett	-32,9144	5,1056	289	-6,4467	4,78E-10	Dunnett	2E-08	117,4821	150,3966	-21,8851	p <0.001
	16	Genotype	S42IL-106	Scarlett	-14,1279	5,1056	289	-2,7671	0,00602	Dunnett	0,139	136,2687	150,3966	-9,3937	p <0.01
	16	Genotype	S42IL-114	Scarlett	-13,8232	5,3141	289	-2,6012	0,00977	Dunnett	0,2026	136,5733	150,3966	-9,1912	p <0.01
	16	Genotype	S42IL-103	Scarlett	-11,5030	5,1056	289	-2,253	0,02501	Dunnett	0,4008	138,8936	150,3966	-7,6484	p <0.05
	16	Genotype	S42IL-109	Scarlett	-12,1633	5,1056	289	-2,3823	0,01785	Dunnett	0,3166	138,2333	150,3966	-8,0875	p <0.05
	16	Genotype	S42IL-113	Scarlett	-13,1472	5,3141	289	-2,474	0,01393	Dunnett	0,2645	137,2493	150,3966	-8,7417	p <0.05
	16	Genotype	S42IL-115	Scarlett	-12,1924	5,1056	289	-2,388	0,01758	Dunnett	0,3132	138,2041	150,3966	-8,1069	p <0.05
RDW	16	Genotype	S42IL-124	Scarlett	-0,0511	0,0173	289	-2,96	0,0034	Dunnett	0,0868	0,0892	0,1403	-36,4220	p <0.01
	16	Genotype	S42IL-134	Scarlett	-0,0492	0,0164	289	-2,99	0,0030	Dunnett	0,0787	0,0911	0,1403	-35,0440	p <0.01
	16	Genotype	S42IL-139	Scarlett	-0,0428	0,0158	289	-2,71	0,0071	Dunnett	0,1582	0,0975	0,1403	-30,4959	p <0.01
	16	Genotype	S42IL-140	Scarlett	-0,0474	0,0158	289	-3,01	0,0029	Dunnett	0,0761	0,0929	0,1403	-33,8153	p <0.01
	16	Genotype	S42IL-143	Scarlett	-0,0450	0,0158	289	-2,86	0,0046	Dunnett	0,1124	0,0953	0,1403	-32,1047	p <0.01
	16	Genotype	S42IL-141	Scarlett	-0,0322	0,0158	289	-2,04	0,0423	Dunnett	0,5639	0,1081	0,1403	-22,9305	p <0.05
	16	Genotype	S42IL-173	Scarlett	0,0342	0,0158	289	2,17	0,0309	Dunnett	0,4620	0,1745	0,1403	24,3865	p <0.05

FWS	16	Genotype	S42IL-124	Scarlett	-0,0121	0,0025	289	-4,8022	2,52E-06	Dunnett	0,0001	0,0097	0,0219	-55,4670	p <0.001
	16	Genotype	S42IL-134	Scarlett	-0,0084	0,0024	289	-3,4877	0,00056	Dunnett	0,0186	0,0135	0,0219	-38,2756	p <0.001
	16	Genotype	S42IL-139	Scarlett	-0,0088	0,0023	289	-3,816	0,00017	Dunnett	0,0061	0,0131	0,0219	-40,2351	p <0.001
	16	Genotype	S42IL-140	Scarlett	-0,0086	0,0023	289	-3,7311	0,00023	Dunnett	0,0083	0,0133	0,0219	-39,3403	p <0.001
	16	Genotype	S42IL-143	Scarlett	-0,0097	0,0023	289	-4,2248	3,21E-05	Dunnett	0,0013	0,0121	0,0219	-44,5460	p <0.001
	16	Genotype	S42IL-135	Scarlett	-0,0068	0,0023	289	-2,9301	0,00366	Dunnett	0,093	0,0151	0,0219	-30,8948	p <0.01
	16	Genotype	S42IL-161	Scarlett	-0,0068	0,0023	289	-2,9611	0,00332	Dunnett	0,0859	0,0150	0,0219	-31,2214	p <0.01
	16	Genotype	S42IL-127	Scarlett	-0,0054	0,0023	289	-2,354	0,01924	Dunnett	0,334	0,0164	0,0219	-24,8204	p <0.05
	16	Genotype	S42IL-141	Scarlett	-0,0058	0,0023	289	-2,4965	0,0131	Dunnett	0,2527	0,0161	0,0219	-26,3227	p <0.05
RSD	16	Genotype	S42IL-124	Scarlett	-7,1141	1,0095	289	-7,0469	1,35E-11	Dunnett	1E-12	10,4458	17,5599	-40,5132	p <0.001
	16	Genotype	S42IL-134	Scarlett	-3,7910	0,9592	289	-3,9523	9,74E-05	Dunnett	0,0037	13,7688	17,5599	-21,5891	p <0.001
	16	Genotype	S42IL-138	Scarlett	-4,2173	0,9216	289	-4,5762	7E-06	Dunnett	0,0003	13,3426	17,5599	-24,0166	p <0.001
	16	Genotype	S42IL-139	Scarlett	-5,0014	0,9216	289	-5,4271	1,21E-07	Dunnett	6E-06	12,5584	17,5599	-28,4822	p <0.001
	16	Genotype	S42IL-140	Scarlett	-4,1241	0,9216	289	-4,4751	1,1E-05	Dunnett	0,0005	13,4357	17,5599	-23,4862	p <0.001
	16	Genotype	S42IL-141	Scarlett	-3,5404	0,9216	289	-3,8417	0,00015	Dunnett	0,0056	14,0194	17,5599	-20,1621	p <0.001
	16	Genotype	S42IL-143	Scarlett	-3,3097	0,9216	289	-3,5914	0,00039	Dunnett	0,0133	14,2501	17,5599	-18,8482	p <0.001
RSW	16	Genotype	S42IL-124	Scarlett	-8,6988	1,3005	289	-6,6888	1,16E-10	Dunnett	5E-09	6,0398	14,7386	-59,0205	p <0.001
	16	Genotype	S42IL-143	Scarlett	-5,1440	1,1872	289	-4,3329	2E-05	Dunnett	0,0009	9,5946	14,7386	-34,9016	p <0.001
	16	Genotype	S42IL-109	Scarlett	-3,4984	1,1872	289	-2,9468	0,00347	Dunnett	0,0891	11,2401	14,7386	-23,7366	p <0.01
	16	Genotype	S42IL-123	Scarlett	3,1201	1,1872	289	2,62818	0,00904	Dunnett	0,191	17,8587	14,7386	21,1699	p <0.01
	16	Genotype	S42IL-102	Scarlett	-3,0149	1,1872	289	-2,5395	0,01163	Dunnett	0,2312	11,7237	14,7386	-20,4556	p <0.05
	16	Genotype	S42IL-131	Scarlett	2,8187	1,1872	289	2,37428	0,01824	Dunnett	0,3215	17,5573	14,7386	19,1247	p <0.05
	16	Genotype	S42IL-133	Scarlett	3,0427	1,1872	289	2,56296	0,01088	Dunnett	0,22	17,7813	14,7386	20,6446	p <0.05
	16	Genotype	S42IL-138	Scarlett	-3,0274	1,1872	289	-2,5501	0,01129	Dunnett	0,2261	11,7111	14,7386	-20,5409	p <0.05
	16	Genotype	S42IL-161	Scarlett	-2,4160	1,1872	289	-2,0351	0,04276	Dunnett	0,5673	12,3226	14,7386	-16,3924	p <0.05
	16	Genotype	S42IL-176	Scarlett	-2,4854	1,1872	289	-2,0935	0,03717	Dunnett	0,5202	12,2531	14,7386	-16,8634	p <0.05
CHA	16	Genotype	S42IL-102	Scarlett	-44,0953	8,4392	289	-5,225	3,34E-07	Dunnett	2E-05	130,8199	174,9151	-25,2095	p <0.001
	16	Genotype	S42IL-110	Scarlett	-40,2827	9,2447	289	-4,3574	1,83E-05	Dunnett	0,0008	134,6324	174,9151	-23,0299	p <0.001
	16	Genotype	S42IL-112	Scarlett	-35,1873	8,7838	289	-4,0059	7,86E-05	Dunnett	0,0031	139,7278	174,9151	-20,1168	p <0.001
	16	Genotype	S42IL-115	Scarlett	28,3207	8,4392	289	3,35585	0,0009	Dunnett	0,0281	203,2359	174,9151	16,1911	p <0.001
	16	Genotype	S42IL-122	Scarlett	-60,1836	8,4392	289	-7,1314	8E-12	Dunnett	1E-12	114,7316	174,9151	-34,4073	p <0.001
	16	Genotype	S42IL-123	Scarlett	62,1644	8,4392	289	7,36614	1,85E-12	Dunnett	1E-12	237,0796	174,9151	35,5398	p <0.001
	16	Genotype	S42IL-124	Scarlett	-151,5333	9,2447	289	-16,391	3,76E-43	Dunnett	1E-12	23,3818	174,9151	-86,6325	p <0.001
	16	Genotype	S42IL-129	Scarlett	-44,3477	8,4392	289	-5,255	2,88E-07	Dunnett	1E-05	130,5674	174,9151	-25,3538	p <0.001
	16	Genotype	S42IL-134	Scarlett	-100,1108	8,7838	289	-11,397	4,24E-25	Dunnett	1E-12	74,8043	174,9151	-57,2339	p <0.001
	16	Genotype	S42IL-135	Scarlett	-71,9656	8,4392	289	-8,5275	8,49E-16	Dunnett	1E-12	102,9496	174,9151	-41,1431	p <0.001
	16	Genotype	S42IL-136	Scarlett	-30,8017	8,4392	289	-3,6498	0,00031	Dunnett	0,0109	144,1134	174,9151	-17,6095	p <0.001
	16	Genotype	S42IL-137	Scarlett	-50,8393	8,4392	289	-6,0242	5,16E-09	Dunnett	2E-07	124,0759	174,9151	-29,0651	p <0.001
	16	Genotype	S42IL-138	Scarlett	-65,2086	8,4392	289	-7,7269	1,83E-13	Dunnett	1E-12	109,7066	174,9151	-37,2801	p <0.001
	16	Genotype	S42IL-139	Scarlett	-85,0694	8,4392	289	-10,08	1,13E-20	Dunnett	1E-12	89,8457	174,9151	-48,6347	p <0.001
	16	Genotype	S42IL-140	Scarlett	-143,8137	8,4392	289	-17,041	1,48E-45	Dunnett	1E-12	31,1014	174,9151	-82,2191	p <0.001
	16	Genotype	S42IL-141	Scarlett	-59,4664	8,4392	289	-7,0464	1,35E-11	Dunnett	1E-12	115,4487	174,9151	-33,9973	p <0.001
	16	Genotype	S42IL-143	Scarlett	-148,9283	8,4392	289	-17,647	8,41E-48	Dunnett	1E-12	25,9869	174,9151	-85,1432	p <0.001
	16	Genotype	S42IL-161	Scarlett	-43,4973	8,4392	289	-5,1542	4,73E-07	Dunnett	2E-05	131,4179	174,9151	-24,8677	p <0.001
	16	Genotype	S42IL-176	Scarlett	-62,5513	8,4392	289	-7,412	1,38E-12	Dunnett	1E-12	112,3639	174,9151	-35,7609	p <0.001
	16	Genotype	S42IL-108	Scarlett	-24,6514	8,4392	289	-2,9211	0,00376	Dunnett	0,0952	150,2637	174,9151	-14,0934	p <0.01
	16	Genotype	S42IL-109	Scarlett	-26,2571	8,4392	289	-3,1113	0,00205	Dunnett	0,0574	148,6580	174,9151	-15,0114	p <0.01
	16	Genotype	S42IL-117	Scarlett	24,1294	8,4392	289	2,8592	0,00456	Dunnett	0,1112	199,0446	174,9151	13,7949	p <0.01
	16	Genotype	S42IL-120	Scarlett	-23,6670	8,4392	289	-2,8044	0,00538	Dunnett	0,1272	151,2481	174,9151	-13,5306	p <0.01
	16	Genotype	S42IL-121	Scarlett	-25,9214	8,4392	289	-3,0715	0,00233	Dunnett	0,064	148,9937	174,9151	-14,8194	p <0.01
	16	Genotype	S42IL-126	Scarlett	-26,5339	8,4392	289	-3,1441	0,00184	Dunnett	0,0523	148,3813	174,9151	-15,1696	p <0.01

	16	Genotype	S42IL-128	Scarlett	-26,9711	8,4392	289	-3,1959	0,00155	Dunnett	0,0452	147,9440	174,9151	-15,4196	p <0.01
	16	Genotype	S42IL-133	Scarlett	25,7086	8,4392	289	3,04632	0,00253	Dunnett	0,0685	200,6237	174,9151	14,6977	p <0.01
	16	Genotype	S42IL-113	Scarlett	17,5775	8,7838	289	2,00113	0,04631	Dunnett	0,5952	192,4927	174,9151	10,0492	p <0.05
	16	Genotype	S42IL-116	Scarlett	-17,1644	8,4392	289	-2,0339	0,04288	Dunnett	0,5683	157,7507	174,9151	-9,8130	p <0.05
	16	Genotype	S42IL-127	Scarlett	-18,9247	8,4392	289	-2,2425	0,02569	Dunnett	0,4082	155,9904	174,9151	-10,8194	p <0.05
	16	Genotype	S42IL-162	Scarlett	-21,3616	8,7838	289	-2,4319	0,01563	Dunnett	0,2876	153,5535	174,9151	-12,2126	p <0.05
1stLLA	16	Genotype	S42IL-124	Scarlett	-2,5371	0,3232	288	-7,85	0,0000	Dunnett	0,0000	1,4200	3,9571	-64,1155	p <0.001
	16	Genotype	S42IL-134	Scarlett	-2,1905	0,3071	288	-7,13	0,0000	Dunnett	0,0000	1,7667	3,9571	-55,3550	p <0.001
	16	Genotype	S42IL-139	Scarlett	-1,8571	0,2950	288	-6,30	0,0000	Dunnett	0,0000	2,1000	3,9571	-46,9314	p <0.001
	16	Genotype	S42IL-140	Scarlett	-2,4429	0,2950	288	-8,28	0,0000	Dunnett	0,0000	1,5143	3,9571	-61,7329	p <0.001
	16	Genotype	S42IL-141	Scarlett	-1,3429	0,2950	288	-4,55	0,0000	Dunnett	0,0003	2,6143	3,9571	-33,9350	p <0.001
	16	Genotype	S42IL-143	Scarlett	-2,4000	0,2950	288	-8,14	0,0000	Dunnett	0,0000	1,5571	3,9571	-60,6498	p <0.001
	16	Genotype	S42IL-173	Scarlett	1,3857	0,2950	288	4,70	0,0000	Dunnett	0,0002	5,3429	3,9571	35,0181	p <0.001
	16	Genotype	S42IL-118	Scarlett	-0,8405	0,3071	288	-2,74	0,0066	Dunnett	0,1494	3,1167	3,9571	-21,2395	p <0.01
	16	Genotype	S42IL-127	Scarlett	-0,9571	0,2950	288	-3,24	0,0013	Dunnett	0,0393	3,0000	3,9571	-24,1877	p <0.01
	16	Genotype	S42IL-138	Scarlett	-0,8571	0,2950	288	-2,91	0,0040	Dunnett	0,0992	3,1000	3,9571	-21,6606	p <0.01
	16	Genotype	S42IL-161	Scarlett	-0,9286	0,2950	288	-3,15	0,0018	Dunnett	0,0519	3,0286	3,9571	-23,4657	p <0.01
	16	Genotype	S42IL-162	Scarlett	0,8595	0,3071	288	2,80	0,0055	Dunnett	0,1290	4,8167	3,9571	21,7208	p <0.01
	16	Genotype	S42IL-119	Scarlett	-0,7071	0,3071	288	-2,30	0,0220	Dunnett	0,3674	3,2500	3,9571	-17,8700	p <0.05
	16	Genotype	S42IL-122	Scarlett	-0,7429	0,2950	288	-2,52	0,0123	Dunnett	0,2421	3,2143	3,9571	-18,7726	p <0.05
RSD/RSW	16	Genotype	S42IL-124	Scarlett	0,6913	0,1250	289	5,53082	7,14E-08	Dunnett	3E-06	1,8942	1,2029	57,4697	p <0.001
	16	Genotype	S42IL-102	Scarlett	0,3081	0,1141	289	2,69988	0,00735	Dunnett	0,1626	1,5109	1,2029	25,6096	p <0.01
	16	Genotype	S42IL-109	Scarlett	0,2638	0,1141	289	2,31162	0,0215	Dunnett	0,3611	1,4666	1,2029	21,9268	p <0.05
	16	Genotype	S42IL-131	Scarlett	-0,2627	0,1141	289	-2,3021	0,02204	Dunnett	0,3674	0,9402	1,2029	-21,8363	p <0.05
	16	Genotype	S42IL-143	Scarlett	0,2848	0,1141	289	2,49621	0,01311	Dunnett	0,2528	1,4877	1,2029	23,6777	p <0.05
1stLBL	16	Genotype	S42IL-124	Scarlett	-1,8721	0,2461	289	-7,6064	4E-13	Dunnett	1E-12	1,9944	3,8665	-48,4181	p <0.001
	16	Genotype	S42IL-134	Scarlett	-0,9013	0,2338	289	-3,8542	0,00014	Dunnett	0,0054	2,9652	3,8665	-23,3110	p <0.001
	16	Genotype	S42IL-139	Scarlett	-0,8853	0,2247	289	-3,9405	0,0001	Dunnett	0,0039	2,9811	3,8665	-22,8979	p <0.001
	16	Genotype	S42IL-140	Scarlett	-1,0855	0,2247	289	-4,8313	2,2E-06	Dunnett	1E-04	2,7810	3,8665	-28,0738	p <0.001
	16	Genotype	S42IL-142	Scarlett	1,0037	0,2247	289	4,4675	1,14E-05	Dunnett	0,0005	4,8702	3,8665	25,9600	p <0.001
	16	Genotype	S42IL-143	Scarlett	-0,8449	0,2247	289	-3,7606	0,00021	Dunnett	0,0075	3,0216	3,8665	-21,8522	p <0.001
1stLTL	16	Genotype	S42IL-106	Scarlett	1,6443	0,4528	289	3,63099	0,00033	Dunnett	0,0116	9,2471	7,6029	21,6267	p <0.001
	16	Genotype	S42IL-115	Scarlett	1,6017	0,4528	289	3,53712	0,00047	Dunnett	0,0159	9,2046	7,6029	21,0675	p <0.001
	16	Genotype	S42IL-124	Scarlett	-1,7000	0,4961	289	-3,427	0,0007	Dunnett	0,0226	5,9029	7,6029	-22,3597	p <0.001
	16	Genotype	S42IL-140	Scarlett	-1,7085	0,4528	289	-3,7728	0,0002	Dunnett	0,0072	5,8944	7,6029	-22,4712	p <0.001
	16	Genotype	S42IL-142	Scarlett	2,1680	0,4528	289	4,78763	2,7E-06	Dunnett	0,0001	9,7709	7,6029	28,5158	p <0.001
	16	Genotype	S42IL-143	Scarlett	-2,1481	0,4528	289	-4,7436	3,3E-06	Dunnett	0,0001	5,4548	7,6029	-28,2536	p <0.001
	16	Genotype	S42IL-119	Scarlett	-1,2771	0,4713	289	-2,7096	0,00714	Dunnett	0,159	6,3258	7,6029	-16,7979	p <0.01
	16	Genotype	S42IL-161	Scarlett	-1,1751	0,4528	289	-2,595	0,00994	Dunnett	0,2054	6,4278	7,6029	-15,4564	p <0.01
	16	Genotype	S42IL-173	Scarlett	1,3864	0,4528	289	3,06167	0,00241	Dunnett	0,0657	8,9893	7,6029	18,2357	p <0.01
	16	Genotype	S42IL-102	Scarlett	1,1398	0,4528	289	2,51698	0,01238	Dunnett	0,2423	8,7427	7,6029	14,9915	p <0.05
	16	Genotype	S42IL-111	Scarlett	0,9880	0,4528	289	2,18173	0,02993	Dunnett	0,4522	8,5909	7,6029	12,9947	p <0.05
	16	Genotype	S42IL-114	Scarlett	0,9607	0,4713	289	2,03824	0,04244	Dunnett	0,5647	8,5636	7,6029	12,6357	p <0.05
	16	Genotype	S42IL-116	Scarlett	1,1739	0,4528	289	2,59228	0,01002	Dunnett	0,2066	8,7768	7,6029	15,4400	p <0.05
	16	Genotype	S42IL-121	Scarlett	-0,9488	0,4528	289	-2,0953	0,03701	Dunnett	0,5188	6,6541	7,6029	-12,4799	p <0.05
	16	Genotype	S42IL-123	Scarlett	1,0576	0,4528	289	2,33551	0,0202	Dunnett	0,3457	8,6605	7,6029	13,9106	p <0.05

	16	Genotype	S42IL-125	Scarlett	-1,0820	0,4528	289	-2,3893	0,01752	Dunnett	0,3124	6,5209	7,6029	-14,2309	p <0.05
	16	Genotype	S42IL-129	Scarlett	-0,9110	0,4528	289	-2,0118	0,04517	Dunnett	0,5864	6,6919	7,6029	-11,9824	p <0.05
	16	Genotype	S42IL-138	Scarlett	1,1448	0,4528	289	2,52795	0,01201	Dunnett	0,2368	8,7476	7,6029	15,0568	p <0.05
2ndLTL	16	Genotype	S42IL-106	Scarlett	1,6443	0,4528	289	3,63099	0,00033	Dunnett	0,0116	9,2471	7,6029	21,6267	p <0.001
	16	Genotype	S42IL-115	Scarlett	1,6017	0,4528	289	3,53712	0,00047	Dunnett	0,0159	9,2046	7,6029	21,0675	p <0.001
	16	Genotype	S42IL-124	Scarlett	-1,7000	0,4961	289	-3,427	0,0007	Dunnett	0,0226	5,9029	7,6029	-22,3597	p <0.001
	16	Genotype	S42IL-140	Scarlett	-1,7085	0,4528	289	-3,7728	0,0002	Dunnett	0,0072	5,8944	7,6029	-22,4712	p <0.001
	16	Genotype	S42IL-142	Scarlett	2,1680	0,4528	289	4,78763	2,7E-06	Dunnett	0,0001	9,7709	7,6029	28,5158	p <0.001
	16	Genotype	S42IL-143	Scarlett	-2,1481	0,4528	289	-4,7436	3,3E-06	Dunnett	0,0001	5,4548	7,6029	-28,2536	p <0.001
	16	Genotype	S42IL-119	Scarlett	-1,2771	0,4713	289	-2,7096	0,00714	Dunnett	0,159	6,3258	7,6029	-16,7979	p <0.01
	16	Genotype	S42IL-161	Scarlett	-1,1751	0,4528	289	-2,595	0,00994	Dunnett	0,2054	6,4278	7,6029	-15,4564	p <0.01
	16	Genotype	S42IL-173	Scarlett	1,3864	0,4528	289	3,06167	0,00241	Dunnett	0,0657	8,9893	7,6029	18,2357	p <0.01
	16	Genotype	S42IL-102	Scarlett	1,1398	0,4528	289	2,51698	0,01238	Dunnett	0,2423	8,7427	7,6029	14,9915	p <0.05
	16	Genotype	S42IL-111	Scarlett	0,9880	0,4528	289	2,18173	0,02993	Dunnett	0,4522	8,5909	7,6029	12,9947	p <0.05
	16	Genotype	S42IL-114	Scarlett	0,9607	0,4713	289	2,03824	0,04244	Dunnett	0,5647	8,5636	7,6029	12,6357	p <0.05
	16	Genotype	S42IL-116	Scarlett	1,1739	0,4528	289	2,59228	0,01002	Dunnett	0,2066	8,7768	7,6029	15,4400	p <0.05
	16	Genotype	S42IL-121	Scarlett	-0,9488	0,4528	289	-2,0953	0,03701	Dunnett	0,5188	6,6541	7,6029	-12,4799	p <0.05
	16	Genotype	S42IL-123	Scarlett	1,0576	0,4528	289	2,33551	0,0202	Dunnett	0,3457	8,6605	7,6029	13,9106	p <0.05
	16	Genotype	S42IL-125	Scarlett	-1,0820	0,4528	289	-2,3893	0,01752	Dunnett	0,3124	6,5209	7,6029	-14,2309	p <0.05
	16	Genotype	S42IL-129	Scarlett	-0,9110	0,4528	289	-2,0118	0,04517	Dunnett	0,5864	6,6919	7,6029	-11,9824	p <0.05
	16	Genotype	S42IL-138	Scarlett	1,1448	0,4528	289	2,52795	0,01201	Dunnett	0,2368	8,7476	7,6029	15,0568	p <0.05

Table S13. S42ILs showing significant effects (*p*<0.05) for the observed root traits and shoot traits at 24°C

trait	Treatment	Effect	Genotype	Parent	Estimate	StdErr	DF	tValue	Probt	Adjustment	Adjp	LSMeans_genotype	LSMeans_Scarlett	RP_PCT	significance
RSAL	24	Genotype	S42IL-124	Scarlett	18,2178	5,2423	289	3,48	0,0006	Dunnett	0,0199	80,4125	62,1947	29,2915	p <0.001
	24	Genotype	S42IL-113	Scarlett	-15,0980	5,0366	289	-3,00	0,0030	Dunnett	0,0803	47,0967	62,1947	-24,2754	p <0.01
	24	Genotype	S42IL-107	Scarlett	12,4796	5,2423	289	2,38	0,0179	Dunnett	0,3267	74,6743	62,1947	20,0654	p <0.05
	24	Genotype	S42IL-112	Scarlett	-11,8393	5,0366	289	-2,35	0,0194	Dunnett	0,3456	50,3554	62,1947	-19,0358	p <0.05
	24	Genotype	S42IL-161	Scarlett	10,1931	5,0366	289	2,02	0,0439	Dunnett	0,5902	72,3879	62,1947	16,3891	p <0.05
RSAR	24	Genotype	S42IL-103	Scarlett	-30,3693	5,4739	289	-5,55	0,0000	Dunnett	0,0000	43,8018	74,1711	-40,9449	p <0.001
	24	Genotype	S42IL-110	Scarlett	-20,4584	5,2592	289	-3,89	0,0001	Dunnett	0,0048	53,7127	74,1711	-27,5827	p <0.001
	24	Genotype	S42IL-113	Scarlett	-24,1940	5,2592	289	-4,60	0,0000	Dunnett	0,0003	49,9771	74,1711	-32,6192	p <0.001
	24	Genotype	S42IL-127	Scarlett	-17,8697	5,2592	289	-3,40	0,0008	Dunnett	0,0254	56,3014	74,1711	-24,0925	p <0.001
	24	Genotype	S42IL-130	Scarlett	-19,7764	5,2592	289	-3,76	0,0002	Dunnett	0,0077	54,3947	74,1711	-26,6632	p <0.001
	24	Genotype	S42IL-133	Scarlett	-20,4281	5,2592	289	-3,88	0,0001	Dunnett	0,0049	53,7430	74,1711	-27,5419	p <0.001
	24	Genotype	S42IL-137	Scarlett	-21,8631	5,4739	289	-3,99	0,0001	Dunnett	0,0033	52,3080	74,1711	-29,4766	p <0.001
	24	Genotype	S42IL-104	Scarlett	-14,6046	5,2592	289	-2,78	0,0058	Dunnett	0,1398	59,5666	74,1711	-19,6904	p <0.01
	24	Genotype	S42IL-105	Scarlett	-16,1181	5,2592	289	-3,06	0,0024	Dunnett	0,0670	58,0530	74,1711	-21,7310	p <0.01
	24	Genotype	S42IL-108	Scarlett	-14,8834	5,2592	289	-2,83	0,0050	Dunnett	0,1230	59,2877	74,1711	-20,0663	p <0.01
	24	Genotype	S42IL-117	Scarlett	-17,1619	5,2592	289	-3,26	0,0012	Dunnett	0,0382	57,0093	74,1711	-23,1382	p <0.01
	24	Genotype	S42IL-140	Scarlett	-14,9723	5,4739	289	-2,74	0,0066	Dunnett	0,1542	59,1988	74,1711	-20,1862	p <0.01
	24	Genotype	S42IL-162	Scarlett	-15,3305	5,4739	289	-2,80	0,0054	Dunnett	0,1321	58,8407	74,1711	-20,6691	p <0.01
	24	Genotype	S42IL-176	Scarlett	-16,5184	5,2592	289	-3,14	0,0019	Dunnett	0,0543	57,6527	74,1711	-22,2707	p <0.01
	24	Genotype	S42IL-116	Scarlett	-12,2754	5,2592	289	-2,33	0,0203	Dunnett	0,3563	61,8957	74,1711	-16,5501	p <0.05
	24	Genotype	S42IL-121	Scarlett	-11,6646	5,2592	289	-2,22	0,0273	Dunnett	0,4372	62,5066	74,1711	-15,7266	p <0.05
	24	Genotype	S42IL-123	Scarlett	-11,6215	5,4739	289	-2,12	0,0346	Dunnett	0,5097	62,5497	74,1711	-15,6685	p <0.05
	24	Genotype	S42IL-125	Scarlett	-11,7357	5,2592	289	-2,23	0,0264	Dunnett	0,4273	62,4354	74,1711	-15,8225	p <0.05
	24	Genotype	S42IL-126	Scarlett	-13,5307	5,2592	289	-2,57	0,0106	Dunnett	0,2217	60,6404	74,1711	-18,2426	p <0.05
	24	Genotype	S42IL-131	Scarlett	-11,6424	5,2592	289	-2,21	0,0276	Dunnett	0,4403	62,5287	74,1711	-15,6967	p <0.05
	24	Genotype	S42IL-132	Scarlett	-12,4561	5,2592	289	-2,37	0,0185	Dunnett	0,3343	61,7150	74,1711	-16,7938	p <0.05
	24	Genotype	S42IL-135	Scarlett	-12,5343	5,2592	289	-2,38	0,0178	Dunnett	0,3250	61,6369	74,1711	-16,8991	p <0.05
	24	Genotype	S42IL-136	Scarlett	-11,0940	5,4739	289	-2,03	0,0436	Dunnett	0,5878	63,0772	74,1711	-14,9573	p <0.05
	24	Genotype	S42IL-138	Scarlett	-11,5350	5,2592	289	-2,19	0,0291	Dunnett	0,4555	62,6361	74,1711	-15,5519	p <0.05
RSALR	24	Genotype	S42IL-103	Scarlett	-35,6257	8,8957	289	-4,00	0,0001	Dunnett	0,0032	100,7402	136,3659	-26,1251	p <0.001
	24	Genotype	S42IL-113	Scarlett	-39,2920	8,5467	289	-4,60	0,0000	Dunnett	0,0003	97,0739	136,3659	-28,8137	p <0.001
	24	Genotype	S42IL-130	Scarlett	-29,2303	8,5467	289	-3,42	0,0007	Dunnett	0,0237	107,1356	136,3659	-21,4352	p <0.001
	24	Genotype	S42IL-133	Scarlett	-29,7166	8,5467	289	-3,4769	0,0006	Dunnett	0,0198	106,6493	136,3659	-21,7918	p <0.001
	24	Genotype	S42IL-127	Scarlett	-24,9937	8,5467	289	-2,9244	0,0037	Dunnett	0,0971	111,3721	136,3659	-18,3284	p <0.01
	24	Genotype	S42IL-137	Scarlett	-26,9739	8,8957	289	-3,0322	0,0026	Dunnett	0,0732	109,3920	136,3659	-19,7805	p <0.01
	24	Genotype	S42IL-176	Scarlett	-23,7250	8,5467	289	-2,7759	0,0059	Dunnett	0,1401	112,6409	136,3659	-17,3980	p <0.01
	24	Genotype	S42IL-108	Scarlett	-20,5793	8,5467	289	-2,41	0,0167	Dunnett	0,3101	115,7866	136,3659	-15,0912	p <0.05
	24	Genotype	S42IL-110	Scarlett	-21,2957	8,5467	289	-2,49	0,0133	Dunnett	0,2626	115,0701	136,3659	-15,6166	p <0.05
	24	Genotype	S42IL-112	Scarlett	-20,4797	8,5467	289	-2,40	0,0172	Dunnett	0,3171	115,8861	136,3659	-15,0182	p <0.05
	24	Genotype	S42IL-117	Scarlett	-17,4864	8,5467	289	-2,05	0,0417	Dunnett	0,5719	118,8794	136,3659	-12,8232	p <0.05
	24	Genotype	S42IL-124	Scarlett	20,7331	8,8957	289	2,3307	0,0205	Dunnett	0,3586	157,0990	136,3659	15,2041	p <0.05
	24	Genotype	S42IL-126	Scarlett	-18,4710	8,5467	289	-2,1612	0,0315	Dunnett	0,4800	117,8949	136,3659	-13,5452	p <0.05
	24	Genotype	S42IL-135	Scarlett	-17,6113	8,5467	289	-2,0606	0,0402	Dunnett	0,5600	118,7546	136,3659	-12,9147	p <0.05
	24	Genotype	S42IL-162	Scarlett	-19,7015	8,8957	289	-2,2147	0,0276	Dunnett	0,4396	116,6643	136,3659	-14,4475	p <0.05

NSR	24	Genotype	S42IL-124	Scarlett	-0,9286	0,2403	289	-3,86	0,0001	Dunnett	0,0053	5,5000	6,4286	-14,4444	p <0.001
	24	Genotype	S42IL-127	Scarlett	-0,8571	0,2309	289	-3,71	0,0002	Dunnett	0,0090	5,5714	6,4286	-13,3333	p <0.001
	24	Genotype	S42IL-128	Scarlett	-1,0000	0,2309	289	-4,33	0,0000	Dunnett	0,0009	5,4286	6,4286	-15,5556	p <0.001
	24	Genotype	S42IL-129	Scarlett	-1,4286	0,2309	289	-6,19	0,0000	Dunnett	0,0000	5,0000	6,4286	-22,2222	p <0.001
	24	Genotype	S42IL-140	Scarlett	-0,9286	0,2403	289	-3,86	0,0001	Dunnett	0,0053	5,5000	6,4286	-14,4444	p <0.001
	24	Genotype	S42IL-143	Scarlett	-2,4286	0,2309	289	-10,52	0,0000	Dunnett	0,0000	4,0000	6,4286	-37,7778	p <0.001
	24	Genotype	S42IL-176	Scarlett	-1,1429	0,2309	289	-4,95	0,0000	Dunnett	0,0001	5,2857	6,4286	-17,7778	p <0.001
	24	Genotype	S42IL-105	Scarlett	-0,7143	0,2309	289	-3,09	0,0022	Dunnett	0,0618	5,7143	6,4286	-11,1111	p <0.01
	24	Genotype	S42IL-107	Scarlett	-0,7619	0,2403	289	-3,17	0,0017	Dunnett	0,0499	5,6667	6,4286	-11,8519	p <0.01
	24	Genotype	S42IL-110	Scarlett	-0,7143	0,2309	289	-3,09	0,0022	Dunnett	0,0618	5,7143	6,4286	-11,1111	p <0.01
	24	Genotype	S42IL-139	Scarlett	-0,7619	0,2403	289	-3,17	0,0017	Dunnett	0,0499	5,6667	6,4286	-11,8519	p <0.01
	24	Genotype	S42IL-109	Scarlett	-0,5714	0,2309	289	-2,48	0,0139	Dunnett	0,2715	5,8571	6,4286	-8,8889	p <0.05
	24	Genotype	S42IL-111	Scarlett	-0,5714	0,2309	289	-2,48	0,0139	Dunnett	0,2715	5,8571	6,4286	-8,8889	p <0.05
	24	Genotype	S42IL-112	Scarlett	-0,5714	0,2309	289	-2,48	0,0139	Dunnett	0,2715	5,8571	6,4286	-8,8889	p <0.05
	24	Genotype	S42IL-117	Scarlett	-0,5714	0,2309	289	-2,48	0,0139	Dunnett	0,2715	5,8571	6,4286	-8,8889	p <0.05
	24	Genotype	S42IL-122	Scarlett	-0,5714	0,2309	289	-2,48	0,0139	Dunnett	0,2715	5,8571	6,4286	-8,8889	p <0.05
NLR	24	Genotype	S42IL-115	Scarlett	233,8571	57,6661	289	4,06	0,0001	Dunnett	0,0026	903,0000	669,1429	34,9488	p <0.001
	24	Genotype	S42IL-118	Scarlett	222,0000	57,6661	289	3,85	0,0001	Dunnett	0,0056	891,1429	669,1429	33,1768	p <0.001
	24	Genotype	S42IL-124	Scarlett	-325,6429	60,0208	289	-5,43	0,0000	Dunnett	0,0000	343,5000	669,1429	-48,6657	p <0.001
	24	Genotype	S42IL-136	Scarlett	226,6905	60,0208	289	3,78	0,0002	Dunnett	0,0072	895,8333	669,1429	33,8777	p <0.001
	24	Genotype	S42IL-140	Scarlett	-298,1429	60,0208	289	-4,97	0,0000	Dunnett	0,0001	371,0000	669,1429	-44,5559	p <0.001
	24	Genotype	S42IL-143	Scarlett	-416,7143	57,6661	289	-7,23	0,0000	Dunnett	0,0000	252,4286	669,1429	-62,2758	p <0.001
	24	Genotype	S42IL-162	Scarlett	263,8571	60,0208	289	4,40	0,0000	Dunnett	0,0007	933,0000	669,1429	39,4321	p <0.001
	24	Genotype	S42IL-106	Scarlett	161,8571	57,6661	289	2,81	0,0053	Dunnett	0,1301	831,0000	669,1429	24,1887	p <0.01
	24	Genotype	S42IL-129	Scarlett	-162,5714	57,6661	289	-2,82	0,0051	Dunnett	0,1263	506,5714	669,1429	-24,2955	p <0.01
	24	Genotype	S42IL-132	Scarlett	174,2857	57,6661	289	3,02	0,0027	Dunnett	0,0752	843,4286	669,1429	26,0461	p <0.01
	24	Genotype	S42IL-176	Scarlett	179,4286	57,6661	289	3,11	0,0020	Dunnett	0,0589	848,5714	669,1429	26,8147	p <0.01
	24	Genotype	S42IL-113	Scarlett	134,0000	57,6661	289	2,32	0,0208	Dunnett	0,3632	803,1429	669,1429	20,0256	p <0.05
	24	Genotype	S42IL-122	Scarlett	-115,2857	57,6661	289	-2,00	0,0465	Dunnett	0,6106	553,8571	669,1429	-17,2289	p <0.05
	24	Genotype	S42IL-131	Scarlett	139,4286	57,6661	289	2,42	0,0162	Dunnett	0,3042	808,5714	669,1429	20,8369	p <0.05
	24	Genotype	S42IL-142	Scarlett	126,4286	57,6661	289	2,19	0,0291	Dunnett	0,4562	795,5714	669,1429	18,8941	p <0.05
	24	Genotype	S42IL-170	Scarlett	123,8571	57,6661	289	2,15	0,0326	Dunnett	0,4903	793,0000	669,1429	18,5098	p <0.05
LSR/NSR	24	Genotype	S42IL-109	Scarlett	7,9065	2,0749	289	3,81	0,0002	Dunnett	0,0064	36,6126	28,7061	27,5428	p <0.001
	24	Genotype	S42IL-106	Scarlett	6,0214	2,0749	289	2,90	0,0040	Dunnett	0,1028	34,7275	28,7061	20,9758	p <0.01
	24	Genotype	S42IL-132	Scarlett	6,1472	2,0749	289	2,96	0,0033	Dunnett	0,0880	34,8534	28,7061	21,4144	p <0.01
	24	Genotype	S42IL-134	Scarlett	5,4678	2,0749	289	2,64	0,0089	Dunnett	0,1936	34,1740	28,7061	19,0477	p <0.01
	24	Genotype	S42IL-162	Scarlett	5,7348	2,1596	289	2,66	0,0084	Dunnett	0,1851	34,4409	28,7061	19,9777	p <0.01
	24	Genotype	S42IL-170	Scarlett	6,6969	2,0749	289	3,23	0,0014	Dunnett	0,0424	35,4030	28,7061	23,3290	p <0.01
	24	Genotype	S42IL-176	Scarlett	6,7482	2,0749	289	3,25	0,0013	Dunnett	0,0394	35,4543	28,7061	23,5079	p <0.01
	24	Genotype	S42IL-104	Scarlett	4,1609	2,0749	289	2,01	0,0459	Dunnett	0,6054	32,8670	28,7061	14,4949	p <0.05
	24	Genotype	S42IL-107	Scarlett	4,9807	2,1596	289	2,31	0,0218	Dunnett	0,3748	33,6868	28,7061	17,3507	p <0.05
	24	Genotype	S42IL-113	Scarlett	4,1884	2,0749	289	2,02	0,0444	Dunnett	0,5944	32,8945	28,7061	14,5906	p <0.05
	24	Genotype	S42IL-117	Scarlett	5,0229	2,0749	289	2,42	0,0161	Dunnett	0,3024	33,7290	28,7061	17,4977	p <0.05
	24	Genotype	S42IL-118	Scarlett	5,1358	2,0749	289	2,48	0,0139	Dunnett	0,2715	33,8420	28,7061	17,8911	p <0.05
	24	Genotype	S42IL-121	Scarlett	4,5221	2,0749	289	2,18	0,0301	Dunnett	0,4660	33,2282	28,7061	15,7531	p <0.05
	24	Genotype	S42IL-126	Scarlett	4,3203	2,0749	289	2,08	0,0382	Dunnett	0,5424	33,0264	28,7061	15,0501	p <0.05
	24	Genotype	S42IL-136	Scarlett	5,2817	2,1596	289	2,45	0,0151	Dunnett	0,2880	33,9878	28,7061	18,3992	p <0.05

LLR/NLR	24	Genotype	S42IL-101	Scarlett	-0,2286	0,0510	289	-4,48	0,0000	Dunnett	0,0005	0,5934	0,8220	-27,8098	p <0.001
	24	Genotype	S42IL-102	Scarlett	-0,2972	0,0531	289	-5,60	0,0000	Dunnett	0,0000	0,5248	0,8220	-36,1504	p <0.001
	24	Genotype	S42IL-103	Scarlett	-0,3811	0,0531	289	-7,18	0,0000	Dunnett	0,0000	0,4408	0,8220	-46,3677	p <0.001
	24	Genotype	S42IL-104	Scarlett	-0,2793	0,0510	289	-5,48	0,0000	Dunnett	0,0000	0,5427	0,8220	-33,9822	p <0.001
	24	Genotype	S42IL-105	Scarlett	-0,2546	0,0510	289	-4,99	0,0000	Dunnett	0,0000	0,5674	0,8220	-30,9682	p <0.001
	24	Genotype	S42IL-106	Scarlett	-0,2921	0,0510	289	-5,73	0,0000	Dunnett	0,0000	0,5299	0,8220	-35,5382	p <0.001
	24	Genotype	S42IL-107	Scarlett	-0,2807	0,0531	289	-5,29	0,0000	Dunnett	0,0000	0,5412	0,8220	-34,1536	p <0.001
	24	Genotype	S42IL-108	Scarlett	-0,3303	0,0510	289	-6,47	0,0000	Dunnett	0,0000	0,4917	0,8220	-40,1827	p <0.001
	24	Genotype	S42IL-109	Scarlett	-0,2761	0,0510	289	-5,41	0,0000	Dunnett	0,0000	0,5458	0,8220	-33,5941	p <0.001
	24	Genotype	S42IL-110	Scarlett	-0,2211	0,0510	289	-4,33	0,0000	Dunnett	0,0009	0,6009	0,8220	-26,8940	p <0.001
	24	Genotype	S42IL-111	Scarlett	-0,2698	0,0510	289	-5,29	0,0000	Dunnett	0,0000	0,5522	0,8220	-32,8220	p <0.001
	24	Genotype	S42IL-112	Scarlett	-0,2263	0,0510	289	-4,44	0,0000	Dunnett	0,0006	0,5957	0,8220	-27,5283	p <0.001
	24	Genotype	S42IL-113	Scarlett	-0,3208	0,0510	289	-6,29	0,0000	Dunnett	0,0000	0,5012	0,8220	-39,0254	p <0.001
	24	Genotype	S42IL-114	Scarlett	-0,2519	0,0531	289	-4,74	0,0000	Dunnett	0,0001	0,5701	0,8220	-30,6484	p <0.001
	24	Genotype	S42IL-115	Scarlett	-0,3545	0,0510	289	-6,95	0,0000	Dunnett	0,0000	0,4675	0,8220	-43,1238	p <0.001
	24	Genotype	S42IL-116	Scarlett	-0,3594	0,0510	289	-7,04	0,0000	Dunnett	0,0000	0,4626	0,8220	-43,7243	p <0.001
	24	Genotype	S42IL-117	Scarlett	-0,2763	0,0510	289	-5,42	0,0000	Dunnett	0,0000	0,5456	0,8220	-33,6182	p <0.001
	24	Genotype	S42IL-118	Scarlett	-0,2567	0,0510	289	-5,03	0,0000	Dunnett	0,0000	0,5653	0,8220	-31,2304	p <0.001
	24	Genotype	S42IL-119	Scarlett	-0,2726	0,0510	289	-5,34	0,0000	Dunnett	0,0000	0,5494	0,8220	-33,1621	p <0.001
	24	Genotype	S42IL-120	Scarlett	-0,3565	0,0510	289	-6,99	0,0000	Dunnett	0,0000	0,4655	0,8220	-43,3735	p <0.001
	24	Genotype	S42IL-121	Scarlett	-0,2348	0,0510	289	-4,60	0,0000	Dunnett	0,0003	0,5872	0,8220	-28,5595	p <0.001
	24	Genotype	S42IL-122	Scarlett	-0,3003	0,0510	289	-5,89	0,0000	Dunnett	0,0000	0,5216	0,8220	-36,5384	p <0.001
	24	Genotype	S42IL-123	Scarlett	-0,2744	0,0531	289	-5,17	0,0000	Dunnett	0,0000	0,5476	0,8220	-33,3813	p <0.001
	24	Genotype	S42IL-124	Scarlett	-0,4666	0,0531	289	-8,79	0,0000	Dunnett	0,0000	0,3554	0,8220	-56,7658	p <0.001
	24	Genotype	S42IL-125	Scarlett	-0,1974	0,0510	289	-3,87	0,0001	Dunnett	0,0052	0,6246	0,8220	-24,0151	p <0.001
	24	Genotype	S42IL-126	Scarlett	-0,2976	0,0510	289	-5,83	0,0000	Dunnett	0,0000	0,5244	0,8220	-36,2073	p <0.001
	24	Genotype	S42IL-127	Scarlett	-0,3108	0,0510	289	-6,09	0,0000	Dunnett	0,0000	0,5112	0,8220	-37,8146	p <0.001
	24	Genotype	S42IL-128	Scarlett	-0,1886	0,0510	289	-3,70	0,0003	Dunnett	0,0095	0,6334	0,8220	-22,9449	p <0.001
	24	Genotype	S42IL-129	Scarlett	-0,2488	0,0510	289	-4,88	0,0000	Dunnett	0,0001	0,5732	0,8220	-30,2628	p <0.001
	24	Genotype	S42IL-131	Scarlett	-0,2573	0,0510	289	-5,04	0,0000	Dunnett	0,0000	0,5647	0,8220	-31,2965	p <0.001
	24	Genotype	S42IL-132	Scarlett	-0,2371	0,0510	289	-4,65	0,0000	Dunnett	0,0002	0,5849	0,8220	-28,8445	p <0.001
	24	Genotype	S42IL-134	Scarlett	-0,3962	0,0510	289	-7,7665	0,0000	Dunnett	0,0000	0,4258	0,8220	-48,2037	p <0.001
	24	Genotype	S42IL-136	Scarlett	-0,1913	0,0531	289	-3,6034	0,0004	Dunnett	0,0131	0,6306	0,8220	-23,2783	p <0.001
	24	Genotype	S42IL-137	Scarlett	-0,2911	0,0531	289	-5,4823	0,0000	Dunnett	0,0000	0,5309	0,8220	-35,4159	p <0.001
	24	Genotype	S42IL-138	Scarlett	-0,3575	0,0510	289	-7,0073	0,0000	Dunnett	0,0000	0,4645	0,8220	-43,4915	p <0.001
	24	Genotype	S42IL-139	Scarlett	-0,2974	0,0531	289	-5,6006	0,0000	Dunnett	0,0000	0,5246	0,8220	-36,1801	p <0.001
	24	Genotype	S42IL-140	Scarlett	-0,2456	0,0531	289	-4,6249	0,0000	Dunnett	0,0003	0,5764	0,8220	-29,8770	p <0.001
	24	Genotype	S42IL-141	Scarlett	-0,3337	0,0510	289	-6,5417	0,0000	Dunnett	0,0000	0,4882	0,8220	-40,6019	p <0.001
	24	Genotype	S42IL-142	Scarlett	-0,1792	0,0510	289	-3,5132	0,0005	Dunnett	0,0176	0,6428	0,8220	-21,8048	p <0.001
	24	Genotype	S42IL-143	Scarlett	-0,2743	0,0510	289	-5,3758	0,0000	Dunnett	0,0000	0,5477	0,8220	-33,3656	p <0.001
	24	Genotype	S42IL-161	Scarlett	-0,3457	0,0510	289	-6,7755	0,0000	Dunnett	0,0000	0,4763	0,8220	-42,0527	p <0.001
	24	Genotype	S42IL-162	Scarlett	-0,3179	0,0531	289	-5,986	0,0000	Dunnett	0,0000	0,5041	0,8220	-38,6694	p <0.001
	24	Genotype	S42IL-170	Scarlett	-0,2592	0,0510	289	-5,0797	0,0000	Dunnett	0,0000	0,5628	0,8220	-31,5278	p <0.001
	24	Genotype	S42IL-173	Scarlett	-0,2060	0,0510	289	-4,0376	0,0001	Dunnett	0,0028	0,6160	0,8220	-25,0597	p <0.001
	24	Genotype	S42IL-176	Scarlett	-0,2942	0,0510	289	-5,7676	0,0000	Dunnett	0,0000	0,5277	0,8220	-35,7970	p <0.001
	24	Genotype	S42IL-130	Scarlett	-0,1597	0,0510	289	-3,13	0,0019	Dunnett	0,0561	0,6623	0,8220	-19,4236	p <0.01
	24	Genotype	S42IL-135	Scarlett	-0,1617	0,0510	289	-3,1694	0,0017	Dunnett	0,0501	0,6603	0,8220	-19,6711	p <0.01
	24	Genotype	S42IL-133	Scarlett	-0,1320	0,0510	289	-2,5879	0,0101	Dunnett	0,2147	0,6900	0,8220	-16,0620	p <0.05

TRL	24	Genotype	S42IL-103	Scarlett	-229,7607	42,8895	289	-5,36	0,0000	Dunnett	0,0000	495,9852	725,7459	-31,6586	p <0.001
	24	Genotype	S42IL-105	Scarlett	-141,7793	41,2069	289	-3,44	0,0007	Dunnett	0,0222	583,9666	725,7459	-19,5357	p <0.001
	24	Genotype	S42IL-108	Scarlett	-150,5524	41,2069	289	-3,65	0,0003	Dunnett	0,0111	575,1934	725,7459	-20,7445	p <0.001
	24	Genotype	S42IL-110	Scarlett	-172,0171	41,2069	289	-4,17	0,0000	Dunnett	0,0016	553,7287	725,7459	-23,7021	p <0.001
	24	Genotype	S42IL-111	Scarlett	-159,3967	41,2069	289	-3,87	0,0001	Dunnett	0,0052	566,3491	725,7459	-21,9632	p <0.001
	24	Genotype	S42IL-114	Scarlett	-149,1442	42,8895	289	-3,48	0,0006	Dunnett	0,0198	576,6017	725,7459	-20,5505	p <0.001
	24	Genotype	S42IL-116	Scarlett	-220,7663	41,2069	289	-5,36	0,0000	Dunnett	0,0000	504,9796	725,7459	-30,4192	p <0.001
	24	Genotype	S42IL-119	Scarlett	-148,6853	41,2069	289	-3,61	0,0004	Dunnett	0,0129	577,0606	725,7459	-20,4872	p <0.001
	24	Genotype	S42IL-120	Scarlett	-264,7899	41,2069	289	-6,43	0,0000	Dunnett	0,0000	460,9560	725,7459	-36,4852	p <0.001
	24	Genotype	S42IL-122	Scarlett	-259,6644	41,2069	289	-6,30	0,0000	Dunnett	0,0000	466,0814	725,7459	-35,7790	p <0.001
	24	Genotype	S42IL-123	Scarlett	-491,4722	42,8895	289	-11,46	0,0000	Dunnett	0,0000	234,2737	725,7459	-67,7196	p <0.001
	24	Genotype	S42IL-124	Scarlett	-456,2655	42,8895	289	-10,64	0,0000	Dunnett	0,0000	269,4803	725,7459	-62,8685	p <0.001
	24	Genotype	S42IL-127	Scarlett	-254,1417	41,2069	289	-6,17	0,0000	Dunnett	0,0000	471,6041	725,7459	-35,0180	p <0.001
	24	Genotype	S42IL-128	Scarlett	-196,9193	41,2069	289	-4,78	0,0000	Dunnett	0,0001	528,8266	725,7459	-27,1334	p <0.001
	24	Genotype	S42IL-129	Scarlett	-286,9363	41,2069	289	-6,96	0,0000	Dunnett	0,0000	438,8096	725,7459	-39,5367	p <0.001
	24	Genotype	S42IL-134	Scarlett	-202,3313	41,2069	289	-4,91	0,0000	Dunnett	0,0001	523,4146	725,7459	-27,8791	p <0.001
	24	Genotype	S42IL-135	Scarlett	-185,8373	41,2069	289	-4,51	0,0000	Dunnett	0,0004	539,9086	725,7459	-25,6064	p <0.001
	24	Genotype	S42IL-137	Scarlett	-174,3262	42,8895	289	-4,06	0,0001	Dunnett	0,0025	551,4197	725,7459	-24,0203	p <0.001
	24	Genotype	S42IL-138	Scarlett	-228,4593	41,2069	289	-5,54	0,0000	Dunnett	0,0000	497,2866	725,7459	-31,4792	p <0.001
	24	Genotype	S42IL-139	Scarlett	-264,5274	42,8895	289	-6,17	0,0000	Dunnett	0,0000	461,2185	725,7459	-36,4490	p <0.001
	24	Genotype	S42IL-140	Scarlett	-377,9510	42,8895	289	-8,81	0,0000	Dunnett	0,0000	347,7948	725,7459	-52,0776	p <0.001
	24	Genotype	S42IL-141	Scarlett	-237,2663	41,2069	289	-5,76	0,0000	Dunnett	0,0000	488,4796	725,7459	-32,6928	p <0.001
	24	Genotype	S42IL-143	Scarlett	-480,8610	41,2069	289	-11,67	0,0000	Dunnett	0,0000	244,8849	725,7459	-66,2575	p <0.001
	24	Genotype	S42IL-161	Scarlett	-223,9873	41,2069	289	-5,44	0,0000	Dunnett	0,0000	501,7586	725,7459	-30,8630	p <0.001
	24	Genotype	S42IL-101	Scarlett	-107,9181	41,2069	289	-2,62	0,0093	Dunnett	0,2007	617,8277	725,7459	-14,8700	p <0.01
	24	Genotype	S42IL-102	Scarlett	-128,9179	42,8895	289	-3,01	0,0029	Dunnett	0,0785	596,8280	725,7459	-17,7635	p <0.01
	24	Genotype	S42IL-104	Scarlett	-112,9821	41,2069	289	-2,74	0,0065	Dunnett	0,1519	612,7637	725,7459	-15,5677	p <0.01
	24	Genotype	S42IL-107	Scarlett	-123,3805	42,8895	289	-2,88	0,0043	Dunnett	0,1096	602,3653	725,7459	-17,0005	p <0.01
	24	Genotype	S42IL-113	Scarlett	-110,3929	41,2069	289	-2,68	0,0078	Dunnett	0,1755	615,3530	725,7459	-15,2110	p <0.01
	24	Genotype	S42IL-117	Scarlett	-135,2663	41,2069	289	-3,28	0,0012	Dunnett	0,0360	590,4796	725,7459	-18,6382	p <0.01
	24	Genotype	S42IL-121	Scarlett	-115,5244	41,2069	289	-2,80	0,0054	Dunnett	0,1312	610,2214	725,7459	-15,9184	p <0.01
	24	Genotype	S42IL-125	Scarlett	-111,7820	41,2069	289	-2,71	0,0071	Dunnett	0,1625	613,9639	725,7459	-15,4024	p <0.01
	24	Genotype	S42IL-126	Scarlett	-128,8214	41,2069	289	-3,13	0,0020	Dunnett	0,0566	596,9244	725,7459	-17,7502	p <0.01
	24	Genotype	S42IL-131	Scarlett	-112,7351	41,2069	289	-2,74	0,0066	Dunnett	0,1540	613,0107	725,7459	-15,5337	p <0.01
	24	Genotype	S42IL-109	Scarlett	-100,7596	41,2069	289	-2,45	0,0151	Dunnett	0,2883	624,9863	725,7459	-13,8836	p <0.05
	24	Genotype	S42IL-112	Scarlett	-88,6776	41,2069	289	-2,15	0,0322	Dunnett	0,4871	637,0683	725,7459	-12,2188	p <0.05
	24	Genotype	S42IL-115	Scarlett	-93,4986	41,2069	289	-2,27	0,0240	Dunnett	0,4005	632,2473	725,7459	-12,8873	p <0.05
	24	Genotype	S42IL-176	Scarlett	-94,4999	41,2069	289	-2,29	0,0225	Dunnett	0,3837	631,2460	725,7459	-13,0211	p <0.05
RDW	24	Genotype	S42IL-124	Scarlett	-0,1165	0,0341	289	-3,41	0,0007	Dunnett	0,0243	0,1787	0,2951	-39,4671	p <0.001
	24	Genotype	S42IL-139	Scarlett	-0,1292	0,0341	289	-3,79	0,0002	Dunnett	0,0070	0,1659	0,2951	-43,7872	p <0.001
	24	Genotype	S42IL-143	Scarlett	-0,1676	0,0328	289	-5,11	0,0000	Dunnett	0,0000	0,1275	0,2951	-56,7936	p <0.001
	24	Genotype	S42IL-129	Scarlett	-0,0982	0,0328	289	-2,99	0,0030	Dunnett	0,0812	0,1969	0,2951	-33,2688	p <0.01
	24	Genotype	S42IL-140	Scarlett	-0,0935	0,0341	289	-2,74	0,0065	Dunnett	0,1529	0,2016	0,2951	-31,6851	p <0.01
	24	Genotype	S42IL-109	Scarlett	-0,0793	0,0328	289	-2,42	0,0162	Dunnett	0,3038	0,2158	0,2951	-26,8793	p <0.05
	24	Genotype	S42IL-120	Scarlett	-0,0658	0,0328	289	-2,01	0,0457	Dunnett	0,6045	0,2293	0,2951	-22,3002	p <0.05
	24	Genotype	S42IL-127	Scarlett	-0,0787	0,0328	289	-2,40	0,0170	Dunnett	0,3148	0,2164	0,2951	-26,6760	p <0.05
	24	Genotype	S42IL-128	Scarlett	-0,0820	0,0328	289	-2,50	0,0130	Dunnett	0,2580	0,2131	0,2951	-27,7893	p <0.05
	24	Genotype	S42IL-132	Scarlett	0,0649	0,0328	289	1,98	0,0488	Dunnett	0,6277	0,3600	0,2951	21,9904	p <0.05
	24	Genotype	S42IL-161	Scarlett	-0,0801	0,0328	289	-2,44	0,0152	Dunnett	0,2906	0,2151	0,2951	-27,1310	p <0.05

FWS	24	Genotype	S42IL-124	Scarlett	-0,0215	0,0048	289	-4,50	0,0000	Dunnett	0,0004	0,0274	0,0489	-44,0177	p <0.001
	24	Genotype	S42IL-140	Scarlett	-0,0204	0,0048	289	-4,27	0,0000	Dunnett	0,0011	0,0285	0,0489	-41,7689	p <0.001
	24	Genotype	S42IL-143	Scarlett	-0,0317	0,0046	289	-6,89	0,0000	Dunnett	0,0000	0,0172	0,0489	-64,7488	p <0.001
	24	Genotype	S42IL-127	Scarlett	-0,0119	0,0046	289	-2,60	0,0099	Dunnett	0,2099	0,0370	0,0489	-24,4159	p <0.01
	24	Genotype	S42IL-128	Scarlett	-0,0122	0,0046	289	-2,64	0,0086	Dunnett	0,1895	0,0368	0,0489	-24,8540	p <0.01
	24	Genotype	S42IL-129	Scarlett	-0,0153	0,0046	289	-3,32	0,0010	Dunnett	0,0320	0,0336	0,0489	-31,2208	p <0.01
	24	Genotype	S42IL-135	Scarlett	-0,0123	0,0046	289	-2,67	0,0081	Dunnett	0,1805	0,0367	0,0489	-25,0584	p <0.01
	24	Genotype	S42IL-139	Scarlett	-0,0154	0,0048	289	-3,21	0,0015	Dunnett	0,0444	0,0336	0,0489	-31,4106	p <0.01
	24	Genotype	S42IL-162	Scarlett	0,0129	0,0048	289	2,69	0,0076	Dunnett	0,1726	0,0618	0,0489	26,2753	p <0.01
	24	Genotype	S42IL-123	Scarlett	0,0100	0,0048	289	2,10	0,0368	Dunnett	0,5300	0,0590	0,0489	20,5169	p <0.05
	24	Genotype	S42IL-134	Scarlett	-0,0105	0,0046	289	-2,28	0,0235	Dunnett	0,3942	0,0384	0,0489	-21,4077	p <0.05
	24	Genotype	S42IL-141	Scarlett	-0,0108	0,0046	289	-2,34	0,0198	Dunnett	0,3503	0,0381	0,0489	-22,0210	p <0.05
	24	Genotype	S42IL-161	Scarlett	-0,0108	0,0046	289	-2,36	0,0192	Dunnett	0,3423	0,0381	0,0489	-22,1379	p <0.05
RSD	24	Genotype	S42IL-124	Scarlett	-4,6133	1,3591	289	-3,39	0,0008	Dunnett	0,0257	27,9127	32,5260	-14,1835	p <0.001
	24	Genotype	S42IL-143	Scarlett	-6,5513	1,3058	289	-5,02	0,0000	Dunnett	0,0000	25,9747	32,5260	-20,1417	p <0.001
RSW	24	Genotype	S42IL-143	Scarlett	-6,2119	1,7101	289	-3,63	0,0003	Dunnett	0,0119	12,6094	18,8213	-33,0044	p <0.001
	24	Genotype	S42IL-113	Scarlett	3,5626	1,7101	289	2,08	0,0381	Dunnett	0,5416	22,3839	18,8213	18,9284	p <0.05
	24	Genotype	S42IL-117	Scarlett	3,5910	1,7101	289	2,10	0,0366	Dunnett	0,5282	22,4123	18,8213	19,0795	p <0.05
	24	Genotype	S42IL-124	Scarlett	-4,2136	1,7800	289	-2,37	0,0186	Dunnett	0,3351	14,6077	18,8213	-22,3875	p <0.05
	24	Genotype	S42IL-130	Scarlett	4,2563	1,7101	289	2,49	0,0134	Dunnett	0,2641	23,0776	18,8213	22,6142	p <0.05
	24	Genotype	S42IL-133	Scarlett	3,6731	1,7101	289	2,15	0,0326	Dunnett	0,4903	22,4944	18,8213	19,5159	p <0.05
	24	Genotype	S42IL-137	Scarlett	3,7789	1,7800	289	2,12	0,0346	Dunnett	0,5098	22,6002	18,8213	20,0777	p <0.05
CHA	24	Genotype	S42IL-124	Scarlett	-233,9746	45,8884	289	-5,10	0,0000	Dunnett	0,0000	179,2005	413,1751	-56,6284	p <0.001
	24	Genotype	S42IL-143	Scarlett	-212,3786	44,0881	289	-4,82	0,0000	Dunnett	0,0001	200,7966	413,1751	-51,4016	p <0.001
	24	Genotype	S42IL-170	Scarlett	150,7616	44,0881	289	3,42	0,0007	Dunnett	0,0237	563,9367	413,1751	36,4885	p <0.001
	24	Genotype	S42IL-130	Scarlett	117,2109	44,0881	289	2,66	0,0083	Dunnett	0,1838	530,3860	413,1751	28,3683	p <0.01
	24	Genotype	S42IL-136	Scarlett	145,2959	45,8884	289	3,17	0,0017	Dunnett	0,0505	558,4710	413,1751	35,1657	p <0.01
	24	Genotype	S42IL-104	Scarlett	104,9590	44,0881	289	2,38	0,0179	Dunnett	0,3267	518,1341	413,1751	25,4030	p <0.05
	24	Genotype	S42IL-113	Scarlett	101,5221	44,0881	289	2,30	0,0220	Dunnett	0,3773	514,6973	413,1751	24,5712	p <0.05
	24	Genotype	S42IL-115	Scarlett	90,2616	44,0881	289	2,05	0,0415	Dunnett	0,5708	503,4367	413,1751	21,8458	p <0.05
	24	Genotype	S42IL-117	Scarlett	111,9137	44,0881	289	2,54	0,0117	Dunnett	0,2385	525,0889	413,1751	27,0863	p <0.05
	24	Genotype	S42IL-123	Scarlett	99,1334	45,8884	289	2,16	0,0316	Dunnett	0,4807	512,3085	413,1751	23,9931	p <0.05
	24	Genotype	S42IL-133	Scarlett	96,6849	44,0881	289	2,19	0,0291	Dunnett	0,4558	509,8600	413,1751	23,4005	p <0.05
	24	Genotype	S42IL-162	Scarlett	117,0555	45,8884	289	2,55	0,0113	Dunnett	0,2323	530,2307	413,1751	28,3307	p <0.05
	24	Genotype	S42IL-173	Scarlett	91,5289	44,0881	289	2,08	0,0388	Dunnett	0,5474	504,7040	413,1751	22,1526	p <0.05
1stLLA	24	Genotype	S42IL-109	Scarlett	-1,4429	0,4030	289	-3,58	0,0004	Dunnett	0,0141	4,1714	5,6143	-25,6997	p <0.001
	24	Genotype	S42IL-124	Scarlett	-3,4976	0,4195	289	-8,34	0,0000	Dunnett	0,0000	2,1167	5,6143	-62,2986	p <0.001
	24	Genotype	S42IL-127	Scarlett	-1,4429	0,4030	289	-3,58	0,0004	Dunnett	0,0141	4,1714	5,6143	-25,6997	p <0.001
	24	Genotype	S42IL-134	Scarlett	-1,5714	0,4030	289	-3,90	0,0001	Dunnett	0,0047	4,0429	5,6143	-27,9898	p <0.001
	24	Genotype	S42IL-137	Scarlett	-1,6310	0,4195	289	-3,89	0,0001	Dunnett	0,0049	3,9833	5,6143	-29,0500	p <0.001
	24	Genotype	S42IL-139	Scarlett	-2,4810	0,4195	289	-5,91	0,0000	Dunnett	0,0000	3,1333	5,6143	-44,1900	p <0.001
	24	Genotype	S42IL-143	Scarlett	-4,1000	0,4030	289	-10,17	0,0000	Dunnett	0,0000	1,5143	5,6143	-73,0280	p <0.001
	24	Genotype	S42IL-161	Scarlett	-1,4857	0,4030	289	-3,69	0,0003	Dunnett	0,0099	4,1286	5,6143	-26,4631	p <0.001
	24	Genotype	S42IL-110	Scarlett	-1,3000	0,4030	289	-3,23	0,0014	Dunnett	0,0426	4,3143	5,6143	-23,1552	p <0.01
	24	Genotype	S42IL-138	Scarlett	-1,0857	0,4030	289	-2,69	0,0075	Dunnett	0,1697	4,5286	5,6143	-19,3384	p <0.01
	24	Genotype	S42IL-140	Scarlett	-1,1310	0,4195	289	-2,70	0,0074	Dunnett	0,1688	4,4833	5,6143	-20,1442	p <0.01
	24	Genotype	S42IL-141	Scarlett	-1,1571	0,4030	289	-2,87	0,0044	Dunnett	0,1111	4,4571	5,6143	-20,6107	p <0.01
	24	Genotype	S42IL-142	Scarlett	-1,2857	0,4030	289	-3,19	0,0016	Dunnett	0,0472	4,3286	5,6143	-22,9008	p <0.01
	24	Genotype	S42IL-112	Scarlett	-0,9429	0,4030	289	-2,34	0,0200	Dunnett	0,3528	4,6714	5,6143	-16,7939	p <0.05

	24	Genotype	S42IL-113	Scarlett	-0,8143	0,4030	289	-2,02	0,0443	Dunnett	0,5929	4,8000	5,6143	-14,5038	p <0.05
	24	Genotype	S42IL-117	Scarlett	-0,8000	0,4030	289	-1,99	0,0481	Dunnett	0,6224	4,8143	5,6143	-14,2494	p <0.05
	24	Genotype	S42IL-120	Scarlett	-1,0286	0,4030	289	-2,55	0,0112	Dunnett	0,2317	4,5857	5,6143	-18,3206	p <0.05
	24	Genotype	S42IL-122	Scarlett	-0,8143	0,4030	289	-2,02	0,0443	Dunnett	0,5929	4,8000	5,6143	-14,5038	p <0.05
	24	Genotype	S42IL-128	Scarlett	-0,8714	0,4030	289	-2,16	0,0314	Dunnett	0,4792	4,7429	5,6143	-15,5216	p <0.05
	24	Genotype	S42IL-129	Scarlett	-0,9000	0,4030	289	-2,23	0,0263	Dunnett	0,4261	4,7143	5,6143	-16,0305	p <0.05
	24	Genotype	S42IL-133	Scarlett	-1,0143	0,4030	289	-2,52	0,0124	Dunnett	0,2495	4,6000	5,6143	-18,0662	p <0.05
	24	Genotype	S42IL-135	Scarlett	-1,0429	0,4030	289	-2,59	0,0102	Dunnett	0,2148	4,5714	5,6143	-18,5751	p <0.05
RSD/RSW	24	Genotype	S42IL-143	Scarlett	0,6931	0,1912	289	3,6259	0,0003	Dunnett	0,0121	2,5127	1,8196	38,0905	p <0.001
	24	Genotype	S42IL-128	Scarlett	-0,3911	0,1912	289	-2,0463	0,0416	Dunnett	0,5717	1,4284	1,8196	-21,4962	p <0.05
1stLBL	24	Genotype	S42IL-106	Scarlett	-4,9692	1,1329	289	-4,39	0,0000	Dunnett	0,0007	9,9062	14,8754	-33,4054	p <0.001
	24	Genotype	S42IL-107	Scarlett	-4,3278	1,1792	289	-3,67	0,0003	Dunnett	0,0105	10,5476	14,8754	-29,0936	p <0.001
	24	Genotype	S42IL-108	Scarlett	-4,2961	1,1329	289	-3,79	0,0002	Dunnett	0,0068	10,5793	14,8754	-28,8806	p <0.001
	24	Genotype	S42IL-124	Scarlett	-7,7562	1,1792	289	-6,58	0,0000	Dunnett	0,0000	7,1192	14,8754	-52,1413	p <0.001
	24	Genotype	S42IL-125	Scarlett	-3,8453	1,1329	289	-3,39	0,0008	Dunnett	0,0257	11,0301	14,8754	-25,8498	p <0.001
	24	Genotype	S42IL-129	Scarlett	-5,2784	1,1329	289	-4,66	0,0000	Dunnett	0,0002	9,5970	14,8754	-35,4841	p <0.001
	24	Genotype	S42IL-132	Scarlett	-4,1119	1,1329	289	-3,63	0,0003	Dunnett	0,0120	10,7635	14,8754	-27,6421	p <0.001
	24	Genotype	S42IL-134	Scarlett	-4,2777	1,1329	289	-3,78	0,0002	Dunnett	0,0073	10,5977	14,8754	-28,7570	p <0.001
	24	Genotype	S42IL-138	Scarlett	-6,3531	1,1329	289	-5,61	0,0000	Dunnett	0,0000	8,5223	14,8754	-42,7089	p <0.001
	24	Genotype	S42IL-140	Scarlett	-4,2608	1,1792	289	-3,61	0,0004	Dunnett	0,0127	10,6146	14,8754	-28,6434	p <0.001
	24	Genotype	S42IL-141	Scarlett	-4,2641	1,1329	289	-3,76	0,0002	Dunnett	0,0076	10,6113	14,8754	-28,6652	p <0.001
	24	Genotype	S42IL-143	Scarlett	-9,9224	1,1329	289	-8,76	0,0000	Dunnett	0,0000	4,9530	14,8754	-66,7034	p <0.001
	24	Genotype	S42IL-113	Scarlett	-3,1992	1,1329	289	-2,82	0,0051	Dunnett	0,1248	11,6762	14,8754	-21,5066	p <0.01
	24	Genotype	S42IL-114	Scarlett	-3,3649	1,1792	289	-2,85	0,0046	Dunnett	0,1161	11,5105	14,8754	-22,6203	p <0.01
	24	Genotype	S42IL-115	Scarlett	-3,1103	1,1329	289	-2,75	0,0064	Dunnett	0,1506	11,7651	14,8754	-20,9091	p <0.01
	24	Genotype	S42IL-120	Scarlett	-3,2475	1,1329	289	-2,87	0,0045	Dunnett	0,1124	11,6279	14,8754	-21,8312	p <0.01
	24	Genotype	S42IL-126	Scarlett	-3,3519	1,1329	289	-2,96	0,0033	Dunnett	0,0889	11,5235	14,8754	-22,5334	p <0.01
	24	Genotype	S42IL-128	Scarlett	-3,3229	1,1329	289	-2,93	0,0036	Dunnett	0,0950	11,5525	14,8754	-22,3379	p <0.01
	24	Genotype	S42IL-136	Scarlett	-3,1000	1,1792	289	-2,63	0,0090	Dunnett	0,1963	11,7754	14,8754	-20,8398	p <0.01
	24	Genotype	S42IL-139	Scarlett	-3,2130	1,1792	289	-2,72	0,0068	Dunnett	0,1580	11,6624	14,8754	-21,5992	p <0.01
	24	Genotype	S42IL-101	Scarlett	-2,6173	1,1329	289	-2,31	0,0216	Dunnett	0,3722	12,2581	14,8754	-17,5949	p <0.05
	24	Genotype	S42IL-103	Scarlett	-2,3989	1,1792	289	-2,03	0,0428	Dunnett	0,5815	12,4765	14,8754	-16,1266	p <0.05
	24	Genotype	S42IL-109	Scarlett	-2,4866	1,1329	289	-2,19	0,0290	Dunnett	0,4544	12,3888	14,8754	-16,7163	p <0.05
	24	Genotype	S42IL-111	Scarlett	-2,3379	1,1329	289	-2,06	0,0399	Dunnett	0,5575	12,5375	14,8754	-15,7168	p <0.05
	24	Genotype	S42IL-112	Scarlett	-2,2926	1,1329	289	-2,02	0,0439	Dunnett	0,5903	12,5828	14,8754	-15,4118	p <0.05
	24	Genotype	S42IL-118	Scarlett	-2,3141	1,1329	289	-2,04	0,0420	Dunnett	0,5747	12,5613	14,8754	-15,5565	p <0.05
	24	Genotype	S42IL-121	Scarlett	-2,3984	1,1329	289	-2,12	0,0351	Dunnett	0,5145	12,4770	14,8754	-16,1233	p <0.05
	24	Genotype	S42IL-123	Scarlett	2,9027	1,1792	289	2,46	0,0144	Dunnett	0,2790	17,7781	14,8754	19,5134	p <0.05
	24	Genotype	S42IL-127	Scarlett	-2,2462	1,1329	289	-1,98	0,0484	Dunnett	0,6243	12,6292	14,8754	-15,0998	p <0.05
	24	Genotype	S42IL-135	Scarlett	-2,8879	1,1329	289	-2,55	0,0113	Dunnett	0,2332	11,9875	14,8754	-19,4139	p <0.05
1stLTL	24	Genotype	S42IL-106	Scarlett	-5,1718	1,3105	289	-3,95	0,0001	Dunnett	0,0039	14,7477	19,9195	-25,9635	p <0.001
	24	Genotype	S42IL-107	Scarlett	-4,9606	1,3640	289	-3,64	0,0003	Dunnett	0,0117	14,9590	19,9195	-24,9031	p <0.001
	24	Genotype	S42IL-124	Scarlett	-8,9146	1,3640	289	-6,54	0,0000	Dunnett	0,0000	11,0049	19,9195	-44,7533	p <0.001
	24	Genotype	S42IL-129	Scarlett	-5,4356	1,3105	289	-4,15	0,0000	Dunnett	0,0018	14,4840	19,9195	-27,2876	p <0.001
	24	Genotype	S42IL-138	Scarlett	-5,9912	1,3105	289	-4,57	0,0000	Dunnett	0,0003	13,9283	19,9195	-30,0772	p <0.001
	24	Genotype	S42IL-141	Scarlett	-4,3628	1,3105	289	-3,33	0,0010	Dunnett	0,0313	15,5567	19,9195	-21,9021	p <0.001
	24	Genotype	S42IL-143	Scarlett	-12,3712	1,3105	289	-9,44	0,0000	Dunnett	0,0000	7,5484	19,9195	-62,1056	p <0.001
	24	Genotype	S42IL-108	Scarlett	-4,0765	1,3105	289	-3,11	0,0021	Dunnett	0,0591	15,8430	19,9195	-20,4651	p <0.01
	24	Genotype	S42IL-125	Scarlett	-3,7653	1,3105	289	-2,87	0,0044	Dunnett	0,1105	16,1542	19,9195	-18,9026	p <0.01
	24	Genotype	S42IL-132	Scarlett	-3,4336	1,3105	289	-2,62	0,0093	Dunnett	0,2001	16,4859	19,9195	-17,2374	p <0.01
	24	Genotype	S42IL-134	Scarlett	-3,9271	1,3105	289	-3,00	0,0030	Dunnett	0,0805	15,9925	19,9195	-19,7147	p <0.01
	24	Genotype	S42IL-140	Scarlett	-3,7366	1,3640	289	-2,74	0,0065	Dunnett	0,1527	16,1829	19,9195	-18,7587	p <0.01

	24	Genotype	S42IL-111	Scarlett	-2,8688	1,3105	289	-2,19	0,0294	Dunnett	0,4587	17,0507	19,9195	-14,4019	p <0.05
	24	Genotype	S42IL-113	Scarlett	-2,9585	1,3105	289	-2,26	0,0247	Dunnett	0,4086	16,9611	19,9195	-14,8521	p <0.05
	24	Genotype	S42IL-115	Scarlett	-2,5842	1,3105	289	-1,97	0,0496	Dunnett	0,6332	17,3353	19,9195	-12,9731	p <0.05
	24	Genotype	S42IL-120	Scarlett	-3,0030	1,3105	289	-2,29	0,0226	Dunnett	0,3848	16,9165	19,9195	-15,0758	p <0.05
	24	Genotype	S42IL-123	Scarlett	3,4340	1,3640	289	2,52	0,0124	Dunnett	0,2490	23,3535	19,9195	17,2393	p <0.05
	24	Genotype	S42IL-126	Scarlett	-3,0151	1,3105	289	-2,30	0,0221	Dunnett	0,3786	16,9044	19,9195	-15,1364	p <0.05
	24	Genotype	S42IL-128	Scarlett	-3,1387	1,3105	289	-2,40	0,0173	Dunnett	0,3178	16,7809	19,9195	-15,7567	p <0.05
	24	Genotype	S42IL-139	Scarlett	-2,8919	1,3640	289	-2,12	0,0348	Dunnett	0,5120	17,0276	19,9195	-14,5181	p <0.05
2ndLTL	24	Genotype	S42IL-103	Scarlett	4,9883	1,3624	289	3,66	0,0003	Dunnett	0,0108	21,3551	16,3668	30,4779	p <0.001
	24	Genotype	S42IL-108	Scarlett	4,6501	1,3089	289	3,55	0,0004	Dunnett	0,0155	21,0169	16,3668	28,4117	p <0.001
	24	Genotype	S42IL-113	Scarlett	4,5015	1,3089	289	3,44	0,0007	Dunnett	0,0223	20,8683	16,3668	27,5037	p <0.001
	24	Genotype	S42IL-114	Scarlett	6,2507	1,3624	289	4,59	0,0000	Dunnett	0,0003	22,6175	16,3668	38,1915	p <0.001
	24	Genotype	S42IL-115	Scarlett	5,9917	1,3089	289	4,58	0,0000	Dunnett	0,0003	22,3585	16,3668	36,6089	p <0.001
	24	Genotype	S42IL-118	Scarlett	7,1348	1,3089	289	5,45	0,0000	Dunnett	0,0000	23,5016	16,3668	43,5933	p <0.001
	24	Genotype	S42IL-120	Scarlett	5,4671	1,3089	289	4,18	0,0000	Dunnett	0,0016	21,8339	16,3668	33,4037	p <0.001
	24	Genotype	S42IL-121	Scarlett	5,6522	1,3089	289	4,32	0,0000	Dunnett	0,0009	22,0190	16,3668	34,5345	p <0.001
	24	Genotype	S42IL-132	Scarlett	6,6070	1,3089	289	5,05	0,0000	Dunnett	0,0000	22,9738	16,3668	40,3682	p <0.001
	24	Genotype	S42IL-134	Scarlett	4,7122	1,3089	289	3,60	0,0004	Dunnett	0,0132	21,0790	16,3668	28,7909	p <0.001
	24	Genotype	S42IL-136	Scarlett	7,4672	1,3624	289	5,48	0,0000	Dunnett	0,0000	23,8340	16,3668	45,6238	p <0.001
	24	Genotype	S42IL-138	Scarlett	6,2850	1,3089	289	4,80	0,0000	Dunnett	0,0001	22,6518	16,3668	38,4008	p <0.001
	24	Genotype	S42IL-139	Scarlett	5,9483	1,3624	289	4,37	0,0000	Dunnett	0,0008	22,3151	16,3668	36,3436	p <0.001
	24	Genotype	S42IL-142	Scarlett	5,5878	1,3089	289	4,27	0,0000	Dunnett	0,0011	21,9546	16,3668	34,1407	p <0.001
	24	Genotype	S42IL-143	Scarlett	-6,7513	1,3089	289	-5,16	0,0000	Dunnett	0,0000	9,6156	16,3668	-41,2497	p <0.001
	24	Genotype	S42IL-162	Scarlett	5,9423	1,3624	289	4,36	0,0000	Dunnett	0,0008	22,3091	16,3668	36,3067	p <0.001
	24	Genotype	S42IL-107	Scarlett	3,6618	1,3624	289	2,69	0,0076	Dunnett	0,1720	20,0286	16,3668	22,3734	p <0.01
	24	Genotype	S42IL-112	Scarlett	4,2954	1,3089	289	3,28	0,0012	Dunnett	0,0361	20,6622	16,3668	26,2443	p <0.01
	24	Genotype	S42IL-130	Scarlett	4,0316	1,3089	289	3,08	0,0023	Dunnett	0,0643	20,3984	16,3668	24,6328	p <0.01
	24	Genotype	S42IL-135	Scarlett	3,4367	1,3089	289	2,63	0,0091	Dunnett	0,1978	19,8035	16,3668	20,9977	p <0.01
	24	Genotype	S42IL-101	Scarlett	3,2832	1,3089	289	2,51	0,0127	Dunnett	0,2538	19,6500	16,3668	20,0599	p <0.05
	24	Genotype	S42IL-109	Scarlett	2,8084	1,3089	289	2,15	0,0327	Dunnett	0,4921	19,1752	16,3668	17,1592	p <0.05
	24	Genotype	S42IL-125	Scarlett	2,6736	1,3089	289	2,04	0,0420	Dunnett	0,5747	19,0405	16,3668	16,3358	p <0.05
	24	Genotype	S42IL-126	Scarlett	2,7237	1,3089	289	2,08	0,0383	Dunnett	0,5434	19,0906	16,3668	16,6419	p <0.05
	24	Genotype	S42IL-141	Scarlett	2,7620	1,3089	289	2,11	0,0357	Dunnett	0,5200	19,1288	16,3668	16,8757	p <0.05

Table S14. putative quantitative trait loci (QTL) for A) root and B) shoot traits tested.

A

Trait	S42IL	QTL	chromosome	LSMeans_24°C_genotype	StdErr_24°C_genotype	LSMeans_24°C_Scarlett	StdErr_24°C_Scarlett	Diff	p-value (DT)	position [cM]
RSAL	-124	QRSAL.S42IL.4H	-4H	80,4125	5,2423	62,1947	3,1457	29,2915	0,0006	113.4-115.2
			-5H	80,4125	5,2423	62,1947	3,1457	29,2915	0,0006	not unambiguous
			-7H	80,4125	5,2423	62,1947	3,1457	29,2915	0,0006	not unambiguous
	-107		-2H	74,6743	5,2423	62,1947	3,1457	20,0654	0,0179	not unambiguous
RSAR	-103		-1H	43,8018	5,4739	74,1711	3,6827	-40,9449	0,0000	not unambiguous
	-110	QRSAR.S42IL.2Ha	-2H	53,7127	5,2592	74,1711	3,6827	-27,5827	0,0001	89.15-91
		QRSAR.S42IL.2Hb	-2H	53,7127	5,2592	74,1711	3,6827	-27,5827	0,0001	147,5-149,5
	-127	QRSAR.S42IL.5Hc	-5H	56,3014	5,2592	74,1711	3,6827	-24,0925	0,0008	138.5-140.1
		QRSAR.S42IL.5Hd	-5H	56,3014	5,2592	74,1711	3,6827	-24,0925	0,0008	142-152.6
	-176		-1H	57,6527	5,2592	74,1711	3,6827	-22,2707	0,0019	not unambiguous
		QRSAR.S42IL.3Ha	-3H	57,6527	5,2592	74,1711	3,6827	-22,2707	0,0019	0-8.9
		QRSAR.S42IL.5Hc	-5H	57,6527	5,2592	74,1711	3,6827	-22,2707	0,0019	138.5-140.1
		QRSAR.S42IL.5Ha	-5H	57,6527	5,2592	74,1711	3,6827	-22,2707	0,0019	106-121.3
		QRSAR.S42IL.5Hb	-5H	57,6527	5,2592	74,1711	3,6827	-22,2707	0,0019	121.3-138.3
	-140	QRSAR.S42IL.3Hb	-3H	59,1988	5,4739	74,1711	3,6827	-20,1862	0,0066	96.5-98.7
	-108		-2H	59,2877	5,2592	74,1711	3,6827	-20,0663	0,0050	not unambiguous
	-126	QRSAR.S42IL.5Ha	-5H	60,6404	5,2592	74,1711	3,6827	-18,2426	0,0106	106-121.3
	-135	QRSAR.S42IL.7H	-7H	61,6369	5,2592	74,1711	3,6827	-16,8991	0,0178	70.2-74.4
	-132		-6H	61,7150	5,2592	74,1711	3,6827	-16,7938	0,0185	not unambiguous
	-116	QRSAR.S42IL.4Ha	-4H	61,8957	5,2592	74,1711	3,6827	-16,5501	0,0203	1.3-15
		QRSAR.S42IL.4Hb	-4H	61,8957	5,2592	74,1711	3,6827	-16,5501	0,0203	17,8-22,2
			-6H	61,8957	5,2592	74,1711	3,6827	-16,5501	0,0203	not unambiguous
	-125		-5H	62,4354	5,2592	74,1711	3,6827	-15,8225	0,0264	not unambiguous
	-131		-6H	62,5287	5,2592	74,1711	3,6827	-15,6967	0,0276	not unambiguous
			-3H	62,5287	5,2592	74,1711	3,6827	-15,6967	0,0276	not unambiguous
	-123		-1H	62,5497	5,4739	74,1711	3,6827	-15,6685	0,0346	not unambiguous
		QRSAR.S42IL.2Hc	-2H	62,5497	5,4739	74,1711	3,6827	-15,6685	0,0346	120.7-129.8
		QRSAR.S42IL.4Hc	-4H	62,5497	5,4739	74,1711	3,6827	-15,6685	0,0346	100,8-110,2
	-136		-4H	63,0772	5,4739	74,1711	3,6827	-14,9573	0,0436	not unambiguous
			-7H	63,0772	5,4739	74,1711	3,6827	-14,9573	0,0436	not unambiguous
RSALR	-124	QRSALR.S42IL.4H	-4H	157,0990	8,8957	136,3659	3,1249	15,2041	0,0205	113.4-115.2
			-5H	157,0990	8,8957	136,3659	3,1249	15,2041	0,0205	not unambiguous
			-7H	157,0990	8,8957	136,3659	3,1249	15,2041	0,0205	not unambiguous
	-126	QRSALR.S42IL.5Ha	-5H	117,8949	8,5467	136,3659	3,1249	-13,5452	0,0315	106-121.25
	-108		-2H	115,7866	8,5467	136,3659	3,1249	-15,0912	0,0167	not unambiguous
	-176		-1H	112,6409	8,5467	136,3659	3,1249	-17,3980	0,0059	not unambiguous
		QRSALR.S42IL.3H	-3H	112,6409	8,5467	136,3659	3,1249	-17,3980	0,0059	0-8.9
		QRSALR.S42IL.5Ha	-5H	112,6409	8,5467	136,3659	3,1249	-17,3980	0,0059	106-121.25
		QRSALR.S42IL.5Hb	-5H	112,6409	8,5467	136,3659	3,1249	-17,3980	0,0059	121.3-138.3
	-103		-1H	100,7402	8,8957	136,3659	3,1249	-26,1251	0,0001	not unambiguous
NSR	-105	QNSR.S42IL.1H	-1H	5,7143	0,2309	6,4286	0,2020	-11,1111	0,0022	54.4-56
	-109	QNSR.S42IL.2H	-2H	5,8571	0,2309	6,4286	0,2020	-8,8889	0,0139	59.5-62.5

	-111		-1H	5,8571	0,2309	6,4286	0,2020	-8,8889	0,0139	not unambiguous
			-2H	5,8571	0,2309	6,4286	0,2020	-8,8889	0,0139	not unambiguous
		QNSR.S42IL.3Ha	-3H	5,8571	0,2309	6,4286	0,2020	-8,8889	0,0139	47.3-54.5
	-112	QNSR.S42IL.3Hb	-3H	5,8571	0,2309	6,4286	0,2020	-8,8889	0,0139	64.5-76.3
	-117		-4H	5,8571	0,2309	6,4286	0,2020	-8,8889	0,0139	not unambiguous
NLR	-131		-3H	808,5714	57,6661	669,1429	32,4532	20,8369	0,0162	not unambiguous
			-6H	808,5714	57,6661	669,1429	32,4532	20,8369	0,0162	not unambiguous
LSR/NSR	**-104**		-1H	32,8670	2,0749	28,7061	1,0774	14,4949	0,0459	not unambiguous
		QLSR/NSR.S42IL.2H	-2H	32,8670	2,0749	28,7061	1,0774	14,4949	0,0459	0-7.8
	-107		-2H	33,6868	2,1596	28,7061	1,0774	17,3507	0,0218	not unambiguous
	-117		-4H	33,7290	2,0749	28,7061	1,0774	17,4977	0,0161	not unambiguous
	-121		-3H	33,2282	2,0749	28,7061	1,0774	15,7531	0,0301	not unambiguous
			-4H	33,2282	2,0749	28,7061	1,0774	15,7531	0,0301	not unambiguous
	-126		-5H	33,0264	2,0749	28,7061	1,0774	15,0501	0,0382	not unambiguous
	-162		-4H	34,4409	2,1596	28,7061	1,0774	19,9777	0,0084	not unambiguous
LLR/NLR	**-134**	QLLR/NLR.S42IL.2Hc	-7H	0,4258	0,0510	0,8220	0,0487	-48,2037	0,0000	61,5-67,4
	-116	QLLR/NLR.S42IL.4Ha	-4H	0,4626	0,0510	0,8220	0,0487	-43,7243	0,0000	1,3-15
		QLLR/NLR.S42IL.4Hb	-4H	0,4626	0,0510	0,8220	0,0487	-43,7243	0,0000	17,8-22,2
			-6H	0,4626	0,0510	0,8220	0,0487	-43,7243	0,0000	not unambiguous
	-138	QLLR/NLR.S42IL.1Hf	-1H	0,4645	0,0510	0,8220	0,0487	-43,4915	0,0000	82.6-100.1
		QLLR/NLR.S42IL.7Hb	-7H	0,4645	0,0510	0,8220	0,0487	-43,4915	0,0000	119,5-126,7
		QLLR/NLR.S42IL.7Hc	-7H	0,4645	0,0510	0,8220	0,0487	-43,4915	0,0000	128,3-129,7
	-120		-4H	0,4655	0,0510	0,8220	0,0487	-43,3735	0,0000	not unambiguous
	-161		-3H	0,4763	0,0510	0,8220	0,0487	-42,0527	0,0000	not unambiguous
	-141	QLLR/NLR.S42IL.1Hc	-1H	0,4882	0,0510	0,8220	0,0487	-40,6019	0,0000	58.4-62.3
		QLLR/NLR.S42IL.1Hd	-1H	0,4882	0,0510	0,8220	0,0487	-40,6019	0,0000	62.8-80.2
		QLLR/NLR.S42IL.5Hd	-5H	0,4882	0,0510	0,8220	0,0487	-40,6019	0,0000	165,8-189,4
	-108	QLLR/NLR.S42IL.2Hb	-2H	0,4917	0,0510	0,8220	0,0487	-40,1827	0,0000	18,5-33,5
	-162		-4H	0,5041	0,0531	0,8220	0,0487	-38,6694	0,0000	not unambiguous
	-127	QLLR/NLR.S42IL.5Hb	-5H	0,5112	0,0510	0,8220	0,0487	-37,8146	0,0000	138.5-140.1
		QLLR/NLR.S42IL.5Hc	-5H	0,5112	0,0510	0,8220	0,0487	-37,8146	0,0000	143,1-152,6
	-122		-4H	0,5216	0,0510	0,8220	0,0487	-36,5384	0,0000	not unambiguous
		QLLR/NLR.S42IL.6He	-6H	0,5216	0,0510	0,8220	0,0487	-36,5384	0,0000	113,2-126,6
		QLLR/NLR.S42IL.7Ha	-7H	0,5216	0,0510	0,8220	0,0487	-36,5384	0,0000	2,5-11
	-102	QLLR/NLR.S42IL.1Ha	-1H	0,5248	0,0531	0,8220	0,0487	-36,1504	0,0000	15.1-32.2
		QLLR/NLR.S42IL.1Hc	-1H	0,5248	0,0531	0,8220	0,0487	-36,1504	0,0000	58.4-62.3
	-137		-2H	0,5309	0,0531	0,8220	0,0487	-35,4159	0,0000	not unambiguous
			-3H	0,5309	0,0531	0,8220	0,0487	-35,4159	0,0000	not unambiguous
			-4H	0,5309	0,0531	0,8220	0,0487	-35,4159	0,0000	not unambiguous
		QLLR/NLR.S42IL.7Hb	-7H	0,5309	0,0531	0,8220	0,0487	-35,4159	0,0000	119,5-126,7
	-107	QLLR/NLR.S42IL.2Hb	-2H	0,5412	0,0531	0,8220	0,0487	-34,1536	0,0000	18,5-33,5
	-104		-1H	32,8670	2,0749	28,7061	1,0774	14,4949	0,0459	not unambiguous
		QLSR/NSR.S42IL.2H	-2H	32,8670	2,0749	28,7061	1,0774	14,4949	0,0459	0-7.8
			-6H	0,5427	0,0510	0,8220	0,0487	-33,9822	0,0000	not unambiguous
	-117		-4H	0,5456	0,0510	0,8220	0,0487	-33,6182	0,0000	not unambiguous

Group	ID	Name	H	Col1	Col2	Col3	Col4	Col5	Col6	Range
		QLLR/NLR.S42IL.1He	-1H	0,5477	0,0510	0,8220	0,0487	-33,3656	0,0000	82.6-100.1
		QLLR/NLR.S42IL.1Hf	-1H	0,5477	0,0510	0,8220	0,0487	-33,3656	0,0000	100.35-116.3
			-5H	0,5477	0,0510	0,8220	0,0487	-33,3656	0,0000	not unambiguous
			-7H	0,5477	0,0510	0,8220	0,0487	-33,3656	0,0000	not unambiguous
	-119		-3H	0,5494	0,0510	0,8220	0,0487	-33,1621	0,0000	not unambiguous
			-4H	0,5494	0,0510	0,8220	0,0487	-33,1621	0,0000	not unambiguous
	-170		-7H	0,5628	0,0510	0,8220	0,0487	-31,5278	0,0000	not unambiguous
	-131		-3H	0,5647	0,0510	0,8220	0,0487	-31,2965	0,0000	not unambiguous
		QLLR/NLR.S42IL.6Hd	-6H	0,5647	0,0510	0,8220	0,0487	-31,2965	0,0000	91,1-91,7
	-118		-3H	0,5653	0,0510	0,8220	0,0487	-31,2304	0,0000	not unambiguous
			-4H	0,5653	0,0510	0,8220	0,0487	-31,2304	0,0000	not unambiguous
	-105	QLLR/NLR.S42IL.1Hb	-1H	0,5674	0,0510	0,8220	0,0487	-30,9682	0,0000	54.4-56
	-114		-3H	0,5701	0,0531	0,8220	0,0487	-30,6484	0,0000	not unambiguous
		QLLR/NLR.S42IL.5Ha	-5H	0,5701	0,0531	0,8220	0,0487	-30,6484	0,0000	48,8-50
			-7H	0,5701	0,0531	0,8220	0,0487	-30,6484	0,0000	not unambiguous
	-129	QLLR/NLR.S42IL.6Ha	-6H	0,5732	0,0510	0,8220	0,0487	-30,2628	0,0000	38.1-59.6
	-140	QLLR/NLR.S42IL.3H	-3H	0,5764	0,0531	0,8220	0,0487	-29,8770	0,0000	96.5-98.7
	-121		-3H	0,5872	0,0510	0,8220	0,0487	-28,5595	0,0000	not unambiguous
			-4H	0,5872	0,0510	0,8220	0,0487	-28,5595	0,0000	not unambiguous
	-110	QLLR/NLR.S42IL.2Hd	-2H	0,6009	0,0510	0,8220	0,0487	-26,8940	0,0000	89,15-91
		QLLR/NLR.S42IL.2He	-2H	0,6009	0,0510	0,8220	0,0487	-26,8940	0,0000	147,5-149,5
	-142		-1H	0,6428	0,0510	0,8220	0,0487	-21,8048	0,0005	not unambiguous
	-130		-3H	0,6623	0,0510	0,8220	0,0487	-19,4236	0,0019	not unambiguous
		QLLR/NLR.S42IL.6Hd	-6H	0,6623	0,0510	0,8220	0,0487	-19,4236	0,0019	91,1-91,7
		QLLR/NLR.S42IL.6Hb	-6H	0,6623	0,0510	0,8220	0,0487	-19,4236	0,0019	62,7-63,5
		QLLR/NLR.S42IL.6Hc	-6H	0,6623	0,0510	0,8220	0,0487	-19,4236	0,0019	64,3-65,7
TRL	-123	QTRL.S42IL.2H	-2H	234,2737	42,8895	725,7459	15,8731	-67,7196	0,0000	120.7-129.8
		QTRL.S42IL.4H	-4H	234,2737	42,8895	725,7459	15,8731	-67,7196	0,0000	100,8-110,2
	-105	QTRL.S42IL.1Hb	-1H	583,9666	41,2069	725,7459	15,8731	-19,5357	0,0007	54.4-56
	-117		-4H	590,4796	41,2069	725,7459	15,8731	-18,6382	0,0012	not unambiguous
	-102	QTRL.S42IL.1Ha	-1H	596,8280	42,8895	725,7459	15,8731	-17,7635	0,0029	15.1-32.2
	-107		-2H	602,3653	42,8895	725,7459	15,8731	-17,0005	0,0043	not unambiguous
	-131		-3H	613,0107	41,2069	725,7459	15,8731	-15,5337	0,0066	not unambiguous
			-6H	613,0107	41,2069	725,7459	15,8731	-15,5337	0,0066	not unambiguous
RDW	-129	QRDW.S42IL.6Hb	-6H	0,1969	0,0328	0,2951	0,0296	-33,2688	0,0030	46.7-59.6
		QRDW.S42IL.6Hc	-6H	0,1969	0,0328	0,2951	0,0296	-33,2688	0,0030	76.1
	-128	QRDW.S42IL.6Ha	-6H	0,2131	0,0328	0,2951	0,0296	-27,7893	0,0130	38-46.7
		QRDW.S42IL.6Hb	-6H	0,2131	0,0328	0,2951	0,0296	-27,7893	0,0130	46.7-59.6
	-161		-3H	0,2151	0,0328	0,2951	0,0296	-27,1310	0,0152	not unambiguous
	-109	QRDW.S42IL.2H	-2H	0,2158	0,0328	0,2951	0,0296	-26,8793	0,0162	59.5-62.5
	-127	QRDW.S42IL.5Ha	-5H	0,2164	0,0328	0,2951	0,0296	-26,6760	0,0170	138.5-140.1
		QRDW.S42IL.5Hb	-5H	0,2164	0,0328	0,2951	0,0296	-26,6760	0,0170	143.1-152.6
	-120		-4H	0,2293	0,0328	0,2951	0,0296	-22,3002	0,0457	not unambiguous
	-132		-6H	0,3600	0,0328	0,2951	0,0296	21,9904	0,0488	not unambiguous
RSW	-130		-3H	23,0776	1,7101	18,8213	1,6357	22,6142	0,0134	not unambiguous
		QRSW.S42IL.6H	-6H	23,0776	1,7101	18,8213	1,6357	22,6142	0,0134	62,7-63,5
	-137		-7H	22,6002	1,7800	18,8213	1,6357	20,0777	0,0346	not unambiguous

	-117		-4H	22,4123	1,7101	18,8213	1,6357	19,0795	0,0366	not unambiguous
RSW	-113		-3H	22,3839	1,7101	18,8213	1,6357	18,9284	0,0381	not unambiguous
CHA	-170		-7H	563,9367	44,0881	413,1751	42,8215	36,4885	0,0007	not unambiguous
	-130		-3H	530,3860	44,0881	413,1751	42,8215	28,3683	0,0083	not unambiguous
		QCHA.S42IL.6H	-6H	530,3860	44,0881	413,1751	42,8215	28,3683	0,0083	62.7-63.5
	-104	QCHA.S42IL.2H	-2H	518,1341	44,0881	413,1751	42,8215	25,4030	0,0179	0-7.8

B

Trait	S42IL		chromosome	LSMeans_24°C_genotype	StdErr_24°C_genotype	LSMeans_24°C_Scarlett	StdErr_24°C_Scarlett	Diff	p-value (DT)	position [cM]
1stLLA	-137		-7H	3,9833	0,4195	5,6143	0,2075	-29,0500	0,0001	not unambiguous
	-109	Q1stLLA.S42IL.2H	-2H	4,1714	0,4030	5,6143	0,2075	-25,6997	0,0004	59.5-60.8
	-110		-2H	4,3143	0,4030	5,6143	0,2075	-23,1552	0,0014	not unambiguous
	-142		-1H	4,3286	0,4030	5,6143	0,2075	-22,9008	0,0016	not unambiguous
	-135	Q1stLLA.S42IL.7Hb	-7H	4,5714	0,4030	5,6143	0,2075	-18,5751	0,0102	70.2-74.4
	-120		-4H	4,5857	0,4030	5,6143	0,2075	-18,3206	0,0112	not unambiguous
	-133		-1H	4,6000	0,4030	5,6143	0,2075	-18,0662	0,01238685	not unambiguous
		Q1stLLA.S42IL.3Ha	-3H	4,6000	0,4030	5,6143	0,2075	-18,0662	0,0124	36,8-40,7
		Q1stLLA.S42IL.5H	-5H	4,6000	0,4030	5,6143	0,2075	-18,0662	0,0124	0-0,1
		Q1stLLA.S42IL.6Hc	-6H	4,6000	0,4030	5,6143	0,2075	-18,0662	0,0124	76,1
		Q1stLLA.S42IL.7Ha	-7H	4,6000	0,4030	5,6143	0,2075	-18,0662	0,0124	11.8-34.3
	-112	Q1stLLA.S42IL.3Hb	-3H	4,6714	0,4030	5,6143	0,2075	-16,7939	0,0200	64.5-76.3
	-129	Q1stLLA.S42IL.6Hb	-6H	4,7143	0,4030	5,6143	0,2075	-16,0305	0,0263	47.5-55.7
		Q1stLLA.S42IL.6Hc	-6H	4,7143	0,4030	5,6143	0,2075	-16,0305	0,0263	76,1
	-128		-1H	4,7429	0,4030	5,6143	0,2075	-15,5216	0,0314	not unambiguous
		Q1stLLA.S42IL.6Hb	-6H	4,7429	0,4030	5,6143	0,2075	-15,5216	0,0314	47.5-55.7
		Q1stLLA.S42IL.6Ha	-6H	4,7429	0,4030	5,6143	0,2075	-15,5216	0,0314	38.1-46.7
	-113		-3H	4,8000	0,4030	5,6143	0,2075	-14,5038	0,0443	not unambiguous
	-117		-4H	4,8143	0,4030	5,6143	0,2075	-14,2494	0,0481	not unambiguous
1stLBL	**-138**	Q1stLBL.S42IL.7Hb	-7H	8,5223	1,1329	14,8754	0,1618	-42,7089	0,0000	128.3-129.4
	-129	Q1stLBL.S42IL.6Hb	-6H	9,5970	1,1329	14,8754	0,1618	-35,4841	0,0000	47.5-55.7
		Q1stLBL.S42IL.6Hc	-6H	9,5970	1,1329	14,8754	0,1618	-35,4841	0,0000	76.1
	-106	Q1stLBL.S42IL.2Ha	-2H	9,9062	1,1329	14,8754	0,1618	-33,4054	0,0000	8,9-12,1
		Q1stLBL.S42IL.2Hb	-2H	9,9062	1,1329	14,8754	0,1618	-33,4054	0,0000	12,5-16,5
	-107	Q1stLBL.S42IL.2Hb	-2H	10,5476	1,1792	14,8754	0,1618	-29,0936	0,0003	12,5-16,5
		Q1stLBL.S42IL.2Hc	-2H	10,5476	1,1792	14,8754	0,1618	-29,0936	0,0003	18,9-33,5
		Q1stLBL.S42IL.2Hd	-2H	10,5476	1,1792	14,8754	0,1618	-29,0936	0,0003	33,9-41,2
	-108	Q1stLBL.S42IL.2Hc	-2H	10,5793	1,1329	14,8754	0,1618	-28,8806	0,0002	12,5-16,5
		Q1stLBL.S42IL.2Hd	-2H	10,5793	1,1329	14,8754	0,1618	-28,8806	0,0002	33,9-41,2
		Q1stLBL.S42IL.2He	-2H	10,5793	1,1329	14,8754	0,1618	-28,8806	0,0002	41,9-52,2
	-141	Q1stLBL.S42IL.1Hb	-1H	10,6113	1,1329	14,8754	0,1618	-28,6652	0,0002	62,8-80.2
		Q1stLBL.S42IL.5Hc	-5H	10,6113	1,1329	14,8754	0,1618	-28,6652	0,0002	165,8-189,4
	-132		-6H	10,7635	1,1329	14,8754	0,1618	-27,6421	0,0003	not unambiguous
	-125		-5H	11,0301	1,1329	14,8754	0,1618	-25,8498	0,0008	not unambiguous
	-114		-3H	11,5105	1,1792	14,8754	0,1618	-22,6203	0,0046	not unambiguous
		Q1stLBL.S42IL.5Ha	-5H	11,5105	1,1792	14,8754	0,1618	-22,6203	0,0046	48,8-50
			-6H	11,5105	1,1792	14,8754	0,1618	-22,6203	0,0046	not unambiguous
	-126		-5H	11,5235	1,1329	14,8754	0,1618	-22,5334	0,0033	not unambiguous
	-128		-1H	11,5525	1,1329	14,8754	0,1618	-22,3379	0,0036	not unambiguous
		Q1stLBL.S42IL.6Hb	-6H	11,5525	1,1329	14,8754	0,1618	-22,3379	0,0036	38-46.7
		Q1stLBL.S42IL.6Hc	-6H	11,5525	1,1329	14,8754	0,1618	-22,3379	0,0036	47.5-55.7
	-120		-4H	11,6279	1,1329	14,8754	0,1618	-21,8312	0,0045	not unambiguous
	-113		-3H	11,6762	1,1329	14,8754	0,1618	-21,5066	0,0051	not unambiguous
	-115		-3H	11,7651	1,1329	14,8754	0,1618	-20,9091	0,0064	not unambiguous
			-6H	11,7651	1,1329	14,8754	0,1618	-20,9091	0,0064	not unambiguous
	-136		-4H	11,7754	1,1792	14,8754	0,1618	-20,8398	0,0090	not unambiguous
			-7H	11,7754	1,1792	14,8754	0,1618	-20,8398	0,0090	not unambiguous
	-135	Q1stLBL.S42IL.7Ha	-7H	11,9875	1,1329	14,8754	0,1618	-19,4139	0,0113	70.2-74,4
	-101	Q1stLBL.S42IL.1Ha	-1H	12,2581	1,1329	14,8754	0,1618	-17,5949	0,0216	0-9.9
	-109	Q1stLBL.S42IL.2Hd	-2H	12,3888	1,1329	14,8754	0,1618	-16,7163	0,0290	33,9-41,2
		Q1stLBL.S42IL.2He	-2H	12,3888	1,1329	14,8754	0,1618	-16,7163	0,0290	41,9-52,2
		Q1stLBL.S42IL.2Hf	-2H	12,3888	1,1329	14,8754	0,1618	-16,7163	0,0290	59,5-60,7
	-121		-3H	12,4770	1,1329	14,8754	0,1618	-16,1233	0,0351	not unambiguous
			-4H	12,4770	1,1329	14,8754	0,1618	-16,1233	0,0351	not unambiguous
	-111		-1H	12,5375	1,1329	14,8754	0,1618	-15,7168	0,0399	not unambiguous
			-2H	12,5375	1,1329	14,8754	0,1618	-15,7168	0,0399	not unambiguous
		Q1stLBL.S42IL.3Ha	-3H	12,5375	1,1329	14,8754	0,1618	-15,7168	0,0399	47.3-54.5
		Q1stLBL.S42IL.3Hb	-3H	12,5375	1,1329	14,8754	0,1618	-15,7168	0,0399	54,5-55,2

	-118		-3H	12,5613	1,1329	14,8754	0,1618	-15,5565	0,0420	not unambiguous
			-4H	12,5613	1,1329	14,8754	0,1618	-15,5565	0,0420	not unambiguous
	-112	**Q1stLBL.S42IL.3Hc**	-3H	12,5828	1,1329	14,8754	0,1618	-15,4118	0,0439	64.5-76.3
	-127	**Q1stLBL.S42IL.5Hb**	-5H	12,6292	1,1329	14,8754	0,1618	-15,0998	0,0484	142-152.6
	-123	**Q1stLBL.S42IL.2Hg**	-2H	17,7781	1,1792	14,8754	0,1618	19,5134	0,0144	120.7-129.8
		Q1stLBL.S42IL.4H	-4H	17,7781	1,1792	14,8754	0,1618	19,5134	0,0144	100,8-110,2
1stLTL	**-107**	**Q1stLTL.S42IL.2H**	-2H	14,9590	1,3640	19,9195	0,1713	-24,9031	0,0003	18.5-33.5
	-141	**Q1stLTL.S42IL.1H**	-1H	15,5567	1,3105	19,9195	0,1713	-21,9021	0,0010	62,8-80.2
		Q1stLTL.S42IL.5H	-5H	15,5567	1,3105	19,9195	0,1713	-21,9021	0,0010	165,8-189,4
	-108	**Q1stLTL.S42IL.2H**	-2H	15,8430	1,3105	19,9195	0,1713	-20,4651	0,0021	18.5-33.5
	-134	**Q1stLTL.S42IL.7H**	-7H	15,9925	1,3105	19,9195	0,1713	-19,7147	0,0030	67.8-70.2
	-132		-6H	16,4859	1,3105	19,9195	0,1713	-17,2374	0,0093	not unambiguous
	-128		-1H	16,7809	1,3105	19,9195	0,1713	-15,7567	0,0173	not unambiguous
		Q1stLTL.S42IL.6H	-6H	16,7809	1,3105	19,9195	0,1713	-15,7567	0,0173	38-46.7
	-126		-5H	16,9044	1,3105	19,9195	0,1713	-15,1364	0,0221	not unambiguous
	-120		-4H	16,9165	1,3105	19,9195	0,1713	-15,0758	0,0226	not unambiguous
	-113		-3H	16,9611	1,3105	19,9195	0,1713	-14,8521	0,0247	not unambiguous
	-139		-7H	17,0276	1,3640	19,9195	0,1713	-14,5181	0,0348	not unambiguous
2ndLTL	-136		-4H	23,8340	1,3624	16,3668	0,5432	45,6238	0,0000	not unambiguous
			-7H	23,8340	1,3624	16,3668	0,5432	45,6238	0,0000	not unambiguous
	-118		-3H	23,5016	1,3089	16,3668	0,5432	43,5933	0,0000	not unambiguous
			-4H	23,5016	1,3089	16,3668	0,5432	43,5933	0,0000	not unambiguous
	-132		-6H	22,9738	1,3089	16,3668	0,5432	40,3682	0,0000	not unambiguous
	-139		-7H	22,3151	1,3624	16,3668	0,5432	36,3436	0,0000	not unambiguous
	-162		-4H	22,3091	1,3624	16,3668	0,5432	36,3067	0,0000	not unambiguous
	-120		-4H	21,8339	1,3089	16,3668	0,5432	33,4037	0,0000	not unambiguous
	-103		-1H	21,3551	1,3624	16,3668	0,5432	30,4779	0,0003	not unambiguous
	-134	**Q2ndLTL.S42IL.7Ha**	-7H	21,0790	1,3089	16,3668	0,5432	28,7909	0,0004	67.8-70.2
	-108	**Q2ndLTL.S42IL.2Ha**	-2H	21,0169	1,3089	16,3668	0,5432	28,4117	0,0004	18.5-33.5
		Q2ndLTL.S42IL.2Hb	-2H	21,0169	1,3089	16,3668	0,5432	28,4117	0,0004	33.9-41.2
		Q2ndLTL.S42IL.2Hc	-2H	21,0169	1,3089	16,3668	0,5432	28,4117	0,0004	41.9-51.9
	-113		-3H	20,8683	1,3089	16,3668	0,5432	27,5037	0,0007	not unambiguous
	-112	**Q2ndLTL.S42IL.3H**	-3H	20,6622	1,3089	16,3668	0,5432	26,2443	0,0012	64.6-76.3
	-130		-3H	20,3984	1,3089	16,3668	0,5432	24,6328	0,0023	not unambiguous
		Q2ndLTL.S42IL.6H	-6H	20,3984	1,3089	16,3668	0,5432	24,6328	0,0023	62.7-63.5
	-107	**Q2ndLTL.S42IL.2Ha**	-2H	20,0286	1,3624	16,3668	0,5432	22,3734	0,0076	18.5-33.5
		Q2ndLTL.S42IL.2Hb	-2H	20,0286	1,3624	16,3668	0,5432	22,3734	0,0076	33.9-41.2
	-135	**Q2ndLTL.S42IL.7Hb**	-7H	19,8035	1,3089	16,3668	0,5432	20,9977	0,0091	70.2-74.4
	-101	**Q2ndLTL.S42IL.1Ha**	-1H	19,6500	1,3089	16,3668	0,5432	20,0599	0,0127	0-9.9
	-109	**Q2ndLTL.S42IL.2Hb**	-2H	19,1752	1,3089	16,3668	0,5432	17,1592	0,0327	33.9-41.2
		Q2ndLTL.S42IL.2Hc	-2H	19,1752	1,3089	16,3668	0,5432	17,1592	0,0327	41.9-51.9
		Q2ndLTL.S42IL.2Hd	-2H	19,1752	1,3089	16,3668	0,5432	17,1592	0,0327	59,5-60,7
	-141	**Q2ndLTL.S42IL.1Hb**	-1H	19,1288	1,3089	16,3668	0,5432	16,8757	0,0357	62,8--80.2
		Q2ndLTL.S42IL.5H	-5H	19,1288	1,3089	16,3668	0,5432	16,8757	0,0357	165,8-189,4
	-126		-5H	19,0906	1,3089	16,3668		16,6419	0,0383	not unambiguous
FWS	**-129**	**QFWS.S42IL.6Hb**	-6H	0,0336	0,0046	0,0489	0,0030	-31,2208	0,0010	47.5-55.7
		QFWS.S42IL.6Hc	-6H	0,0336	0,0046	0,0489	0,0030	-31,2208		76.1
	-128		-1H	0,0368	0,0046	0,0489	0,0030	-24,8540	0,0086	not unambiguous
		QFWS.S42IL.6Hb	-6H	0,0368	0,0046	0,0489	0,0030	-24,8540	0,0086	47.5-55.7
		QFWS.S42IL.6Ha	-6H	0,0368	0,0046	0,0489	0,0030	-24,8540	0,0086	38.1-55.7
	-123	**QFWS.S42IL.2H**	-2H	17,7781	0,0046	14,8754	0,0030	19,5134	0,0144	120.7-129.8
		QFWS.S42IL.4H	-4H	0,0590	0,0048	0,0489	0,0030	20,5169	0,0368	100.8-110.2
	-162		-4H	0,0618	0,0048	0,0489	0,0030	26,2753	0,0076	not unambiguous

significant different response to Scarlett (*p*<0.05)

Tables S15 overlapping and non-overlapping subsets of genotypes

A rootspecific_no overlap

S42IL	QTL	chromosome	LSMeans_24°C_genotype	StdErr_24°C_genotype	LSMeans_24°C_Scarlett	StdErr_24°C_Scarlett	Diff	p-value (DT)	position [cM]
-102	QLLR/NLR.S42IL.1Ha	-1H	0,5248	0,0531	0,8220	0,0487	-36,1504	0,0000	15,1-32,2
	QTRL.S42IL.1Ha		596,8280	42,8895	725,7459	15,8731	-17,7635	0,0029	
-105	QNSR.S42IL.1H	-1H	5,7143	0,2309	6,4286	0,2020	-11,1111	0,0022	54,4-57,3
	QLLR/NLR.S42IL.1Hb		0,5674	0,0510	0,8220	0,0487	-30,9682	0,0000	
	QTRL.S42IL.1Hb		583,9666	41,2069	725,7459	15,8731	-19,5357	0,0007	
-104	QLLR/NLR.S42IL.2Ha	-2H	0,5427	0,0510	0,8220	0,0487	-33,9822	0,0000	0-7,8
	QLSR/NSR.S42IL.2H		32,8670	2,0749	28,7061	1,0774	14,4949	0,0459	
	QCHA.S42IL.2H		518,1341	44,0881	413,1751	42,8215	25,4030	0,0179	
-110	QRSAR.S42IL.2Ha	-2H	53,7127	5,2592	74,1711	3,6827	-27,5827	0,0001	89,15-91
	QLLR/NLR.S42IL.2Hd		0,6009	0,0510	0,8220	0,0487	-26,8940	0,0000	
-110	QRSAR.S42IL.2Hb	-2H	53,7127	5,2592	74,1711	3,6827	-27,5827	0,0001	147,5-149,5
	QLLR/NLR.S42IL.2He		0,6009	0,0510	0,8220	0,0487	-26,8940	0,0000	
-176	QRSAR.S42IL.3Ha	-3H	57,6527	5,2592	74,1711	3,6827	-22,2707	0,0019	0-8.9
	QRSALR.S42IL.3H		112,6409	8,5467	136,3659	3,1249	-17,3980	0,0059	
-124	QRSAL.S42IL.4H	-4H	80,4125	5,2423	62,1947	3,1457	29,2915	0,0006	113.4-115.2
	QRSALR.S42IL.4H		157,0990	8,8957	136,3659	3,1249	15,2041	0,0205	

B shootspecific_no overlap

S42IL	QTL	chromosome	LSMeans_24°C_genotype	StdErr_24°C_genotype	LSMeans_24°C_Scarlett	StdErr_24°C_Scarlett	Diff	p-value (DT)	position [cM]
-101	Q1stLBL.S42IL.1Ha	-1H	12,2581	1,1329	14,8754	0,1618	-17,5949	0,0216	0-9.9
	Q2ndLTL.S42IL.1Ha		19,6500	1,3089	16,3668	0,5432	20,0599	0,0127	
-134	Q1stLTL.S42IL.7H	-7H	15,9925	1,3105	19,9195	0,1713	-19,7147	0,0030	67.8-70,2
	Q2ndLTL.S42IL.7Ha		21,0790	1,3089	16,3668	0,5432	28,7909	0,0004	

C rootspecific_overlap

S42IL	QTL	chromosome	LSMeans_24°C_genotype	StdErr_24°C_genotype	LSMeans_24°C_Scarlett	StdErr_24°C_Scarlett	Diff	p-value (DT)	position [cM]
-126	QRSALR.S42IL.5H	-5H	117,8949	8,5467	136,3659	3,1249	-13,5452	0,0315	
-176	QRSALR.S42IL.5H	-5H	112,6409	8,5467	136,3659	3,1249	-17,3980	0,0059	106-121.25
	QRSAR.S42IL.5Ha	-5H	57,6527	5,2592	74,1711	3,6827	-22,2707	0,0019	

D shootspecific_overlap

S42IL	QTL	chromosome	LSMeans_24°C_genotype	StdErr_24°C_genotype	LSMeans_24°C_Scarlett	StdErr_24°C_Scarlett	Diff	p-value (DT)	position [cM]
-107	Q1stLBL.S42IL.2Hd	-2H	10,5476	1,1792	14,8754	0,1618	-29,0936	0,0003	33,9-41,2
-108			10,5793	1,1329	14,8754	0,1618	-28,8806	0,0002	
-109			12,3888	1,1329	14,8754	0,1618	-16,7163	0,0290	
-108	Q2ndLTL.S42IL.2Hb		21,0169	1,3089	16,3668	0,5432	28,4117	0,0004	
-107			20,0286	1,3624	16,3668	0,5432	22,3734	0,0076	
-109			19,1752	1,3089	16,3668	0,5432	17,1592	0,0327	
-108	Q1stLBL.S42IL.2He	-2H	10,5793	1,1329	14,8754	0,1618	-28,8806	0,0002	41,9-52,2
-109			12,3888	1,1329	14,8754	0,1618	-16,7163	0,0290	
-108	Q2ndLTL.S42IL.2Hc		21,0169	1,3089	16,3668	0,5432	28,4117	0,0004	
-109			19,1752	1,3089	16,3668	0,5432	17,1592	0,0327	

E both_ overlap

S42IL	QTL	chromosome	LSMeans_24°C_genotype	StdErr_24°C_genotype	LSMeans_24°C_Scarlett	StdErr_24°C_Scarlett	Diff	p-value (DT)	position [cM]
-108	QLLR/NLR.S42IL.2Hb	-2H	0,4917	0,0510	0,8220	0,0487	-40,1827	0,0000	18,5-33,5
-107			0,5412	0,0531	0,8220	0,0487	-34,1536	0,0000	
-107	Q1stLBL.S42IL.2Hc		10,5476	1,1792	14,8754	0,1618	-29,0936	0,0003	
-107	Q1stLTL.S42IL.2H		14,9590	1,3640	19,9195	0,1713	-24,9031	0,0003	
-108			15,8430	1,3105	19,9195	0,1713	-20,4651	0,0021	
-108	Q2ndLTL.S42IL.2Ha		21,0169	1,3089	16,3668	0,5432	28,4117	0,0004	
-107			20,0286	1,3624	16,3668	0,5432	22,3734	0,0076	
-128	Q1stLBL.S42IL.6Hb	-6H	11,5525	1,1329	14,8754	0,1618	-22,3379	0,0036	38-46.7
	Q1stLTL.S42IL.6H		16,7809	1,3105	19,9195	0,1713	-15,7567	0,0173	
	Q1stLLA.S42IL.6Ha		0,2131	0,0328	0,2951	0,0296	-27,7893	0,0130	
	QFWS.S42IL.6Ha		1,4282	0,1912	1,8196	0,1882	-21,4962	0,0416	
	QRDW.S42IL.6H		4,7429	0,4030	5,6143	0,2075	-15,5216	0,0314	
	QRSD/RSW.S42IL.6H		0,0368	0,0046	0,0489	0,0030	-24,8540	0,0086	
-129	QLLR/NLR.S42IL.6Ha		0,5732	0,0510	0,8220	0,0487	-30,2628	0,0000	
-129	Q1stLLA.S42IL.6Hb	-6H	4,7143	0,4030	5,6143	0,2075	-16,0305	0,0263	47.5-55.7
-128			4,7429	0,4030	5,6143	0,2075	-15,5216	0,0314	
-129	Q1stLBL.S42IL.6Hb		9,5970	1,1329	14,8754	0,1618	-35,4841	0,0000	
-128			11,5525	1,1329	14,8754	0,1618	-22,3379	0,0036	
-129	QFWS.S42IL.6Hb		0,0336	0,0046	0,0489	0,0030	-31,2208	0,0010	
-128			0,0368	0,0046	0,0489	0,0030	-24,8540	0,0086	
-129	QRDW.S42IL.6Hb		0,1969	0,0328	0,2951	0,0296	-33,2688	0,0030	
-128			0,2131	0,0328	0,2951	0,0296	-27,7893	0,0130	
-129	Q1stLBL.S42IL.6Hc	-6H	9,5970	1,1329	14,8754	0,1618	-35,4841	0,0000	76.1
	QFWS.S42IL.6Hc		0,0336	0,0046	0,0489	0,0030	-31,2208	0,0010	
	QRDW.S42IL.6Ha		0,1969	0,0328	0,2951	0,0296	-33,2688	0,0030	
-133	Q1stLLA.S42IL.6Hc		4,6000	0,4030	5,6143	0,2075	-18,0662	0,0124	
-129			4,7143	0,4030	5,6143	0,2075	-16,0305	0,0263	

F both_no overlap

S42IL	QTL	chromosome	LSMeans_24°C_genotype	StdErr_24°C_genotype	LSMeans_24°C_Scarlett	StdErr_24°C_Scarlett	Diff	p-value (DT)	position [cM]
-141	Q2ndLTL.S42IL.1Hb	-1H	19,1288	1,3089	16,3668	0,5432	16,8757	0,0357	70.5--80.2
	Q1stLBL.S42IL.1Hb		10,6113	1,1329	14,8754	0,1618	-28,6652	0,0002	
	Q1stLTL.S42IL.1H		15,5567	1,3105	19,9195	0,1713	-21,9021	0,0010	
	QLLR/NLR.S42IL.1Hc		0,4882	0,0510	0,8220	0,0487	-40,6019	0,0000	
-123	Q1stLBL.S42IL.2Hg	-2H	17,7781	1,1792	14,8754	0,1618	19,5134	0,0144	120.7-129.8
	QFWS.S42IL.2H		17,7781	0,0046	14,8754	0,0030	19,5134	0,0144	
	QTRL.S42IL.2H		234,2737	42,8895	725,7459	15,8731	-67,7196	0,0000	
-109	Q1stLBL.S42IL.2Hf	-2H	12,3888	1,1329	14,8754	0,1618	-16,7163	0,0290	59,5-60,7
	Q2ndLTL.S42IL.2Hd		19,1752	1,3089	16,3668	0,5432	17,1592	0,0327	
	Q1stLLA.S42IL.2H		4,1714	0,4030	5,6143	0,2075	-25,6997	0,0004	
	QRDW.S42IL.2H		0,2158	0,0328	0,2951	0,0296	-26,8793	0,0162	
	QNSR.S42IL.2H		5,8571	0,2309	6,4286	0,2020	-8,8889	0,0139	
-111	Q1stLBL.S42IL.3Ha	-3H	12,5375	1,1329	14,8754	0,1618	-15,7168	0,0399	47.3-54.5
	QNSR.S42IL.3Ha		5,8571	0,2309	6,4286	0,2020	-8,8889	0,0139	
-112	Q1stLLA.S42IL.3Hb	-3H	4,6714	0,4030	5,6143	0,2075	-16,7939	0,0200	64.5-76.3
	Q1stLBL.S42IL.3Hc		12,5828	1,1329	14,8754	0,1618	-15,4118	0,0439	
	Q2ndLTL.S42IL.3H		20,6622	1,3089	16,3668	0,5432	26,2443	0,0012	
	QNSR.S42IL.3Hb		5,8571	0,2309	6,4286	0,2020	-8,8889	0,0139	
-123	Q1stLBL.S42IL.4H	-4H	17,7781	1,1792	14,8754	0,1618	19,5134	0,0144	100,8-110,2
	QRSAR.S42IL.4Hb		62,5497	5,4739	74,1711	3,6827	-15,6685	0,0346	
	QTRL.S42IL.4H		234,2737	42,8895	725,7459	15,8731	-67,7196	0,0000	
	QFWS.S42IL.4H		0,0590	0,0048	0,0489	0,0030	20,5169	0,0368	
-114	Q1stLBL.S42IL.5Ha	-5H	11,5105	1,1792	14,8754	0,1618	-22,6203	0,0046	48,8-50
	QLLR/NLR.S42IL.5Ha		0,5701	0,0531	0,8220	0,0487	-30,6484	0,0000	
-127	Q1stLBL.S42IL.5Hb	-5H	12,6292	1,1329	14,8754	0,1618	-15,0998	0,0484	142-152.6
	QRSAR.S42IL.5Hd		56,3014	5,2592	74,1711	3,6827	-24,0925	0,0008	
	QLLR/NLR.S42IL.5Hb		0,5112	0,0510	0,8220	0,0487	-37,8146	0,0000	
	QRDW.S42IL.5H		0,2164	0,0328	0,2951	0,0296	-26,6760	0,0170	
-141	Q1stLBL.S42IL.5Hc	-5H	10,6113	1,1329	14,8754	0,1618	-28,6652	0,0002	165,8-169,4
	Q1stLTL.S42IL.5H		15,5567	1,3105	19,9195	0,1713	-21,9021	0,0010	
	Q2ndLTL.S42IL.5H		19,1288	1,3089	16,3668	0,5432	16,8757	0,0357	
	QLLR/NLR.S42IL.5Hc		0,4882	0,0510	0,8220	0,0487	-40,6019	0,0000	

S42IL	QTL	chromosome	LSMeans_24°C_genotype	StdErr_24°C_genotype	LSMeans_24°C_Scarlett	StdErr_24°C_Scarlett	Diff	p-value (DT)	position [cM]
-130	Q2ndLTL.S42IL.6H	-6H	20,3984	1,3089	16,3668	0,5432	24,6328	0,0023	62.7-63.5
	QRSW.S42IL.6H		23,0776	1,7101	18,8213	1,6357	22,6142	0,0134	
	QCHA.S42IL.6H		530,3860	44,0881	413,1751	42,8215	28,3683	0,0083	
	QLLR/NLR.S42IL.6Hd		0,6623	0,0510	0,8220	0,0487	-19,4236	0,0019	
-135	Q1stLBL.S42IL.7Ha	-7H	11,9875	1,1329	14,8754	0,1618	-19,4139	0,0113	70.2-74,4
	Q1stLLA.S42IL.7Hb		4,5714	0,4030	5,6143	0,2075	-18,5751	0,0102	
	Q2ndLTL.S42IL.7Hb		19,8035	1,3089	16,3668	0,5432	20,9977	0,0091	
	QRSAR.S42IL.7H		61,6369	5,2592	74,1711	3,6827	-16,8991	0,0178	
-138	QLLR/NLR.S42IL.7Hc	-7H	0,4645	0,0510	0,8220	0,0487	-43,4915	0,0000	128,3-129,4
	Q1stLBL.S42IL.7Hb		8,5223	1,1329	14,8754	0,1618	-42,7089	0,0000	

G rootspecific_overlap_one trait

S42IL	QTL	chromosome	LSMeans_24°C_genotype	StdErr_24°C_genotype	LSMeans_24°C_Scarlett	StdErr_24°C_Scarlett	Diff	p-value (DT)	position [cM]
-127	QRSAR.S42IL.5Hc	-5H	56,3014	5,2592	74,1711	3,6827	-24,0925	0,0008	138.5-140.1
-176			57,6527	5,2592	74,1711	3,6827	-22,2707	0,0019	
-131	QLLR/NLR.S42IL.6Hb	-6H	0,5647	0,0510	0,8220	0,0487	-31,2965	0,0000	91,1-91,7
-130			0,6623	0,0510	0,8220	0,0487	-19,4236	0,0019	
-138	QLLR/NLR.S42IL.7Hb	-7H	0,4645	0,0510	0,8220	0,0487	-43,4915	0,0000	119,5-126,7
-137			0,5309	0,0531	0,8220	0,0487	-35,4159	0,0000	

H shootspecific_overlap_one trait

S42IL	QTL	chromosome	LSMeans_24°C_genotype	StdErr_24°C_genotype	LSMeans_24°C_Scarlett	StdErr_24°C_Scarlett	Diff	p-value (DT)	position [cM]
-106	Q1stLBL.S42IL.2Hb	-2H	9,9062	1,1329	14,8754	0,1618	-33,4054	0,0000	12,5-16,5
-107			10,5476	1,1792	14,8754	0,1618	-29,0936	0,0003	
-108			10,5793	1,1329	14,8754	0,1618	-28,8806	0,0002	

Table S16. Statistical differences for the relative temperature responses for all significantly tested ILs based on Dunnett test were assessed by two-way ANOVA (*p*< 0.05) of the absolute data.

Trait	S42IL	*P*-value
RSAL	-124	0.053
RSAR	-110	0.254
	-127	0.254
	-176	0.078
	-140	0.078
	-135	0.463
	-116	0.254
	-123	0.666
RSALR	-124	0.108
	-126	0.382
	-108	0.29
	-176	0.048
NSR	-105	0.248
	-109	0.678
	-111	0.678
	-112	0.301
LSR/NSR	-104	0.222
LLR/NLR	-134	5e−04
	-116	1e−04
	-138	1e−04
	-141	5e−05
	-108	6e−03
	-127	9e−05
	-122	1e−01
	-102	6e−04
	-137	1e−01
	-107	1e−02
	-104	6e−05
	-143	3e−03
	-131	8e−04
	-105	2e−01
	-114	4e−02
	-129	2e−04
	-110	8e−03
	-130	3e−03
TRL	-123	4e−18
	-105	1e−02
	-102	9e−04
RDW	-129	0.094
	-128	0.419
	-109	0.123
	-127	0.419
RSW	-130	0.466
CHA	-130	0.302
	-104	0.302
RSD/RSW	-128	0,4190

Trait	S42IL	*P*-values
1stLLA	-109	0,028
	-135	0,691
	-133	0,389
	-112	0,382
	-129	0,564
	-128	0,697
	-138	1e−02
	-129	6e−03
1stLBL	-106	7e−03
	-107	1e−02
	-108	5e−02
	-141	1e−01
	-114	2e−01
	-128	3e−01
	-135	2e−01
	-101	3e−01
	-109	2e−01
	-111	4e−01
	-112	4e−01
	-127	5e−01
	-123	3e−01
	-107	4e−03
	-141	1e−02
	-108	1e−02
1stLTL	-134	5e−01
	-128	4e−01
2ndLTL	-134	7e−04
	-108	3e−01
	-112	4e−02
	-130	1e−02
	-107	4e−01
	-135	1e−01
	-101	1e−01
	-109	4e−01
	-141	3e−01
	-129	0,138
	-128	0,703
	-123	0,022
FWS	-123	0,022

significant different response to Scarlett (*p*<0.05)

Table S17. In the repetition selected S42ILs showing significant effects (*p*<0.05) for the observed root traits and shoot traits at 16°C

trait	Treatment	Effect	Genotype	parent	Estimate	StdErr	DF	tValue	probt	Adjustment	Adjp	LSMeans_genotype	LSMeans_Scarlett	Rp_pCT	significance
1stLLA	16	line	S42IL-109	Scarlett	-1,34	0,49	65	-2,76	0,0076	Dunnett	0,0426	2,75	4,08	-32,77	p <0.01
	16	line	S42IL-123	Scarlett	-1,28	0,49	65	-2,64	0,0104	Dunnett	0,0574	2,8	4,08	-31,36	p <0.05
	16	line	S42IL-129	Scarlett	-0,5	0,49	65	-1,02	0,3116	Dunnett	0,8540	3,59	4,08	-12,12	
	16	line	S42IL-137	Scarlett	-0,99	0,5	65	-1,97	0,0536	Dunnett	0,2459	3,1	4,08	-24,13	
CHA	16	line	S42IL-109	Scarlett	-49,21	19,7	65	-2,50	0,0151	Dunnett	0,0804	50,77	99,98	-49,22	p <0.05
	16	line	S42IL-123	Scarlett	-50,22	19,7	65	-2,55	0,0132	Dunnett	0,0713	49,76	99,98	-50,23	p <0.05
	16	line	S42IL-129	Scarlett	-28,6	19,7	65	-1,45	0,1515	Dunnett	0,5579	71,38	99,98	-28,61	
	16	line	S42IL-137	Scarlett	-34,08	20,34	65	-1,68	0,0987	Dunnett	0,4048	65,9	99,98	-34,09	
FWS	16	line	S42IL-109	Scarlett	-0,05	0,01	65	-4,15	0,0001	Dunnett	0,0006	0,07	0,12	-40,17	p <0.001
	16	line	S42IL-123	Scarlett	-0,05	0,01	65	-4,16	0,0001	Dunnett	0,0006	0,07	0,12	-40,21	p <0.001
	16	line	S42IL-129	Scarlett	-0,02	0,01	65	-1,54	0,1283	Dunnett	0,4946	0,11	0,12	-14,9	
	16	line	S42IL-137	Scarlett	-0,04	0,01	65	-2,98	0,0041	Dunnett	0,0239	0,09	0,12	-29,74	p <0.01
1stLBL	16	line	S42IL-109	Scarlett	-9,46	8,74	65	-1,08	0,2832	Dunnett	0,8173	67,84	77,29	-12,24	
	16	line	S42IL-123	Scarlett	-18,5	8,74	65	-2,12	0,0380	Dunnett	0,1835	58,79	77,29	-23,94	p <0.05
	16	line	S42IL-129	Scarlett	-1,26	8,74	65	-0,14	0,8858	Dunnett	1,0000	76,03	77,29	-1,63	
	16	line	S42IL-137	Scarlett	-3,52	9,02	65	-0,39	0,6974	Dunnett	0,9992	73,77	77,29	-4,56	
2ndLBL	16	line	S42IL-109	Scarlett	-20,81	5,97	65	-3,48	0,0009	Dunnett	0,0056	27,5	48,31	-43,07	p <0.001
	16	line	S42IL-123	Scarlett	-23,06	5,97	65	-3,86	0,0003	Dunnett	0,0017	25,25	48,31	-47,73	p <0.001
	16	line	S42IL-129	Scarlett	-6,19	5,97	65	-1,04	0,3040	Dunnett	0,8448	42,13	48,31	-12,81	
	16	line	S42IL-137	Scarlett	-8,92	6,16	65	-1,45	0,1527	Dunnett	0,5612	39,39	48,31	-18,46	
LSL	16	line	S42IL-109	Scarlett	-10,29	5,65	65	-1,82	0,0733	Dunnett	0,3193	34,58	44,86	-22,93	
	16	line	S42IL-123	Scarlett	-11	5,65	65	-1,95	0,0560	Dunnett	0,2553	33,87	44,86	-24,51	

Trait					Estimate	Std Err	df	t	p	Method	Adj p	Mean1	Mean2	% diff	Sig
	16	line	S42IL-129	Scarlett	-9,17	5,65	65	-1,62	0,1094	Dunnett	0,4388	35,69	44,86	-20,45	
	16	line	S42IL-137	Scarlett	0,7	5,84	65	0,12	0,9053	Dunnett	1,0000	45,56	44,86	1,55	
LSR/NSR	16	line	S42IL-109	Scarlett	-2,61	2,77	65	-0,94	0,3497	Dunnett	0,8942	16,09	18,71	-13,97	
	16	line	S42IL-123	Scarlett	-1,44	2,77	65	-0,52	0,6056	Dunnett	0,9952	17,27	18,71	-7,69	
	16	line	S42IL-129	Scarlett	-0,78	2,77	65	-0,28	0,7796	Dunnett	0,9999	17,93	18,71	-4,17	
	16	line	S42IL-137	Scarlett	2,76	2,86	65	0,96	0,3390	Dunnett	0,8839	21,46	18,71	14,74	
NSR	16	line	S42IL-109	Scarlett	-0,93	0,59	65	-1,59	0,1177	Dunnett	0,4639	5,67	6,6	-14,14	
	16	line	S42IL-123	Scarlett	-0,6	0,59	65	-1,02	0,3119	Dunnett	0,8543	6	6,6	-9,09	
	16	line	S42IL-129	Scarlett	-0,82	0,59	65	-1,40	0,1673	Dunnett	0,5977	5,78	6,6	-12,46	
	16	line	S42IL-137	Scarlett	-1,72	0,61	65	-2,84	0,0060	Dunnett	0,0346	4,88	6,6	-26,14	p <0.01
RDW	16	line	S42IL-109	Scarlett	-0,01	0	65	-1,89	0,0634	Dunnett	0,2832	0,01	0,01	-42,98	
	16	line	S42IL-123	Scarlett	0	0	65	0,67	0,5071	Dunnett	0,9800	0,02	0,01	15,18	
	16	line	S42IL-129	Scarlett	0,01	0	65	3,08	0,0030	Dunnett	0,0179	0,02	0,01	70,19	p <0.01
	16	line	S42IL-137	Scarlett	-0,01	0	65	-2,15	0,0349	Dunnett	0,1703	0,01	0,01	-50,62	p <0.05
RDW/TW	16	line	S42IL-109	Scarlett	0,03	0,07	65	0,40	0,6905	Dunnett	0,9990	0,47	0,44	6,19	
	16	line	S42IL-123	Scarlett	0,19	0,07	65	2,79	0,0069	Dunnett	0,0394	0,63	0,44	43,18	p <0.01
	16	line	S42IL-129	Scarlett	0,15	0,07	65	2,27	0,0263	Dunnett	0,1327	0,6	0,44	35,2	p <0.05
	16	line	S42IL-137	Scarlett	-0,04	0,07	65	-0,55	0,5832	Dunnett	0,9931	0,4	0,44	-8,82	
RSD	16	line	S42IL-109	Scarlett	-29,35	16,65	65	-1,76	0,0827	Dunnett	0,3520	139,71	169,06	-17,36	
	16	line	S42IL-123	Scarlett	-39,32	16,65	65	-2,36	0,0212	Dunnett	0,1095	129,73	169,06	-23,26	p <0.05
	16	line	S42IL-129	Scarlett	-26,24	16,65	65	-1,58	0,1199	Dunnett	0,4702	142,81	169,06	-15,52	
	16	line	S42IL-137	Scarlett	-42,84	17,19	65	-2,49	0,0153	Dunnett	0,0814	126,22	169,06	-25,34	p <0.05
RSD/RSW	16	line	S42IL-109	Scarlett	-0,83	0,47	65	-1,78	0,0796	Dunnett	0,3413	2,37	3,2	-26,06	
	16	line	S42IL-123	Scarlett	-0,88	0,47	65	-1,88	0,0650	Dunnett	0,2891	2,32	3,2	-27,46	

Trait	N		Line	Control	Diff	SE	df	t	p	Method	adj p	Mean	Control Mean	%	Sig
	16	line	S42IL-129	Scarlett	-0,86	0,47	65	-1,85	0,0696	Dunnett	0,3057	2,34	3,2	-27	
	16	line	S42IL-137	Scarlett	-1,7	0,48	65	-3,52	0,0008	Dunnett	0,0049	1,5	3,2	-53,23	p <0.001
RSW	16	line	S42IL-109	Scarlett	-12,01	15,77	65	-0,76	0,4491	Dunnett	0,9604	62,87	74,87	-16,04	
	16	line	S42IL-123	Scarlett	-2,4	15,77	65	-0,15	0,8796	Dunnett	1,0000	72,47	74,87	-3,2	
	16	line	S42IL-129	Scarlett	6,64	15,77	65	0,42	0,6751	Dunnett	0,9987	81,51	74,87	8,87	
	16	line	S42IL-137	Scarlett	18,96	16,28	65	1,16	0,2484	Dunnett	0,7638	93,83	74,87	25,32	
SDW	16	line	S42IL-109	Scarlett	-0,01	0	65	-4,40	0,0000	Dunnett	0,0003	0,01	0,02	-46,32	p <0.001
	16	line	S42IL-123	Scarlett	-0,01	0	65	-3,98	0,0002	Dunnett	0,0011	0,01	0,02	-41,94	p <0.001
	16	line	S42IL-129	Scarlett	0	0	65	-1,81	0,0755	Dunnett	0,3269	0,01	0,02	-19,04	
	16	line	S42IL-137	Scarlett	-0,01	0	65	-3,29	0,0016	Dunnett	0,0099	0,01	0,02	-35,81	p <0.01
SDW/TW	16	line	S42IL-109	Scarlett	-0,03	0,07	65	-0,40	0,6905	Dunnett	0,9990	0,53	0,56	-4,87	
	16	line	S42IL-123	Scarlett	-0,19	0,07	65	-2,79	0,0069	Dunnett	0,0394	0,37	0,56	-33,96	p <0.01
	16	line	S42IL-129	Scarlett	-0,15	0,07	65	-2,27	0,0263	Dunnett	0,1327	0,4	0,56	-27,69	p <0.05
	16	line	S42IL-137	Scarlett	0,04	0,07	65	0,55	0,5832	Dunnett	0,9931	0,6	0,56	6,93	
SRL	16	line	S42IL-109	Scarlett	12027,27	101863,51	65	0,12	0,9064	Dunnett	1,0000	89867,65	77840,37	15,45	
	16	line	S42IL-123	Scarlett	-33475,32	101863,51	65	-0,33	0,7435	Dunnett	0,9997	44365,06	77840,37	-43,01	
	16	line	S42IL-129	Scarlett	-39239,68	101863,51	65	-0,39	0,7013	Dunnett	0,9992	38600,69	77840,37	-50,41	
	16	line	S42IL-137	Scarlett	4950,01	105160,91	65	0,05	0,9626	Dunnett	1,0000	82790,39	77840,37	6,36	
1stLTL	16	line	S42IL-109	Scarlett	-19,75	10,45	65	-1,89	0,0632	Dunnett	0,2824	102,41	122,16	-16,16	
	16	line	S42IL-123	Scarlett	-29,5	10,45	65	-2,82	0,0063	Dunnett	0,0359	92,66	122,16	-24,15	p <0.01
	16	line	S42IL-129	Scarlett	-6,52	10,45	65	-0,62	0,5349	Dunnett	0,9862	115,64	122,16	-5,33	
	16	line	S42IL-137	Scarlett	-2,83	10,78	65	-0,26	0,7941	Dunnett	0,9999	119,33	122,16	-2,31	
TRL	16	line	S42IL-109	Scarlett	-322,29	124,5	65	-2,59	0,0119	Dunnett	0,0647	523,08	845,36	-38,12	p <0.05
	16	line	S42IL-123	Scarlett	-211,28	124,5	65	-1,70	0,0945	Dunnett	0,3913	634,08	845,36	-24,99	

| | 16 | line | S42IL-129 | Scarlett | -181,61 | 124,5 | 65 | -1,46 | 0,1494 | Dunnett | 0,5526 | 663,75 | 845,36 | -21,48 | |
| | 16 | line | S42IL-137 | Scarlett | -323,7 | 128,53 | 65 | -2,52 | 0,0143 | Dunnett | 0,0765 | 521,66 | 845,36 | -38,29 | p <0.05 |

Table S18. In the repetition selected S42ILs showing significant effects (*p*<0.05) for the observed root traits and shoot traits at 24°C

trait	Treatment	Effect	Genotype	parent	Estimate	StdErr	DF	tValue	probt	Adjustment	Adjp	LSMeans_genotype	LSMeans_Scarlett	Rp_pCT	significance
1stLLA	24	line	S42IL-109	Scarlett	-2,92	0,64	62	-4,59	0,0000	Dunnett	0,0001	3,81	6,73	-43,38	p <0.001
	24	line	S42IL-123	Scarlett	-0,08	0,64	62	-0,12	0,9019	Dunnett	1,0000	6,65	6,73	-1,17	
	24	line	S42IL-129	Scarlett	-2,12	0,64	62	-3,33	0,0015	Dunnett	0,0089	4,61	6,73	-31,44	p <0.01
	24	line	S42IL-137	Scarlett	-3,86	0,66	62	-5,90	0,0000	Dunnett	0,0000	2,87	6,73	-57,4	p <0.001
CHA	24	line	S42IL-109	Scarlett	-173,29	224,91	62	-0,77	0,4439	Dunnett	0,9554	75,63	248,92	-69,62	
	24	line	S42IL-123	Scarlett	-54,21	224,91	62	-0,24	0,8103	Dunnett	1,0000	194,71	248,92	-21,78	
	24	line	S42IL-129	Scarlett	-81,8	224,91	62	-0,36	0,7173	Dunnett	0,9994	167,11	248,92	-32,86	
	24	line	S42IL-137	Scarlett	-146,01	231,83	62	-0,63	0,5311	Dunnett	0,9844	102,91	248,92	-58,66	
FWS	24	line	S42IL-109	Scarlett	-0,09	0,02	62	-3,83	0,0003	Dunnett	0,0019	0,13	0,22	-42,53	p <0.001
	24	line	S42IL-123	Scarlett	-0,06	0,02	62	-2,65	0,0101	Dunnett	0,0547	0,15	0,22	-29,51	p <0.05
	24	line	S42IL-129	Scarlett	-0,09	0,02	62	-3,71	0,0004	Dunnett	0,0028	0,13	0,22	-41,25	p <0.001
	24	line	S42IL-137	Scarlett	-0,12	0,03	62	-4,67	0,0000	Dunnett	0,0001	0,1	0,22	-53,45	p <0.001
1stLBL	24	line	S42IL-109	Scarlett	-27,95	12,13	62	-2,30	0,0246	Dunnett	0,1228	81,28	109,23	-25,59	p <0.05
	24	line	S42IL-123	Scarlett	6,25	12,13	62	0,52	0,6083	Dunnett	0,9950	115,48	109,23	5,72	
	24	line	S42IL-129	Scarlett	-3,28	12,13	62	-0,27	0,7880	Dunnett	0,9999	105,95	109,23	-3	
	24	line	S42IL-137	Scarlett	-45,53	12,51	62	-3,64	0,0006	Dunnett	0,0035	63,7	109,23	-41,68	p <0.001
2ndLBL	24	line	S42IL-109	Scarlett	-55,03	16,06	62	-3,43	0,0011	Dunnett	0,0067	90,71	145,73	-37,76	p <0.01
	24	line	S42IL-123	Scarlett	-23,78	16,06	62	-1,48	0,1438	Dunnett	0,5292	121,95	145,73	-16,32	
	24	line	S42IL-129	Scarlett	-56,58	16,06	62	-3,52	0,0008	Dunnett	0,0050	89,15	145,73	-38,82	p <0.001

	24	line	S42IL-137	Scarlett	-41,08	16,56	62	-2,48	0,0158	Dunnett	0,0826	104,65	145,73	-28,19	p <0.05
LSL	24	line	S42IL-109	Scarlett	-14,65	5,98	62	-2,45	0,0172	Dunnett	0,0892	34,52	49,16	-29,79	p <0.05
	24	line	S42IL-123	Scarlett	0,45	5,98	62	0,08	0,9399	Dunnett	1,0000	49,62	49,16	0,92	
	24	line	S42IL-129	Scarlett	3,15	5,98	62	0,53	0,6009	Dunnett	0,9944	52,31	49,16	6,4	
	24	line	S42IL-137	Scarlett	-15,3	6,17	62	-2,48	0,0158	Dunnett	0,0826	33,86	49,16	-31,12	p <0.05
LSR/NSR	24	line	S42IL-109	Scarlett	0,18	6,49	62	0,03	0,9776	Dunnett	1,0000	36,29	36,11	0,51	
	24	line	S42IL-123	Scarlett	4,03	6,49	62	0,62	0,5375	Dunnett	0,9856	40,13	36,11	11,15	
	24	line	S42IL-129	Scarlett	-1,48	6,49	62	-0,23	0,8208	Dunnett	1,0000	34,63	36,11	-4,09	
	24	line	S42IL-137	Scarlett	0,18	6,69	62	0,03	0,9791	Dunnett	1,0000	36,28	36,11	0,49	
NSR	24	line	S42IL-109	Scarlett	-1,33	0,51	62	-2,60	0,0117	Dunnett	0,0627	5,78	7,11	-18,75	p <0.05
	24	line	S42IL-123	Scarlett	-1,33	0,51	62	-2,60	0,0117	Dunnett	0,0627	5,78	7,11	-18,75	p <0.05
	24	line	S42IL-129	Scarlett	-1,22	0,51	62	-2,38	0,0203	Dunnett	0,1036	5,89	7,11	-17,19	p <0.05
	24	line	S42IL-137	Scarlett	-3,36	0,53	62	-6,35	0,0000	Dunnett	0,0000	3,75	7,11	-47,27	p <0.001
RDW	24	line	S42IL-109	Scarlett	-0,02	0,01	62	-3,54	0,0008	Dunnett	0,0048	0,02	0,04	-44,7	p <0.001
	24	line	S42IL-123	Scarlett	-0,01	0,01	62	-2,70	0,0090	Dunnett	0,0494	0,03	0,04	-34,07	p <0.01
	24	line	S42IL-129	Scarlett	-0,02	0,01	62	-3,44	0,0010	Dunnett	0,0064	0,02	0,04	-43,47	p <0.01
	24	line	S42IL-137	Scarlett	-0,03	0,01	62	-5,14	0,0000	Dunnett	0,0000	0,01	0,04	-66,89	p <0.001
RDW/TW	24	line	S42IL-109	Scarlett	0	0,05	62	-0,09	0,9257	Dunnett	1,0000	0,57	0,58	-0,74	
	24	line	S42IL-123	Scarlett	-0,02	0,05	62	-0,43	0,6722	Dunnett	0,9985	0,56	0,58	-3,35	
	24	line	S42IL-129	Scarlett	0	0,05	62	-0,08	0,9368	Dunnett	1,0000	0,57	0,58	-0,63	
	24	line	S42IL-137	Scarlett	-0,1	0,05	62	-2,07	0,0429	Dunnett	0,1999	0,48	0,58	-16,79	p <0.05
RSD	24	line	S42IL-109	Scarlett	-55,19	35,28	62	-1,56	0,1229	Dunnett	0,4710	289,09	344,28	-16,03	
	24	line	S42IL-123	Scarlett	-30,01	35,28	62	-0,85	0,3983	Dunnett	0,9289	314,27	344,28	-8,72	
	24	line	S42IL-129	Scarlett	-66,83	35,28	62	-1,89	0,0629	Dunnett	0,2762	277,46	344,28	-19,41	

	24	line	S42IL-137	Scarlett	-115,63	36,37	62	-3,18	0,0023	Dunnett	0,0137	228,65	344,28	-33,59	p <0.01
RSD/RSW	24	line	S42IL-109	Scarlett	2,21	0,5	62	4,45	0,0000	Dunnett	0,0002	4,57	2,37	93,17	p <0.001
	24	line	S42IL-123	Scarlett	0,24	0,5	62	0,48	0,6311	Dunnett	0,9967	2,61	2,37	10,09	
	24	line	S42IL-129	Scarlett	0,75	0,5	62	1,51	0,1351	Dunnett	0,5056	3,12	2,37	31,67	
	24	line	S42IL-137	Scarlett	0,24	0,51	62	0,47	0,6391	Dunnett	0,9971	2,61	2,37	10,16	
RSW	24	line	S42IL-109	Scarlett	-88,55	26,58	62	-3,33	0,0015	Dunnett	0,0089	67,61	156,16	-56,71	p <0.01
	24	line	S42IL-123	Scarlett	-18,15	26,58	62	-0,68	0,4973	Dunnett	0,9759	138,01	156,16	-11,62	
	24	line	S42IL-129	Scarlett	-49,94	26,58	62	-1,88	0,0649	Dunnett	0,2836	106,21	156,16	-31,98	
	24	line	S42IL-137	Scarlett	-62,81	27,4	62	-2,29	0,0253	Dunnett	0,1258	93,35	156,16	-40,22	p <0.05
SDW	24	line	S42IL-109	Scarlett	-0,01	0	62	-4,08	0,0001	Dunnett	0,0008	0,02	0,03	-43,61	p <0.001
	24	line	S42IL-123	Scarlett	-0,01	0	62	-2,84	0,0061	Dunnett	0,0342	0,02	0,03	-30,37	p <0.01
	24	line	S42IL-129	Scarlett	-0,01	0	62	-4,15	0,0001	Dunnett	0,0007	0,02	0,03	-44,33	p <0.001
	24	line	S42IL-137	Scarlett	-0,02	0	62	-4,80	0,0000	Dunnett	0,0001	0,01	0,03	-52,92	p <0.001
SDW/TW	24	line	S42IL-109	Scarlett	0	0,05	62	0,09	0,9257	Dunnett	1,0000	0,43	0,42	1	
	24	line	S42IL-123	Scarlett	0,02	0,05	62	0,43	0,6722	Dunnett	0,9985	0,44	0,42	4,55	
	24	line	S42IL-129	Scarlett	0	0,05	62	0,08	0,9368	Dunnett	1,0000	0,43	0,42	0,85	
	24	line	S42IL-137	Scarlett	0,1	0,05	62	2,07	0,0429	Dunnett	0,1999	0,52	0,42	22,8	p <0.05
SRL	24	line	S42IL-109	Scarlett	9714,41	7483,34	62	1,30	0,1990	Dunnett	0,6615	52767,05	43052,64	22,56	
	24	line	S42IL-123	Scarlett	7489,27	7483,34	62	1,00	0,3208	Dunnett	0,8585	50541,91	43052,64	17,4	
	24	line	S42IL-129	Scarlett	10448,74	7483,34	62	1,40	0,1676	Dunnett	0,5899	53501,37	43052,64	24,27	
	24	line	S42IL-137	Scarlett	-2482,5	7713,65	62	-0,32	0,7487	Dunnett	0,9997	40570,13	43052,64	-5,77	
1stLTL	24	line	S42IL-109	Scarlett	-65,34	17,84	62	-3,66	0,0005	Dunnett	0,0033	131	196,34	-33,28	p <0.001
	24	line	S42IL-123	Scarlett	-10,68	17,84	62	-0,60	0,5514	Dunnett	0,9882	185,66	196,34	-5,44	
	24	line	S42IL-129	Scarlett	-38,74	17,84	62	-2,17	0,0337	Dunnett	0,1622	157,61	196,34	-19,73	p <0.05

trait	Treatment	Effect	Genotype	parent	Estimate	StdErr	DF	tValue	probt	Adjustment	Adjp	LSMeans_genotype	LSMeans_Scarlett	Rp_pCT	significance
	24	line	S42IL-137	Scarlett	-53,95	18,39	62	-2,93	0,0047	Dunnett	0,0268	142,39	196,34	-27,48	p <0.01
TRL	24	line	S42IL-109	Scarlett	-633,77	216,24	62	-2,93	0,0047	Dunnett	0,0270	1175,83	1809,6	-35,02	p <0.01
	24	line	S42IL-123	Scarlett	-490,15	216,24	62	-2,27	0,0269	Dunnett	0,1329	1319,45	1809,6	-27,09	p <0.05
	24	line	S42IL-129	Scarlett	-602,48	216,24	62	-2,79	0,0071	Dunnett	0,0394	1207,12	1809,6	-33,29	p <0.01
	24	line	S42IL-137	Scarlett	-1250,35	222,89	62	-5,61	0,0000	Dunnett	0,0000	559,25	1809,6	-69,1	p <0.001

Table S19 In the repetition significant effects in root and shoot traits ($p<0.05$) for selected S42ILs were reproducible

trait	Treatment	Effect	Genotype	parent	Estimate	StdErr	DF	tValue	probt	Adjustment	Adjp	LSMeans_genotype	LSMeans_Scarlett	Rp_pCT	significance
1stLBL	24	line	S42IL-109	Scarlett	-27,95	12,13	62	-2,30	0,0246	Dunnett	0,1228	81,28	109,23	-25,59	p <0.05
	24	line	S42IL-137	Scarlett	-45,53	12,51	62	-3,64	0,0006	Dunnett	0,0035	63,7	109,23	-41,68	p <0.001
1stLLA	24	line	S42IL-129	Scarlett	-2,12	0,64	62	-3,33	0,0015	Dunnett	0,0089	4,61	6,73	-31,44	p <0.01
	24	line	S42IL-137	Scarlett	-3,86	0,66	62	-5,90	0,0000	Dunnett	0,0000	2,87	6,73	-57,4	p <0.001
1stLTL	24	line	S42IL-109	Scarlett	-65,34	17,84	62	-3,66	0,0005	Dunnett	0,0033	131	196,34	-33,28	p <0.001
	24	line	S42IL-129	Scarlett	-38,74	17,84	62	-2,17	0,0337	Dunnett	0,1622	157,61	196,34	-19,73	p <0.05
	24	line	S42IL-137	Scarlett	-53,95	18,39	62	-2,93	0,0047	Dunnett	0,0268	142,39	196,34	-27,48	p <0.01
FWS	24	line	S42IL-129	Scarlett	-0,09	0,02	62	-3,71	0,0004	Dunnett	0,0028	0,13	0,22	-41,25	p <0.001
NSR	24	line	S42IL-109	Scarlett	-1,33	0,51	62	-2,60	0,0117	Dunnett	0,0627	5,78	7,11	-18,75	p <0.05
	24	line	S42IL-123	Scarlett	-1,33	0,51	62	-2,60	0,0117	Dunnett	0,0627	5,78	7,11	-18,75	p <0.05
	24	line	S42IL-129	Scarlett	-1,22	0,51	62	-2,38	0,0203	Dunnett	0,1036	5,89	7,11	-17,19	p <0.05
RDW	24	line	S42IL-109	Scarlett	-0,02	0,01	62	-3,54	0,0008	Dunnett	0,0048	0,02	0,04	-44,7	p <0.001
	24	line	S42IL-123	Scarlett	-0,01	0,01	62	-2,70	0,0090	Dunnett	0,0494	0,03	0,04	-34,07	p <0.01
RSD/RSW	24	line	S42IL-109	Scarlett	2,21	0,5	62	4,45	0,0000	Dunnett	0,0002	4,57	2,37	93,17	p <0.001
RSW	24	line	S42IL-109	Scarlett	-88,55	26,58	62	-3,33	0,0015	Dunnett	0,0089	67,61	156,16	-56,71	p <0.01
	24	line	S42IL-137	Scarlett	-62,81	27,4	62	-2,29	0,0253	Dunnett	0,1258	93,35	156,16	-40,22	p <0.05
TRL	24	line	S42IL-123	Scarlett	-490,15	216,24	62	-2,27	0,0269	Dunnett	0,1329	1319,45	1809,6	-27,09	p <0.05
	24	line	S42IL-129	Scarlett	-602,48	216,24	62	-2,79	0,0071	Dunnett	0,0394	1207,12	1809,6	-33,29	p <0.01

☐ Reproduced   ☐ ILs revealed a new significant phenotypic effect

Table S20 The correspondence of those QTL in the S42IL-population associated with shoot traits with QTL previously identified in field

Trait	S42IL	chromosome	QTL	posit on [cM]	RP%	Studies with corresponding QTL	Candidate genes
1stLLA	-109	-2H	Q1stLLA.S42IL.2H	59.5-60.8	-25.69975	I, II, VII, VIII, X	HvFT4 HvCEN
	-135	-7Hb	Q1stLLA.S42IL.7Hb	70.2-74.4	-18.57506	VII	HvCO1
	-133	-3Ha	Q1stLLA.S42IL.3Ha	36,8-40,7	-18.06616		
		-5H	Q1stLLA.S42IL.5H	0-0,1	-18.06616		
		-6Hc	Q1stLLA.S42IL.6Hc	76,1	-18.06616		
		-7Ha	Q1stLLA.S42IL.7Ha	11.8-34.3	-18.06616	III, IV, V, VII, IX	VRN-H3
	-112	-3Hb	Q1stLLA.S42IL.3H	64.5-76.3	-16.79389	VII	
	-129	-6Ha	Q1stLLA.S42IL.6Ha	38.1-55.7	-16.03053	VI, VII	HvCO2
		-6Hb	Q1stLLA.S42IL.6Hc	76,1	-16.03053		
	-128	-6Ha	Q1stLLA.S42IL.6Hb	47.5-55.7	-15.52163	VI	HvCO2
1stLBL	-138	-7Hb	Q1stLBL.S42IL.7Hb	128.3-129.4	-42.7089	VII	HvFT3
	-129	-6H	Q1stLBL.S42IL.6H	38.1-55.7	-35.48414	VI, VII	HvCO2
	-106	-2Ha	Q1stLBL.S42IL2Ha	8,9-12,1	-33.40536		
		-2Hb	Q1stLBL.S42IL2Hb	12,5-16,5	-33.40536		
	-107	-2Ha	Q1stLBL.S42IL2Ha	12,5-16,5	-29.09363	I, II, III, IV, VI, VII, X	Ppd-H1
		-2Hb	Q1stLBL.S42IL2Hb	18,5-33,5	-29.09363		
		-2Hc	Q1stLBL.S42IL2Hc	33,9-41,2	-29.09363		
	-108	-2Ha	Q1stLBL.S42IL2Ha	12,5-16,5	-28.88061	I, II, III, IV, V, VI, VII	Ppd-H1 HvFT4
		-2Hb	Q1stLBL.S42IL2Hb	33,9-41,2	-28.88061		
		-2Hc	Q1stLBL.S42IL2Hc	41,9-52,2	-28.88061		
	-141	-1Hb	Q1stLBL.S42IL1Hb	62,8-80.2	-28.66522	III	
		-5Hb	Q1stLBL.S42IL5Hb	165,8-189,4	-28.66522		
	-114	-5Ha	Q1stLBL.S42IL5Ha	48,8-50	-22.62034		
	-128	-6H	Q1stLBL.S42IL.6H	47.5-55.7	-22.33793	VI	HvCO2
	-135	-7Ha	Q1stLBL.S42IL5Ha	70.2-74,4	-19.41386	VII	HvCO1
	-101	-1Ha	Q1stLBL.S42IL1Ha	0-9.9	-17.59487	III, IV	
	-109	-2Ha	Q1stLBL.S42IL2Ha	33,9-41,2	-16.71628	I, II, VII, VIII, X	HvFT4 HvCEN
		-2Hb	Q1stLBL.S42IL2Hb	41,9-52,2	-16.71628		
		-2Hc	Q1stLBL.S42IL2Hc	59,5-60,7	-16.71628		
	-111	-3Ha	Q1stLBL.S42IL3Ha	47.3-54.5	-15.7168	X	
		-3Hb	Q1stLBL.S42IL3Hb	54,5-55,2	-15.7168		
	-112	-3Hc	Q1stLBL.S42IL3Hc	64.5-76.3	-15.41184	VII	
	-127	-5H	Q1stLBL.S42IL5Hb	142-152.6	-15.09983		
1stLTL	-107	-2H	Q1stLTL.S42IL2H	18.5-33.5	-24.90306	I, II, III, IV, V, VI, VII	Ppd-H1
	-141	-1H	Q1stLTLL.S42IL.1H	62,8-80.2	-21.9021	III	
		-5H	Q1stLTLL.S42IL.5H	165,8-189,4	-21.9021		
	-108	-2H	Q1stLTLL.S42IL.2H	18.5-33.5	-20.46507	I, II, III, IV, V, VI, VII	Ppd-H1 HvFT4
	-134	-7H	Q1stLTL.S42IL.7H	67.8-70,2	-19.7147	I, II, III, IV, V, X	HvCO1
	-128	-6H	Q1stLTLL.S42IL.6H	47,5-55.7	-15.75669	VII	HvCO2
2ndLTL	-134	-7H	Q2ndLTL.S42IL.7H	67.8-70,2	28.79093	I, II, III, IV, V, X	HvCO1
	-108	-2Ha	Q2ndLTL.S42IL.2Ha	18.5-33.5	28.41172	I, II, III, IV, V, VI, VII	Ppd-H1 HvFT4
		-2Hb	Q2ndLTL.S42IL.2Hb	33.9-41.2	28.41172		
		-2Hc	Q2ndLTL.S42IL.2Hc	41.9-52.2	28.41172		
	-112	-3H	Q2ndLTL.S42IL.3H	64.6-76.3	26.24434	VII	
	-130	-6H	Q2ndLTL.S42IL.6H	62.7-63.5	24.63277		
	-107	-2Ha	Q2ndLTL.S42IL.2Ha	18.5-33.5	22.37345	I, II, III, IV, V, VI, VII	Ppd-H1
		-2Hb	Q2ndLTL.S42IL.2Hb	33.9-41.2	22.37345		
	-135	-7H	Q2ndLTL.S42IL.7H	70.2-74.4	20.99775	VII	HvCO1
	-101	-1Ha	Q2ndLTL.S42IL.1Ha	0-9.9	20.05989	III, IV	
	-109	-2Ha	Q2ndLTL.S42IL.2Ha	33.9-41.2	17.15923	I, II, VII, VIII, X	HvFT4 HvCEN
		-2Hb	Q2ndLTL.S42IL.2Hb	41.9-51.9	17.15923		
		-2Hc	Q2ndLTL.S42IL.2Hc	59,5-60,7	17.15923		
	-141	-1Hb	Q2ndLTL.S42IL.1Hb	62,8--80.2	16.87572	III	
		-5H	Q2ndLTL.S42IL.5H	165,8-189,4	16.87572		
FWS	-129	-6H	QFWS.S42IL.6H	38.1-55.7	-31.22079	VI, VII	HvCO2
	-128	-6H	QFWS.S42IL.6H	47.5-55.7	-24.85397	VII	HvCO2
	-123	-4H	QFWS.S42IL.4H	100.8-110.2	20.51694		

von Korff et al. 2006   I   Honsdorf et al. 2017   VII
Schmalenbach et al. 2009   II   Stephan Reinert et al. 2019   VIII
Schmalenbach et al. 2011   III   Amare Kebede et al. 2019   IX
Hoffmann et al. 2012   IV   Zahn et al. 2020   X
Schnaithmann and Pillen 2013   V
Honsdorf et al. 2014 b   VI

Acknowledgements

Curriculum Vitae
Julia Bellstädt

Personal Details

Date and place of birth: 23.03.1989 in Dessau-Roßlau

Marital status: Unmarried, two children

Nationality: German

Education

Since 12/2015	PhD student at the Institute of Agricultural and Nutritional Sciences at MLU Halle-Wittenberg, Supervisor: Prof. Dr. Marcel Quint
1/2014	Teaching degree (High School) in Arts and Biology, Martin Luther University Halle-Wittenberg
10/2009-1/2014	Teacher Training Course for Arts and Biology teacher at Martin Luther University of Halle-Wittenberg and Burg Giebichenstein University of Art and Design
10/2008-9/2009	Start teacher training course for Arts and Biology teacher at Friedrich-Friedrich Schiller University Jena and Bauhaus University Weimar
6/2007	Abitur
8/2001-6/2007	High school at Philanthropinum in Dessau-Roßlau
9/1999-6/2001	Secondary school in Mildensee (Dessau-Roßlau)
8/1995-7/1999	„Grundschule am Luisium" in Dessau-Waldersee

Research experience

4/2020-7/2020	Research assistant, at Institute of Agricultural and Nutritional Sciences at MLU Halle-Wittenberg
5/2019-9/2019	Research assistant, Leibniz Institute of Plant Biochemistry (IPB), Halle
2/2014-8/2014	Research assistant, Leibniz Institute of Plant Biochemistry (IPB), Halle
4/2013-7/2014	Research intern, Leibniz Institute of Plant Biochemistry (IPB), Halle

10/2007-1/2008   **internship at Diakonissenkrankenhaus Dessau (DKD) and Städtischen Klinikum Dessau**

Grants

PhD Scholarship, Rosa-Luxemburg-Stiftung (2015-2019)

Language skills

English, French

IT skills

Word, Excel, PowerPoint, Photoshop, GIMP, basic knowledge of R

List of publication

Bellstaedt, J., Trenner, J., Lippmann, R., Poeschl, Y., Zhang, X., Friml, J., Quint, M., Delker, C. (2019). A mobile auxin signal connects temperature sensing in cotyledons with growth responses in hypocotyls. Plant Physiol.180, 757-766,

Ibañez, C., Poeschl, Y., Peterson, T., **Bellstädt, J.**, Denk, K., Gogol-Döring, A., Quint, M., Delker, C. (2017). Ambient temperature and genotype differentially affect developmental and phenotypic plasticity in *Arabidopsis thaliana*, BMC Plant Biol. *17*, 114.

Drost, H.G., **Bellstädt, J.**, O'Maoileidigh, D.S., Silva, A.T., Gabel, A., Weinholdt, C., Ryan, P.T., Dekkers, B.J.W., Bentsink, L., Hilhorst, H., Ligterink, W., Wellmer, F., Grosse, I., Quint, M. (2016). Post-embryonic hourglass patterns mark ontogenetic transitions in plant development. Mol. Biol. Evol. *33*, 1158-63.

Eidesstatliche Erklärung / Declaration under Oath

Ich erkläre an Eides statt, dass ich die Arbeit selbstständig und ohne fremde Hilfe verfasst, keine anderen als die von mir angegebenen Quellen und Hilfsmittel benutzt und die den benutzten Werken wörtlich oder inhaltlich entnommenen Stellen als solche kenntlich gemacht habe.

I declare under penalty of perjury that this thesis is my own work entirely and has been written without any help from other people. I used only the sources mentioned and included all the citations correctly both in word or content.

Halle, 14.12.2021   _____

Unterschrift / Signature